U.S. DEPARTMENT OF ENERGY

PNNL- 18985

Prepared for the
U.S. Nuclear Regulatory Commission
under a Related Services Agreement
with the U.S. Department of Energy
Contract DE-AC05-76RL01830

Program for the Inspection of Nickel Alloy Components

Report from the Program's Steering Committee: Inspection of Bottom-Mounted Instrumentation Nozzles Round Robin

SE Cumblidge
PG Heasler
SR Doctor
TT Taylor

November 2009

Pacific Northwest
NATIONAL LABORATORY

Proudly Operated by Battelle *Since 1965*

DISCLAIMER

PACIFIC NORTHWEST NATIONAL LABORATORY
operated by
BATTELLE
for the
UNITED STATES DEPARTMENT OF ENERGY
under Contract DE-AC05-76RL01830

Printed in the United States of America

Available to DOE and DOE contractors from the
Office of Scientific and Technical Information,
P.O. Box 62, Oak Ridge, TN 37831-0062;
ph: (865) 576-8401
fax: (865) 576-5728
email: reports@adonis.osti.gov

Available to the public from the National Technical Information Service,
U.S. Department of Commerce, 5285 Port Royal Rd., Springfield, VA 22161
ph: (800) 553-6847
fax: (703) 605-6900
email: orders@ntis.fedworld.gov
online ordering: http://www.ntis.gov/ordering.htm

This document was printed on recycled paper.
(9/2003)

PNNL- 18985

Program for the Inspection of Nickel Alloy Components

Report from the Program's Steering Committee: Inspection of Bottom-Mounted Instrumentation Nozzles Round Robin

SE Cumblidge SR Doctor
PG Heasler TT Taylor

November 2009

Prepared for
U.S. Nuclear Regulatory Commission
under a Related Services Agreement
with the U.S. Department of Energy
Contract DE-AC05-76RL01830

Pacific Northwest National Laboratory
Richland, Washington 99352

Summary

The U.S. Nuclear Regulatory Commission (NRC) executed agreements with organizations in Japan, Sweden, South Korea, Finland, and the United States to establish the Program for the Inspection of Nickel Alloy Components (PINC). The objectives of the PINC program participants are:

- To join together for cooperative research.
- To address the problem of primary water stress corrosion cracking (PWSCC), a form of degradation observed in some pressurized water reactor pressure boundary components. Specifically, the research was designed primarily to understand the morphology of PWSCC cracks, to assess nondestructive evaluation (NDE) techniques for detecting and characterizing cracks with such morphology, and to distinguish them from other types of flaws or other innocuous weld conditions. This program provided data that enabled a quantitative assessment of available NDE techniques to detect and size PWSCC in nickel-based alloys.

The PINC participants identified and ranked all PWSCC and component configurations for consideration for study in the PINC framework. The three areas that were ranked highest were bottom-mounted instrumentation (BMIs), dissimilar metal welds (DMWs), and control rod drive mechanisms (CRDMs). The BMIs were identified as top priority because it is not easy to replace a reactor pressure vessel bottom head and repairs are challenging, as was learned at the South Texas Project. The issue of dissimilar metal welds was considered to also be very important based on the cracking that had been experienced at V.C. Summer and Ringhals. The CRDM issue was also assigned a high priority because of the number of plants world wide that have experienced cracking and the Davis-Besse event. However, the low availability of CRDM assemblies and the need to complete the PINC round robin in a timely fashion made it possible to address only the dissimilar metal welds and the bottom-mounted instrumentation nozzles. Dissimilar metal piping weld assemblies were available immediately so this round-robin study was able to start first.

The PINC was focused on studying two aspects of PWSCC. One was to document the crack morphology and NDE responses of PWSCC and compare these data with methods to simulate PWSCC for NDE capability studies. The other was to study the capability of various NDE methods to detect and size the through-wall extent of PWSCC. The studies involving NDE capability were carried out as international round robins with PINC participants. The results are, in some cases, discussed with reference to the requirements of ASME Code, Section XI, Appendix VIII. It should be noted that the round robin study was not designed to constitute an Appendix VIII compliant demonstration.

This report describes the efforts of the PINC participants to assess the capability of NDE techniques to detect and characterize the through-wall depth and length of PWSCC in bottom-mounted instrumentation penetration tubes and J-groove welds. Based upon the information that was developed from conducting round-robin exercises on BMI nozzles, this study provided the following conclusions. The conclusions and recommendations presented in this report are based on the probability of detection, false call rate, and sizing statistics measured in the round robin studies.

Probability of Detection Performance

For the test samples used in the PINC BMI round robin, two techniques proved to have a high probability of detection for flaws greater than 5 mm in length: eddy current using a single cross coil probe at 300-400 kHz and adaptive phased array ultrasonic testing at 5 MHz. The array eddy current examinations carried out in this BMI round robin using frequencies of 100-200 kHz had relatively poor performance, with a large number of false calls. There were not enough long flaws in the potential drop inspections to determine their effectiveness with statistical significance.

Sizing Performance

The cross coil eddy current techniques, adaptive phased array ultrasonic test, and the closely coupled probe potential drop tests all achieved length sizing root mean square errors of less than 5 mm. The array eddy current techniques in this BMI round robin were less effective at length sizing, and the induced current potential drop technique did not have a sufficient number of inspections to draw any conclusions on the technique's length sizing capability. There was insufficient information on depth sizing to draw meaningful conclusions.

Acknowledgments

There have been significant contributions made by a number of people and organizations to accomplish this study. The authors acknowledge special appreciation to Deborah Jackson and Carol Moyer of the NRC for their leadership in helping organize and start the PINC and Iouri Prokofiev for his leadership. George Schuster (retired) of Pacific Northwest National Laboratory (PNNL) was the initial leader and chairman of the Data Analysis Group and the Atlas Information Tool task group. The authors also acknowledge the hard work and effort of the round-robin invigilators who reviewed inspection procedures and monitored the work of inspection teams, and they thank members of the Data Analysis Group who worked diligently to ensure that the very large set of data was correct and suggested the analysis that was performed.

The following companies participated in the PINC dissimilar metal weld round robin and should be acknowledged for their significant contributions:

- European Inspection Teams
  a. FORCE Institute
  b. Wesdyne TRC (two teams)
  c. Tecnatom
  d. VTT (two teams)
- Korean Inspection Teams
  a. Korea Plant Service and Engineering Company
  b. Doosan Heavy Industries
  c. Sean-UMI-ANSCO
  d. Seoul National University
  e. Korea Hydro & Nuclear Power Company
- Japanese Inspection Teams
  f. Tohoku University – Three Teams
     - Fracture and Reliability Research Institute
     - Institute of Fluid Science
     - Department of Nanomechanics
  g. Mitsubishi Heavy Industries, Ltd., Takasago Research & Development Center – Two Teams
     - Ultrasonic testing team
     - Eddy-current testing team

The following companies participated in the PINC BMI weld round robin and are acknowledged for their significant contributions:

- European Inspection Team
  - Wesdyne TRC

- Korean Inspection Team
  - Korea Plant Service and Engineering Company
- Japanese Inspection Teams
  h. Tohoku University – Three Teams
     - Fracture and Reliability Research Institute
     - Institute of Fluid Science
     - Department of Nanomechanics
  i. Mitsubishi Heavy Industries, Ltd, Takasago Research & Development Center – Two Teams
     - Ultrasonic testing team
     - Eddy-current testing team
- United States Inspection Team
  - The Electric Power Research Institute

The authors acknowledge the following organizations who have participated in the PINC.

Organizations from Japan

- Japan Nuclear Energy Safety Organization (JNES)
- Japan Power Engineering and Inspection Corporation (JAPEIC)
- Tohoku University
- Mitsubishi Heavy Industries, Ltd. (MHI)
- KANSAI Electric Power Company

Organizations from Europe

- Swedish Radiation Safety Authority (SSM)
- Swedish Qualification Centre (SQC)
- Wesdyne TRC, Sweden
- VTT, Finland
- Force Institute, Denmark
- Wesdyne TRC, Sweden
- Tecnatom, Spain
- Helsinki University of Technology

Organizations from South Korea

- Korea Institute of Nuclear Safety (KINS)
- Korea Atomic Energy Research Institute (KAERI)

- Korea Plant Services & Engineering Co. Ltd. (KPS)
- Sungkunkwan University
- Korea Electric Power Research Institute (KEPRI)

Organization from the United States

- Electric Power Research Institute

Finally, the authors thank Ms. Kay Hass for typing and editing the seemingly endless versions and revisions of this document.

Acronyms and Abbreviations

AC	alternating current
ASME	American Society of Mechanical Engineers
BMI	bottom-mounted instrumentation
CCPPD	closely coupled probe potential drop method
COD	crack opening displacement
CRDM	control rod drive mechanism
DAG	Data Analysis Task Group
DC	direct current
DMW	dissimilar metal welds
ECT	eddy current testing
EPRI	Electric Power Research Institute
FCP	false call probability
ICPD	induced current potential drop method
JAPEIC	Japan Power Engineering and Inspection Corporation
JNES	Japan Nuclear Energy Safety Organization
KAERI	Korea Atomic Energy Research Institute
KEPRI	Korea Electric Power Research Institute
KINS	Korea Institute of Nuclear Safety
KPS	Korea Plant Services & Engineering Co. Ltd.
LOCA	loss-of-coolant accident
MHI	Mitsubishi Heavy Industries, Ltd.
NDE	nondestructive evaluation
NRC	Nuclear Regulatory Commission
PINC	Program for the Inspection of Nickel Alloy Components
POD	probability of detection
PNNL	Pacific Northwest National Laboratory
PWR	pressurized water reactor
PWSCC	primary water stress corrosion cracking
RMSE	root mean square error
RPV	reactor pressure vessel
RRT	round robin test
SCC	stress corrosion cracking
SQC	Swedish Qualification Center
SSM	Swedish Radiation Safety Authority
TG	Task Group
TOFD	time-of-flight diffraction
UT	ultrasonic testing

Contents

Figures

Tables

1.0 Introduction

Stress corrosion cracking in nickel alloy material has occurred world-wide in a number of nuclear power plants and is seen as a serious issue affecting the reliable and safe operation of nuclear power plants. Stress corrosion cracking in dissimilar metal welds is often referred to as primary water stress corrosion cracking (PWSCC) or interdendritic stress corrosion cracking (IDSCC). For this report the term primary water stress corrosion cracking (PWSCC) will be used. PWSCC degradation has resulted in breaches of the pressure boundary and caused leakage in several dissimilar metal welds (Bamford 2000; Bamford et al. 2002; Jenssen et al. 2002a; Jenssen et al. 2002b), control rod drive mechanism nozzle penetration weldments (Frye et al. 2002; Lang 2003), and bottom-mounted instrumentation nozzle penetration weldments (Halpin 2003). Reliable detection of PWSCC is challenging because the geometries, materials, and configurations are not conducive to reliable nondestructive evaluation (NDE) and the service-induced cracking exhibits very tight and very complex branching in the nickel-based welds.

The U.S. Nuclear Regulatory Commission (NRC) executed agreements with organizations in Japan, Sweden, South Korea, the United States, and Finland to establish the Program for the Inspection of Nickel Alloy Components (PINC). The objectives of the PINC program participants are:

- To join together for cooperative research.
- To address the problem of PWSCC. Specifically, the research was designed primarily to understand the morphology of PWSCC cracks, to assess NDE techniques for detecting and characterizing cracks with such morphology, and to distinguish them from other types of flaws or other innocuous weld conditions. This program provided data that enabled a quantitative assessment of available NDE techniques to detect and size PWSCC in dissimilar metal welds.

PINC program participants organized the project into a Steering Committee, two task groups, and the Data Analysis Group, as illustrated in the following organizational chart (Figure 1.1).

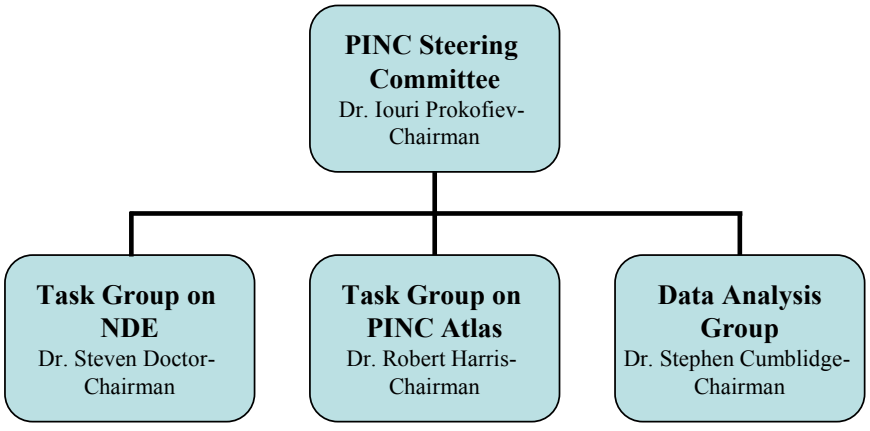

Figure 1.1. Organization Chart for Steering Committee and Task Groups

1.1 PINC Steering Committee

Steering Committee Members

Deborah Jackson was the original Chairman from the NRC. In 2004 she was replaced by *Carol Moyer,* and in 2007 *Carol Moyer* was replaced by *Iouri Prokofiev*
Katsumi Kono
Suck-Chull Kang was the initial representative from KINS. In May 2007 he was replaced by *Myungho Song* and in May 2008 he was replaced by *Haedong Chung*
Pentti Kauppinen
Peter Merck
Naoki Chigusa was the initial representative from Kansai Electric Power Company. He was replaced by *Mr. Hiraoka.*
Masanobu Iwasaki was the substitute for *Dr. Chigusa*. In June 2008, he was replaced by *Mr. Taniguchi*.
Tetsuo Shoji
Jack Spanner

Non-Voting Members
Rob Harris
Steven Doctor
Stephen Cumblidge

The Steering Committee of the Program provides guidance for the project and its implementation and:

- Advises the Task Groups on program implementation and recommends related actions.
- Monitors the program progress, collects, coordinates, and assimilates the results of projects (Task Groups) addressing specific aspects of the problem, and promotes practical implementation of program results at the national level.
- Provides a forum for exchanging information among group members on related work underway and planned activities. The Steering Committee develops strategies to deal with matters requiring coordination with members.
- Assures that the efforts of the Task Groups and of the program as a whole remain focused on specific technical issues that have been agreed to by PINC members as well as ensuring that the work is progressing to an agreed-upon time schedule.
- Provides a final report documenting the results of this program and providing specific recommendations for inspection of PWSCC.

1.2 Task Group on NDE

Task Group (TG) NDE Members

Steven Doctor – Chairman
Ichiro Komura
Katsumi Kono
Kwangsik Yoon

Kyungcho Kim
Sung Sik Kang
Pentti Kauppinen
Peter Merck
Tommy Zettervall
Shuji Tanioka
Jack Spanner

This Task Group (TG)-NDE has the following objectives:

- Develop designs of round-robin studies that need to be conducted in order to quantify the effectiveness of NDE for the detection and characterization of PWSCC.
- Review and assess methods to simulate the NDE responses from implanted flaws that will mimic the NDE response from service-induced PWSCC for use in round-robin studies.
- Review available mockups for use in the round-robin studies and, if new assemblies are needed, ensure that they are developed.
- Develop a test plan for each intended round-robin study.
- Coordinate the PINC inspection teams so that a schedule can be developed for circulating the assemblies and ensure it is followed.
- Use invigilators to oversee the round-robin inspections in each country and to ensure uniformity of guidance for each team.
- Coordinate receipt of inspection results.

1.3 Task Group on PINC Atlas

Task Group Atlas Members

Robert Harris – Chairman
Seiji Asada
Joo Youl Hong
Tae Hyun Lee
Iouri Prokofiev
Brian Rassler
Myung Ho Song
Boyd Taylor
Kwangsik Yoon
Masanobu Iwasaki
Kyungcho Kim
Sung Sik Kang
Tetsuo Shoji
Shuji Tanioka
Hännu Hanninen
Karen Gott

The objective of the TG-Atlas technical subgroup is to produce a final product of the PINC program that is an electronic resource of information on PWSCC in nickel-based alloys used in nuclear power

plant applications. This will include documenting the material that has been generated in support of an improved understanding of (1) the morphology of PWSCC, (2) NDE responses to PWSCC, and (3) the capability of NDE to reliably detect and accurately size PWSCC.

- The TG-Atlas group is taking the following as input:
  - Results of the activities of the other task groups
  - Presentations of PINC members
  - Submissions from PINC members
  - Available open literature
- The TG-Atlas will produce an Atlas in electronic form as output that will be provided to all PINC participants.
- The Atlas will be user-friendly and permit additions by users.
- The Atlas will document the following:
  - PWSCC morphology
  - PWSCC NDE results from real PWSCC and simulated PWSCC
  - Round-robin test results
  - To the extent practicable, contrasting morphology and NDE results from other types of cracking and noise sources that are likely to be confused with PWSCC
  - References and links to the open literature.

1.4 Data Analysis Group

Data Analysis Group Members

Stephen Cumblidge – Chairman
Steven Doctor, Invigilator U.S.
Pat Heasler
Peter Merck
Tommy Zetterwall, Invigilator Europe
Ichiro Komura, Invigilator Japan
Kazunobu Sakamoto
Kyung-Cho Kim, Invigilator Korea
Myung Ho Song
Yongsik Kim
Sung Sik Kang
Pentti Kauppinen
Jack Spanner
Anders Brunn

This group is responsible for:

- Coordinating the analysis of the data that was generated during the round-robin trials conducted under TG-NDE

- Coordinating the need for oversight of destructive testing
- Assembling the data and information for inclusion into the Atlas
- Developing a final report on the round-robin trials for submitting to the Steering Committee.

The PINC surveyed the program participants to identify and rank all PWSCC and component configurations for consideration to be studied in the PINC framework. The three areas that were ranked highest were the bottom-mounted instrumentation, dissimilar metal piping welds, and control rod drive mechanisms. The bottom-mounted instrumentation (BMI) areas were identified as top priority because it is not easy to replace a reactor pressure vessel bottom head and repairs are challenging, as learned at the South Texas Project nuclear power plant. The issue of dissimilar metal welds (DMWs) was considered to also be very important, based on the cracking experienced at the V.C. Summer and Ringhals plants. The control rod drive mechanism (CRDM) issue was also ranked high because of the Davis-Besse event and the number of plants worldwide that have experienced cracking. However, the limited availability of CRDM assemblies and the need to complete the PINC round robin in a timely fashion made it possible to address only the DMWs and the BMI nozzles. It was also thought that the NDE techniques used for BMIs would be used on CRDMs and, as a result, would be addressing the CRDM inspection issues. DMW assemblies were available immediately, so this round-robin study was able to start first.

The PINC program focused on studying two aspects of PWSCC: (1) document the crack morphology of PWSCC and (2) study the capability of various NDE methods to detect and size the through-wall extent of PWSCC. The studies involving NDE capability were carried out as international round robins with PINC program participants.

This report documents the study of NDE inspection capability to detect and length the through-wall extent of PWSCC in bottom mounted instrumentation penetrations (BMI). The report is organized as follows.

Section 1 provides introductory material and explains the organization of the PINC program. Section 2 provides background information for the round-robin study. The availability of test blocks offered to the PINC program is reviewed in Section 3 along with photographs of the test blocks, schematic drawings of product forms, and dimensions of the test blocks. Section 3 also gives the coordinate system used in the round-robin test. Section 4 describes the manufacturing process for the flaws used in the test blocks. Section 5 describes the scoring procedure used for the analysis in this report. Section 6 presents information on the NDE methods that were used by PINC participants in this round-robin study along with probability of detection (POD) results. Section 7 covers the sizing performance for the NDE techniques/procedures used. Section 8 discusses the results and highlights the conclusions that can be drawn. Section 9 provides literature references. Appendices A, B, and C provide detailed results from the round-robin testing and detailed descriptions of the test blocks.

2.0 Background

Cracking observed in the early 1990s in reactor components in France and other countries was attributed to PWSCC, leading to replacement of reactor vessel heads, piping, etc. The problem resurfaced in 2000 when, at the Oconee plant in the United States, leakage was discovered from a control rod drive mechanism penetration fabricated using Alloy 600, resulting in deposits of boric-acid crystals on the vessel head. Further investigation led to the identification of PWSCC cracks in the reactor penetration tubes and attachment J-groove welds. Circumferential cracking of CRDM nozzles has been identified at Oconee Units 2 and 3 and Crystal River Unit 3. An extreme consequence of such cracking was illustrated by the discovery of wastage on the Davis-Besse reactor vessel head. More recently, boric-acid deposits and NDE indications found on the South Texas Project BMI nozzles have been attributed to PWSCC. Cracks also have been found in reactor nozzle hot leg dissimilar metal welds at the V.C. Summer plant in the United States and at the Ringhals plant in Sweden, providing further evidence that PWSCC is a generic concern.

The cracking associated with safe-end piping welds is important because of the potential for a large loss of coolant inventory, and the cracking of CRDM nozzle welds and circumferential cracking of CRDM nozzle base metal is important because of the potential for control rod ejection and loss-of-coolant accident (LOCA). Recent events at nuclear stations related to damage in Alloy 600 base material and Alloy 182/82 welds have prompted industry initiatives directed at reexamining the damage mechanisms, damage morphology, and examination practices of the affected components. These events have given high visibility to the PWSCC phenomenon, and high priority to work on understanding this cracking mechanism and detecting its occurrence.

Some data describing the failure of Alloys 600/182/82 due to PWSCC have been developed by Westinghouse and the French utility Électricité de France. Various aspects of the problem have also been addressed by a number of research programs within the United States and in other countries. The data collected to date, however, are sparse, and the significant factors leading to crack initiation and governing crack growth rate are not well understood. Complicating factors include chemistry variations in the nickel-base alloy components, evolution of the primary water chemistry within an operating cycle, and residual stresses and possible embedded flaws resulting from weld repairs. In addition, detection and characterization of PWSCC-related flaws through NDE have proven to be particularly difficult in these materials and in components with complicated geometries. The occurrences of cracking in the United States have been identified initially through indirect means, specifically the discovery of boric-acid deposits resulting from through-wall cracking in the primary system pressure boundary. Such leakage degrades a layer of plant defense-in-depth, and should be prevented whenever possible.

Although there are many different aspects of this issue that need to be addressed, NRC proposed research concentrated in two interrelated areas. Task 1 focuses on characterizing the morphology of PWSCC cracks, which has been identified as a contributing factor to the difficulties experienced in detecting and sizing cracks in the field. As part of the characterization, work will address refining the ability to distinguish PWSCC cracks from other flaws with similar features, such as hot cracks in welds. Task 2 will focus on the nondestructive testing aspects, including such topics as the manufacture and simulation of PWSCC cracks in test assemblies for use in assessing the effectiveness and reliability of NDE techniques.

The research addresses the nickel-base alloys used as pressurized water reactor (PWR) pressure boundary components including dissimilar metal welds and reactor pressure vessel (RPV) head penetrations. Primarily, the research focused on the Alloy 600/182/82 group of materials, but replacement materials (Alloys 690/152/52) were not excluded.

3.0 Test Plan for Bottom-Mounted Instrumentation Round Robin

This section of the report describes the test plan used for conducting the PINC BMI round robin. Fourteen test blocks were selected for the round-robin test on NDE effectiveness for degradation in BMI nozzle penetration seal welds. The purpose of this test plan is to provide the scope and schedule for use of the new mockup. The proposed test blocks for use in the BMI round-robin test are reviewed in Section 3.1. Available photographs of the test blocks are shown. Section 3.2 provides the schematic drawings of product forms and dimensions of the test blocks. Section 3.3 gives the coordinate system used in the round-robin test. Section 3.4 describes the cracks that are being made available in the test blocks and Section 3.5 covers the round robin test methodology.

3.1 BMI Round-Robin Test Blocks

All available photographs for BMI seal weld test blocks are shown in this section. Table 3.1 references the photographs and drawings for the test blocks. Fourteen test blocks were selected for the round robin. Test blocks 5.4 and 5.5 did not contain cracks in the weld metal and were not used in the round robin test studies.

Table 3.1. Test Blocks for BMI Round Robin

ID	Participant	Test Block	Photograph	Drawing
PINC 5.1	KINS	Penetration W17	Figure 3.11	Figure 3.15
PINC 5.2	KINS	Penetration W22	Figure 3.12	Figure 3.16
PINC 5.3	KINS	Penetration W46	Figure 3.13	Figure 3.17
PINC 5.6	SSM/SQC	F3.537.2	No Photograph	Figure 3.18
PINC 5.7	NRC/PNNL	WNP1.BMI.1	Figure 3.1	Figure 3.19
PINC 5.8	NRC/PNNL	WNP1.BMI.2	Figure 3.2	Figure 3.20
PINC 5.9	NRC/PNNL	WNP1.BMI.3	Figure 3.3	Figure 3.21
PINC 5.10	NRC/PNNL	WNP1.BMI.4	Figure 3.4	Figure 3.22
PINC 5.11	NRC/PNNL	WNP1.BMI.5	Figure 3.5	Figure 3.23
PINC 5.12	NRC/PNNL	WNP1.BMI.6	Figure 3.6	Figure 3.24
PINC 5.13	JNES	BMI No 1	Figure 3.7	Figures 3.25 & 3.26
PINC 5.14	JNES	BMI No 2	Figure 3.8	Figures 3.25 & 3.26
PINC 5.15	JNES	BMI No 3	Figure 3.9	Figures 3.25 & 3.26
PINC 5.16	JNES	BMI No 4	Figure 3.10	Figures 3.25 & 3.26

Figure 3.1. Photograph of PINC 5.7 from PNNL – WNP-1 BMI Nozzle Penetration #1

Figure 3.2. Photograph of PINC 5.8 from PNNL – WNP-1 BMI Nozzle Penetration #2

Figure 3.3. Photograph of PINC 5.9 from PNNL – WNP-1 BMI Nozzle Penetration #3

Figure 3.4. Photograph of PINC 5.10 from PNNL – WNP-1 BMI Nozzle Penetration #4

Figure 3.5. Photograph of PINC 5.11 from PNNL – WNP-1 BMI Nozzle Penetration #5

Figure 3.6. Photograph of PINC 5.12 from PNNL – WNP-1 BMI Nozzle Penetration #6

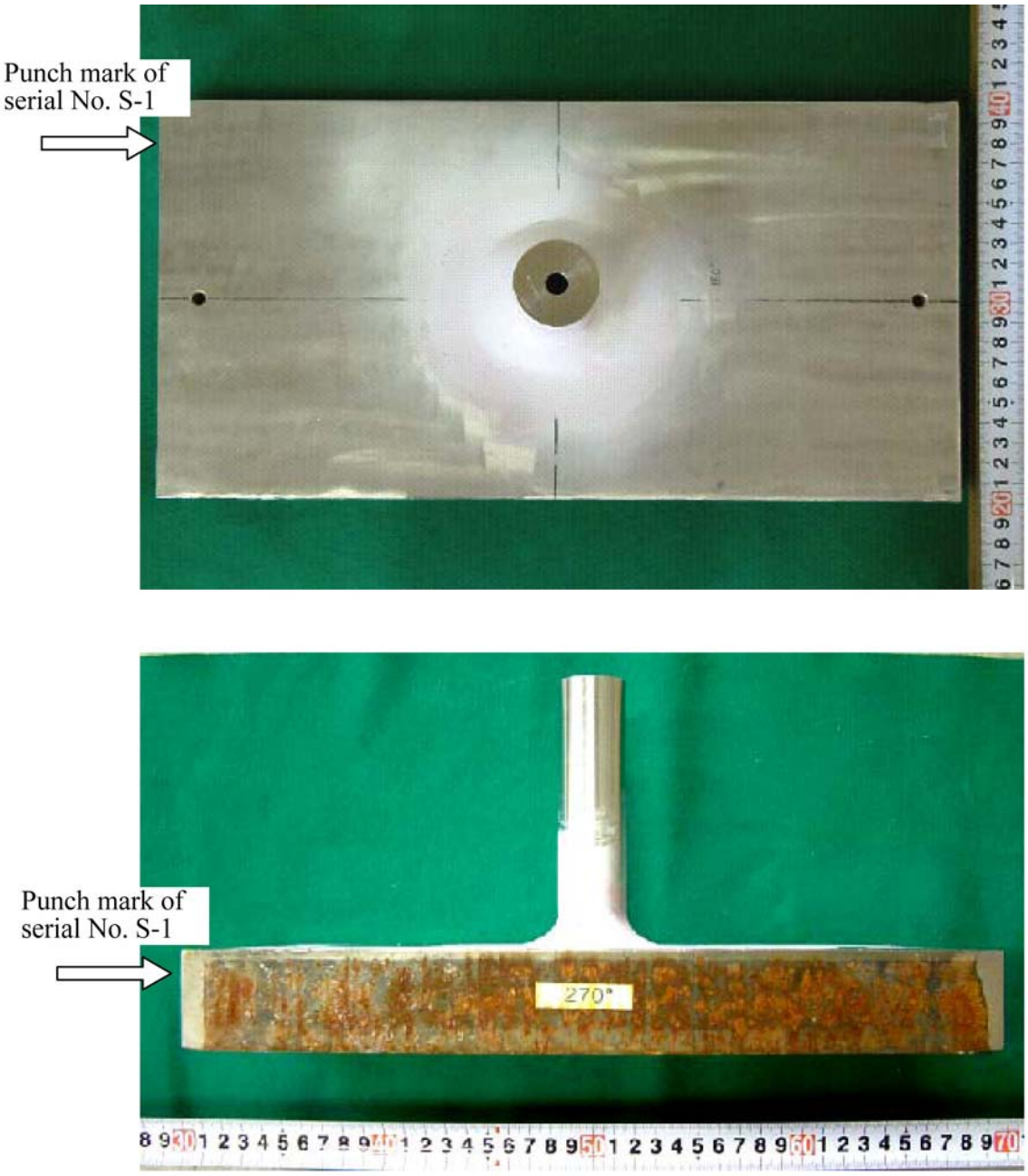

Figure 3.7. Photograph of PINC 5.13 from JNES – BMI Nozzle Test Block No. 1

Figure 3.8. Photograph of PINC 5.14 from JNES – BMI Nozzle Test Block No. 2

Figure 3.9. Photograph of PINC 5.15 from JNES – BMI Nozzle Test Block No. 3

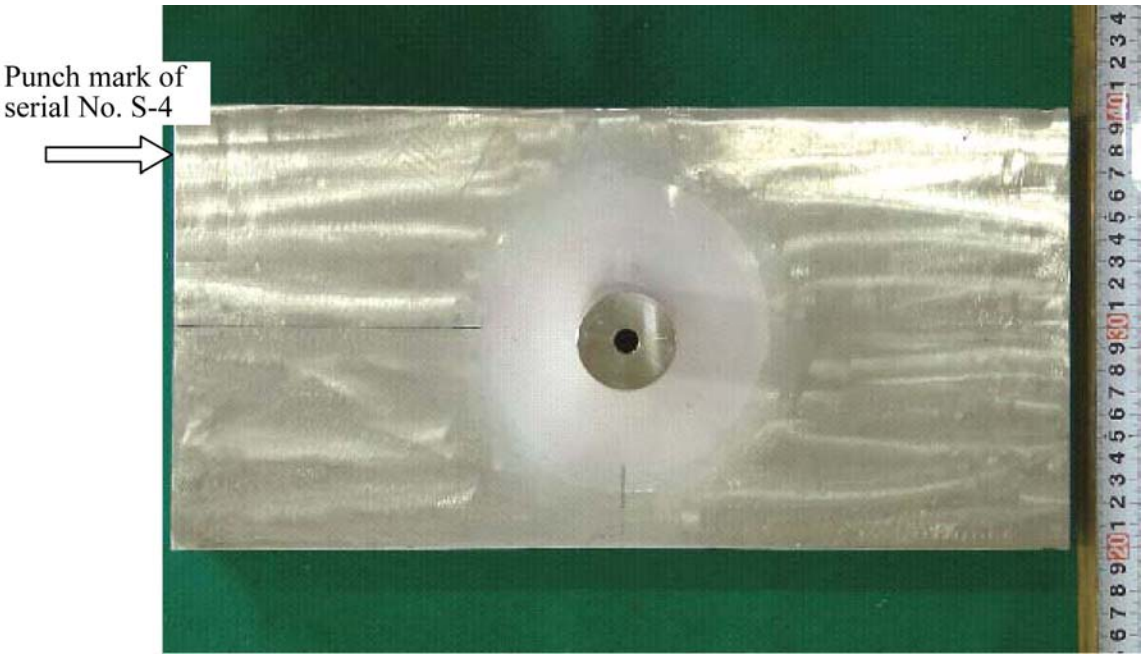

Figure 3.10. Photograph of PINC 5.16 from JNES – BMI Nozzle Test Block No. 4

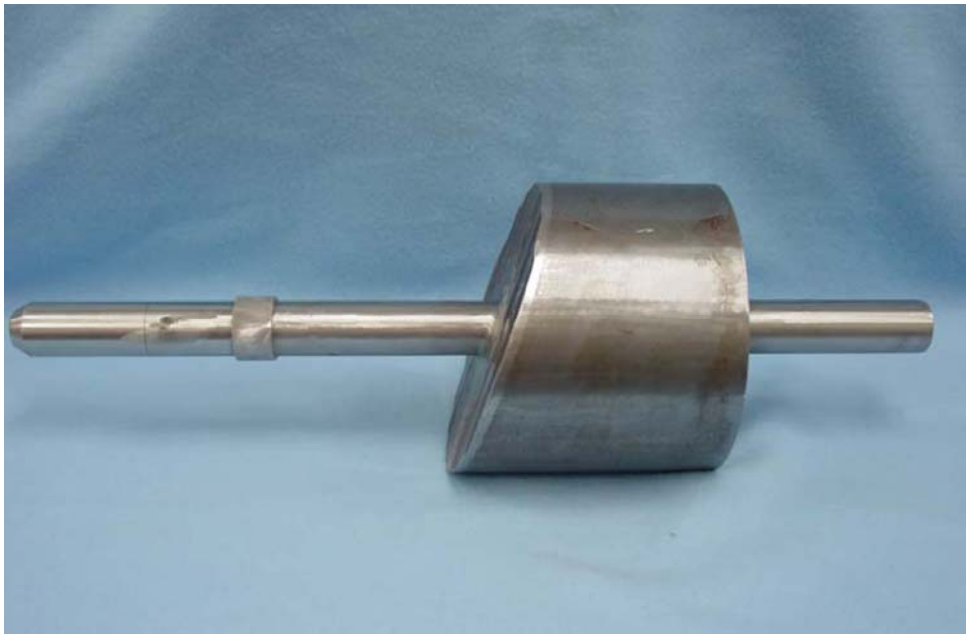

Figure 3.11. Photograph of PINC 5.1 from KINS – BMI Nozzle Test Block

Figure 3.12. Photograph of PINC 5.2 from KINS – BMI Nozzle Test Block

Figure 3.13. Photograph of PINC 5.3 from KINS – BMI Nozzle Test Block

Figure 3.14. Photograph of an Extra Block from KINS – BMI Nozzle Test Block. Since this was not in the original test design, it is optional whether the teams chose to inspect this block. While the test sample was optional, all teams were encouraged to include this test sample in their inspection schedule.

3.2 Schematic Drawings for BMI Test Blocks

Schematic drawings are provided to give product form configuration and dimensions for the test blocks. The first three test blocks from KINS have the configurations shown in Figures 3.15, 3.16, and 3.17. The outside diameter of the BMI penetration tubes is 38 mm and the inside diameter is 15.5 mm. PINC 5.6 has the configuration shown in Figure 3.18. The outside diameter of the tube is 47 mm and the inside diameter is 25 mm. The six test blocks PINC 5.7–5.12 are similar to each other and, as shown in Figures 3.19 to 3.24, the outside diameter of the tube is 44 mm and the inside diameter is 15.9 mm. The four test blocks from JNES have a tube outside diameter of 38.1 mm and an inside diameter of 9.5 mm. Their configuration is shown in Figures 3.25 and 3.26.

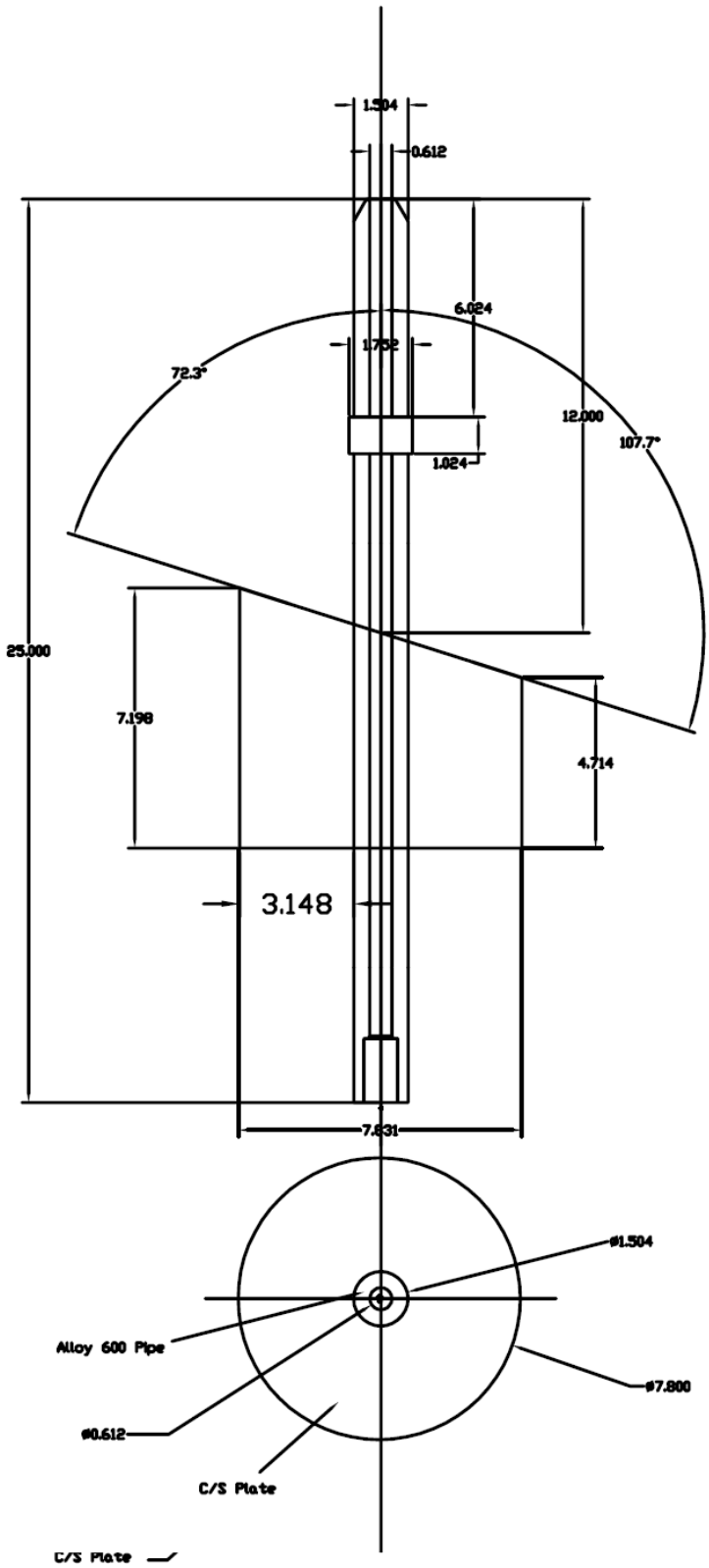

Figure 3.15. Drawing of PINC 5.1 from KINS

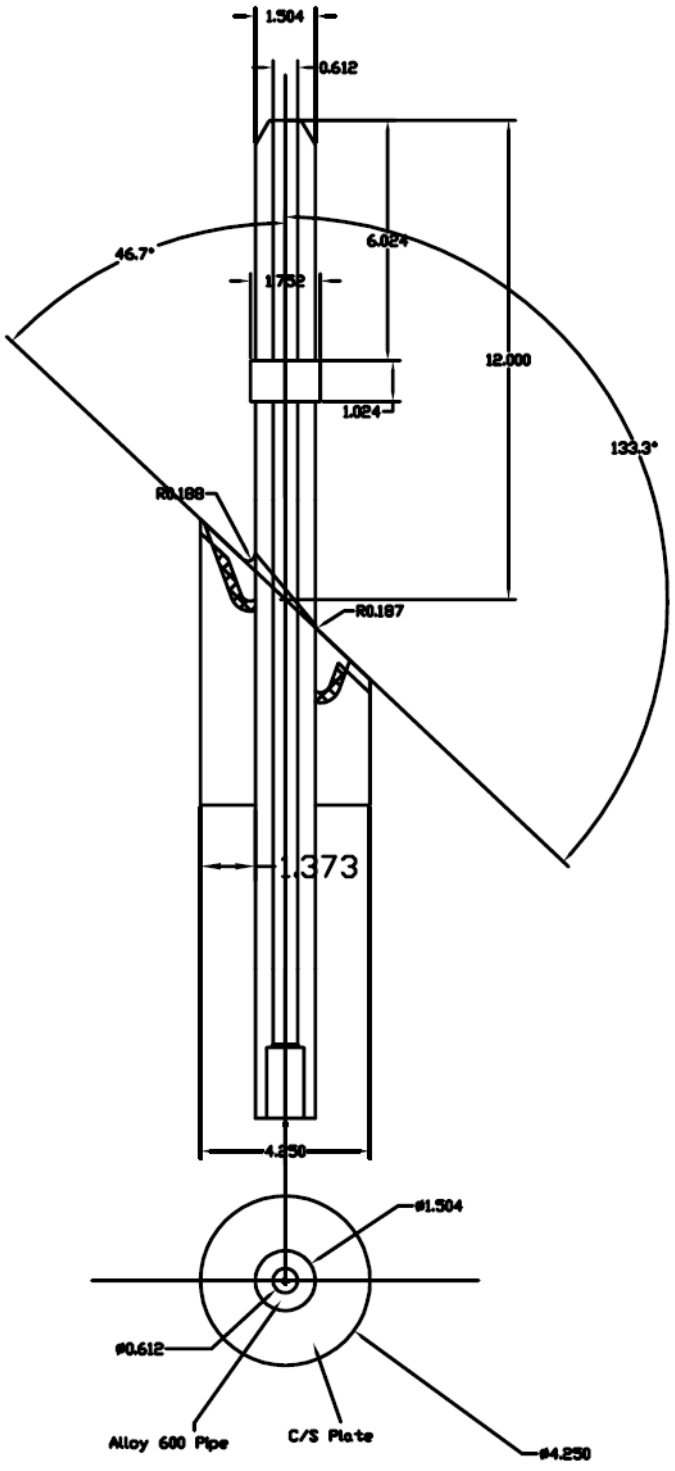

Figure 3.16. Drawing of PINC 5.2 from KINS

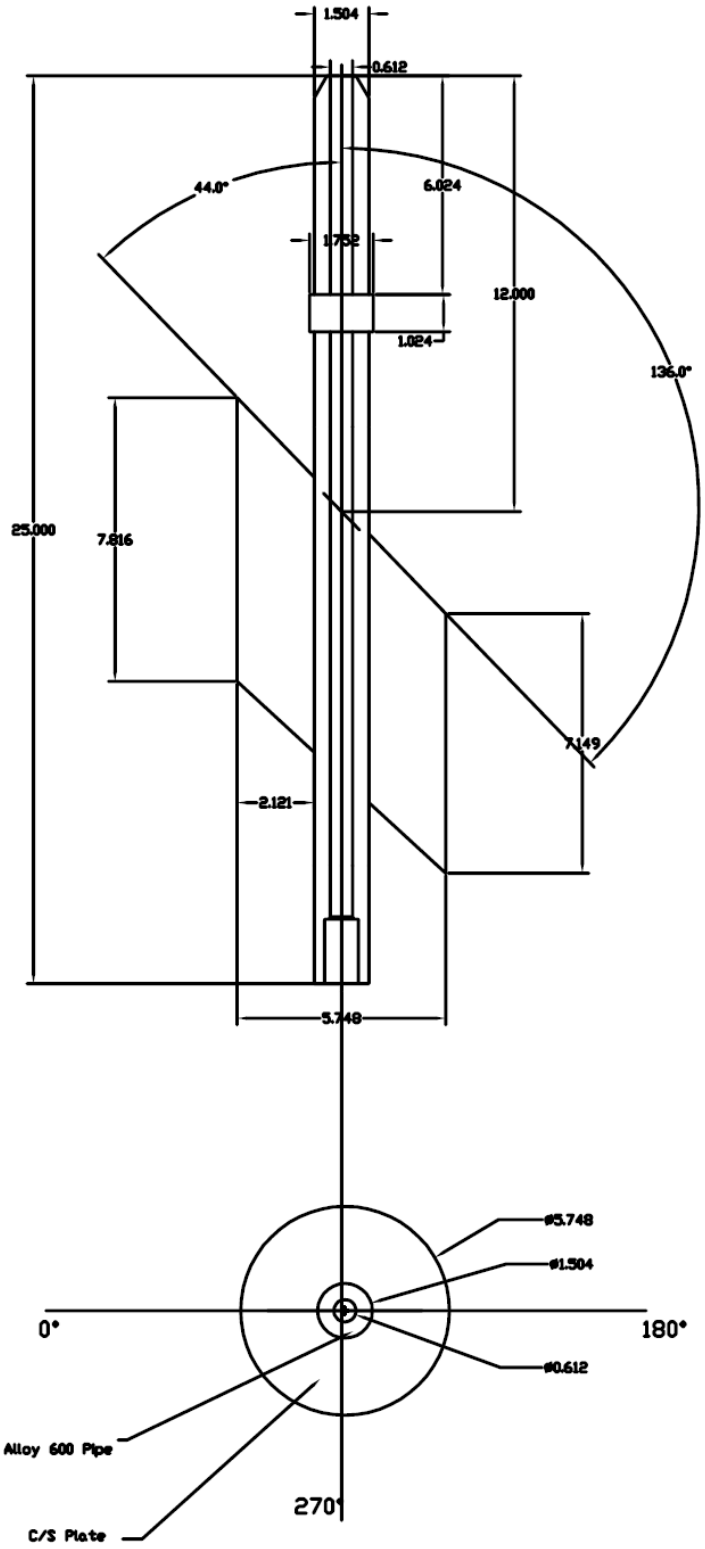

Figure 3.17. Drawing of PINC 5.3 from KINS

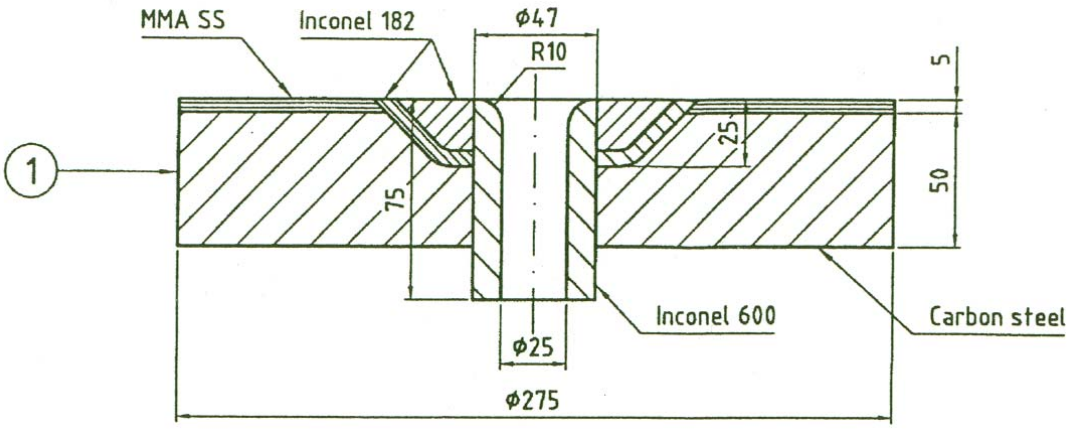

Figure 3.18. Drawing of PINC 5.6 from SSM/SQC

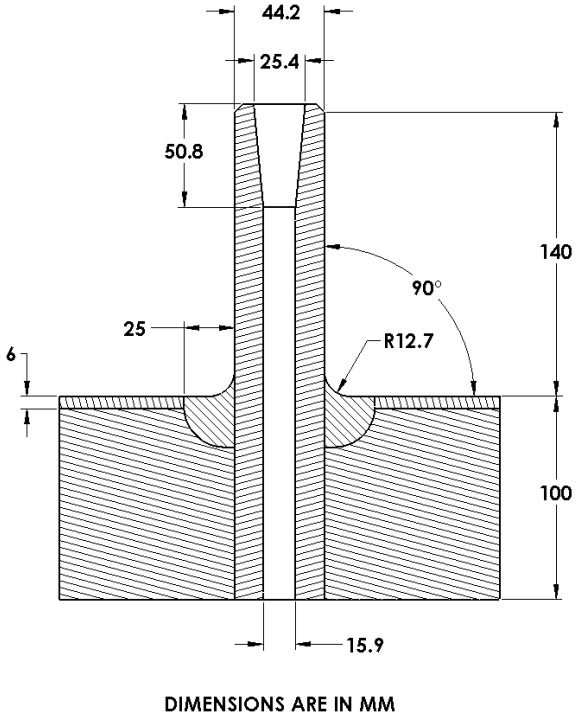

Figure 3.19. Drawing of PINC 5.7 from NRC/PNNL

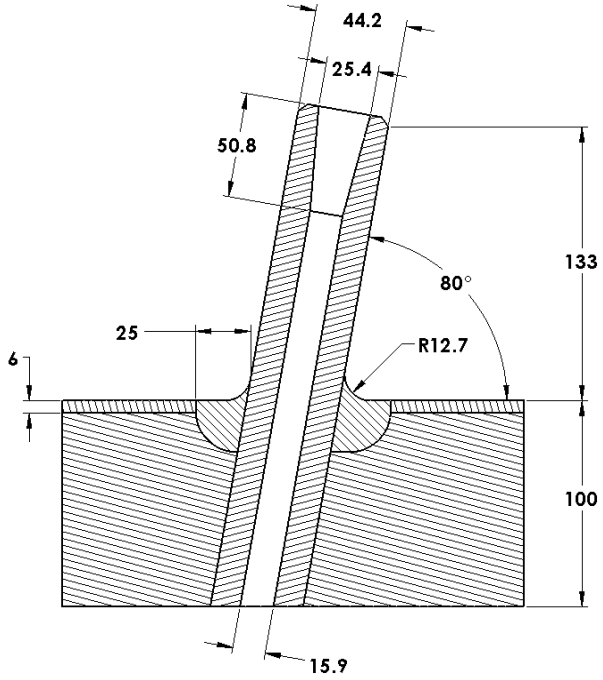

Figure 3.20. Drawing of PINC 5.8 from NRC/PNNL

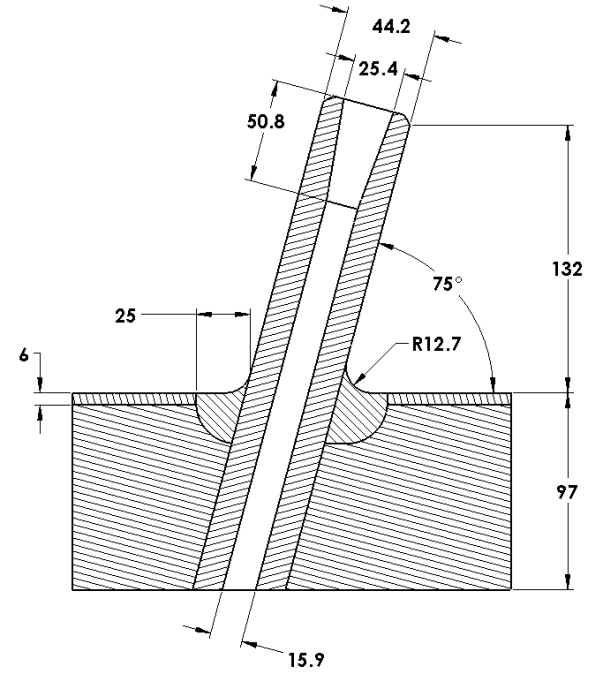

Figure 3.21. Drawing of PINC 5.9 from NRC/PNNL

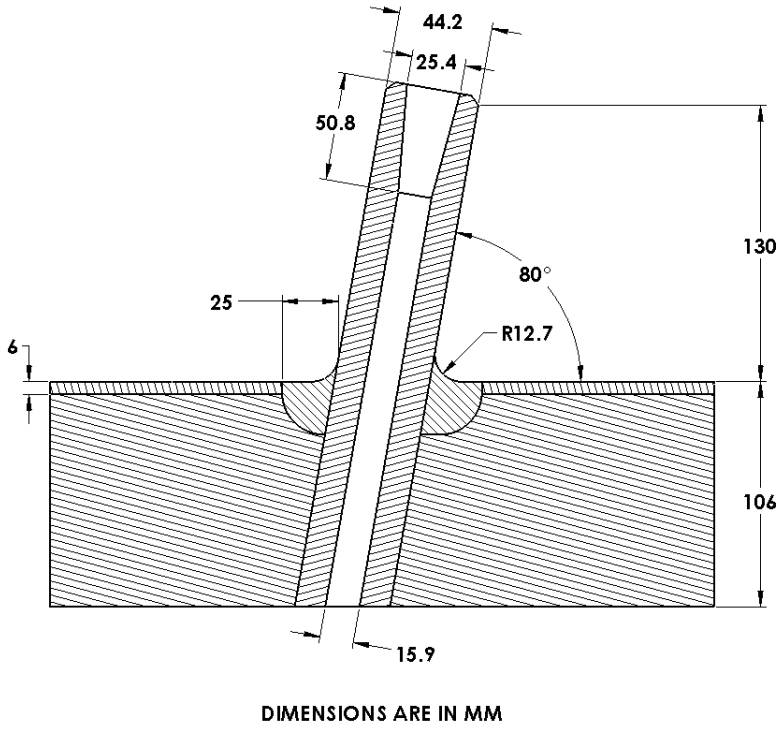

Figure 3.22. Drawing of PINC 5.10 from NRC/PNNL

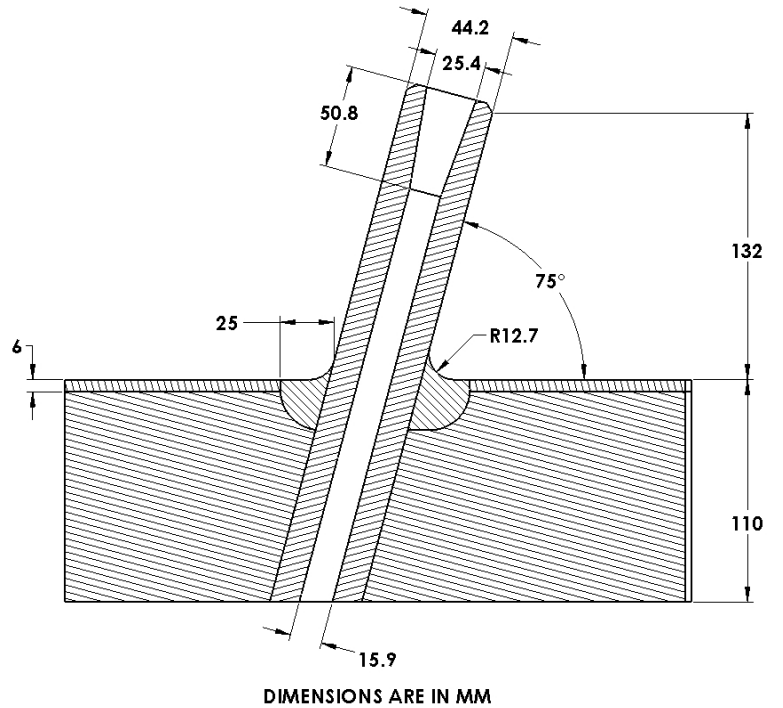

Figure 3.23. Drawing of PINC 5.11 from NRC/PNNL

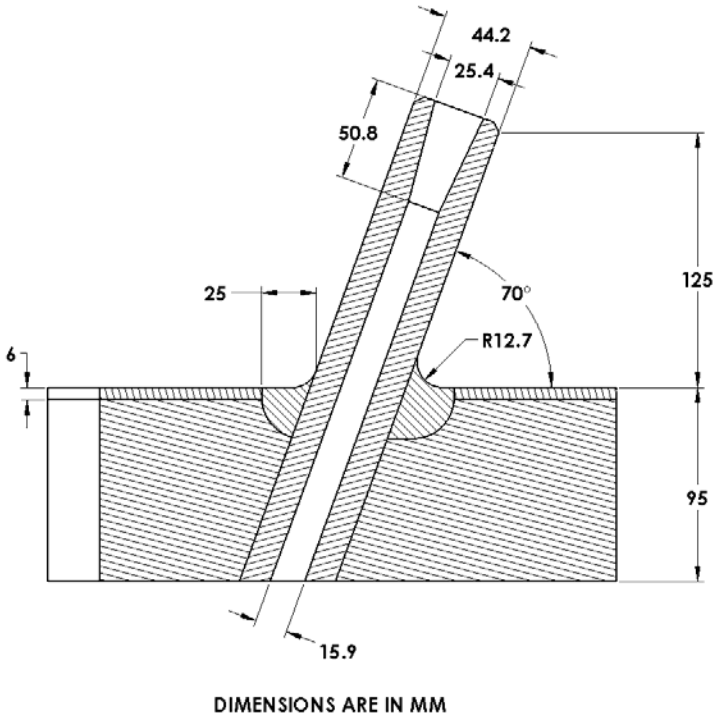

Figure 3.24. Drawing of PINC 5.12 from NRC/PNNL

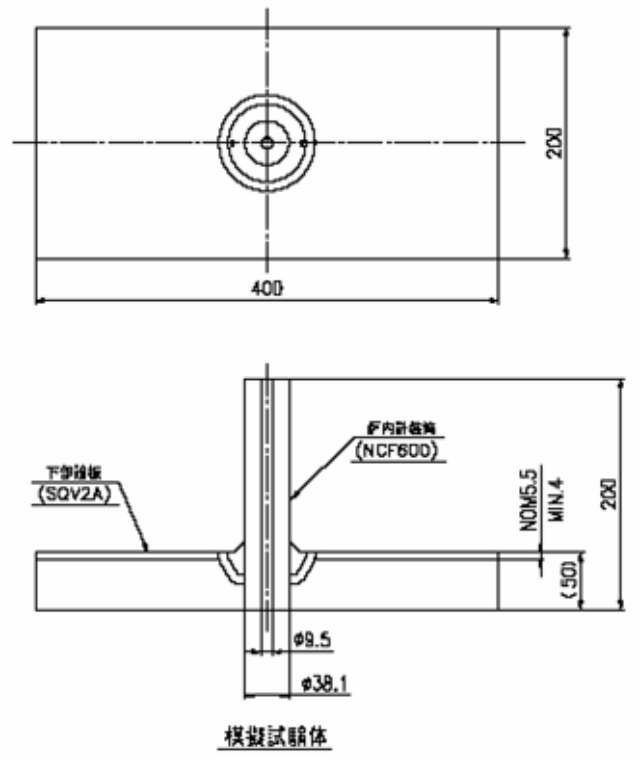

Figure 3.25. Drawing of Test Blocks PINC 5.13 through 5.16 from JNES

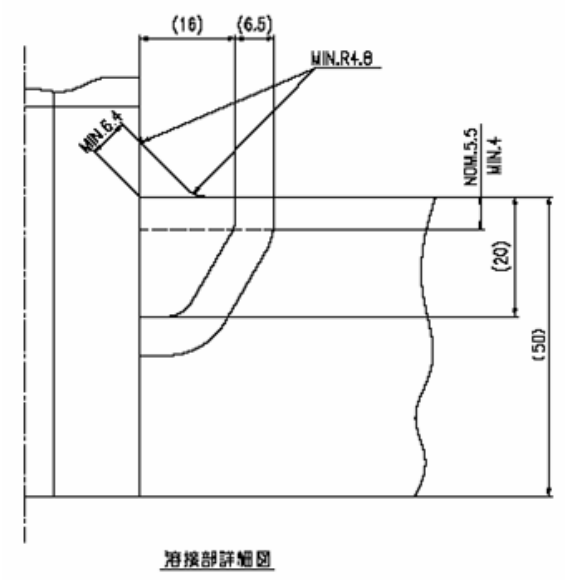

Figure 3.26. Drawing of Seal Weld Configuration for PINC 5.13 through 5.16 from JNES

3.3 Coordinate Systems for BMI Round Robin

This section documents the coordinate system for use in the bottom-mounted instrumentation nozzle penetration seal weld round-robin test. Figure 3.27 shows the coordinate system for the first three test blocks, PINC 5.1 through 5.3. The circumferential axis increases clockwise when viewed from the top of the test block and starts at the 0° mark on the part. The radial axis starts at the center of the tube. The Z dimension for PINC 5.1 through 5.3 is measured from one of two areas as follows.

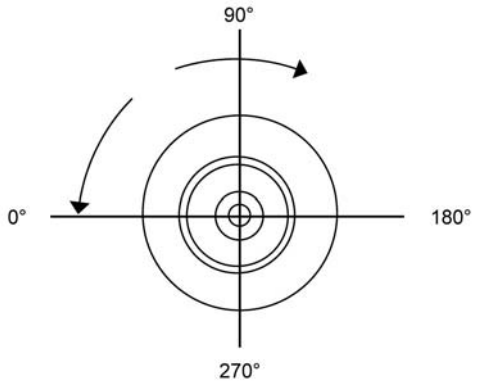

Figure 3.27. Coordinate System for PINC 5.1 through 5.3 from KINS

For measuring defects in the J-groove weld, the Z dimension should be measured from the top (surface that is facing the reactor core) wetted surface that is clad, has a J-groove weld, and may or may not have buttering. The surface is curved; therefore, the Z dimension is reported relative to the angular location around the specimen. Figure 3.28 is an illustration of the Z dimension.

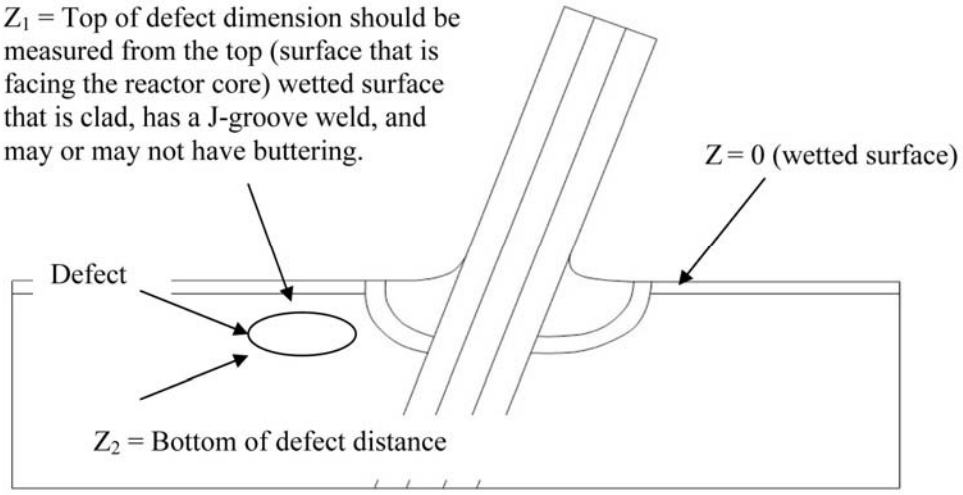

Figure 3.28. Illustration of Z Dimension

For measuring defects within the BMI tube, the Z dimension should be measured from the top of the tube down as shown in Figure 3.29.

Figure 3.30 shows the coordinate system for the fourth test block, PINC 5.6. The circumferential axis increases counter-clockwise when viewed from the top of the test block and starts at the 0° mark on the part. The radial axis starts at the center of the tube.

For PINC specimens 5.7–5.12, the zero Θ is defined by a hole drilled into the cladding, with Θ going clockwise when looking down on the specimen as shown in Figure 3.31. The radial axis starts at the center of the tube. For PINC specimens 5.7–5.12, when measuring defects in the J-groove weld, the Z dimension should be measured from the top (surface that is facing the reactor core) wetted surface that is clad, J-groove, and has buttering. The surface is curved; therefore, the Z dimension is reported relative to the angular location around the specimen.

For PINC specimens 5.13–5.16, the circumferential axis increases clockwise around the part when viewed from the top of the test block and starts at the 0° punch mark direction on the side surface of the test block as shown in Figure 3.32. The radial axis starts at the center of the tube.

For the axial coordinate system of PINC 5.13–5.16, Y=0 position is the top of the test block, and the length for "Y+" is measured along the surface of test block, as shown in Figure 3.33.

For PINC specimens 5.13–5.16, when measuring defects in the J-groove weld, the Z dimension should be measured from the top (surface that is facing the reactor core) wetted surface that is clad, J-groove, and has buttering. The surface is curved; therefore, the Z dimension is reported relative to the angular location around the specimen.

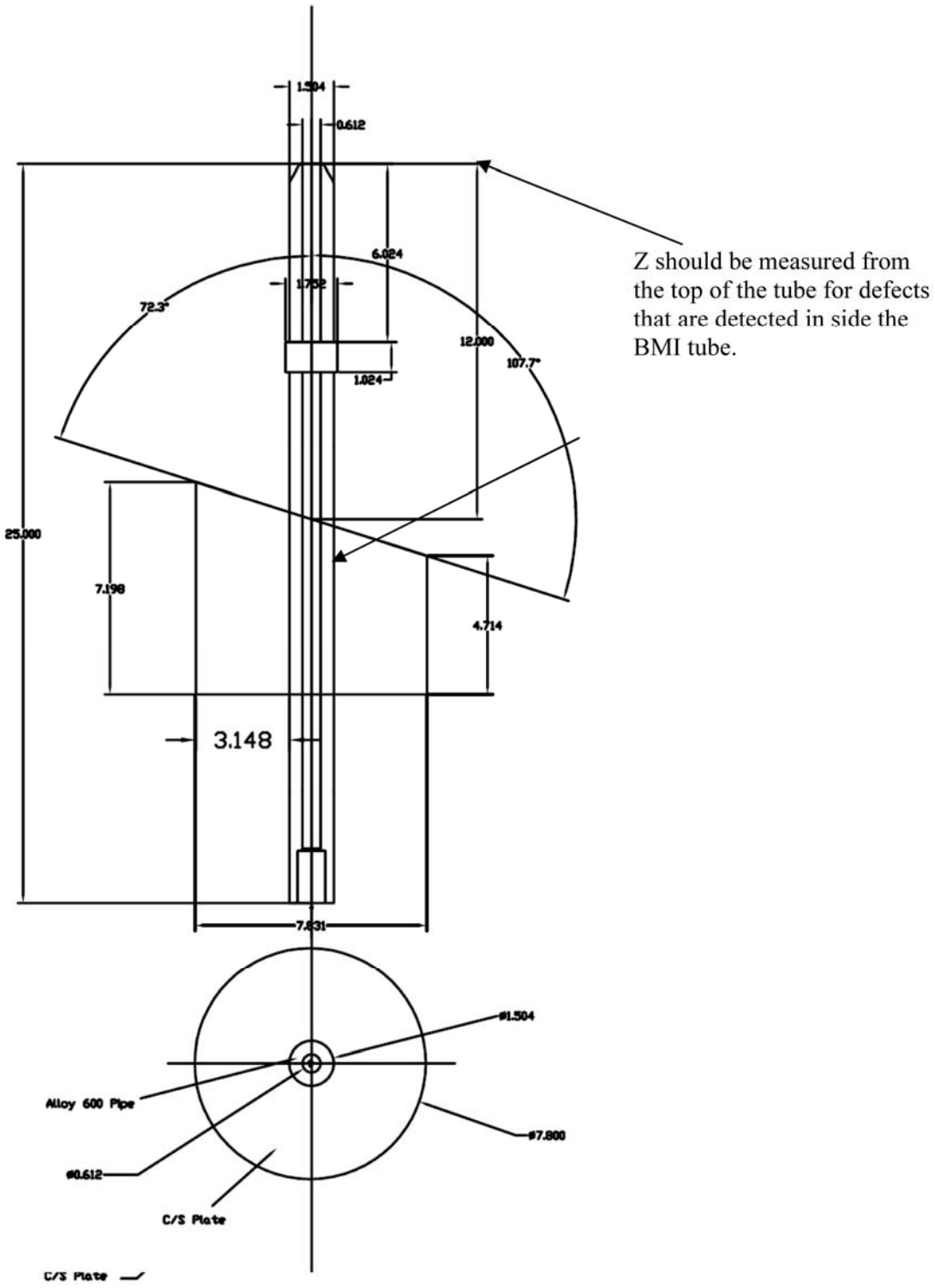

Figure 3.29. Coordinate System for PINC 5.1–5.3

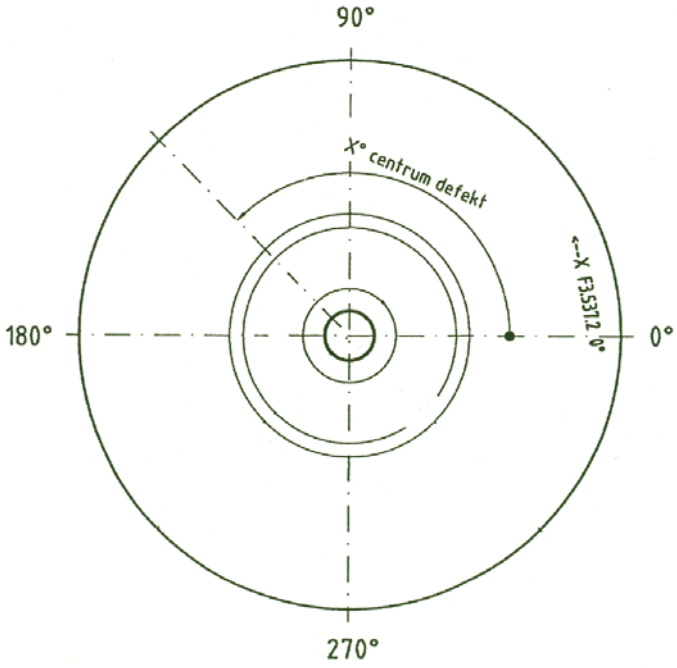

Figure 3.30. Coordinate System for PINC 5.6 – SSM/SQC F3.537.2

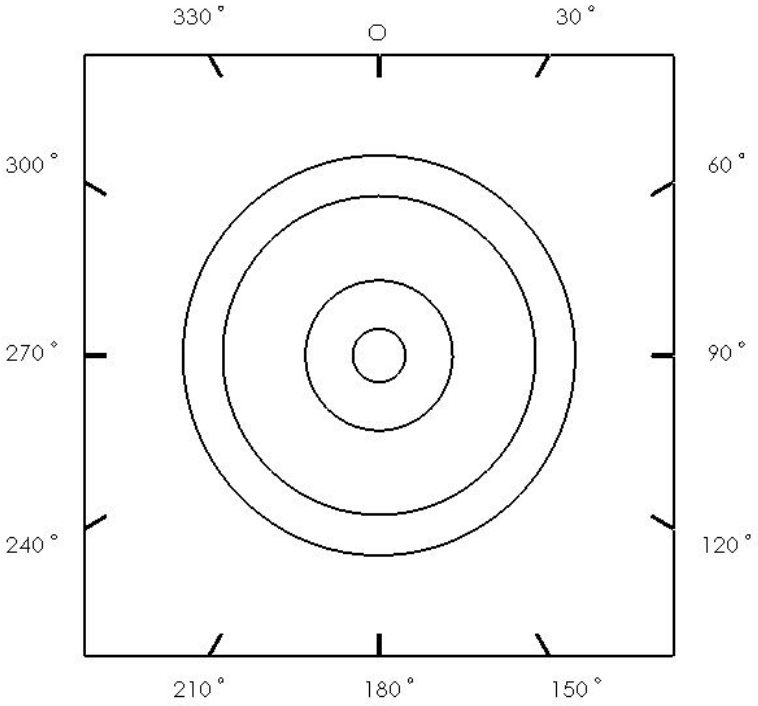

Figure 3.31. Coordinate System for the Six Test Blocks, PINC 5.7–5.12

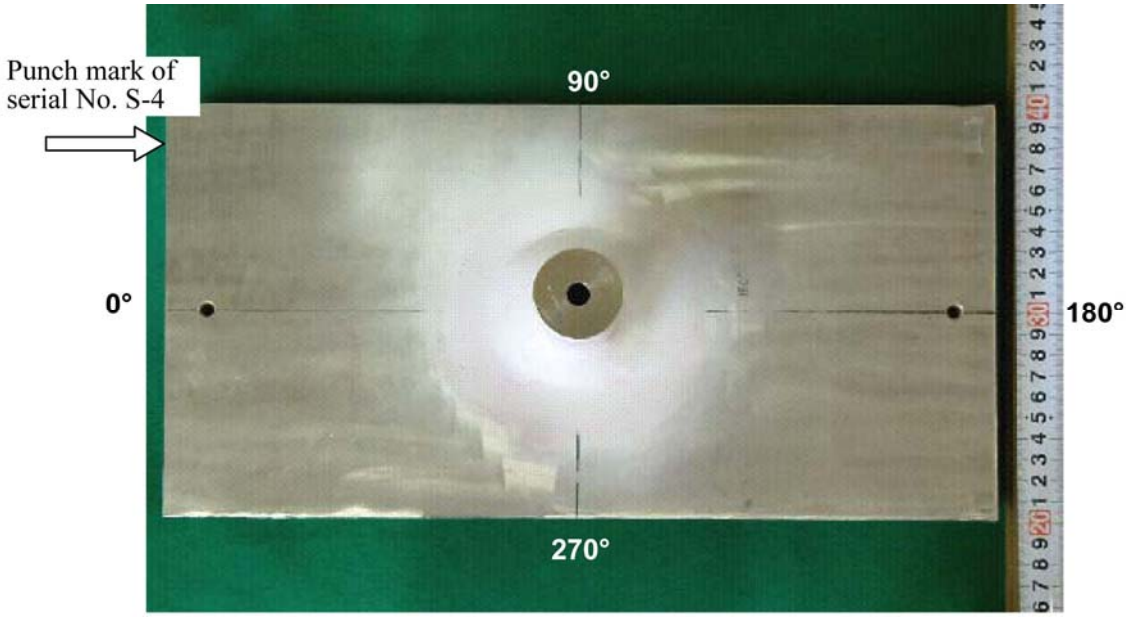

Figure 3.32. Circumferential Coordinate System for the Four Test Blocks, PINC 5.13–5.16

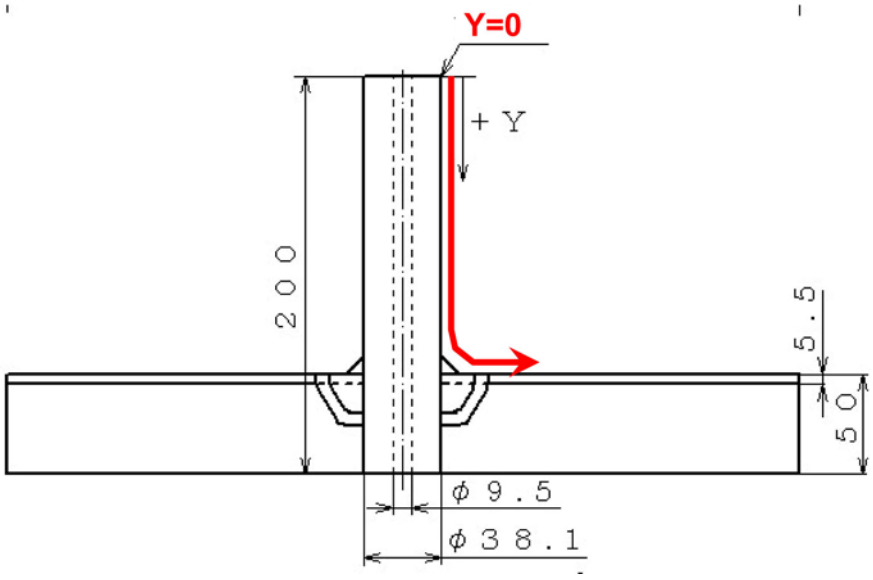

Figure 3.33. Axial Coordinate System for the Four Test Blocks, PINC 5.13–5.16

3.4 Available Cracks

The objectives of the round-robin test include simulating the NDE responses from PWSCC by selecting manufactured cracks with appropriate NDE responses. This includes both peak response and indication length. The degradation initiation sites associated with through-wall leaks from observed PWSCC show cracks as short as 4 mm. Therefore, fabricated cracks in the test blocks will have a range of crack lengths including some short cracks in order to simulate this condition. Some unexpected

fabrication flaws will be present in the test blocks and PNNL will fingerprint the blocks, locating the cracks to separate them from the unexpected fabrication flaws. Inspection teams should expect fabrication flaws and a range of crack properties in the test blocks.

The test assemblies from Sweden, Japan, and the United States all have the cracks located in the J-groove weld or buttering. Three of the Korean assemblies have cracks in the penetration tubes and at the interface between the penetration tube and the J-groove weld and in one additional assembly provided by Korea, the location of the cracks is unknown.

Table 3.2 and 3.3 show the samples and cracks that were used in the BMI study. The destructive validation for the flaws in Samples 5.2, 5.10, and 5.13-5.16 are given in Appendix B.

Table 3.2. Flaws Used for Surface Inspections

Test Block	Flaw	Θ1, °	Θ2, °	r1, mm	r2, mm	Z1, mm	Z2, mm	SB*	Orient
5.1	Surf5.1.5	268	304	20	23.6	1	10	no	Circ.
5.2	Surf5.2.3	148	155	19.3	27.3	0	14.1	yes	Axial
5.3	Surf5.3.3	130	160	19.1	27.7	0	8	yes	Circ.
5.3	Surf5.3.6	338	338	19.1	30	0	10	yes	Axial
5.6	Surf5.6.1	45	45	24	28	0	2	yes	Axial
5.6	Surf5.6.2	131	139	34	34	0	2	yes	Circ.
5.6	Surf5.6.3	225	225	55	60	0	2	yes	Axial
5.6	Surf5.6.4	310	320	58	58	0	5	yes	Circ.
5.6	Surf5.6.5	245	265	30	30	0	5	yes	Circ.
5.6	Surf5.6.6	180	180	35	41	0	1.5	yes	Axial
5.7	Surf5.7.1	162	168	42	42	0	2	yes	Circ.
5.7	Surf5.7.2	15	15	34	37	0	3	yes	Axial
5.7	Surf5.7.3	300	300	32	40	0	NA	Yes	Axial
5.8	No Flaw	NA	NA	NA	NA	NA	NA	NA	NA
5.9	Surf5.9.1	15	15	43	47	0	1	yes	Axial
5.9	Surf5.9.2	75	75	33	36	0	6	yes	Axial
5.9	Surf5.9.3	193	197	44	44	0	3	yes	Circ.
5.9	Surf5.9.4	345	345	45	49	0	7	yes	Axial
5.10	Surf5.10.1	39	51	33	33	0	9	yes	Circ.
5.10	Surf5.10.2	72	78	45	45	0	7	yes	Circ.
5.10	Surf5.10.3†	225	225	39	41	0	0.4	yes	Axial
5.10	Surf5.10.4	251	259	46	46	0	2	yes	Circ.
5.10	Surf5.10.5	285	285	36	40	0	2	yes	Axial
5.10	Surf5.10.6†	315	315	46	48	0	4.5	yes	Axial
5.11	No Flaw	NA	NA	NA	NA	NA	NA	NA	NA
5.12	No Flaw	NA	NA	NA	NA	NA	NA	NA	NA
5.13	Surf5.13.1	349	7.8	34.7	36.9	0	2.2	yes	Circ.
5.13	Surf5.13.2	175	188	33.3	36.1	0	2.4	yes	Circ.
5.14	Surf5.14.1	340.1	22.5	29.8	36.6	0	10.5	yes	Circ.
5.14	Surf5.14.2	166.9	194.8	29	31.4	0	2.1	yes	Circ.
5.15	Surf5.15.1	87.7	91.1	25.1	36.4	0	3.5	yes	Axial
5.15	Surf5.15.2	265.3	270.8	25	35.2	0	3.3	yes	Axial
5.16	Surf5.16.1	88.9	95.5	22.4	38.8	0	10.9	yes	Axial
5.16	Surf5.16.2	268.9	275.9	23.2	36.6	0	5.8	yes	Axial

*SB = surface-breaking, † Determined by destructive evaluation to be too small for use in scoring

Table 3.3. Flaws Used for Penetration Tube Inspections

Test Block	Flaw	Θ1, °	Θ2, °	r1, mm	r2, mm	Z1, mm	Z2, mm	SB	Orient
5.1	Tube5.1.1	8	44	19.1	21.7	299.1	306.4	no	Circ.
5.1	Tube5.1.2	68	112	10.3	19.1	304.8	304.8	no	Circ.
5.1	Tube5.1.3	202	202	7.8	12.2	310.7	338.6	yes	Axial
5.1	Tube5.1.4	209	245	15	19.1	309.1	315.7	no	Circ.
5.1	Tube5.1.5	268	304	19.8	23.6	303	303	no	Circ.
5.1	Tube5.1.6	303	339	14.7	19.1	299.9	299.9	no	Circ.
5.2	Tube5.2.1	15	70	17.4	23.7	294.1	307.9	no	Circ.
5.2	Tube5.2.2	90	93	18.6	21.1	305.2	352.7	no	Axial
5.2	Tube5.2.3	100	107	7.5	10.7	296	321.6	yes	Axial
5.2	Tube5.2.4	148	155	19.3	27.3	327.1	341.2	no	Axial
5.2	Tube5.2.5	220	290	7.5	19.1	304.5	317	yes	Circ.
5.2	Tube5.2.6	305	350	14.4	19.7	290.4	297.6	no	Circ.
5.3	Tube5.3.1	13	43	16.3	19.1	293.5	293.5	no	Circ.
5.3	Tube5.3.2	86	116	21.6	27.7	307.2	313.3	no	Circ.
5.3	Tube5.3.3	130	160	19.1	27.7	315.2	322.8	no	Circ.
5.3	Tube5.3.4	191	227	7.5	21.7	315.9	315.9	yes	Circ.
5.3	Tube5.3.5	269	313	19.1	29.6	300.2	310.4	no	Circ.
5.3	Tube5.3.6	338	338	19.1	29.9	293	303.8	no	Axial

*SB = surface-breaking

3.5 Round-Robin Trial Methodology

As in the DMW RRT (described in a separate report), there are two reporting forms the teams were requested to use to report their data. The first is used to report the results from a single inspection technique such as ultrasonic testing (UT) at a specific frequency and inspection angle. The second is a combination of techniques that are used to report the results for a single indication where multiple techniques were employed. If only one technique is used, there is no need for the second form.

Because of the geometry of the BMIs, it was decided that a more useful way to report this data was to use another coordinate system: Θ, r, and Z. The definition of this coordinate system is:

Θ is the angular measurement around the sample from the marked zero datum (see the description of the coordinate system below).

r is the radial axis and is a measurement in millimeters from the center of the tube.

Z is depth of an indication and is measured in millimeters from the wetted surface of the sample [for the J-groove weld and buttering, this is the air-to-weld location (Z = 0) and if it is the nozzle penetration tube, then this will be from the top of the penetration tube (Z = 0 at the top of the tube)].

PINC RRT – Technique DATA SHEET for BMI Test Pieces

Inspection Results, <u>One Technique Data for all Indications in Test Piece</u>

Data Sheet No:

<u>Test piece:</u> **<u>Date:</u>** **<u>Team code:</u>** **<u>Weld volume Inspected:</u>**

<u>Scanned surface (inside, outside):</u> **Θ1 (unit) =** **Θ2 (unit) =**

<u>TECHNIQUE DESCRIPTION</u> **r1 (unit) =** **r2 (unit) =**

Detection: **Z1 (unit) =** **Z2 (unit) =**

Characterization:

Length sizing:

Depth sizing:

Θ1	Θ2	r1	r2	Z1	Z2	Θ_{max}	r_{max}	Z_{max}	Ampl 100% ± dB	Surface breaking	Comments	Defect No:
										Yes/No		

PINC RRT – Indication DATA SHEET for BMI Test Pieces

Inspection Results, Integrated Inspection Results of One Indication from Several Techniques

Test piece: **Date:** **Team code:** **Based on Data sheets No:**

Projection surface (inside/outside):

TECHNIQUES DESCRIPTION

Detection:
Characterization:
Length sizing:
Depth sizing:

Defect No:	Θ1	Θ2	r1	r2	Z1	Z2	Θ_{max}	r_{max}	Z_{max}	Ampl 100% ± dB	Surface breaking Yes/No	Comments

4.0 Description of Manufacturing Process for Defects Used to Simulate NDE Responses of PWSCC for the PINC Round Robin

This section describes how the flaws were introduced into the various PINC test specimens. The implantation techniques are important because one of the goals of the PINC is to understand what makes the flaws easier or more challenging to detect. Each flaw manufacturing technique produces flaws with a different morphology. The variety of flaw manufacturing techniques used in the PINC BMI test blocks allows for an analysis of the difficulty in detecting the different types of cracks.

4.1.1 Flaw Fabrication in Test Blocks 5.1–5.3

Most of the cracks used in test blocks 5.1, 5.2, and 5.3 were produced by first creating the flaws in coupons and then welding the coupons containing the flaws into the welds. One example of a crack that was fabricated into the weld is shown in Figure 4.1.

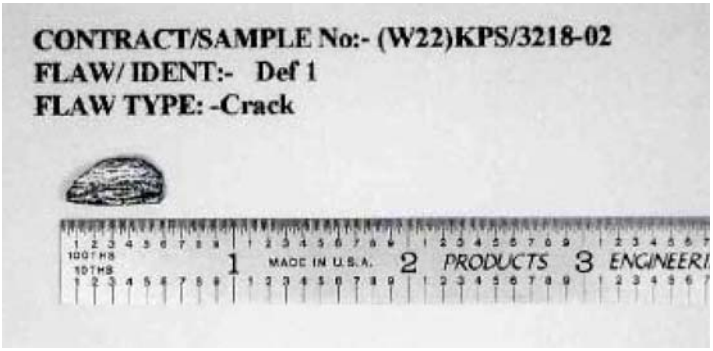

Figure 4.1. Example Flaw Coupon as Used for Test Blocks 5.1–5.3

Other flaw types such as porosity and lack of fusion were introduced into the weld using the same technique. Other flaw types, such as weld undercut, were cut directly into the penetration tube. The undercut flaw is shown in Figure 4.2.

This method of crack fabrication is commonly used and is well understood. The use of coupons does pose one possible issue—the effects of the additional welding on the ultrasonic and electromagnetic properties of the weld–sample interface.

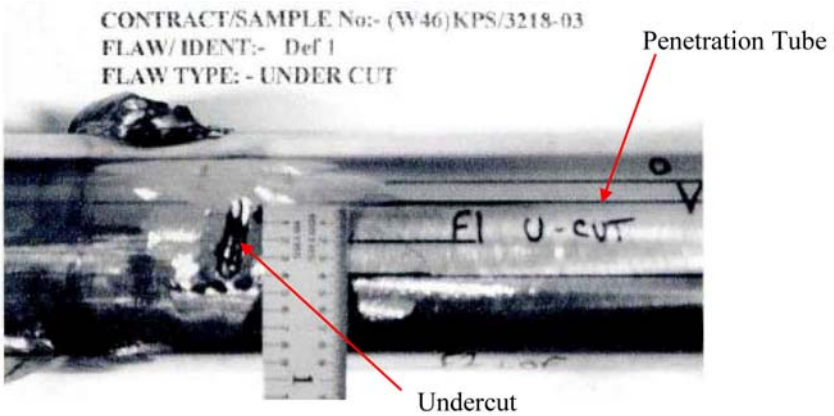

Figure 4.2. Example Weld Undercut Flaw as Used in Test Blocks 5.1–5.3

4.1.2 Flaw Fabrication in Test Blocks 5.9, 5.10 and 5.6

The flaws in test blocks 5.9, 5.10, and 5.6 were fabricated via a weld-solidification process. The region where the crack was fabricated was excised and then filled in with "poisoned" weld metal that is designed to crack on cooling. The cracks in these test blocks were designed to simulate the eddy current responses found for cracks in the 182 weld metal in the Ringhals 4 reactor (SQC 2003). The eddy current responses for the fabricated cracks were checked to ensure they were similar to the responses in real stress corrosion cracks (SCC) that occurred in nickel alloy material.

Possible issues with this style of crack fabrication are similar to those for the fabricated flaws used in test blocks 5.1–5.3—the weld fabrication zone can possibly be detected in an eddy current or a visual examination. A visual examination of the cracked areas showed no disturbance of the surface caused by the implantation process and that the weld solidification cracks were surface-breaking. The flaws in Block 5.6 at 45, 180, 225, 255, and 315 degrees were clearly detected in photographs, and the flaw at 135 degrees had a possible crack-like indication. A sample weld solidification crack in test block 5.6 is shown in Figure 4.3.

4.1.3 Flaw Fabrication in Test Block 5.7

The flaws in test block 5.7 were fabricated using an in situ thermal fatigue process. This process is able to introduce flaws into the material without the weld fabrication problems associated with the coupon insertion or weld-solidification cracking. It is also possible to control crack properties such as crack opening displacement (COD) and crack depth with a high level of precision. The thermal fatigue cracks are very expensive, however, so only two such flaws were ordered. Because of an accident during the fabrication of one of the flaws, three flaws are present in test block 5.7. Only two have the proper pedigree involving length and depth, however. All three flaws in test block 5.7 were confirmed as surface-breaking using visual examination. Photography of the flaws showed that the flaws at 15 degrees and 300 degrees consisted of multiple small cracks spaced closely together. The flaw at 15 degrees is shown in Figure 4.4.

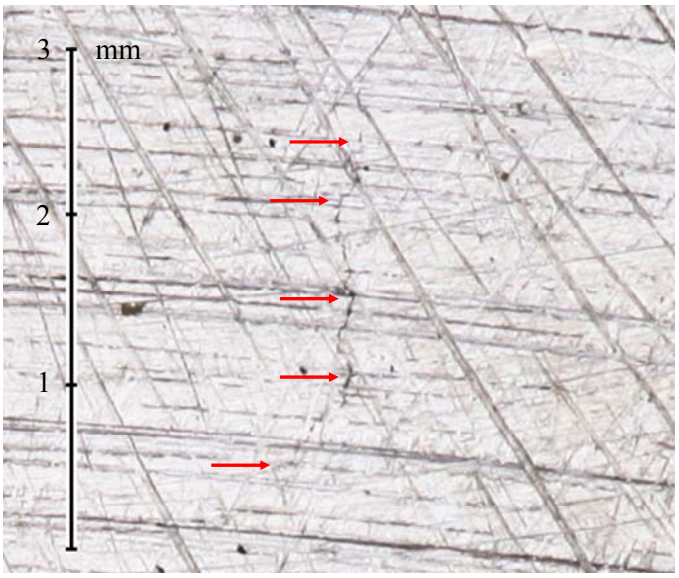

Figure 4.3. Weld Solidification Crack in Test Block 5.6 at 45 Degrees

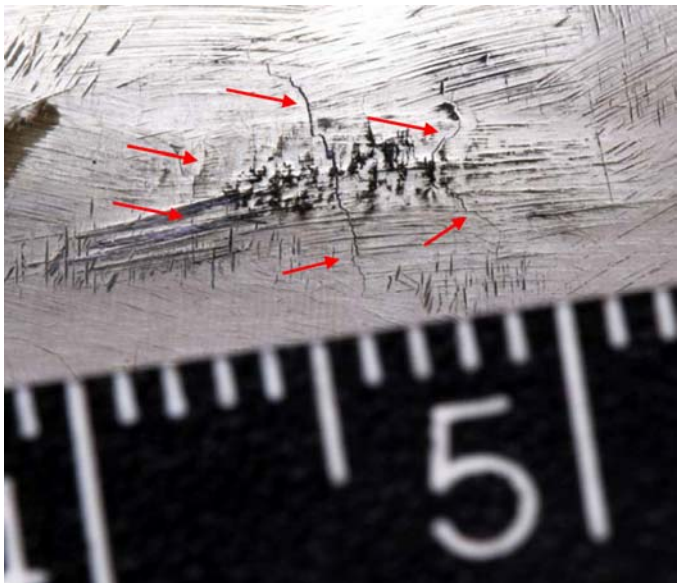

Figure 4.4. Thermal Fatigue Cracks in Test Block 5.7

4.1.4 Flaw Fabrication in Test Block 5.8

Test block 5.8 had a weld repair, but no crack or other flaws, fabricated into the weld. This test block is designed to deal with the issues caused by the flaws fabricated via welding flawed coupons into the test blocks and the weld-solidification cracks. The inspection of test block 5.8 provides important insight to determine if the inspectors are finding the fabrication regions and not the cracks themselves.

4.1.5 Flaw Fabrication in Test Blocks 5.9 and 5.10

The flaws in test blocks 5.9 and 5.10 were fabricated using a weld-solidification cracking process similar to the process used in test block 5.6. The difference between test block 5.6 and test blocks 5.9 and 5.10 is that the flaws in test blocks 5.9 and 5.10 were tailored to be more challenging to detect. These flaws are designed to mimic difficult-to-detect indications such as those found in the North Anna 2 nozzle 31. It is worth noting that the indications with low NDE responses in North Anna 2 were later found to be less than 8 mm deep.

A careful visual examination using high-resolution macro photography found no evidence of surface-breaking flaws in test blocks 5.9 or 5.10. This is in contrast to the weld solidification flaws in test block 5.6, where flaws were visible on the surface. Test blocks 5.9 and 5.10 were then examined using fluorescent dye penetrant testing. The penetrant testing of test block 5.9 showed no indications of any surface-breaking flaws. The penetrant testing of test block 5.10 found no linear indications, but two small spots of penetrant appeared at locations consistent with the crack implantation regions of 255 and 315 degrees. During the destructive examination of sample 5.10 the crack was revealed to have a limited surface-breaking component, and it is now believed that the PT indication near 315 degrees may have come from a welding defect such as porosity. The results of the penetrant testing are shown in Figure 4.5.

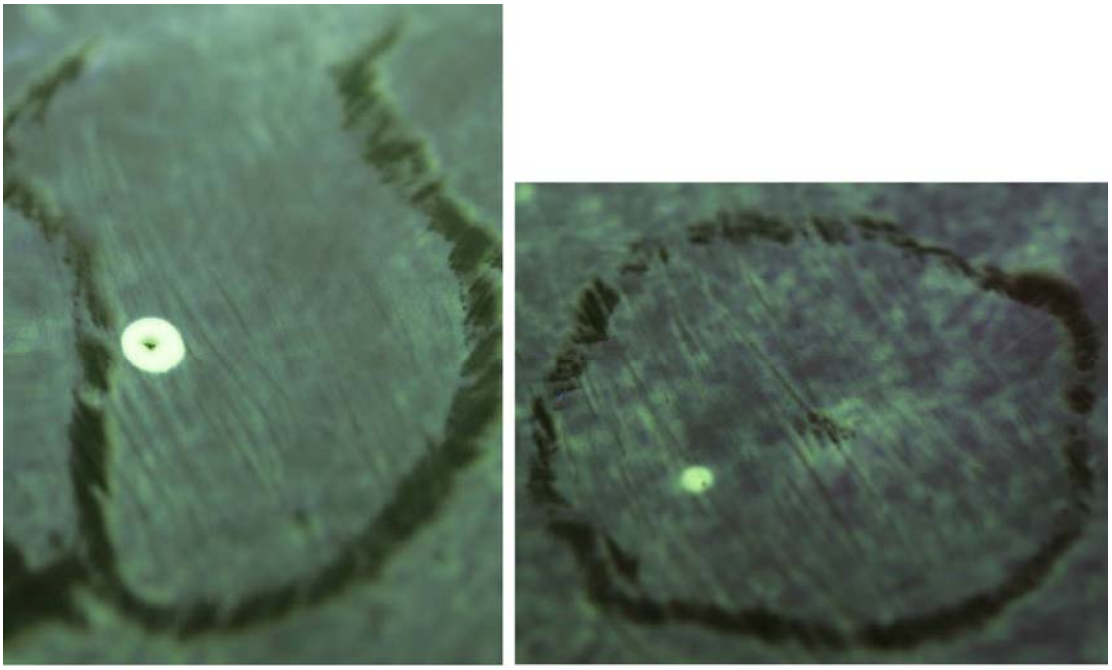

Figure 4.5. Penetrant Testing Results for Test Block 5.10

4.1.6 Test Blocks 5.11 and 5.12

No flaws were present in test blocks 5.11 or 5.12. These test blocks were included in the study to provide blank BMI specimens to help discern the false call rate for the inspectors.

4.1.7 Flaw Fabrication in Test Blocks 5.13–5.16

For the test blocks 5.13–5.16, the flaws were fabricated using laboratory-grown stress corrosion cracking (SCC). The geometry of the test blocks before preparing the SCC is shown in Figure 4.6. The penetration tubes were cut off before preparing the SCC, and the tubes were re-welded after preparing the SCC. Figure 4.7 shows the procedure for preparing laboratory SCC in a piping sample. Figure 4.8 and Figure 4.9 show typical examples of laboratory-induced SCC in these BMI test blocks.

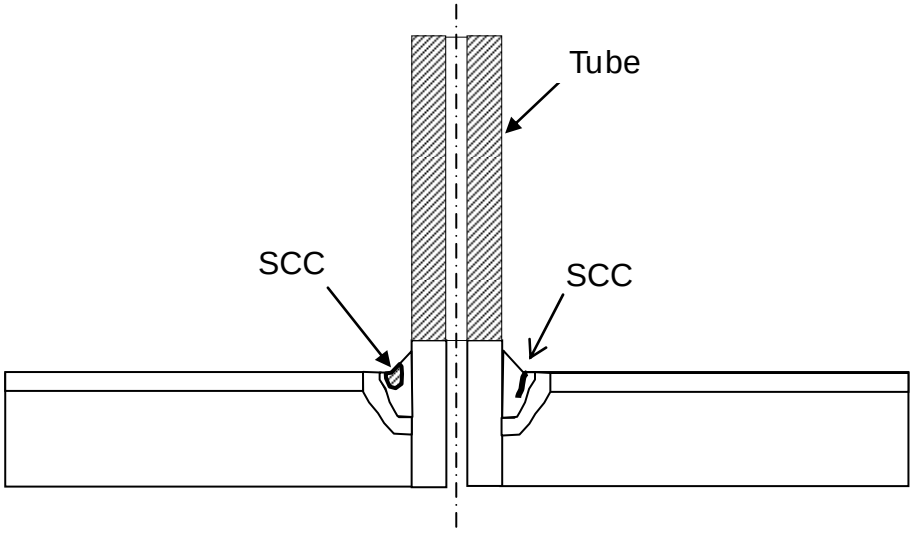

Figure 4.6. BMI Test Blocks for Preparing SCC

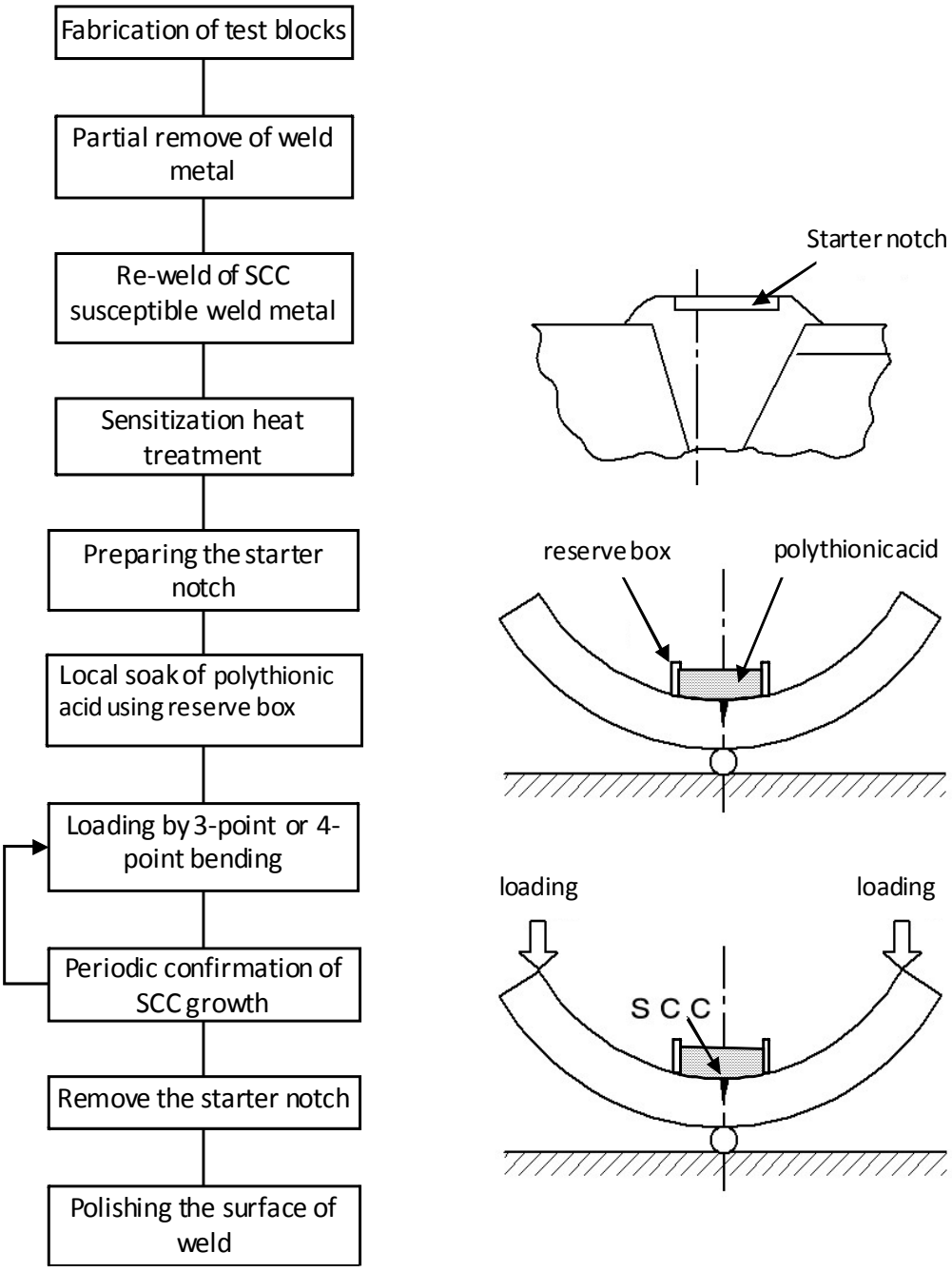

Figure 4.7. Procedure for Preparing Laboratory SCC in a Sample Piping Specimen

Figure 4.8. Example of Laboratory-Induced SCC in BMI Test Block (parallel to the weld)

Figure 4.9. Example of Laboratory-Induced SCC in BMI Test Block (perpendicular to the weld)

5.0 Scoring Procedure for PINC BMI Round Robin

Two types of scoring techniques are described in this section. Section 5.1 describes the general scoring methodology used for single flaws. Section 5.2 describes the scoring methodologies for multiple flaws that fall very close together.

5.1 Scoring Process for Strict Tolerance Single Crack POD

This section describes how inspection results are compared to the test block data to determine whether or not an individual flaw was detected. This section also describes how false calls (i.e., indications not associated with any flaw) are determined.

Scoring merges the inspection results with the true-state results by associating inspection indications with true-state flaws. The scoring procedure is summarized by the flowchart in Figure 5.1.

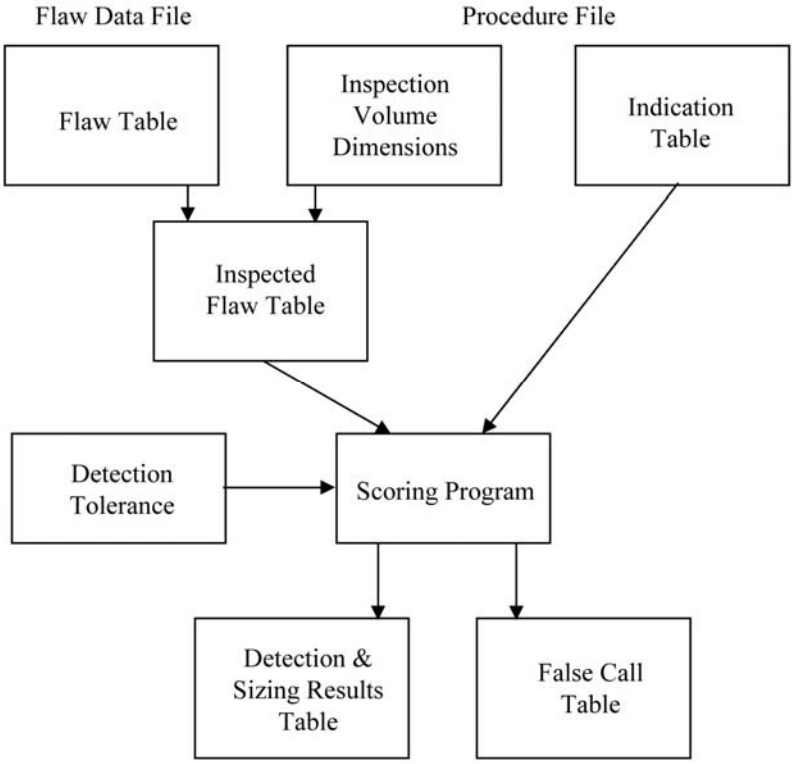

Figure 5.1. Flowchart of Scoring Procedure

The first step of the scoring process consists of uniquely identifying the flaws in the inspected volume of the weld. For this analysis, a table of flaws was developed for each test specimen. The *inspection volume* field indicated in the PDF file record for inspections was then compared with the flaw table for each specimen to determine which flaws are within the inspected volume. These flaws are then placed in the *inspected flaw table*.

The next step of the scoring process compares the entries in the *inspected flaw table* to the entries in the *indication table* (the indications that are recorded on inspection data sheets) to determine which flaw cuboids intersect with which indication cuboids.

A tolerance box of 10 mm was defined around each flaw to account for possible location error. Figure 5.2 shows the probability of detection versus size of tolerance. As can be seen in Figure 5.2, there is not a clear point that shows little improvement in detection for tolerances larger than 10 mm. The tolerance of 10 mm was chosen based mainly upon judgment. A tolerance below 10 mm shows that POD drops significantly and it was judged, for the specimens used in the PINC BMI, that a tolerance greater than 10 mm allowed possible material property variations to interfere with the reported flaw location. Therefore, for the analysis used in this report, a tolerance of 10 mm is used. Without use of a tolerance, location errors might be confused for non-detections. Once the tolerance is defined, ΔX, ΔY, and ΔZ, then the flaw cuboid (X1,X2; Y1,Y2; Z1,Z2) becomes

$$(X_1 - \Delta X, X_2 + \Delta X, Y_1 - \Delta Y, Y_2 + \Delta Y, Z_1 - \Delta Z, Z_2 + \Delta Z) \quad (5.1)$$

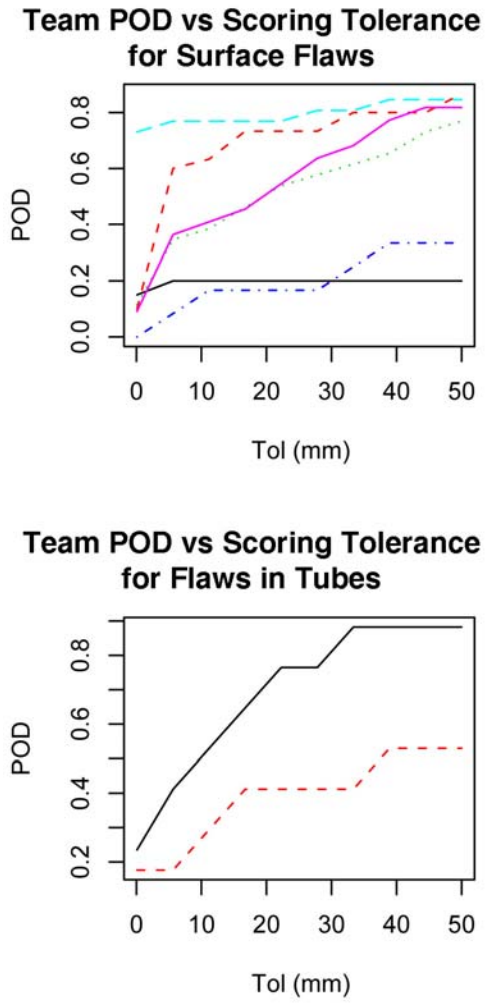

Figure 5.2. Probability of Detection versus Scoring Tolerance for All Teams and Flaws

A list of all indications not intersecting with any flaws is compiled and this list is called the *false call table*. The *false call table* is compiled after the intersecting flaw/indication cuboids have been identified for each indication. The scoring process therefore has two outputs—the detection of flaws, including the length and through-wall depth determined for each flaw, and a list of false calls. Finally, detection and sizing information is appended to all flaws in the *inspected flaw table*, using the intersection information, to produce the *detection and sizing results table*.

It is hoped that there will be few multiple intersections, so that the strategy used for dealing with multiple indications will not have a great effect on the evaluation. However, if this is not the case, we will consider other aggregation schemes.

5.1.1 Scoring Example

This section presents the scoring results for a single inspection, so the reader can more easily understand the scoring process. The data for an example inspection of the surface flaws in test block PINC 5.16 listed in Table 5.1.

Table 5.1. Surface Flaws from Test Block PINC 5.16 Example Inspection Results

Indication ID	Θ 1	Θ 2	r1	r2	z1	z2	Θ Max	r Max	Z Max
1	42	42	32	48	0	8.1	42	39	8.1
2	268	268	35	47	0	3.1	268	42	3.8

This test sample was chosen because there are few flaws and the scoring is relatively simple. Test block 5.16 contains two flaws. The team has inspected the whole block (and this is the case for almost all inspections in the round robin), so all flaws in the block should be included in the scoring procedure.

The scoring result is visually summarized by Figure 5.3. Figure 5.3 shows the results in the r, **Θ** plane, the plane most relevant to our scoring definition. If one examines the results in Figure 5.3, one can determine that the test block contains two flaws (shown in red), one is detected (call intersects with the red rectangle) and one is missed. The figure shows that the example also includes one false call. The flaw cuboid dimensions have been expanded by the scoring tolerance of 10 mm. Appendix A of this report provides the scoring results (similar to Figure 5.3) of all teams that participated in the PINC BMI round robin as plots of indications versus flaw location.

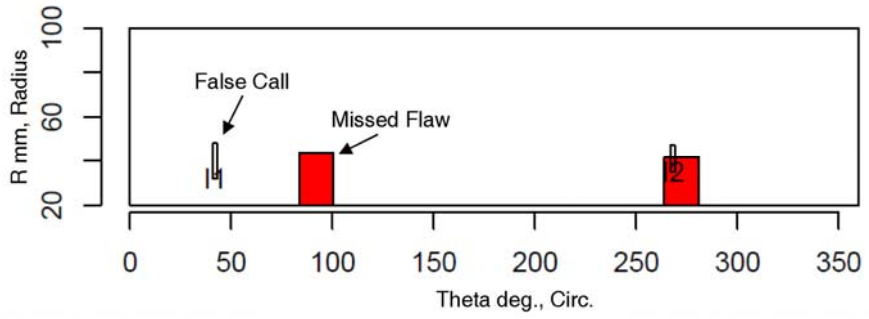

Figure 5.3. Scoring Inspection Results of Test Block 5.16 with 10-mm Tolerance

5.2 Scoring Process for Detection of Degradation for Multiple Cracks

As the Data Analysis Task Group (DAG) reviewed the data from the PINC round-robin exercise, members of the DAG recognized that the samples used in the BMI did not contain a single crack; rather, the test samples contained multiple cracks. In fact, many cracks in the test samples used for the PINC BMI were close together. The DAG decided to analyze the PINC BMI data using a set of proximity rules that would account for the multiple flaws in the test samples.

The DAG decided to use the American Society of Mechanical Engineers (ASME) Section XI IWA-3400 rules for linear surface flaws to account for the multiple flaws in each sample that were close together. The scoring process was the same as that described in Section 5.1, "Scoring Process for Strict Tolerance Single Crack POD."

Section XI, IWA-3400 of the ASME Code states the following:

> *(a)* Linear flaws detected by surface (PT/MT) or volumetric (RT) examination methods shall be considered single linear surface flaws provided the separation distance between flaws is equal to or less than the dimension *S*, where *S* is determined as shown in Figure IWA-3400-1.
> *(b)* The overall length of a single and discontinuous linear flaw shall be determined as shown in Figure IWA-3400-1.

Figure 5.4 is a reproduction of IWA-3400-1 to show the methodology used to determine whether multiple flaws in a PINC BMI sample should be combined as one flaw with length *l* or whether the flaws should be considered as single individual flaws.

Once the rules of IWA-3400 were applied to the test samples, the same scoring process was used on the samples described under Section 5.1.

Figure 5.6 shows the result of combining flaws under the rules of IWA-3400.

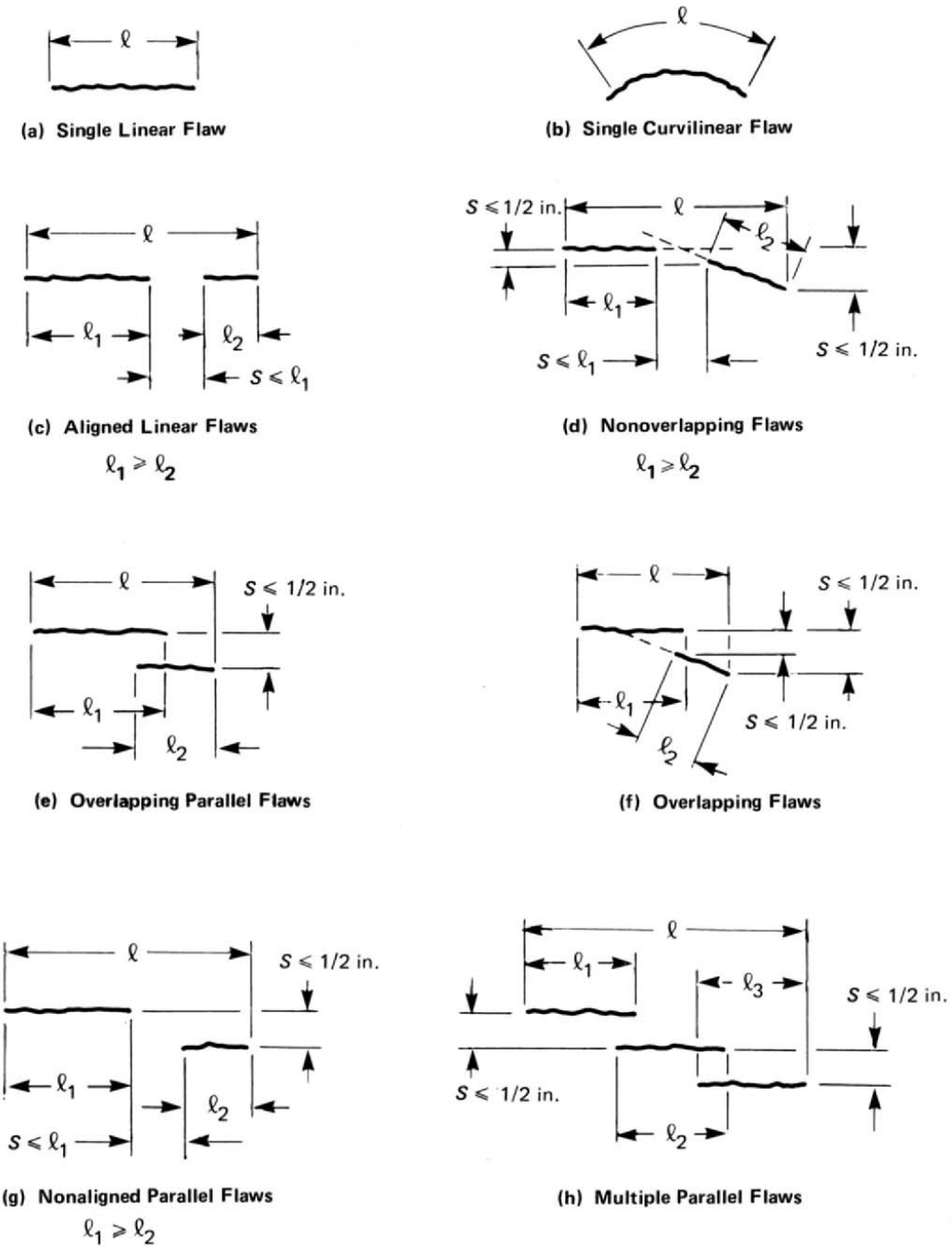

Figure 5.4. Methodology for Determining Singularity or Multiplicity of Linear Surface Flaws. Source: ASME 2007, Figure IWA-3400-1. Copyright American Society of Mechanical Engineers; reproduced with permission.

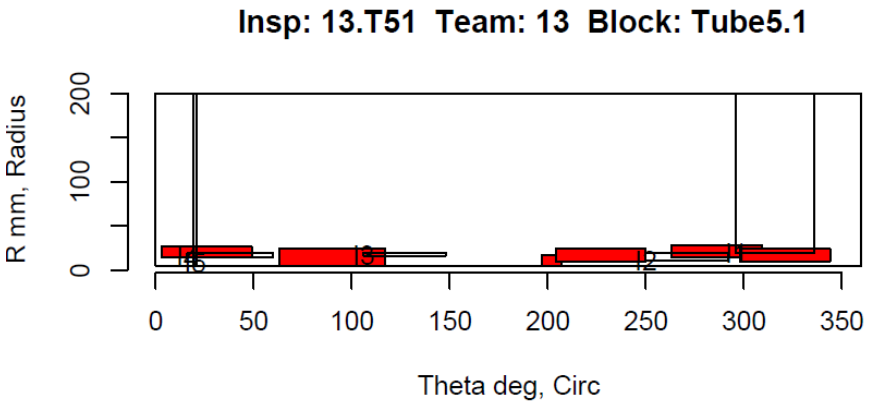

Figure 5.5. Test Sample 5.1 – Individual Flaws

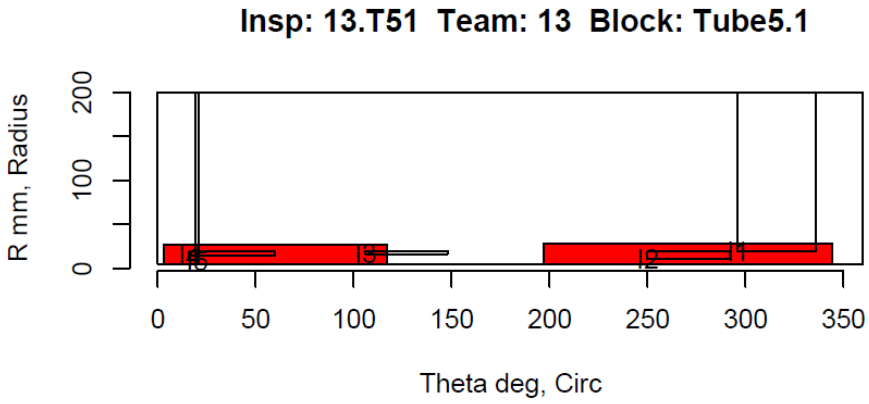

Figure 5.6. Test Sample 5.1 – Individual Flaws Combined Under Rules of IWA-3400

One can see from Figure 5.5 that test sample 5.1 has six individual flaws that are very close in proximity. Figure 5.6 shows that using the rules of IWA-3400, the six individual flaws in test sample 5.1 could be considered as two flaws using the proximity rules of IWA-3400. Based on the destructive evaluation results, this procedure was not used for Sample 5.2.

6.0 Evaluation of NDE Inspection Techniques and Their Performance in Round Robin Tests

This section contains the following information:

- Section 6.1 describes the NDE techniques used in the BMI round-robin examinations.
- Section 6.2 details the ultrasonic inspection techniques used in the round-robin examinations.
- Section 6.3 has information on the electromagnetic techniques used to examine the BMI specimens.
- Section 6.4 describes the process used to ensure that the data were accurate and the interpretation reflects the intent of the inspectors. Also of importance is that the results reflect the reliability of the technique and do not contain errors caused by the test procedures.
- Section 6.5 describes the results of the scoring and some discussion on the effectiveness of the techniques used in the BMI round-robin tests.

6.1 Summary of Nondestructive Techniques Used in PINC BMI Round Robin

The teams conducting the examinations used a wide mix of nondestructive techniques, ranging from standard methods such as conventional ultrasonic inspection to experimental techniques such as potential drop. Because there was a wide variety in techniques and the application of those techniques, comparing the effectiveness of the individual techniques would result in a very complex matrix. PNNL has divided the different techniques used in the DMW and BMI round-robin tests into two broad categories—ultrasonic and electromagnetic.

Within the ultrasonic category, the following methods were used:

- conventional ultrasound
- conventional phased array
- adaptive phased array
- time-of-flight diffraction (TOFD).

Within the electromagnetic category, the following methods were used:

- eddy current
- potential-drop methods, including both direct current (DC) and alternating current (AC) methods, and modified variations of these techniques.

6.2 Ultrasonic Techniques

Ultrasonic techniques use beams of high-frequency sound to interrogate the materials. Ultrasonic techniques are capable of inspecting a volume of material to determine the location, size, and depth of

flaws. During inservice inspection (ISI) outages at nuclear power plants, ultrasonic methods are used in the examination of piping welds; hence, their use in the PINC BMI round robin.

6.2.1 Conventional Ultrasound

Conventional ultrasonic techniques use a transducer mounted on a wedge to produce an ultrasonic beam with a specific fixed angle in the material. Typical angles used for ultrasonic inspection of nuclear components include 30, 45, and 60 degrees, in both longitudinal and shear wave modes of propagation. The ultrasonic transducers may be used to manually scan a test object, or the search unit may be designed to fit in a mechanized scanning fixture and the data collected electronically. A conventional ultrasonic transducer is diagrammed in Figure 6.1.

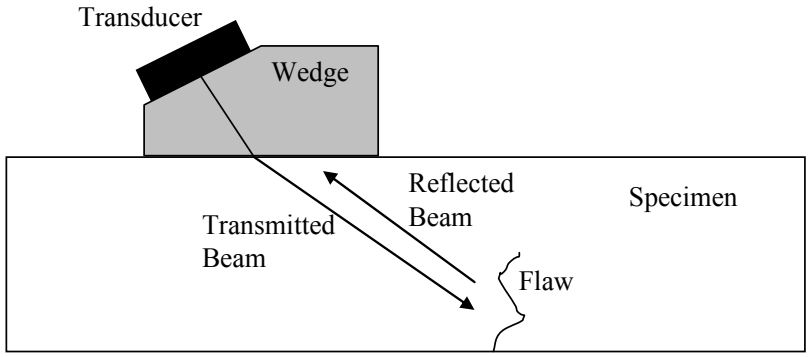

Figure 6.1. Conventional Ultrasonic Testing

Conventional ultrasound is one of the most common and time-tested techniques used to examine reactor components. Inspectors and regulating agencies have a great deal of experience with the capabilities and limitations of conventional ultrasound. A disadvantage of conventional ultrasonic techniques is that they can be time-consuming to apply because a detailed inspection may require many separate examinations using different angles and different frequencies.

6.2.2 Phased Array Ultrasound

Phased array ultrasound is a newer ultrasonic technique that is achieving ever-greater acceptance for performing ISI at nuclear power plants. Unlike a conventional ultrasonic transducer, a phased array ultrasonic transducer consists of several individual elements. These elements are excited to transmit individually at specific time delays, allowing one transducer to emit a beam at many angles and focused at several depths. Phased array beam forming is shown schematically in Figure 6.2.

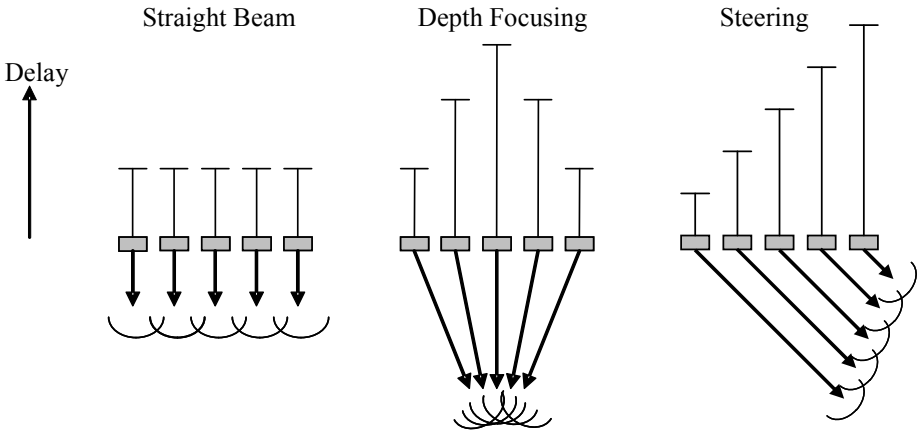

Figure 6.2. Use of Delays to Steer and Focus Ultrasonic Beams in Phased Array Transducers

Phased array ultrasound offers several advantages over conventional ultrasound because a single phased array transducer can be used to emit many angles in quick succession. This versatility allows the inspector to examine a sample much more quickly. Because phased array ultrasound requires sophisticated electronics to control the individual elements, it also provides electronic data-recording capabilities. The main disadvantages of phased array ultrasound are the increased expense of transducers and sophisticated electronics over conventional ultrasonic probes and the relative newness of, and lack of experience with, the technique.

6.2.3 Adaptive Phased Array Ultrasound

Adaptive phased array ultrasound uses the versatility of phased array technology to allow for detailed inspections of samples with irregular surfaces. The system first measures the surface profile using an initial scan and then corrects the delay laws used to focus the beam through the irregular surface. The adaptive phased array technique offers the additional benefit of working on a variety of sample configurations, unlike conventional ultrasonic testing (UT) that would require a custom probe and/or wedge for each surface profile.

6.2.4 Time-of-Flight Diffraction

Time-of-flight diffraction is a well-established ultrasonic technique that is very useful in crack detection and sizing. The TOFD technique uses two transducers that face each other to detect cracks in the material. When arranged properly, a surface lateral wave travels between the two transducers and a back-wall signal is produced by the beam bouncing off of the far side of the sample. If a surface-breaking flaw is present between the two transducers, it will interrupt either the lateral wave or the back-wall wave, and the tip of the flaw will produce a secondary signal, which is also detectable. The TOFD setup is a very powerful technique for detection and length and depth sizing of flaws. A diagram of the TOFD technique is given in Figure 6.3.

TOFD has some disadvantages, however. The TOFD arrangement has a large footprint and is not useful for inspections that have limited access to a component. For TOFD to work properly, the transducers generally need to be on a level and relatively flat surface. The region of interest for most reactor inspections is at or near a weld; if the weld has not been machined flat, the weld crown and other

geometrical features associated with welds may make TOFD unusable. Also, TOFD is less sensitive to flaws that are parallel to the plane of the transducers.

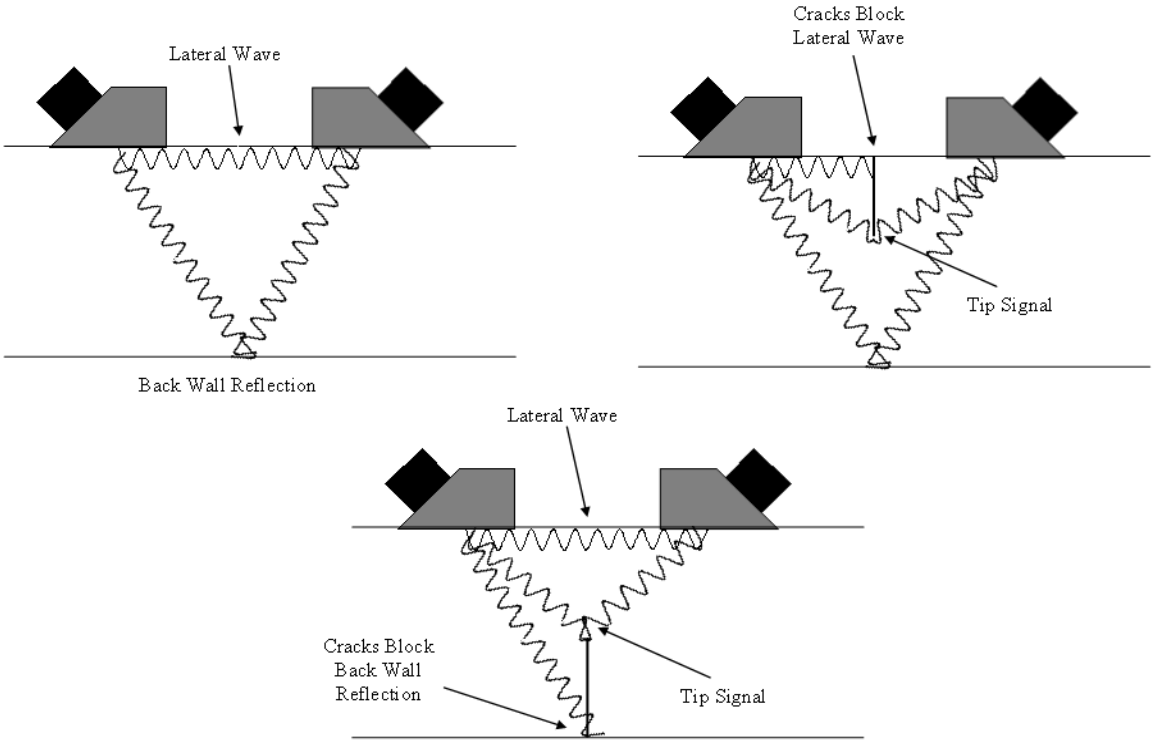

Figure 6.3. Time-of-Flight Diffraction Technique

6.3 Electromagnetic Techniques

Electromagnetic techniques detect flaws by inducing electromagnetic currents in the sample and measuring how the flaws affect the induced current. Electromagnetic techniques are often very useful at detecting surface-breaking flaws but are not typically used to depth-size flaws.

6.3.1 Eddy Current

Eddy current inspection uses a coil or coils held very close to a surface. An AC current is passed through the coil. The AC current creates a cyclical magnetic field around the coil. When this magnetic field intersects with a conducting material, such as steel or stainless steel, electrical currents are induced in the material. These currents make their own magnetic fields, which interact with the magnetic field generated by the coil. The changes in resistance and inductive reactance in the coil allow one to measure the electrical properties of the material. Breaks in the surface, such as cracks, affect the eddy currents in the materials and can be measured using the eddy current system. An eddy current test setup is shown schematically in Figure 6.4.

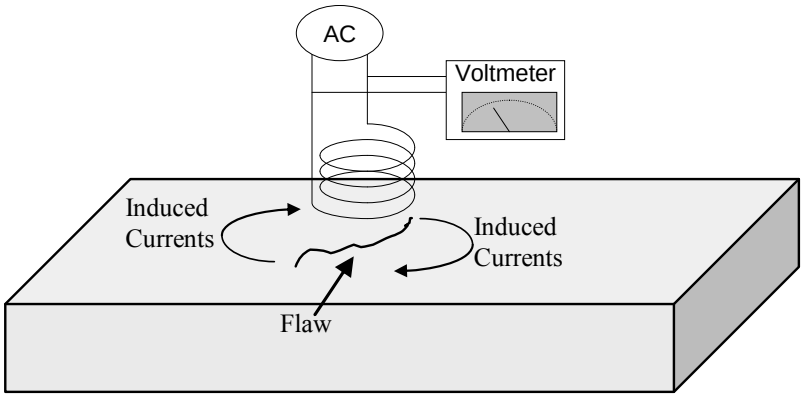

Figure 6.4. Eddy Current Diagram

Eddy current testing (ECT) is very effective at detecting surface-breaking flaws, but usually only from the same surface at which the flaw originates. Using eddy current inspection for through-wall examinations is possible only with thin materials such as steam generator tubes and is not possible for most reactor piping. ECT is one of the most common techniques used to inspect samples where the possible cracked surface is accessible to inspectors. The main weakness of eddy current inspection is that it is a surface and near-surface examination only and cannot be performed through more than a few millimeters of metal. The technique is not capable of characterizing the through-wall size of cracks more than a few millimeters in depth.

6.3.2 Potential-Drop Techniques

Although there are several implementations of potential-drop techniques, they all function by passing a current (AC or DC, depending on the technique) through the specimen and use several probes to measure the electrically induced voltage of the material (see Figure 6.5). Flaws in the material affect the electrical voltage and current, and this effect can be measured. Some potential-drop measurements need to be made from the surface broken by the crack, but some implementations can be used through the entire thickness of a pipe. The potential drop technique has many variations. The variations used in this round-robin test are as follows:

- alternating current potential-drop (ACPD) method
- direct current potential-drop (DCPD) method
- closely coupled probe potential-drop (CCPPD) method using direct current
- induced current potential-drop (ICPD) method using induction alternating current.

Potential-drop techniques are not commonly used in reactor inspections.

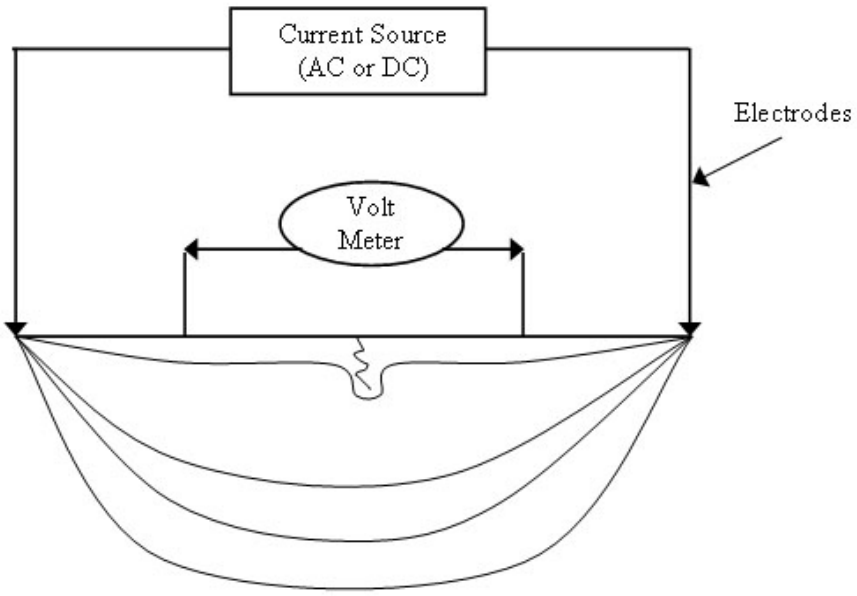

Figure 6.5. Four-Probe Potential-Drop Measurement

6.3.3 Tube Examinations

Only two teams inspected the penetration tubes of Samples 5.1–5.3. Team 13 used TOFD techniques to examine the penetration tubes of the remaining samples, but these had no flaws present in the penetration tubes. The two teams, 13 and 70, that examined the interiors of the penetration tubes used eddy current as a flaw detection technique. Team 13 also used TOFD as a detection technique. The techniques used by Teams 13 and 70 for the penetration tube examinations are as follows:

6.3.3.1 Team 13

Team 13 used a hybrid TOFD/eddy-current testing (ECT) probe. The ECT frequencies used by Team 13 ranged from 75–500 kHz with a probe size of 6 mm (0.25 in.). The TOFD was carried out in the axial and circumferential directions using 5–6 MHz ultrasound. The inspection volume was relatively shallow, covering essentially the penetration tube material and only a millimeter into the J-groove weld metal.

6.3.3.2 Team 70

Team 70 used a cross-coil ECT probe to inspect the interior of the penetration tubes of Samples 5.1-5.3. The coil was mounted on a search unit designed to fit in the penetration tubes while maintaining contact with the wall of the tube. While the ECT coil used for the tube inspection has a nominal frequency range from 5 kHz to 1 MHz, only frequencies ranging from 50–400 kHz were used. The diameter of the coil was 3 mm.

6.3.4 Surface Examinations

The surfaces of the BMI samples were examined with a variety of ECT techniques, one ultrasonic technique, and two potential-drop techniques. The eddy-current techniques can be grouped in two categories – higher-frequency cross-coil probes and lower-frequency array-probe techniques. The potential-drop techniques used different techniques to create the current in the materials, closely coupled probes and induced current. The ultrasonic technique was an immersive adaptive phased-array technique that corrects for sample distance and surface shape to allow for better focusing in the part. The techniques and probe descriptions are given in Table 6.1.

Table 6.1. Techniques and Probes Used by Team

Team	Detection Technique	Probe Description
16	Closely Coupled Probe Potential Drop	2-axis 15 mm × 4 mm, 5-second measurement time
38	Array Eddy Current Probes	100-kHz 48-channel array
66	Adaptive Phased Array Ultrasound	5-MHz 40-element probe, 16 elements used at a time
67	Induced Current Potential Drop	0.3–10 kHz, 2 A, 3-second measurement time
70	Cross Coil Eddy Current Probe	400-kHz, 3-mm coil diameter
99	Array Eddy Current Probe	200 kHz
373	Cross Coil Eddy Current Probe	300-kHz 8-mm coil diameter

6.4 Process Used To Ensure Accuracy of the Inspection Data from the PINC DMW Round Robin

As the data collection was carried out by several teams in several countries, there were inevitable errors in data entry and data transmittal. The data were examined carefully against the true state to determine if any systematic errors were detectable. If a systematic error was found, the appropriate invigilator was contacted to determine an appropriate correction. As there were fewer teams in the BMI RRT than in the DMW RRT and the coordinate system was more consistently followed throughout the round-robin testing, few errors were found. The probability of detection results are therefore often a strong function of how many challenging and how many baseline-difficulty samples the teams inspected.

6.5 Evaluation of Detection Capability

The flaws in the BMI test blocks were evaluated by eight teams using several techniques. The goal of the PINC BMI round robin was to determine which techniques are the most effective and to understand the physical basis for the techniques' performance. No two teams used identical techniques, although some groupings can be made.

There are several approaches to evaluating the abilities of the different teams to detect the fabricated cracks in the test blocks. The data analysis is complicated by two factors—not all teams examined the same test block set, and some of the test blocks had flaws that proved to be more challenging to find than was expected. The average POD, as shown in Table 6.2 for each test block, shows that test blocks 5.9

and 5.10 were the most challenging. The other test blocks have roughly the same POD of close to 0.8. Test blocks 5.1–5.3 are difficult to interpret because there were too few observations and the error was too large to allow one to draw conclusions on their difficulty. The results for each team and each sample are given in Appendix A.

Test blocks 5.6, 5.7, and 5.13–5.16 can be considered "baseline" difficulty, while test blocks 5.9 and 5.10 can be considered "challenging." It should be noted that test blocks 5.9 and 5.10 were designed to mimic difficult-to-detect indications found in the North Anna 2 Nozzle 31 J-groove weld that were not confirmed as actual cracks. The flaw manufacturer for test blocks 5.9 and 5.10 used a process to make the flaws more challenging to detect. All teams inspected the challenging test blocks, 5.9 and 5.10, and the different teams also examined different numbers of the baseline test blocks. To determine which teams are the most affected by the varying proportion of challenging to baseline test blocks, the number of baseline and challenging flaw observations was tallied and is shown in Table 6.3.

Table 6.2. Probability of Detection for Each Test Block in BMI Test Blocks

Test Block	POD	Observations
5.1	0.50	2
5.2	0.50	2
5.3	0.25	4
5.6	0.75	24
5.7	0.81	21
5.9	0.18	28
5.10	0.18	28
5.13	0.70	10
5.14	0.90	10
5.15	0.70	10
5.16	0.90	10

Table 6.3. Number of Baseline and Challenging Flaw Observations for Each Team in BMI Test Blocks

	Flaw Difficulty		
Team	Baseline Flaw Observations	Challenging Flaw Observations	% Baseline Observations
16	11	8	0.58
373	21	8	0.72
38	17	8	0.68
66	11	8	0.58
67	3	8	0.27
70	17	8	0.68
99	13	8	0.62

Most teams appear to have a ratio of 50–60% of baseline flaws. Team 67 faced a more challenging test than the others and this was noted in the data analysis.

6.5.1.1 Probability of Detection Curves for Teams Using a Strict Tolerance Box

The round-robin data were analyzed using a statistical regression to determine the POD for each technique. An upper and lower 95% confidence boundary was calculated using the POD and the number of flaw observations at each flaw size. It is worth noting that the effect of the challenging test blocks is somewhat mitigated in these regressions because all but two of the flaws in the challenging test blocks are less than 5 mm in length. All regressions include the results for both baseline and challenging flaws. The regressions allow one to draw conclusions about the usefulness of the different techniques for finding flaws of various lengths.

6.5.1.2 Probability of Detection for BMI Tube Examinations

The interiors of the penetration tubes were examined by two teams, 13 and 70. Many of the flaws in test blocks 5.1–5.3 were very close to one another, resulting in some flaws being considered one flaw by ASME Code proximity rules. The results for Team 70 (provided in Appendix A) show some calls made on calibration notches in the penetration tubes. These calls on the calibration notches were not considered hits, as the notches are not representative of flaws that would be encountered in the field. The calls on the calibration notches were not counted as false calls because the notches were present in the penetration tubes. Team 70 used a surface technique and is only scored using surface breaking flaws, and thus has fewer observations than Team 13. The results of the tube examinations are presented in Table 6.4.

Table 6.4. Probability of Detection Scores for Tube Examinations in BMI Test Blocks, without using the ASME Code proximity rules

Team	Detection Technique	Observations	POD	False Calls per Test Block	Qualified Team	Data Collection
13	ECT and TOFD	17	0.53	1.7		Automatic
70	ECT	4	0.5	0.67	X	Automatic

Given the low number of observations, it is challenging to draw meaningful results from the examinations. Team 13 achieved a higher POD than Team 70, but with more false calls. An examination of the data shows that the teams made calls that grouped multiple flaws together, which is understandable given the tight flaw spacing. When the tube examinations are scored using ASME Code proximity rules, the POD results improve. The POD results for the combined flaws are given in Table 6.5.

Table 6.5. Probability of Detection Scores for Tube Examinations for Flaws Combined Using ASME Rules in BMI Test Blocks

Team	Detection Technique	Observations	POD	False Calls per Test Block	Qualified Team	Data Collection
13	ECT and TOFD	12	0.83	1.7		Automatic
70	ECT	4	0.5	0.67	X	Automatic

For the tube examinations, the results show low PODs with an insufficient number of observations to draw strong conclusions. Some of the flaws are detectable, but a more extensive test would need to be

performed to quantify the effectiveness of the ECT and TOFD techniques. The regressions for the tube interiors are given in Figure 6.6.

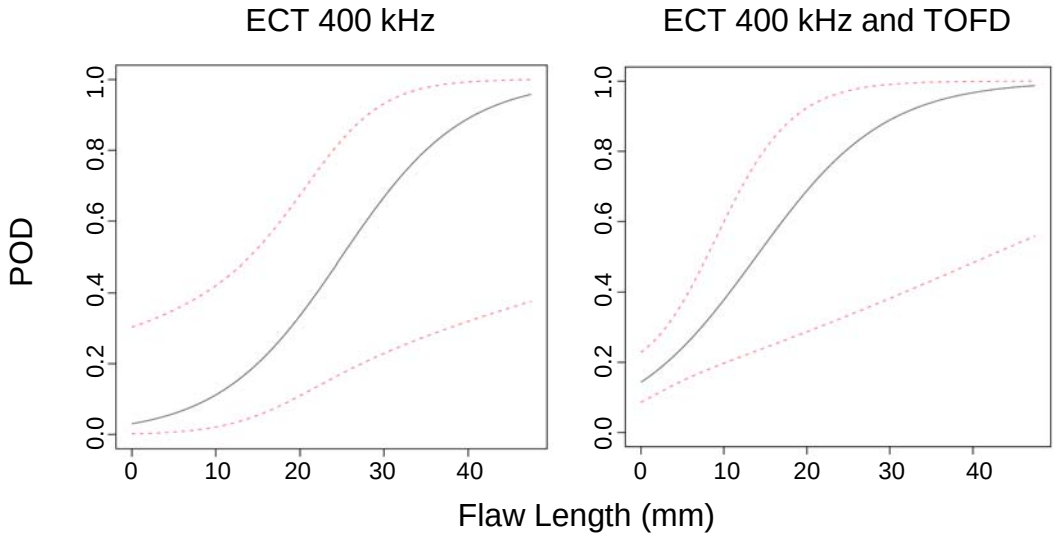

Figure 6.6. Probability of Detection Regression for Examinations of the Penetration Tube Interiors in BMI Test Blocks

6.5.1.3 Probability of Detection for BMI Weld Surface Examinations

The data were analyzed first by comparing the true-state information with fixed scoring boxes with the boxes determined as described in Section 5. This scoring method yields the following results for each team and is given in Table 6.6.

Table 6.6. Probability of Detection and False Call Rates for Each Team Using a 10-mm Tolerance Box in BMI Test Blocks

Team	Detection Technique	Observations	POD	False Calls per Sample	Qualified Team	Data Collection
16	CCPPD	19	0.26	0.00		Manual
373	ECT 300 kHz	29	0.72	0.15		Automatic
38	Array ECT 100 kHz	25	0.4	4.80		Manual
66	Adaptive Phased Array UT	19	0.58	0.00	X	Automatic
67	ICPD	11	0.27	0.67		Automatic
70	ECT 400 kHz	25	0.84	0.00	X	Automatic
99	Array ECT 200 kHz	21	0.43	2.50		Automatic

The straight POD scores correlate very closely with the percentage of baseline flaws examined by each team. When the POD results are analyzed with the baseline and challenging flaws separated out, a trend becomes clear. Teams 66, 70, and 373 were very effective at finding the baseline flaws, with PODs at or near 100%. Teams 16 and 38 showed improved performance on the baseline flaws, but were still below 50%. Teams 67 and 99 showed greatly improved performance on the baseline samples. For the challenging samples, no team performed strongly. The highest scoring team was Team 70, which

achieved a POD of 0.40. Teams 16, 38, 66, and 99 were unable to detect the challenging flaws. The baseline and challenging flaw PODs are given in Table 6.7.

Table 6.7. Probability of Detection Results in BMI Test Blocks for Baseline and Challenging Flaws with Upper and Lower 95% Confidence Levels (CL)

	Baseline	Challenging
Team	POD	POD
16	0.45	0.00
373	0.85	0.38
38	0.59	0.00
66	1.00	0.00
67	0.67	0.13
70	1.00	0.50
99	0.69	0.00

The examinations showed some clear high-performing techniques and techniques that need to be developed further before they are useful for reliably finding flaws in BMIs. The POD regression results for each technique for selected flaw lengths are given in Table 6.8. The false call probability given in Table 6.8 is calculated by extrapolating the POD regression fit to a flaw length of zero.

Cross-coil probe eddy current at 300–400 kHz proved to be very effective at finding the flaws in the test blocks. The high-frequency eddy current was also able to find a small fraction of the challenging flaws as well. The 400-kHz eddy current outperformed the 300-kHz eddy current in both the baseline and in the challenging flaws, and the 400-kHz examinations had a lower false call rate. The POD regressions for the two cross-coil eddy-current inspections are shown in Figure 6.7.

Table 6.8. Probability of Detection Regression Results for 5-, 10-, and 15-mm Flaws in BMI Test Blocks

	Detection	POD for Flaw Lengths of:			
Team	Technique	5	10	15	FCP
16	CCPPD	0.04	0.21	0.59	0.01
373	ECT 300 kHz	0.31	0.83	0.98	0.03
38	Array ECT 100 kHz	0.44	0.55	0.65	0.34
66	Adaptive Phased Array UT	0.21	0.96	1.00	0.00
67	ICPD	0.25	0.79	0.98	0.03
70	ECT 400 kHz	0.80	1.00	1.00	0.01
99	Array ECT 200 kHz	0.37	0.58	0.76	0.21

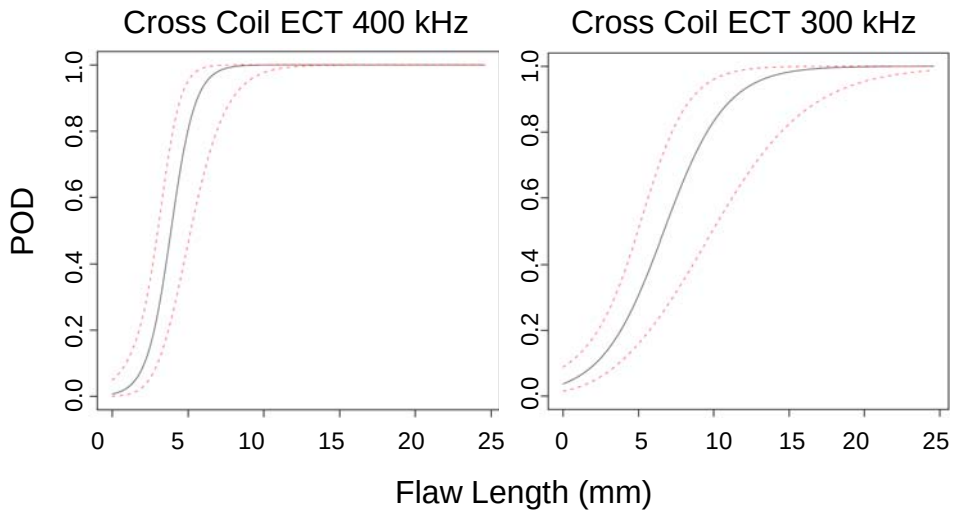

Figure 6.7. Probability of Detection Regressions for Cross-Coil Eddy-Current Techniques with 95% Confidence Intervals in BMI Test Blocks

The results for the array eddy-current techniques were relatively poor. The array probes had difficulty detecting longer flaws, and both array examinations had a very high false call rate. The array eddy current used lower frequencies than the cross-coil probes, which may have contributed to the poor performance. The POD regressions are shown in Figure 6.8.

The POD regressions for the potential-drop techniques show that they are able to detect longer flaws in test blocks, although the 95% confidence interval is very large based on the small number of test blocks in the tests. It is interesting that the potential-drop techniques were able to outperform the array ECT techniques. The POD regressions for the potential-drop techniques are shown in Figure 6.9.

The adaptive phased array ultrasound provided perfect detection of all flaws in the baseline difficulty test blocks and missed all flaws in the challenging test blocks. The POD regression curve shows the adaptive phased array technique has a very high probability of detecting flaws greater than 10 mm in length. The POD results for the adaptive phased array technique for all flaws are shown in Figure 6.10.

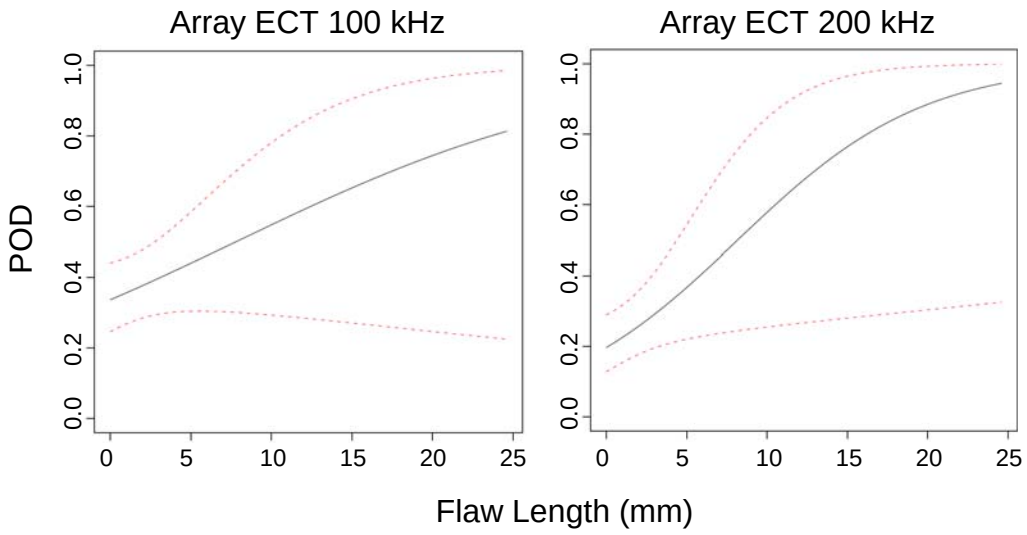

Figure 6.8. Probability of Detection Regressions in BMI Test Blocks for Array Eddy-Current Techniques

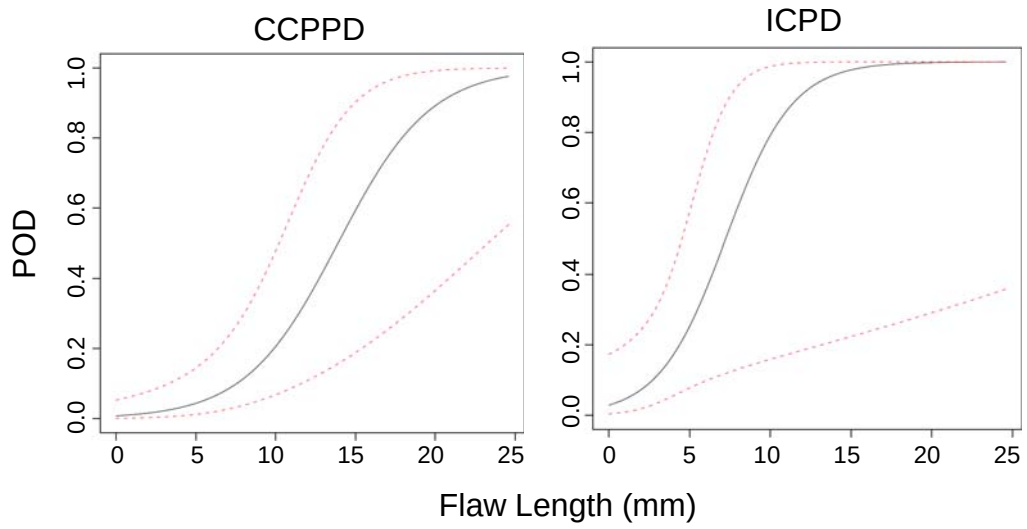

Figure 6.9. Probability of Detection Regressions in BMI Test Blocks for Potential-Drop Techniques

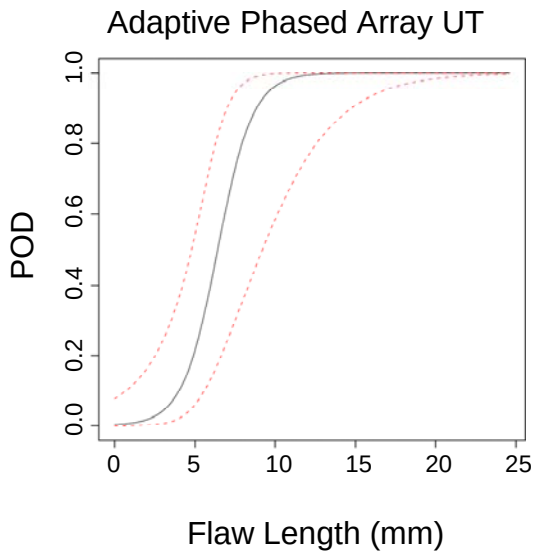

Figure 6.10. Probability of Detection Regression in BMI Test Blocks for Adaptive Phased Array Technique

6.5.1.4 Probability of Detection versus BMI Test Block Flaw Characteristics

It is important to understand the crack morphologies and characteristics that make flaws reliably detectable or challenging to find during inservice inspections. The destructive analysis results of BMI test blocks are shown in Appendix B. The usual crack characteristics that are commonly considered important for NDE reliability include crack length, depth, and COD. The true-state information contained the crack lengths and depths, and the destructive examinations for test blocks 5.13–5.16 contain information on the CODs for these test blocks.

To better understand the crack characteristics, PNNL performed a series of fingerprinting examinations of the surfaces of test blocks 5.6–5.16. These fingerprinting measurements were performed in a laboratory with the true-state information available to the inspectors. A 5-MHz eddy current examination was performed using a pancake-style coil. The eddy current system was calibrated before each examination to ensure consistent results. The flaws were analyzed and the maximum voltage for each flaw was recorded. The PNNL fingerprinting results for the flaws in the surfaces of test blocks 5.6-5.16, along with the crack lengths, depths, crack POD, and flaw fabrication technique, are tabulated in Table 6.9. The complete fingerprinting results are shown in Appendix C.

When the data for the surface examinations were analyzed, the overall POD for each flaw was largely independent of flaw length, depth, or flaw orientation. The single largest influence in the flaw POD was the test block identification. All flaws that were not in test blocks 5.9 and 5.10 have a POD of approximately 0.8, and the flaws in test blocks 5.9 and 5.10 had much lower overall PODs. In test blocks 5.9 and 5.10, the largest influence in the flaw POD was the flaw length. The flaw depth was not an important variable for flaw detection in these test blocks. The crack PODs for the various crack fabrication techniques are plotted against their length in Figure 6.11 and against their depth in Figure 6.12.

Because one of the main goals of the PINC is to discover what makes a crack easy or difficult to detect, the flaws in test blocks 5.9 and 5.10 provided an opportunity to explore what it is about these flaws that make them different from the thermal fatigue, other SCC, and the weld-solidification flaws fabricated into other test blocks. Figures 6.11 and 6.12 indicate that the weld-solidification flaws were the most difficult to detect.

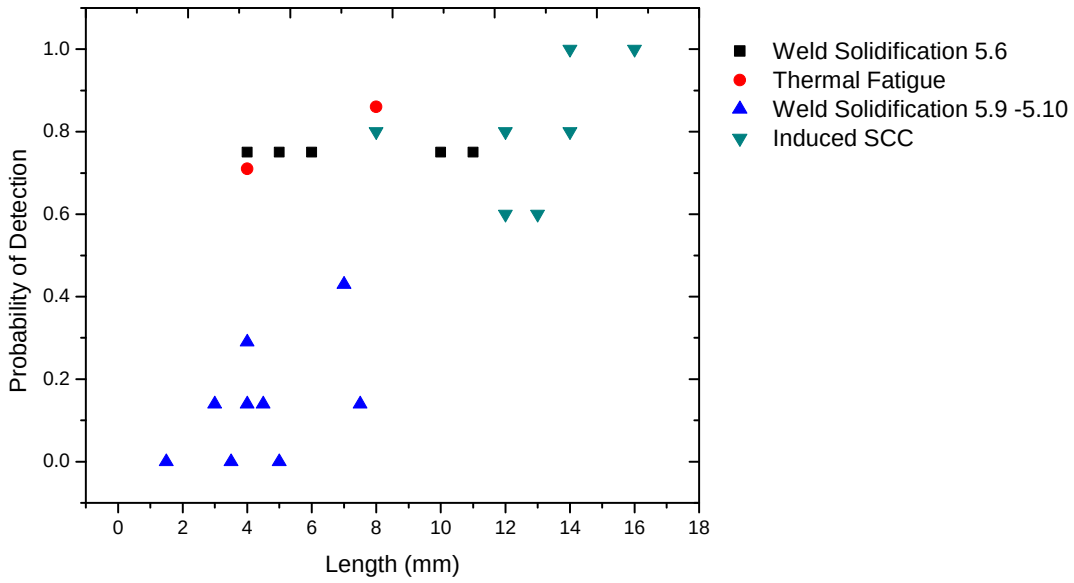

Figure 6.11. BMI Flaw Probability of Detection versus Flaw Length for Each Flaw Fabrication Technique

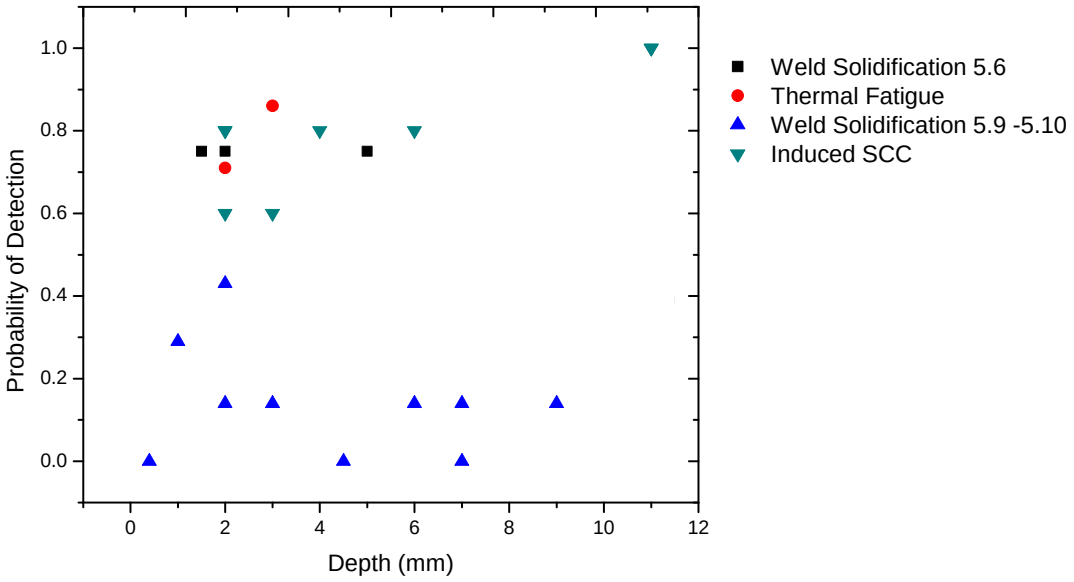

Figure 6.12. BMI Flaw Probability of Detection versus Flaw Depth for Each Flaw Fabrication Technique

Table 6.9. BMI Flaw Probability of Detection and Important Parameters

Test Block	Flaw	Radial Location, °	PNNL ECT Magnitude, V	POD	Flaw Length, mm	Flaw Depth, mm	Flaw Orientation	Fabrication Technique
5.6	1	45	0.72	0.75	4	2	Axial	Weld Solidification
5.6	2	135	1.74	0.75	5	2	Circ.	Weld Solidification
5.6	3	180	1.07	0.75	5	2	Axial	Weld Solidification
5.6	4	225	1.25	0.75	10	5	Circ.	Weld Solidification
5.6	5	255	NR	0.75	11	5	Circ	Weld Solidification
5.6	6	315	1.44	0.75	6	1.5	Axial	Weld Solidification
5.7	1	15	2.35	0.71	4	2	Circ.	Thermal Fatigue
5.7	2	165	1.67	0.86	8	3	Axial	Thermal Fatigue
5.7	3	300	2.32	0.86	NA	NA	Axial	Thermal Fatigue
5.9	1	15	0.51	0.29	4	1	Axial	Weld Solidification
5.9	2	75	NR	0.14	3	6	Axial	Weld Solidification
5.9	3	195	NR	0.14	3	3	Circ.	Weld Solidification
5.9	4	345	1.33	0.14	4	7	Axial	Weld Solidification
5.10	1	45	2.69	0.14	7.5	9	Circ.	Weld Solidification
5.10	2	75	1.79	0.00	5	7	Circ.	Weld Solidification
5.10*	3	225	NR	0.00	3.5	0.4	Axial	Weld Solidification
5.10	4	255	1.9	0.43	7	2	Circ.	Weld Solidification
5.10	5	285	NR	0.14	4.5	2	Axial	Weld Solidification
5.10*	6	315	1.96	0.00	1.5	4.5	Axial	Weld Solidification
5.13	1	0	2.45	0.80	8	2	Circ.	Induced SCC
5.13	2	180	1.62	0.60	12	2	Circ.	Induced SCC
5.14	1	0	3.92	1.00	14	11	Circ.	Induced SCC
5.14	2	180	1.39	0.80	14	2	Circ.	Induced SCC
5.15	1	90	2.94	0.80	12	4	Axial	Induced SCC
5.15	2	270	4.01	0.60	13	3	Axial	Induced SCC
5.16	1	90	4.42	1.00	16	11	Axial	Induced SCC
5.16	2	270	7.08	0.80	19	6	Axial	Induced SCC

* During DE, Flaws 5.10 3 and 5.10 6 were determined to be too small for use in scoring.

7.0 Evaluation of Length Sizing of PWSCC in the PINC BMI Round Robin

For each detected flaw, the ability of the NDE techniques to accurately size the flaw was evaluated. This section describes the length sizing accuracy for the inspections in the round-robin tests. The length sizing results for each inspection was scored using a length-sizing regression and 95% confidence intervals were determined. No analysis of depth sizing is presented, as there were not sufficient data to make such an analysis meaningful.

7.1 Tube Examinations

The small number of flaws detected by the tube examinations makes drawing conclusions from the data difficult. An additional challenge in the flaw length sizing is caused by the close proximity of the flaws to one another, with the result that the teams had occasionally combined multiple flaws together. The length-sizing regression showed that the techniques had a very large root-mean-square error (RMSE) and a large standard deviation. Flaws tended to be undersized by both teams.

Table 7.1. Length Sizing Results for Penetration Tube Examinations

Team	Observations	Technique	RMSE (mm)	Standard Deviation (mm)	Bias (mm)
All	13		19.6	18.17	-7.37
13	8	ECT and TOFD	22.24	19.32	-11
70	5	ECT	16.45	16.37	-1.56

The length sizing regressions show little relationship between the flaw size and the called indication lengths. The 95% confidence bounds for the tube sizing regressions are so large that they are essentially meaningless. Examinations of more flaws by additional teams would be needed for a better length-sizing assessment for examination of flaws in the interior of the penetration tubes.

7.2 Surface Examinations

The length-sizing results for the surface examinations contained enough observations to allow for a complex length-sizing regression. The results for each technique were analyzed and the RMSE, standard deviation, bias, and 95% confidence intervals were determined.

The length-sizing results for the surface examinations showed that some techniques were able to accurately measure the lengths of the flaws. Team 16 had the best score, although they had only five observations in the data set. Several other teams achieved an RMSE of less than 5 mm. The results for each team are given in Table 7.2.

Table 7.2. Length Sizing Results for Surface Examinations

Team	Observations	Technique	RMSE (mm)	Standard Deviation (mm)	Bias (mm)
All	79		11.7	11.53	2.01
16	5	CCPPD	2.45	2.45	-0.1
373	20	Cross Coil ECT 300 kHz	3.94	3.94	-0.18
38	10	Array ET 100 kHz	32.28	28.33	15.48
66	11	UT 5 MHz	4.7	4.55	-1.19
67	3	ICPD	5.46	1.86	-5.13
70	21	Cross Coil ET400 kHz	3.76	2.92	2.37
99	9	Array ET C 200 kHz	4.33	4.07	-1.49

The cross-coil eddy-current tests were able to accurately length size the flaws that were detected, both with RMSEs on the order of 4 mm. The 400-kHz probe examination outperformed the 300 kHz, but not by a statistically significant margin. The POD length sizing regression for the cross-coil ECT is shown in Figure 7.1.

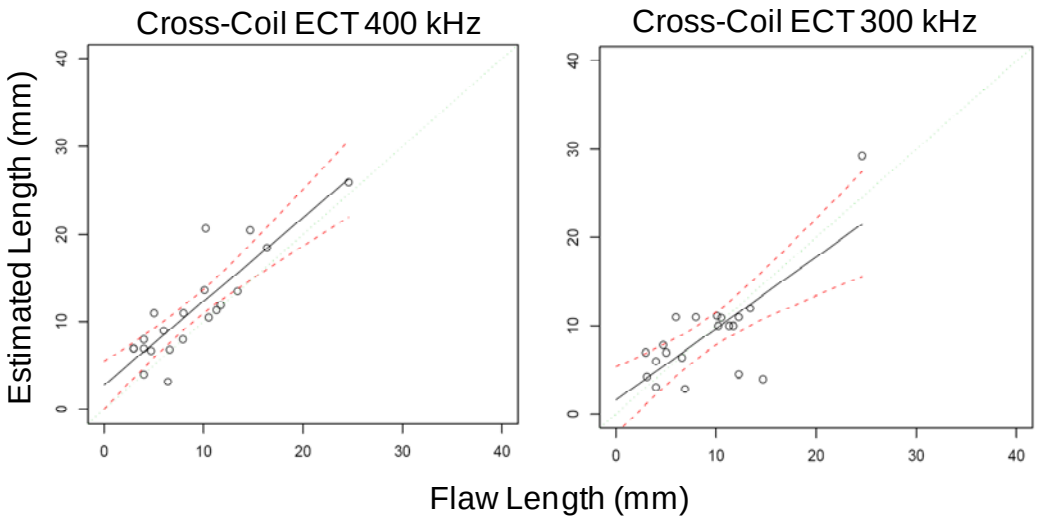

Figure 7.1. Length Sizing Results for Cross-Coil Eddy-Current Probes

The array eddy-current techniques were less effective than the cross-coil probes in this BMI round robin at length sizing the flaws. The 200-kHz array outperformed the 100-kHz array probes. The length-sizing regression for the array probes is given in Figure 7.2.

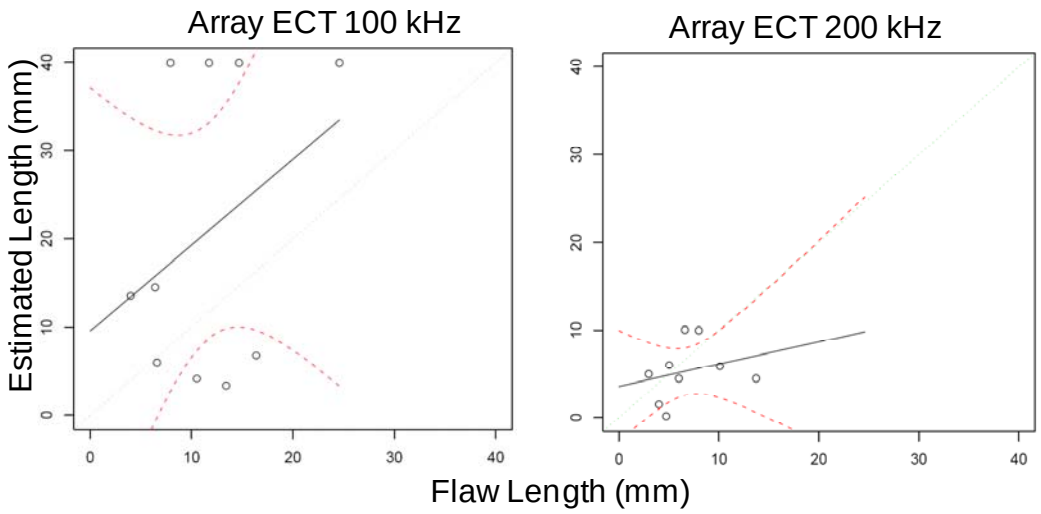

Figure 7.2. Length Sizing Results for Array Eddy-Current Probes

The length sizing results for the CCPPD technique were very good, having the lowest RMSE error and standard deviation of any of the techniques, including the cross-coil eddy-current examinations. There were not enough observations for the ICPD to perform a meaningful analysis. The length sizing results for the potential-drop techniques are presented in Figure 7.3.

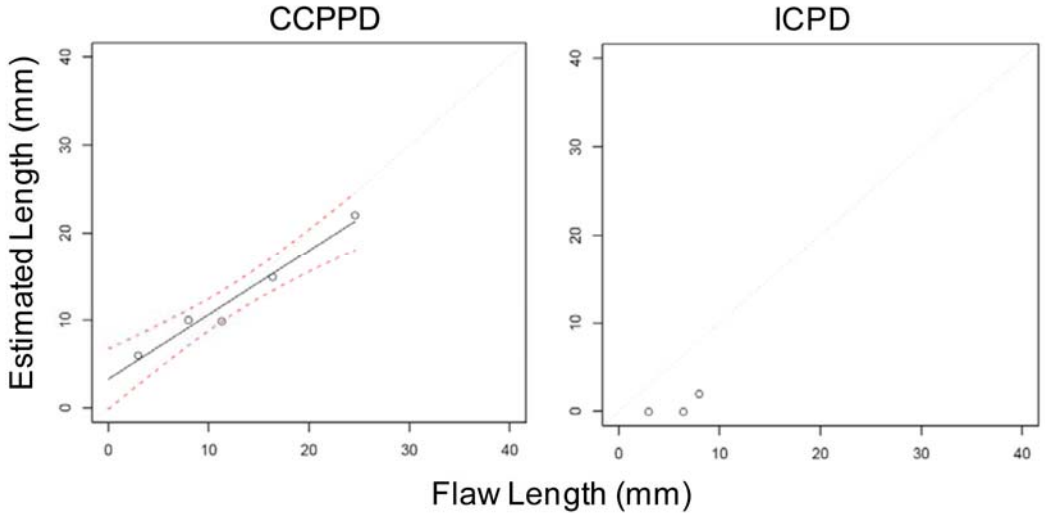

Figure 7.3. Length Sizing Results for Potential-Drop Techniques

The phased-array ultrasonic examinations were also able to accurately size the flaws in the BMI samples. The RMSE was on the order of 5 mm, which is very similar to the results for the cross-coil eddy-current examinations. The length-sizing results for the phased-array examinations are presented in Figure 7.4.

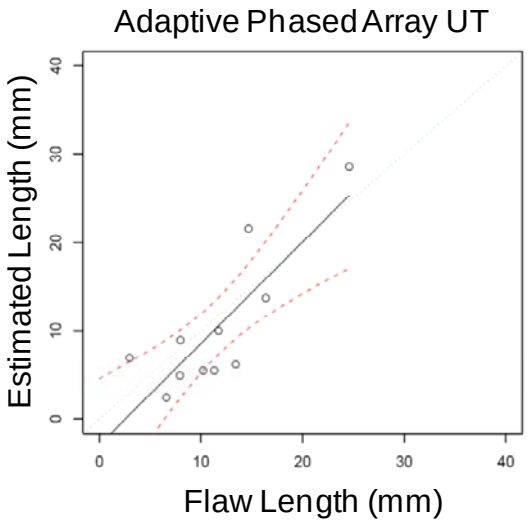

Figure 7.4. Length-Sizing Results for Adaptive Phased-Array Ultrasound Techniques

8.0 Conclusions and Recommendations

The conclusions that may be inferred from the experimental results for the bottom-mounted instrumentation tube specimens are as follows

1. **Conclusion**: Inspections using a single cross-coil eddy-current probe achieved a high POD and a low false call rate. These examinations were performed with multiple frequencies, with the highest frequency used being 300–400 kHz.
    - **Recommendation**: The results of this study suggest that single cross-coil probe eddy current using frequencies of 300–400 kHz should be the preferred method for finding surface-breaking flaws in BMI J-groove welds.

2. **Conclusion**: Inspections using adaptive phased array ultrasound were able to detect all baseline difficulty flaws and none of the challenging flaws (baseline and challenging flaws are defined in Section 4.2.2).
    - **Recommendation**: While adaptive phased array ultrasound was slightly less effective than eddy current testing, the results of this study suggest that adaptive phased array ultrasound can be effectively used to find flaws in BMI welds.

3. **Conclusion**: The inspections using array eddy-current techniques used in this BMI round robin study had a reduced POD and a much higher false call rate compared to the higher frequency cross-coil ECT examinations.
    - **Recommendation**: The results of the BMI round-robin study show that the procedures using array ECT probes operating at 100–200 kHz used in this round robin test require further development before they can be used for the detection of flaws in inservice inspection programs.

4. **Conclusion**: The closely coupled potential-drop technique was able to detect thermal fatigue flaws and SCC flaws with a POD of 50%. For weld solidification flaws, the POD was 0%. No false calls were made by the inspectors using this technique.
    - **Recommendation**: The results of the BMI round-robin study show that the closely coupled potential-drop technique requires further development before it can be used for the detection of flaws in inservice inspection programs.

5. **Conclusion**: Induced-current potential drop was used on only one baseline difficulty test block and two challenging test blocks, possibly skewing the results. There are not enough inspections on baseline difficulty test blocks to draw meaningful conclusions on the POD performance of this technique.
    - **Recommendation**: Further testing needs to be performed to determine if ICPD can be used for inservice inspection.

6. **Conclusion**: Cross-coil eddy current, adaptive phased array ultrasound, and closely coupled probe potential-drop techniques were able to accurately length-size the flaws in the J-groove welds (RMSE of 2.45–4.70 mm).
    - **Recommendation**: These techniques can be used to length-size flaws in BMI J-groove welds.

7. **Conclusion**: The test block geometry made depth-sizing using ultrasound difficult, and not enough data were collected in this round-robin test to accurately determine the effectiveness of the depth-sizing techniques.
    - **Recommendation**: More work should be performed to determine the depth-sizing capabilities of the various techniques.

9.0 References

Bamford WH, et al. 2000. *Integrity Evaluation for Future Operation: Virgil C. Summer Nuclear Plant Reactor Vessel Nozzle to Pipe Weld Regions*. WCAP-15615, Rev. 0. Westinghouse Engineering.

Bamford WH, J Foster, KR Hsu, L Tunon-Sanjur and A McIlree. 2002. "Alloy 182 Crack Growth and Its Impact on Service-Induced Cracking in PWR Plant Piping." In *10th International Conference on Environmental Degradation of Materials in Nuclear Power Systems - Water Reactors*, NACE, Houston, Texas. Paper 34.

Frye CR, ML Arey, RR Robinson and DE Whitaker. 2002. "Evaluation and Repair of Primary Water Stress Corrosion Cracking In Alloy 600/182 Control Rod Drive Mechanism Nozzles." *In Proceedings of ICONE10, 10th International Conference on Nuclear Engineering*, April 14-18, 2002, Arlington, Virginia. American Society of Mechanical Engineers, New York. Paper ICONE10-22653.

Halpin ED. 2003. *Bottom Mounted Instrumentation Penetration Indications.* STP Unit 1 Licensee Event Report (LER) 03-003, ADAMS, ML031681316, June 11, 2003.

Jenssen A, K Norrgard, G Embring, J Lagerstrom and DR Tice. 2002a. "Assessment of Cracking in Dissimilar Metal Welds." *10th International Conference on Environmental Degradation of Materials in Nuclear Power Systems - Water Reactors*. NACE, Houston, Texas. Paper 35.

Jenssen A, K Norrgard, C Jansson, J Lagerstrom, G Embring and P Efsing. 2002b. "Structural Assessment of Defected Nozzle to Safe-End Welds in Ringhals-3 and -4." *Fontevraud V International Symposium*. SFEN. Paper 43.

Lang TA. 2003. "Significant Corrosion of the Davis-Besse Nuclear Reactor Pressure Vessel Head." *ASME Pressure Vessels and Piping Conference*. July 20-24, 2003. Cleveland, Ohio.

Appendix A

Inspection Plots for Bottom-Mounted Instrumentation Samples

Appendix A

Inspection Plots for Bottom-Mounted Instrumentation Samples

Table of Contents

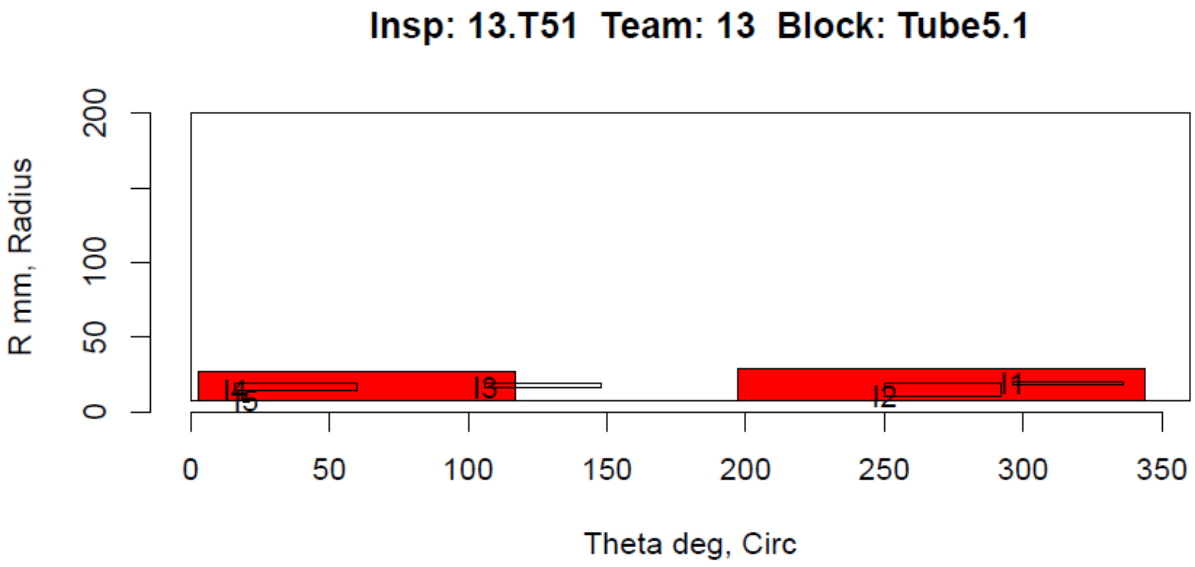
Insp: 13.T51 Team: 13 Block: Tube5.1
R mm, Radius
0
50
100
200
0
50
100
150
200
250
300
350
Theta deg, Circ
1
2
3
4
5

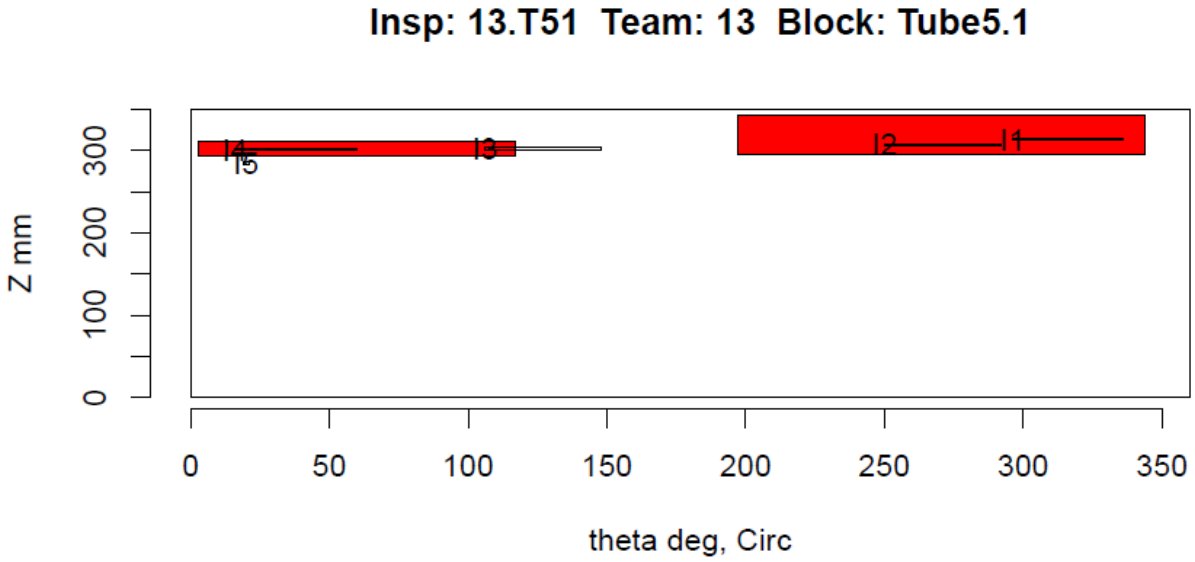
Insp: 13.T51 Team: 13 Block: Tube5.1
Z mm
0
100
200
300
0
50
100
150
200
250
300
350
theta deg, Circ
1
2
3
4
5

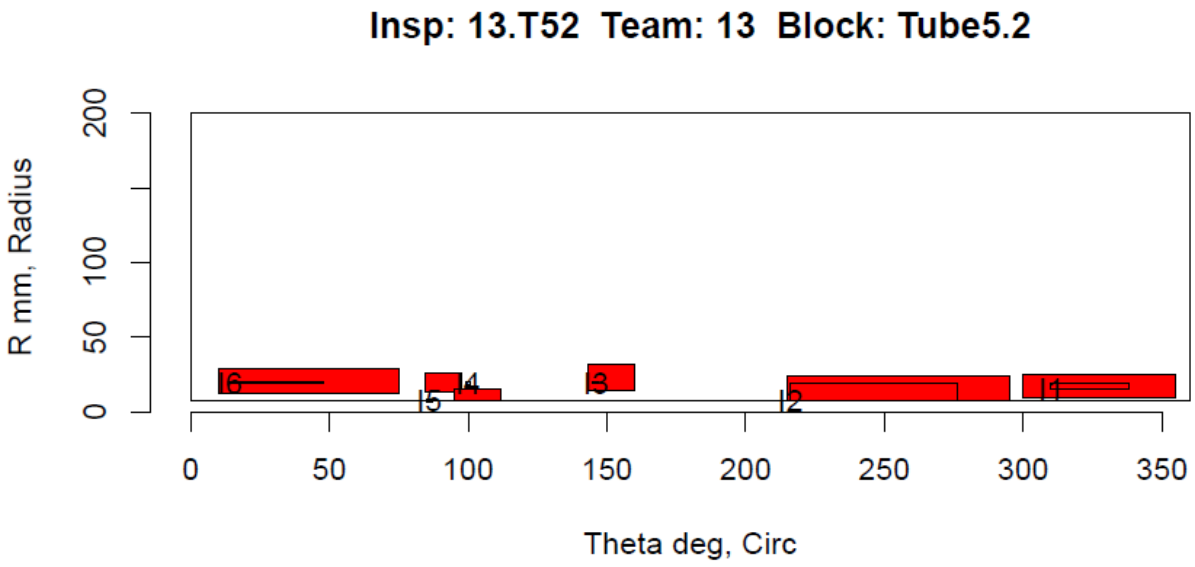
Insp: 13.T52 Team: 13 Block: Tube5.2
R mm, Radius
0
50
100
200
0
50
100
150
200
250
300
350
Theta deg, Circ
6
5
4
3
2
1

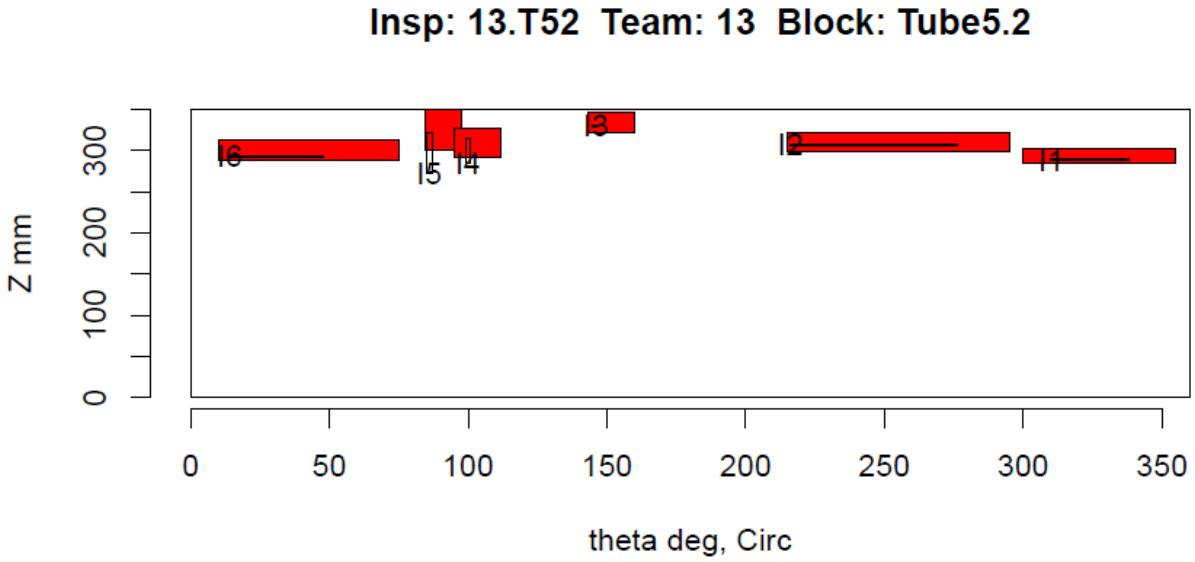
Insp: 13.T52 Team: 13 Block: Tube5.2
Z mm
0
100
200
300
0
50
100
150
200
250
300
350
theta deg, Circ
6
5
4
3
2
1

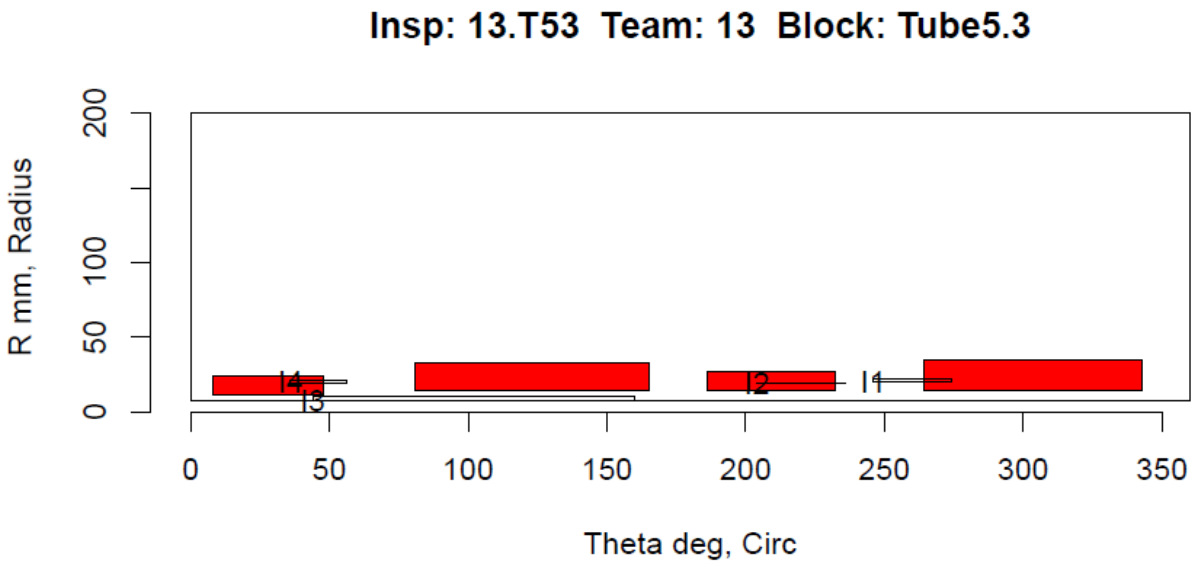
Insp: 13.T53 Team: 13 Block: Tube5.3
R mm, Radius
0
50
100
200
I4
I3
I2
I1
0
50
100
150
200
250
300
350
Theta deg, Circ

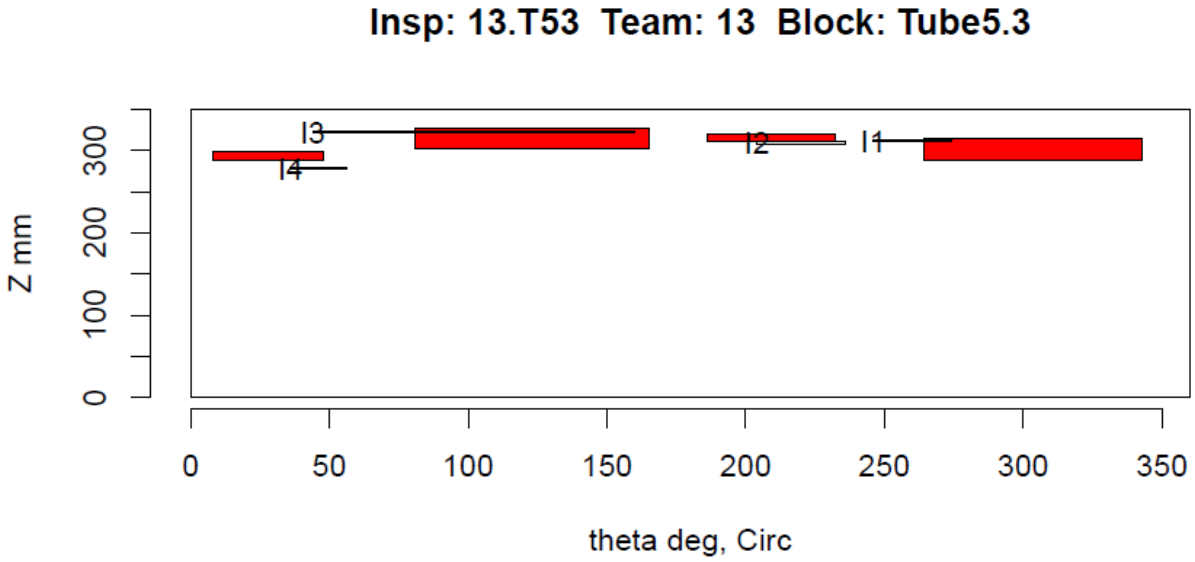
Insp: 13.T53 Team: 13 Block: Tube5.3
Z mm
0
100
200
300
I3
I4
I2
I1
0
50
100
150
200
250
300
350
theta deg, Circ

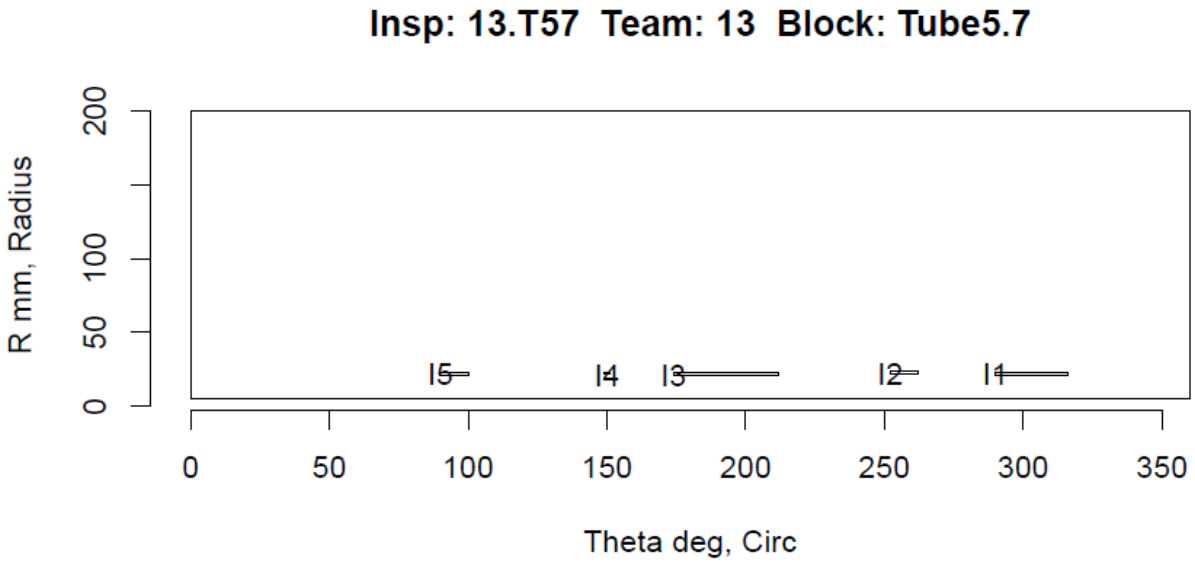
Insp: 13.T57 Team: 13 Block: Tube5.7
R mm, Radius
0
50
100
200
0
50
100
150
200
250
300
350
Theta deg, Circ
5
4
3
2
1

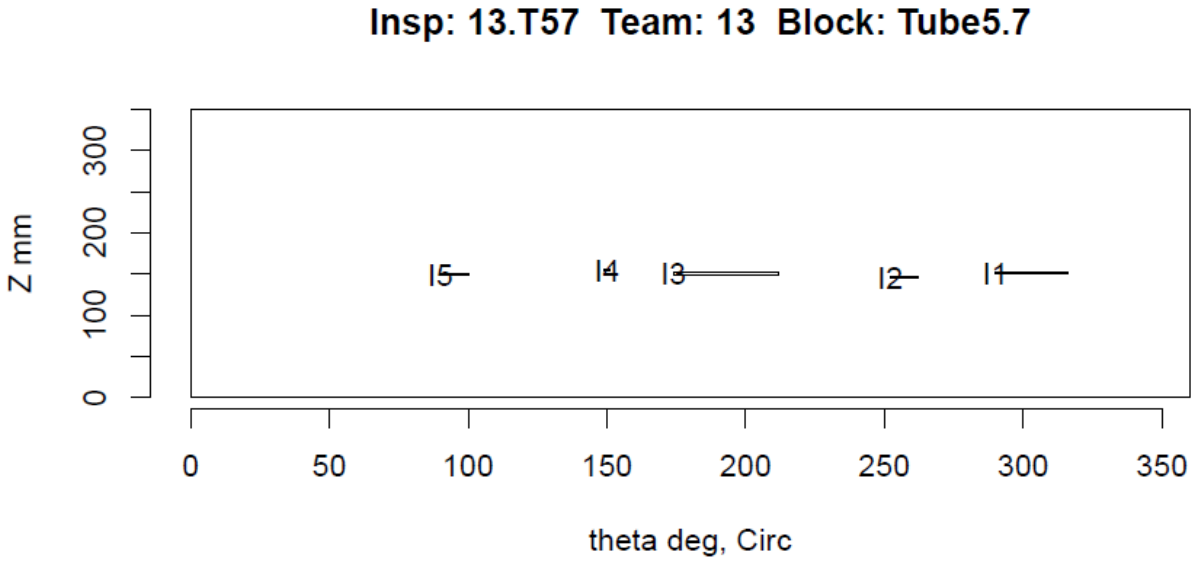
Insp: 13.T57 Team: 13 Block: Tube5.7
Z mm
0
100
200
300
0
50
100
150
200
250
300
350
theta deg, Circ
5
4
3
2
1

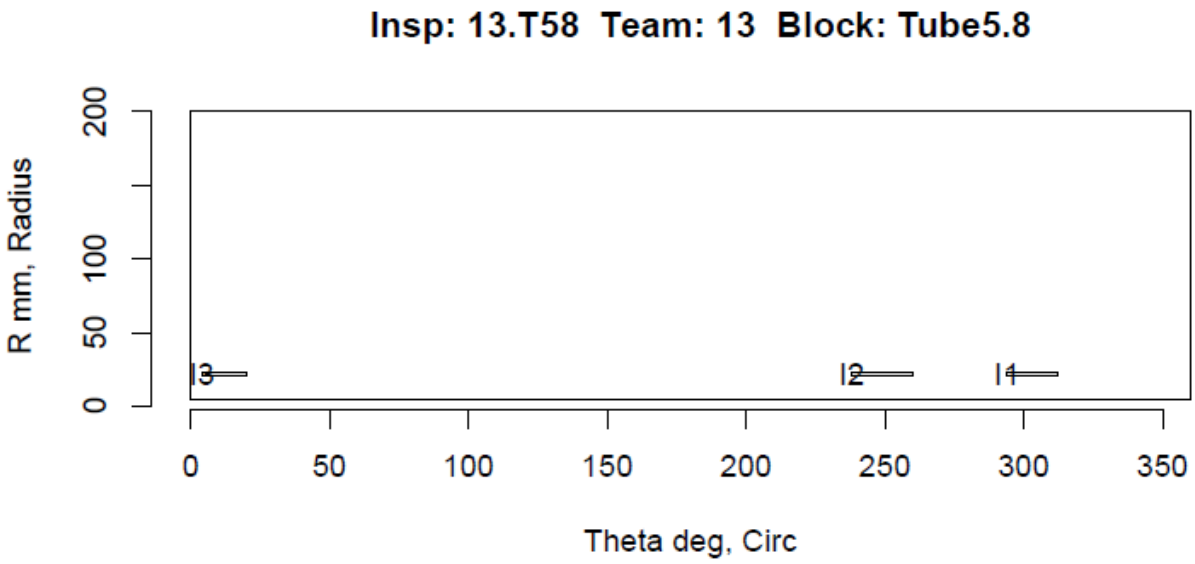
Insp: 13.T58 Team: 13 Block: Tube5.8
R mm, Radius
0
50
100
200
3
2
1
0
50
100
150
200
250
300
350
Theta deg, Circ

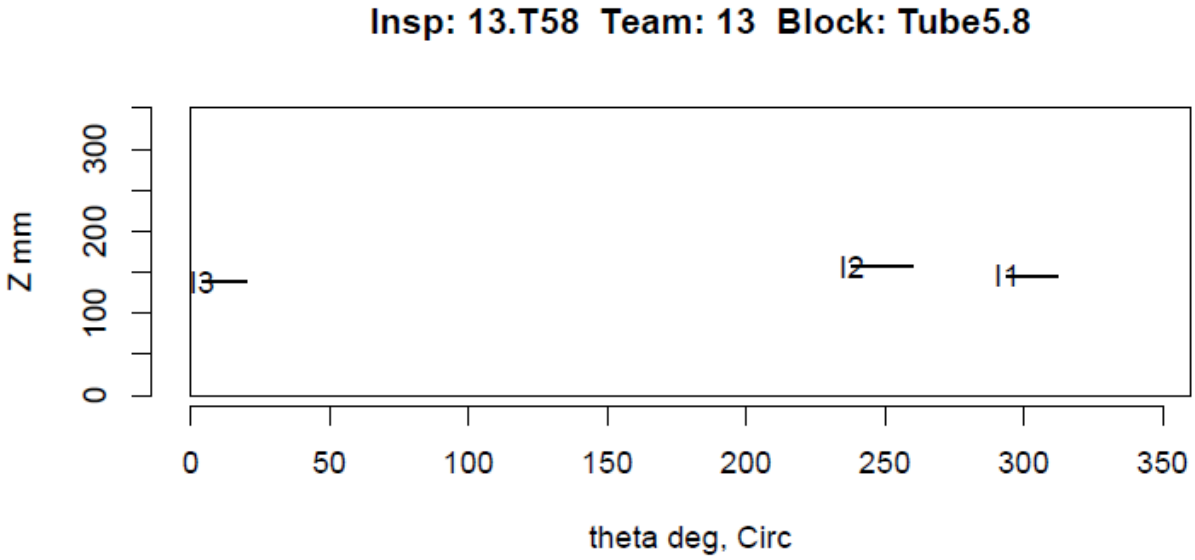
Insp: 13.T58 Team: 13 Block: Tube5.8
Z mm
0
100
200
300
3
2
1
0
50
100
150
200
250
300
350
theta deg, Circ

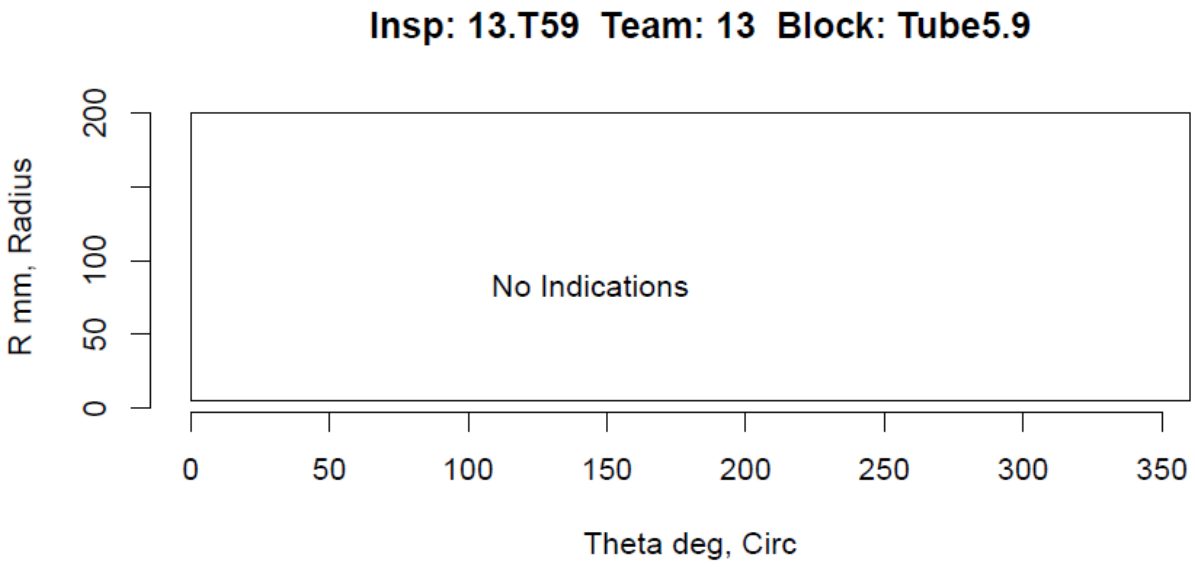
Insp: 13.T59 Team: 13 Block: Tube5.9
R mm, Radius
0
50
100
200
No Indications
0
50
100
150
200
250
300
350
Theta deg, Circ

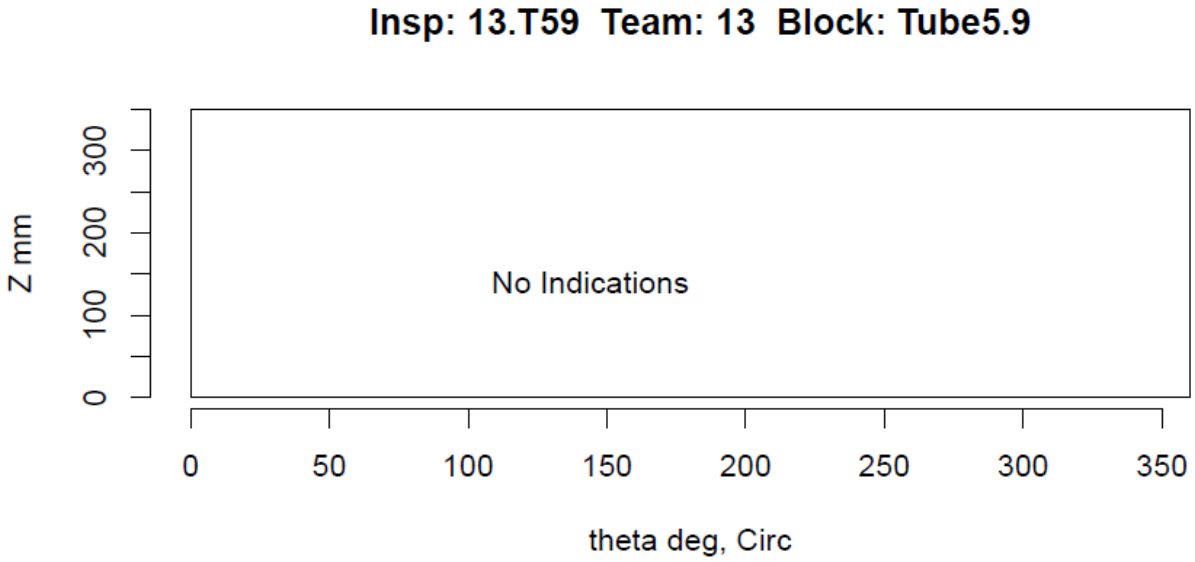
Insp: 13.T59 Team: 13 Block: Tube5.9
Z mm
0
100
200
300
No Indications
0
50
100
150
200
250
300
350
theta deg, Circ

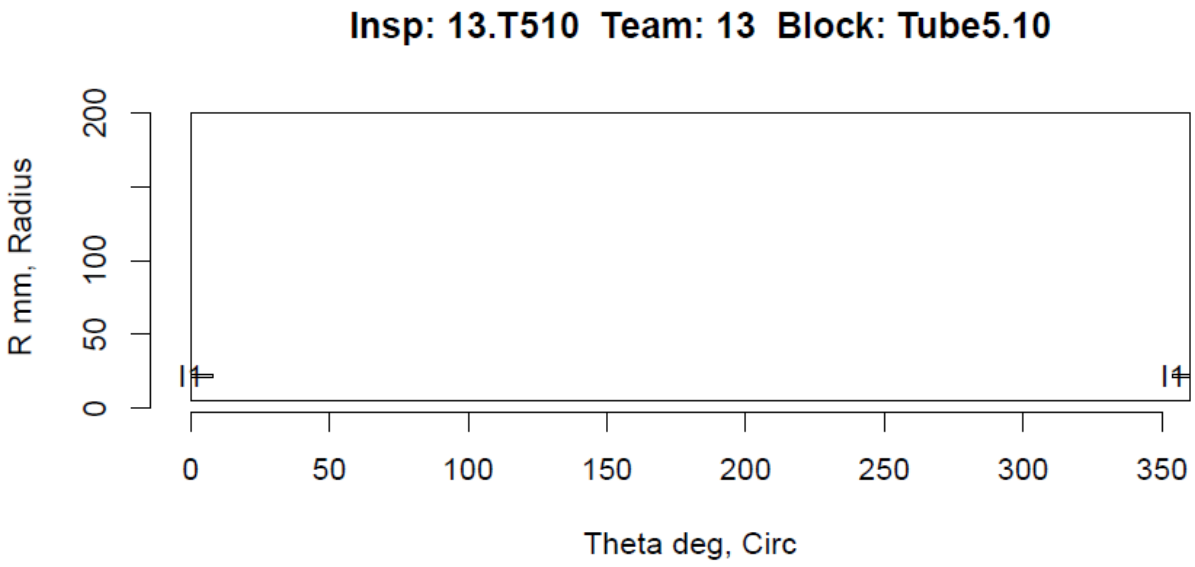
Insp: 13.T510 Team: 13 Block: Tube5.10
R mm, Radius
0
50
100
200
0
50
100
150
200
250
300
350
Theta deg, Circ

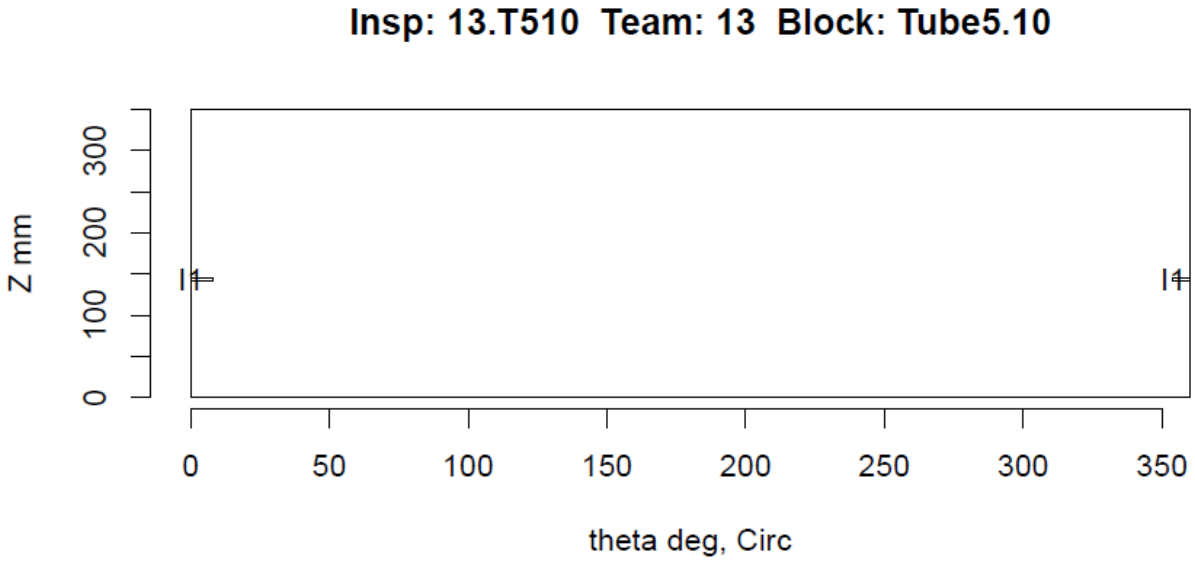
Insp: 13.T510 Team: 13 Block: Tube5.10
Z mm
0
100
200
300
0
50
100
150
200
250
300
350
theta deg, Circ

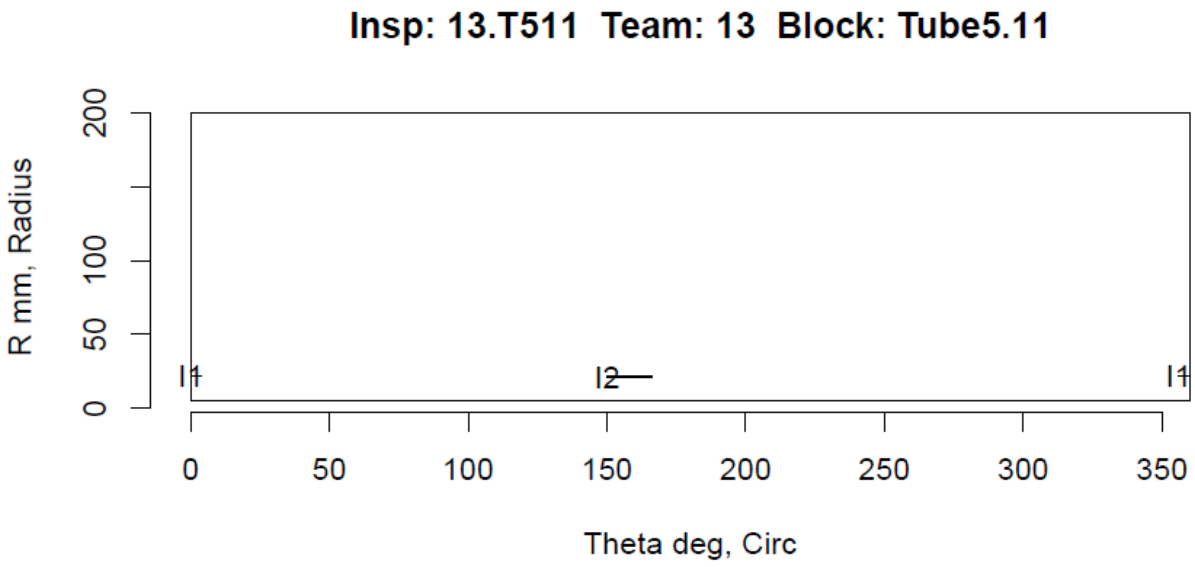
Insp: 13.T511 Team: 13 Block: Tube5.11
R mm, Radius
0
50
100
200
I1
I2
I1
0
50
100
150
200
250
300
350
Theta deg, Circ

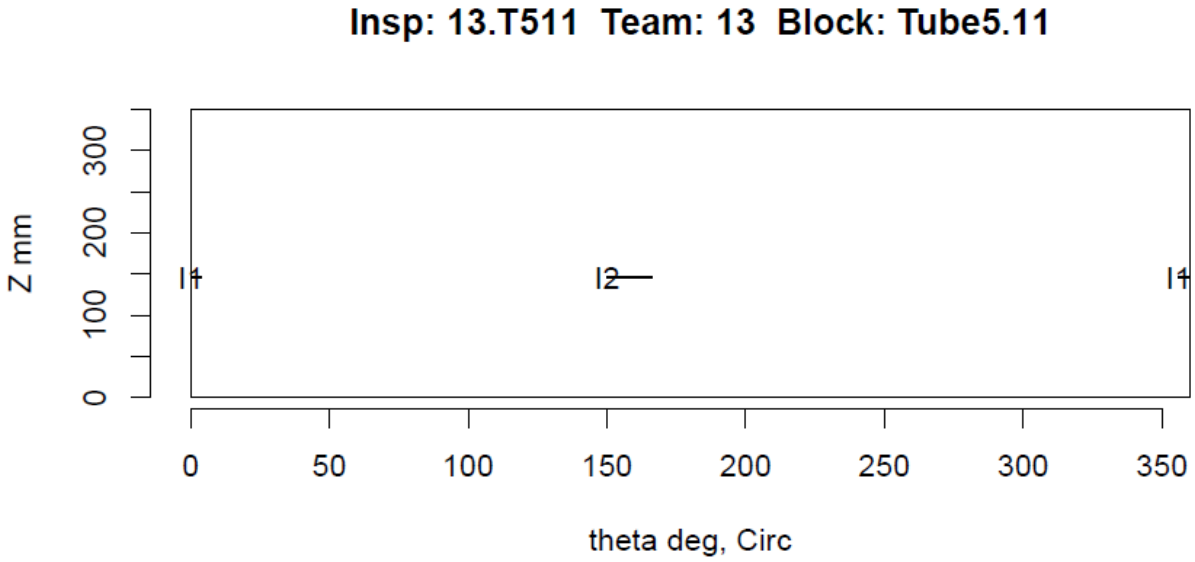
Insp: 13.T511 Team: 13 Block: Tube5.11
Z mm
0
100
200
300
I1
I2
I1
0
50
100
150
200
250
300
350
theta deg, Circ

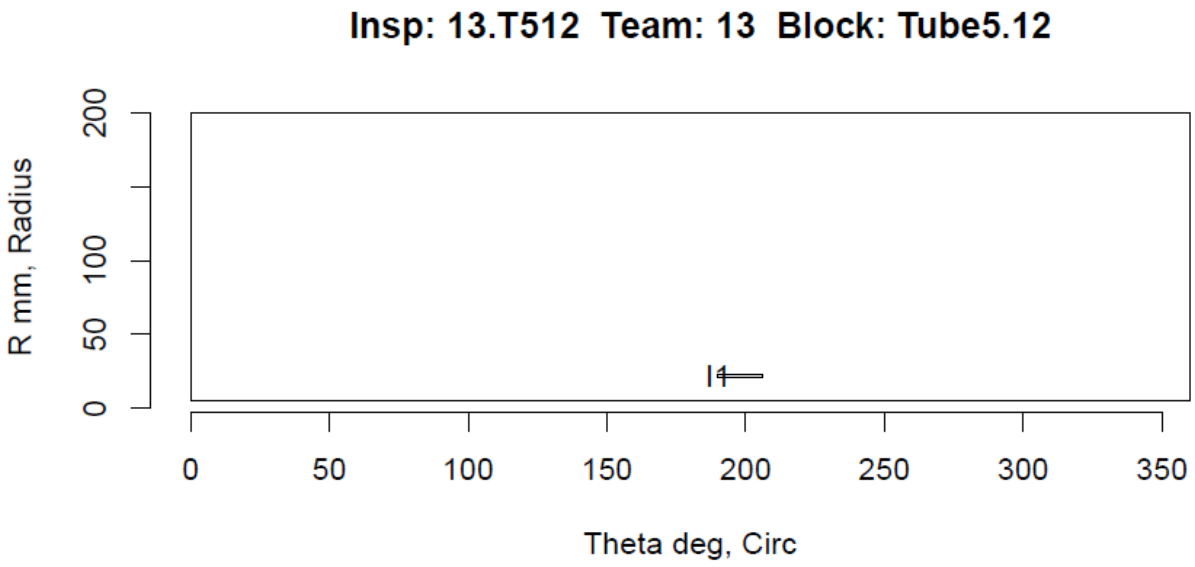
Insp: 13.T512 Team: 13 Block: Tube5.12
R mm, Radius
0
50
100
200
0
50
100
150
200
250
300
350
Theta deg, Circ

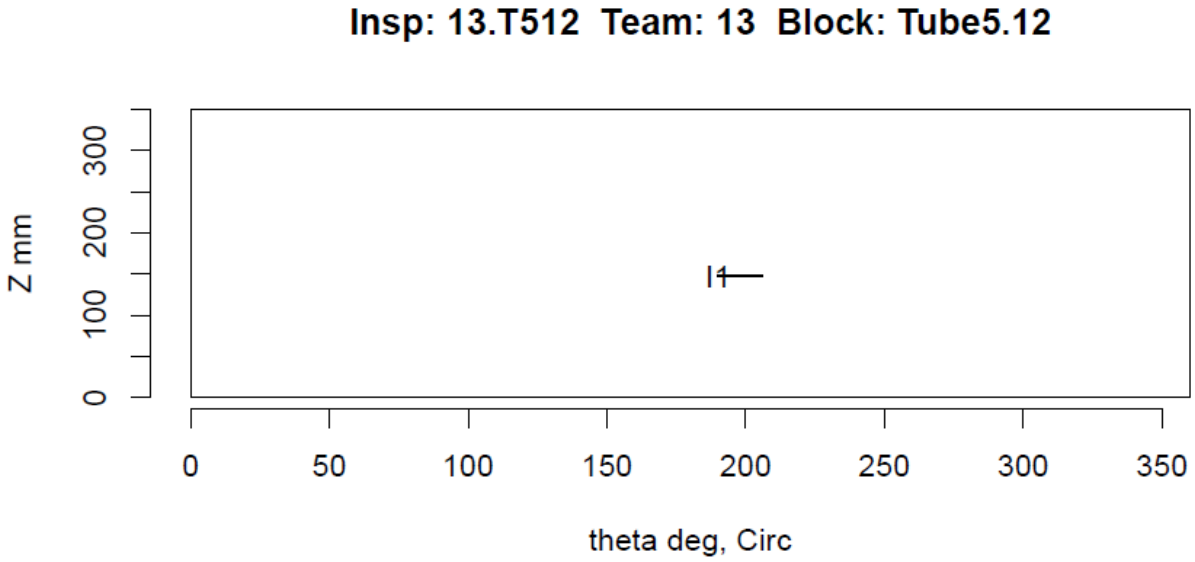
Insp: 13.T512 Team: 13 Block: Tube5.12
Z mm
0
100
200
300
0
50
100
150
200
250
300
350
theta deg, Circ

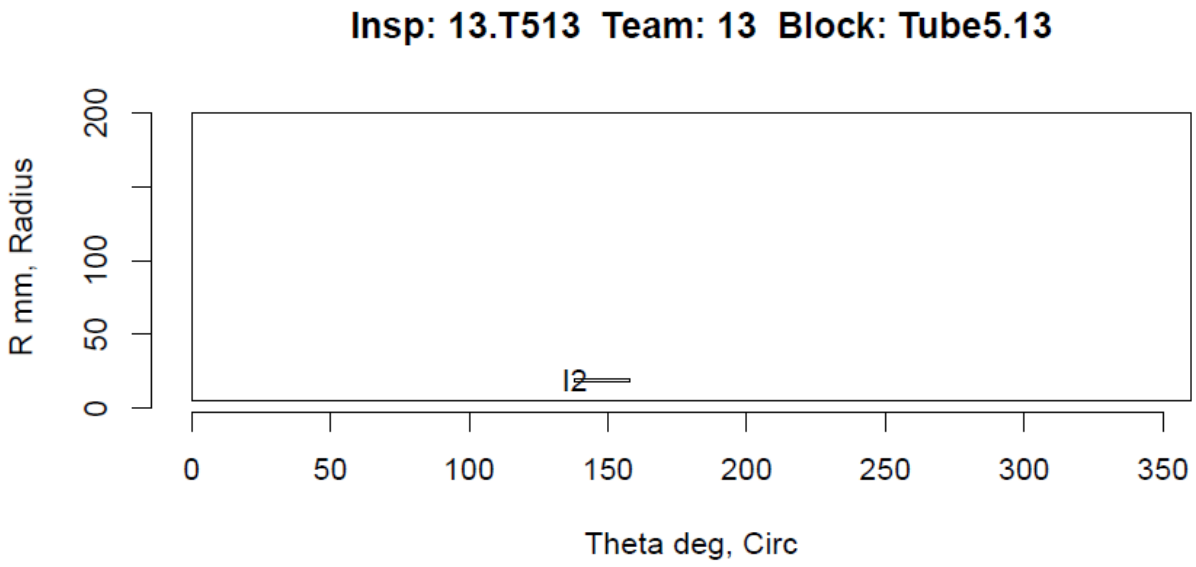
Insp: 13.T513 Team: 13 Block: Tube5.13
R mm, Radius
0
50
100
200
I2
0
50
100
150
200
250
300
350
Theta deg, Circ

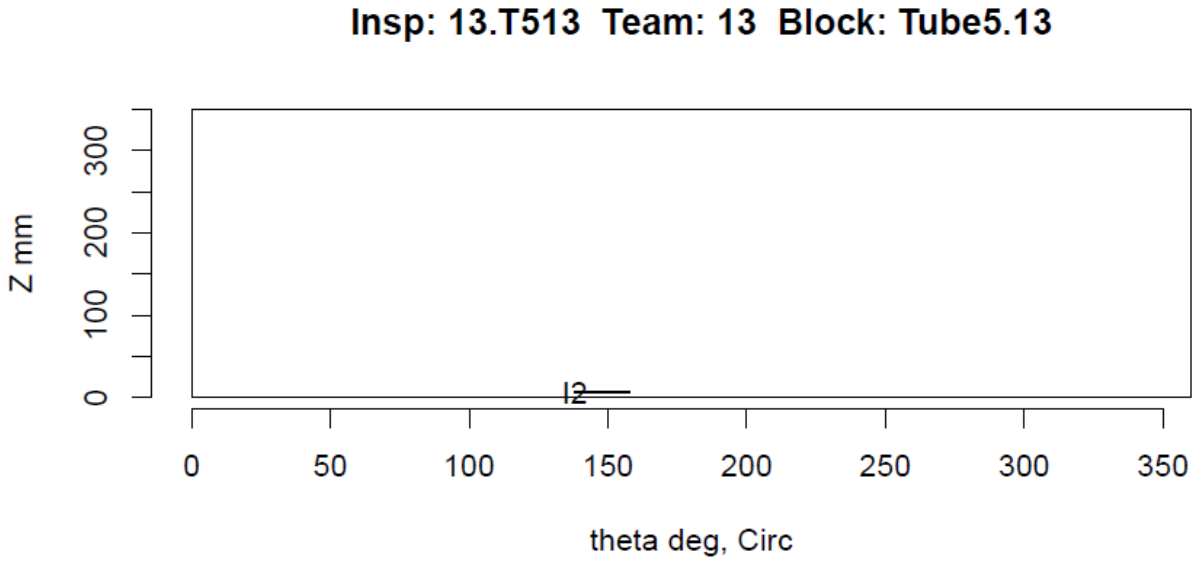
Insp: 13.T513 Team: 13 Block: Tube5.13
Z mm
0
100
200
300
I2
0
50
100
150
200
250
300
350
theta deg, Circ

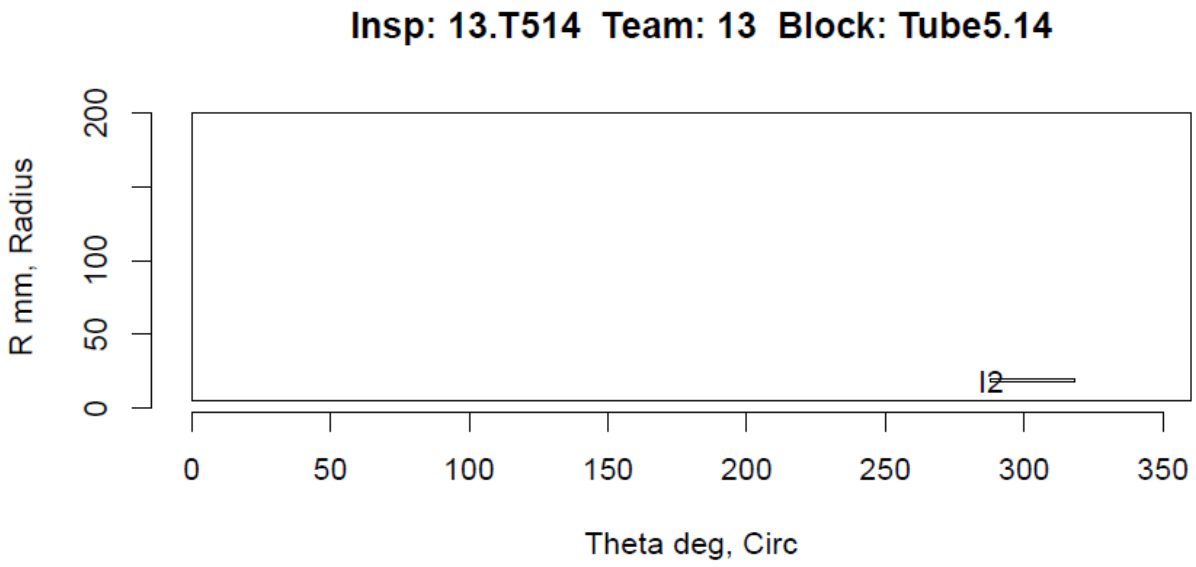
Insp: 13.T514 Team: 13 Block: Tube5.14
R mm, Radius
0
50
100
200
I2
0
50
100
150
200
250
300
350
Theta deg, Circ

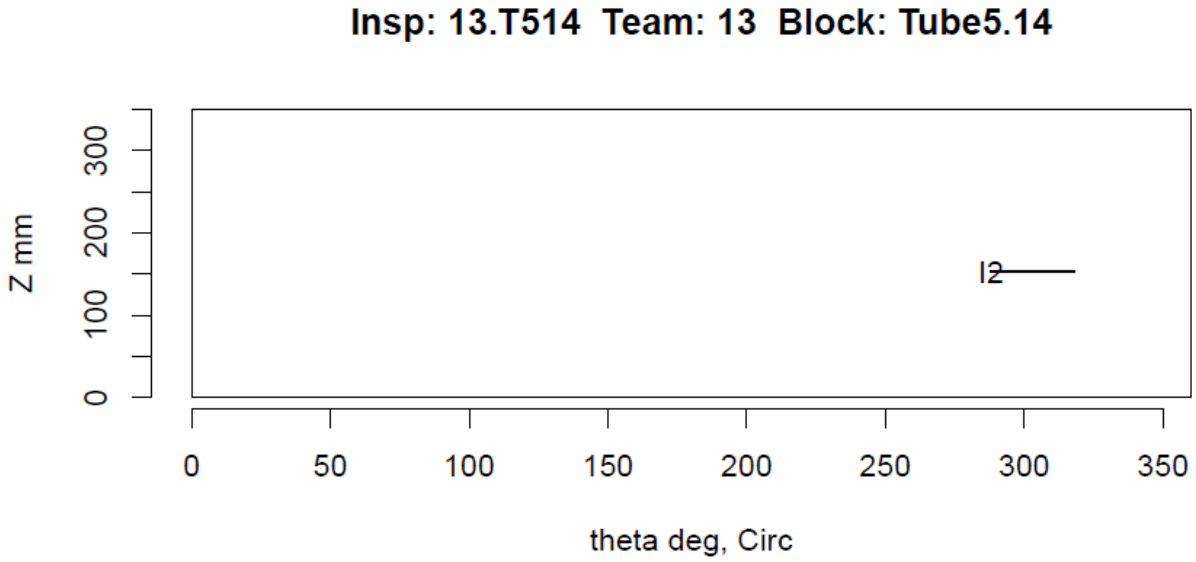
Insp: 13.T514 Team: 13 Block: Tube5.14
Z mm
0
100
200
300
I2
0
50
100
150
200
250
300
350
theta deg, Circ

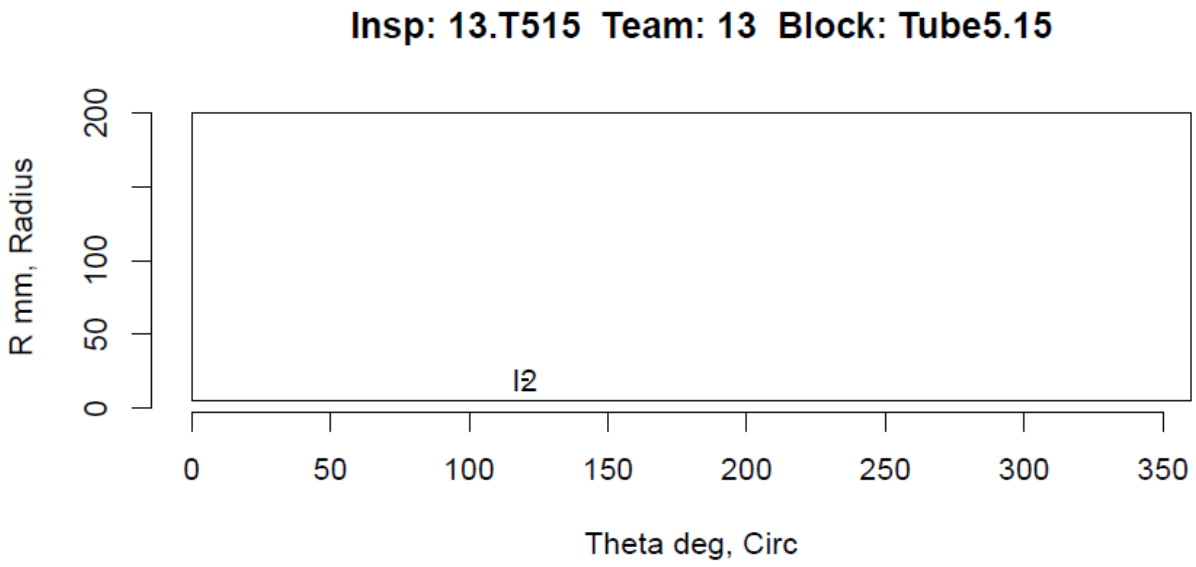
Insp: 13.T515 Team: 13 Block: Tube5.15
R mm, Radius
0
50
100
200
0
50
100
150
200
250
300
350
Theta deg, Circ

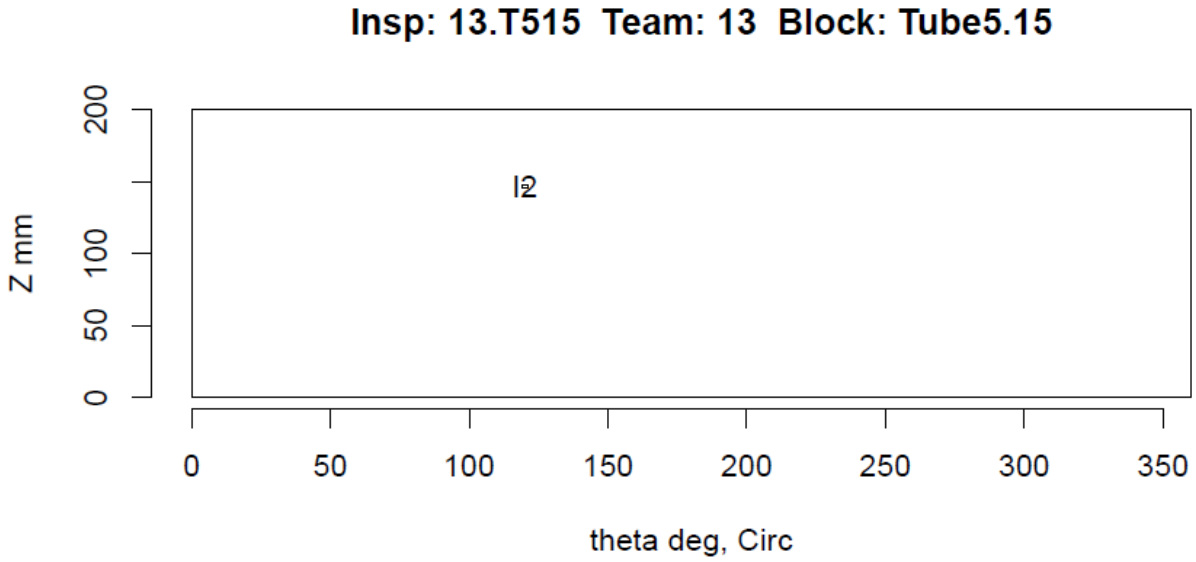
Insp: 13.T515 Team: 13 Block: Tube5.15
Z mm
0
50
100
200
0
50
100
150
200
250
300
350
theta deg, Circ

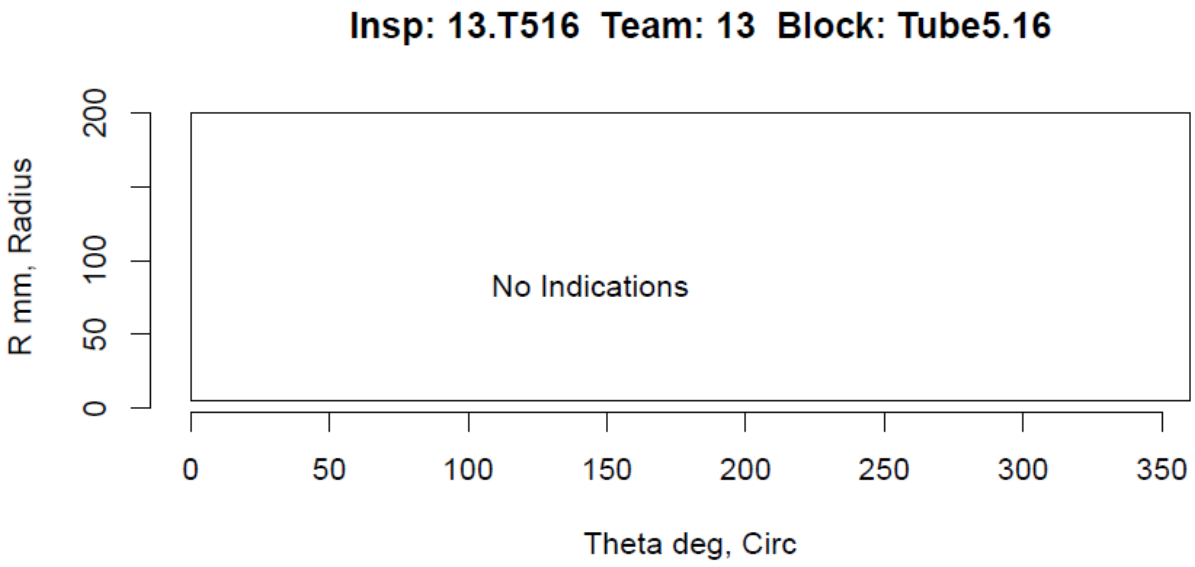
Insp: 13.T516 Team: 13 Block: Tube5.16
R mm, Radius
0
50
100
200
No Indications
0
50
100
150
200
250
300
350
Theta deg, Circ

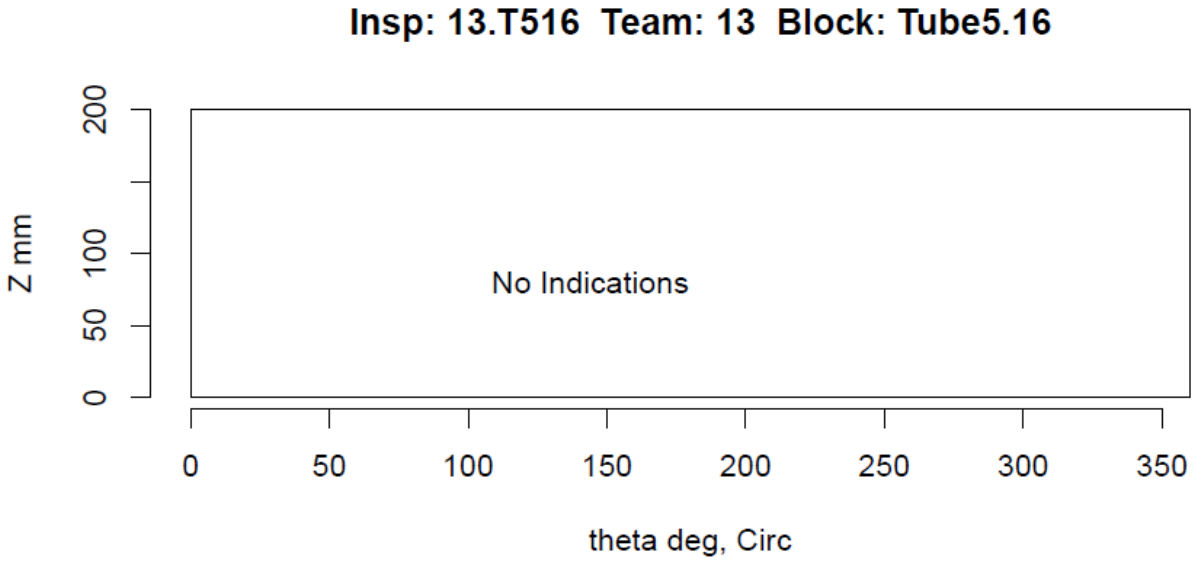
Insp: 13.T516 Team: 13 Block: Tube5.16
Z mm
0
50
100
200
No Indications
0
50
100
150
200
250
300
350
theta deg, Circ

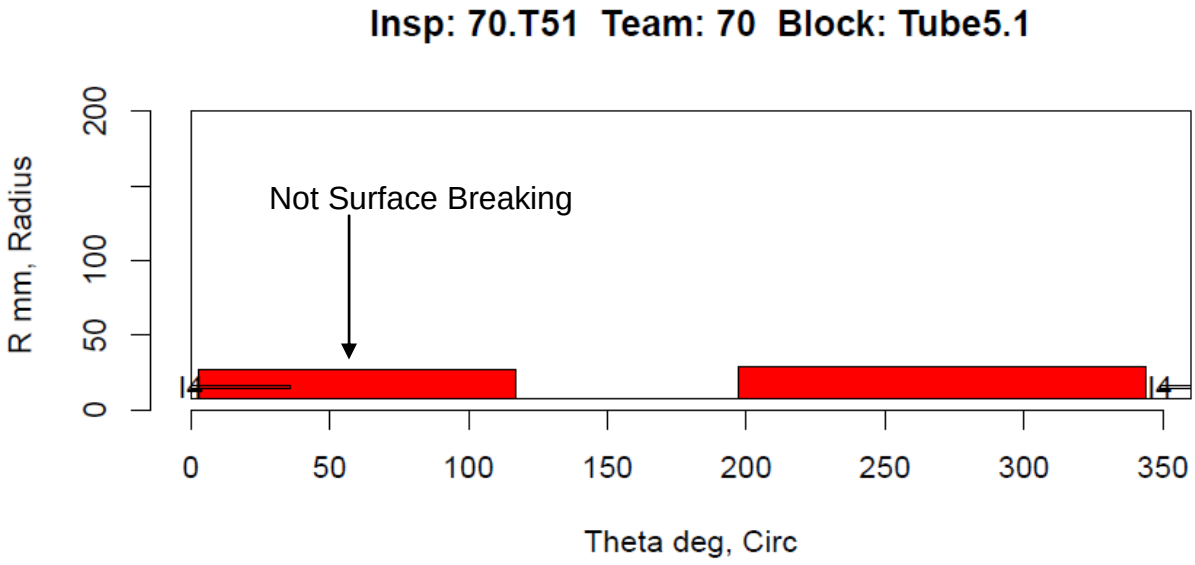
Insp: 70.T51 Team: 70 Block: Tube5.1
R mm, Radius
0
50
100
200
Not Surface Breaking
I4
I4
0
50
100
150
200
250
300
350
Theta deg, Circ

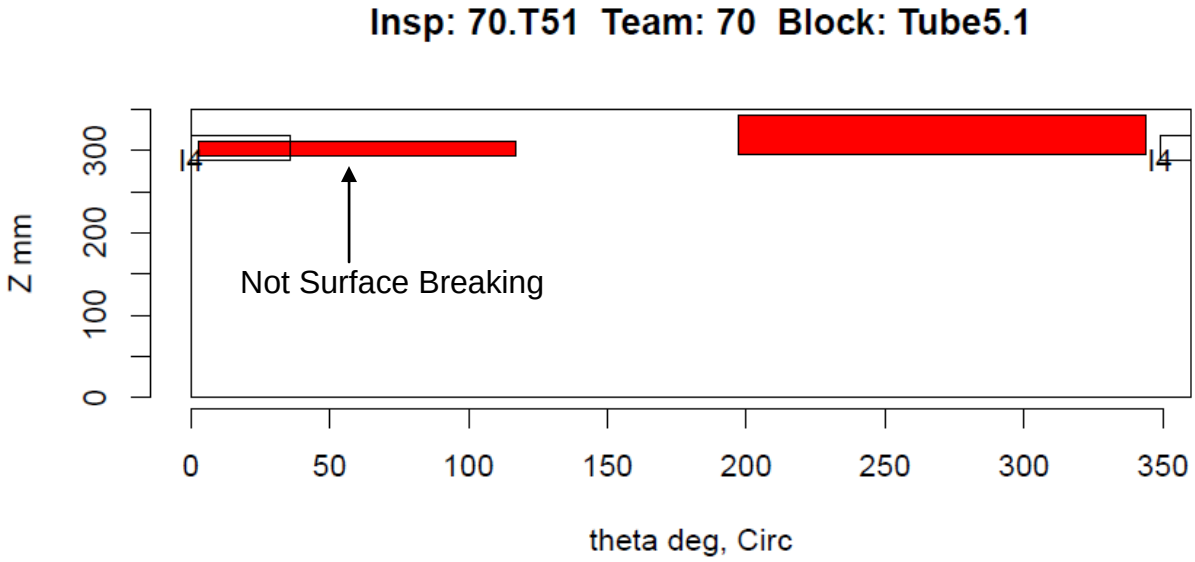
Insp: 70.T51 Team: 70 Block: Tube5.1
Z mm
0
100
200
300
I4
I4
Not Surface Breaking
0
50
100
150
200
250
300
350
theta deg, Circ

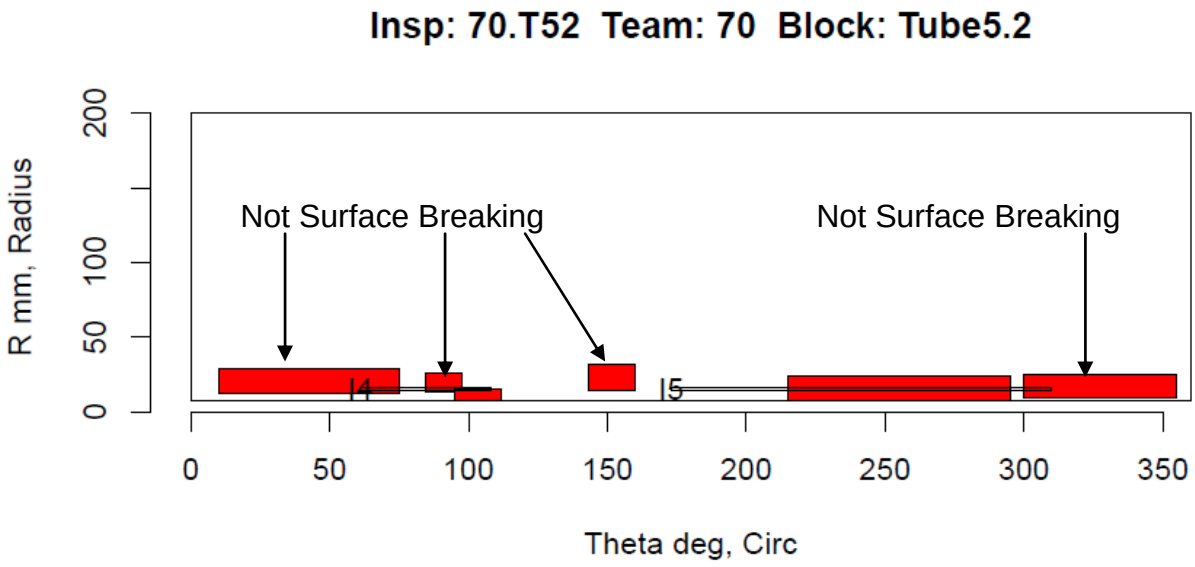
Insp: 70.T52 Team: 70 Block: Tube5.2
R mm, Radius
0
50
100
200
Not Surface Breaking
Not Surface Breaking
I4
I5
0
50
100
150
200
250
300
350
Theta deg, Circ

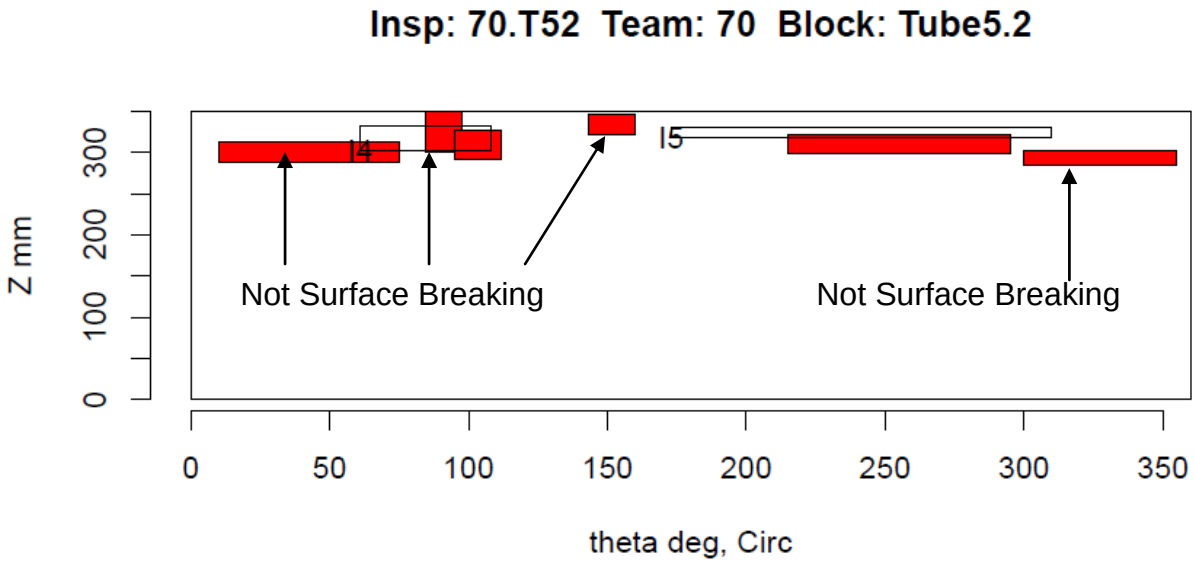
Insp: 70.T52 Team: 70 Block: Tube5.2
Z mm
0
100
200
300
I4
I5
Not Surface Breaking
Not Surface Breaking
0
50
100
150
200
250
300
350
theta deg, Circ

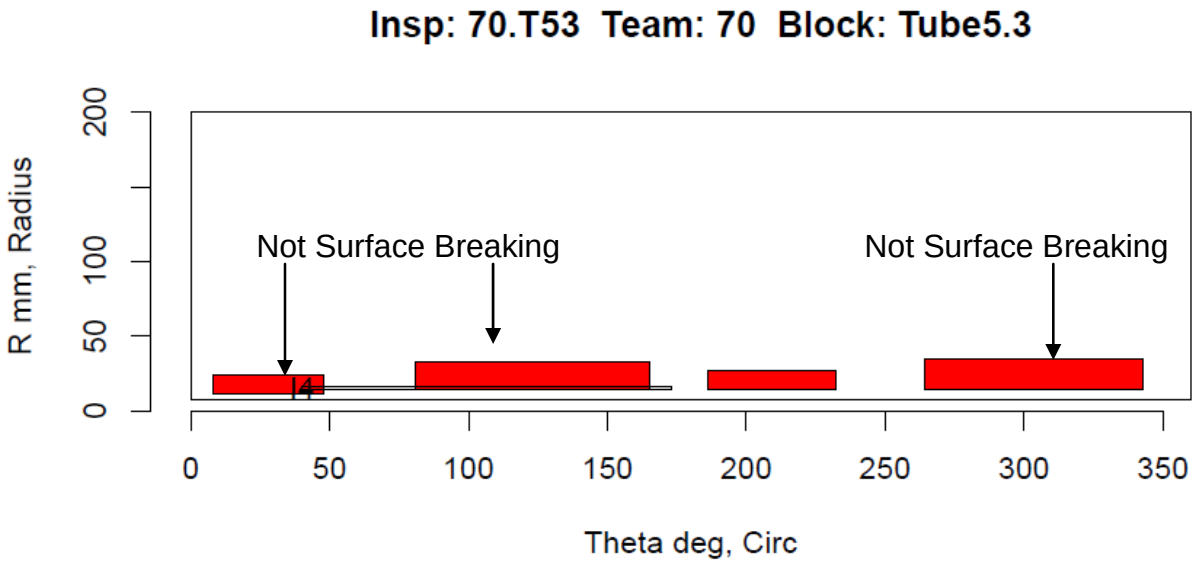
Insp: 70.T53 Team: 70 Block: Tube5.3
R mm, Radius
0
50
100
200
Not Surface Breaking
Not Surface Breaking
0
50
100
150
200
250
300
350
Theta deg, Circ

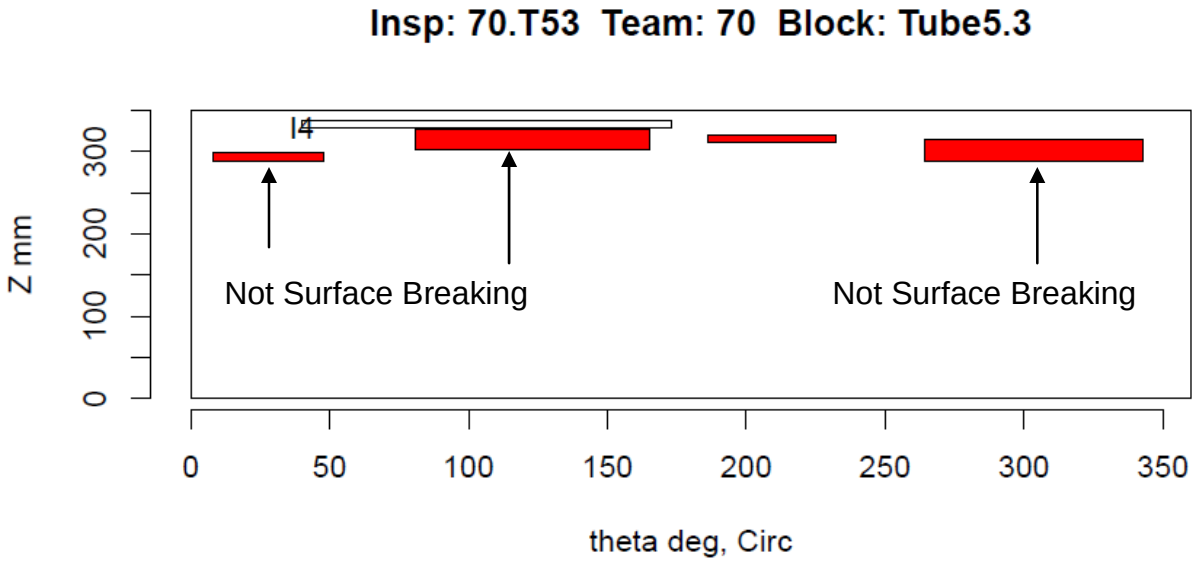
Insp: 70.T53 Team: 70 Block: Tube5.3
Z mm
0
100
200
300
Not Surface Breaking
Not Surface Breaking
0
50
100
150
200
250
300
350
theta deg, Circ

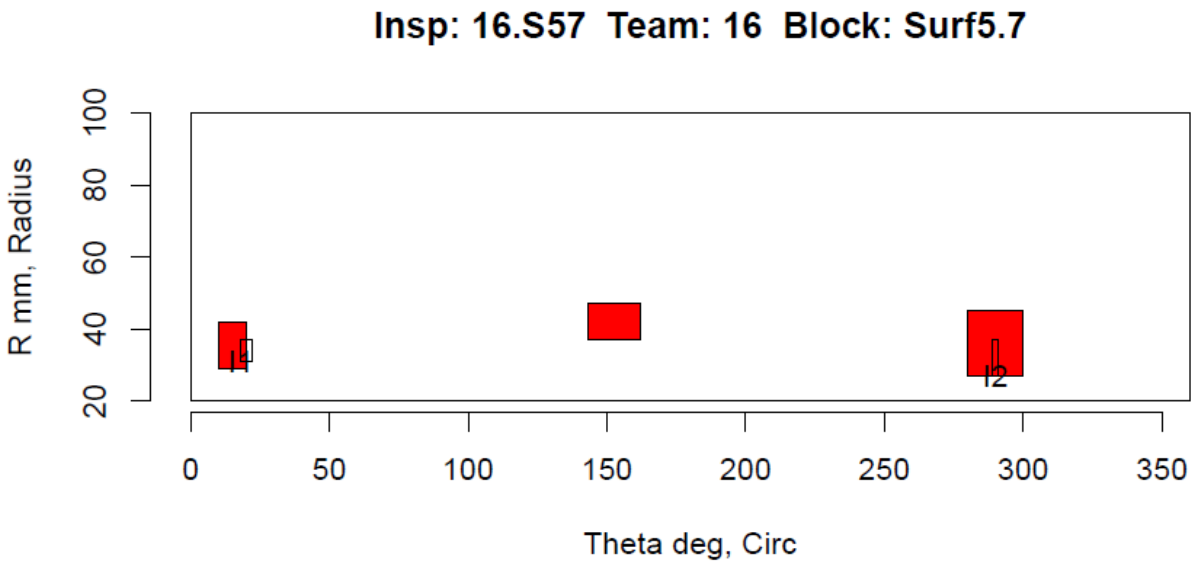
Insp: 16.S57 Team: 16 Block: Surf5.7
R mm, Radius
20
40
60
80
100
0
50
100
150
200
250
300
350
Theta deg, Circ

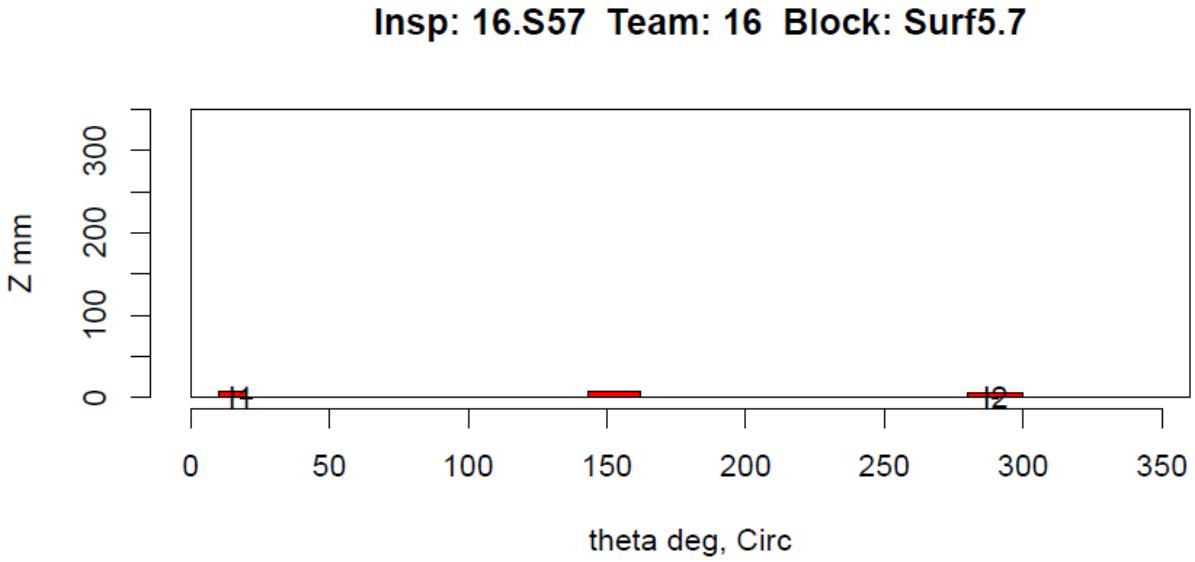
Insp: 16.S57 Team: 16 Block: Surf5.7
Z mm
0
100
200
300
0
50
100
150
200
250
300
350
theta deg, Circ

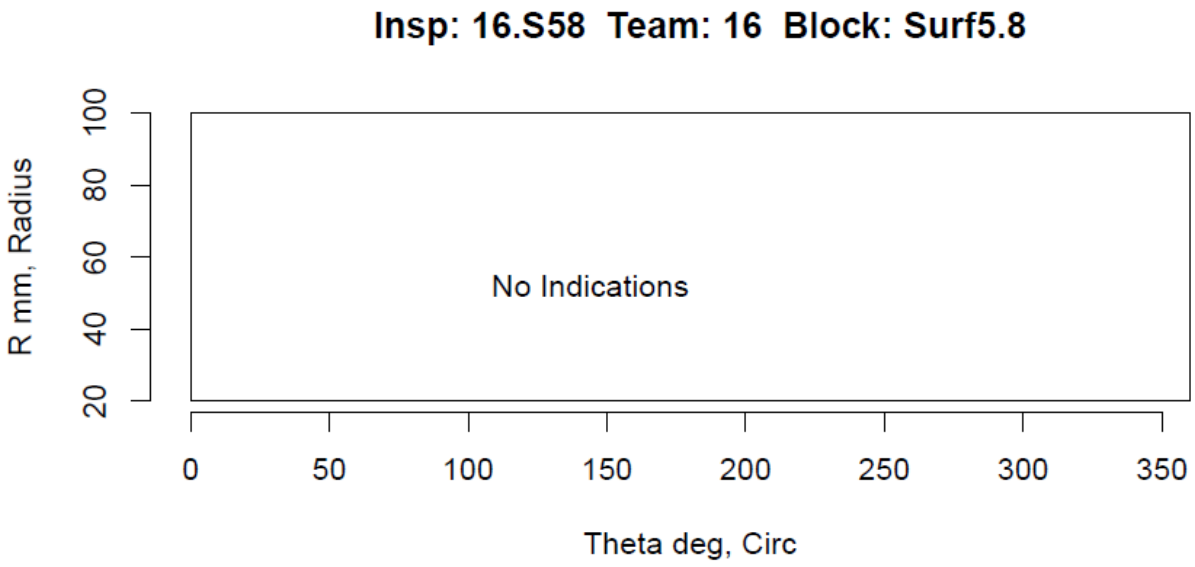
Insp: 16.S58 Team: 16 Block: Surf5.8
R mm, Radius
20
40
60
80
100
No Indications
0
50
100
150
200
250
300
350
Theta deg, Circ

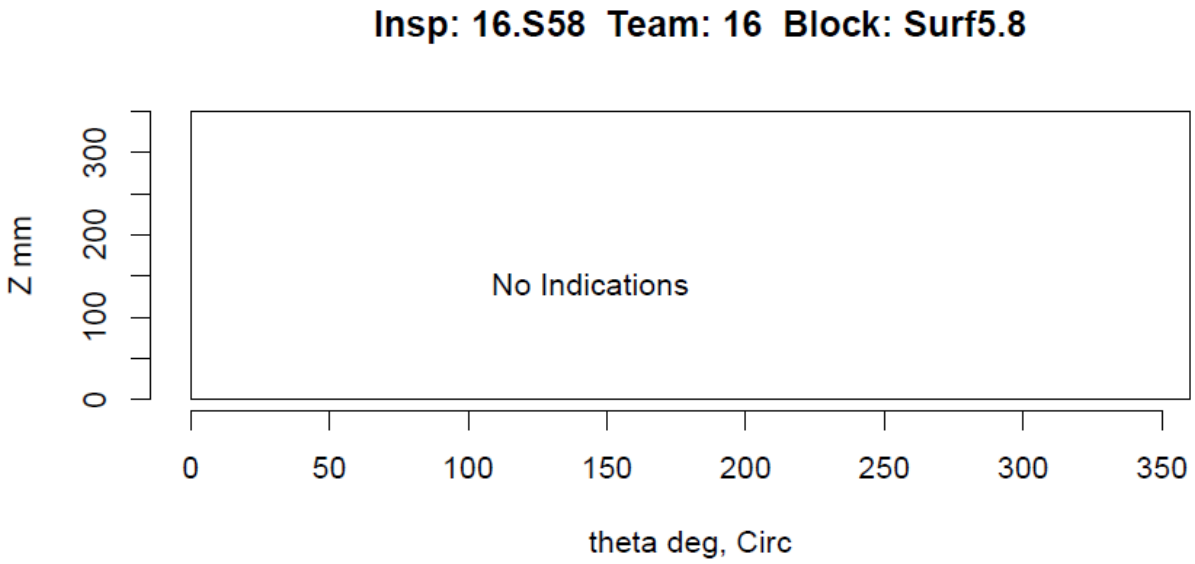
Insp: 16.S58 Team: 16 Block: Surf5.8
Z mm
0
100
200
300
No Indications
0
50
100
150
200
250
300
350
theta deg, Circ

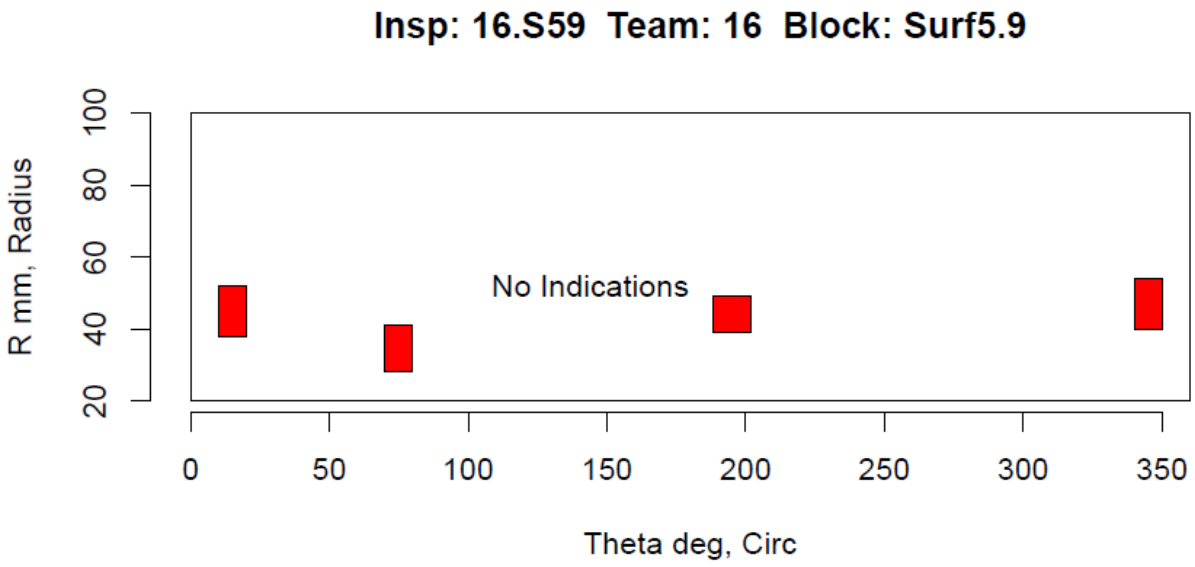
Insp: 16.S59 Team: 16 Block: Surf5.9
R mm, Radius
20
40
60
80
100
No Indications
0
50
100
150
200
250
300
350
Theta deg, Circ

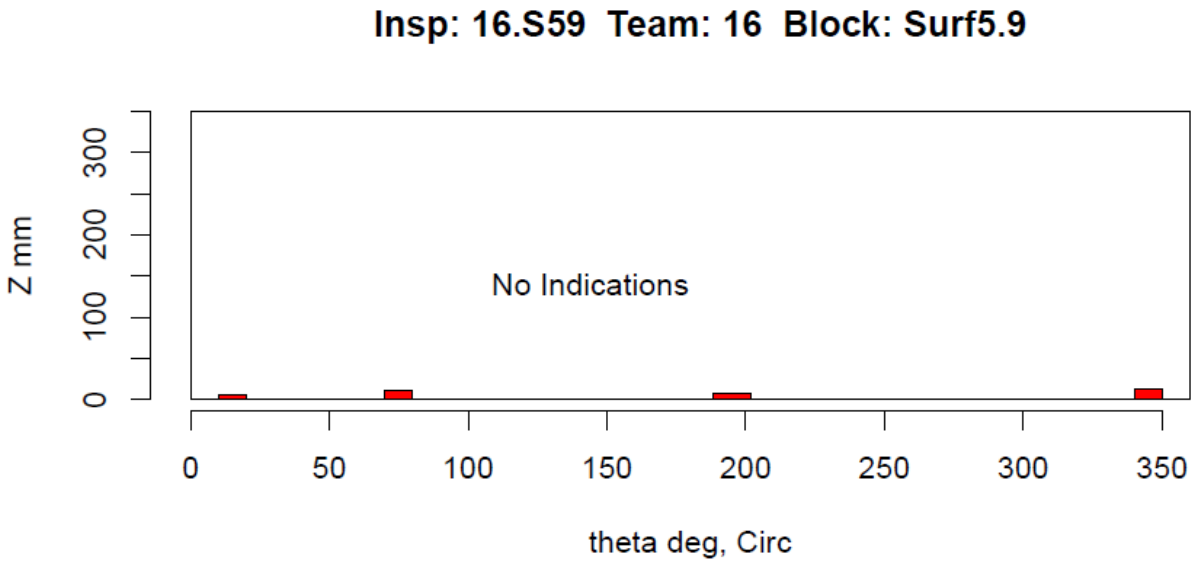
Insp: 16.S59 Team: 16 Block: Surf5.9
Z mm
0
100
200
300
No Indications
0
50
100
150
200
250
300
350
theta deg, Circ

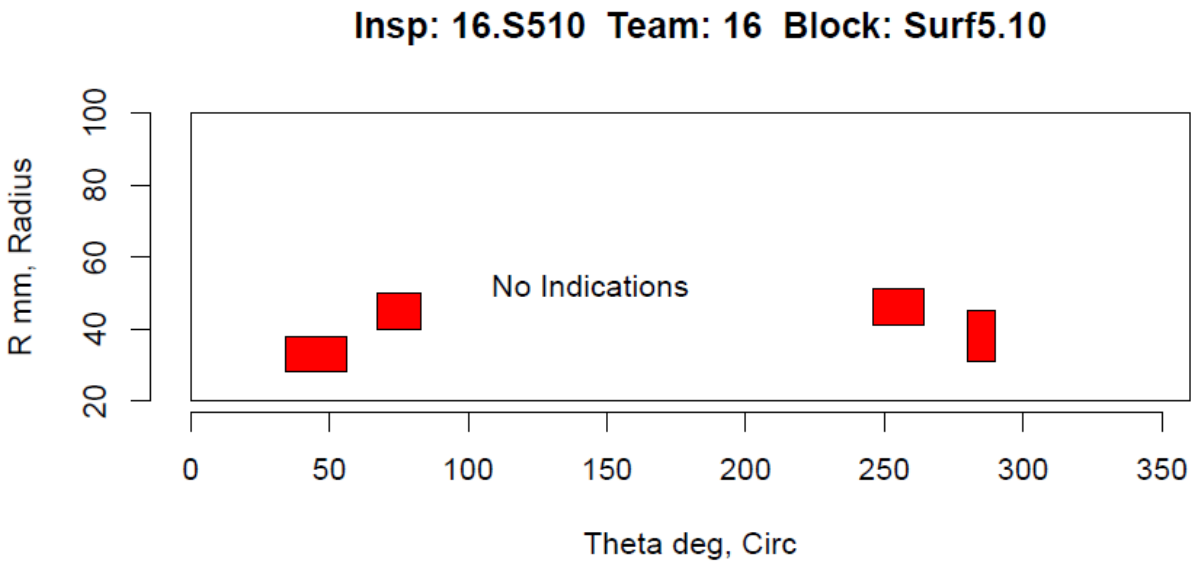
Insp: 16.S510 Team: 16 Block: Surf5.10
R mm, Radius
20
40
60
80
100
No Indications
0
50
100
150
200
250
300
350
Theta deg, Circ

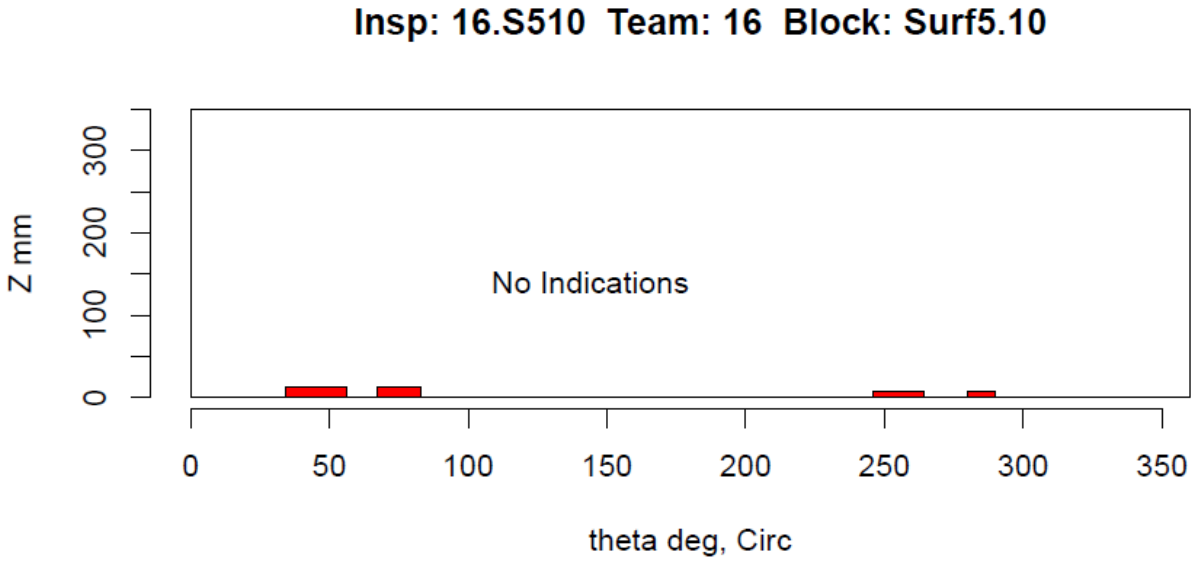
Insp: 16.S510 Team: 16 Block: Surf5.10
Z mm
0
100
200
300
No Indications
0
50
100
150
200
250
300
350
theta deg, Circ

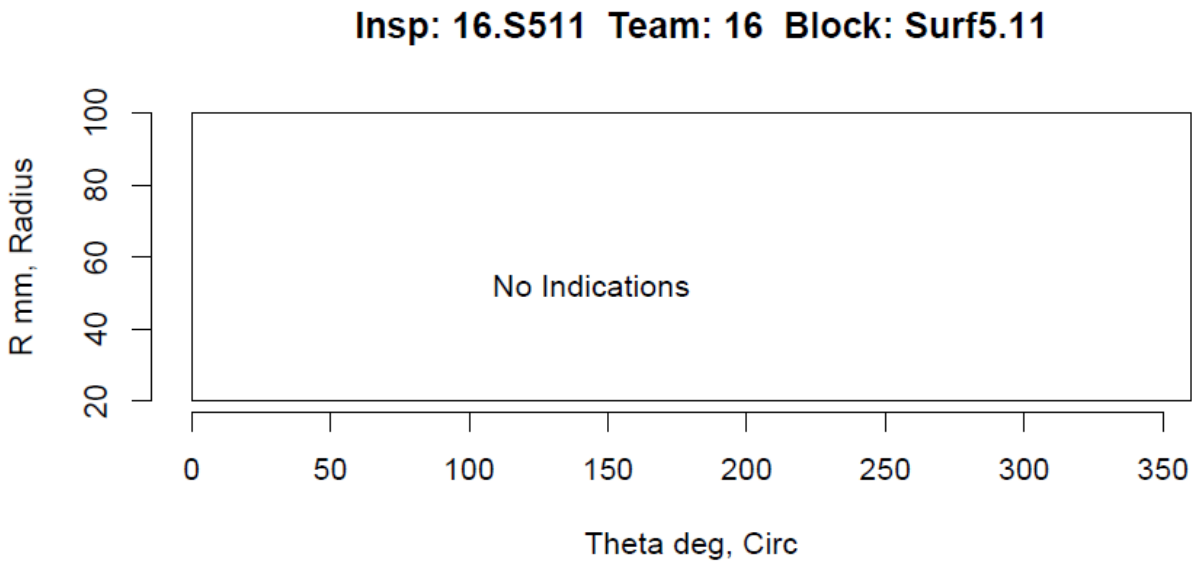
Insp: 16.S511 Team: 16 Block: Surf5.11
R mm, Radius
20
40
60
80
100
No Indications
0
50
100
150
200
250
300
350
Theta deg, Circ

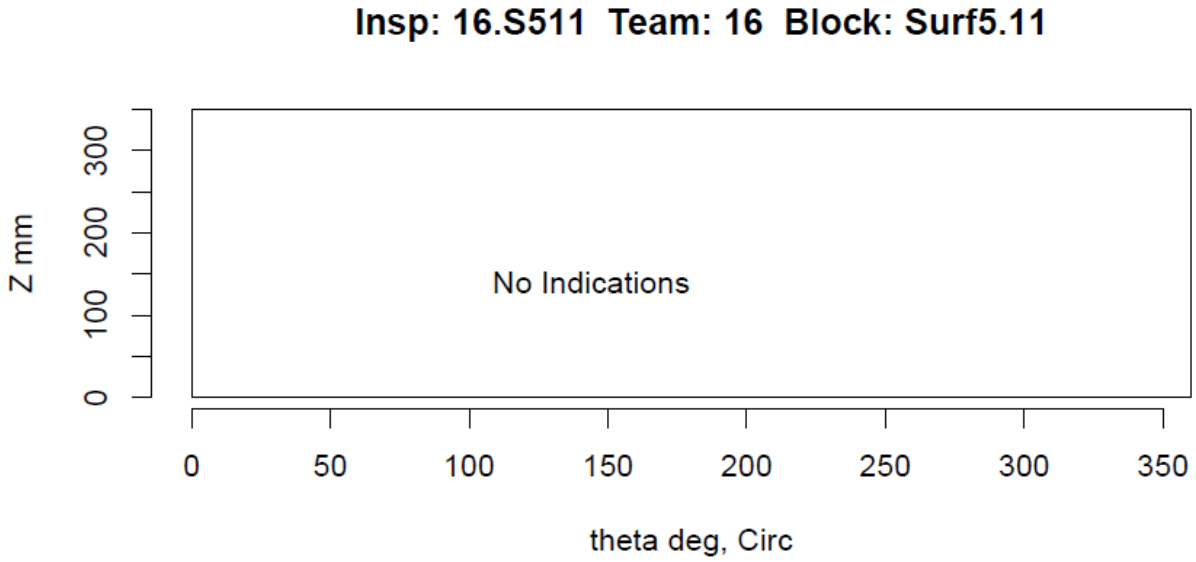
Insp: 16.S511 Team: 16 Block: Surf5.11
Z mm
0
100
200
300
No Indications
0
50
100
150
200
250
300
350
theta deg, Circ

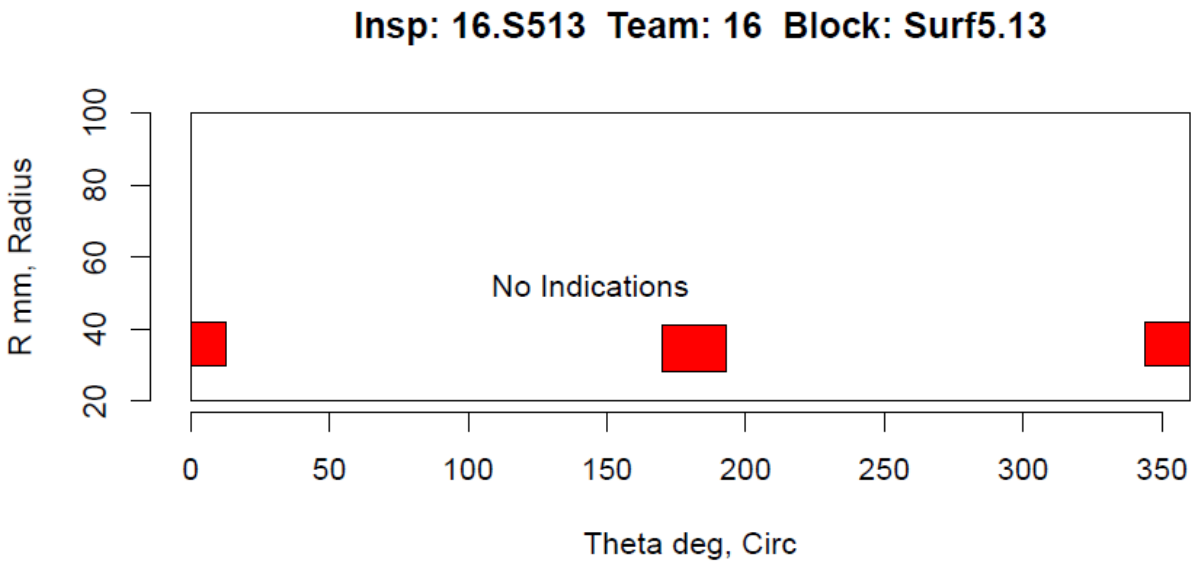
Insp: 16.S513 Team: 16 Block: Surf5.13
R mm, Radius
20
40
60
80
100
No Indications
0
50
100
150
200
250
300
350
Theta deg, Circ

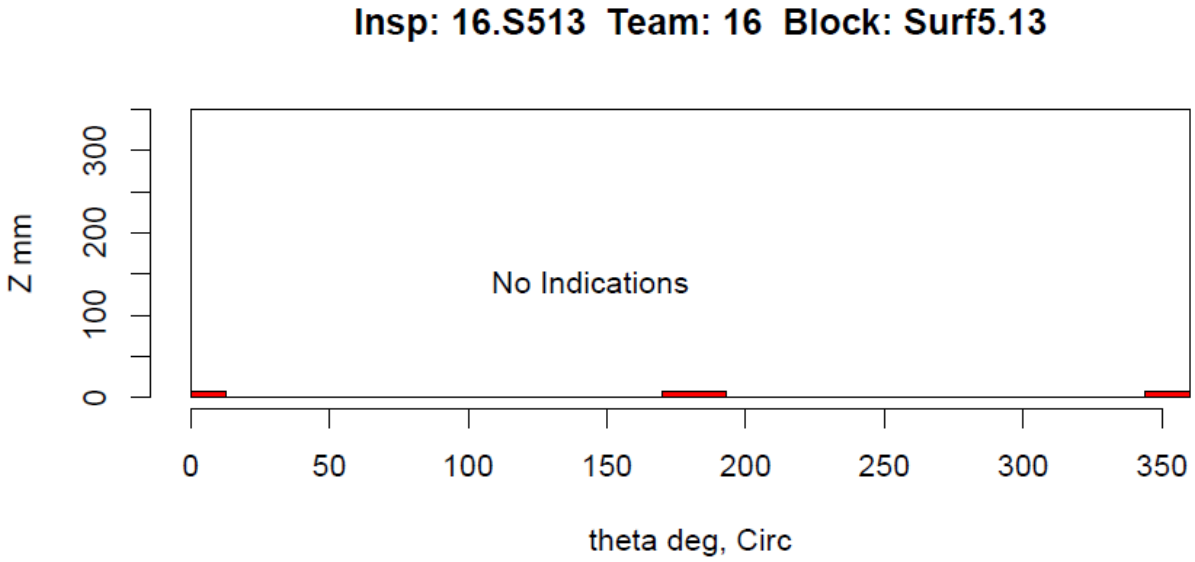
Insp: 16.S513 Team: 16 Block: Surf5.13
Z mm
0
100
200
300
No Indications
0
50
100
150
200
250
300
350
theta deg, Circ

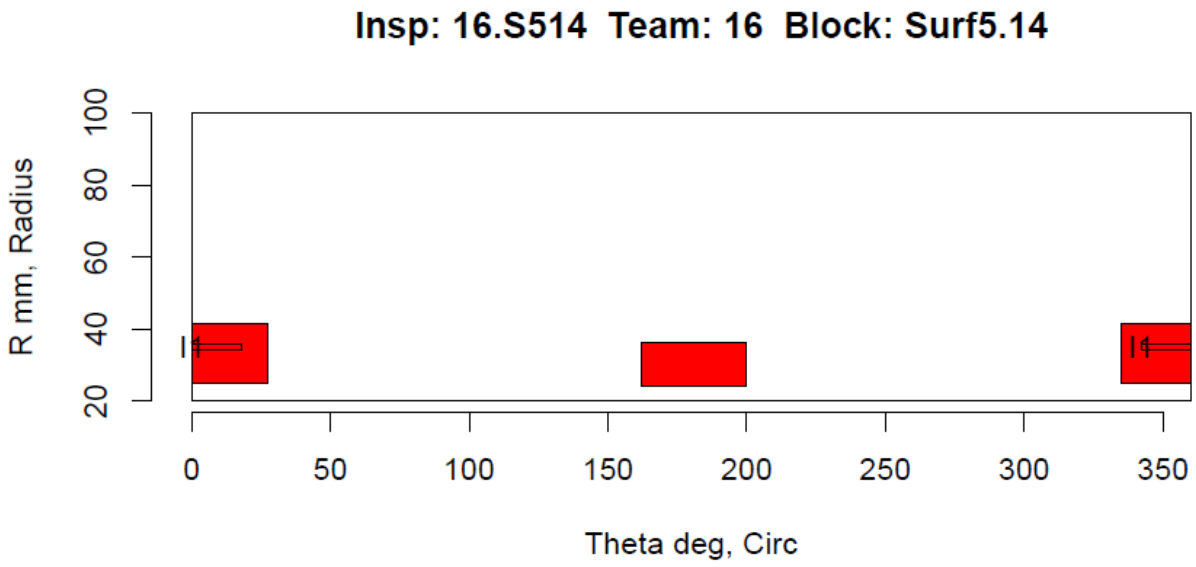
Insp: 16.S514 Team: 16 Block: Surf5.14
R mm, Radius
20
40
60
80
100
0
50
100
150
200
250
300
350
Theta deg, Circ

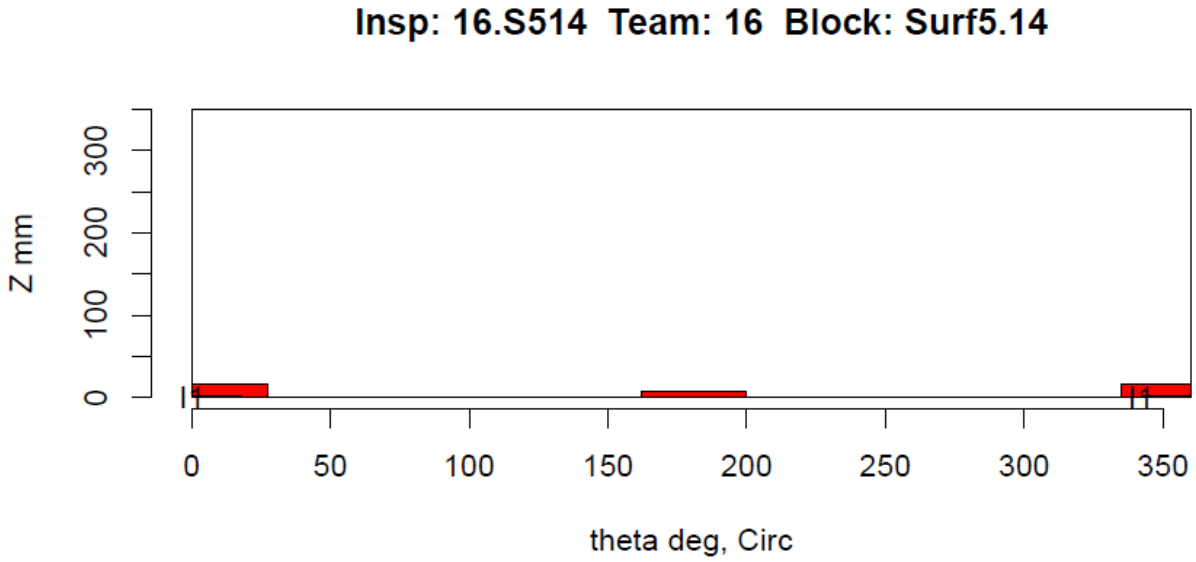
Insp: 16.S514 Team: 16 Block: Surf5.14
Z mm
0
100
200
300
0
50
100
150
200
250
300
350
theta deg, Circ

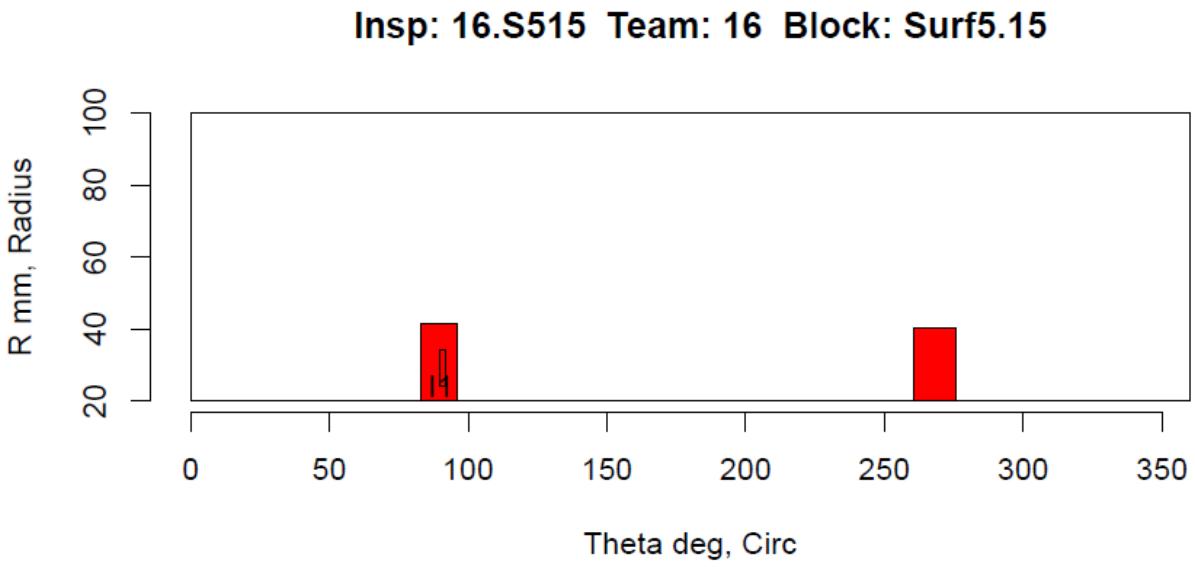
Insp: 16.S515 Team: 16 Block: Surf5.15
R mm, Radius
20
40
60
80
100
0
50
100
150
200
250
300
350
Theta deg, Circ

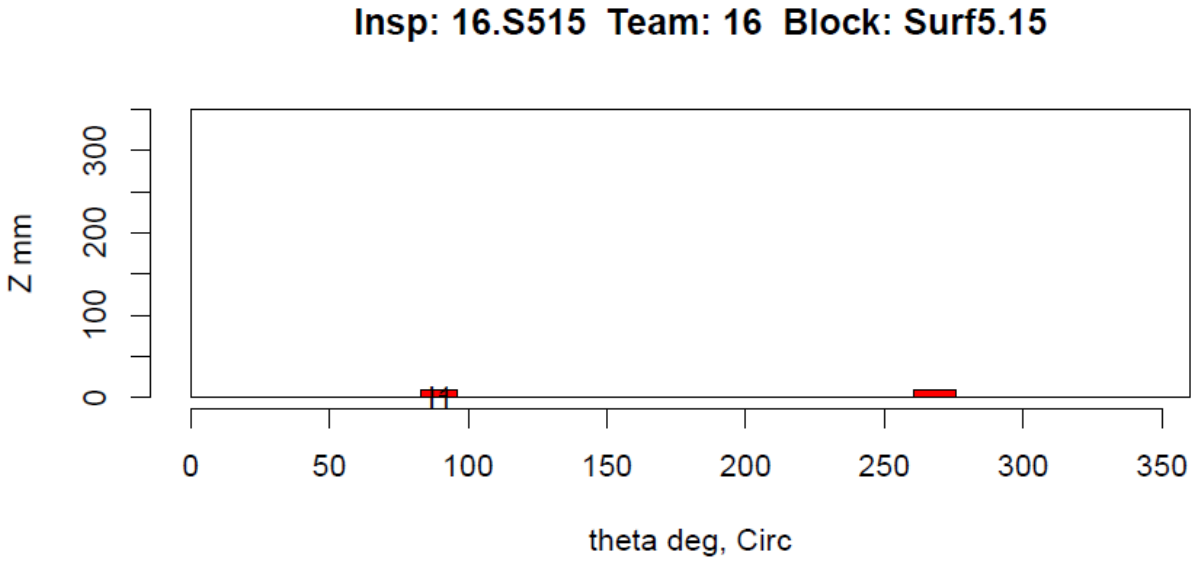
Insp: 16.S515 Team: 16 Block: Surf5.15
Z mm
0
100
200
300
0
50
100
150
200
250
300
350
theta deg, Circ

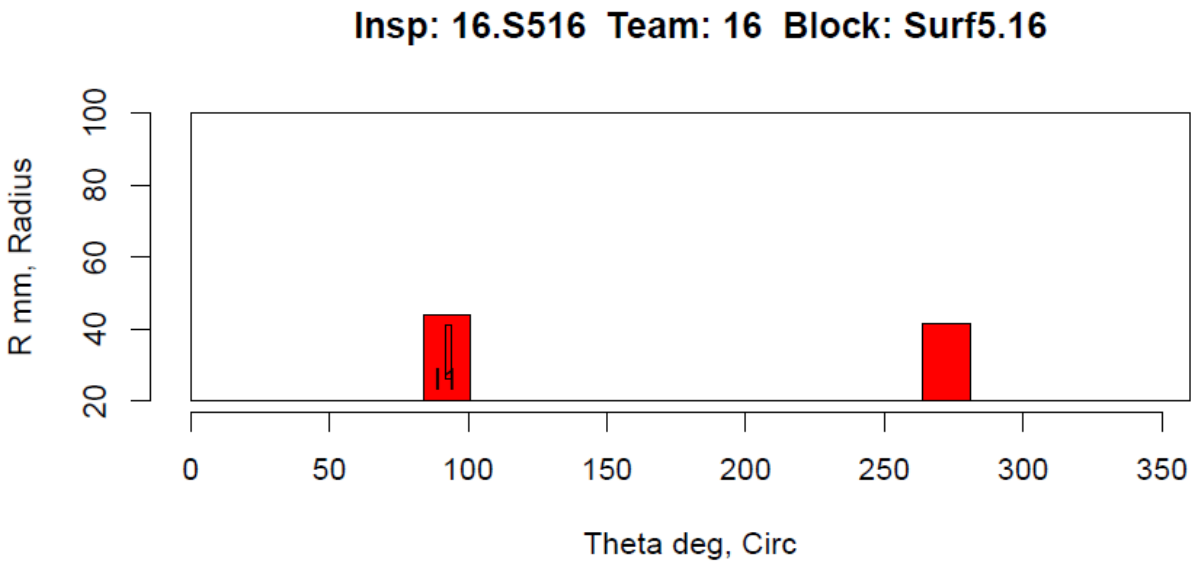
Insp: 16.S516 Team: 16 Block: Surf5.16
R mm, Radius
20
40
60
80
100
0
50
100
150
200
250
300
350
Theta deg, Circ

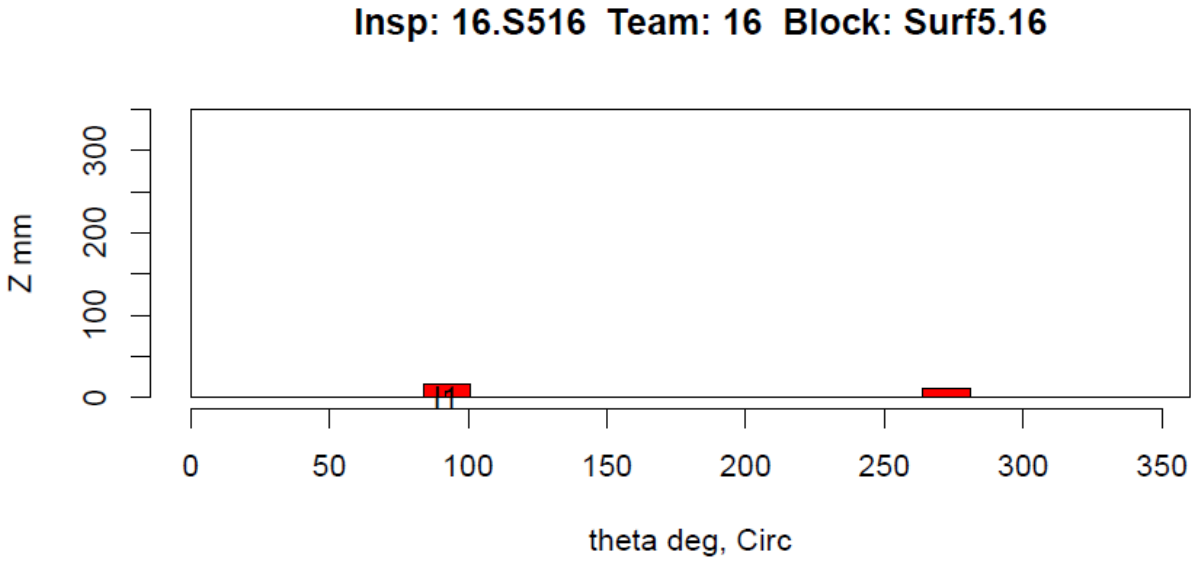
Insp: 16.S516 Team: 16 Block: Surf5.16
Z mm
0
100
200
300
0
50
100
150
200
250
300
350
theta deg, Circ

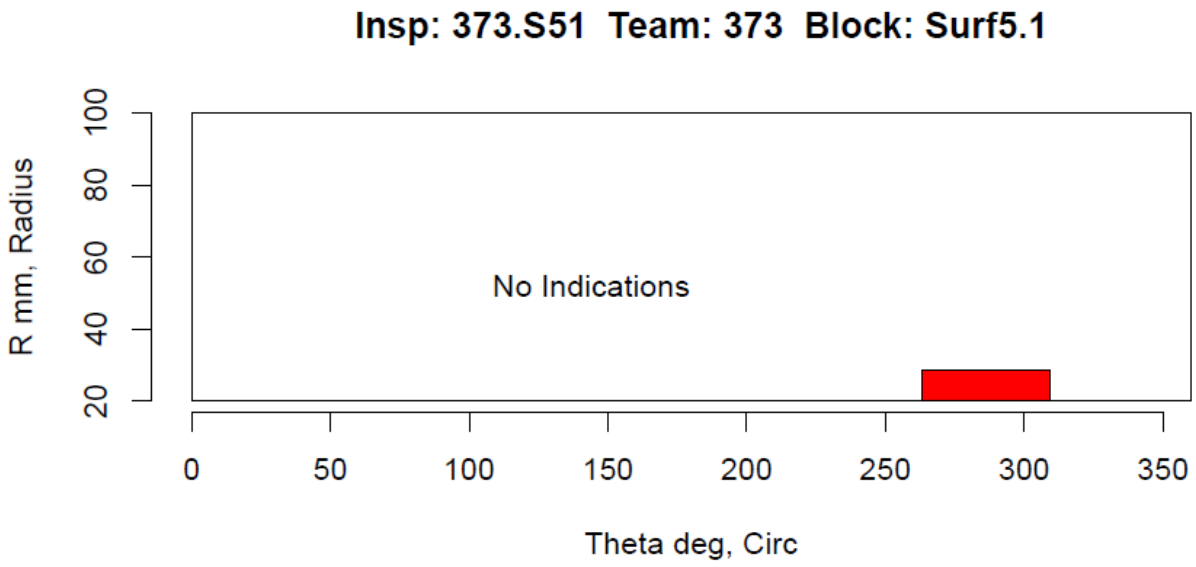
Insp: 373.S51 Team: 373 Block: Surf5.1
R mm, Radius
20
40
60
80
100
No Indications
0
50
100
150
200
250
300
350
Theta deg, Circ

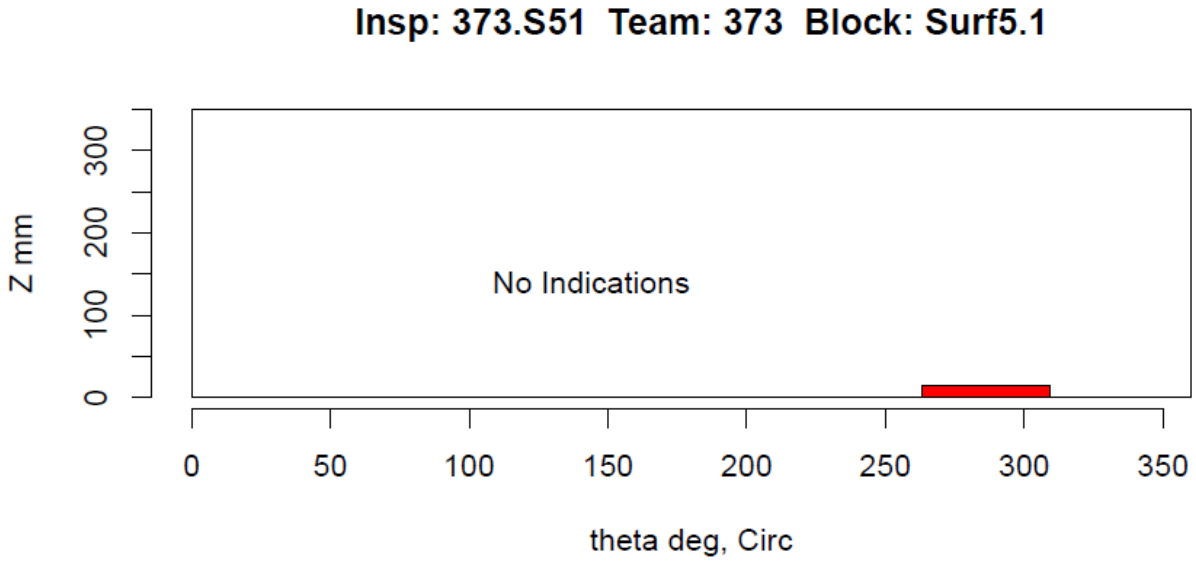
Insp: 373.S51 Team: 373 Block: Surf5.1
Z mm
0
100
200
300
No Indications
0
50
100
150
200
250
300
350
theta deg, Circ

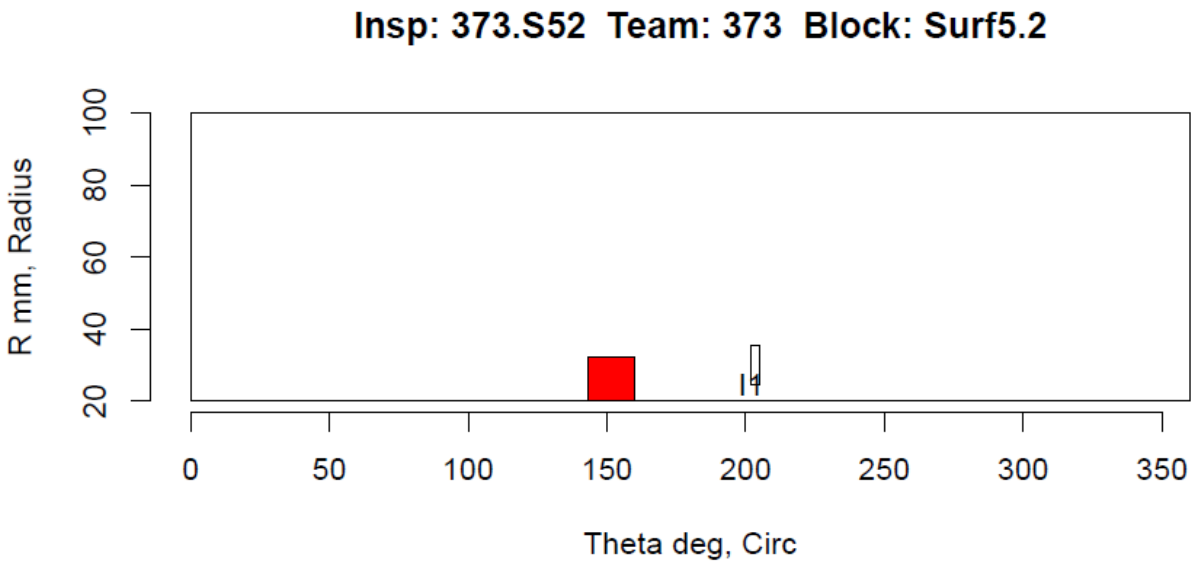
Insp: 373.S52 Team: 373 Block: Surf5.2
R mm, Radius
20
40
60
80
100
0
50
100
150
200
250
300
350
Theta deg, Circ

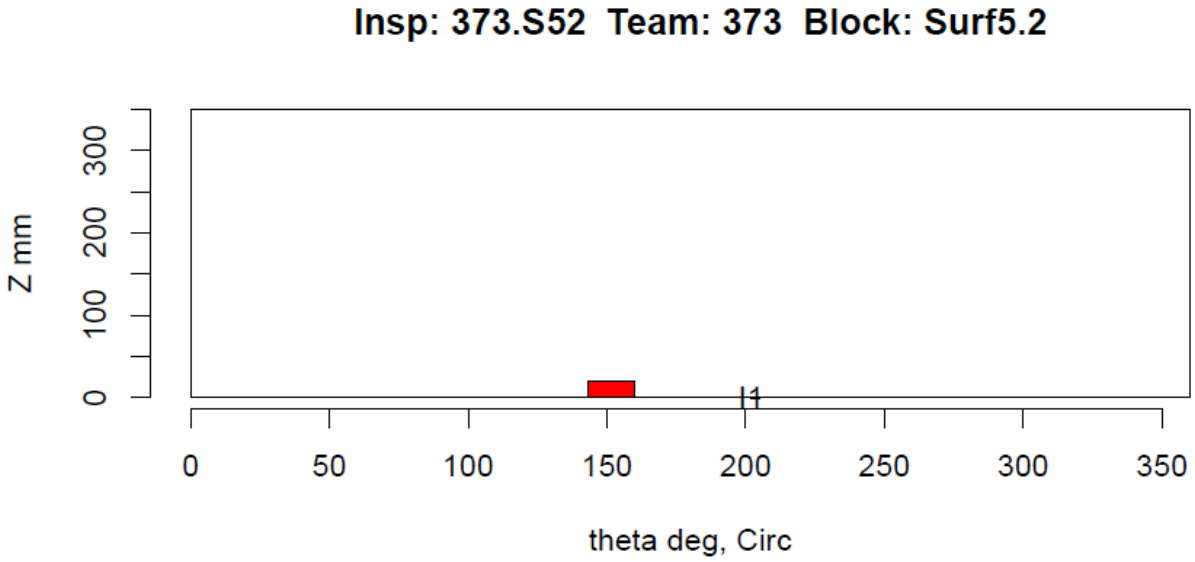
Insp: 373.S52 Team: 373 Block: Surf5.2
Z mm
0
100
200
300
0
50
100
150
200
250
300
350
theta deg, Circ

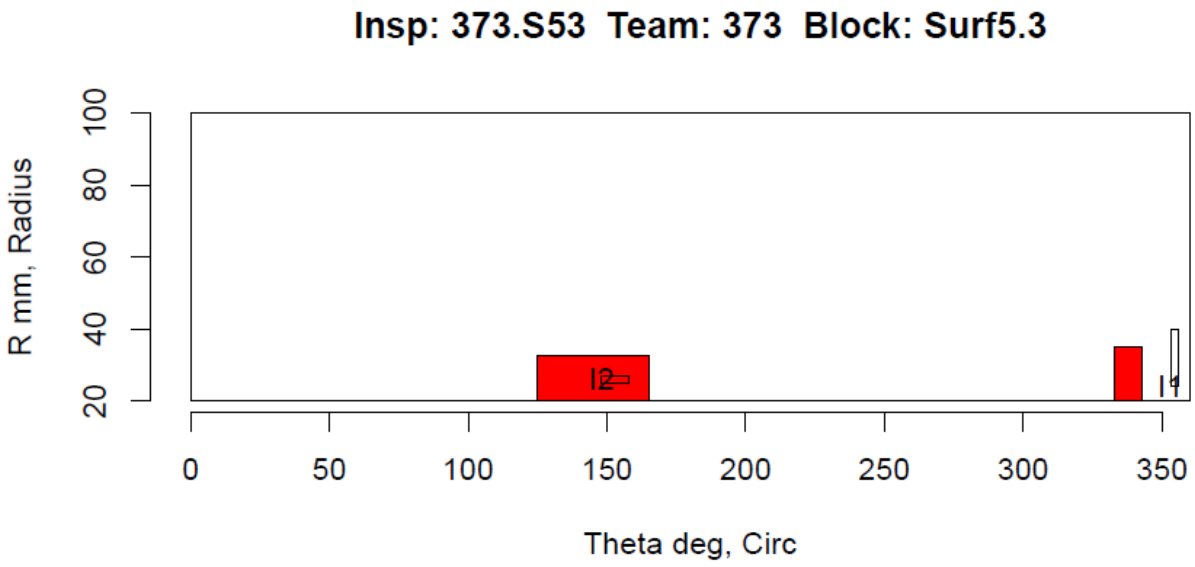
Insp: 373.S53 Team: 373 Block: Surf5.3
R mm, Radius
20
40
60
80
100
0
50
100
150
200
250
300
350
Theta deg, Circ
I2
I1

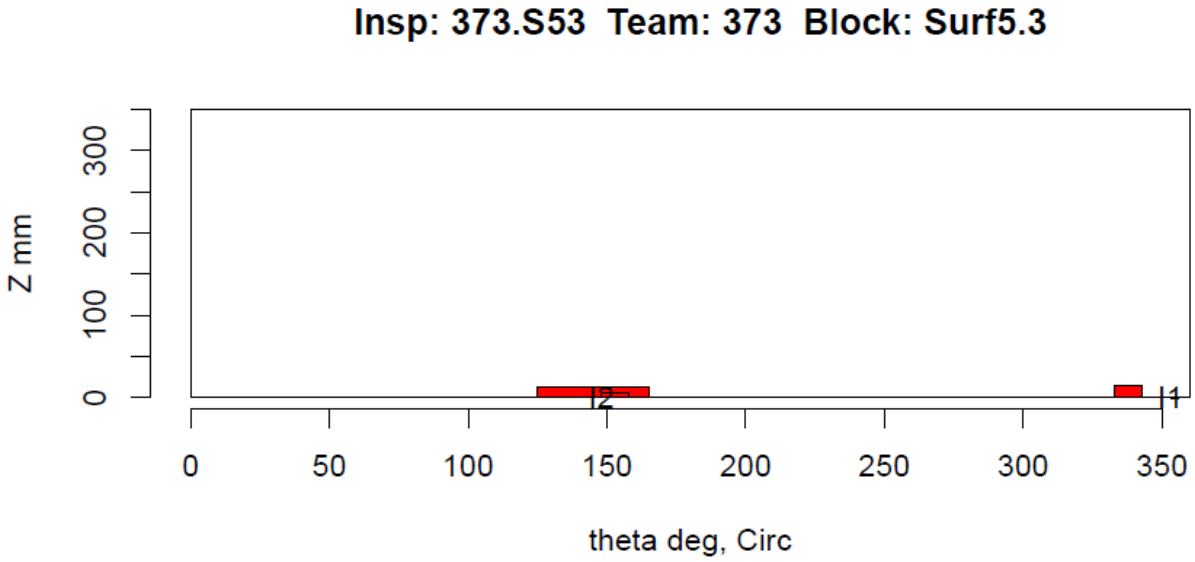
Insp: 373.S53 Team: 373 Block: Surf5.3
Z mm
0
100
200
300
0
50
100
150
200
250
300
350
theta deg, Circ
I2
I1

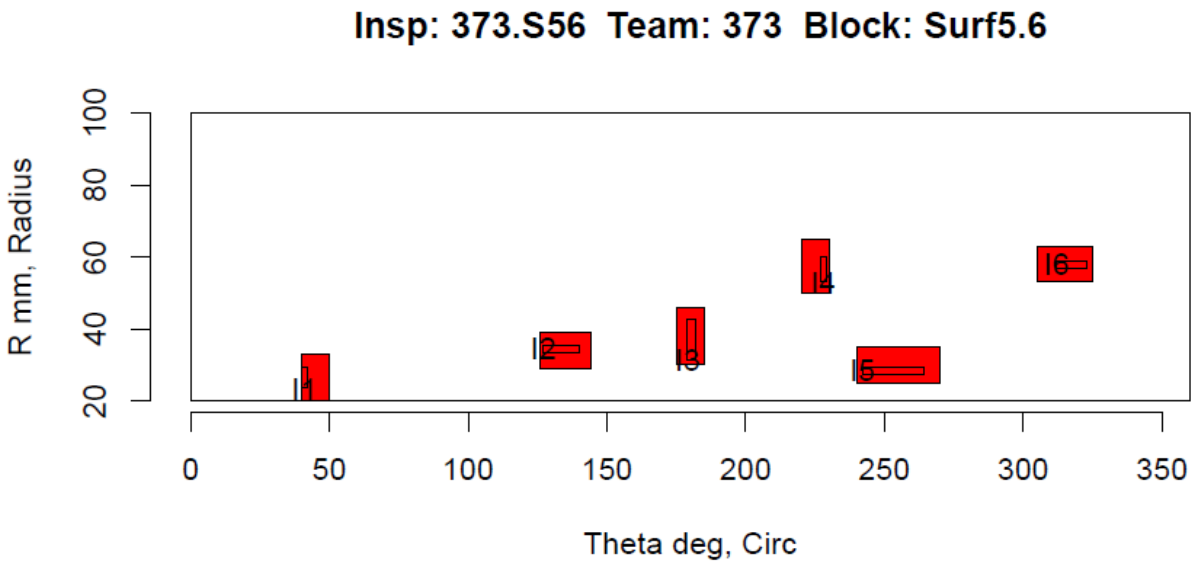
Insp: 373.S56 Team: 373 Block: Surf5.6
R mm, Radius
20
40
60
80
100
0
50
100
150
200
250
300
350
Theta deg, Circ
I1
I2
I3
I4
I5
I6

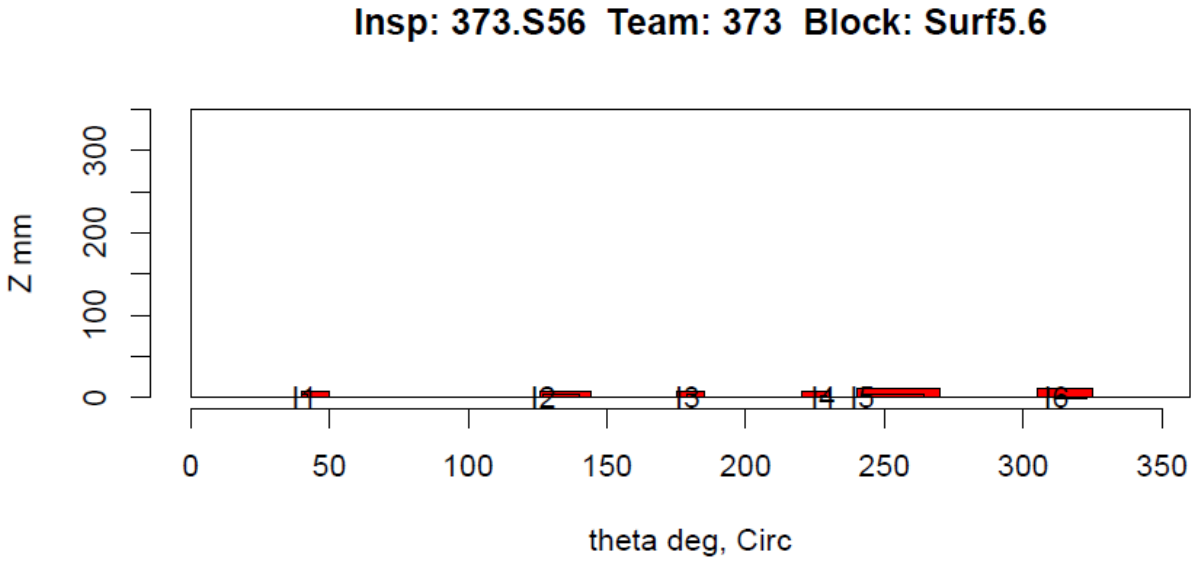
Insp: 373.S56 Team: 373 Block: Surf5.6
Z mm
0
100
200
300
0
50
100
150
200
250
300
350
theta deg, Circ
I1
I2
I3
I4
I5
I6

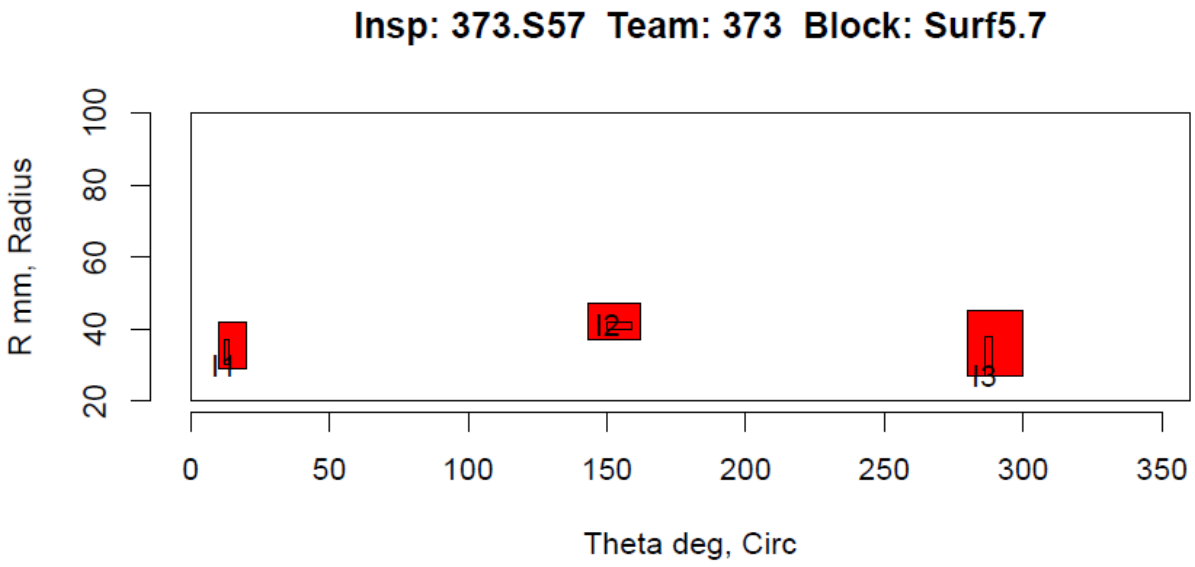
Insp: 373.S57 Team: 373 Block: Surf5.7
R mm, Radius
20
40
60
80
100
I1
I2
I3
0
50
100
150
200
250
300
350
Theta deg, Circ

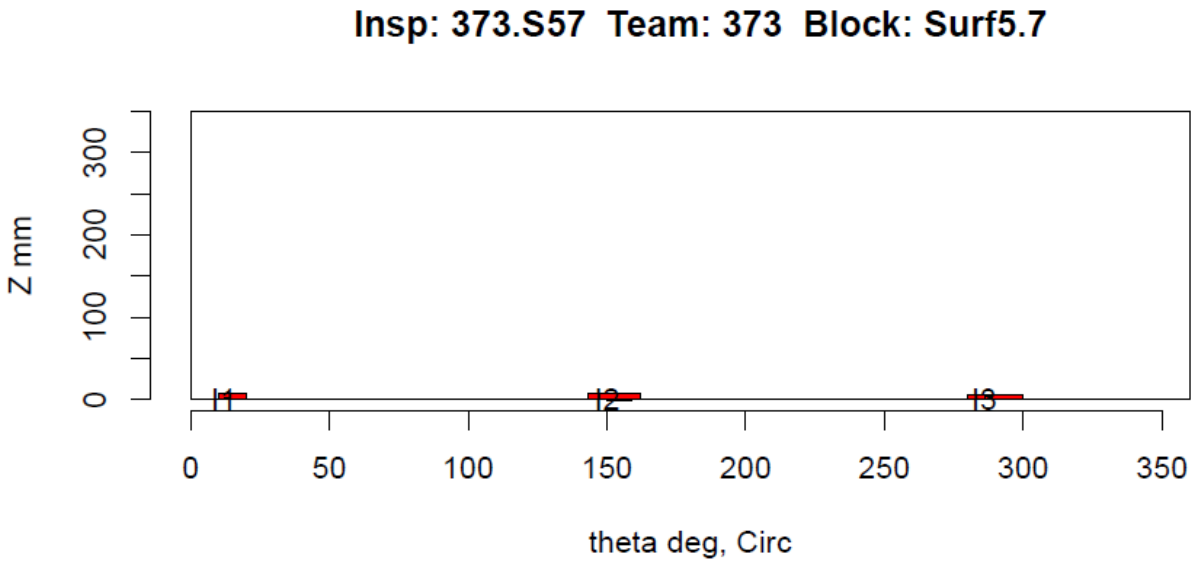
Insp: 373.S57 Team: 373 Block: Surf5.7
Z mm
0
100
200
300
I1
I2
I3
0
50
100
150
200
250
300
350
theta deg, Circ

.

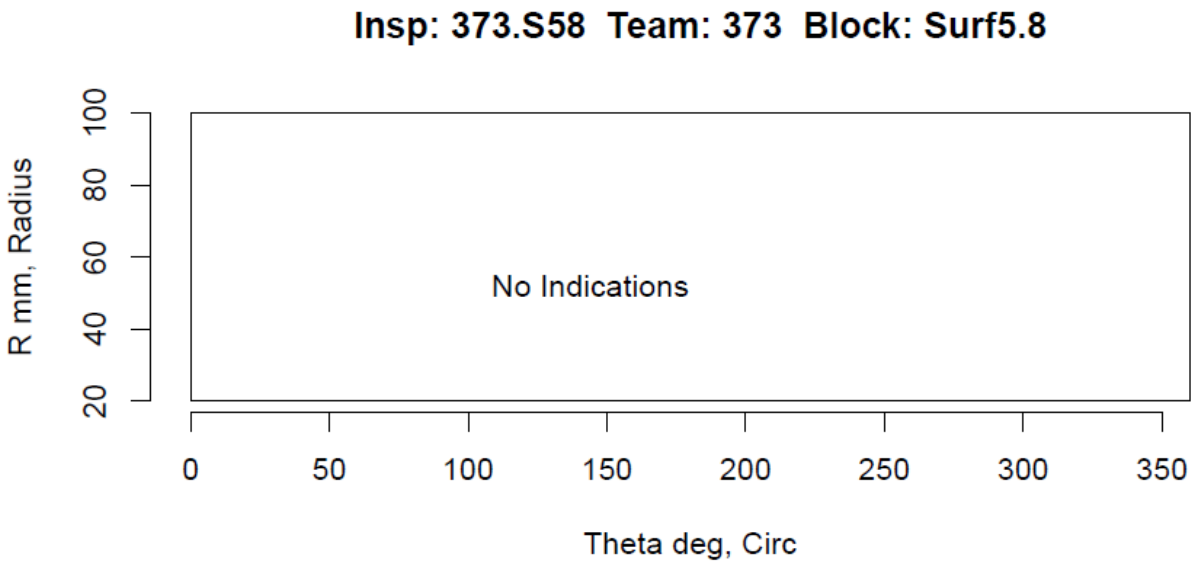
Insp: 373.S58 Team: 373 Block: Surf5.8
R mm, Radius
20
40
60
80
100
No Indications
0
50
100
150
200
250
300
350
Theta deg, Circ

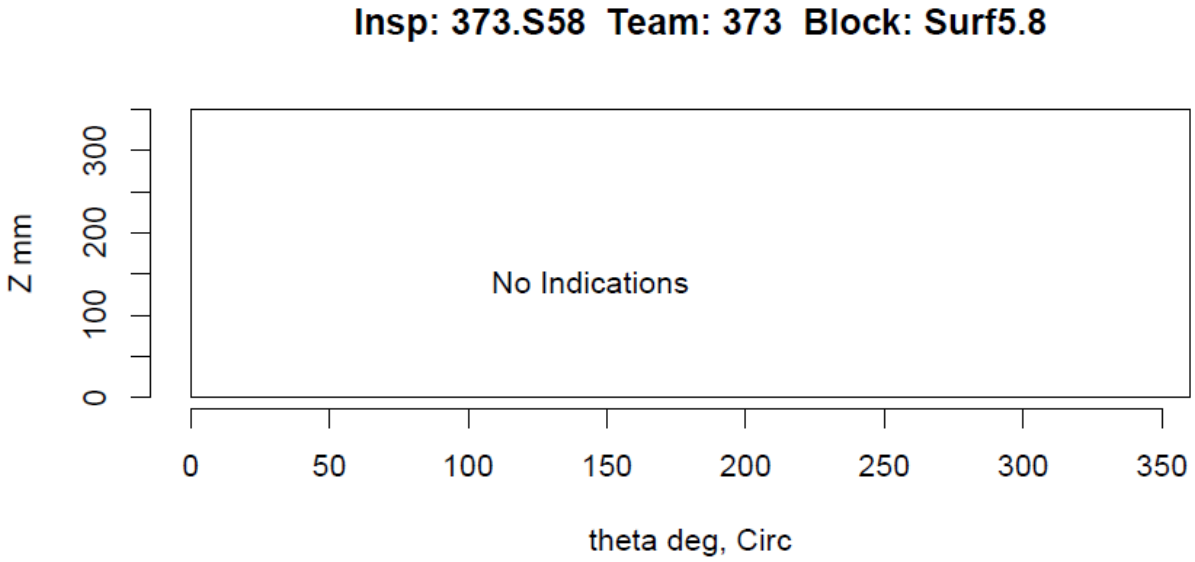
Insp: 373.S58 Team: 373 Block: Surf5.8
Z mm
0
100
200
300
No Indications
0
50
100
150
200
250
300
350
theta deg, Circ

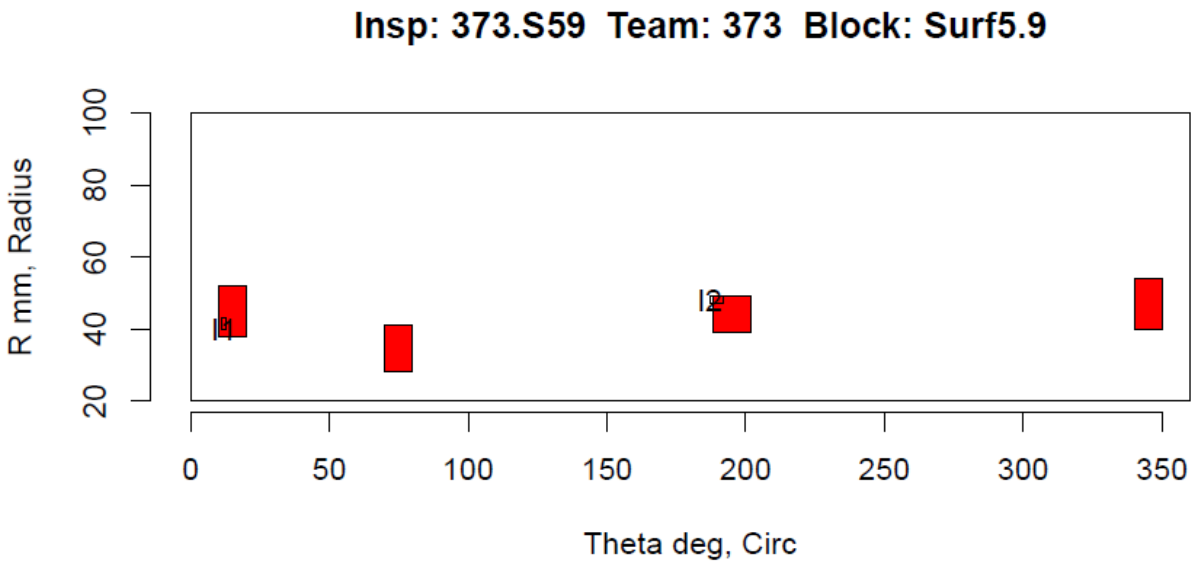
Insp: 373.S59 Team: 373 Block: Surf5.9
R mm, Radius
20
40
60
80
100
0
50
100
150
200
250
300
350
Theta deg, Circ

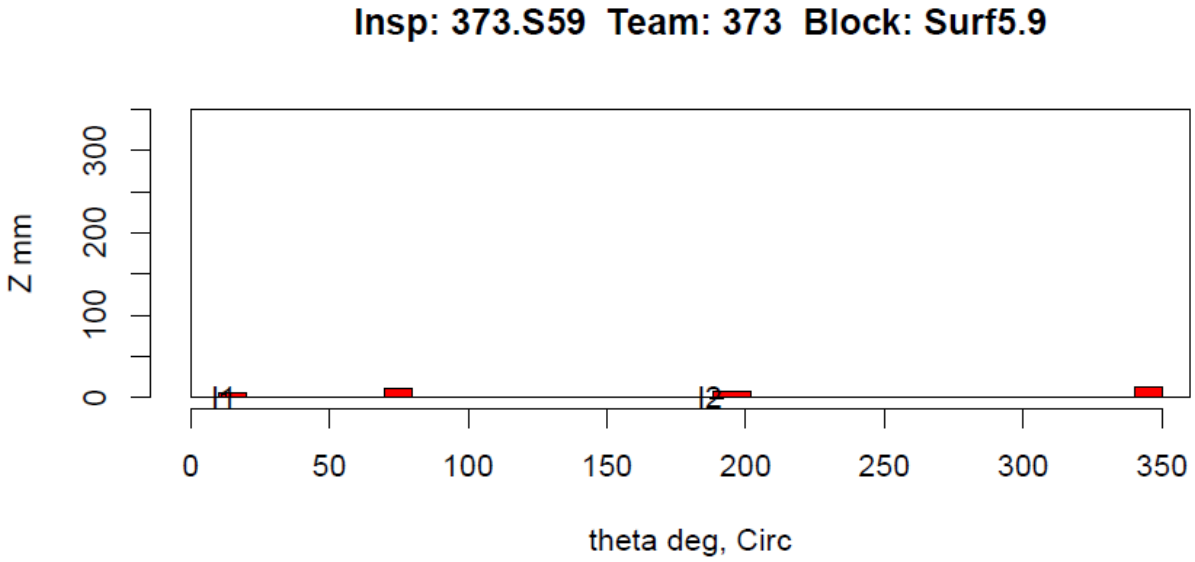
Insp: 373.S59 Team: 373 Block: Surf5.9
Z mm
0
100
200
300
0
50
100
150
200
250
300
350
theta deg, Circ

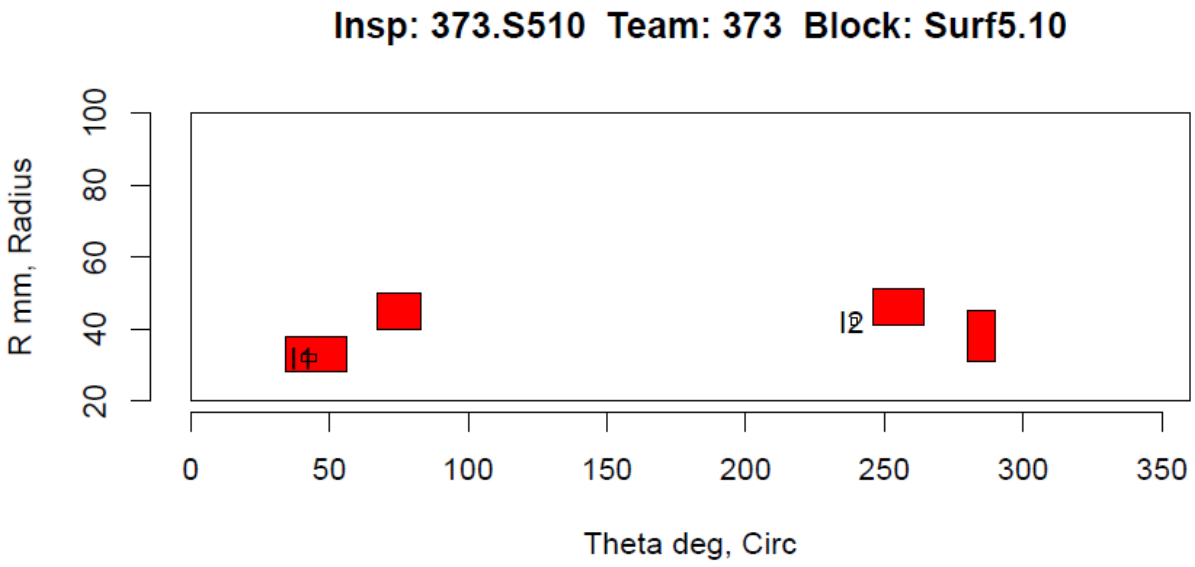
Insp: 373.S510 Team: 373 Block: Surf5.10
R mm, Radius
20
40
60
80
100
0
50
100
150
200
250
300
350
Theta deg, Circ

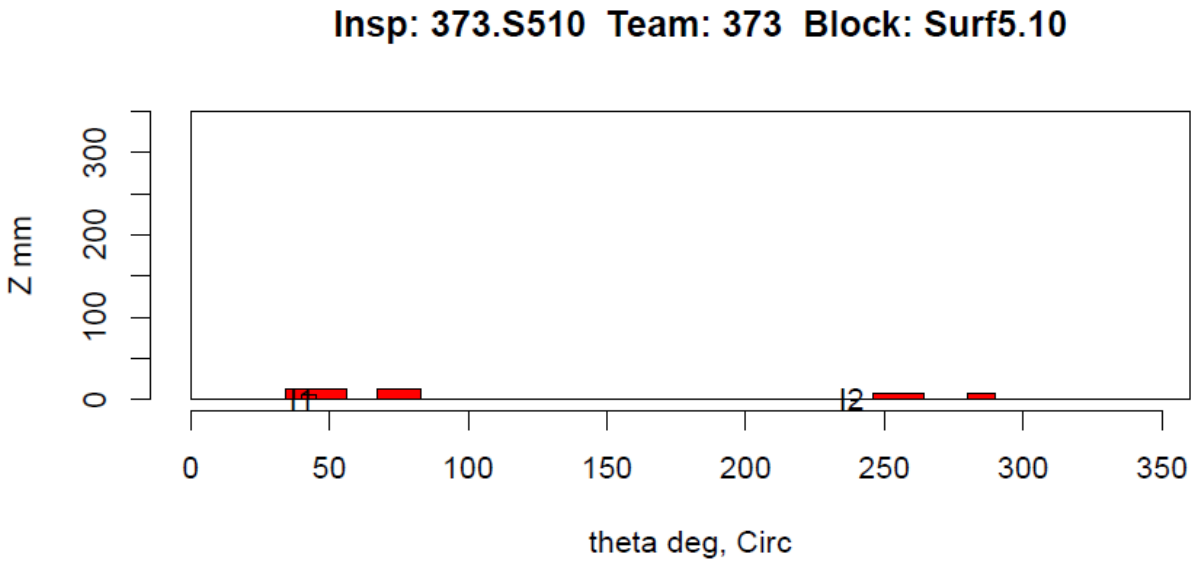
Insp: 373.S510 Team: 373 Block: Surf5.10
Z mm
0
100
200
300
0
50
100
150
200
250
300
350
theta deg, Circ

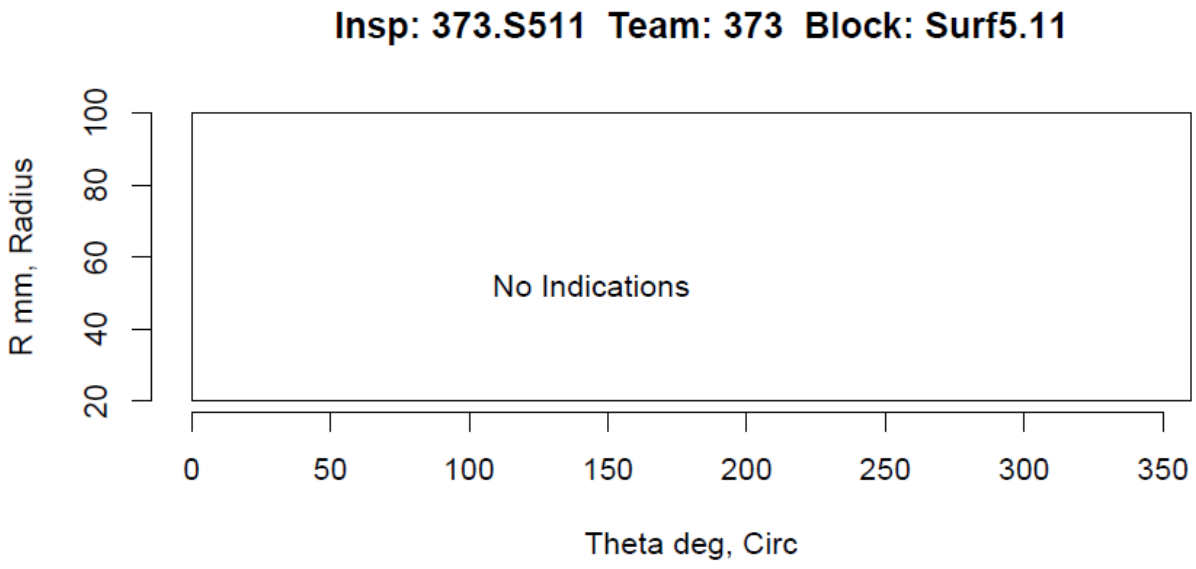
Insp: 373.S511 Team: 373 Block: Surf5.11
R mm, Radius
20
40
60
80
100
No Indications
0
50
100
150
200
250
300
350
Theta deg, Circ

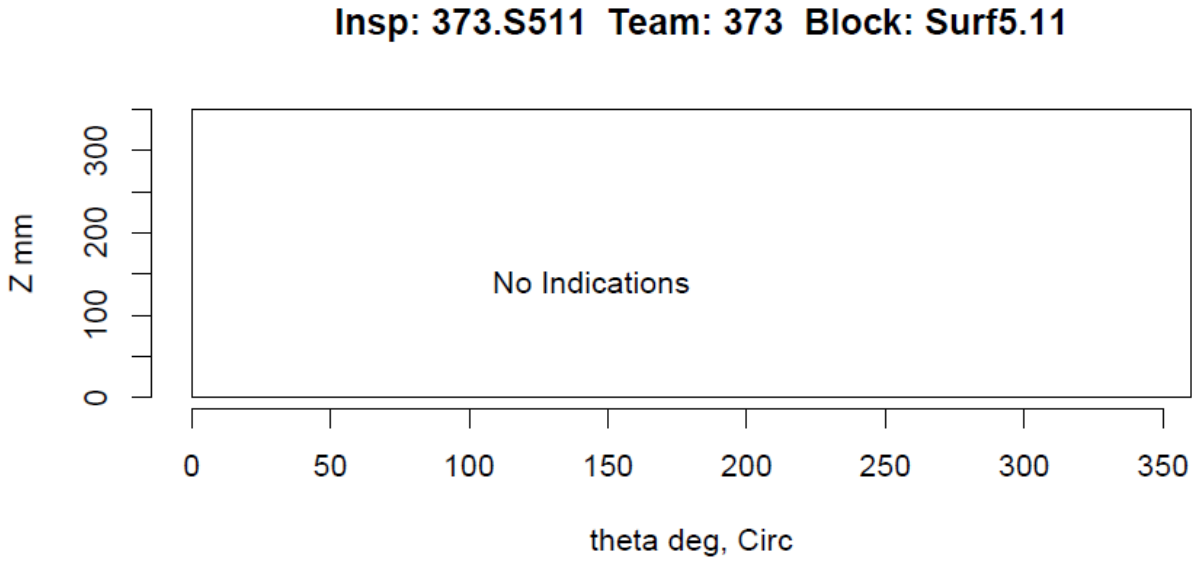
Insp: 373.S511 Team: 373 Block: Surf5.11
Z mm
0
100
200
300
No Indications
0
50
100
150
200
250
300
350
theta deg, Circ

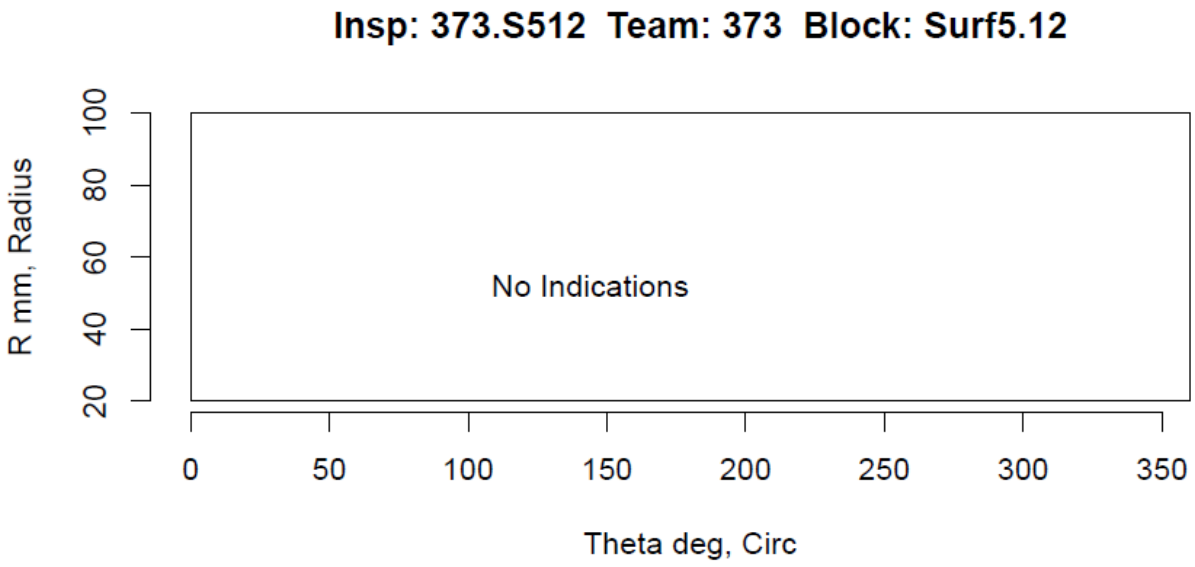
Insp: 373.S512 Team: 373 Block: Surf5.12
R mm, Radius
20
40
60
80
100
No Indications
0
50
100
150
200
250
300
350
Theta deg, Circ

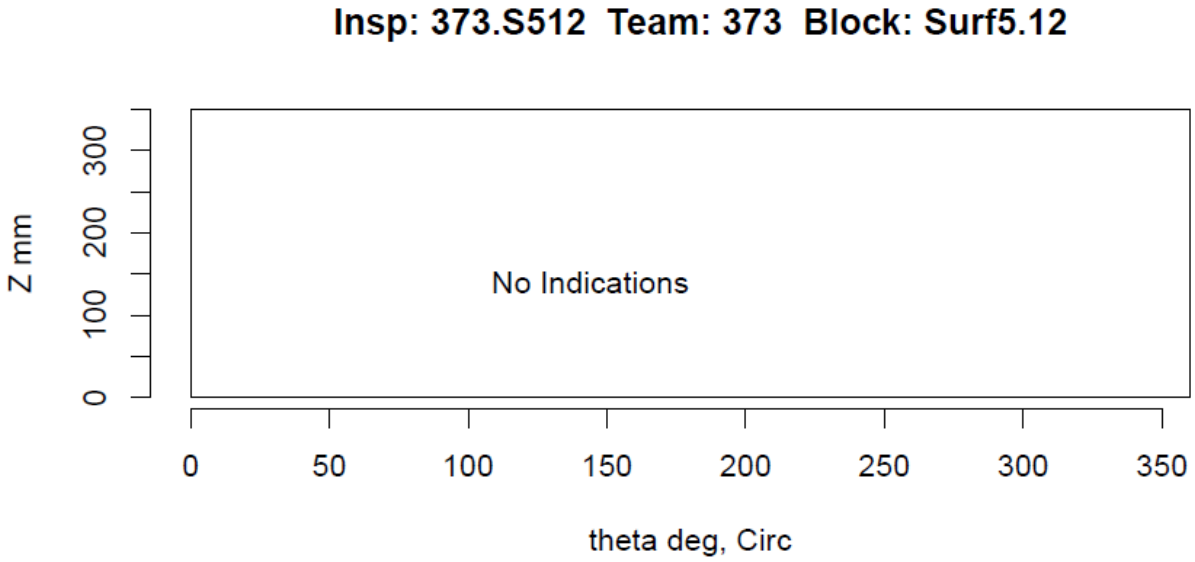
Insp: 373.S512 Team: 373 Block: Surf5.12
Z mm
0
100
200
300
No Indications
0
50
100
150
200
250
300
350
theta deg, Circ

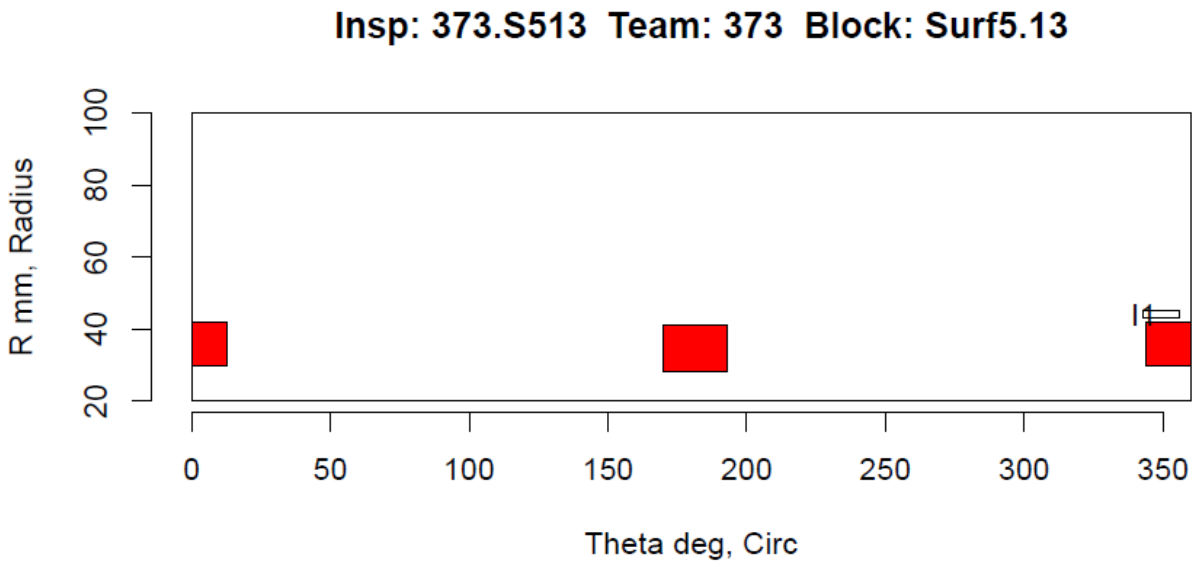
Insp: 373.S513 Team: 373 Block: Surf5.13
R mm, Radius
20
40
60
80
100
0
50
100
150
200
250
300
350
Theta deg, Circ

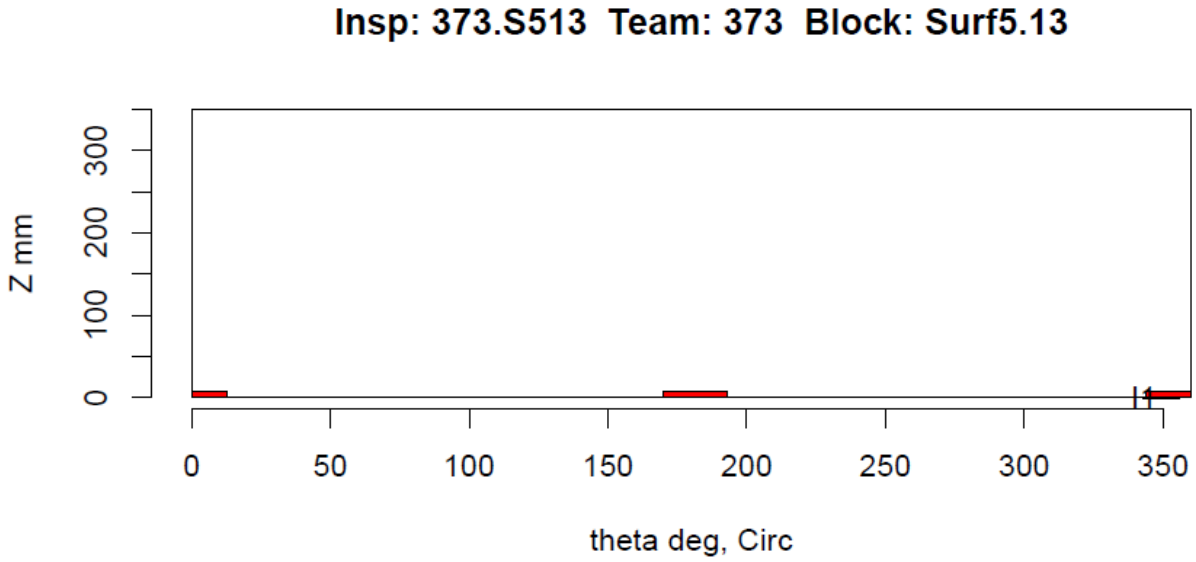
Insp: 373.S513 Team: 373 Block: Surf5.13
Z mm
0
100
200
300
0
50
100
150
200
250
300
350
theta deg, Circ

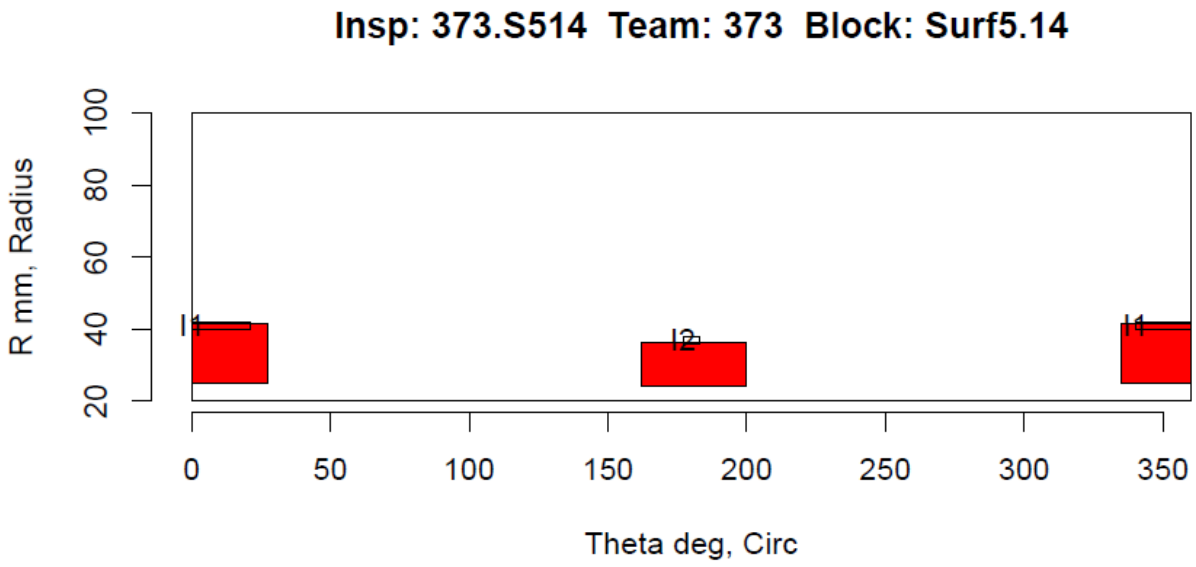
Insp: 373.S514 Team: 373 Block: Surf5.14
R mm, Radius
20
40
60
80
100
0
50
100
150
200
250
300
350
Theta deg, Circ

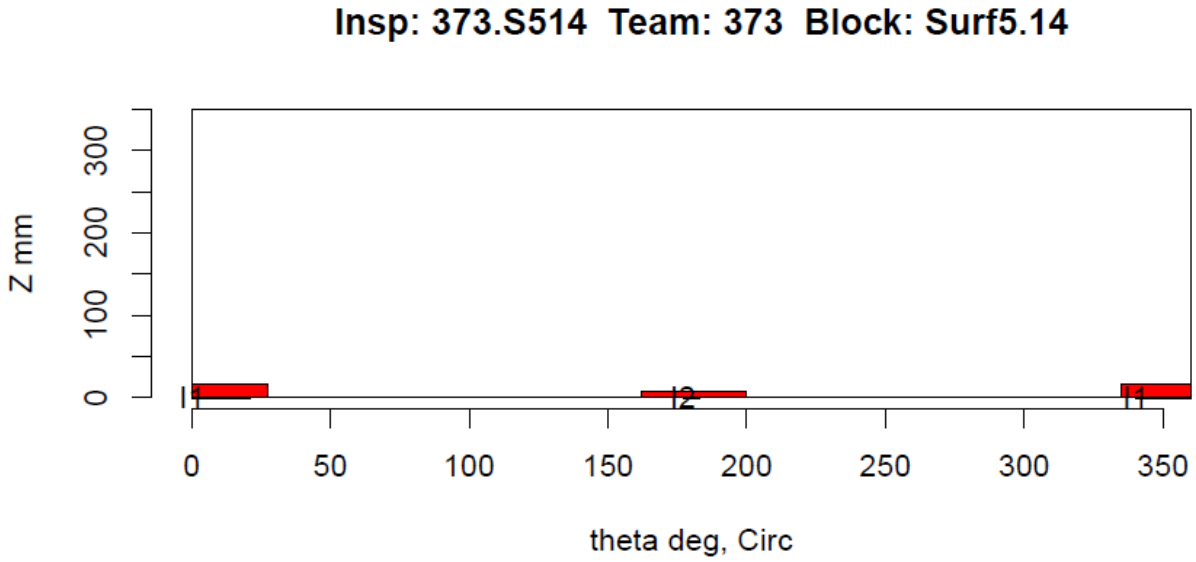
Insp: 373.S514 Team: 373 Block: Surf5.14
Z mm
0
100
200
300
0
50
100
150
200
250
300
350
theta deg, Circ

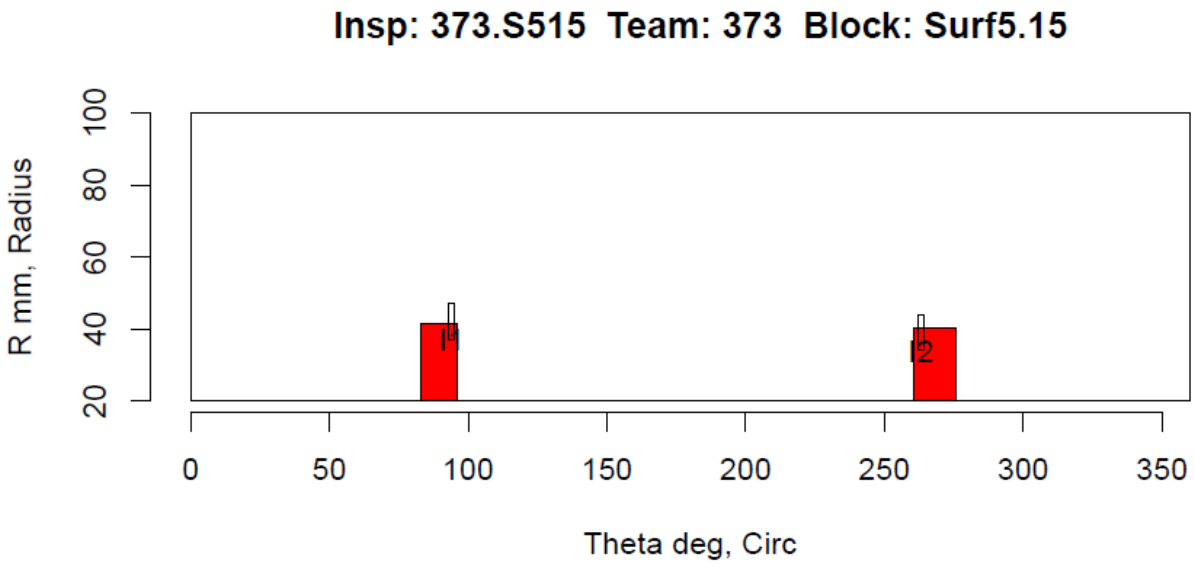
Insp: 373.S515 Team: 373 Block: Surf5.15
R mm, Radius
20
40
60
80
100
0
50
100
150
200
250
300
350
Theta deg, Circ

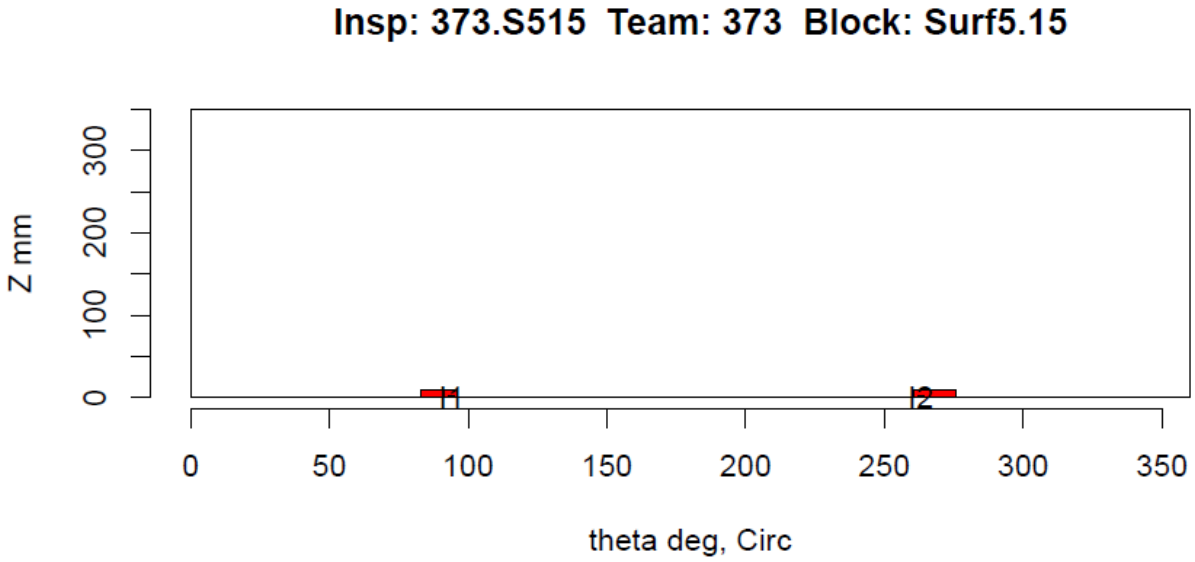
Insp: 373.S515 Team: 373 Block: Surf5.15
Z mm
0
100
200
300
0
50
100
150
200
250
300
350
theta deg, Circ

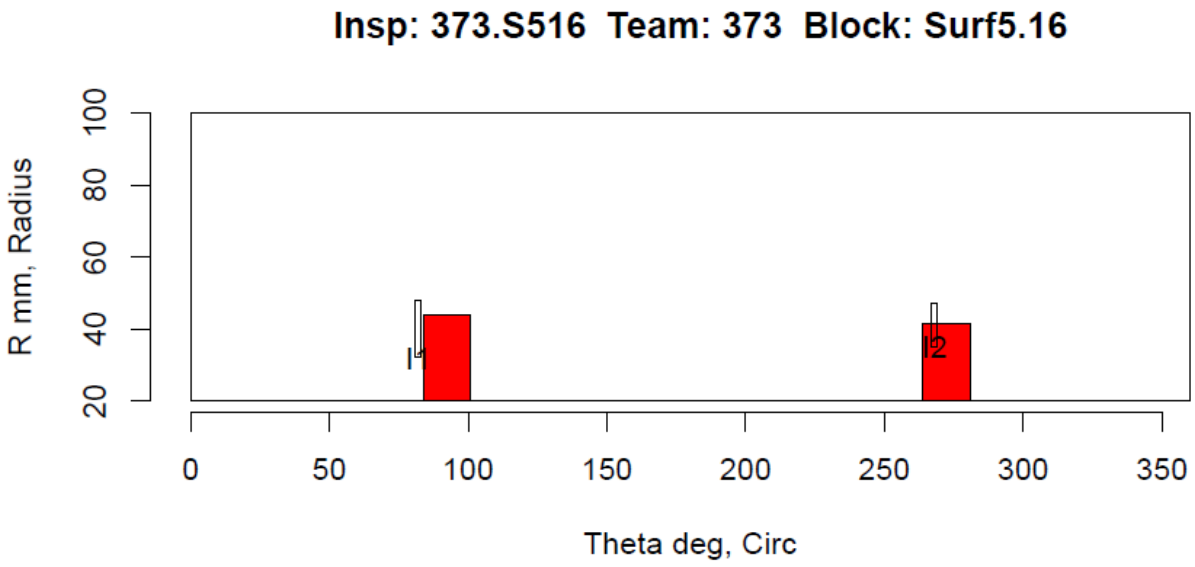
Insp: 373.S516 Team: 373 Block: Surf5.16
R mm, Radius
20
40
60
80
100
0
50
100
150
200
250
300
350
Theta deg, Circ

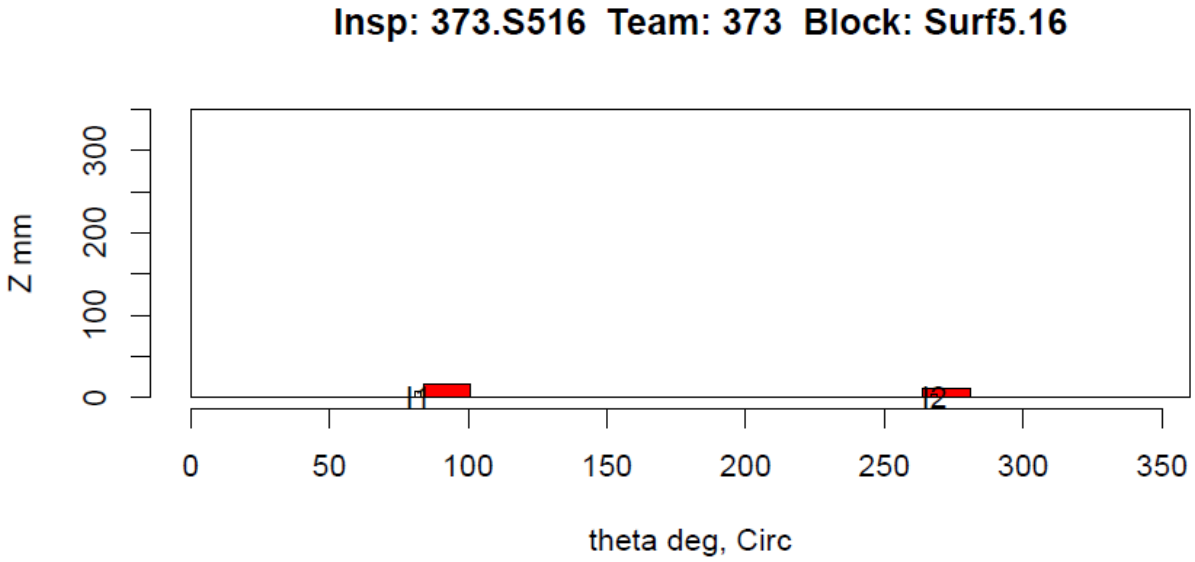
Insp: 373.S516 Team: 373 Block: Surf5.16
Z mm
0
100
200
300
0
50
100
150
200
250
300
350
theta deg, Circ

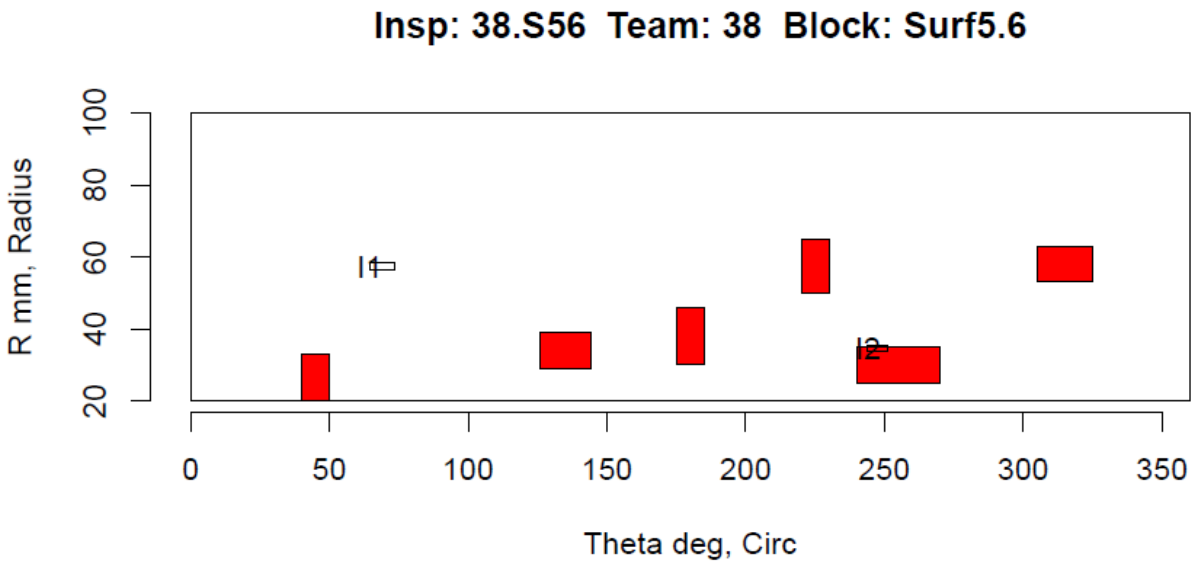
Insp: 38.S56 Team: 38 Block: Surf5.6
R mm, Radius
20
40
60
80
100
I1
I2
0
50
100
150
200
250
300
350
Theta deg, Circ

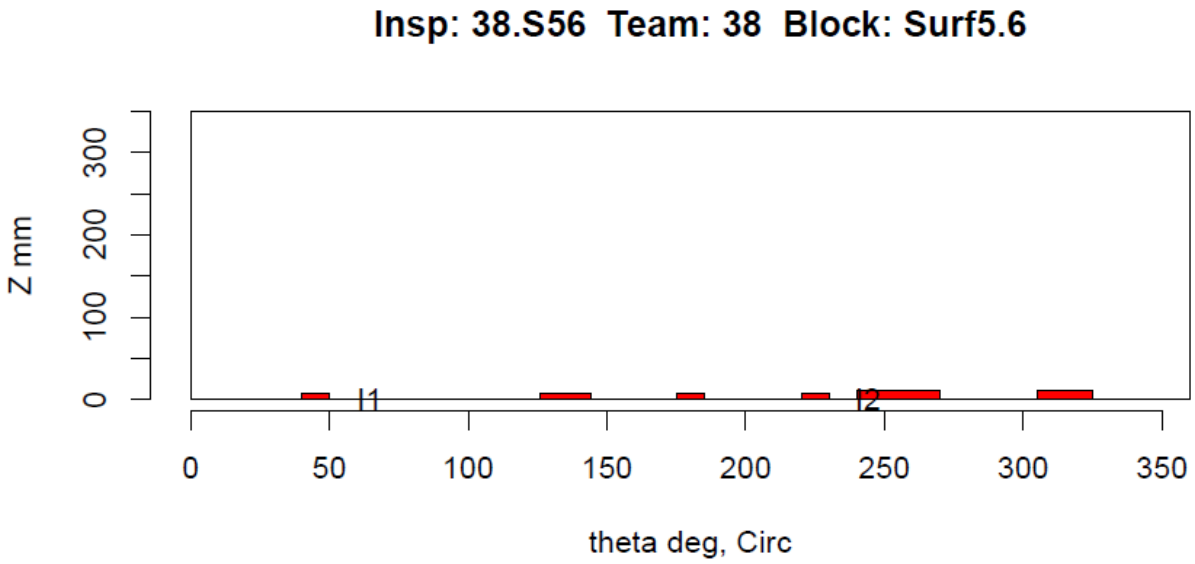
Insp: 38.S56 Team: 38 Block: Surf5.6
Z mm
0
100
200
300
I1
I2
0
50
100
150
200
250
300
350
theta deg, Circ

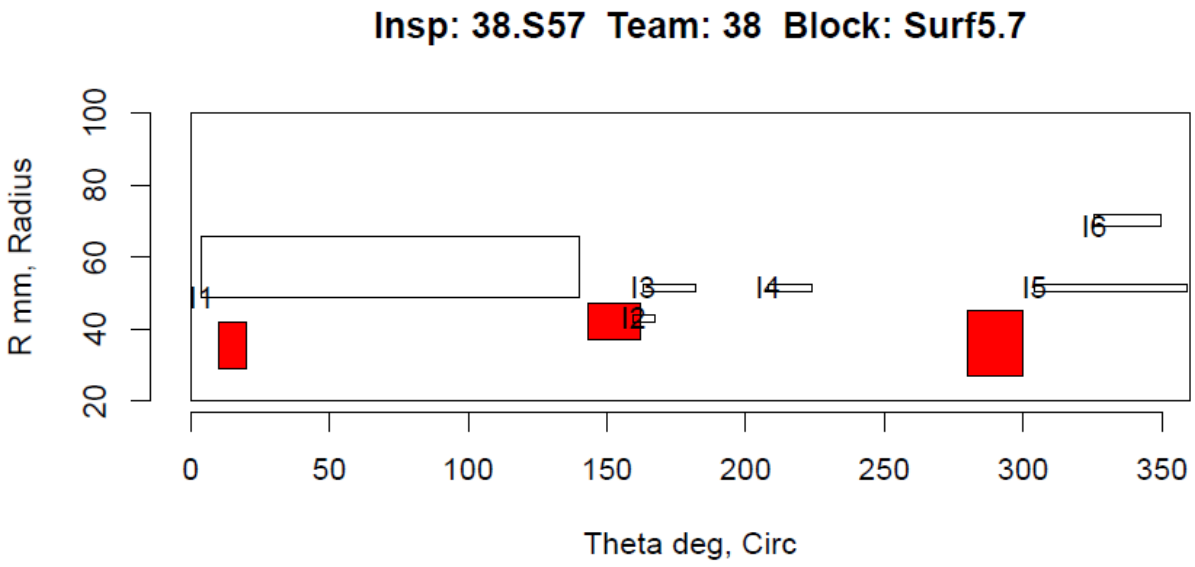
Insp: 38.S57 Team: 38 Block: Surf5.7
R mm, Radius
20
40
60
80
100
0
50
100
150
200
250
300
350
Theta deg, Circ
I1
I2
I3
I4
I5
I6

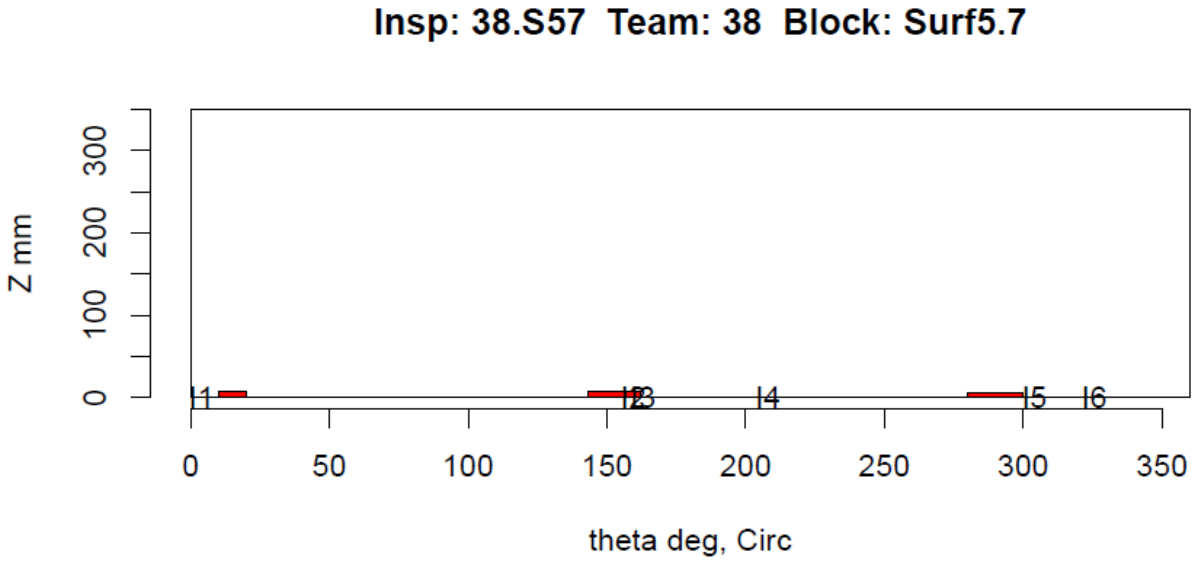
Insp: 38.S57 Team: 38 Block: Surf5.7
Z mm
0
100
200
300
0
50
100
150
200
250
300
350
theta deg, Circ
I1
I2
I3
I4
I5
I6

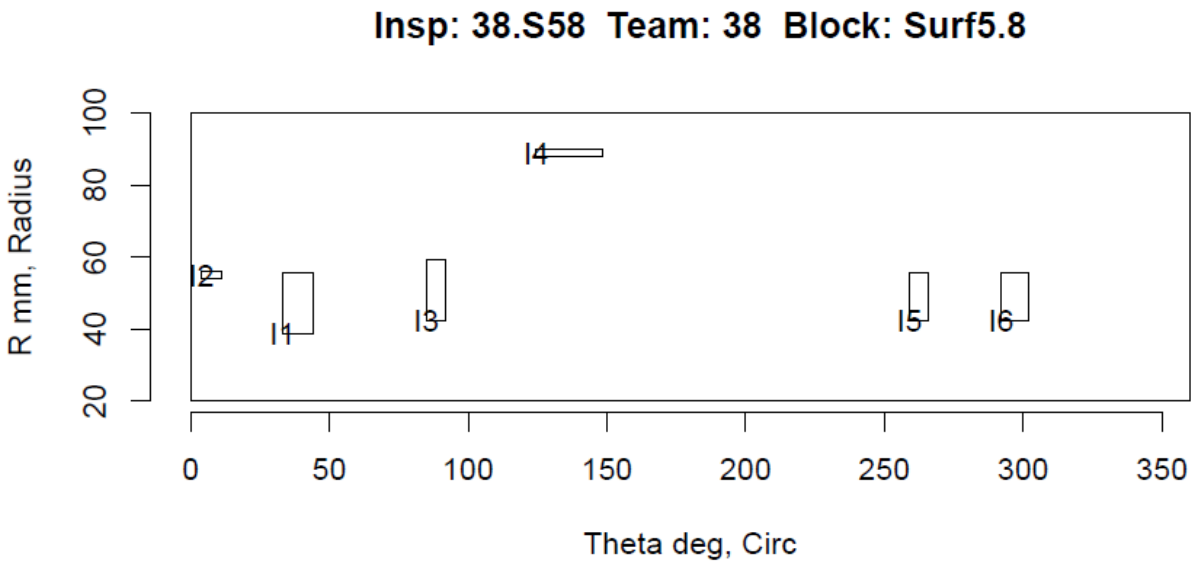
Insp: 38.S58 Team: 38 Block: Surf5.8
R mm, Radius
20
40
60
80
100
I4
I2
I1
I3
I5
I6
0
50
100
150
200
250
300
350
Theta deg, Circ

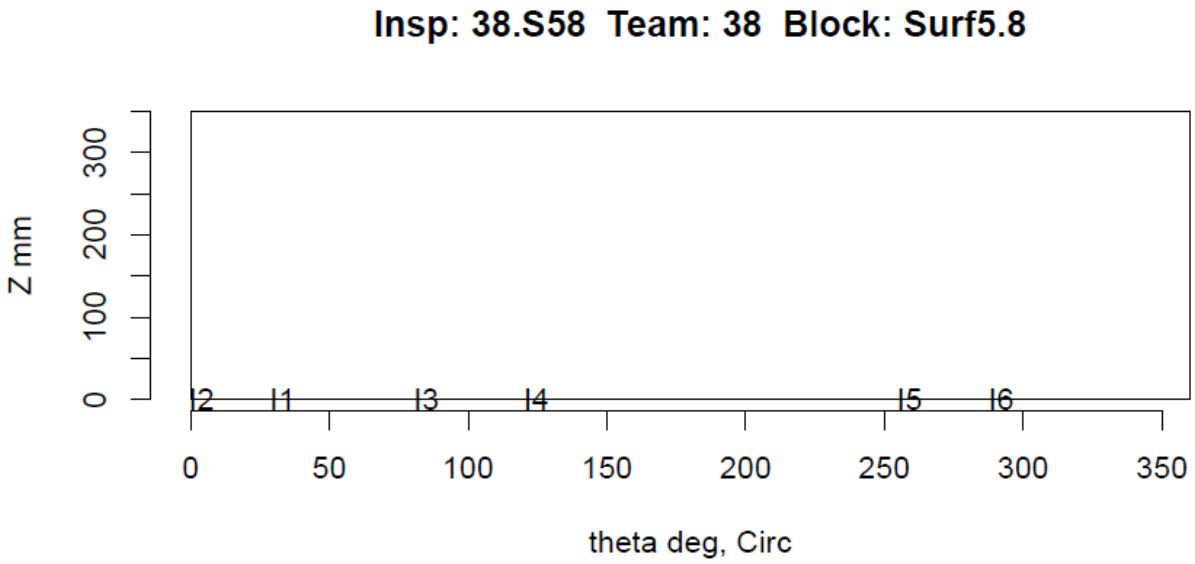
Insp: 38.S58 Team: 38 Block: Surf5.8
Z mm
0
100
200
300
I2
I1
I3
I4
I5
I6
0
50
100
150
200
250
300
350
theta deg, Circ

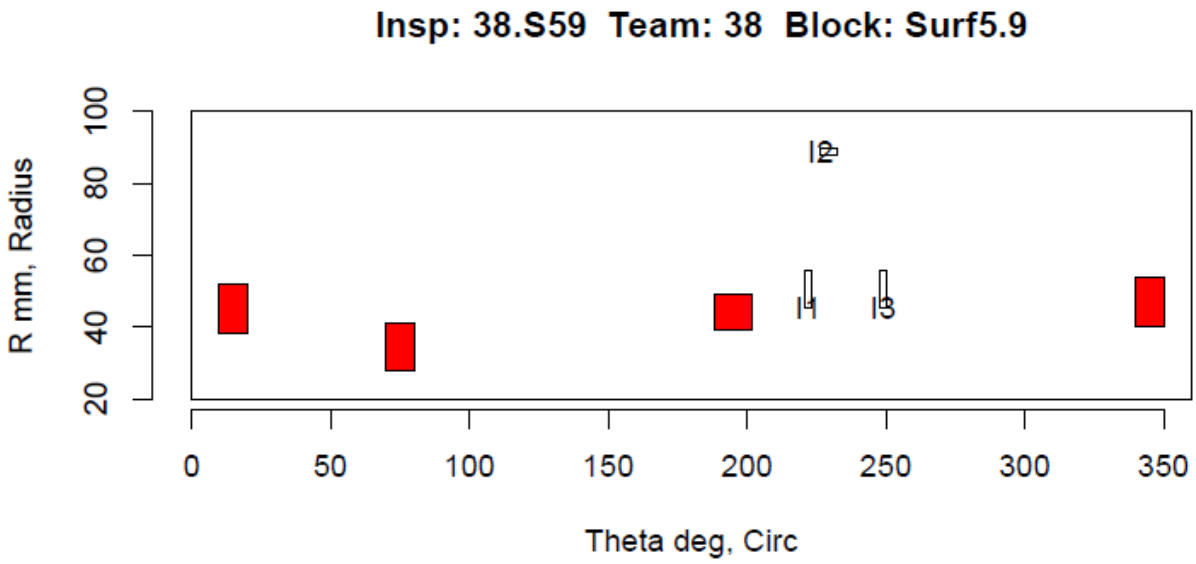
Insp: 38.S59 Team: 38 Block: Surf5.9
R mm, Radius
20
40
60
80
100
0
50
100
150
200
250
300
350
Theta deg, Circ

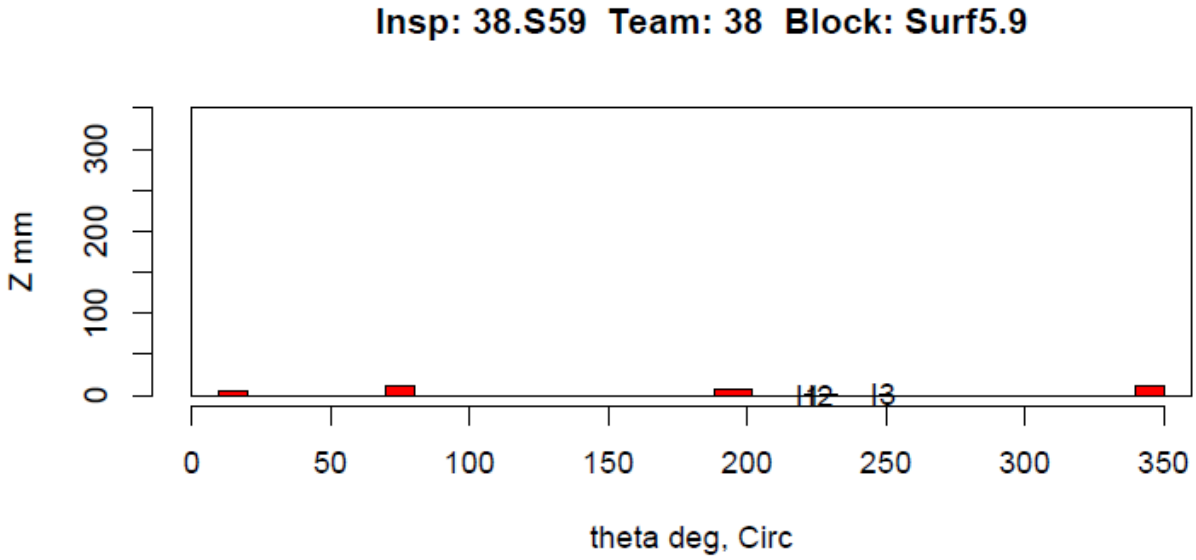
Insp: 38.S59 Team: 38 Block: Surf5.9
Z mm
0
100
200
300
0
50
100
150
200
250
300
350
theta deg, Circ

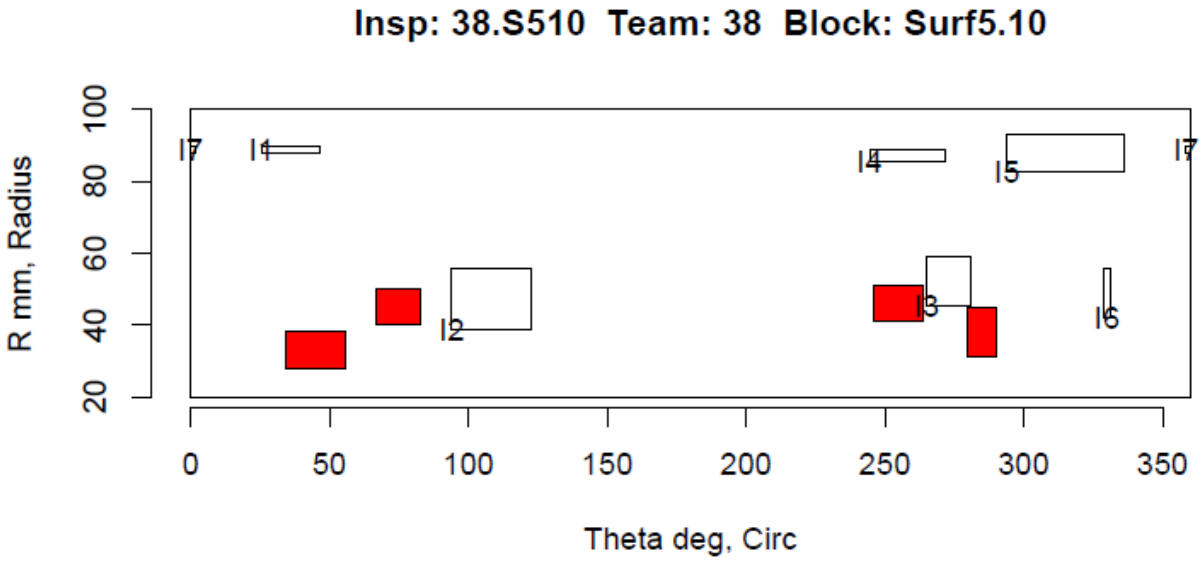
Insp: 38.S510 Team: 38 Block: Surf5.10
R mm, Radius
20
40
60
80
100
I7
I1
I4
I5
I7
I2
I3
I6
0
50
100
150
200
250
300
350
Theta deg, Circ

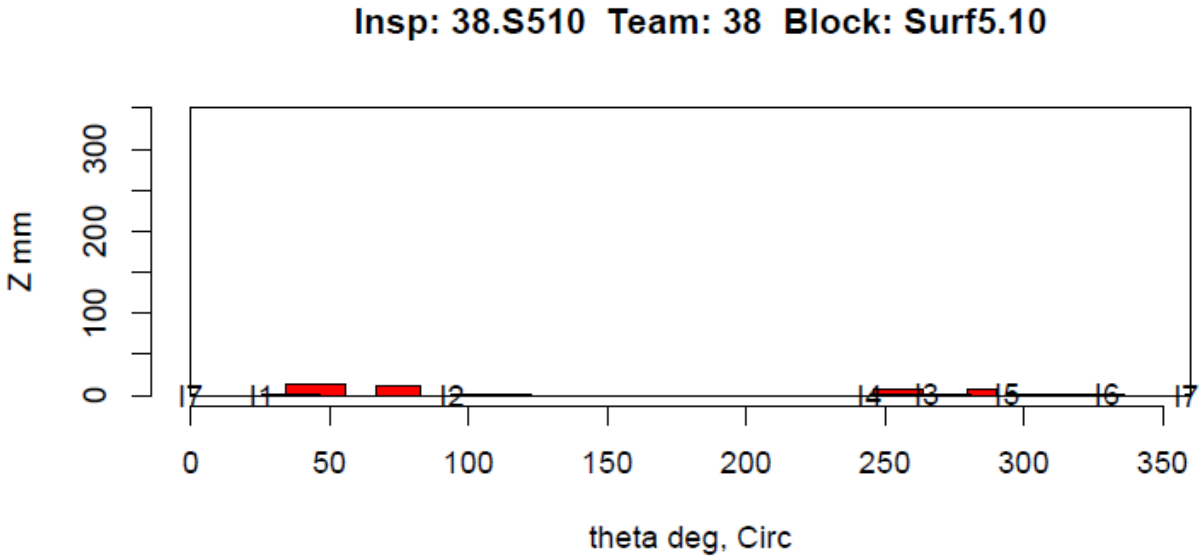
Insp: 38.S510 Team: 38 Block: Surf5.10
Z mm
0
100
200
300
I7
I1
I2
I4
I3
I5
I6
I7
0
50
100
150
200
250
300
350
theta deg, Circ

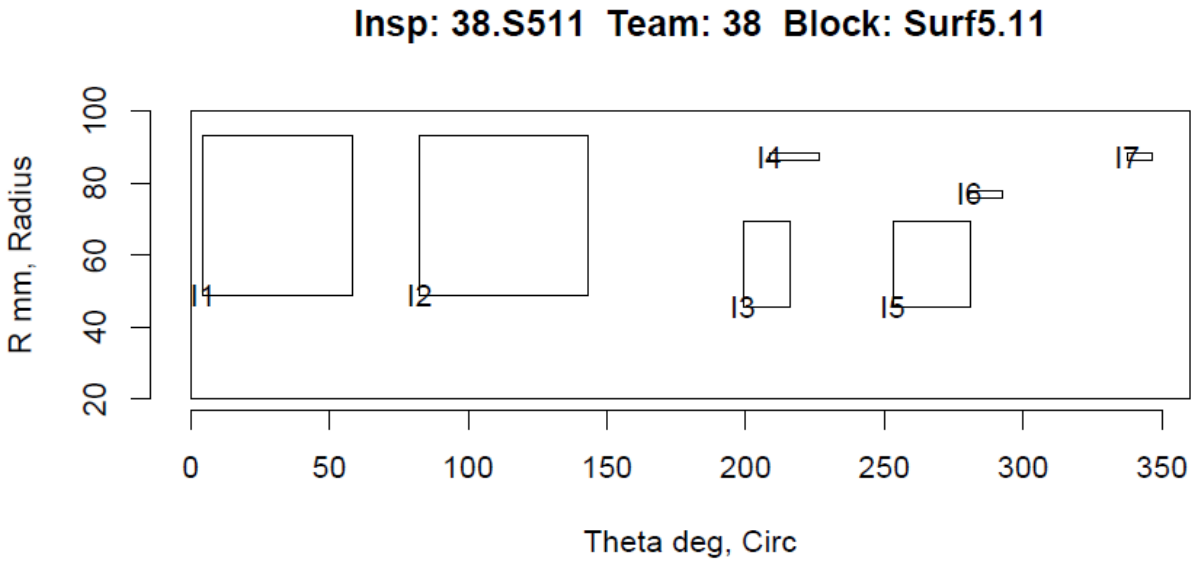
Insp: 38.S511 Team: 38 Block: Surf5.11
R mm, Radius
20
40
60
80
100
I1
I2
I3
I4
I5
I6
I7
0
50
100
150
200
250
300
350
Theta deg, Circ

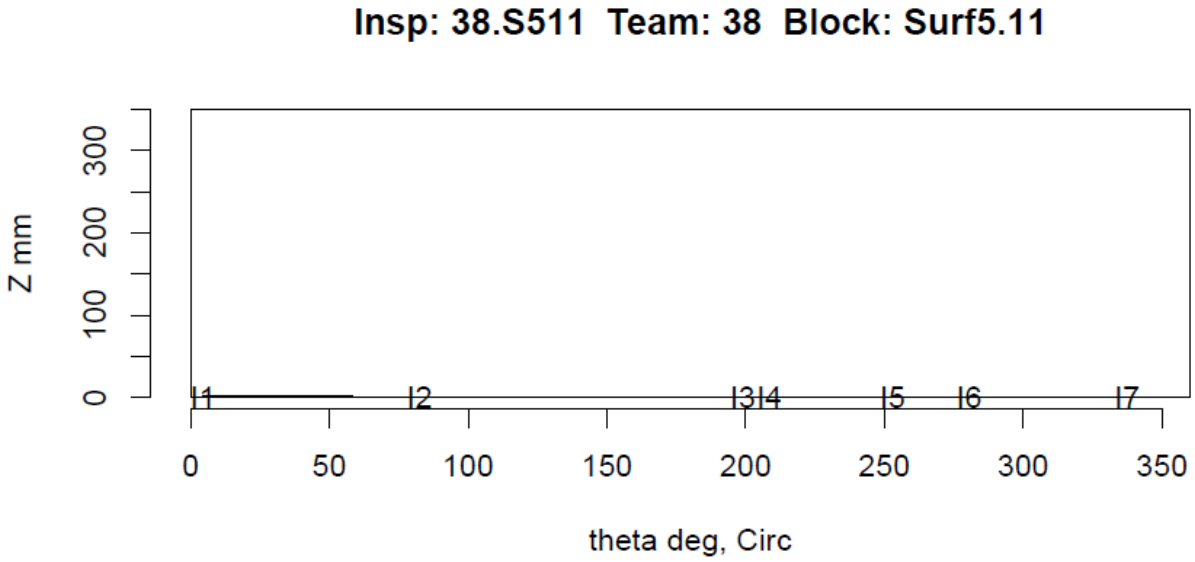
Insp: 38.S511 Team: 38 Block: Surf5.11
Z mm
0
100
200
300
I1
I2
I3I4
I5
I6
I7
0
50
100
150
200
250
300
350
theta deg, Circ

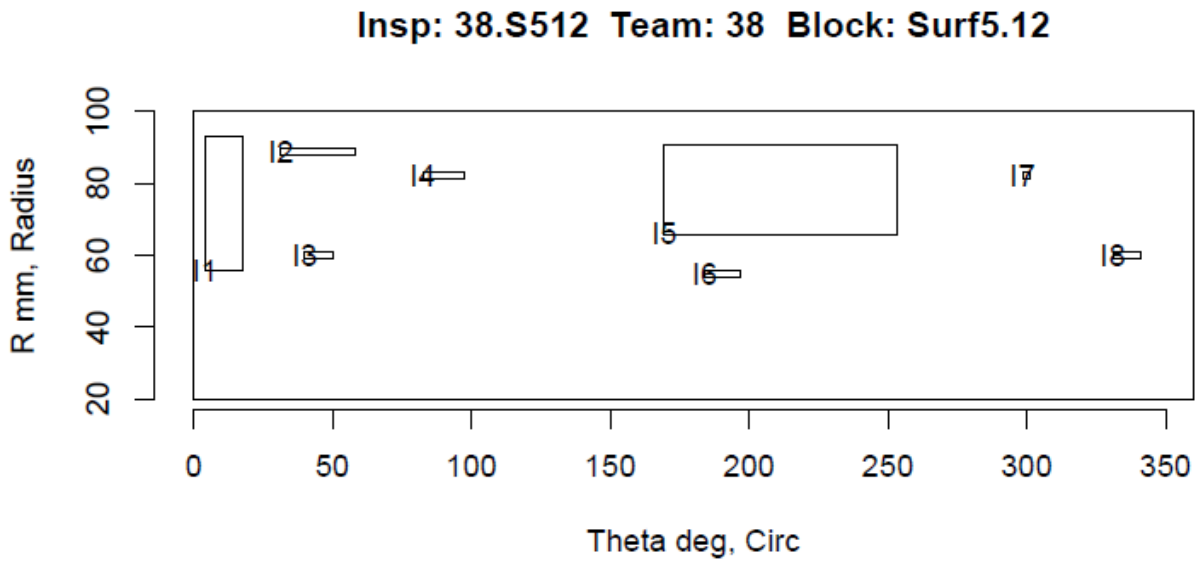
Insp: 38.S512 Team: 38 Block: Surf5.12
R mm, Radius
20
40
60
80
100
0
50
100
150
200
250
300
350
Theta deg, Circ
1
2
3
4
5
6
7
8

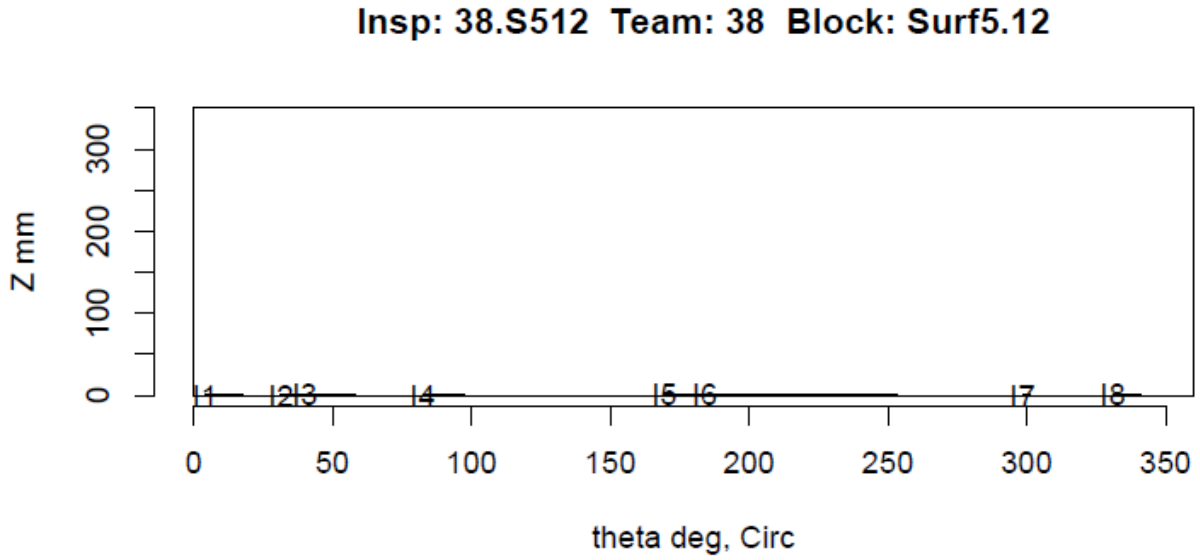
Insp: 38.S512 Team: 38 Block: Surf5.12
Z mm
0
100
200
300
0
50
100
150
200
250
300
350
theta deg, Circ
1
2
3
4
5
6
7
8

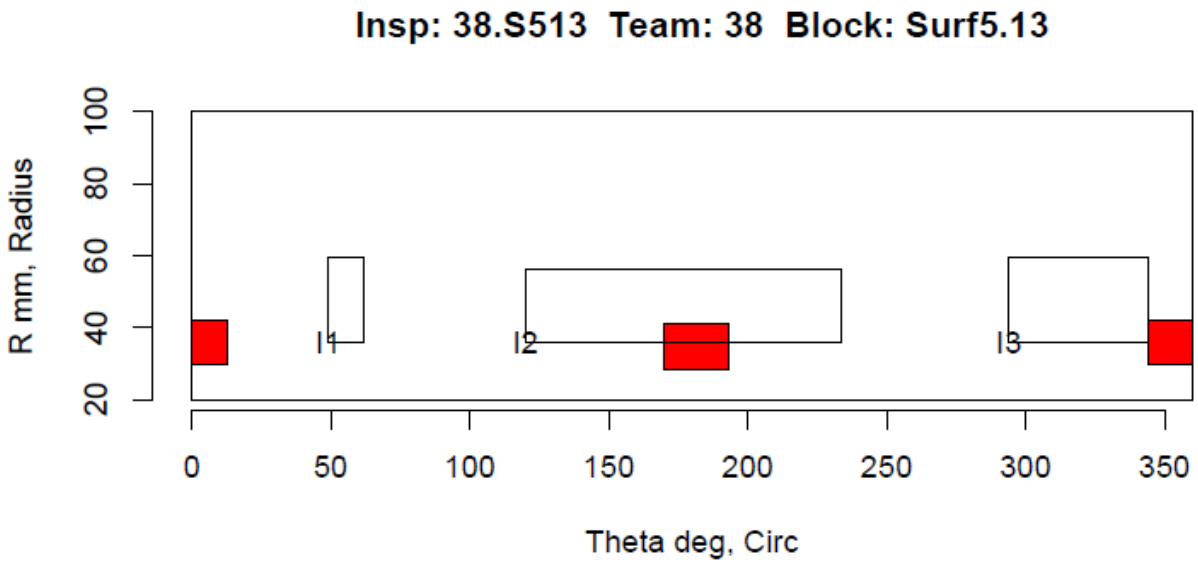
Insp: 38.S513 Team: 38 Block: Surf5.13
R mm, Radius
20
40
60
80
100
I1
I2
I3
0
50
100
150
200
250
300
350
Theta deg, Circ

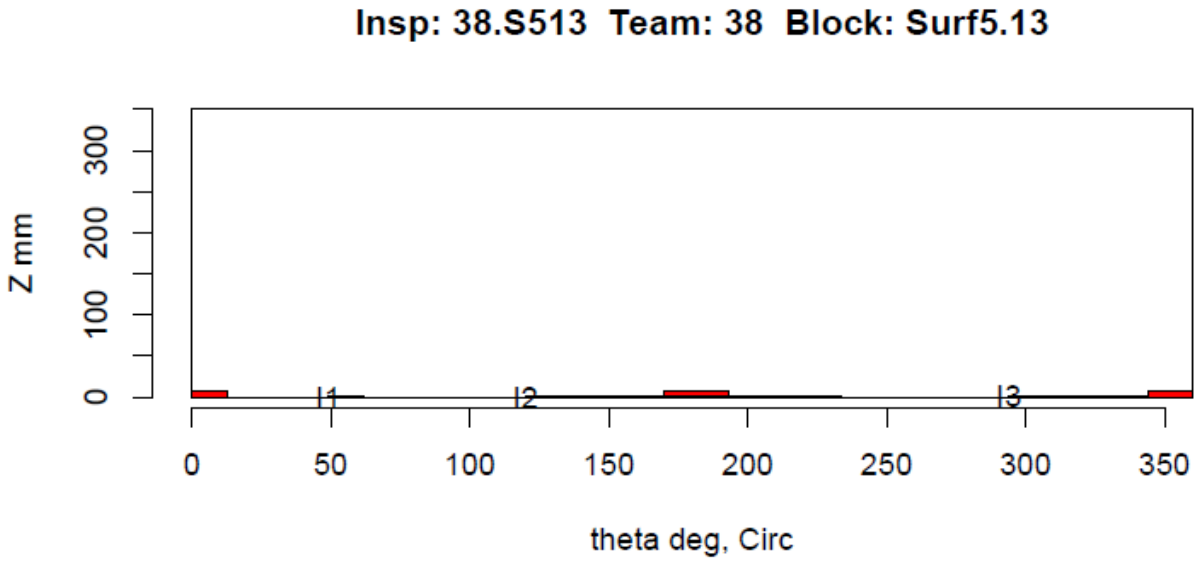
Insp: 38.S513 Team: 38 Block: Surf5.13
Z mm
0
100
200
300
I1
I2
I3
0
50
100
150
200
250
300
350
theta deg, Circ

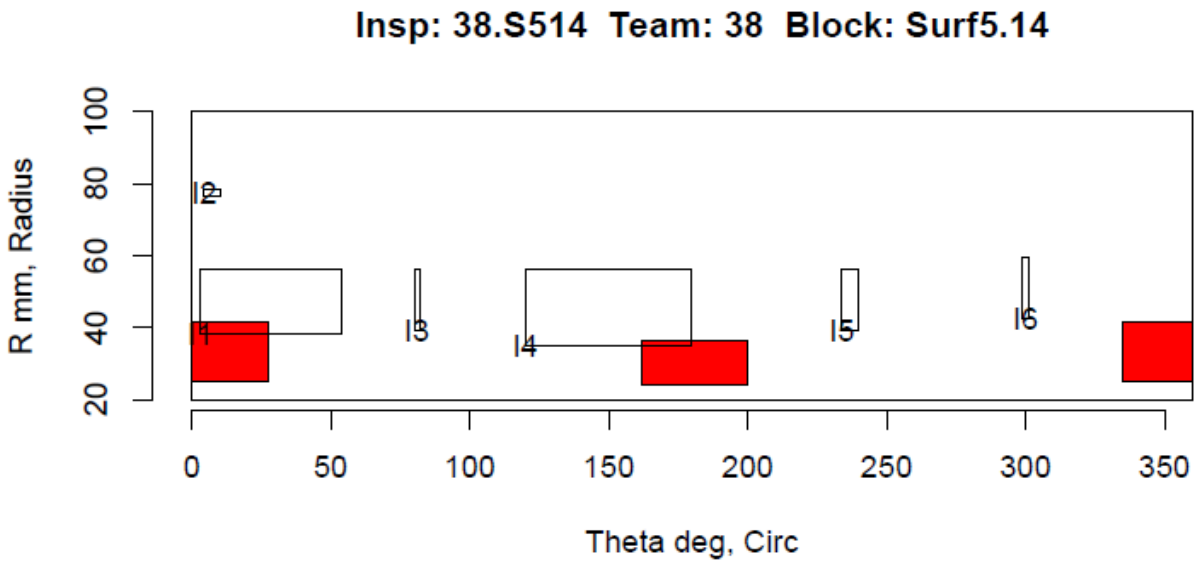
Insp: 38.S514 Team: 38 Block: Surf5.14
R mm, Radius
20
40
60
80
100
0
50
100
150
200
250
300
350
Theta deg, Circ

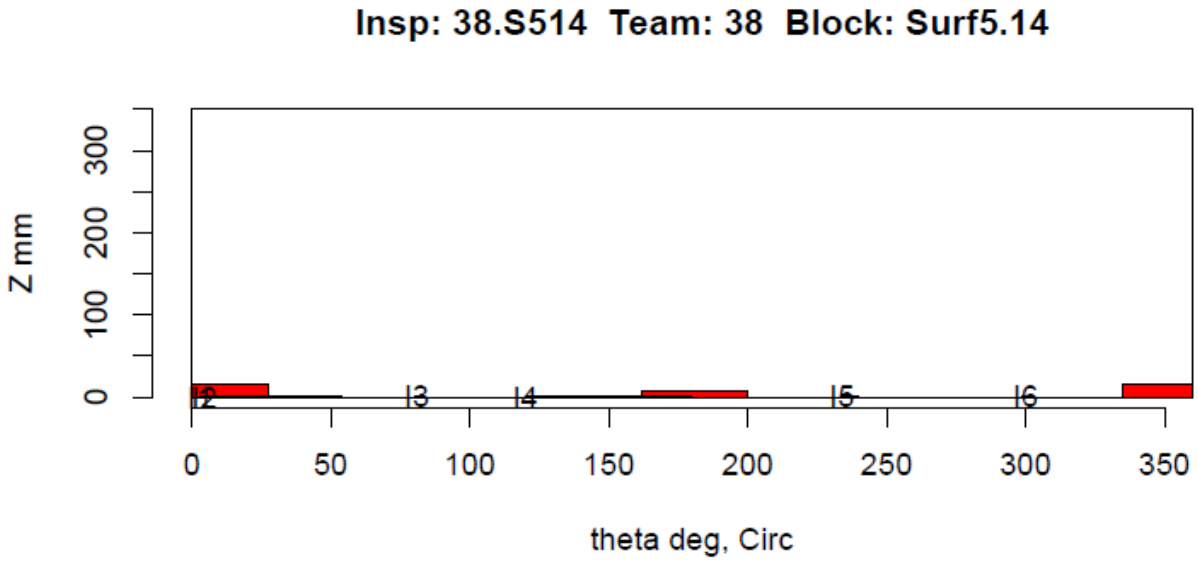
Insp: 38.S514 Team: 38 Block: Surf5.14
Z mm
0
100
200
300
0
50
100
150
200
250
300
350
theta deg, Circ

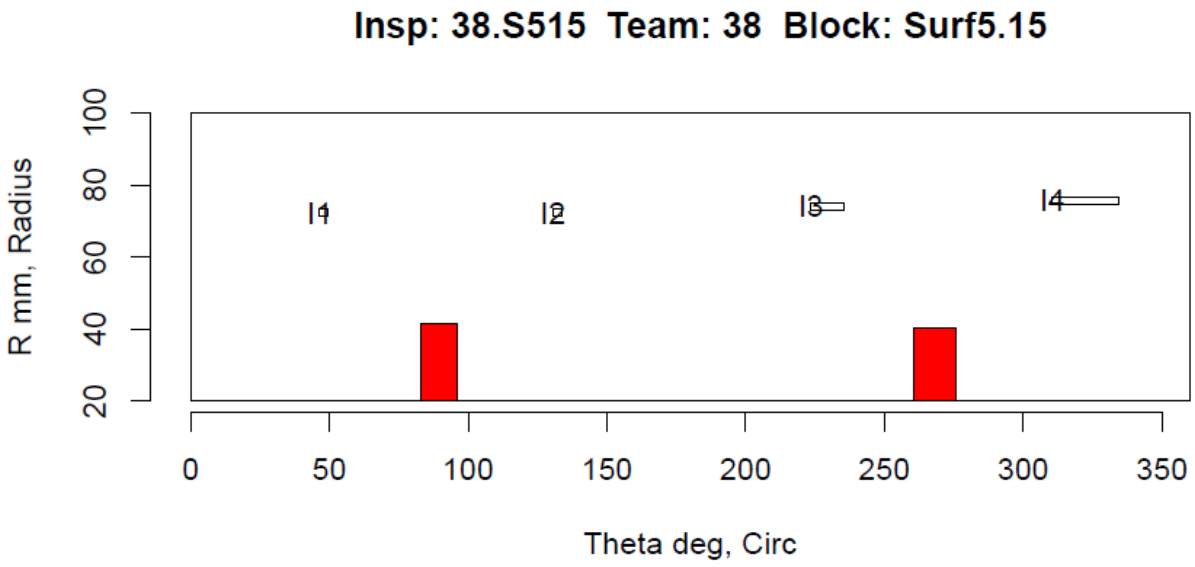
Insp: 38.S515 Team: 38 Block: Surf5.15
R mm, Radius
20
40
60
80
100
I1
I2
I3
I4
0
50
100
150
200
250
300
350
Theta deg, Circ

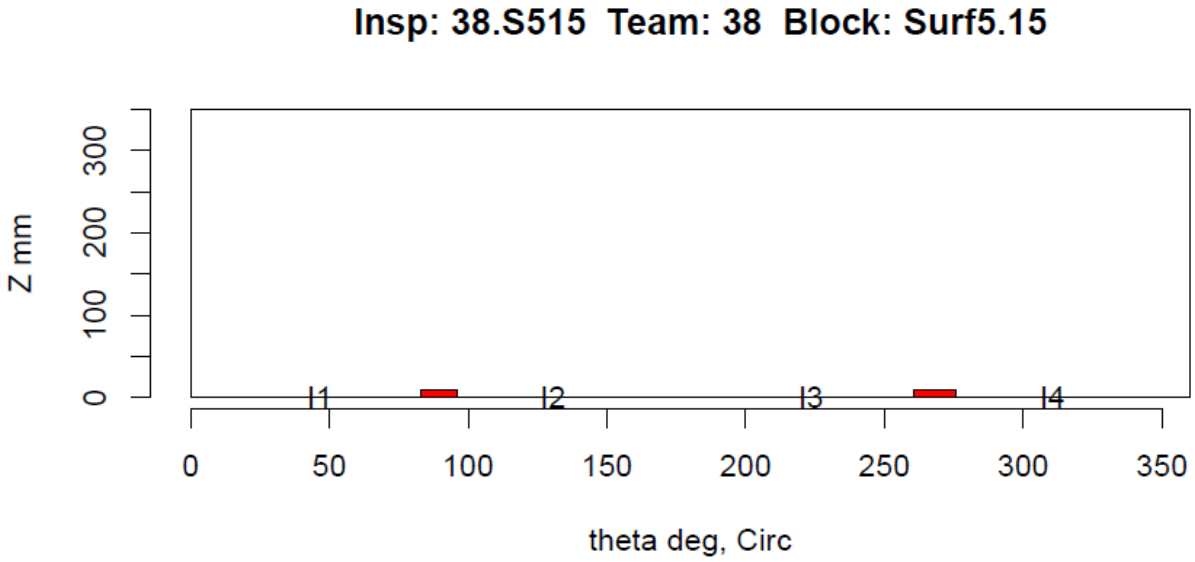
Insp: 38.S515 Team: 38 Block: Surf5.15
Z mm
0
100
200
300
I1
I2
I3
I4
0
50
100
150
200
250
300
350
theta deg, Circ

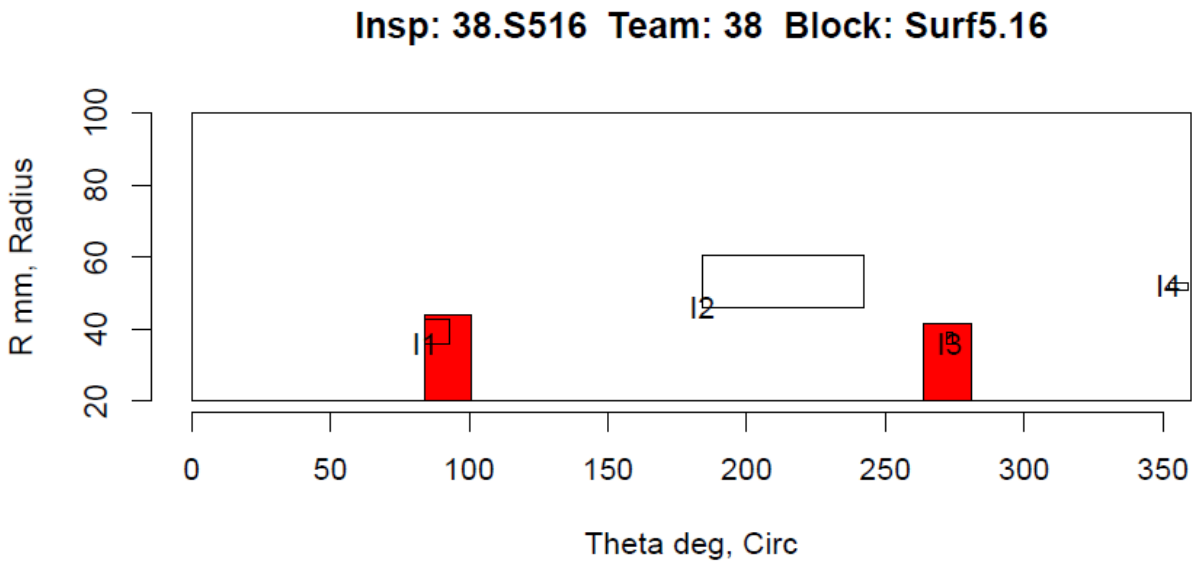
Insp: 38.S516 Team: 38 Block: Surf5.16
R mm, Radius
20
40
60
80
100
I1
I2
I3
I4
0
50
100
150
200
250
300
350
Theta deg, Circ

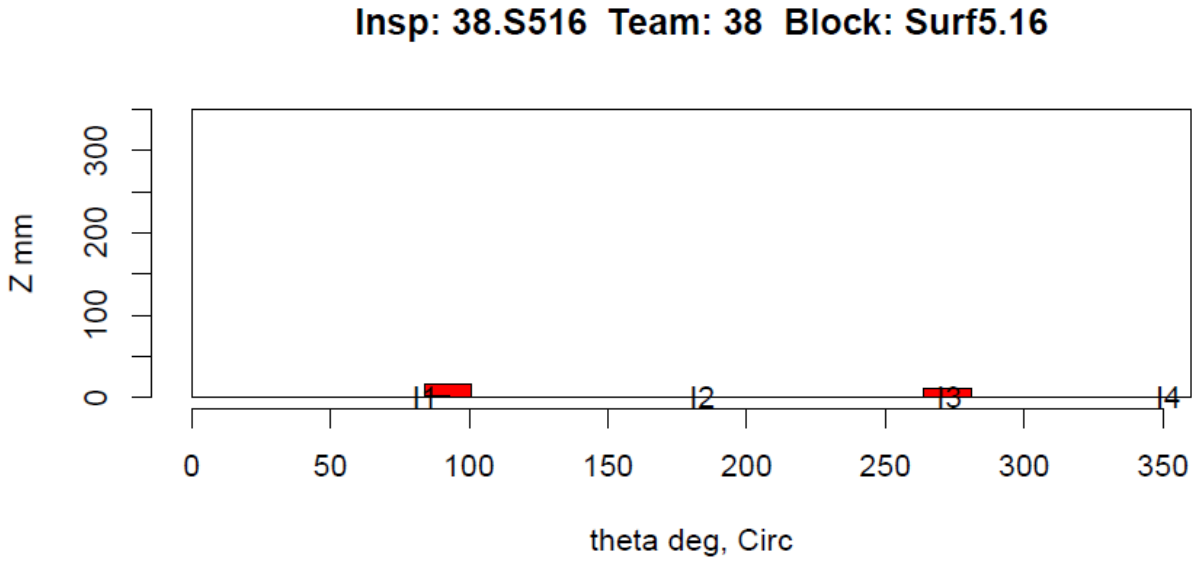
Insp: 38.S516 Team: 38 Block: Surf5.16
Z mm
0
100
200
300
I1
I2
I3
I4
0
50
100
150
200
250
300
350
theta deg, Circ

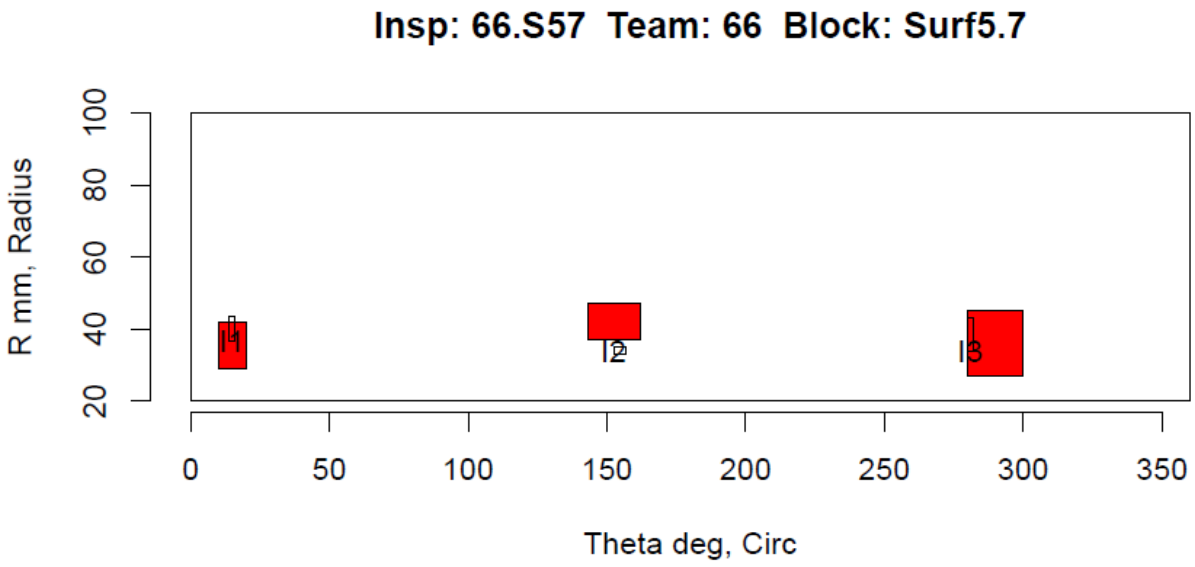
Insp: 66.S57 Team: 66 Block: Surf5.7
R mm, Radius
20
40
60
80
100
0
50
100
150
200
250
300
350
Theta deg, Circ
I1
I2
I3

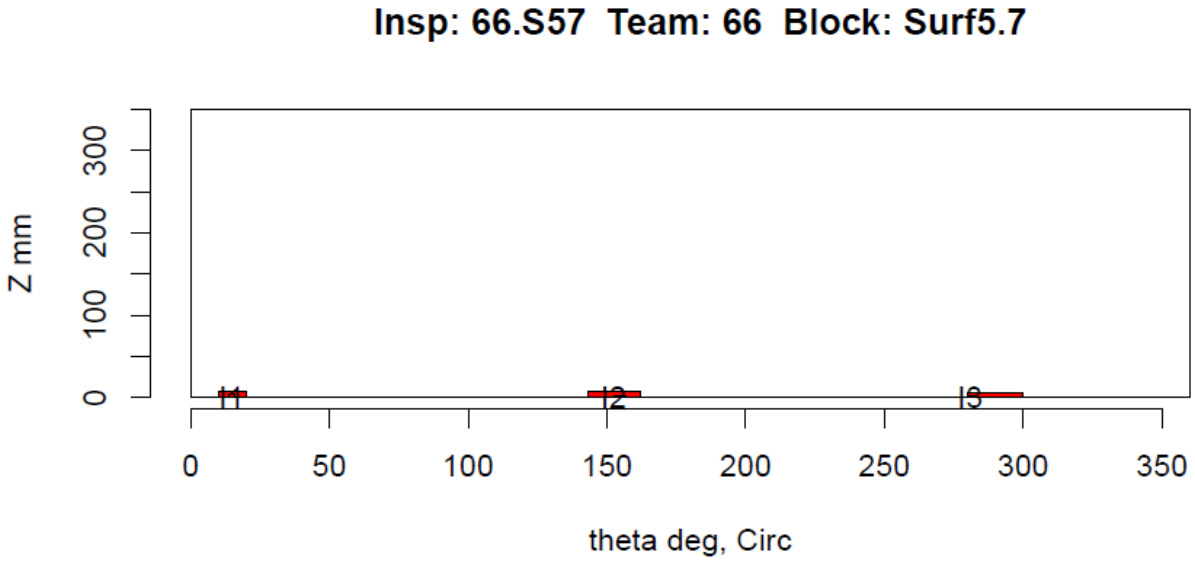
Insp: 66.S57 Team: 66 Block: Surf5.7
Z mm
0
100
200
300
0
50
100
150
200
250
300
350
theta deg, Circ
I1
I2
I3

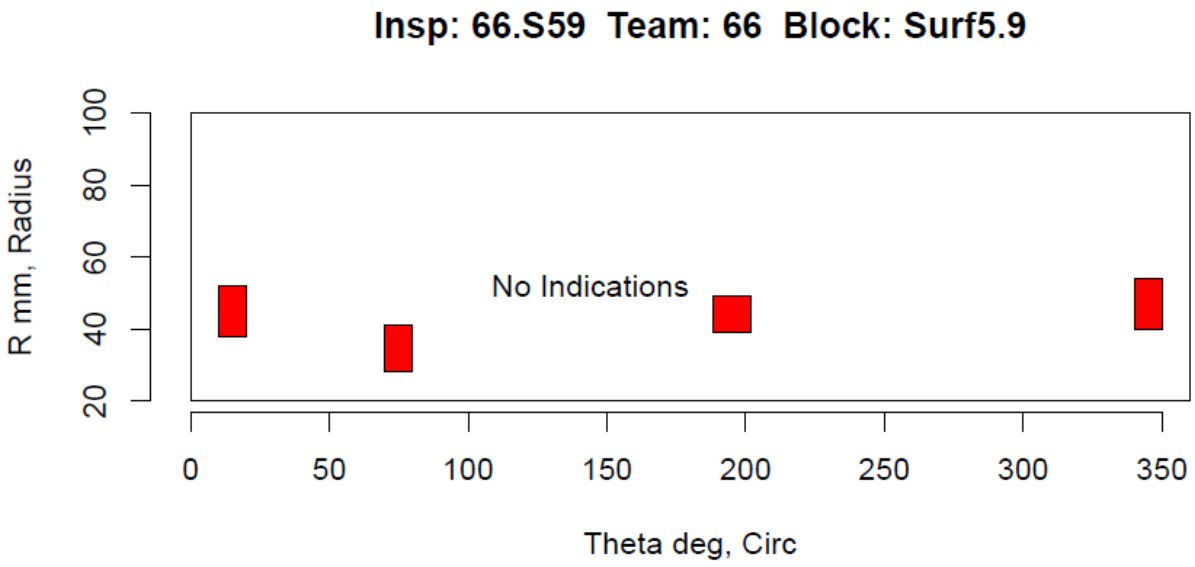
Insp: 66.S59 Team: 66 Block: Surf5.9
R mm, Radius
20
40
60
80
100
No Indications
0
50
100
150
200
250
300
350
Theta deg, Circ

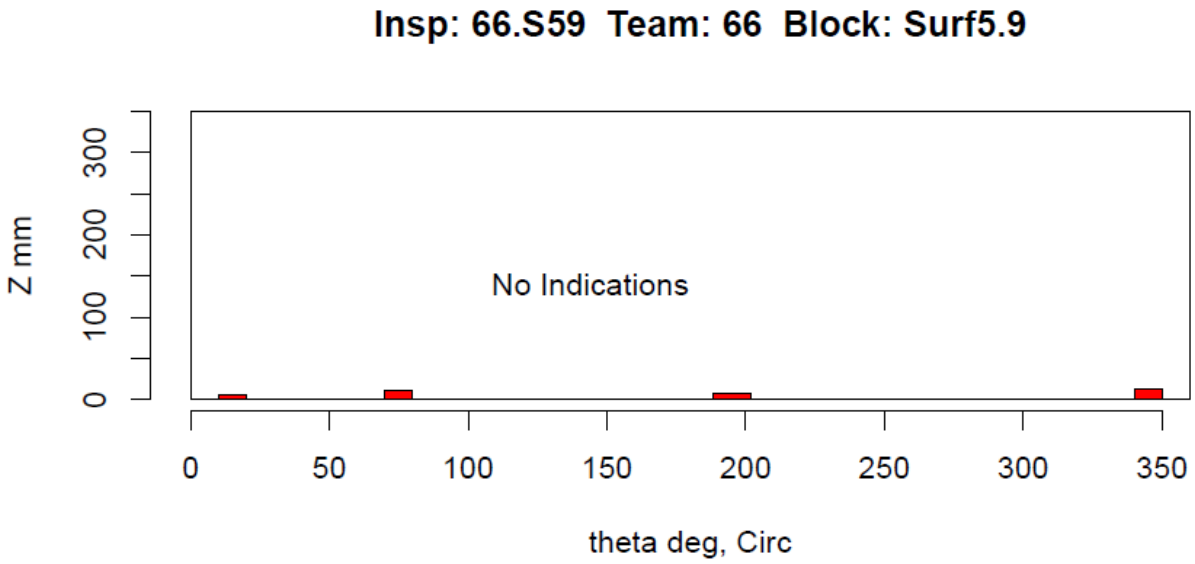
Insp: 66.S59 Team: 66 Block: Surf5.9
Z mm
0
100
200
300
No Indications
0
50
100
150
200
250
300
350
theta deg, Circ

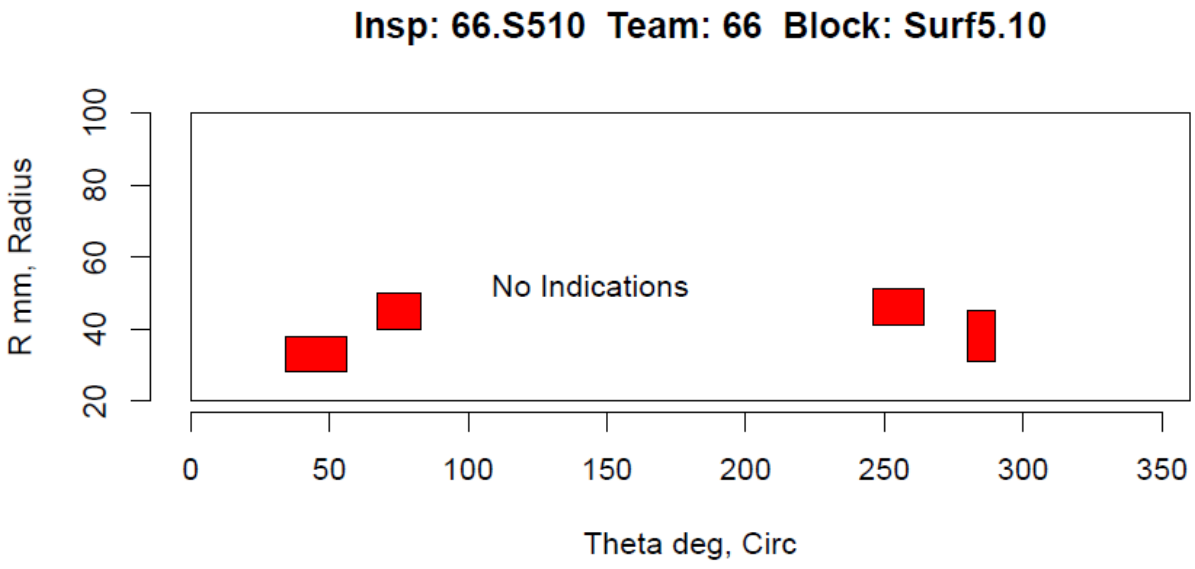
Insp: 66.S510 Team: 66 Block: Surf5.10
R mm, Radius
20
40
60
80
100
No Indications
0
50
100
150
200
250
300
350
Theta deg, Circ

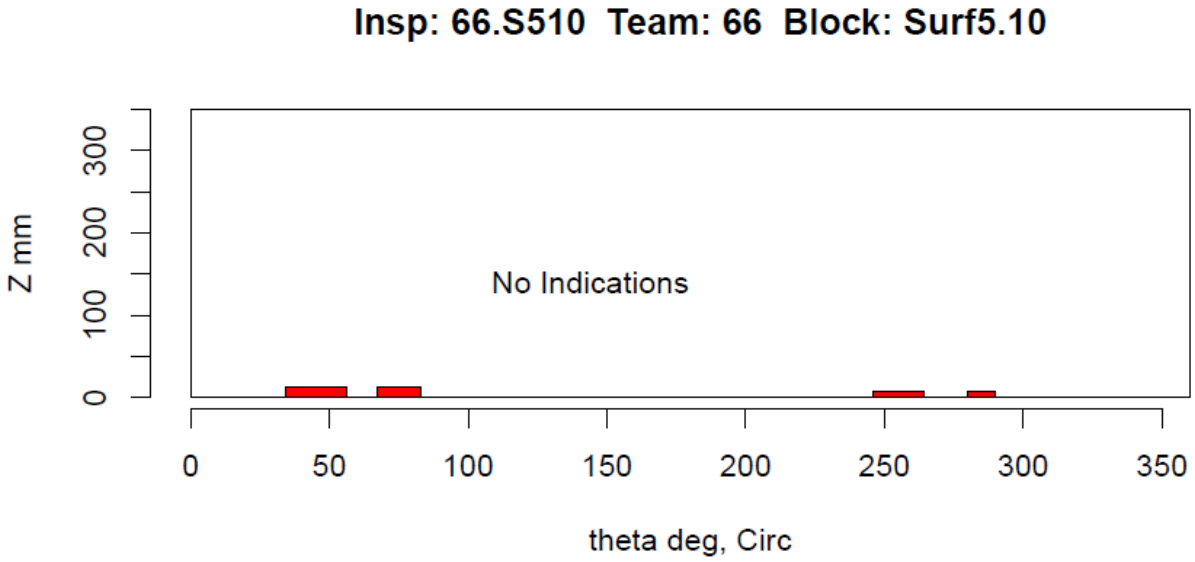
Insp: 66.S510 Team: 66 Block: Surf5.10
Z mm
0
100
200
300
No Indications
0
50
100
150
200
250
300
350
theta deg, Circ

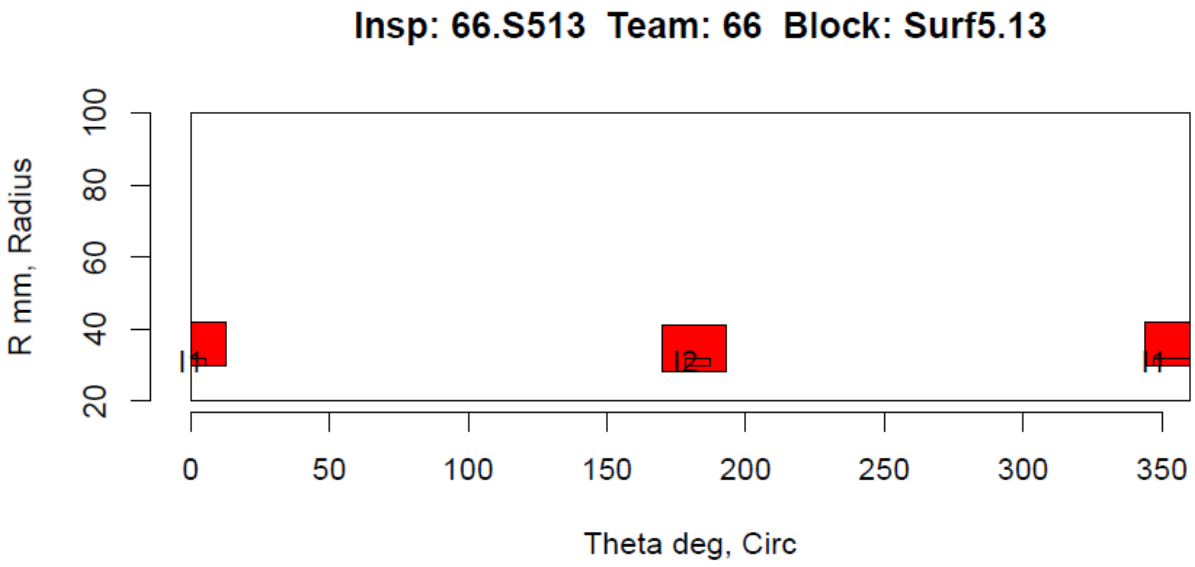
Insp: 66.S513 Team: 66 Block: Surf5.13
R mm, Radius
20
40
60
80
100
I1
I2
I1
0
50
100
150
200
250
300
350
Theta deg, Circ

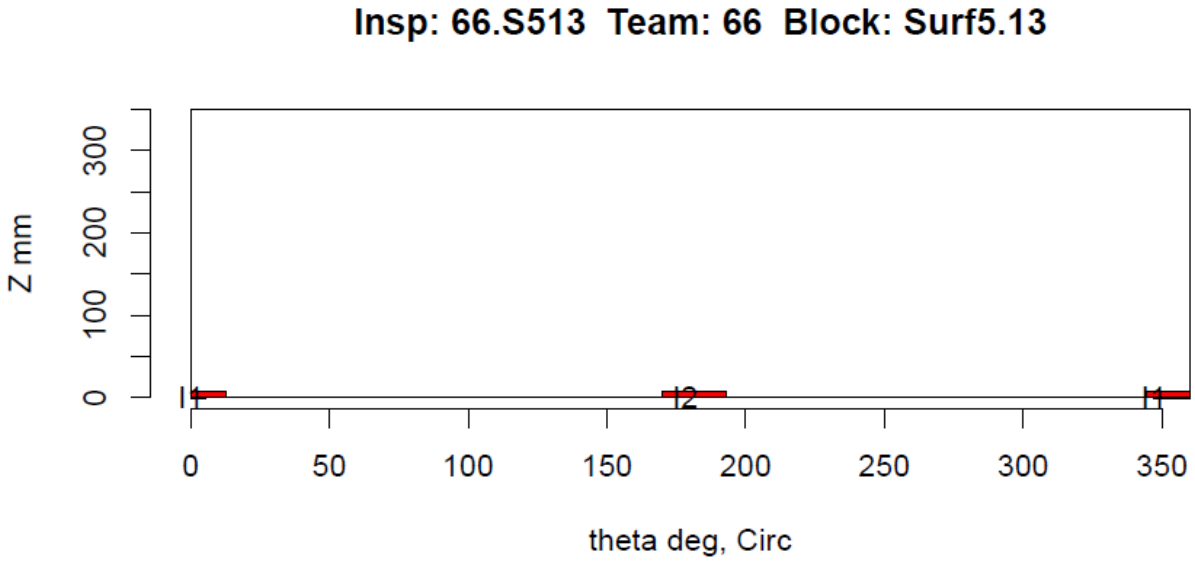
Insp: 66.S513 Team: 66 Block: Surf5.13
Z mm
0
100
200
300
I1
I2
I1
0
50
100
150
200
250
300
350
theta deg, Circ

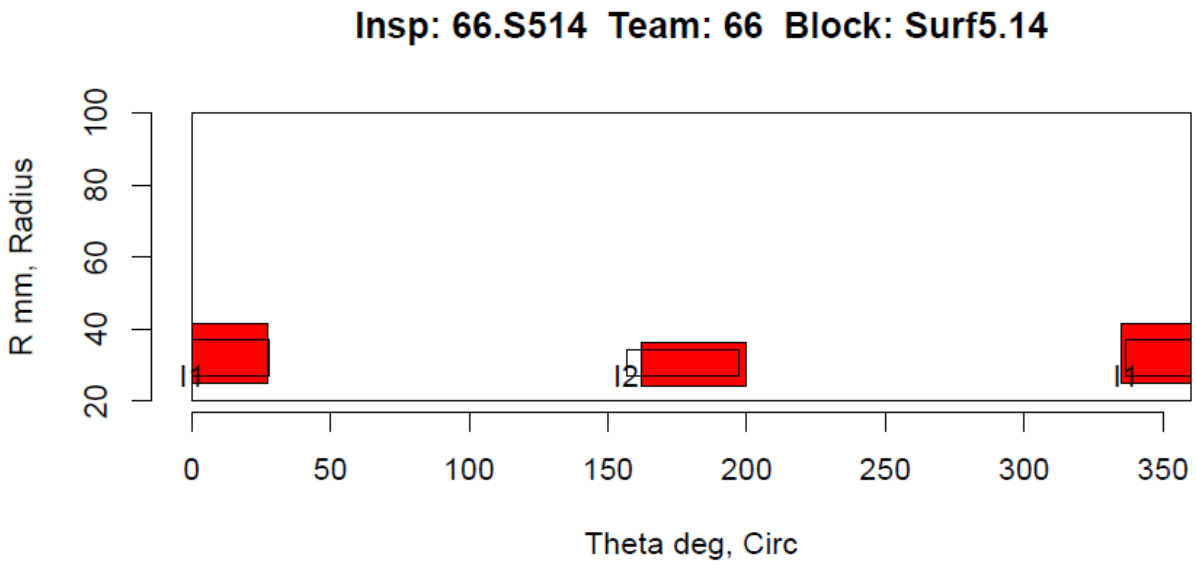
Insp: 66.S514 Team: 66 Block: Surf5.14
R mm, Radius
20
40
60
80
100
0
50
100
150
200
250
300
350
Theta deg, Circ
1
2
1

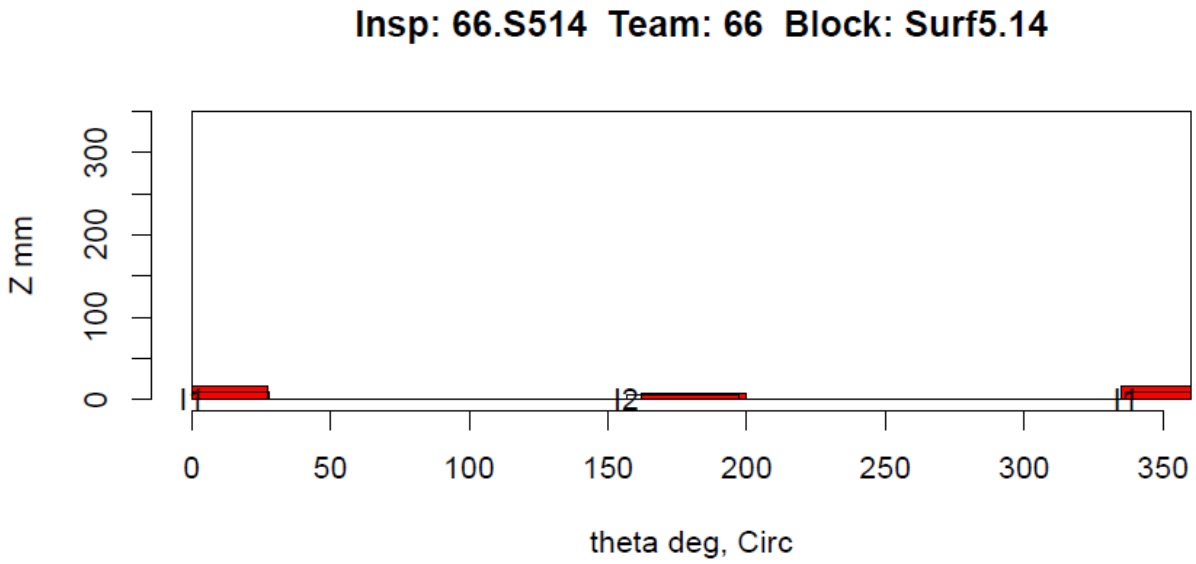
Insp: 66.S514 Team: 66 Block: Surf5.14
Z mm
0
100
200
300
0
50
100
150
200
250
300
350
theta deg, Circ
1
2
1

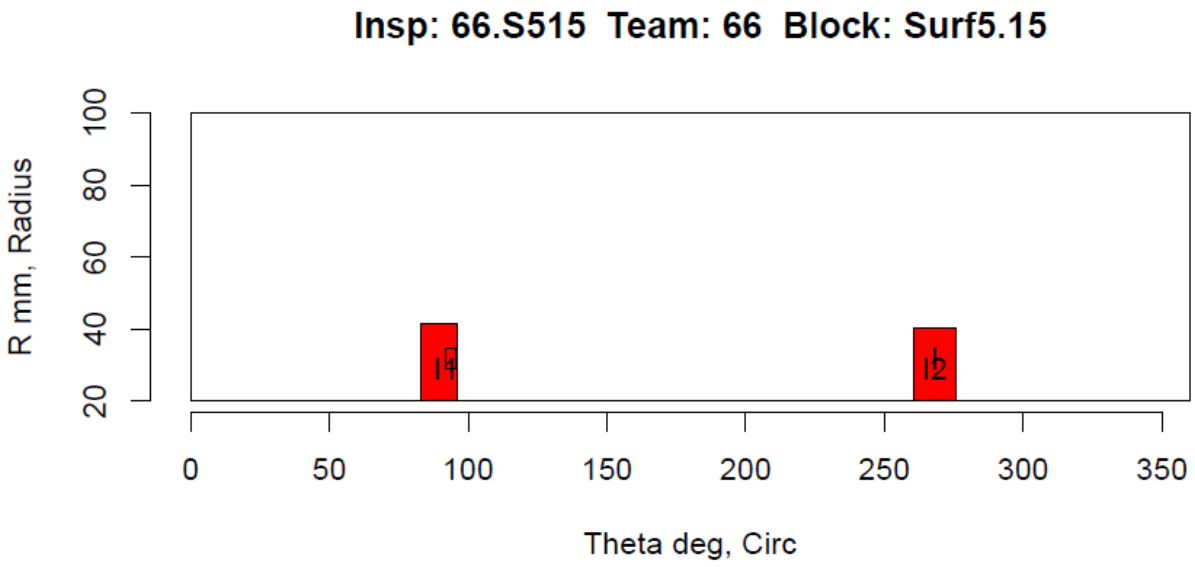
Insp: 66.S515 Team: 66 Block: Surf5.15
R mm, Radius
20
40
60
80
100
0
50
100
150
200
250
300
350
Theta deg, Circ

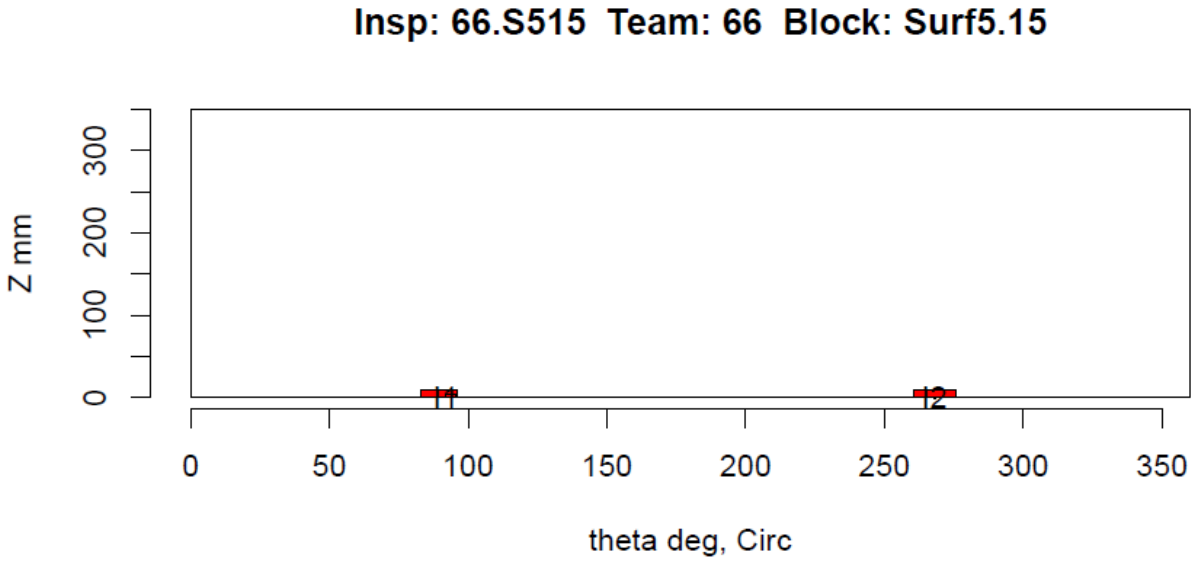
Insp: 66.S515 Team: 66 Block: Surf5.15
Z mm
0
100
200
300
0
50
100
150
200
250
300
350
theta deg, Circ

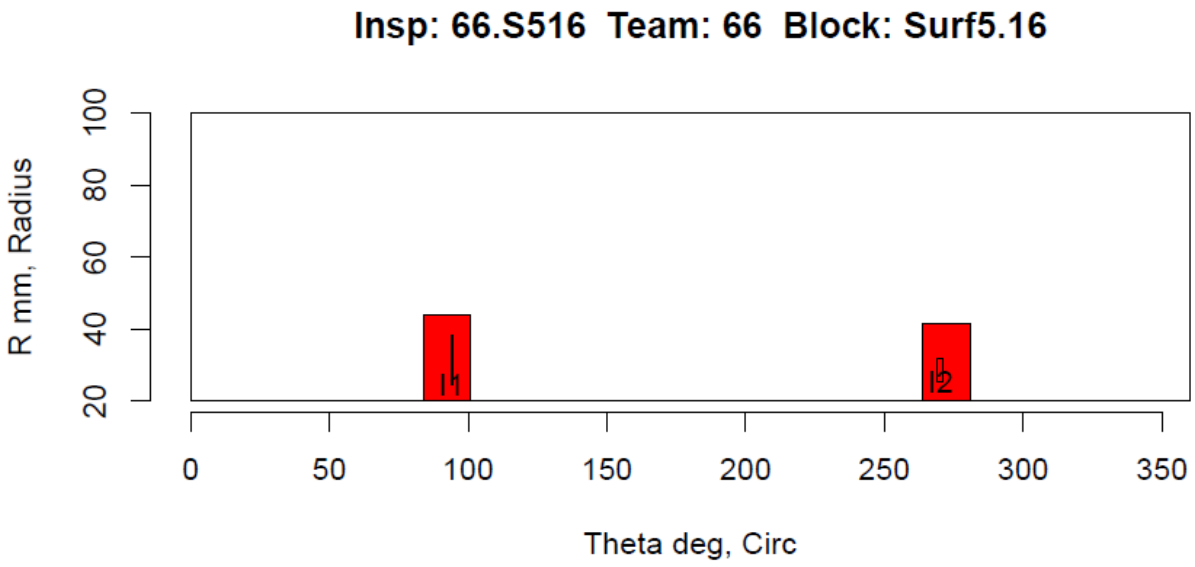
Insp: 66.S516 Team: 66 Block: Surf5.16
R mm, Radius
20
40
60
80
100
0
50
100
150
200
250
300
350
Theta deg, Circ

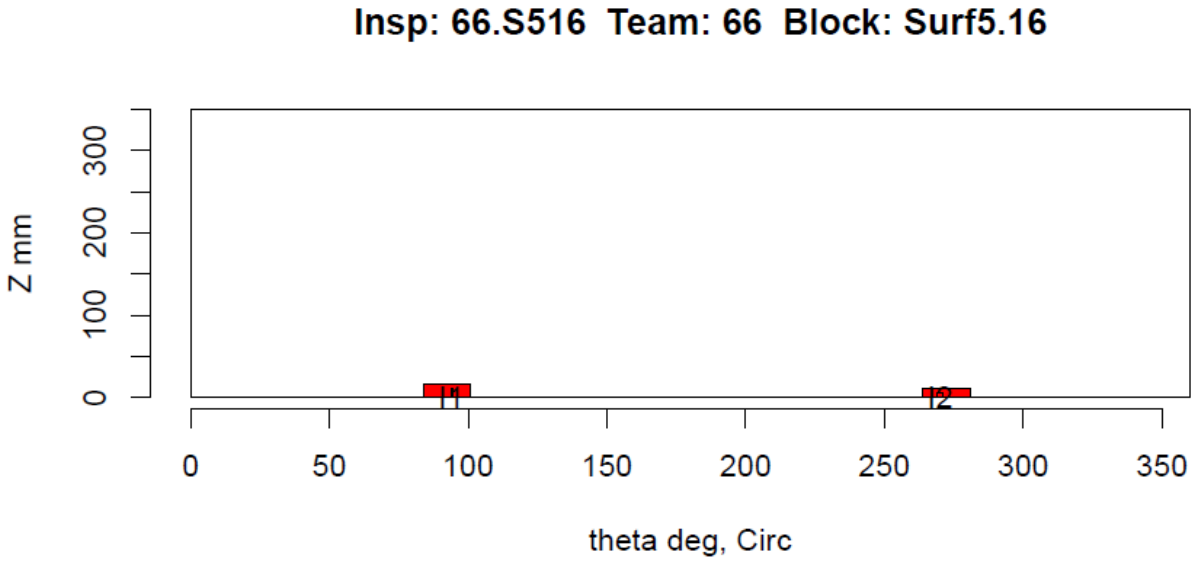
Insp: 66.S516 Team: 66 Block: Surf5.16
Z mm
0
100
200
300
0
50
100
150
200
250
300
350
theta deg, Circ

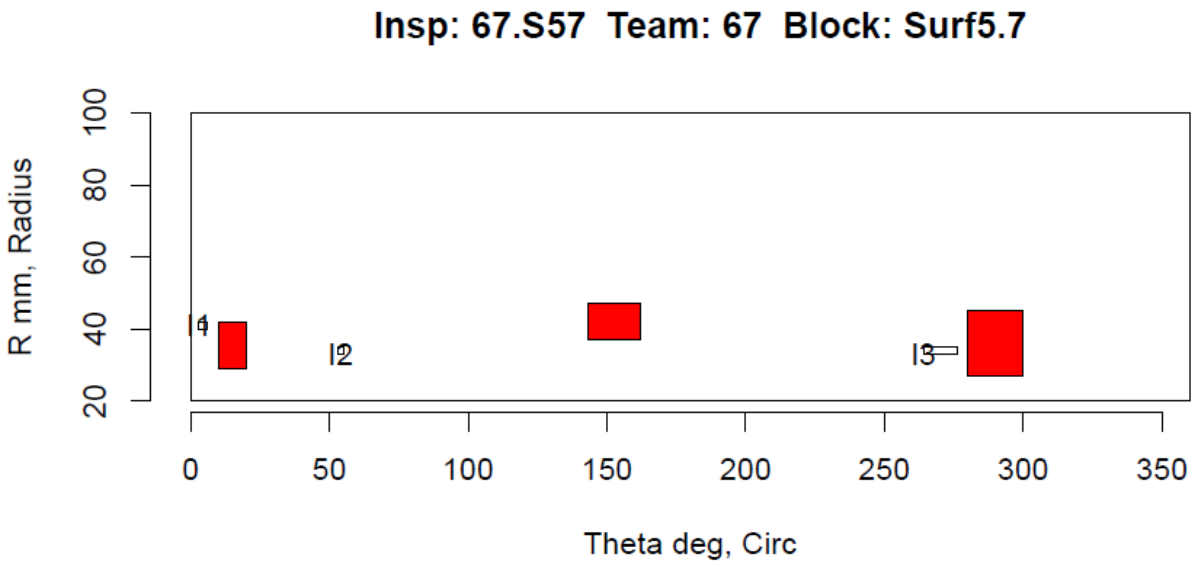
Insp: 67.S57 Team: 67 Block: Surf5.7
R mm, Radius
20
40
60
80
100
I4
I2
I3
0
50
100
150
200
250
300
350
Theta deg, Circ

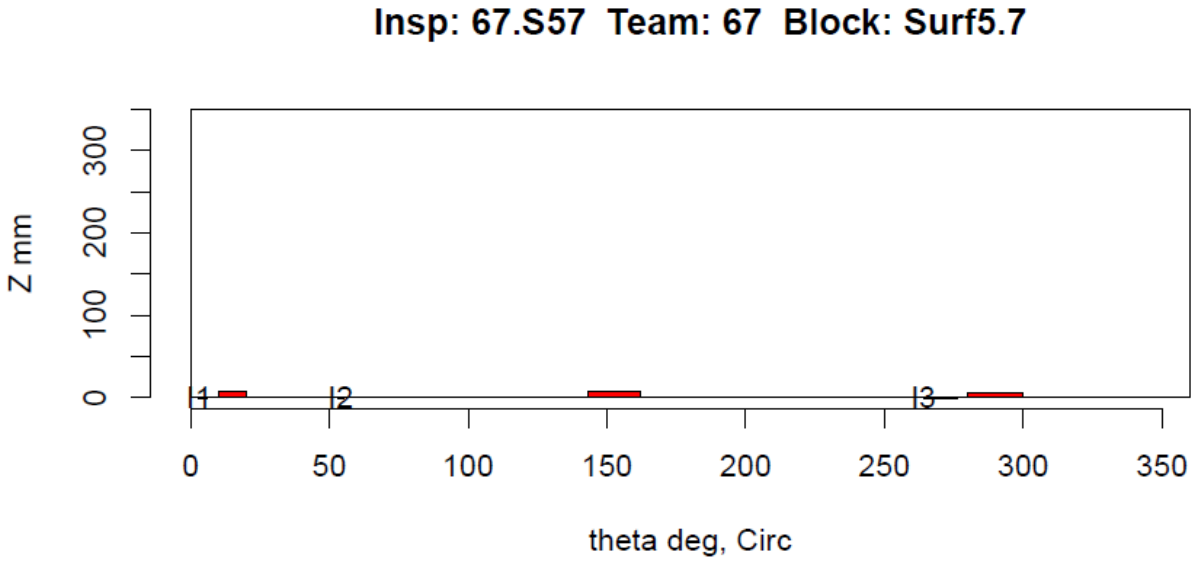
Insp: 67.S57 Team: 67 Block: Surf5.7
Z mm
0
100
200
300
I1
I2
I3
0
50
100
150
200
250
300
350
theta deg, Circ

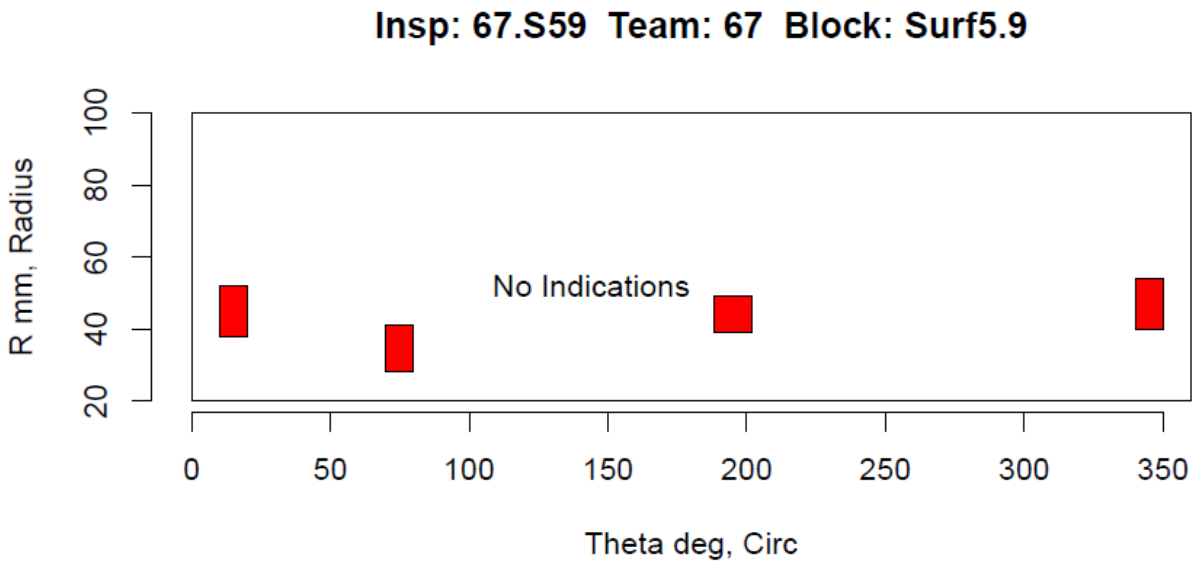
Insp: 67.S59 Team: 67 Block: Surf5.9
R mm, Radius
20
40
60
80
100
No Indications
0
50
100
150
200
250
300
350
Theta deg, Circ

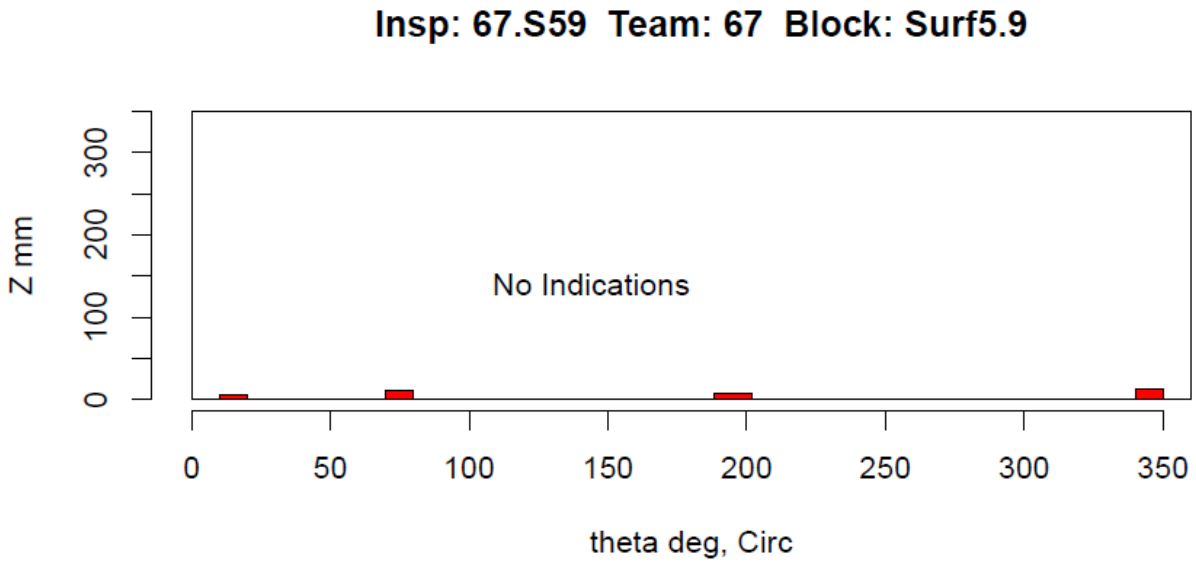
Insp: 67.S59 Team: 67 Block: Surf5.9
Z mm
0
100
200
300
No Indications
0
50
100
150
200
250
300
350
theta deg, Circ

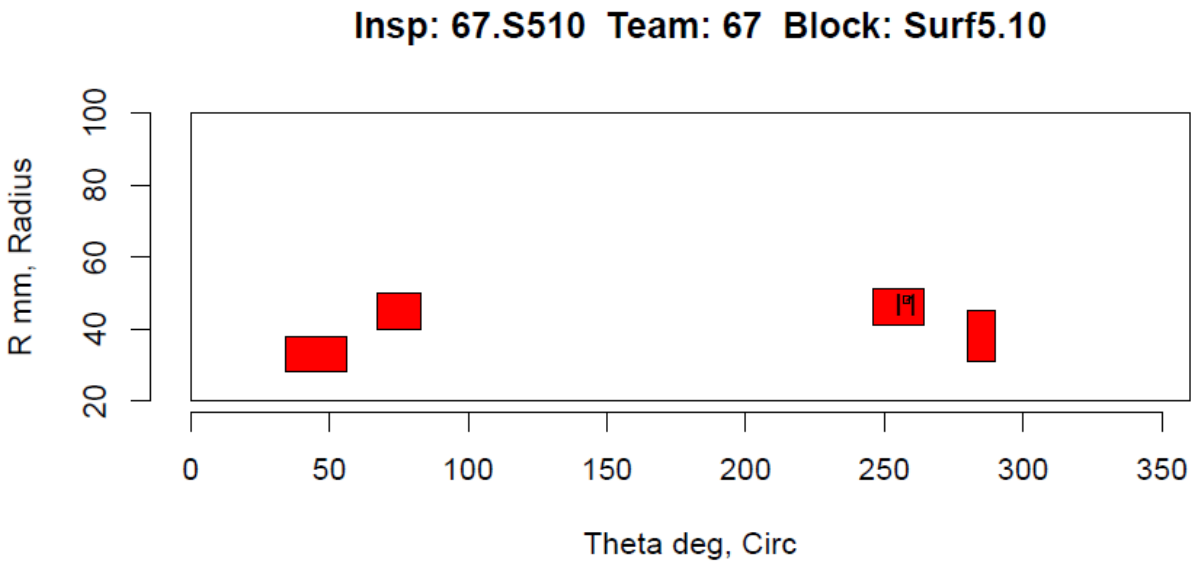
Insp: 67.S510 Team: 67 Block: Surf5.10
R mm, Radius
20
40
60
80
100
0
50
100
150
200
250
300
350
Theta deg, Circ

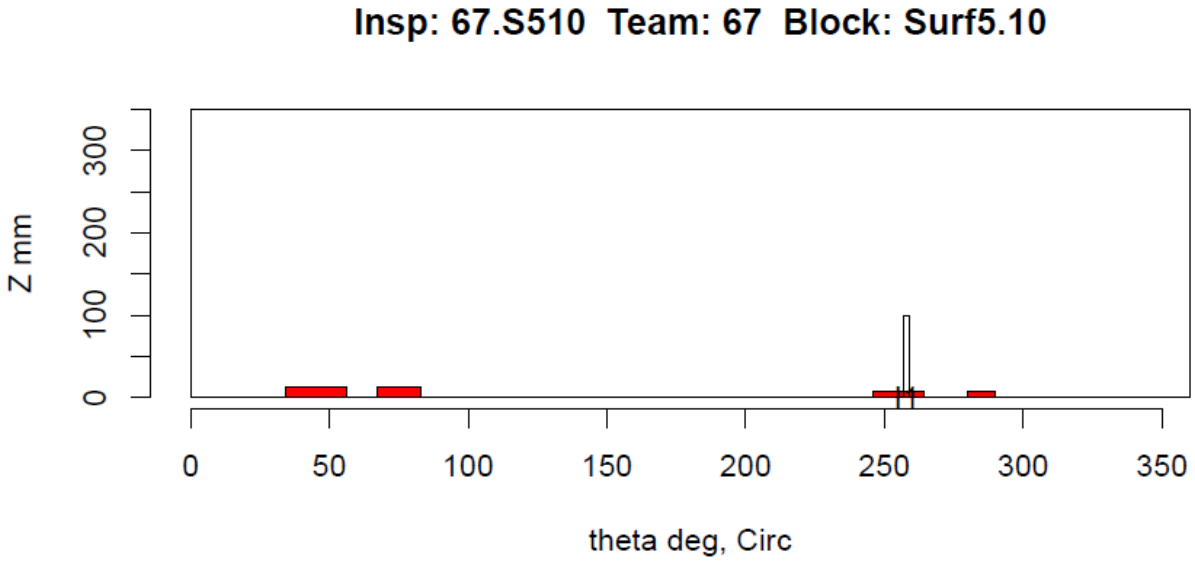
Insp: 67.S510 Team: 67 Block: Surf5.10
Z mm
0
100
200
300
0
50
100
150
200
250
300
350
theta deg, Circ

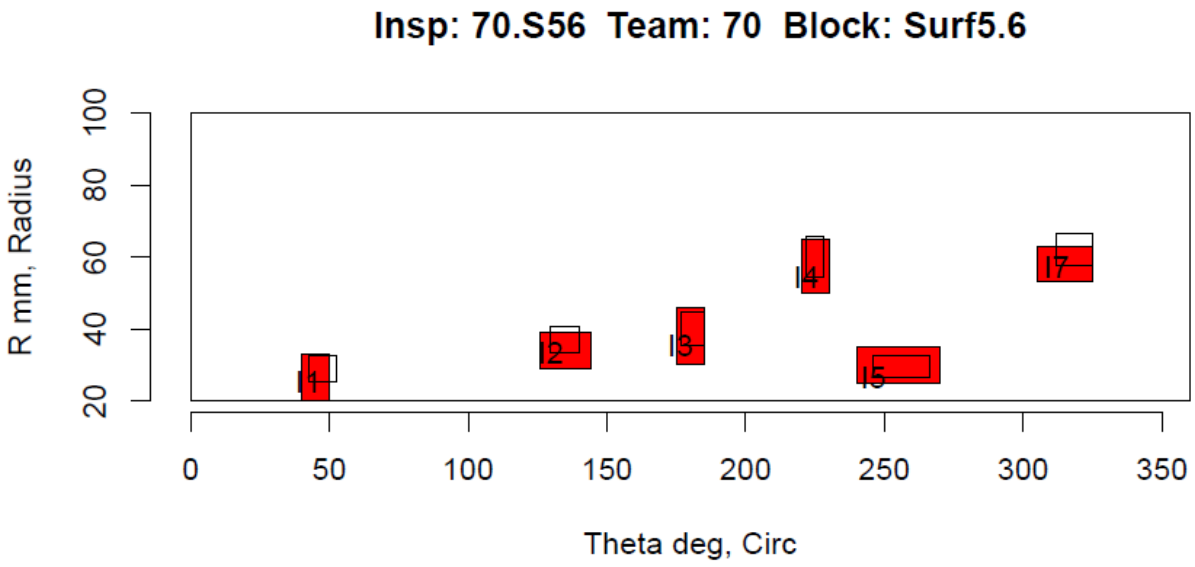
Insp: 70.S56 Team: 70 Block: Surf5.6
R mm, Radius
20
40
60
80
100
0
50
100
150
200
250
300
350
Theta deg, Circ
I1
I2
I3
I4
I5
I7

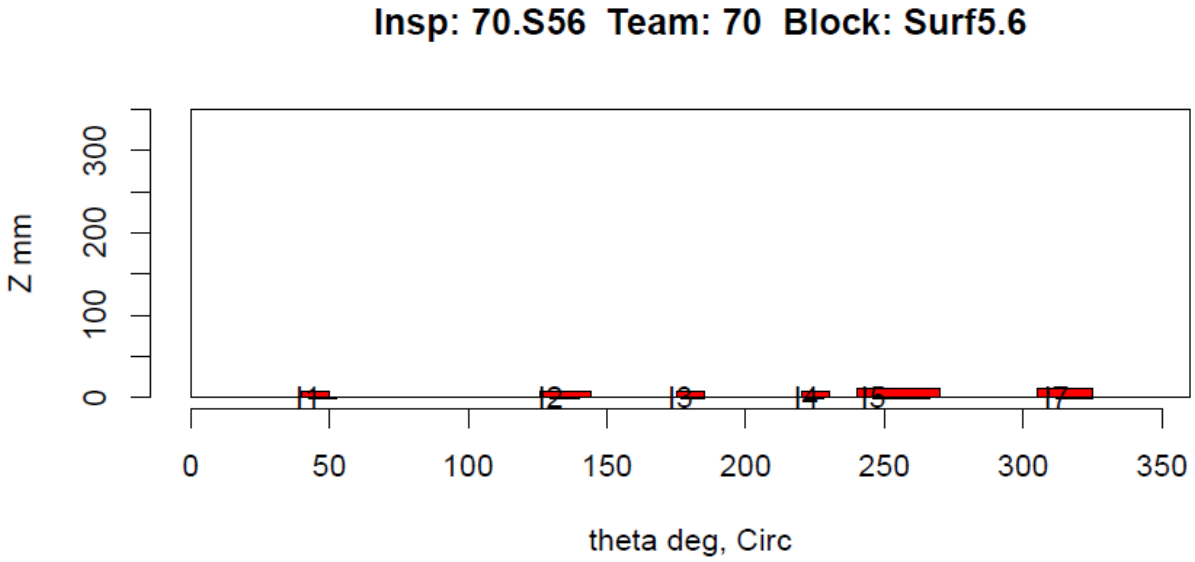
Insp: 70.S56 Team: 70 Block: Surf5.6
Z mm
0
100
200
300
0
50
100
150
200
250
300
350
theta deg, Circ
I1
I2
I3
I4
I5
I7

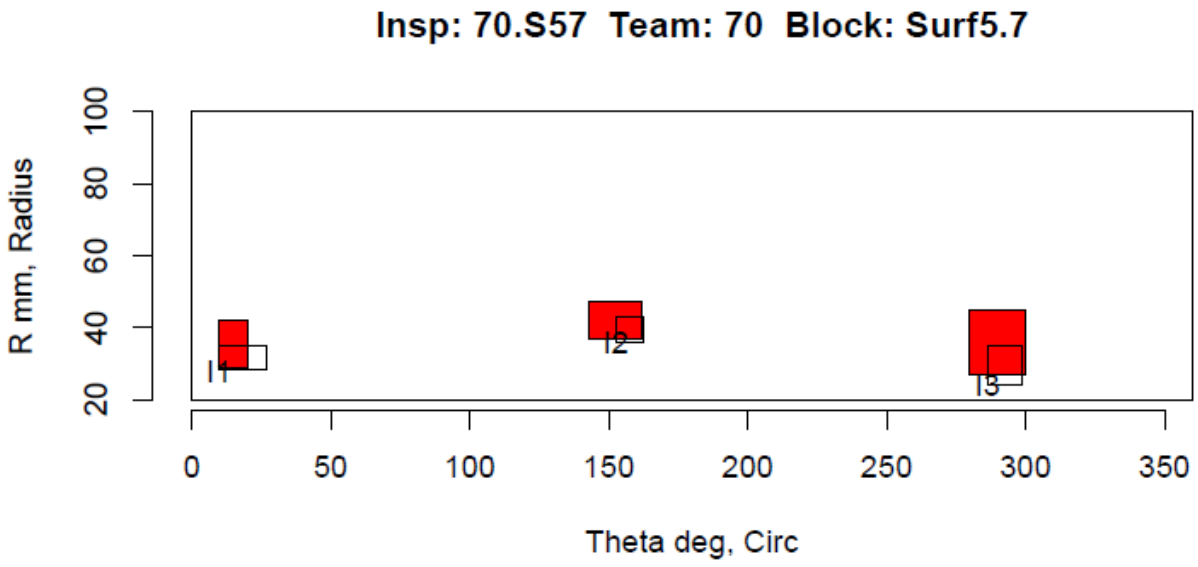
Insp: 70.S57 Team: 70 Block: Surf5.7
R mm, Radius
20
40
60
80
100
0
50
100
150
200
250
300
350
Theta deg, Circ
I1
I2
I3

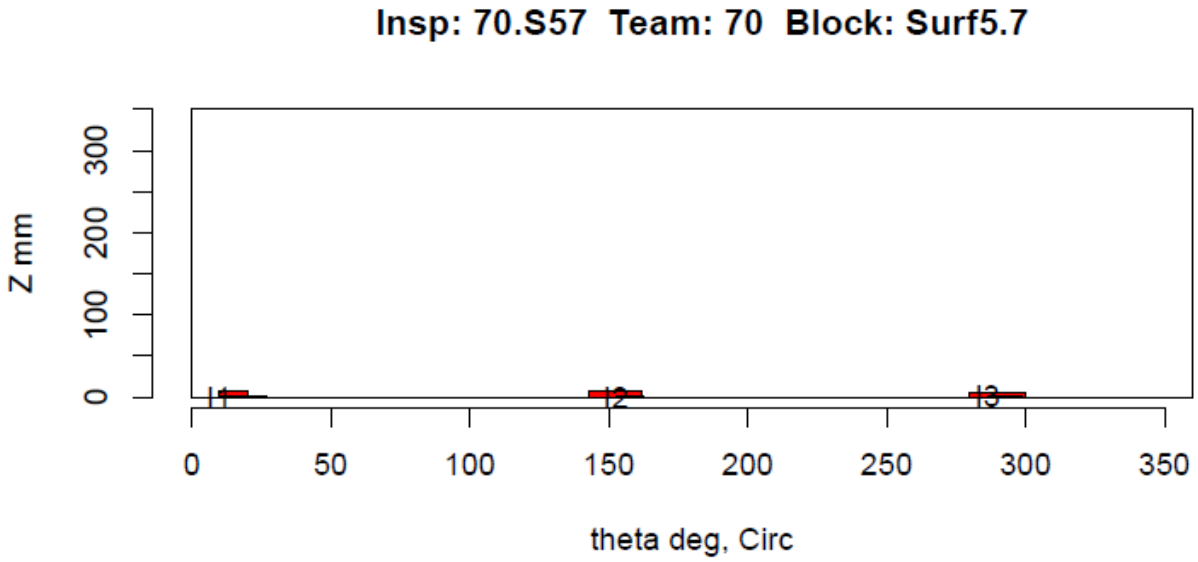
Insp: 70.S57 Team: 70 Block: Surf5.7
Z mm
0
100
200
300
0
50
100
150
200
250
300
350
theta deg, Circ
I1
I2
I3

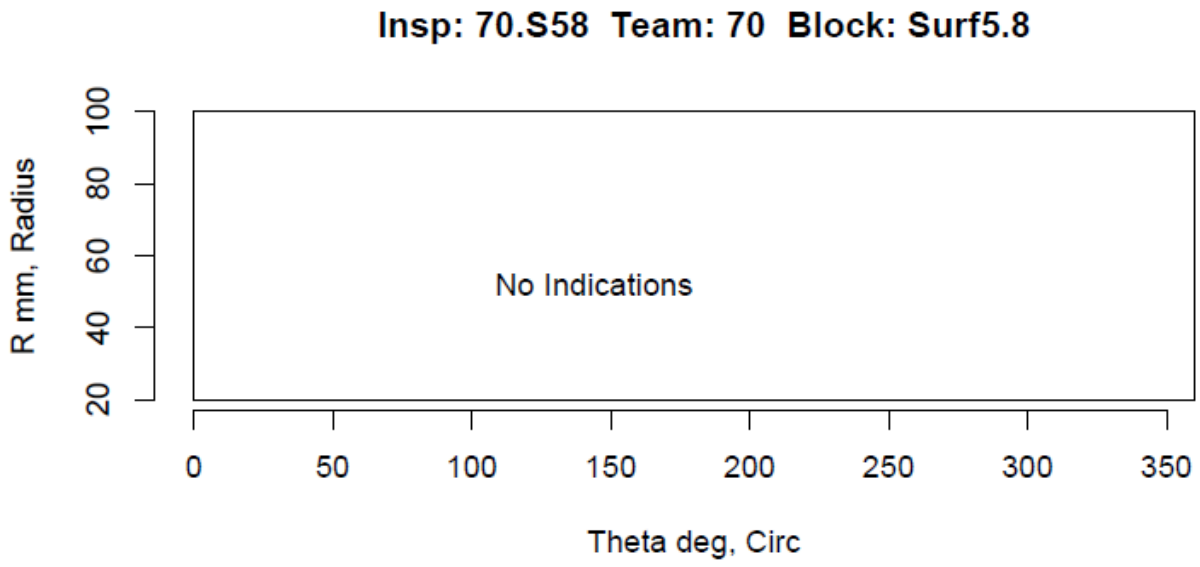
Insp: 70.S58 Team: 70 Block: Surf5.8
R mm, Radius
20
40
60
80
100
No Indications
0
50
100
150
200
250
300
350
Theta deg, Circ

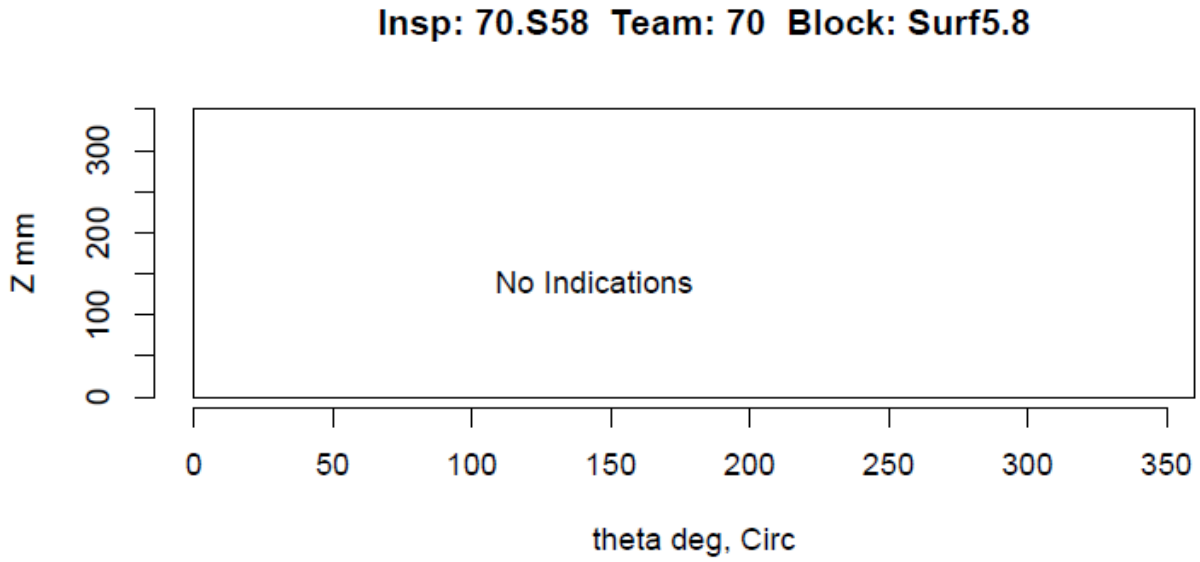
Insp: 70.S58 Team: 70 Block: Surf5.8
Z mm
0
100
200
300
No Indications
0
50
100
150
200
250
300
350
theta deg, Circ

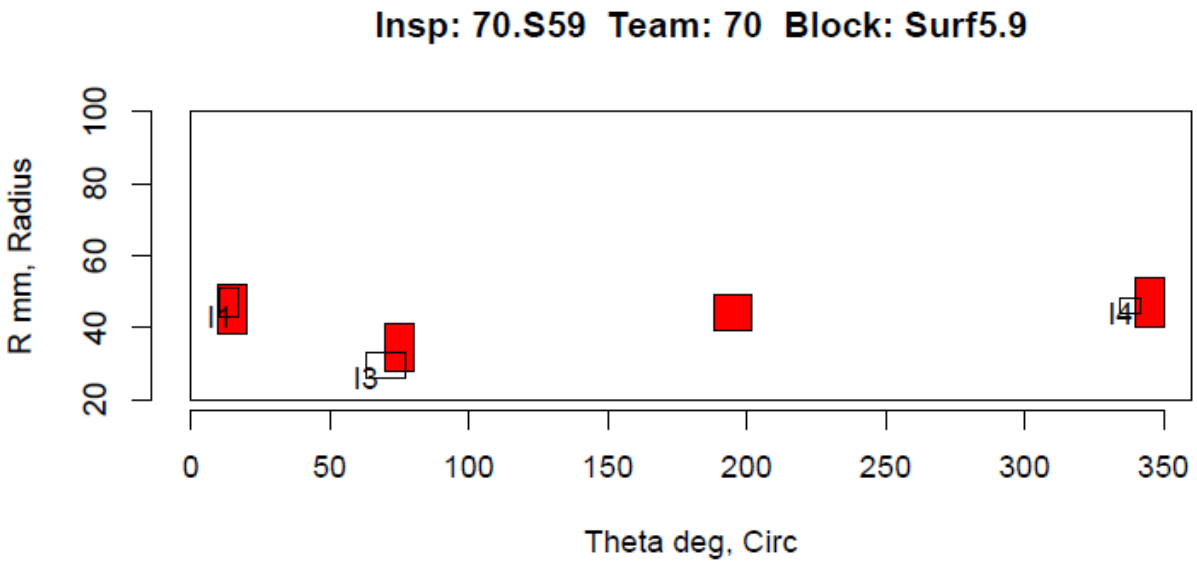
Insp: 70.S59 Team: 70 Block: Surf5.9
R mm, Radius
20
40
60
80
100
0
50
100
150
200
250
300
350
Theta deg, Circ

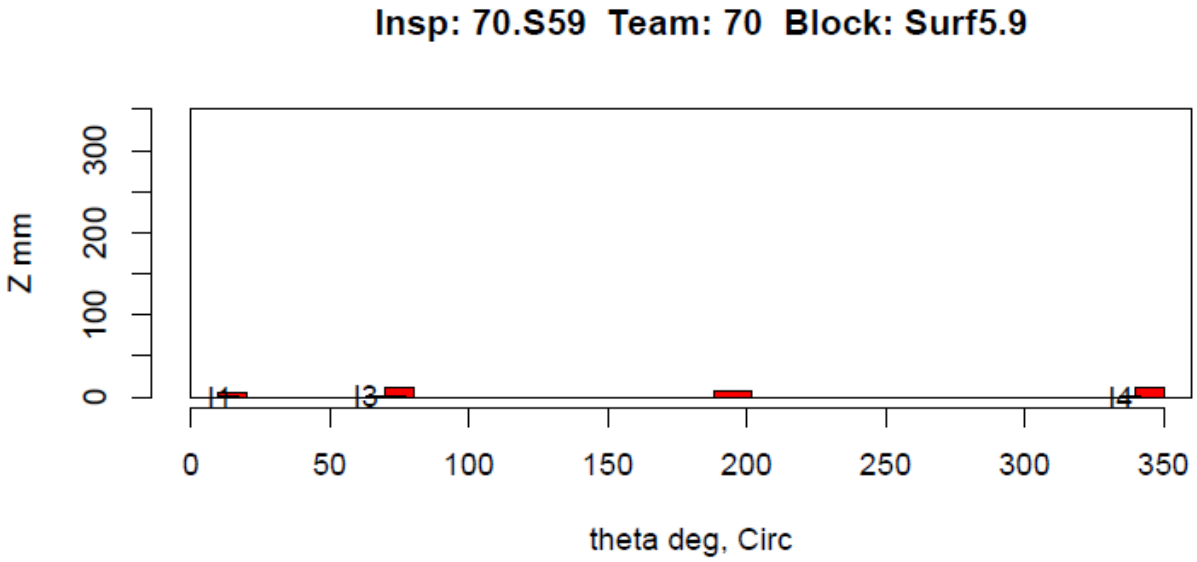
Insp: 70.S59 Team: 70 Block: Surf5.9
Z mm
0
100
200
300
0
50
100
150
200
250
300
350
theta deg, Circ

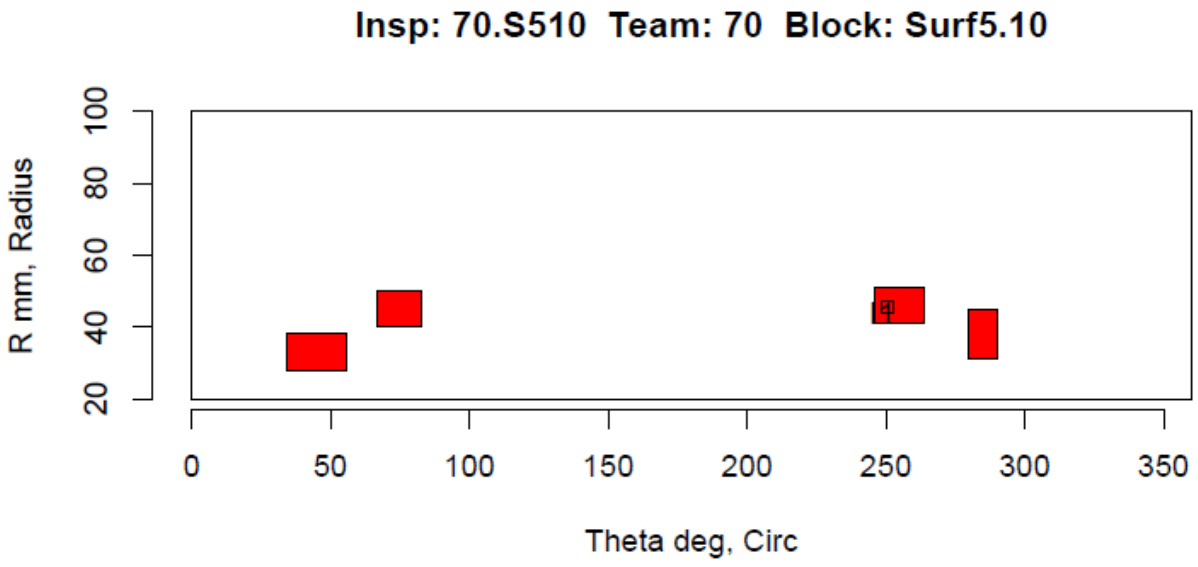
Insp: 70.S510 Team: 70 Block: Surf5.10
R mm, Radius
20
40
60
80
100
0
50
100
150
200
250
300
350
Theta deg, Circ

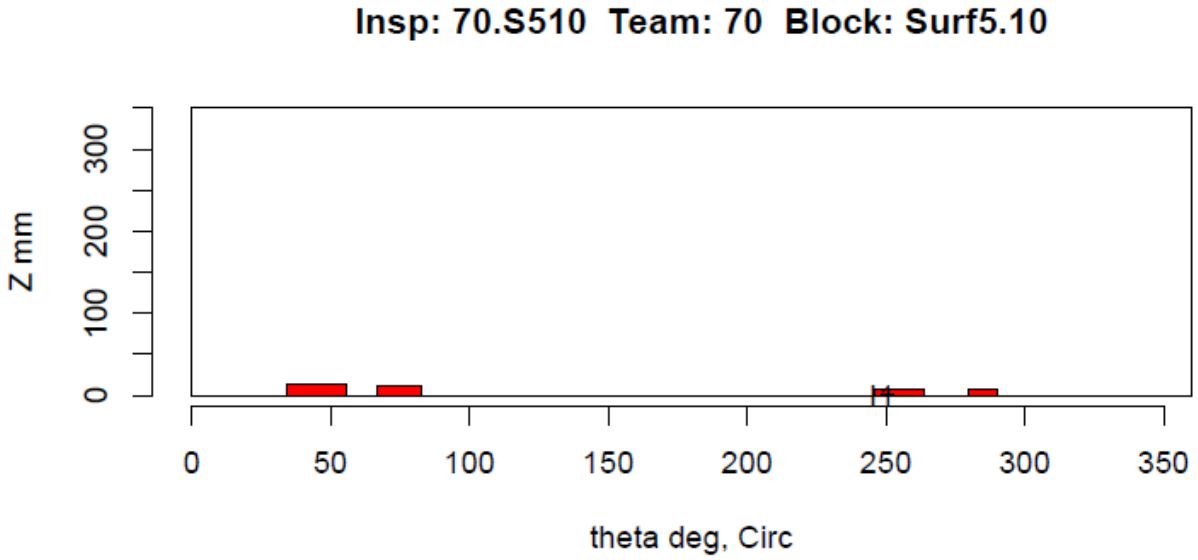
Insp: 70.S510 Team: 70 Block: Surf5.10
Z mm
0
100
200
300
0
50
100
150
200
250
300
350
theta deg, Circ

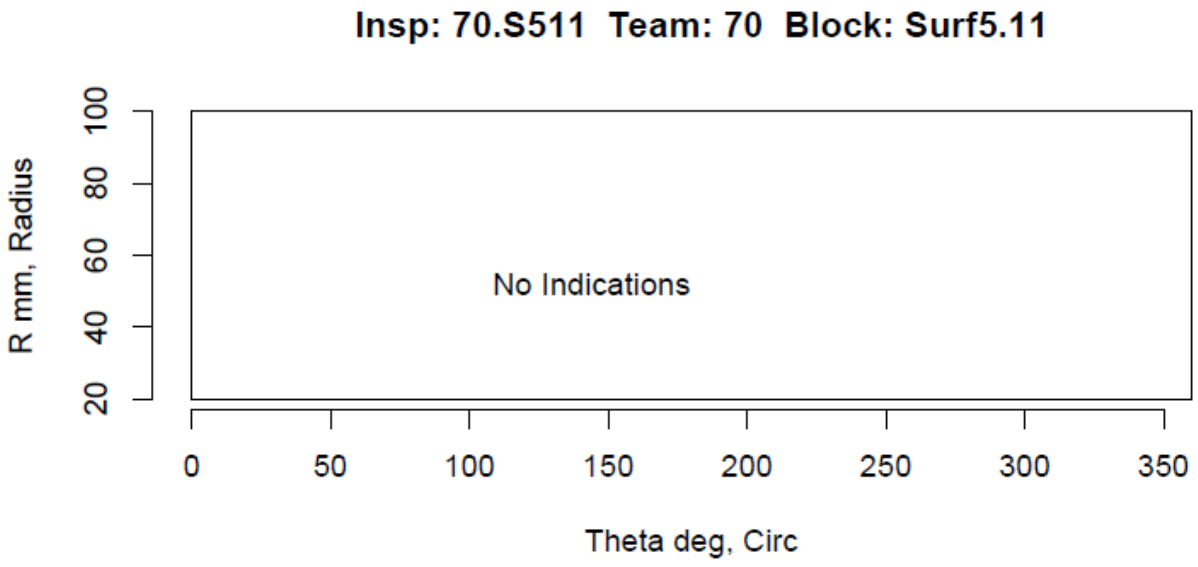
Insp: 70.S511 Team: 70 Block: Surf5.11
R mm, Radius
20
40
60
80
100
No Indications
0
50
100
150
200
250
300
350
Theta deg, Circ

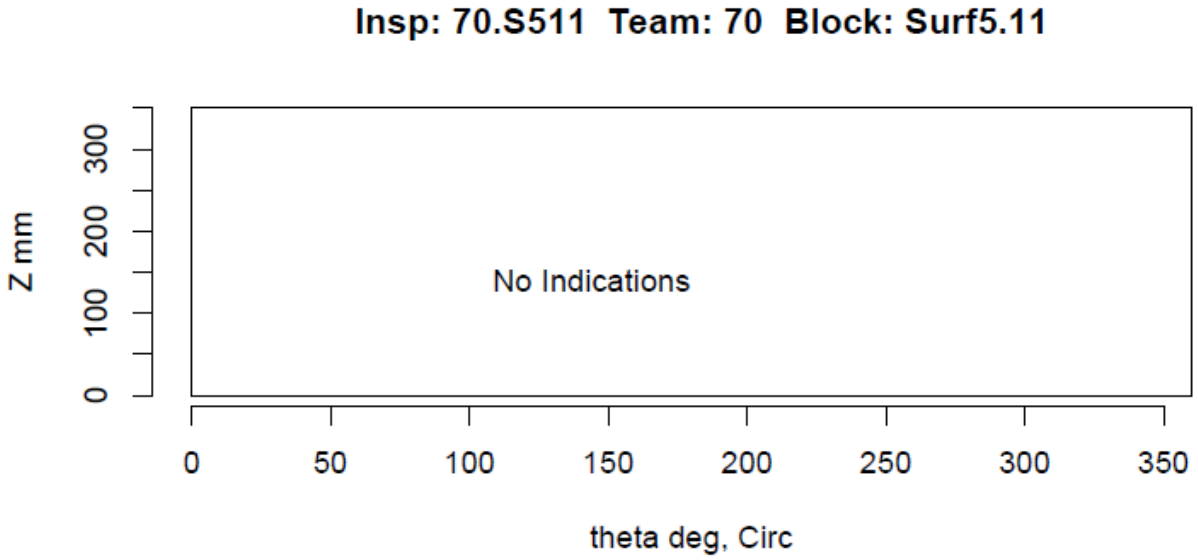
Insp: 70.S511 Team: 70 Block: Surf5.11
Z mm
0
100
200
300
No Indications
0
50
100
150
200
250
300
350
theta deg, Circ

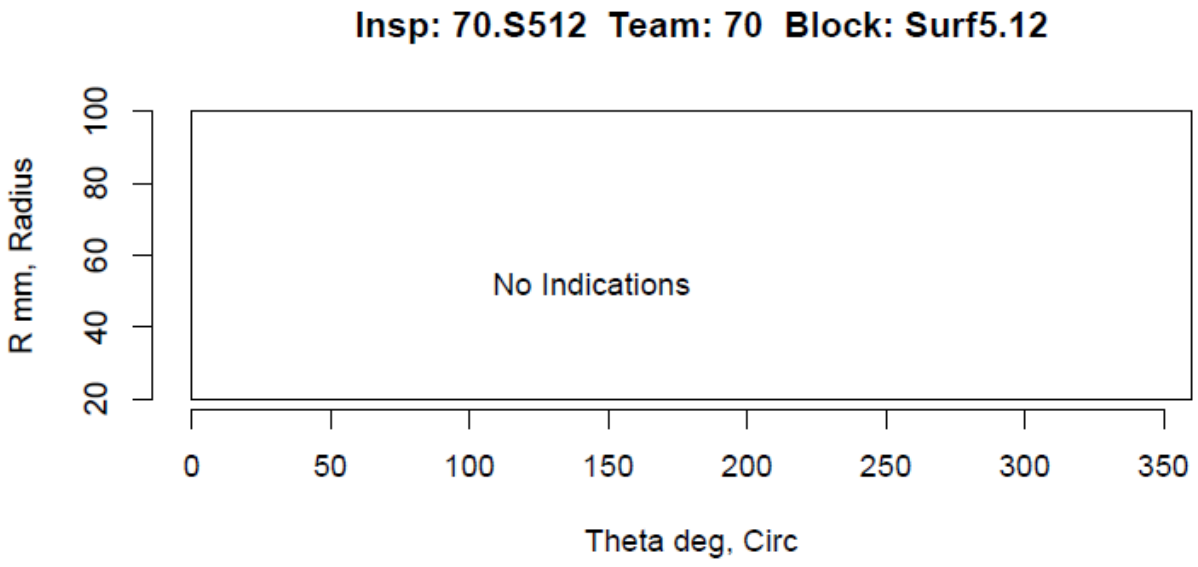
Insp: 70.S512 Team: 70 Block: Surf5.12
R mm, Radius
20
40
60
80
100
No Indications
0
50
100
150
200
250
300
350
Theta deg, Circ

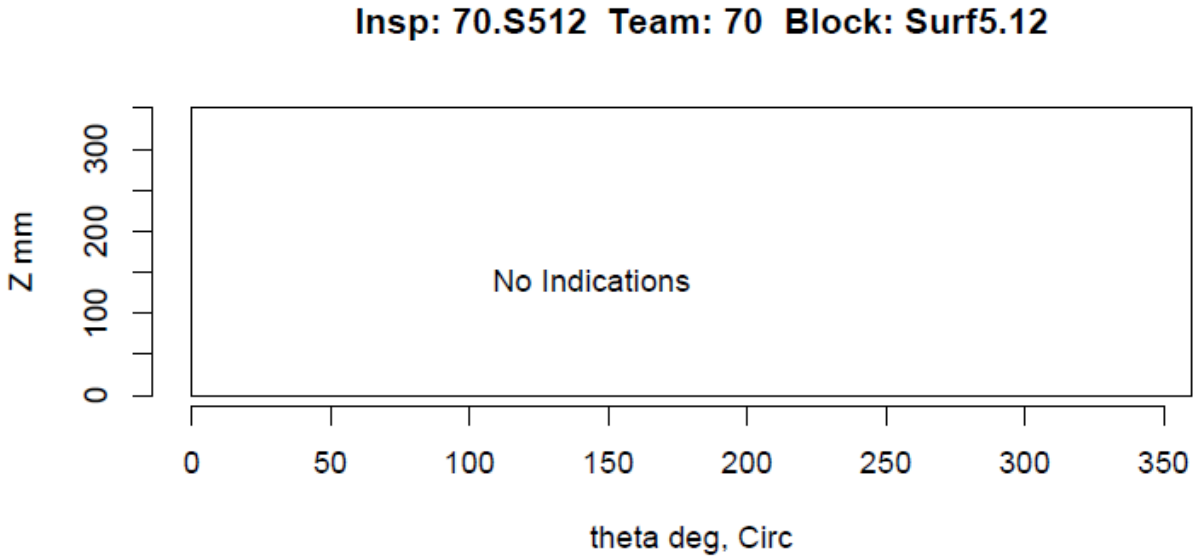
Insp: 70.S512 Team: 70 Block: Surf5.12
Z mm
0
100
200
300
No Indications
0
50
100
150
200
250
300
350
theta deg, Circ

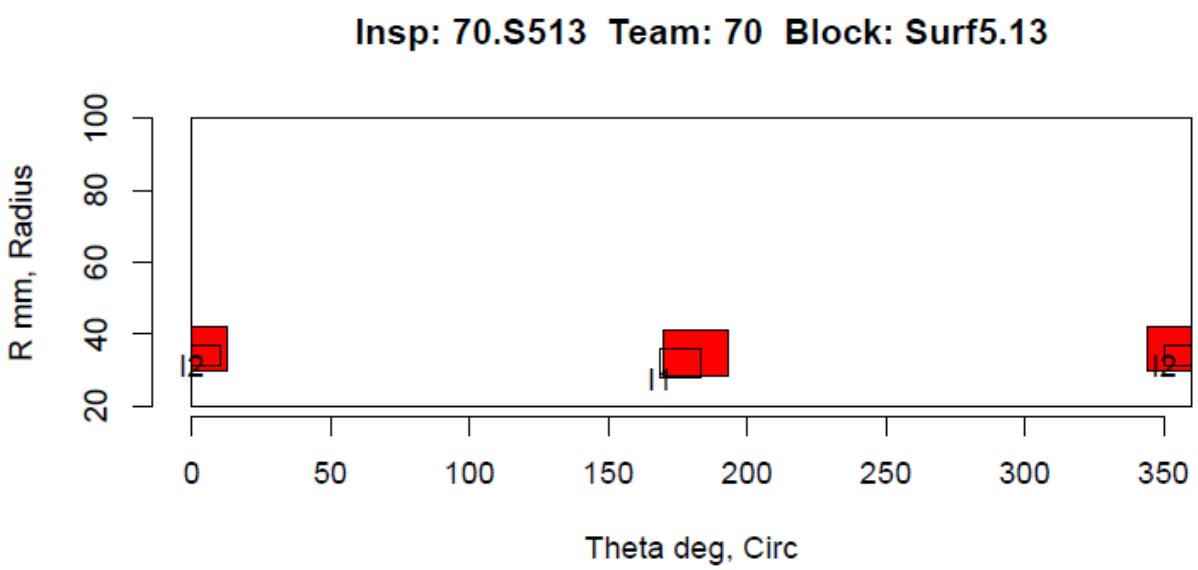
Insp: 70.S513 Team: 70 Block: Surf5.13
R mm, Radius
20
40
60
80
100
0
50
100
150
200
250
300
350
Theta deg, Circ

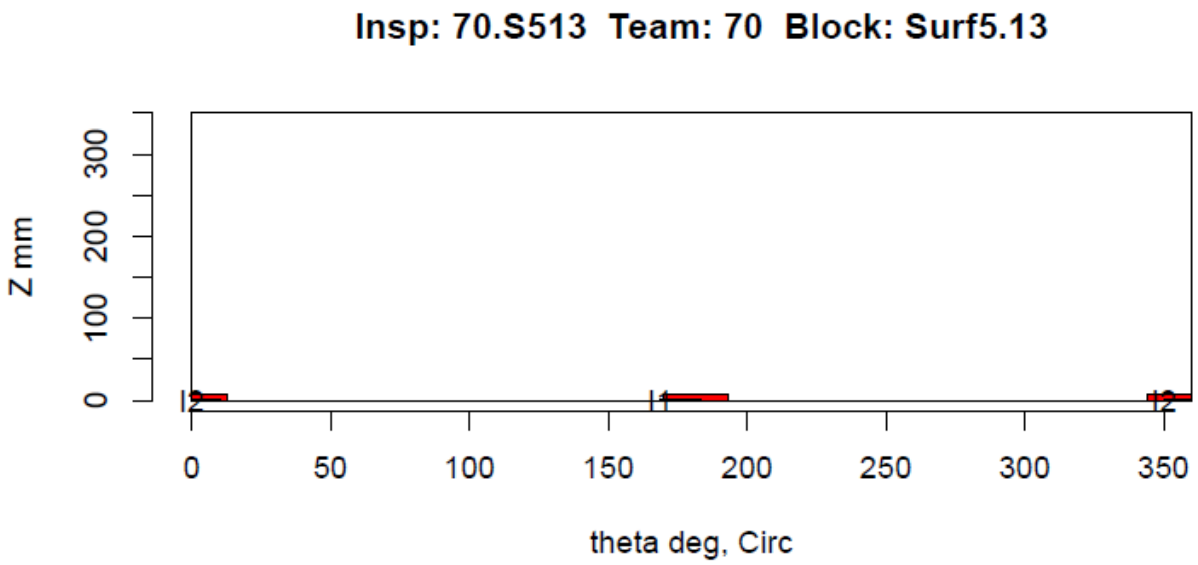
Insp: 70.S513 Team: 70 Block: Surf5.13
Z mm
0
100
200
300
0
50
100
150
200
250
300
350
theta deg, Circ

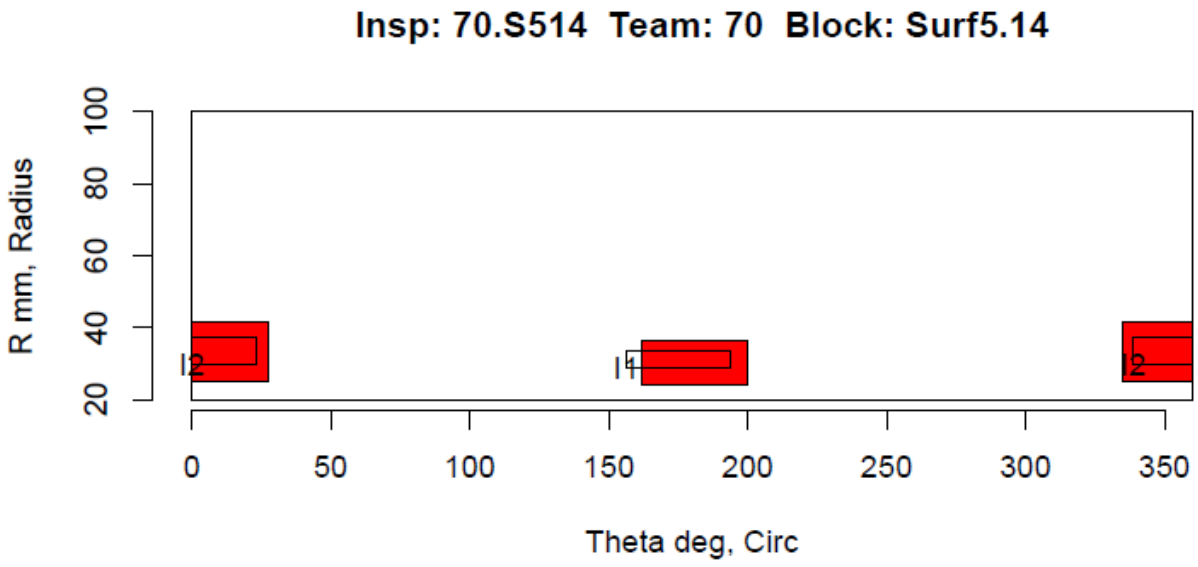
Insp: 70.S514 Team: 70 Block: Surf5.14
R mm, Radius
20
40
60
80
100
0
50
100
150
200
250
300
350
Theta deg, Circ

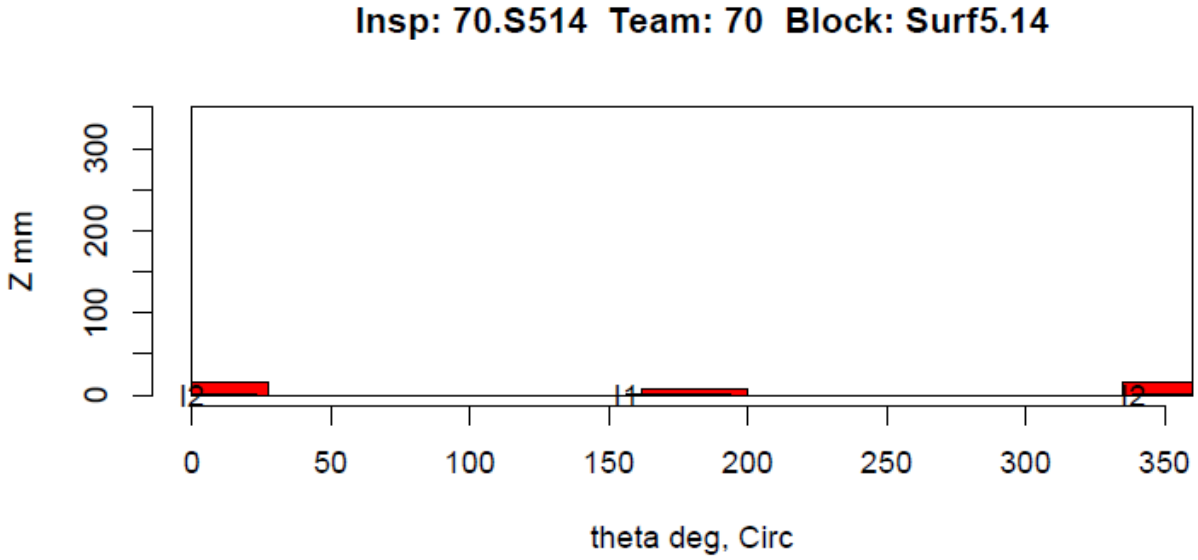
Insp: 70.S514 Team: 70 Block: Surf5.14
Z mm
0
100
200
300
0
50
100
150
200
250
300
350
theta deg, Circ

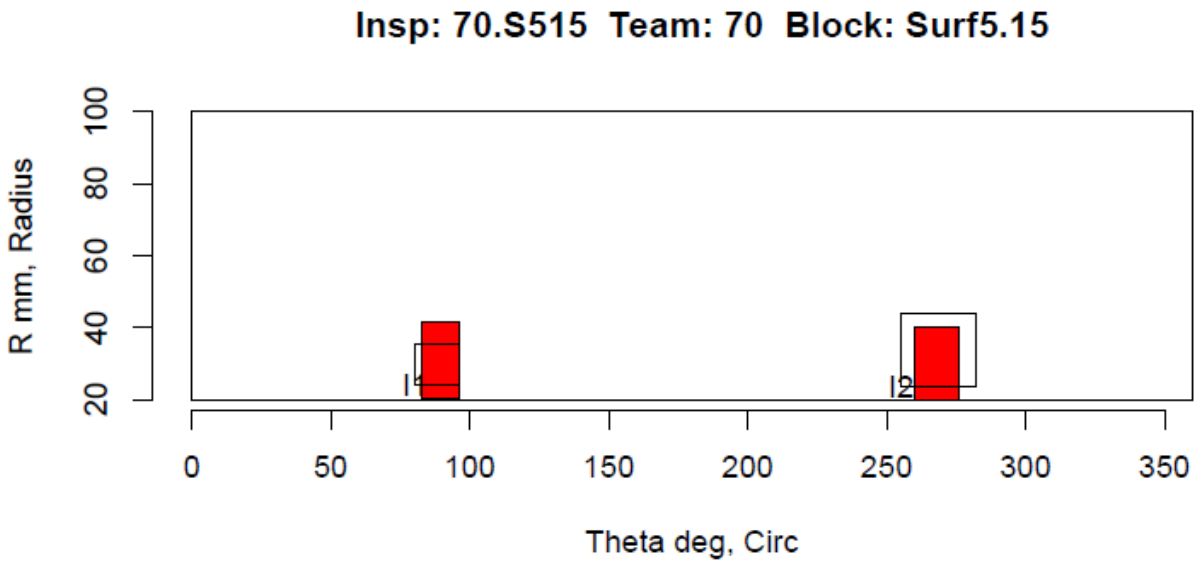
Insp: 70.S515 Team: 70 Block: Surf5.15
R mm, Radius
20
40
60
80
100
0
50
100
150
200
250
300
350
Theta deg, Circ
I1
I2

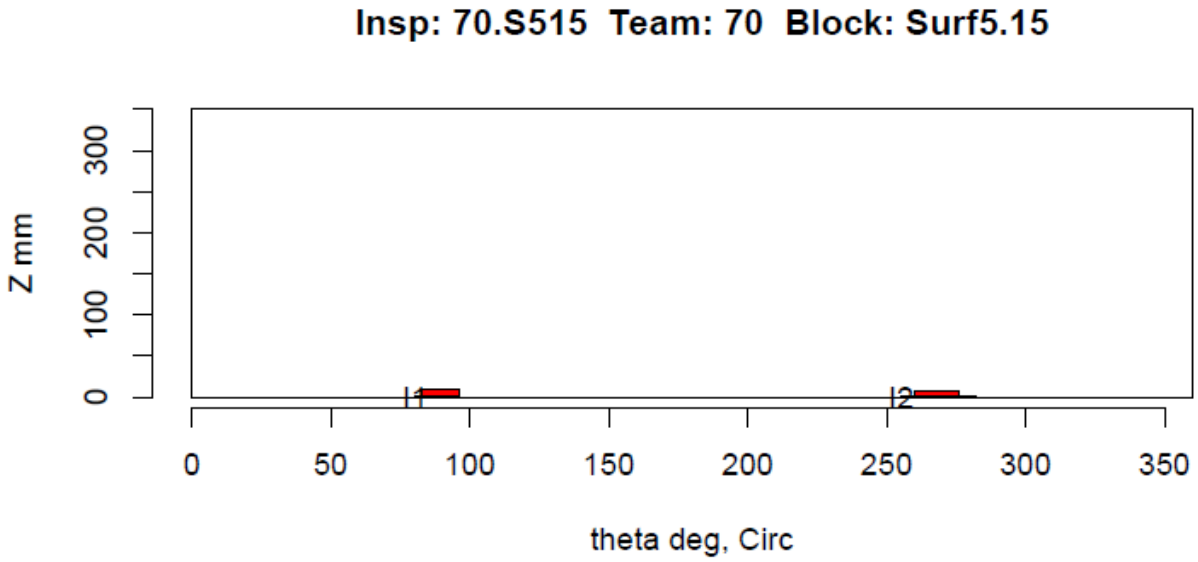
Insp: 70.S515 Team: 70 Block: Surf5.15
Z mm
0
100
200
300
0
50
100
150
200
250
300
350
theta deg, Circ
I1
I2

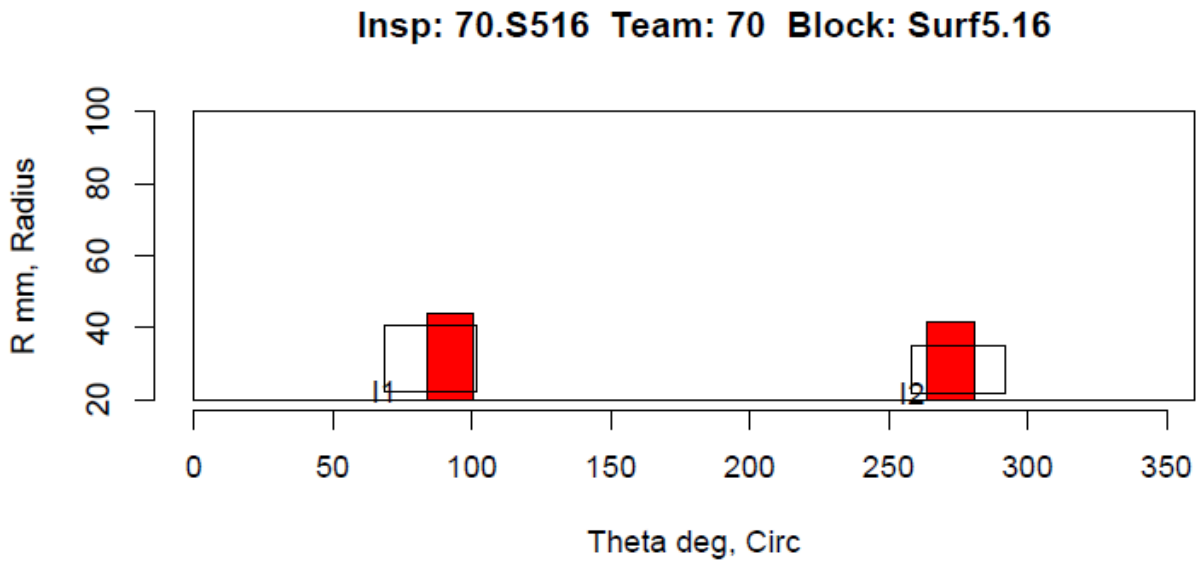
Insp: 70.S516 Team: 70 Block: Surf5.16
R mm, Radius
20
40
60
80
100
0
50
100
150
200
250
300
350
Theta deg, Circ

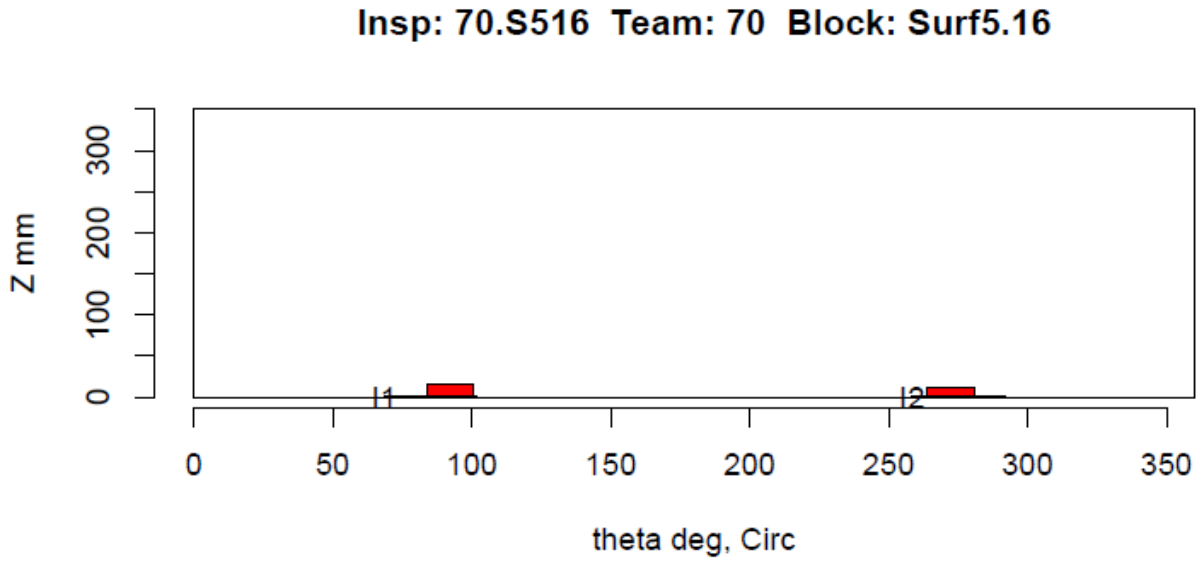
Insp: 70.S516 Team: 70 Block: Surf5.16
Z mm
0
100
200
300
0
50
100
150
200
250
300
350
theta deg, Circ

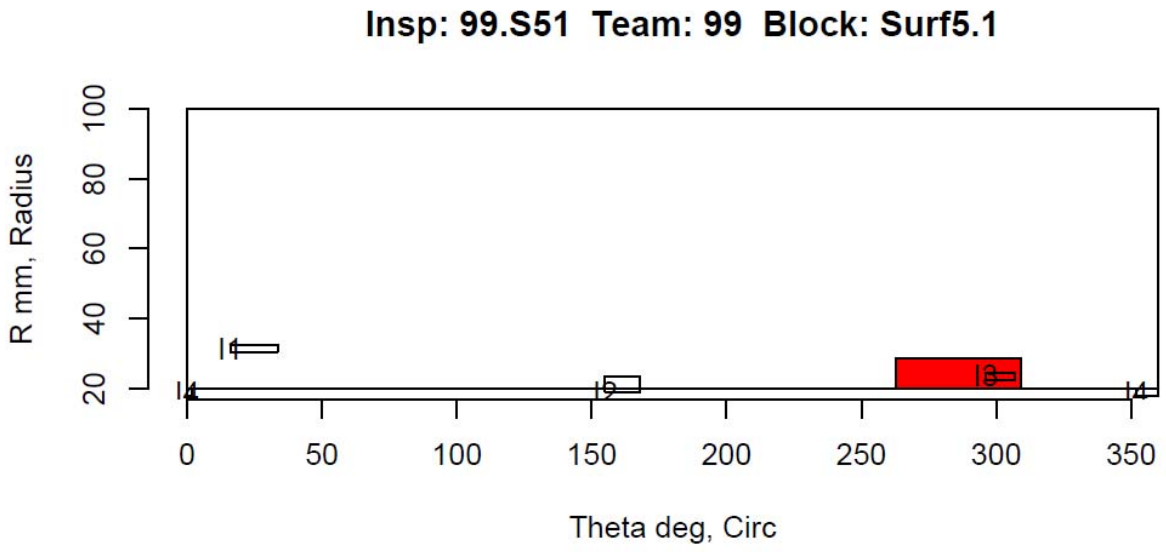
Insp: 99.S51 Team: 99 Block: Surf5.1
R mm, Radius
20
40
60
80
100
0
50
100
150
200
250
300
350
Theta deg, Circ

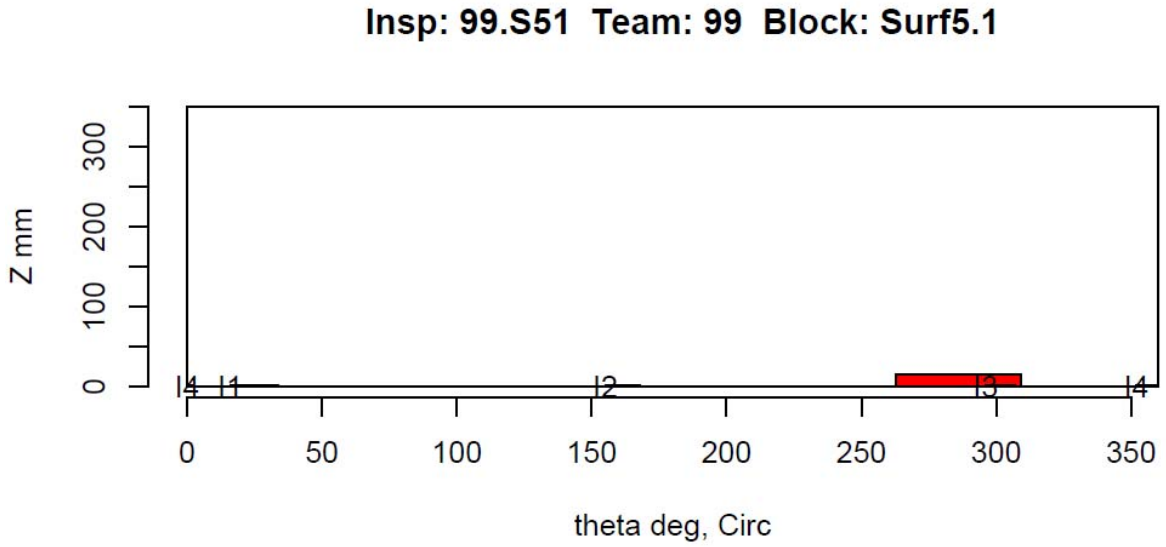
Insp: 99.S51 Team: 99 Block: Surf5.1
Z mm
0
100
200
300
0
50
100
150
200
250
300
350
theta deg, Circ

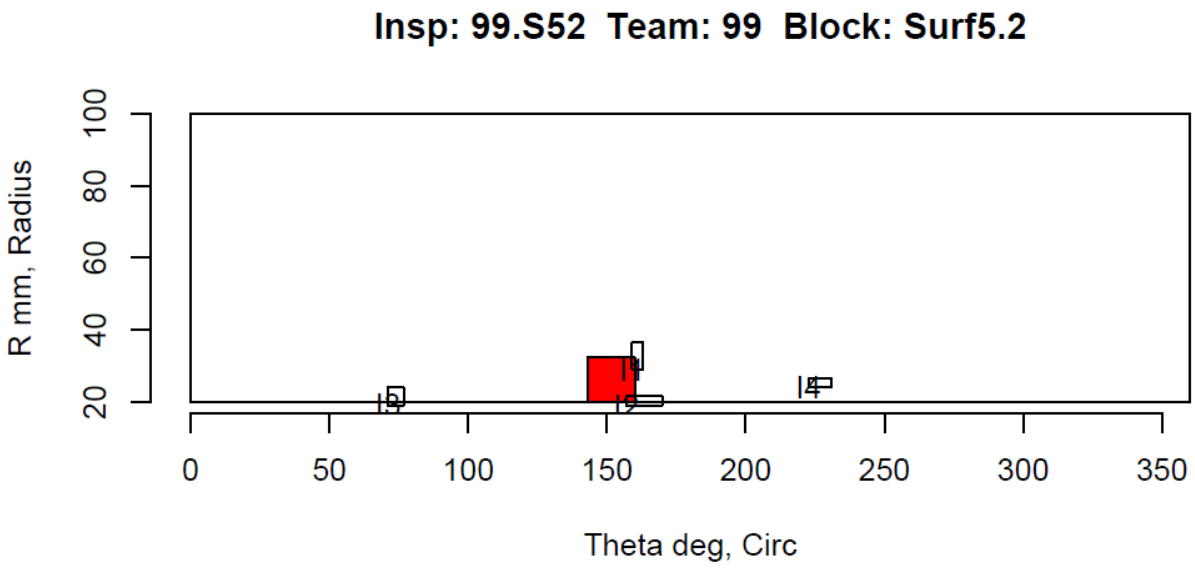
Insp: 99.S52 Team: 99 Block: Surf5.2
R mm, Radius
20
40
60
80
100
0
50
100
150
200
250
300
350
Theta deg, Circ

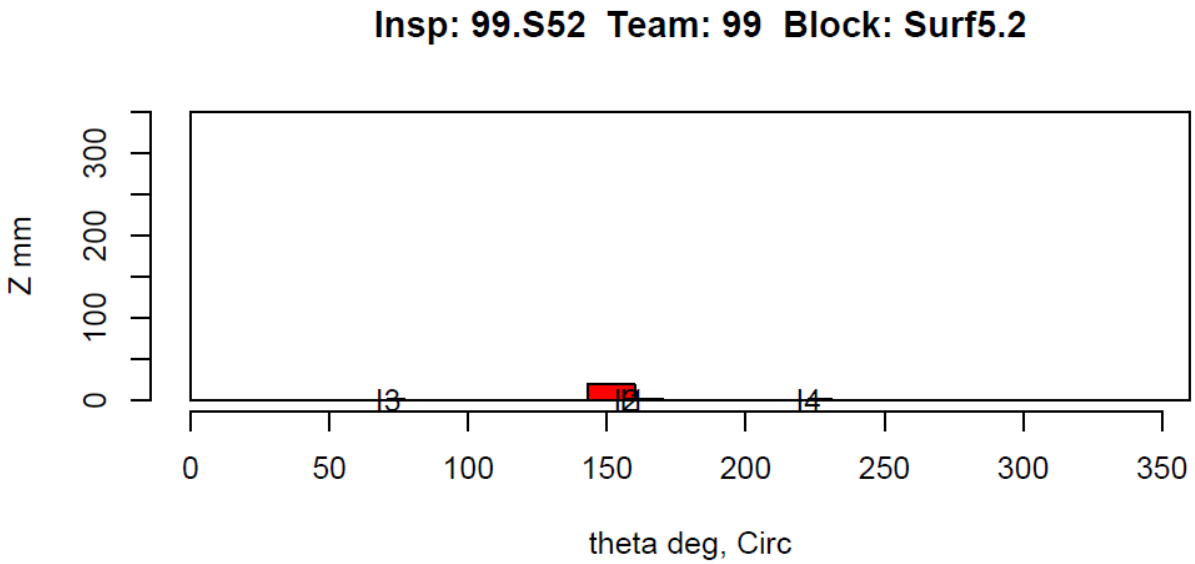
Insp: 99.S52 Team: 99 Block: Surf5.2
Z mm
0
100
200
300
0
50
100
150
200
250
300
350
theta deg, Circ

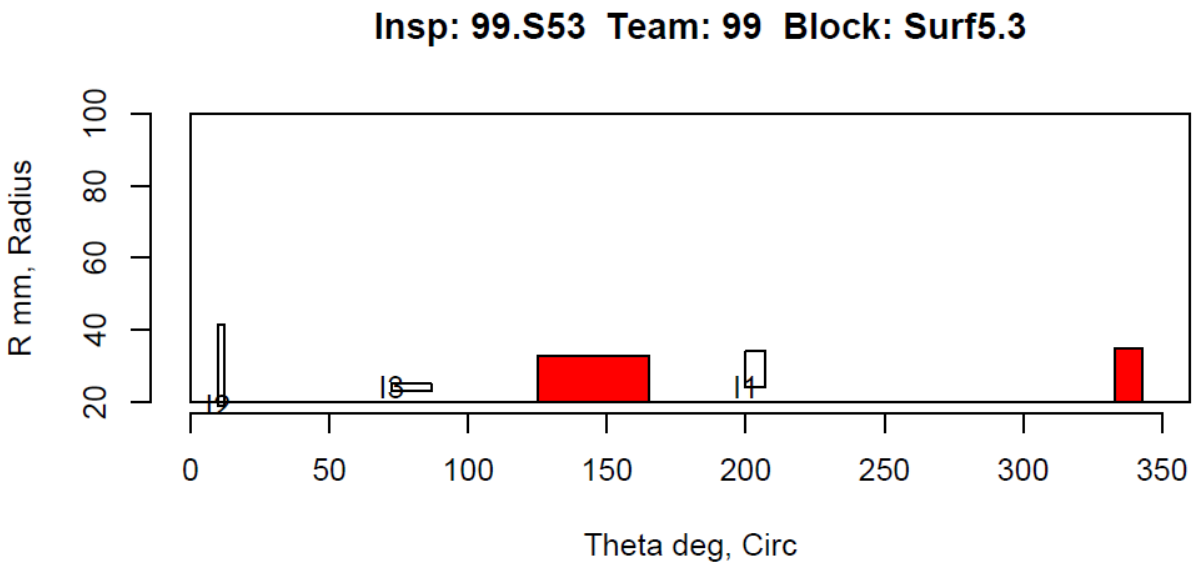
Insp: 99.S53 Team: 99 Block: Surf5.3
R mm, Radius
20
40
60
80
100
0
50
100
150
200
250
300
350
Theta deg, Circ
I5
I4

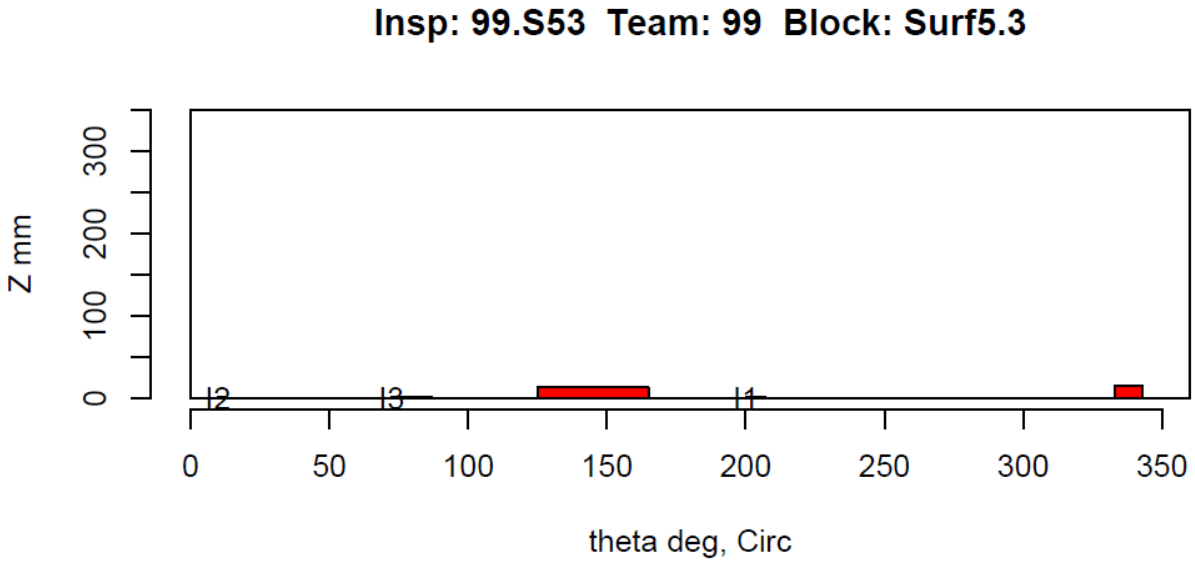
Insp: 99.S53 Team: 99 Block: Surf5.3
Z mm
0
100
200
300
0
50
100
150
200
250
300
350
theta deg, Circ
I2
I3
I1

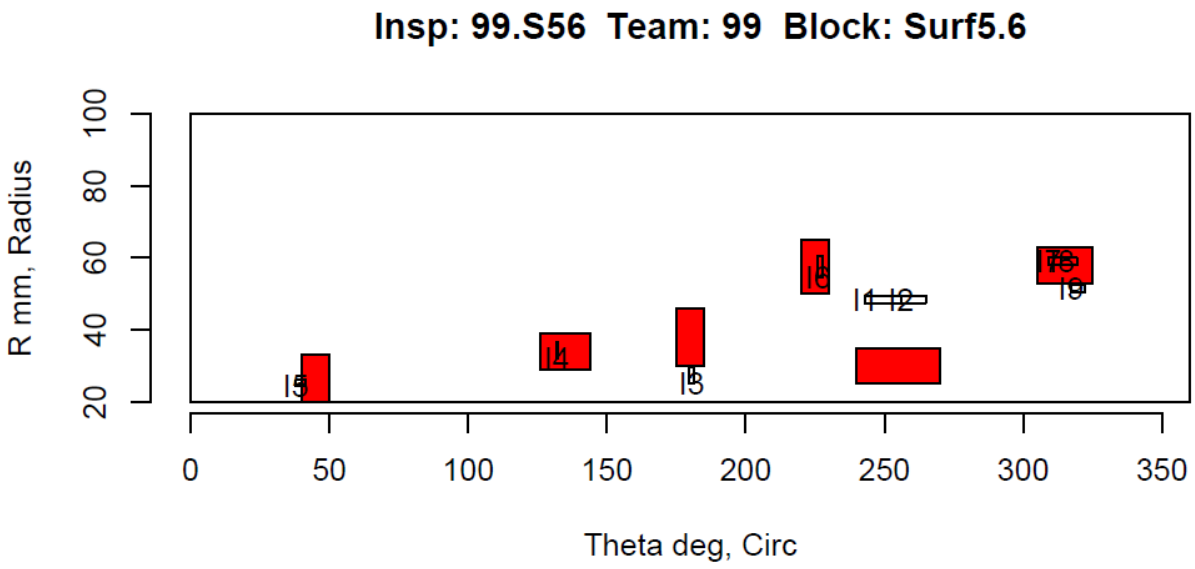
Insp: 99.S56 Team: 99 Block: Surf5.6
R mm, Radius
20
40
60
80
100
0
50
100
150
200
250
300
350
Theta deg, Circ

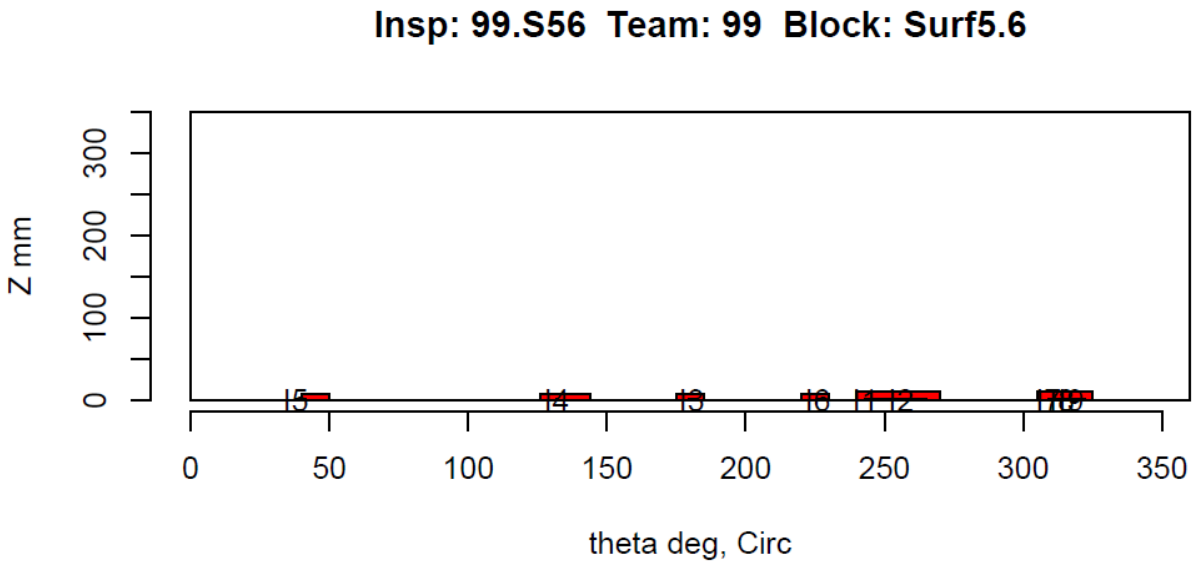
Insp: 99.S56 Team: 99 Block: Surf5.6
Z mm
0
100
200
300
0
50
100
150
200
250
300
350
theta deg, Circ

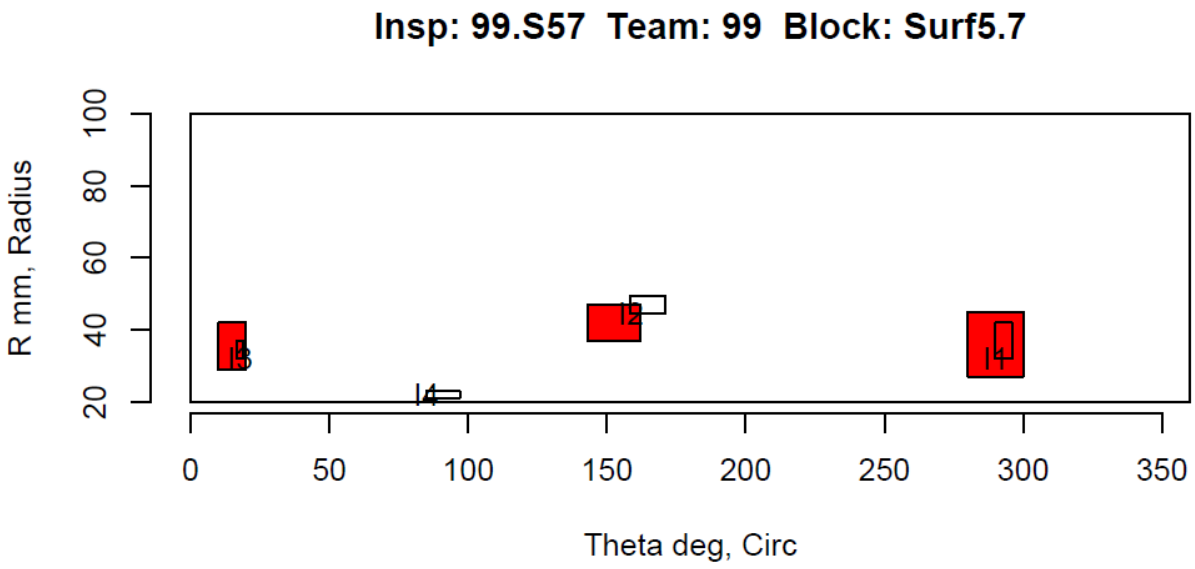
Insp: 99.S57 Team: 99 Block: Surf5.7
R mm, Radius
20
40
60
80
100
0
50
100
150
200
250
300
350
Theta deg, Circ

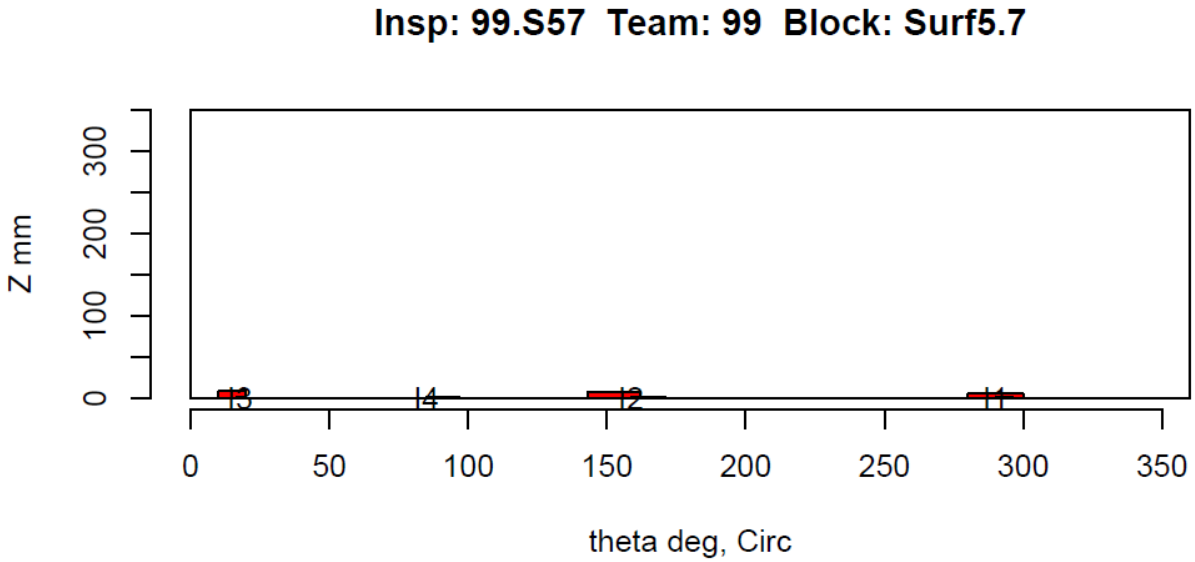
Insp: 99.S57 Team: 99 Block: Surf5.7
Z mm
0
100
200
300
0
50
100
150
200
250
300
350
theta deg, Circ

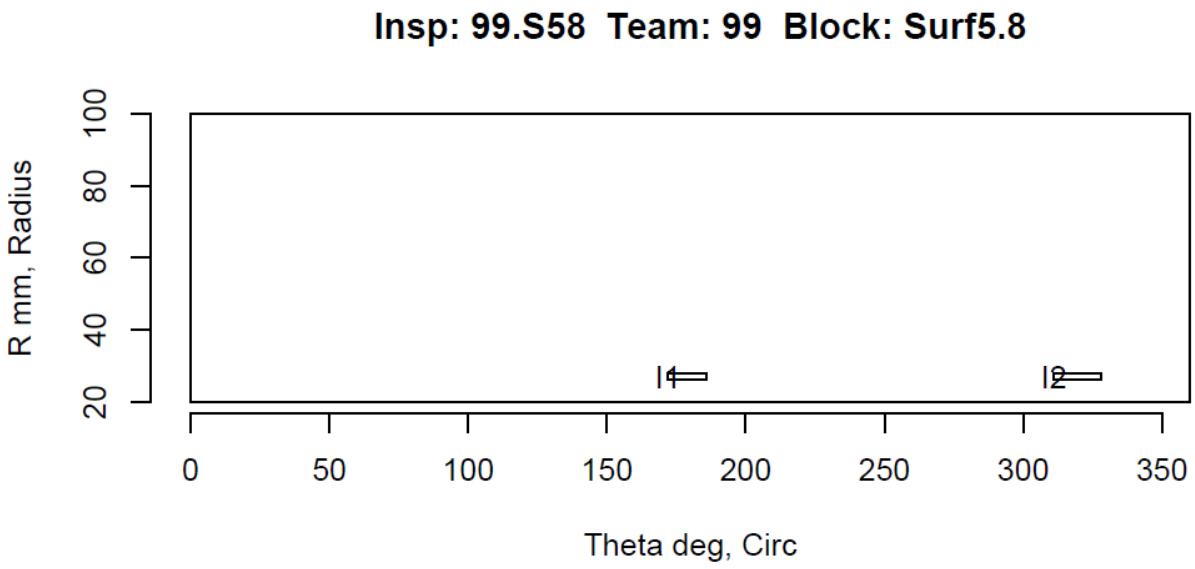
Insp: 99.S58 Team: 99 Block: Surf5.8
R mm, Radius
20
40
60
80
100
1
2
0
50
100
150
200
250
300
350
Theta deg, Circ

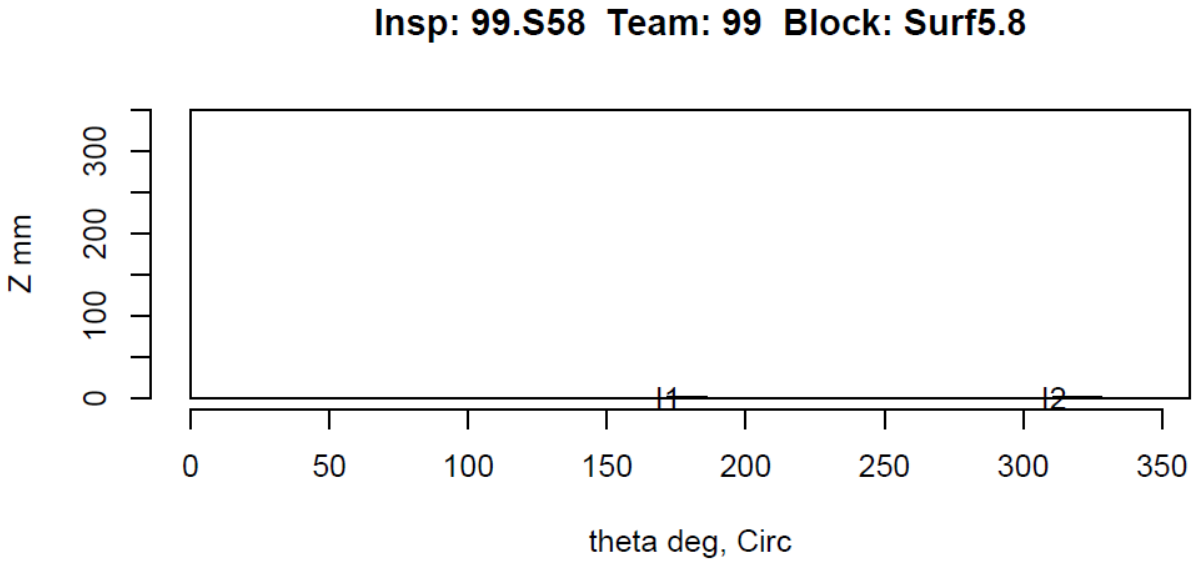
Insp: 99.S58 Team: 99 Block: Surf5.8
Z mm
0
100
200
300
1
2
0
50
100
150
200
250
300
350
theta deg, Circ

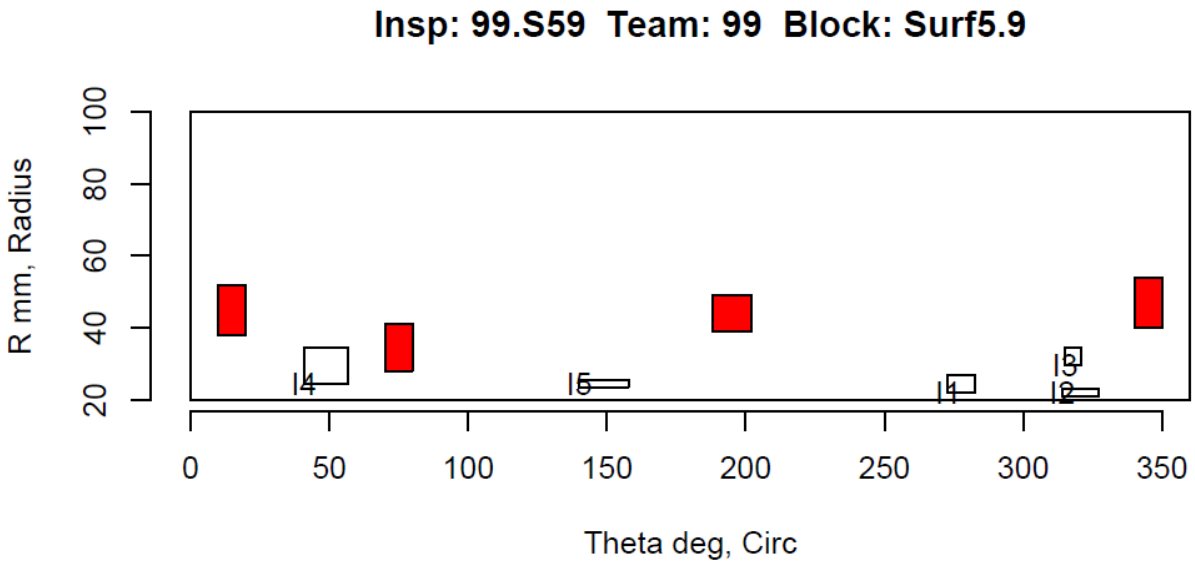
Insp: 99.S59 Team: 99 Block: Surf5.9
R mm, Radius
20
40
60
80
100
0
50
100
150
200
250
300
350
Theta deg, Circ
4
5
1
5
2

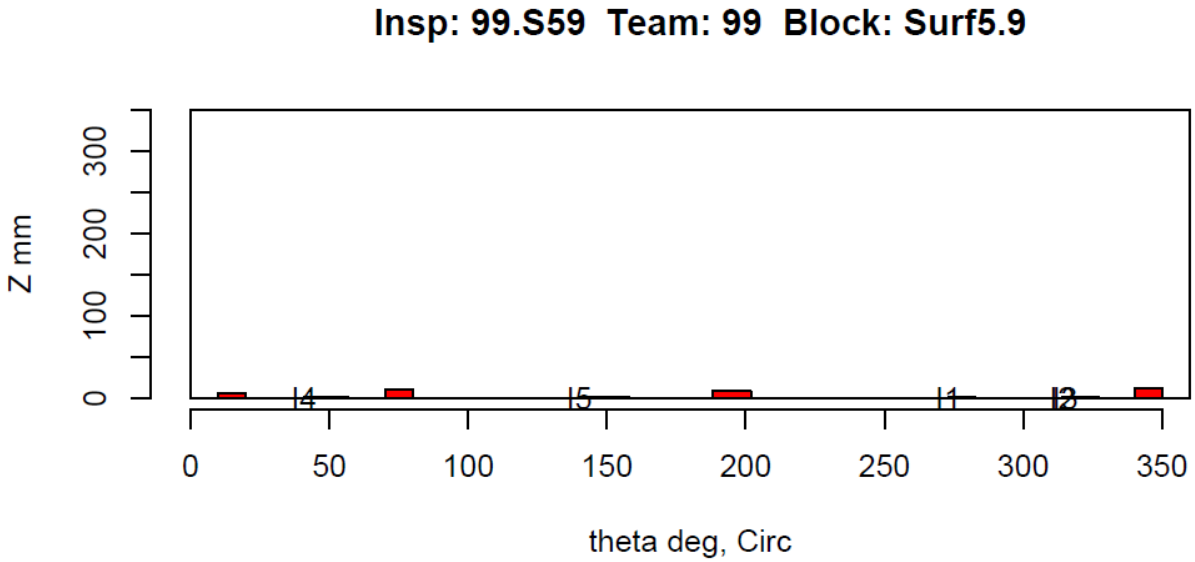
Insp: 99.S59 Team: 99 Block: Surf5.9
Z mm
0
100
200
300
0
50
100
150
200
250
300
350
theta deg, Circ
4
5
1
2

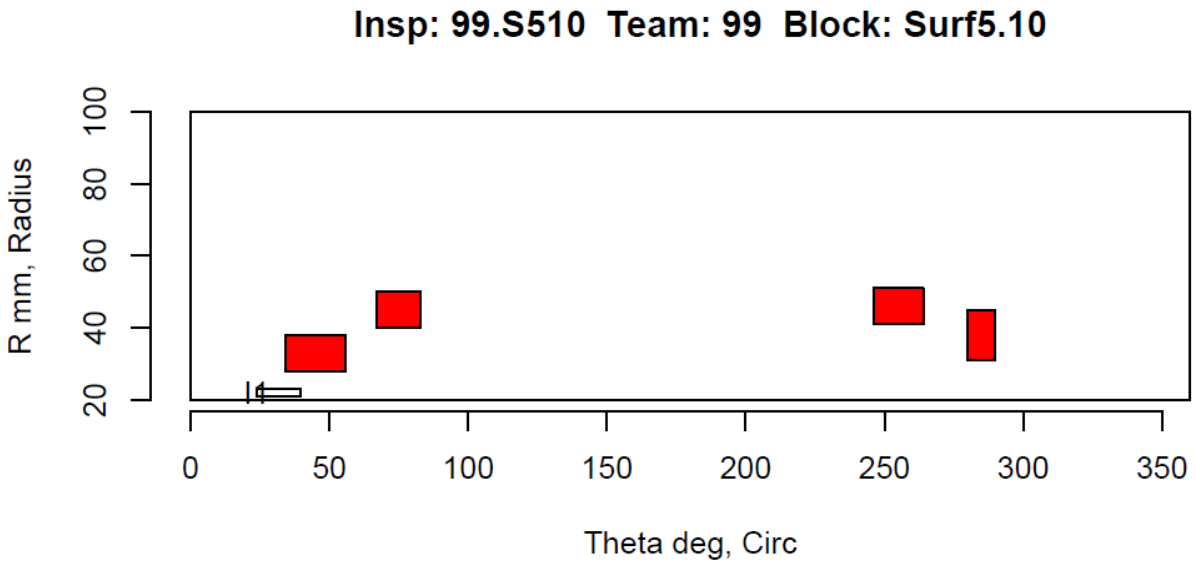
Insp: 99.S510 Team: 99 Block: Surf5.10
R mm, Radius
20
40
60
80
100
0
50
100
150
200
250
300
350
Theta deg, Circ

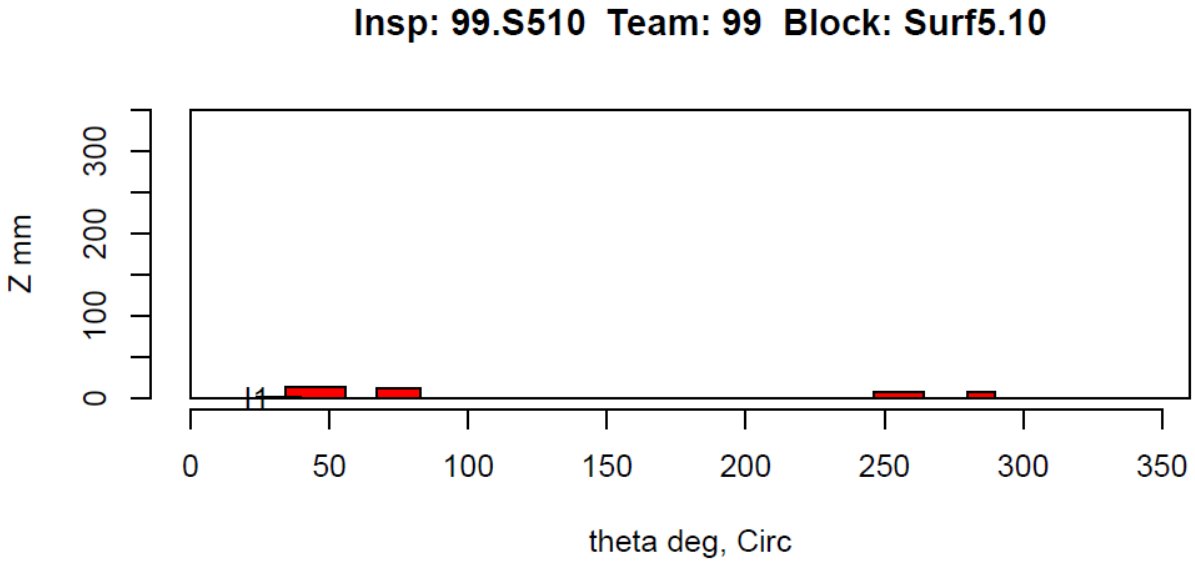
Insp: 99.S510 Team: 99 Block: Surf5.10
Z mm
0
100
200
300
0
50
100
150
200
250
300
350
theta deg, Circ

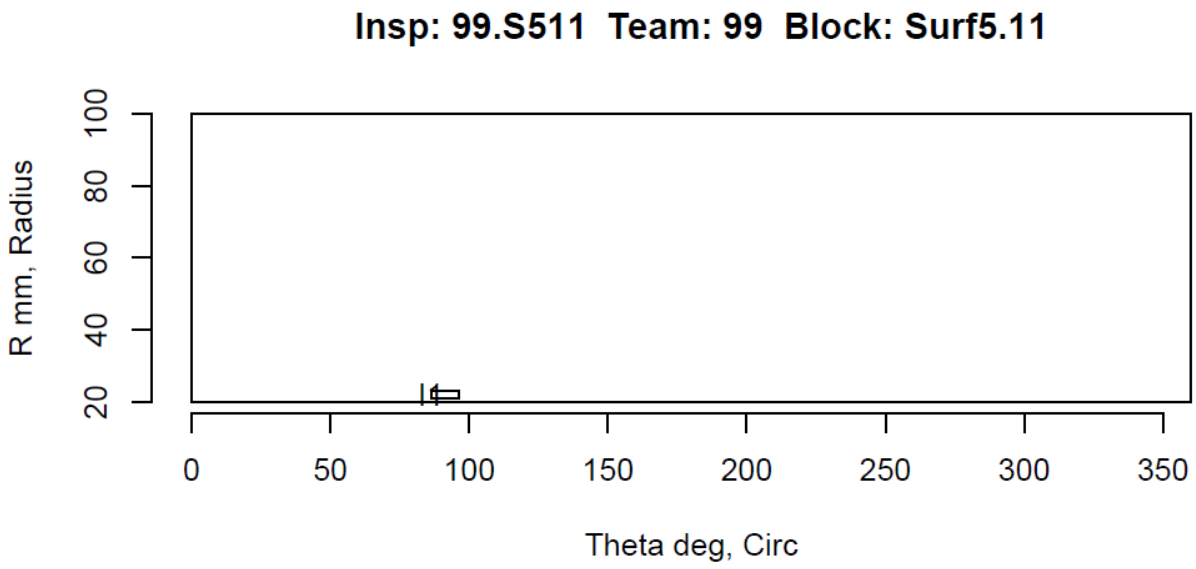
Insp: 99.S511 Team: 99 Block: Surf5.11
R mm, Radius
20
40
60
80
100
0
50
100
150
200
250
300
350
Theta deg, Circ

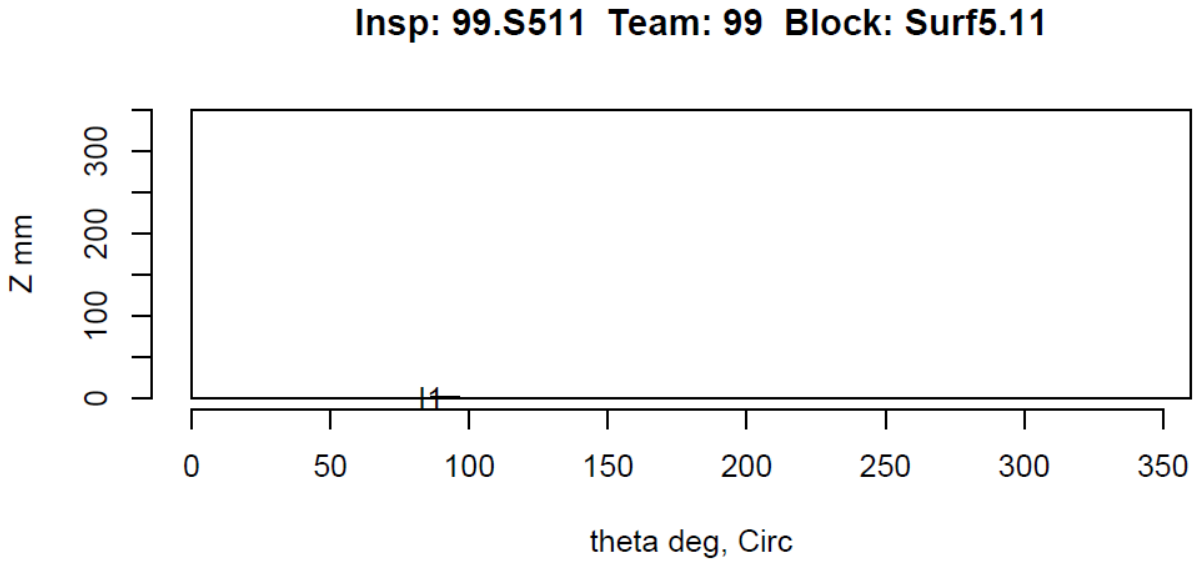
Insp: 99.S511 Team: 99 Block: Surf5.11
Z mm
0
100
200
300
0
50
100
150
200
250
300
350
theta deg, Circ

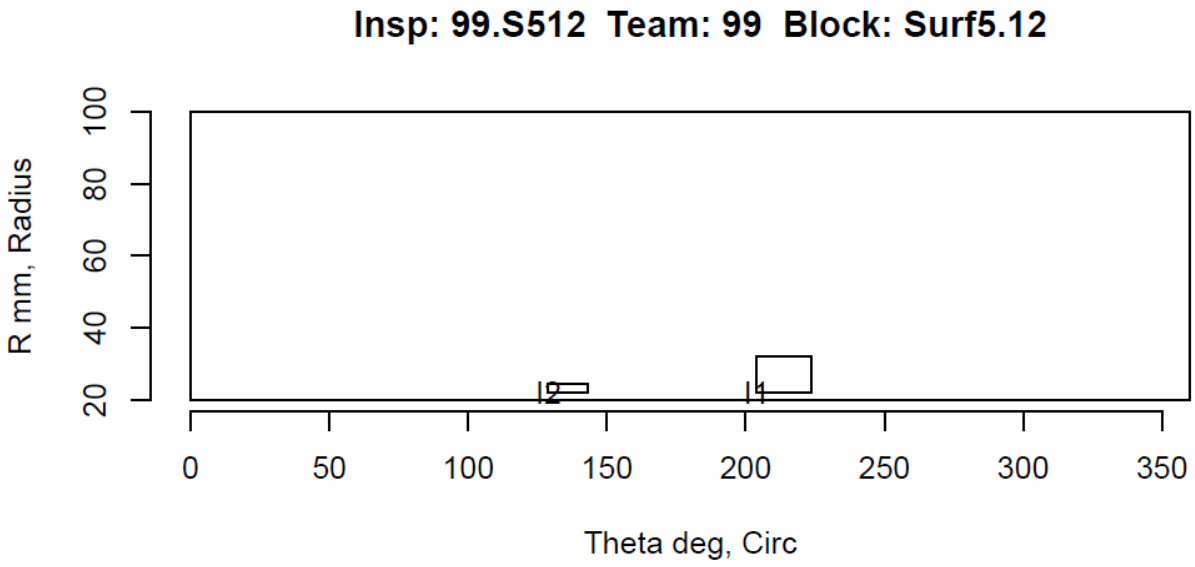
Insp: 99.S512 Team: 99 Block: Surf5.12
R mm, Radius
20
40
60
80
100
2
1
0
50
100
150
200
250
300
350
Theta deg, Circ

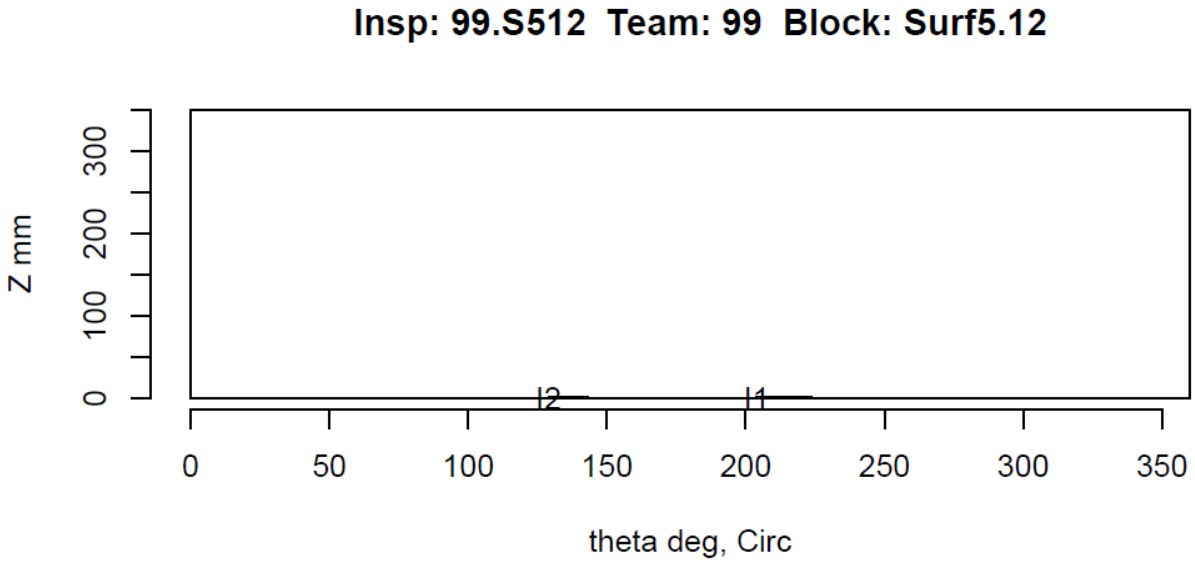
Insp: 99.S512 Team: 99 Block: Surf5.12
Z mm
0
100
200
300
2
1
0
50
100
150
200
250
300
350
theta deg, Circ

Appendix B

Destructive Analysis of BMI Samples

Appendix B

Destructive Analysis of BMI Samples

B.1 Destructive Analysis of Sample 5.2

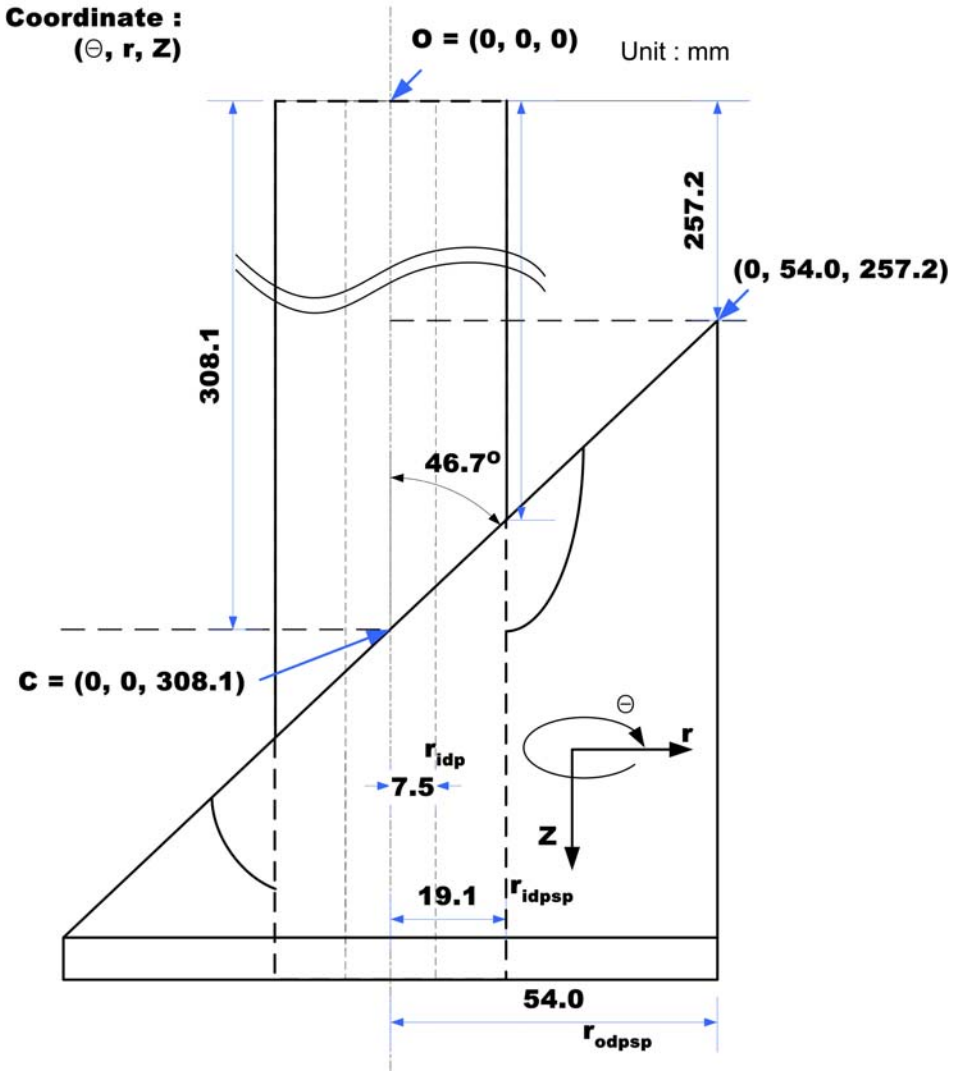

Figure B.1. Analysis of BMI Sample Position

List of Symbols

O	:	Origin coordinate of BMI sample
C	:	Center coordinate
r_{idp}	:	I.D. radius of pipe
r_{idpsp}	:	I.D. radius of pipe support plate
r_{odpsp}	:	O.D. radius of pipe support plate
r_{m1}	:	Minimum radial extent measured from pipe inner surface
r_1	:	Minimum radial extent of flaw, $r_1 = r_{idp} + r_{m1}$
r_{m2}	:	Maximum radial extent measured from pipe inner surface
r_2	:	Maximum radial extent of flaw, $r_2 = r_{idp} + r_{m2}$
Z_{m1}	:	Minimum measured vertical position
Z_{m2}	:	Maximum measured vertical position
Z_1	:	Minimum vertical position of flaw measured from origin O
Z_2	:	Maximum vertical position of flaw measured from origin O
θ_1	:	Minimum measured circumferential extent
θ_2	:	Maximum measured circumferential extent
$\mathbf{r_{min}}$	:	Minimum radial extent
$\mathbf{r_{max}}$	:	Maximum radial extent
$\mathbf{Z_{min}}$	:	Minimum vertical position from origin O
$\mathbf{Z_{max}}$	:	Maximum vertical position from origin O
$\boldsymbol{\theta}_{\mathbf{min}}$	:	Minimum circumferential extent
$\boldsymbol{\theta}_{\mathbf{max}}$	:	Maximum circumferential extent

1. Circumferential Crack, Surface Crack of Pipe O.D.

Position of Flaw

Flaw No.	Circ. Extent (deg)	Radial Extent (mm)		Vertical Position (mm)	
	θ	r_1	r_2	Z_1	Z_2
#1-10	305	-	-	-	-
#1-09	310	15.8	17.1	296.0	297.4
#1-08	315	15.8	18.7	295.8	297.6
#1-07	320	14.4	18.2	294.0	297.1
#1-06	325	15.0	18.9	292.7	296.4
#1-05	330	14.7	19.5	292.0	295.8
#1-04	335	14.9	19.6	291.4	295.6
#1-03	340	15.8	19.7	290.9	294.0
#1-02	345	16.0	19.7	290.4	293.3
#1-01	350	-	-	-	-

Final Results of Destructive Test on BMI Test Sample

BMI Test Block Number	Circ. Extent (deg)		Radial Extent (mm)		Vertical Position (mm)	
	θ_{min}	θ_{max}	r_{min}	r_{max}	Z_{min}	Z_{max}
Flaw No. #1	305	350	14.4	19.7	290.4	297.6

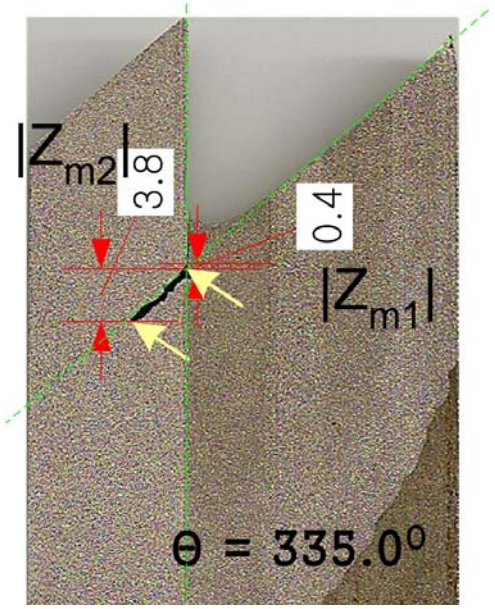

Figure B.2. Flaw #1 Surface Crack of Pipe O.D.

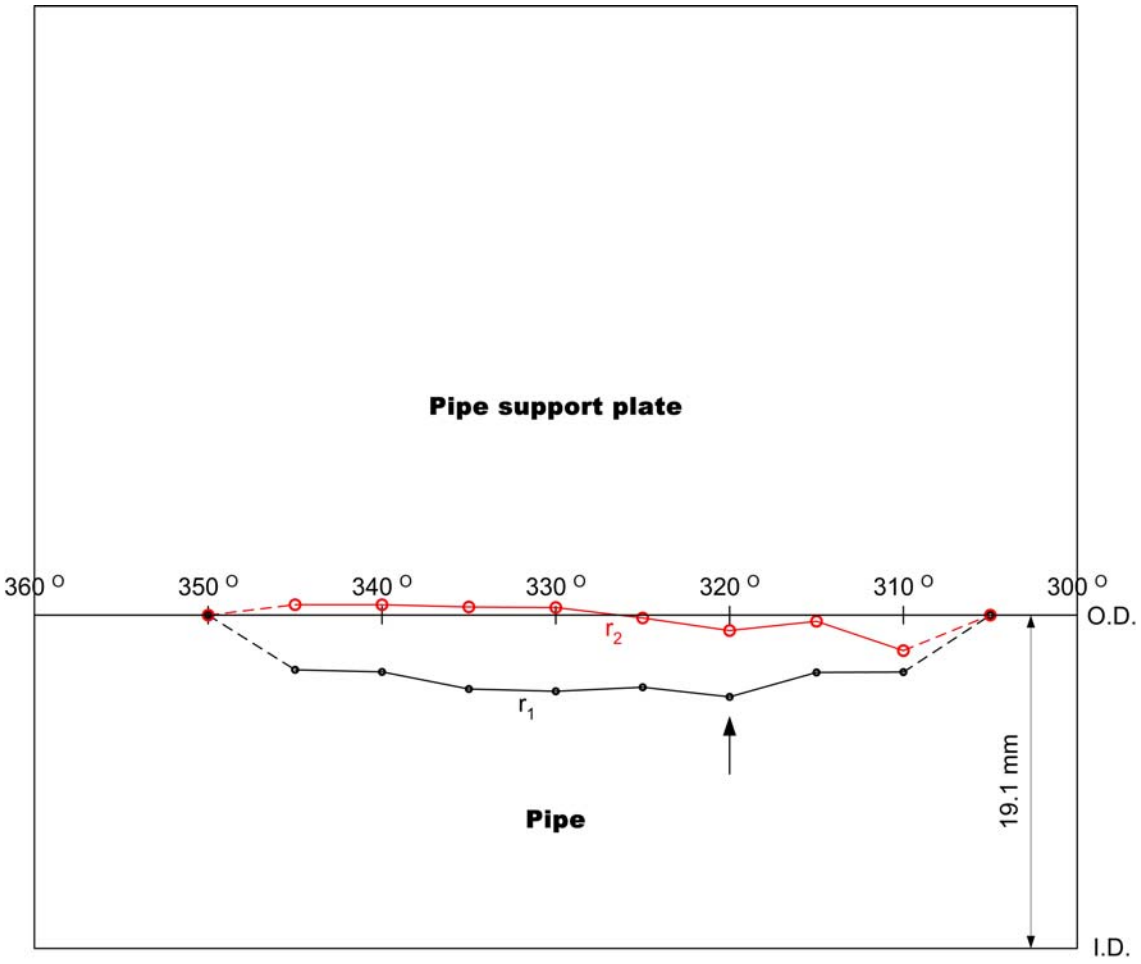

Figure B.3. Depth Profile of Flaw #1 Using r_1 and r_2

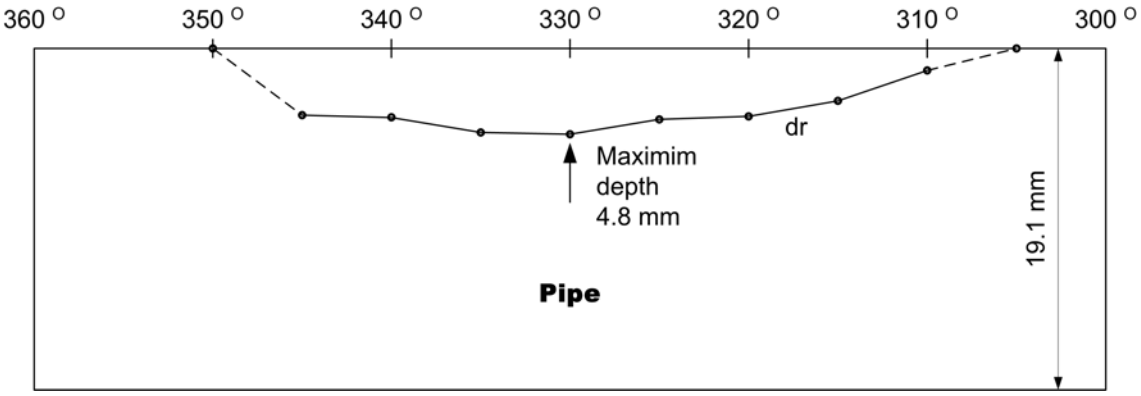

Figure B.4. Depth Profile of Flaw # 1 Using dr (= $r_2 - r_1$)

2. Circumferential Crack, Through Wall Crack

Position of Flaw

Flaw No.	Circ. Extent (deg) θ	Radial Extent (mm) r	Vertical Position (mm) Z_1	Z_2
#2-13*	225	9.2*	314.5	313.9
#2-12*	230	18.9*	317.0	313.5
#2-11	235	19.1	314.7	312.4
#2-10	240	19.1	313.0	312.1
#2-09	245	19.1	311.9	311.5
#2-08	250	19.1	310.6	310.9
#2-07	255	19.1	308.9	310.0
#2-06	260	19.1	307.8	310.1
#2-05	265	19.1	306.4	309.8
#2-04	270	19.1	305.4	309.6
#2-03	275	19.1	304.5	309.2
#2-02*	280	15.8*	305.4	309.8
#2-01*	285	11.3*	307.0	309.6

* : Not perfectly through wall crack

Final Results of Destructive Test on BMI Test Sample

BMI Test Block Number	Circ. Extent (deg)		Radial Extent (mm)		Vertical Position (mm)	
	θ_{min}	θ_{max}	r_{min}	r_{max}	Z_{min}	Z_{max}
Flaw No. #2	220	290	9.2	19.1	304.5	317.0

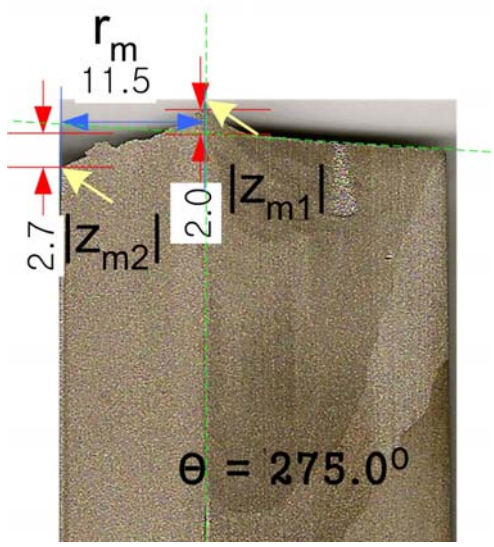

Figure B.5. Flaw #2 Through Wall Crack

3. Axial Crack, 0.05” from Interface J-weld and Nozzle O.D.

Position of Flaw

Flaw No.	Circ. Extent (deg)		Radial Extent (mm)		Vertical Position (mm)	
	θ_1	θ_2	r_1	r_2	Z_1	Z_2
#3-01	-	-	-	-	-	-
#3-02	150	154	19.9	27.3	327.1	334.0
#3-03	149	153	19.8	25.9	329.6	335.3
#3-04	148	155	19.3	24.9	331.7	337.6
#3-05	149	155	19.5	21.9	334.9	337.8
#3-06	151	155	21.2	22.6	339.3	341.2
#3-07	-	-	-	-	-	-

Final Results of Destructive Test on BMI Test Sample

BMI Test Block Number	Circ. Extent (deg)		Radial Extent (mm)		Vertical Position (mm)	
	θ_{min}	θ_{max}	r_{min}	r_{max}	Z_{min}	Z_{max}
Flaw No. #3	148	155	19.3	27.3	327.1	341.2

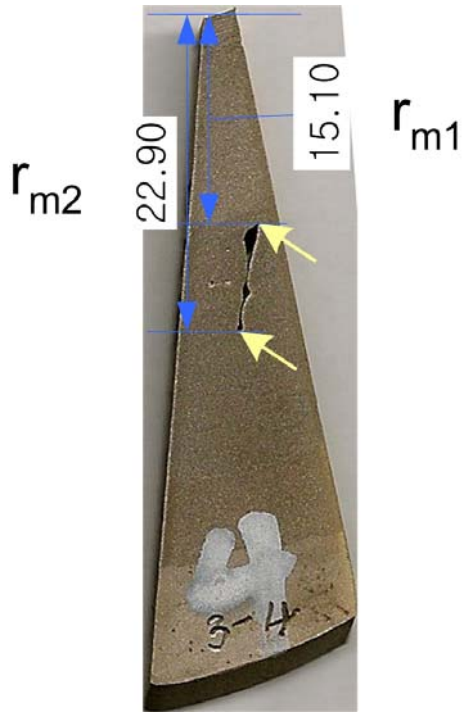

Figure B.6. Flaw #3 Interface J-weld and Nozzle O.D.

3A. Axial Crack, I.D. Notch on Carbon Steel Plate

Position of Flaw

Flaw No.	Circ. Extent (deg)		Radial Extent (mm)		Vertical Position (mm)	
	θ_1	θ_2	r_1	r_2	Z_1	Z_2
#3A-initial	89.6	91.7	19.0	19.7	305.2	305.9
#3A-01	89.6	91.7	19.0	19.7	308.0	308.6
#3A-02	89.7	91.8	19.0	20.5	310.8	311.5
#3A-03	90.0	91.9	19.1	20.8	313.6	314.2
#3A-04	90.2	91.9	19.0	20.7	316.4	317.0
#3A-05	90.5	92.1	18.8	20.4	319.2	319.8
#3A-06	90.5	92.1	19.0	20.7	322.0	322.6
#3A-07	90.5	92.0	19.1	20.8	324.7	325.3
#3A-08	90.5	92.0	19.0	20.8	327.5	328.0
#3A-09	90.6	91.9	19.1	20.9	330.3	330.7
#3A-10	90.7	92.1	19.1	21.1	333.1	333.6
#3A-11	89.7	92.5	18.6	20.4	335.5	336.4
#3A-12	89.9	91.9	18.8	20.0	338.3	339.0
#3A-13	89.9	91.8	18.9	20.2	341.0	341.7
#3A-14	89.9	91.8	18.9	20.2	343.8	344.4
#3A-15	89.9	91.8	18.9	20.3	346.5	347.2
#3A-16	89.9	91.8	18.9	20.4	349.3	349.9
#3A-17	89.9	91.8	18.9	20.3	352.0	352.7

Final Results of Destructive Test on BMI Test Sample

BMI Test Block Number	Circ. Extent (deg)		Radial Extent (mm)		Vertical Position (mm)	
	θ_{min}	θ_{max}	r_{min}	r_{max}	Z_{min}	Z_{max}
Flaw No. #3A	89.6	92.5	18.6	21.1	305.2	352.7

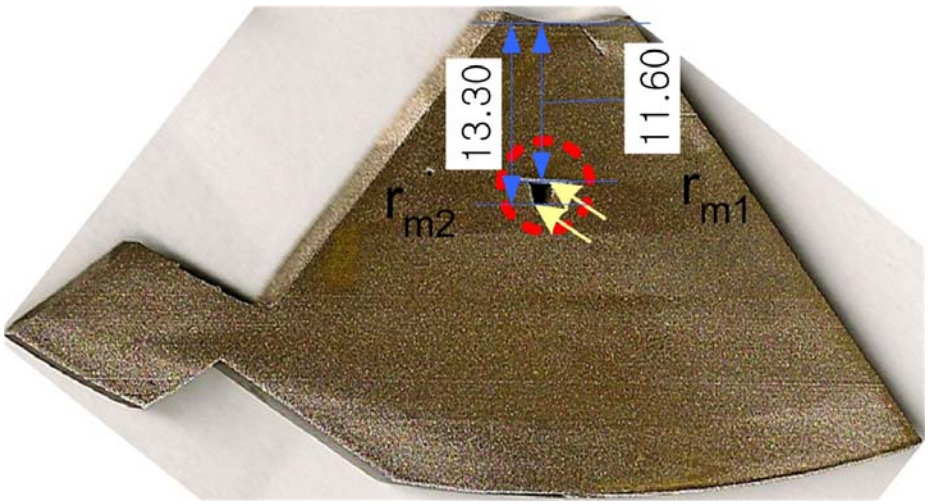

Figure B.7. Flaw #3A I.D. Notch on Carbon Steel Plate

4. Slag Crack, 0.02” from Interface J-weld and Nozzle O.D.

Position of Flaw

Flaw No.	Circ. Extent (deg)	Radial Extent (mm)		Vertical Position (mm)	
	θ	r_1	r_2	Z_1	Z_2
#4-10	20	21.1	22.8	297.4	299.8
#4-09	25	19.9	23.7	294.1	301.9
#4-08	30	19.8	23.7	296.7	304.1
#4-07	35	19.6	23.7	297.2	305.2
#4-06	40	19.7	23.6	297.0	305.7
#4-05	45	19.7	23.5	299.2	306.8
#4-04	50	17.4	21.0	300.9	307.9
#4-03	55	19.8	22.6	300.8	307.9
#4-02	60	21.2	21.5	304.6	305.6
#4-01	65	21.2	21.9	306.1	306.8

Final Results of Destructive Test on BMI Test Sample

BMI Test Block Number	Circ. Extent (deg)		Radial Extent (mm)		Vertical Position (mm)	
	θ_{min}	θ_{max}	r_{min}	r_{max}	Z_{min}	Z_{max}
Flaw No. #4	15	70	17.4	23.7	294.1	307.9

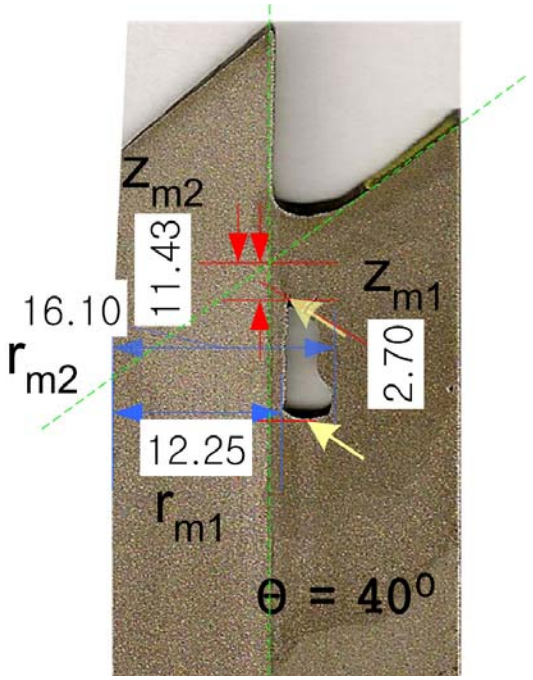

Figure B.8. Flaw #4 508 from Interface J-weld and Nozzle O.D.

5. Axial Crack, Surface Crack of Pipe I.D.

Position of Flaw

Flaw No.	Circ. Extent (deg)		Radial Extent (mm)		Vertical Position (mm)	
	θ_1	θ_2	r_1	r_2	Z_1	Z_2
#5-01	102	106	8.4	9.5	296.0	296.8
#5-02	100	107	7.5	10.7	298.3	300.1
#5-03	100	107	7.5	10.2	301.1	302.6
#5-04	100	107	7.5	10.2	303.8	305.4
#5-05	100	107	7.5	10.2	306.6	308.1
#5-06	100	107	7.5	10.3	309.3	310.9
#5-07	100	107	7.5	9.8	312.1	313.5
#5-08	100	107	7.5	10.3	314.8	316.4
#5-09	100	107	7.5	10.5	317.6	319.2
#5-10	100	107	7.5	9.3	320.3	321.6

Final Results of Destructive Test on BMI Test Sample

BMI Test Block Number	Circ. Extent (deg)		Radial Extent (mm)		Vertical Position (mm)	
	θ_{min}	θ_{max}	r_{min}	r_{max}	Z_{min}	Z_{max}
Flaw No. #5	100	107	7.5	10.7	296.0	321.6

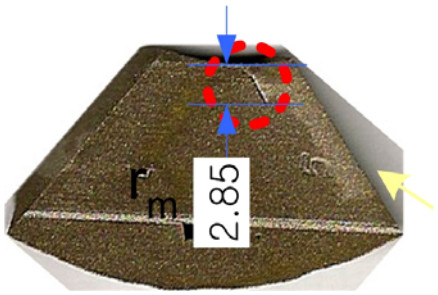

Figure B.9. Flaw #5 Surface Crack of Pipe I.D.

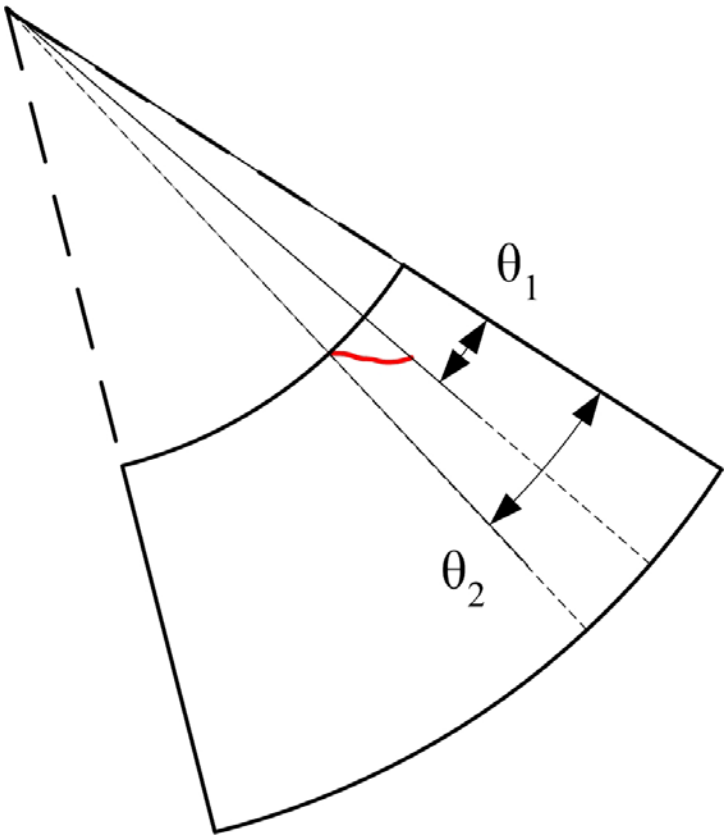

Figure B.10. Flaw #5 Angle of Crack

B.2 Destructive Analysis of Sample 5.10

The six flaws had a consistent profile. Four of the six flaws, 1, 2, 4, and 6, had a shallow surface-breaking component and disconnected segments deeper into the material. Flaw 3 was very shallow and flaw 5 was continuous.

The surface and profile of Flaw 1 showed that the flaw was reasonably discontinuous on the surface and is not continuous until the first 2 mm of weld. The surface-breaking segment measured at the cut surface only penetrated 0.6 mm into the weld. One team was able to detect Flaw 1.

Flaw 2 is very discontinuous at the surface, and the surface-breaking component of the crack is a mere 0.2 mm into the weld. At a depth of 1.5 mm, the flaw becomes continuous and much wider. Flaw 2 can almost be considered an embedded flaw, as the surface-breaking component is so tight and shallow. No teams were able to detect Flaw 2.

Flaw 3 is the smallest measured using DE, with three small surface-breaking components and a measured depth of 0.35 mm. No teams were able to detect Flaw 3.

Flaw 4 had a discontinuous surface profile along the surface and along the cross section, but the surface-breaking segment of the crack was almost 1-mm deep. Also, the flaw has a "T"-shaped profile that would make it more easily detectable by eddy current systems that are sensitive to the orientation of the crack. Three teams detected Flaw 4.

Flaw 5 was continuous along the surface and the cross section into the weld. One team was able to detect Flaw 5.

Flaw 6 was challenging to characterize at the surface with a scanning electron microscope, and is not continuous through the cross section. This flaw may be considered an embedded flaw, as the surface-breaking component penetrates only 0.2 mm into the material.

The measured properties are listed in Table B.1 along with the PINC round-robin PODs for the flaws are summarized in Table B.1. It should be noted that the crack CODs were measured after the surface was polished.

Table B.1. Measured Properties for Flaws in Sample 5.10

Flaw	Length (mm)	Depth	COD	SB Depth	POD
5.10-1	7.5	9	28	0.6	0.14
5.10-2	5	7	12	0.2	0.00
5.10-3	0.8, 3.5	0.35	15	0.35	0.00
5.10-4	7	2	32	0.95	0.43
5.10-5	4.5	2	12	2	0.14
5.10-6	1.6	4.5	10	0.2	0.00

Flaw 1

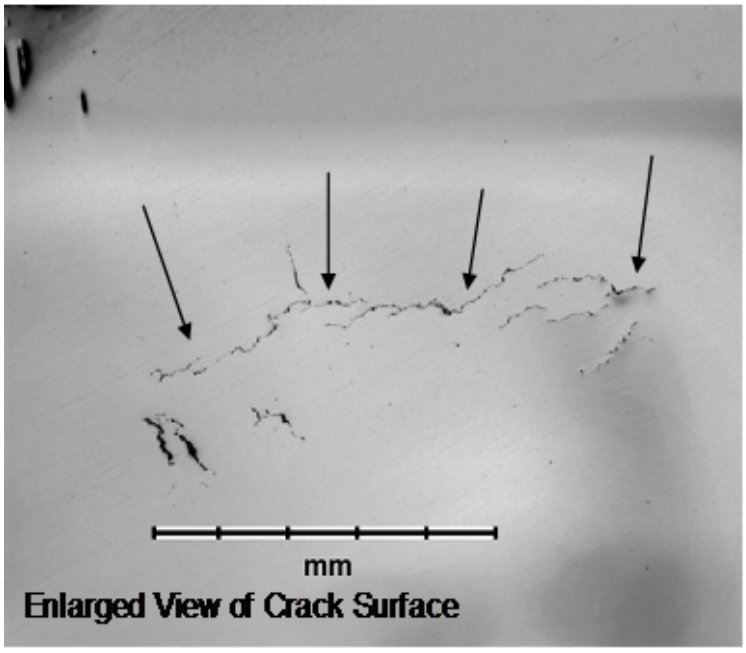

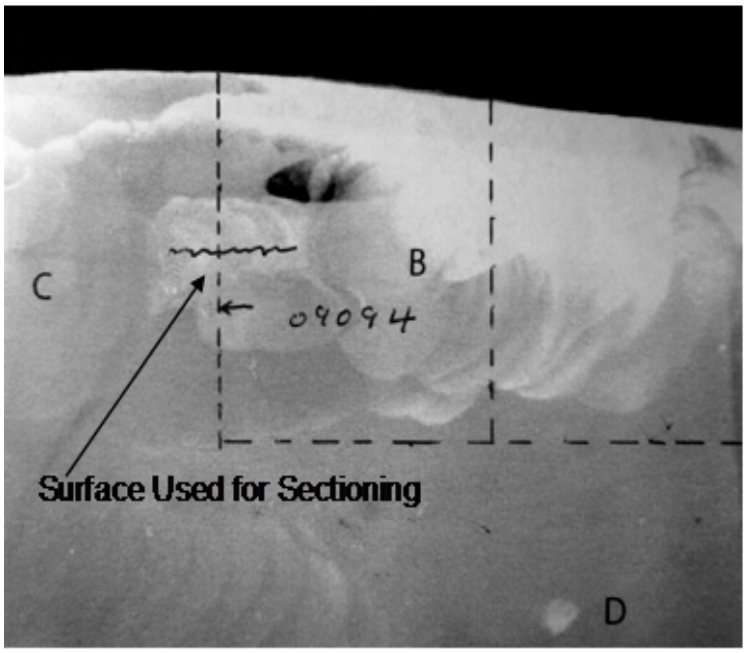

SEM of Cross Section

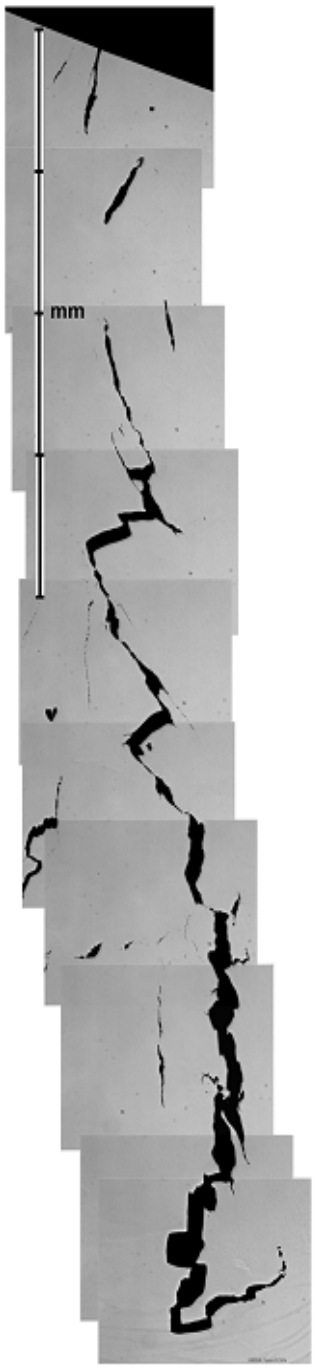

Flaw 1

Measured Length	7.5 mm
COD at Surface	28 μm
Depth of Surface Breaking Segment	0.6 mm
Total Depth	9 mm

Flaw 2

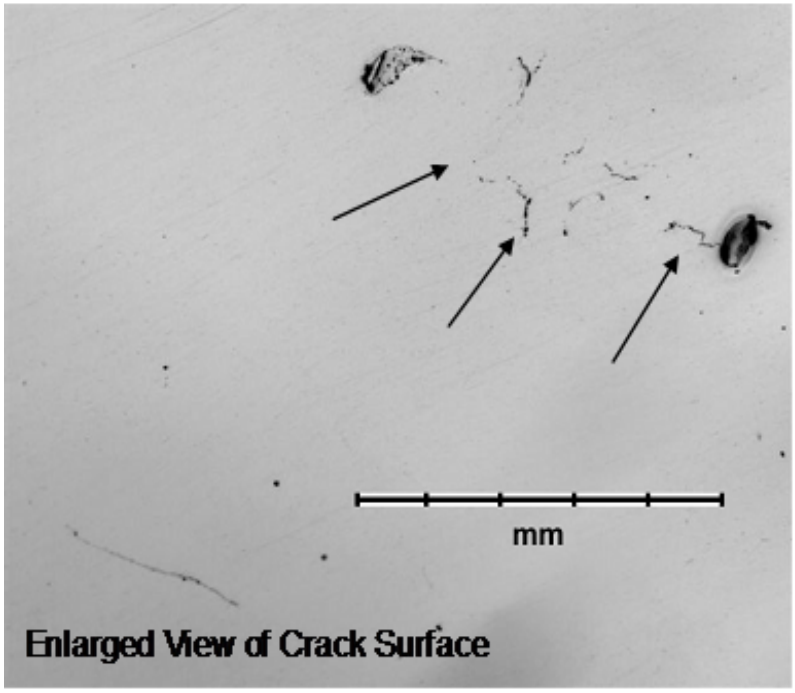

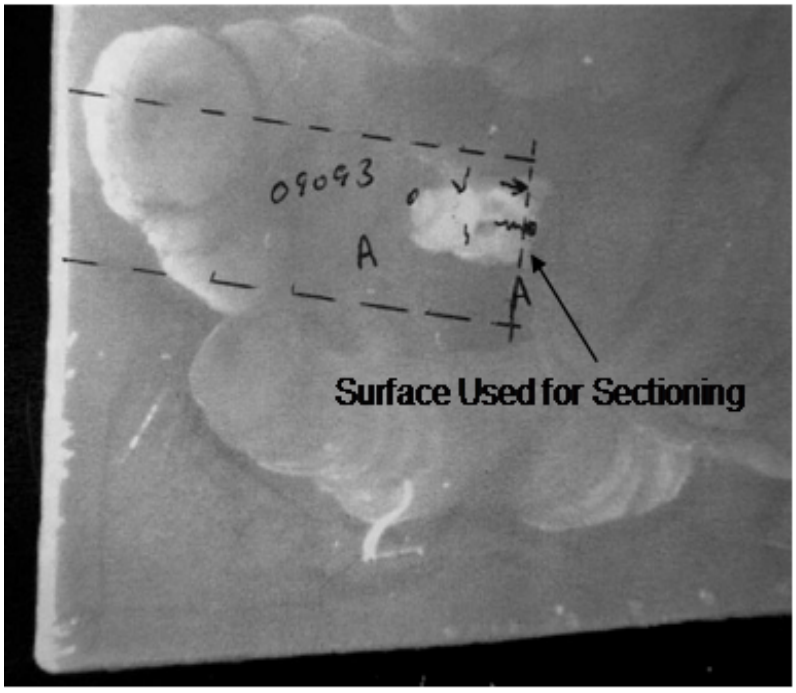

SEM of Cross Section

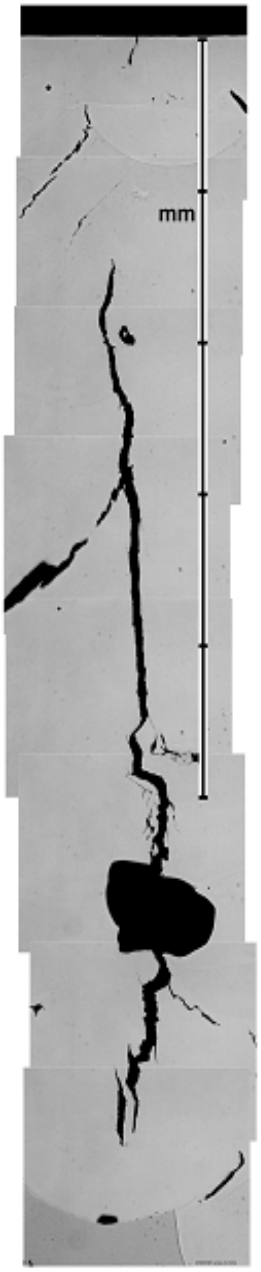

Flaw 2

Measured Length	5 mm
COD at Surface	12 μm
Depth of Surface Breaking Segment	0.2 mm
Total Depth	7 mm

Flaw 3

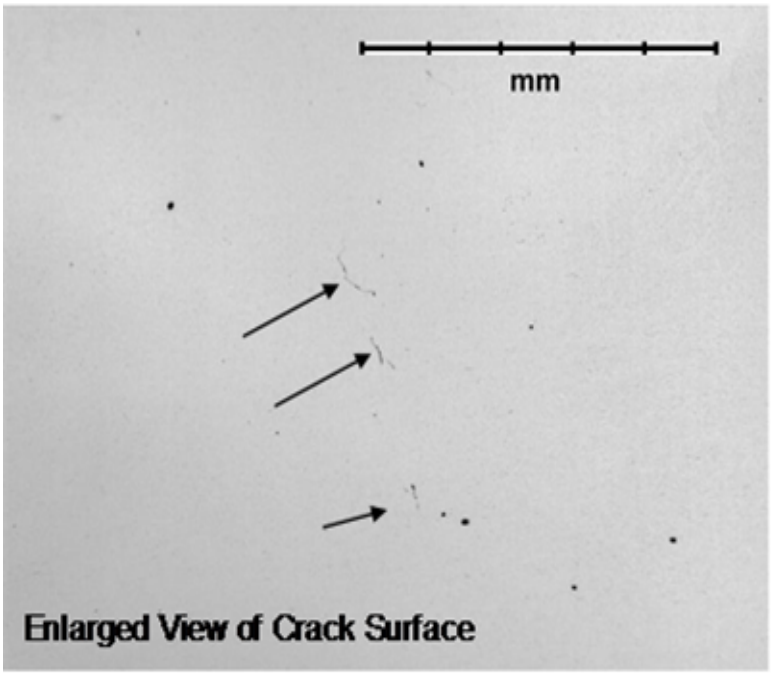

SEM of Cross Section

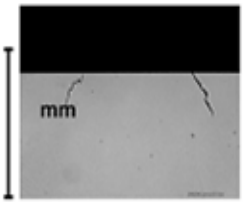

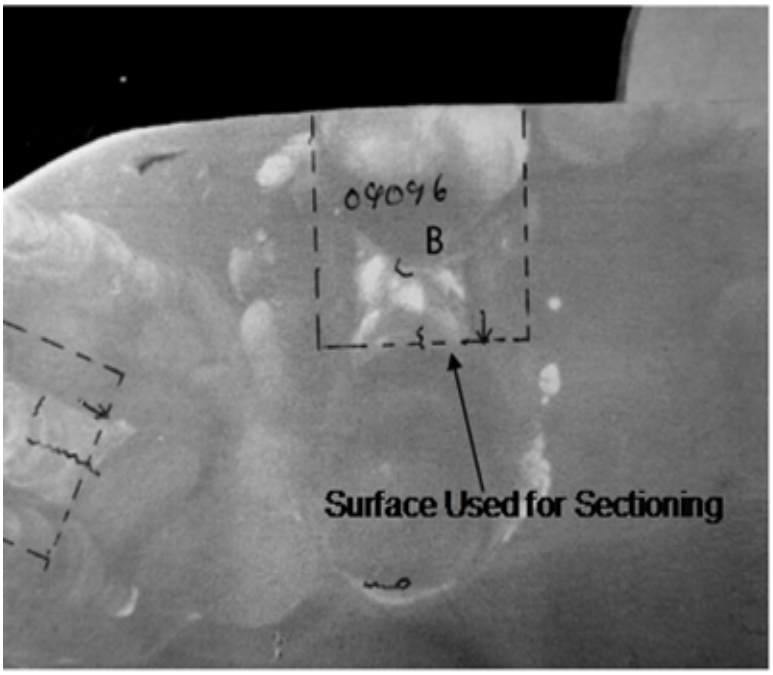

Flaw 3

Measured Length	3.5 mm
COD at Surface	15 µm
Depth of Surface Breaking Segment	0.35 mm
Total Depth	0.35 mm

Flaw 4

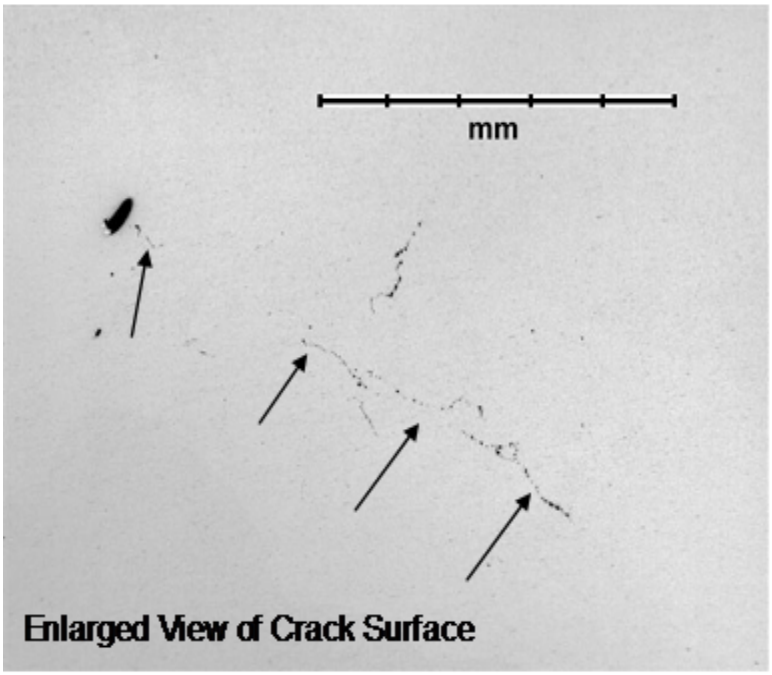

SEM of Cross Section

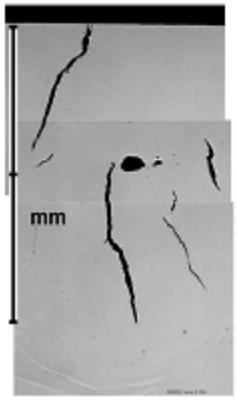

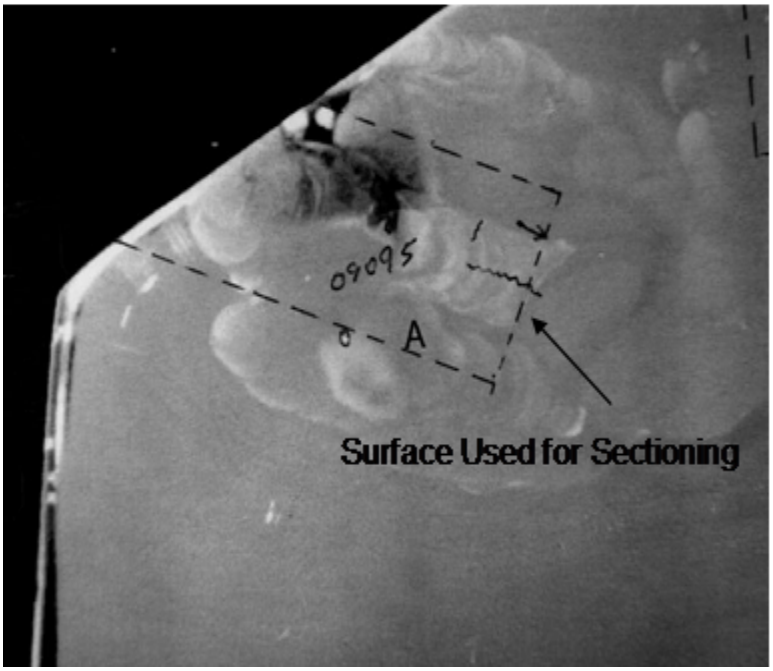

Flaw 4

Measured Length	7 mm
COD at Surface	32 µm
Depth of Surface Breaking Segment	0.9 mm
Total Depth	2 mm

Flaw 5

SEM of Cross Section

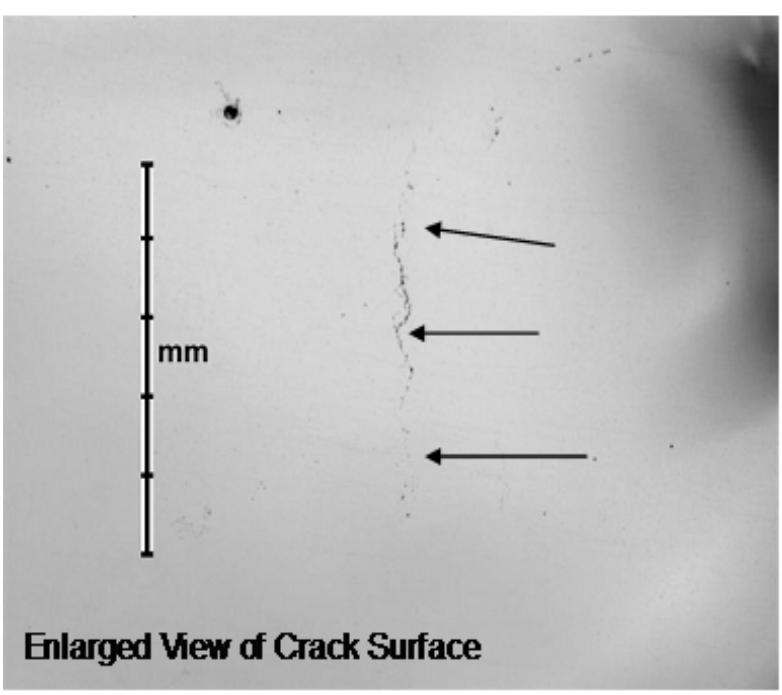

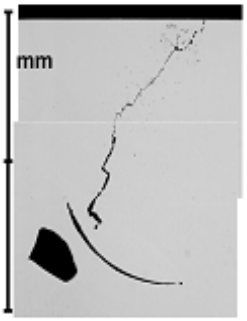

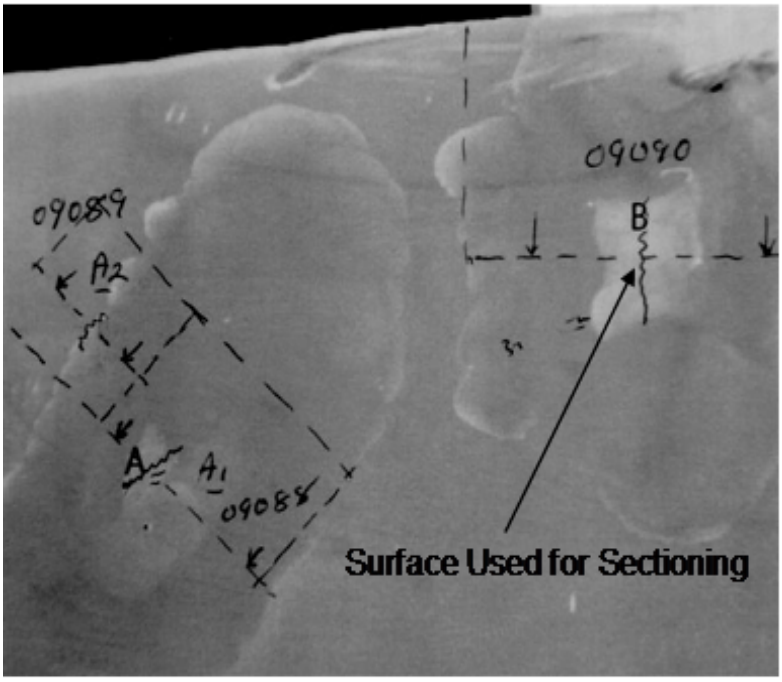

Flaw 5

Measured Length	4.5 mm
COD at Surface	12 μm
Depth of Surface Breaking Segment	1.5 mm
Total Depth	2 mm

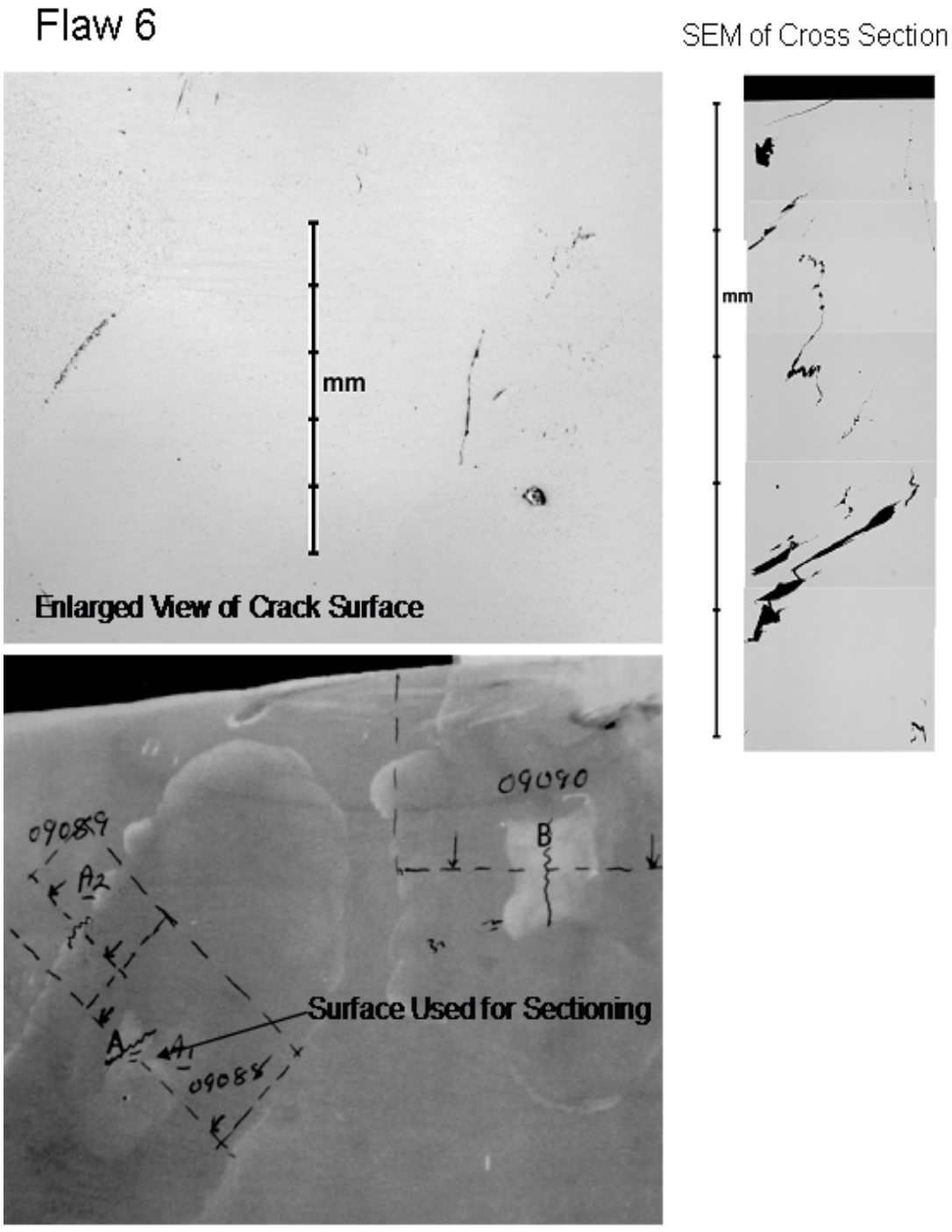

For flaw 6, there was a surface blemish and an apparent crack.

Flaw 6

Measured Length	1.6 mm
COD at Surface	10 μm
Depth of Surface Breaking Segment	0.2 mm
Total Depth	4.5 mm

B.3 Destructive Analysis of Sample 5.11–5.16

Final Results of Destructive Test on JNES BMI Test Block

PINC Test Block Number (Puch mark number)	Defect Number	Circum. Extent (deg.)		Radial extent (mm)		Depth (mm)		Vertical position (mm)	
		Θ1	Θ2	r1	r2	Z1	Z2	Y1	Y2
PINC 5.13 (S-1)	5.13-1	-11.0	7.8	34.7	36.9	0.0	2.2	147.0	149.1
	5.13-2	175.0	188.0	33.3	36.1	0.0	2.4	147.4	150.5
PINC 5.14 (S-2)	5.14-1	-19.9	22.5	29.8	36.6	0.0	10.5	147.2	157.3
	5.14-2	166.9	194.8	29.0	31.4	0.0	2.1	146.8	148.5
PINC 5.15 (S-3)	5.15-1	87.7	91.1	25.1	36.4	0.0	3.5	143.0	148.5
	5.15-2	265.3	270.8	25.0	35.2	0.0	3.3	143.3	149.6
PINC 5.16 (S-4)	5.16-1	88.9	95.5	22.4	38.8	0.0	10.9	138.1	156.5
	5.16-2	268.9	275.9	23.2	36.6	0.0	5.8	139.7	150.8

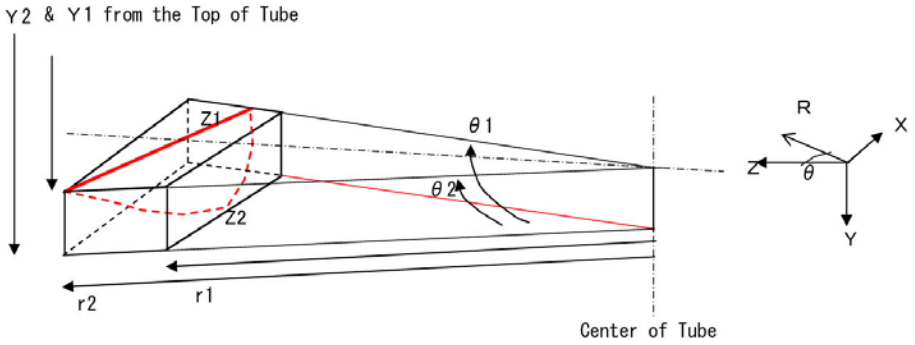

(1) Overview

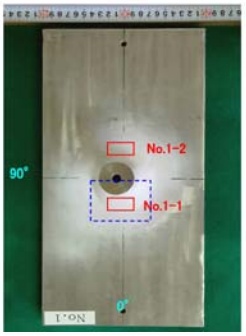

1

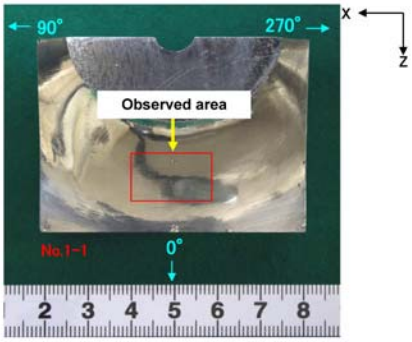

(2) Profile of SCC　　○: Measured on sliced cross section

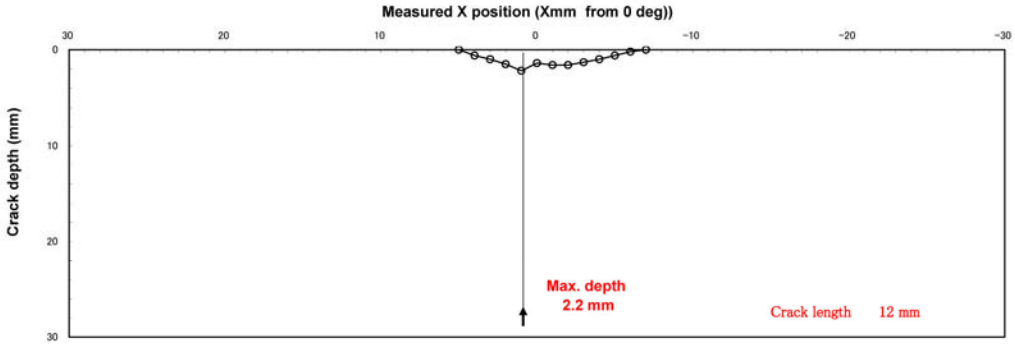

(3) Measured data of SCC

Position (mm)		X=5.0	X=4.0	X=3.0	X=2.0	X=1.0
Depth (mm)	d	0.0	0.6	1.0	1.5	2.2
Opening (μm)		0	2	3	3	2
Tilt (deg) (*)		—	-1	2	14	-27
Position of surf. opening (mm)	X	5.0	4.0	3.0	2.0	1.0
	Y	—	147.4	147.3	147.2	147.1
	Z	—	36.5	36.0	36.0	35.7
Position of crack tip (mm)	X	5.0	4.0	3.0	2.0	1.0
	Y	—	148.1	148.3	148.8	149.1
	Z	—	36.5	36.0	36.4	34.7

Position (mm)		X=0.0	X=-1.0	X=-2.0	X=-3.0	X=-4.0
Depth (mm)	d	1.4	1.6	1.6	1.3	1.0
Opening (μm)		3	31	2	2	2
Tilt (deg) (*)		-5	8	-5	-5	-2
Position of surf. opening (mm)	X	0.0	-1.0	-2.0	-3.0	-4.0
	Y	147.0	147.0	147.2	147.2	147.1
	Z	35.5	35.7	36.1	36.0	35.8
Position of crack tip (mm)	X	0.0	-1.0	-2.0	-3.0	-4
	Y	148.4	148.8	148.8	148.4	148.1
	Z	35.4	35.9	36.0	35.9	35.7

Position (mm)		X=-5.0	X=-6.0	X=-7.0		
Depth (mm)	d	0.6	0.2	0.0		
Opening (μm)		3	1	0		
Tilt (deg) (*)		4	-32	—		
Position of surf. opening (mm)	X	-5.0	-6.0	-7.0		
	Y	147.1	147.3	—		
	Z	35.7	36.1	—		
Position of crack tip (mm)	X	-5.0	-6.0	-7.0		
	Y	147.7	147.4	—		
	Z	35.8	36.0	—		

(*) Measured from Y coordinate (+ : clockwise)

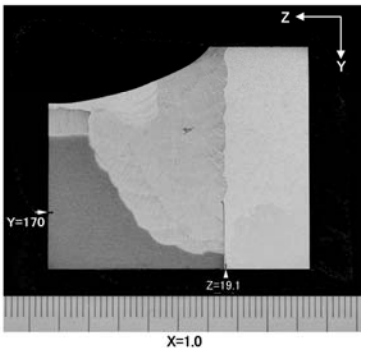

X=1.0

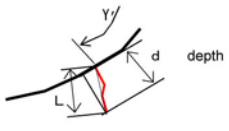

Results of destructive test on PINC 5.13-1 (parallel to weld)

Max depth	Za	Zb	Ya	Yb	L	d
	35.67	34.65	147.1	149.1	2.245	2.2

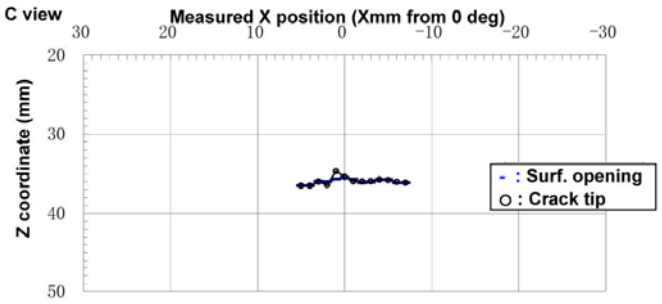

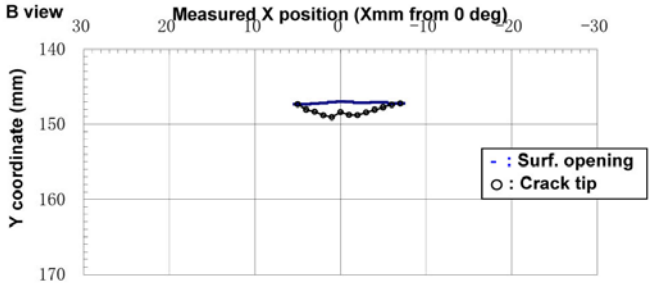

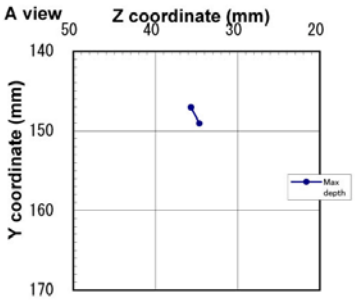

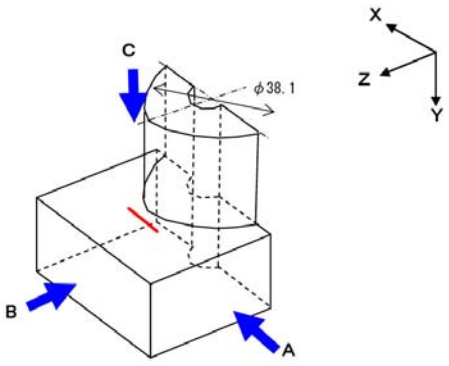

Overview

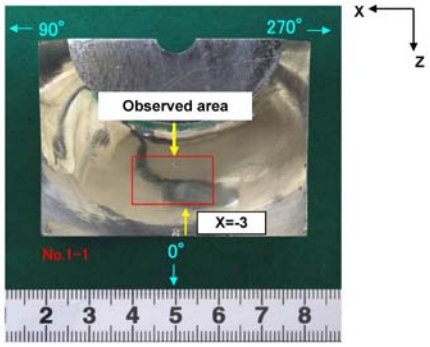

Macro. photo of cross section

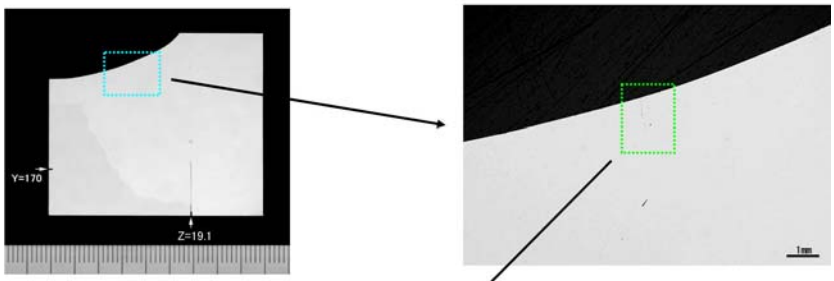

Micro. photo of cross section

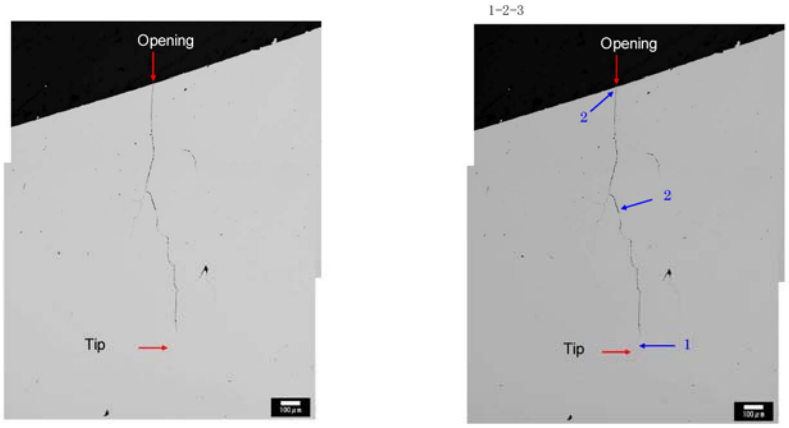

Position (mm)		X=-3.0
Depth (mm)	d	1.3
Opening (μm)		2
Tilt (deg) (°)		-5
Position of surf. opening (mm)	X	-3.0
	Y	147.2
	Z	36.0
Position of crack tip (mm)	X	-3.0
	Y	148.4
	Z	35.9

Typical crack opening data of PINC 5.13-1 (parallel to weld)
(X=- 3.0)

Overview

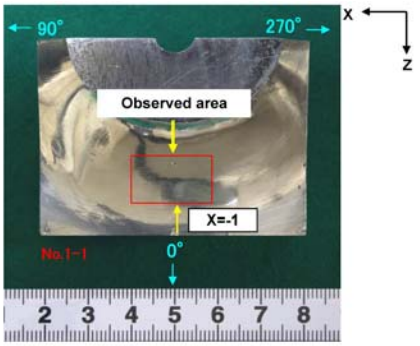

Macro. photo of cross section

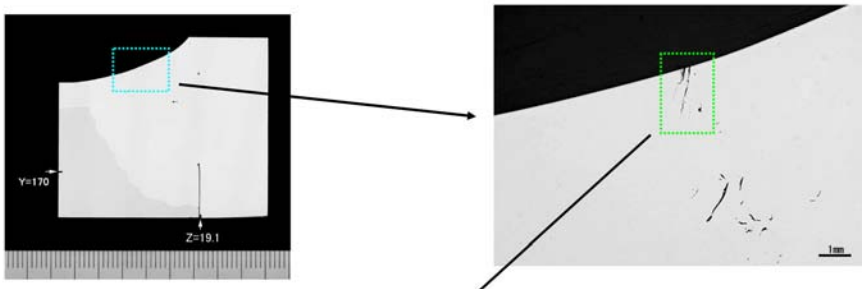

Micro. photo of cross section

1-2-1

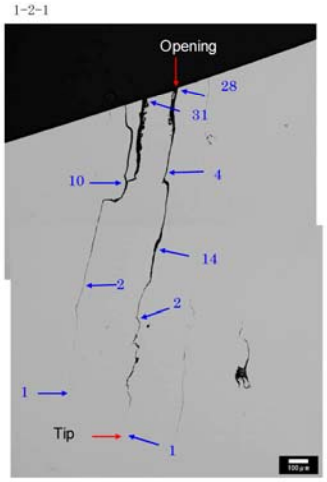

Position (mm)		X=−1.0
Depth (mm)	d	1.6
Opening (μm)		31
Tilt (deg) (°)		8
Position of surf. opening (mm)	X	−1.0
	Y	147.0
	Z	35.7
Position of crack tip (mm)	X	−1.0
	Y	148.8
	Z	35.9

Typical crack opening data of PINC 5.13-1 (parallel to weld)
(X=-1.0)

Overview

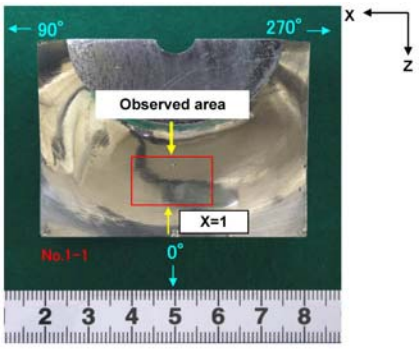

Macro. photo of cross section

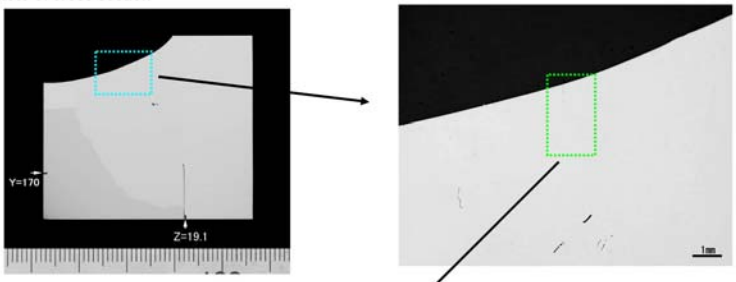

Micro. photo of cross section

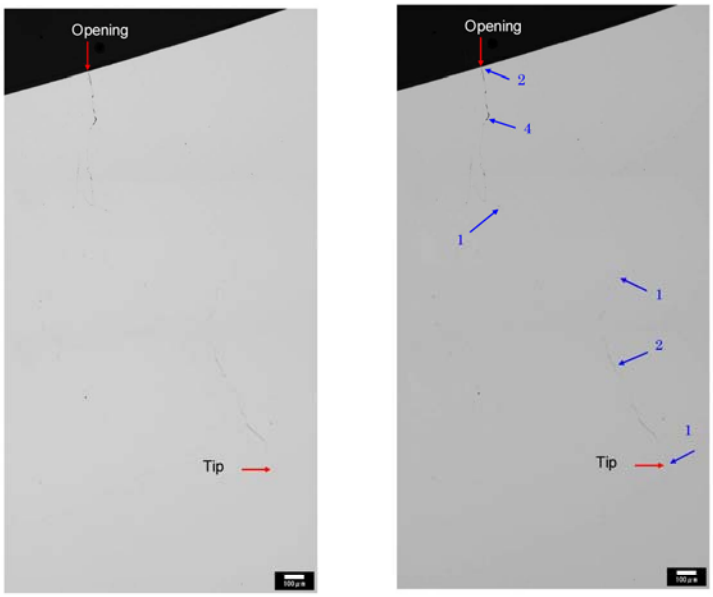

Position (mm)		X=1.0
Depth (mm)	d	2.2
Opening (μm)		2
Tilt (deg) (*)		-27
Position of surf. opening (mm)	X	1.0
	Y	147.1
	Z	35.7
Position of crack tip (mm)	X	1.0
	Y	149.1
	Z	34.7

Typical crack opening data of PINC 5.13-1 (parallel to weld)
(X=1)

Overview

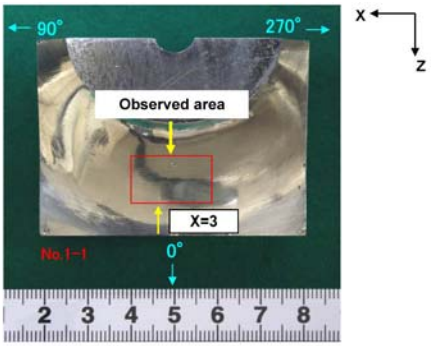

Macro. photo of cross section

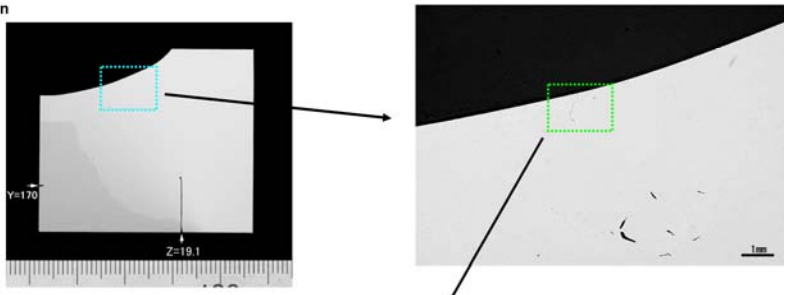

Micro. photo of cross section

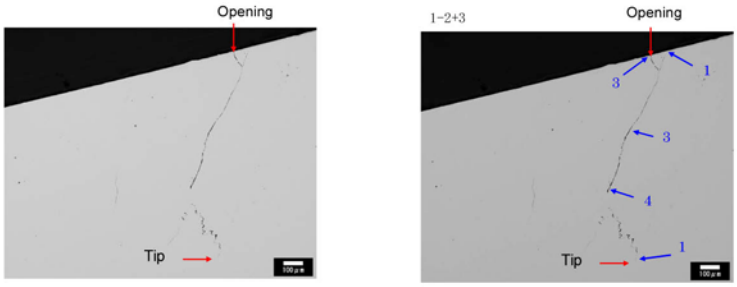

Position (mm)		X=3.0
Depth (mm)	d	1.0
Opening (μm)		3
Tilt (deg) (°)		2
Position of surf. opening (mm)	X	3.0
	Y	147.3
	Z	36.0
Position of crack tip (mm)	X	3.0
	Y	148.3
	Z	36.0

Typical crack opening data of PINC 5.13-1 (parallel to weld)
(X=3)

(1) Overview

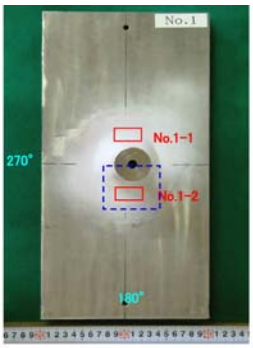

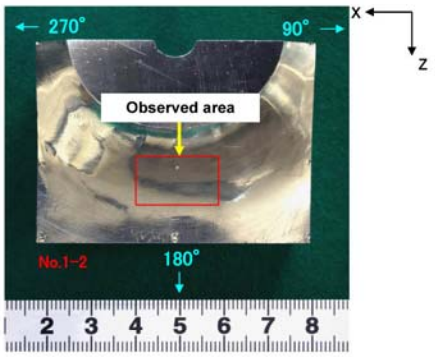

(2) Profile of SCC　　○: Measured on sliced cross section

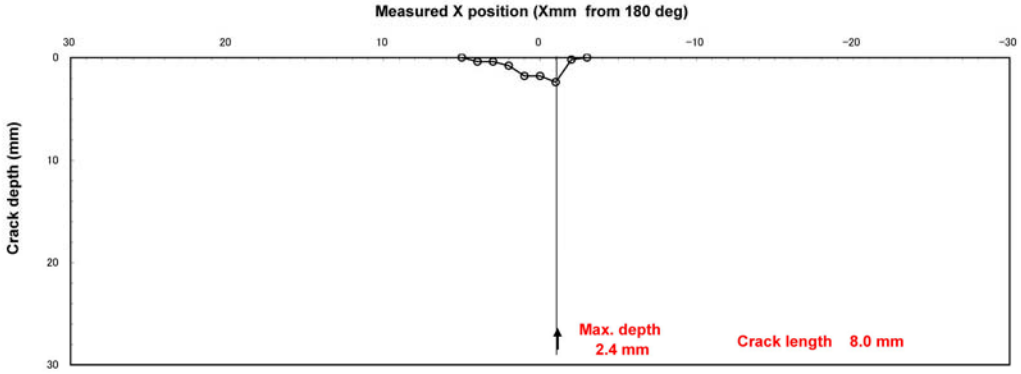

(3) Measured data of SCC

Position (mm)		X=5.0	X=4.0	X=3.0	X=2.0	X=1.0
Depth (mm)	d	0.0	0.4	0.4	0.8	1.8
Opening (μm)		0	3	1	1	2
Tilt (deg) (*)		—	-6	38	-6	8
Position of surf. opening (mm)	X	5.0	4.0	3.0	2.0	1.0
	Y	—	148.3	147.4	147.6	148.1
	Z	—	35.8	33.1	33.7	34.9
Position of crack tip (mm)	X	5.0	4.0	3.0	2.0	1.0
	Y	—	148.8	147.9	148.4	150.1
	Z	—	35.7	33.6	33.6	35.2

Position (mm)		X=0.0	X=-1.0	X=-2.0	X=-3.0	
Depth (mm)	d	1.8	2.4	0.2	0.0	
Opening (μm)		1	2	1	0	
Tilt (deg) (*)		29	20	25	—	
Position of surf. opening (mm)	X	0.0	-1.0	-2.0	-3.0	
	Y	147.8	147.7	147.8	—	
	Z	34.1	34.0	34.3	—	
Position of crack tip (mm)	X	0.0	-1.0	-2.0	-3.0	
	Y	150.3	150.5	148.1	—	
	Z	35.5	35.0	34.5	—	

(*) Measured from Y coordinate (+ : clockwise)

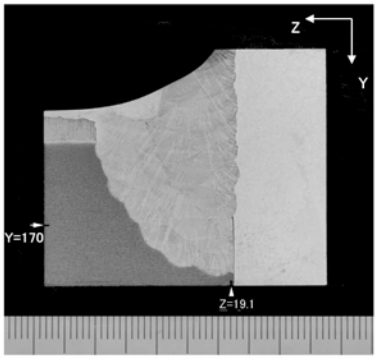

X=5.0

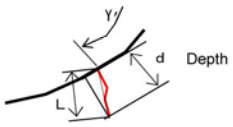

Results of destructive test on PINC 5.13-2 (parallel to weld)

Max depth	Za	Zb	Yb	Yb	L	d
	34.0	35.0	147.7	150.5	2.93	2.4

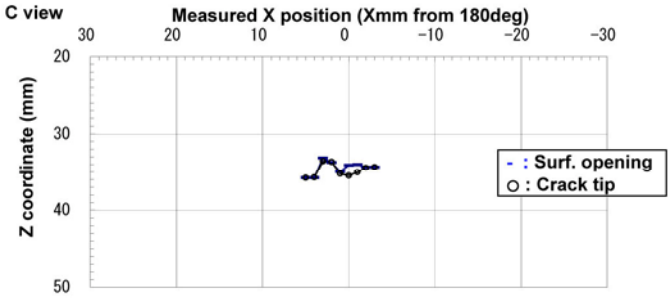

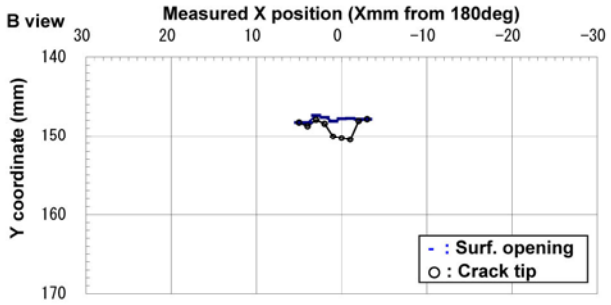

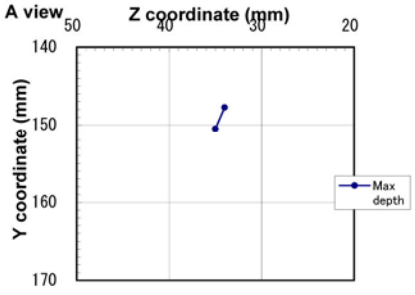

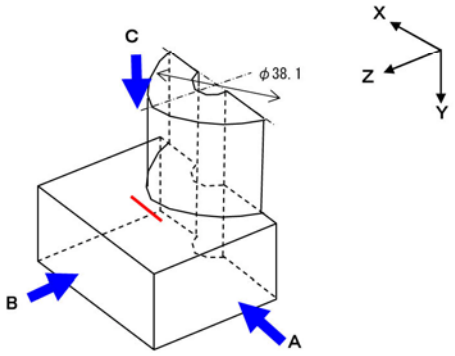

Overview

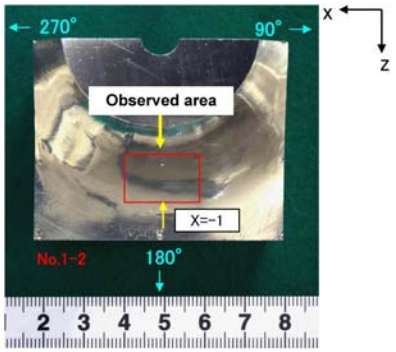

Macro. photo of cross section

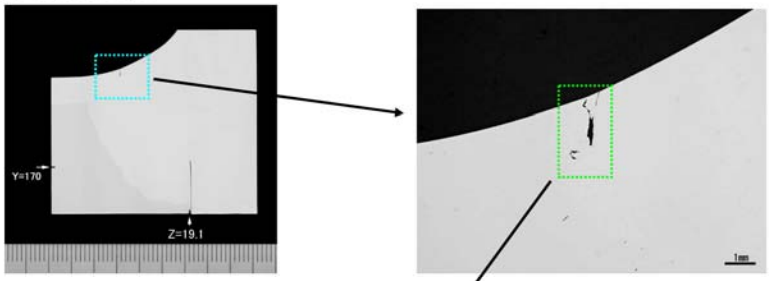

Micro. photo of cross section

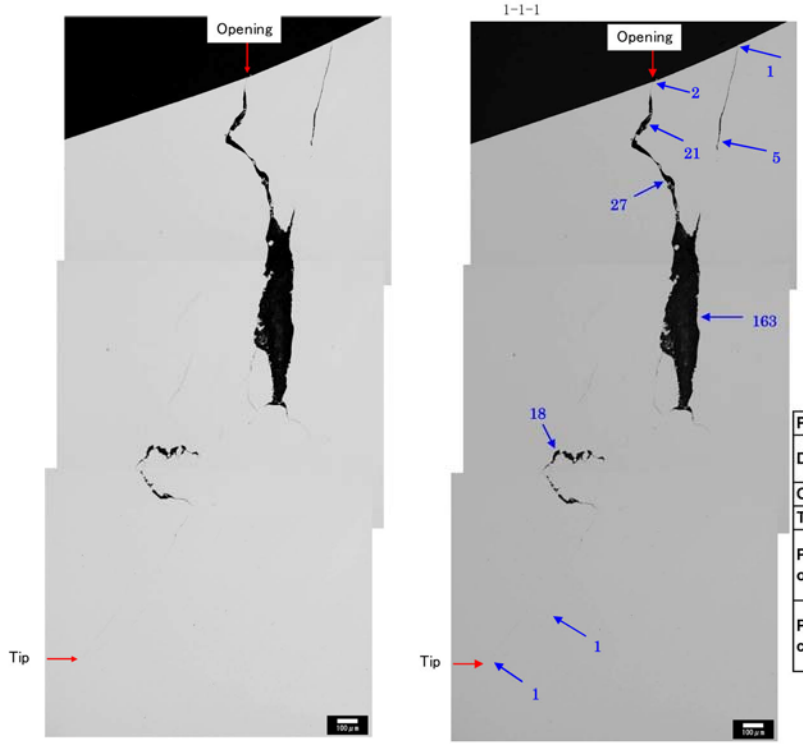

Position (mm)		X=-1.0
Depth (mm)	d	2.4
Opening (μm)		2
Tilt (deg) (*)		20
Position of surf. opening (mm)	X	-1.0
	Y	147.7
	Z	34.0
Position of crack tip (mm)	X	-1.0
	Y	150.5
	Z	35.0

Typical crack opening data of PINC 5.13-2 (parallel to weld)
(X=-1.0)

Overview

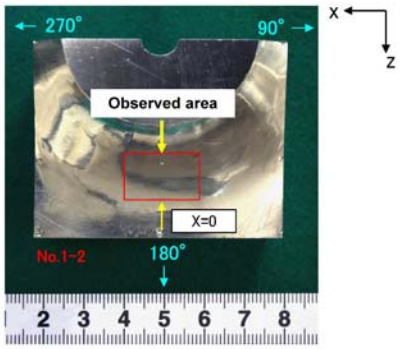

Macro. photo of cross section

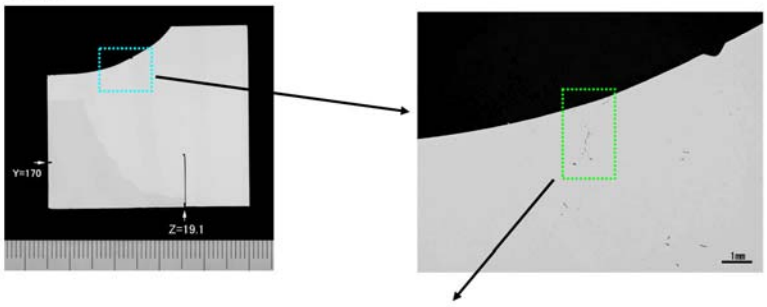

Micro. photo of cross section

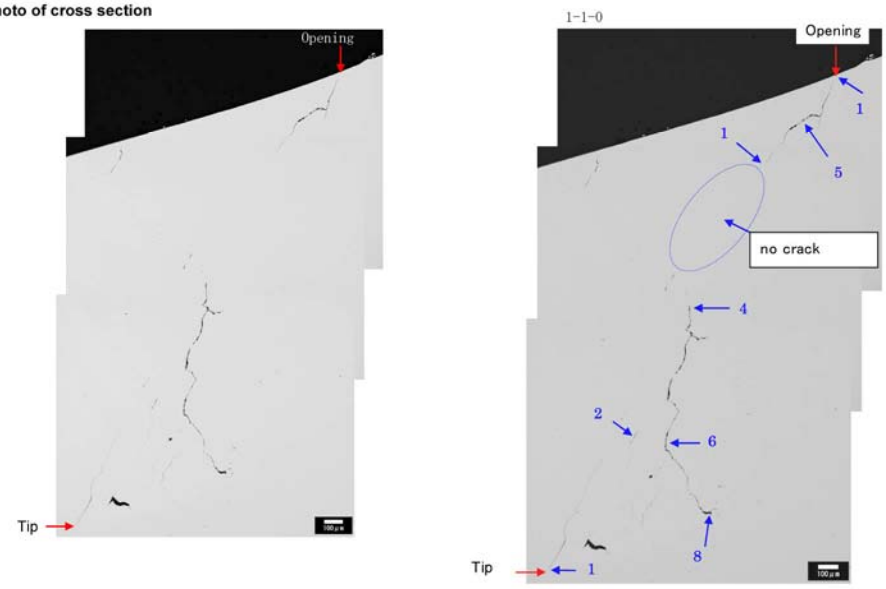

Position (mm)		X=0.0
Depth (mm)	d	1.8
Opening (μm)		1
Tilt (deg) (*)		29
Position of surf. opening (mm)	X	0.0
	Y	147.8
	Z	34.1
Position of crack tip (mm)	X	0.0
	Y	150.3
	Z	35.5

Typical crack opening data of PINC 5.13-2 (parallel to weld)
(X=0)

(1) Overview

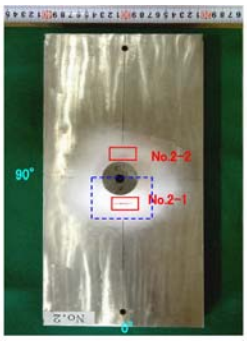

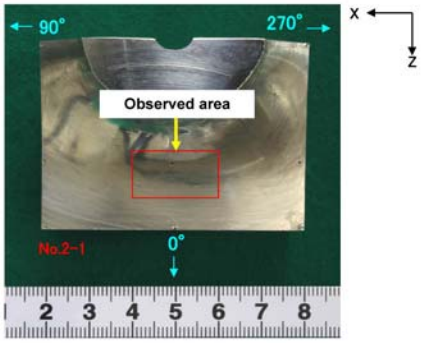

(2) Profile of SCC　　○ : Measured on sliced cross section

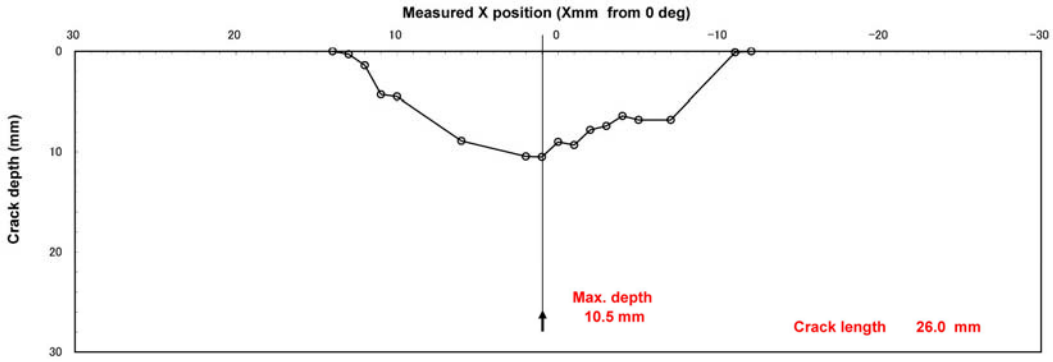

(3) Measured data of SCC

Position (mm)		X=14.0	X=13.0	X=12.0	X=11.0	X=10.0
Depth (mm)	d	0.0	0.3	1.4	4.3	4.5
Opening (μm)		0	2	1	2	4
Tilt (deg) (*)		—	-43	-23	-10	-12
Position of surf. opening (mm)	X	14.0	13.0	12.0	11.0	10.0
	Y	—	147.9	147.9	147.8	147.4
	Z	—	33.8	34.1	33.9	33.1
Position of crack tip (mm)	X	14.0	13.0	12.0	11.0	10.0
	Y	—	148.1	149.2	152.2	151.9
	Z	—	33.6	33.5	33.1	32.2

Position (mm)		X=6.0	X=2.0	X=1.0	X=0.0	X=-1.0
Depth (mm)	d	8.9	10.5	10.5	9.0	9.3
Opening (μm)		8	210	7	17	10
Tilt (deg) (*)		-15	-20	-19	-20	-22
Position of surf. opening (mm)	X	6.0	2.0	1.0	0.0	-1.0
	Y	147.3	147.4	147.3	147.3	147.5
	Z	33.2	33.4	33.2	33.2	33.6
Position of crack tip (mm)	X	6.0	2.0	1.0	0.0	-1.0
	Y	155.9	157.2	157.3	155.8	156.1
	Z	30.8	29.7	29.8	30.1	30.1

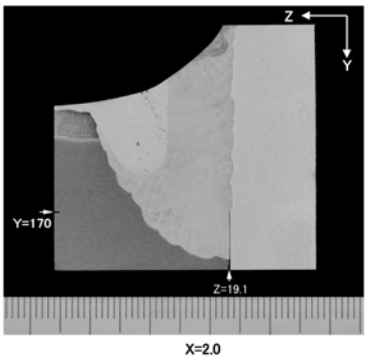

Position (mm)		X=-2.0	X=-3.0	X=-4.0	X=-5.0	X=-7.0	X=-11.0	X=-12.0
Depth (mm)	d	7.8	7.4	6.4	6.8	6.8	0.1	0.0
Opening (μm)		19	38	13	13	8	2	0
Tilt (deg) (*)		-17	-24	-25	-22	-18	20	—
Position of surf. opening (mm)	X	-2.0	-3.0	-4.0	-5.0	-7.0	-11.0	-12.0
	Y	147.2	147.3	147.2	147.2	147.4	147.9	—
	Z	32.9	33.2	32.9	32.8	33.1	33.5	—
Position of crack tip (mm)	X	-2.0	-3.0	-4.0	-5.0	-7.0	-11.0	-12.0
	Y	154.7	154.0	153.0	153.6	153.9	148.0	—
	Z	30.7	30.1	30.2	30.3	30.9	33.5	—

(*) Measured from Y coordinate (+ : clockwise)

Results of destructive test on PINC 5.14-1 (parallel to weld)

Max depth	Za	Zb	Ya	Yb	L	d
	33.15	29.78	147.3	157.3	10.52	10.5

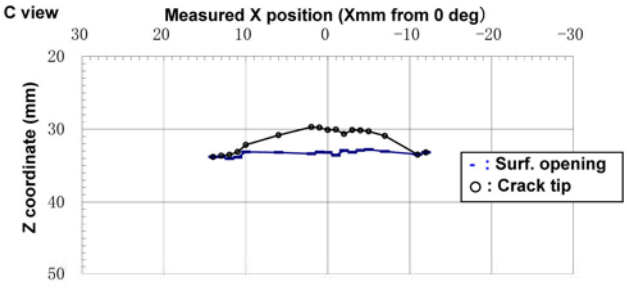

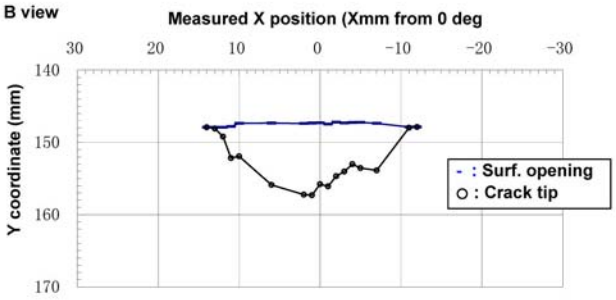

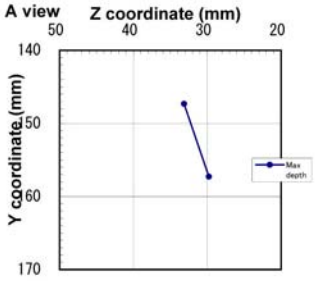

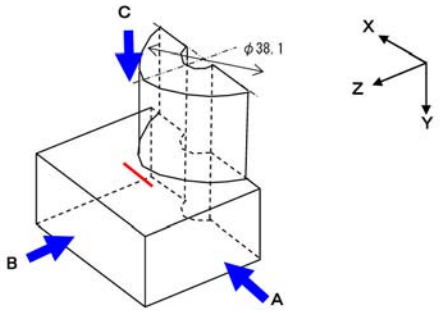

Overview

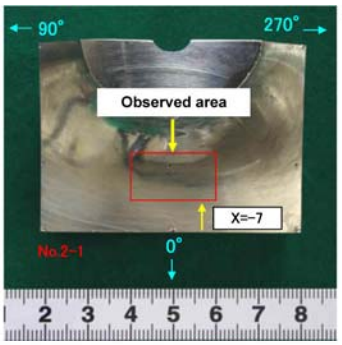

Macro. photo of cross section

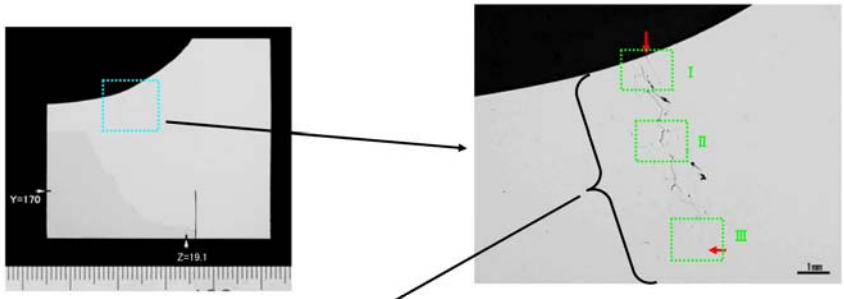

Micro. photo of cross section

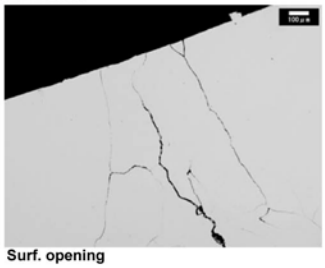

Surf. opening

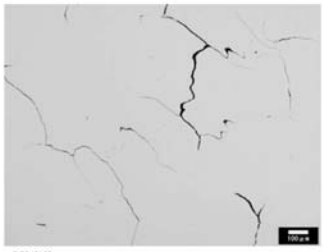

Middle

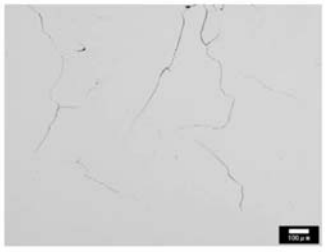

Tip

2-2 -7

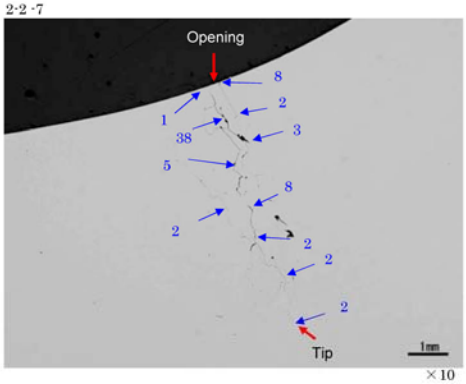

×10

Position (mm)		X=-7.0
Depth (mm)	d	6.8
Opening (μm)		8
Tilt (deg) (°)		-18
Position of surf. opening (mm)	X	-7.0
	Y	147.4
	Z	33.1
Position of crack tip (mm)	X	-7.0
	Y	153.9
	Z	30.9

Typical crack opening data of PINC 5.14-1 (parallel to weld)
(X= -7)

Overview

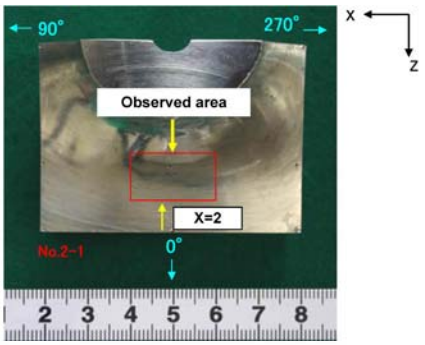

Macro. photo of cross section

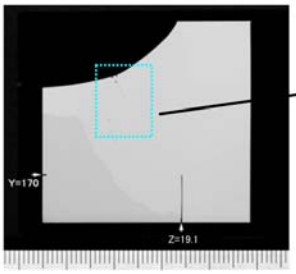

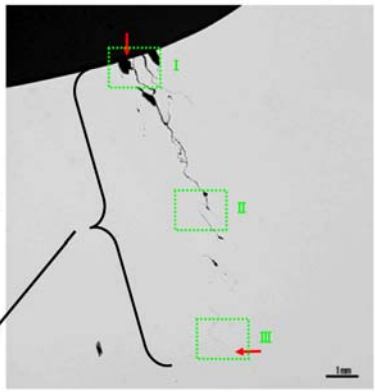

Micro. photo of cross section

Surf. opening

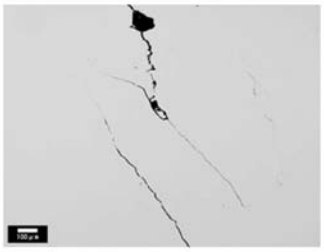

Middle

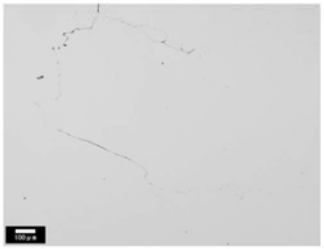

Tip

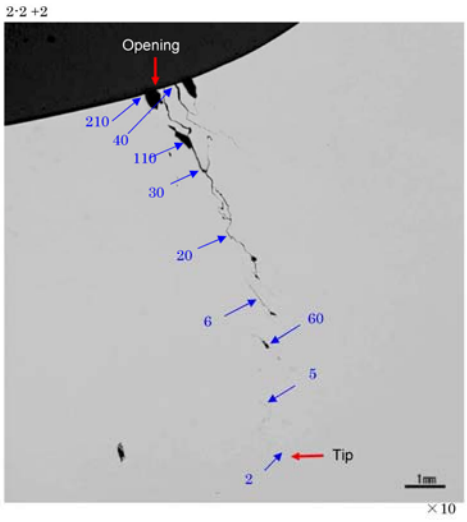

Position (mm)		X=2.0
Depth (mm)	d	10.5
Opening (μm)		210
Tilt (deg) (*)		-20
Position of surf. opening (mm)	X	2.0
	Y	147.4
	Z	33.4
Position of crack tip (mm)	X	2.0
	Y	157.2
	Z	29.7

Typical crack opening data of PINC 5.14-1 (parallel to weld)
(X=2)

(1) Overview

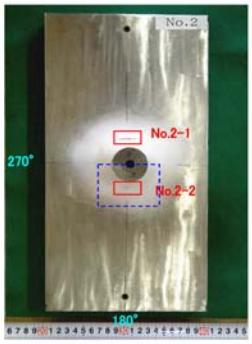

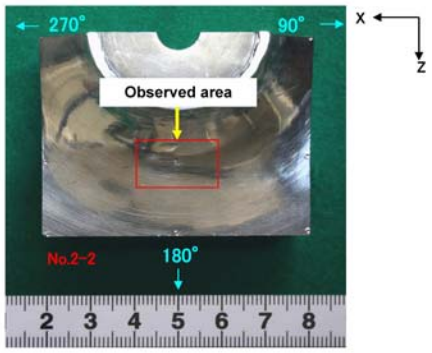

(2) Profile of SCC　　○: Measured on sliced cross section

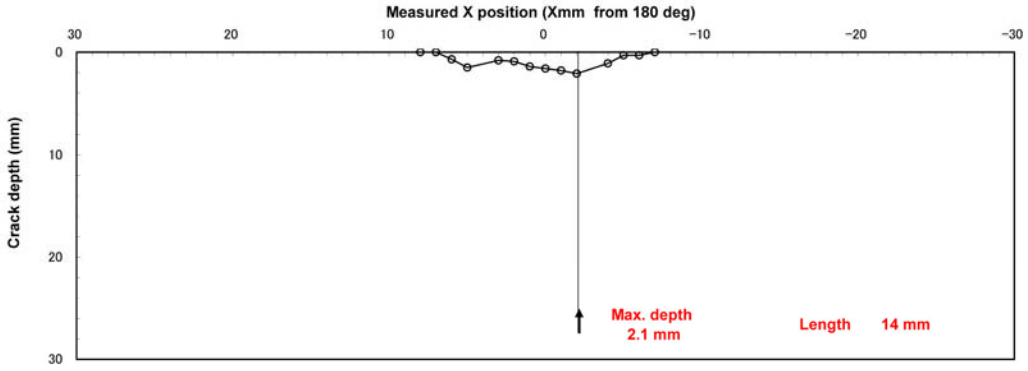

(3) Measured data of SCC

Position (mm)		X=8.0	X=7.0	X=6.0	X=5.0	X=3.0
Depth (mm)	d	0.0	0.0	0.7	1.5	0.8
Opening (μm)		0	0	3	8	7
Tilt (deg) (*)		—	—	-43	-55	-79
Position of surf. opening (mm)	X	8.0	7.0	6.0	5.0	3.0
	Y	—	—	147.1	147.1	147.1
	Z	—	—	30.4	30.3	30.4
Position of crack tip (mm)	X	8.0	7.0	6.0	5.0	3.0
	Y	—	—	147.6	148.1	147.3
	Z	—	—	29.9	28.9	29.1

Position (mm)		X=2.0	X=1.0	X=0.0	X=-1.0	X=-2.0
Depth (mm)	d	0.9	1.4	1.6	1.8	2.1
Opening (μm)		9	2	5	3	17
Tilt (deg) (*)		-65	-36	-64	-54	-56
Position of surf. opening (mm)	X	2.0	1.0	0.0	-1.0	-2.0
	Y	147.0	147.3	147.4	147.3	147.2
	Z	30.3	30.9	31.4	31.1	30.9
Position of crack tip (mm)	X	2.0	1.0	0.0	-1.0	-2.0
	Y	147.5	148.4	148.3	148.5	148.5
	Z	29.4	30.1	29.4	29.5	29.0

Position (mm)		X=-4.0	X=-5.0	X=-6.0	X=-7.0	
Depth (mm)	d	1.1	0.3	0.3	0.0	
Opening (μm)		4	3	3	0	
Tilt (deg) (*)		-67	-48	-76	—	
Position of surf. opening (mm)	X	-4.0	-5.0	-6.0	-7.0	
	Y	147.0	146.8	146.9	—	
	Z	30.5	30.0	30.0	—	
Position of crack tip (mm)	X	-4.0	-5.0	-6.0	-7.0	
	Y	147.6	147.0	147.0	—	
	Z	29.1	29.7	29.6	—	

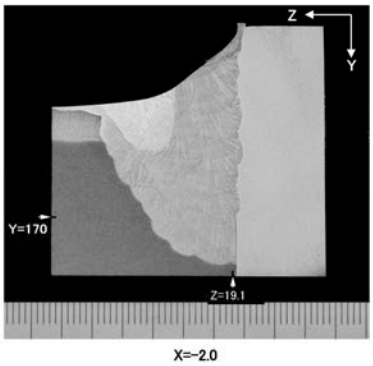

X=-2.0

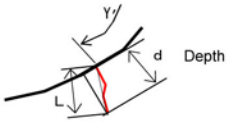

(*) Measured from Y coordinate (+ : clockwise)

Results of destructive test on PINC 5.14-2 (parallel to weld)

Max depth	Za	Zb	Ya	Yb	L	d
	30.9	29.0	147.2	148.5	2.3	2.1

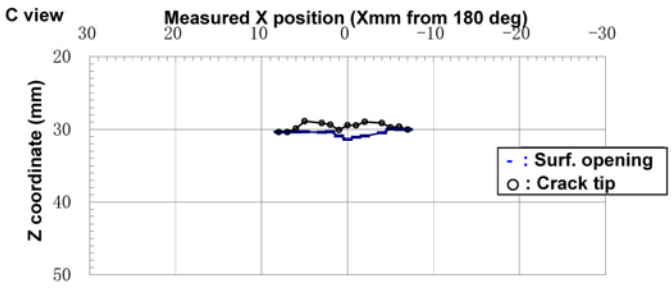

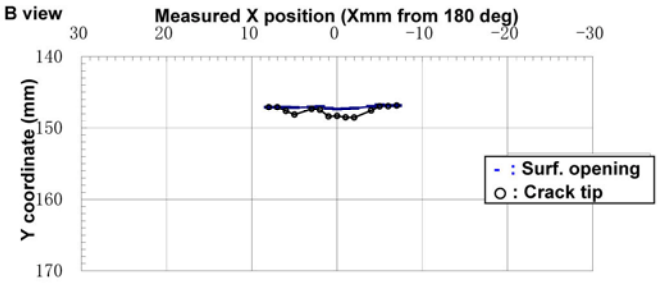

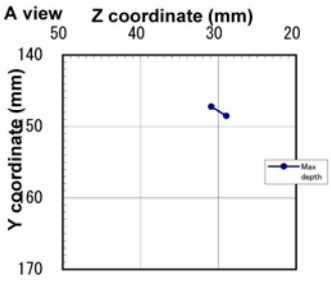

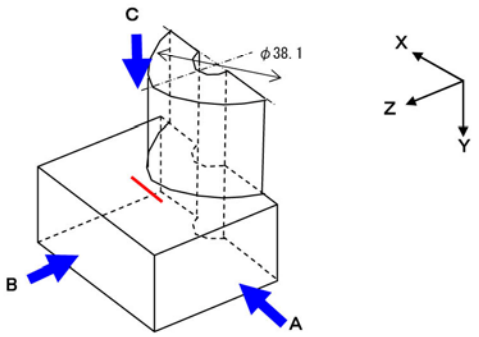

Overview

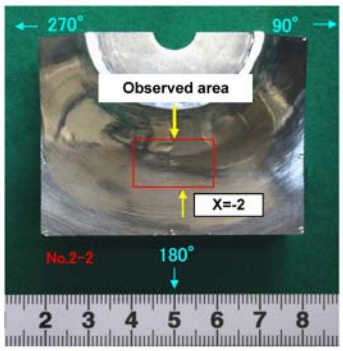

Macro. photo of cross section

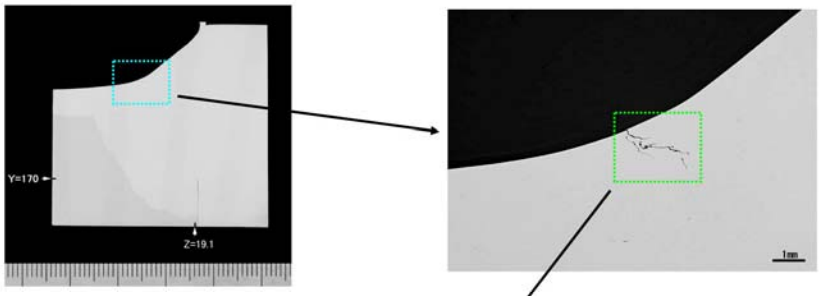

Micro. photo of cross section

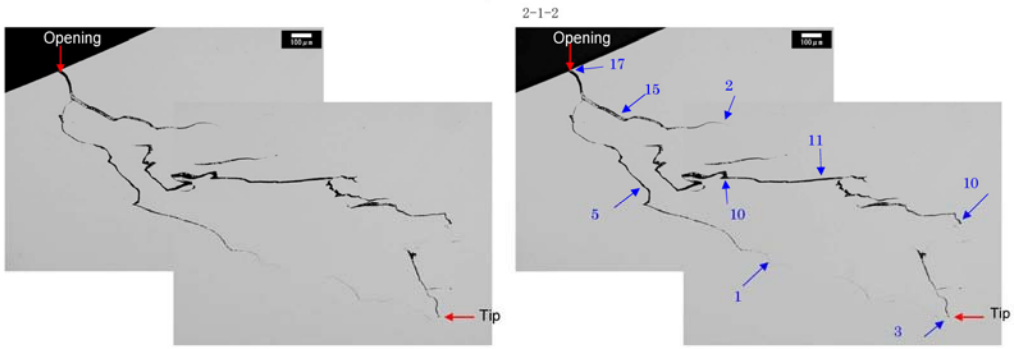

Position (mm)		X=-2.0
Depth (mm)	d	2.1
Opening (μm)		17
Tilt (deg) (*)		-56
Position of surf. opening (mm)	X	-2.0
	Y	147.2
	Z	30.9
Position of crack tip (mm)	X	-2.0
	Y	148.5
	Z	29.0

Typical crack opening data of PINC 5.14-2 (parallel to weld)
(X=-2)

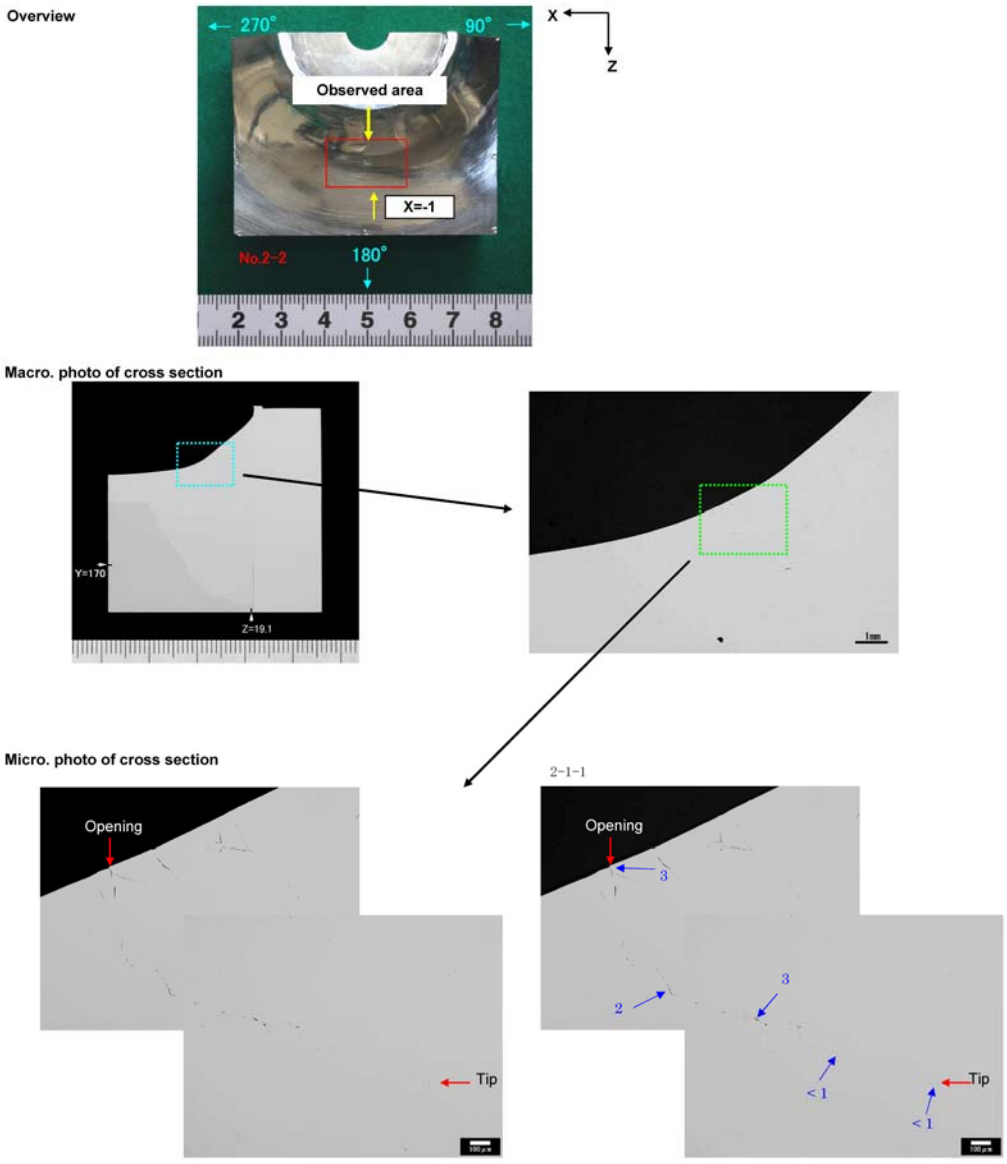

Position (mm)		X=−1.0
Depth (mm)	d	1.8
Opening (μm)		3
Tilt (deg) (*)		−54
Position of surf. opening (mm)	X	−1.0
	Y	147.3
	Z	31.1
Position of crack tip (mm)	X	−1.0
	Y	148.5
	Z	29.5

Typical crack opening data of PINC 5.14-2 (parallel to weld)
(X=-1)

Overview

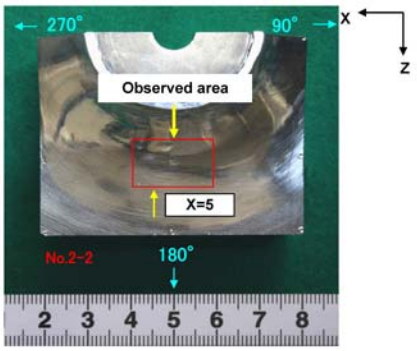

Macro. photo of cross section

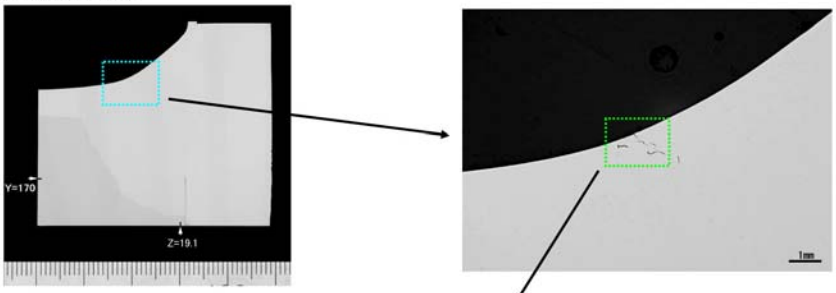

Micro. photo of cross section

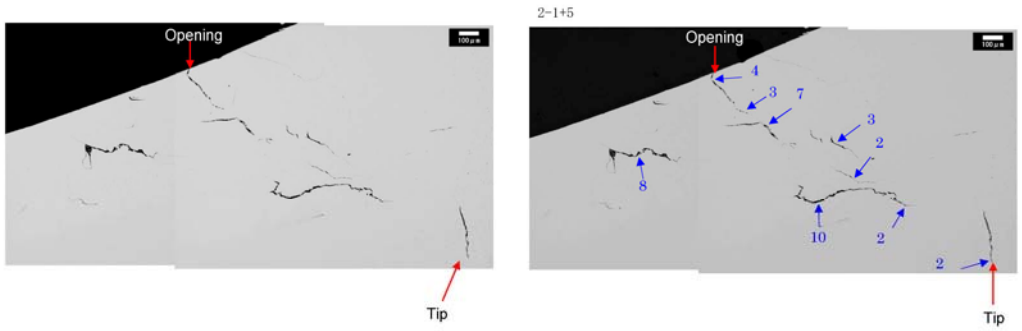

Position (mm)		X=5.0
Depth (mm)	d	1.5
Opening (μm)		8
Tilt (deg) (°)		−55
Position of surf. opening (mm)	X	5.0
	Y	147.1
	Z	30.3
Position of crack tip (mm)	X	5.0
	Y	148.1
	Z	28.9

Typical crack opening data of PINC 5.14-2 (parallel to weld)
(X=5)

(1) Overview

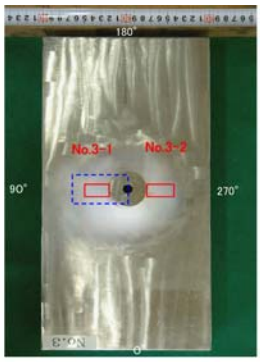

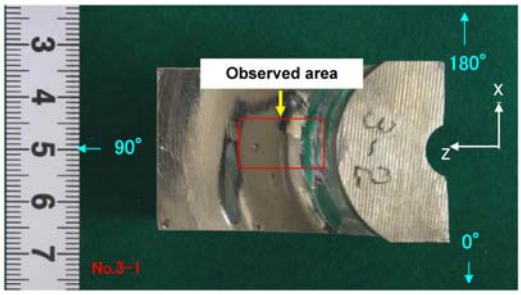

(2) Profile of SCC ○ : Measured on sliced cross section

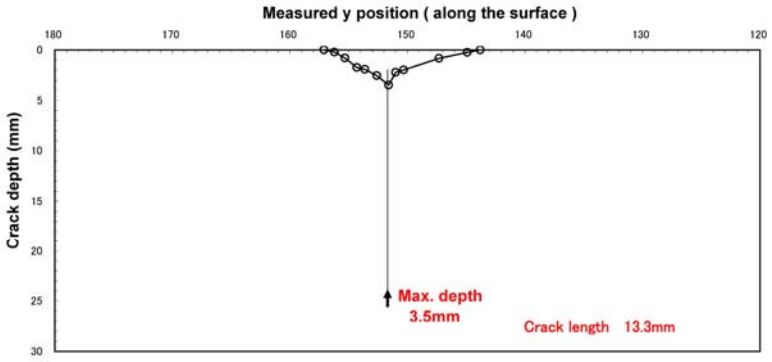

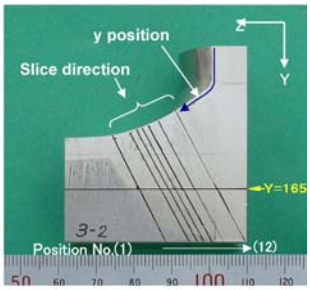

(3) Measured data of SCC

Position		(1)	(2)	(3)	(4)	(5)
Depth (mm)	d	0.0	0.2	0.8	1.7	1.9
Opening (μm)		0	0	3	2	2
Tilt (deg) (*)		—	17	10	-29	-14
Position of surf. opening (mm)	y	157.1	156.2	155.3	154.3	153.6
	X	—	-1.3	-0.7	-1.0	-1.2
	Y	148.5	148.2	147.9	147.7	147.4
	Z	36.3	35.5	34.6	33.7	32.9
Position of crack tip (mm)	X	—	-1.4	-0.9	0.0	-0.7
	Y	—	148.4	148.7	149.2	149.1
	Z	—	35.4	34.2	33.0	32.0

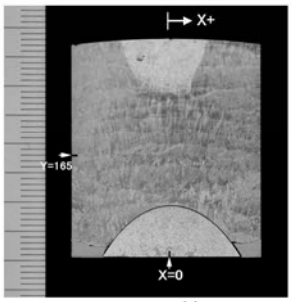

Postition (6)

Position		(6)	(7)	(8)	(9)	(10)	(11)	(12)
Depth (mm)	d	2.5	3.5	2.2	2.0	0.8	0.2	0.0
Opening (μm)		2	6	3	2	2	3	0
Tilt (deg) (*)		-1	10	-10	3	-10	-9	—
Position of surf. opening (mm)	y	152.6	151.6	151.0	150.3	147.3	144.9	143.8
	X	-0.3	-0.5	0.2	-0.9	-0.3	-0.4	—
	Y	146.8	146.6	146.0	145.9	144.9	143.5	143.0
	Z	32.2	31.3	30.6	29.6	28.1	25.8	25.1
Position of crack tip (mm)	X	-0.2	-1.1	0.6	-1.0	-0.2	-0.3	—
	Y	149.0	149.7	148.0	147.6	145.7	143.7	—
	Z	31.0	29.7	29.6	28.7	27.7	25.7	—

(*) Measured from radial coordinate of 90 deg. (+ : clockwise)

Results of destructive test on PINC 5.15-1 (perpendicular to weld)

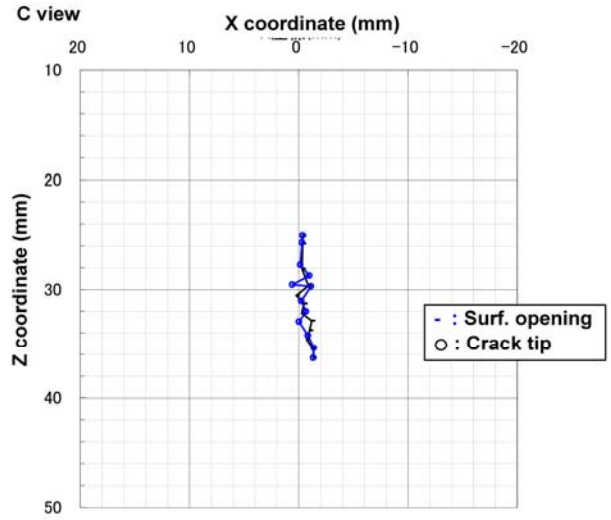
C view
X coordinate (mm)
20
10
0
−10
−20
10
20
30
40
50
Z coordinate (mm)
- : Surf. opening
○ : Crack tip

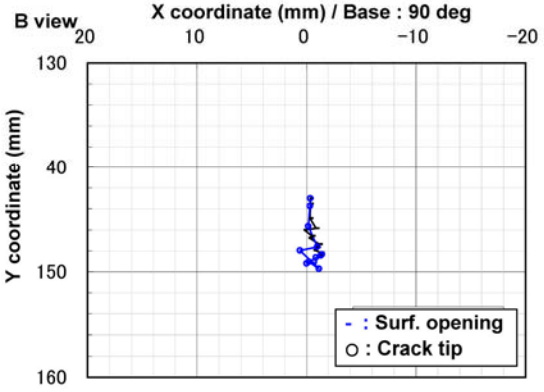
B view
X coordinate (mm) / Base : 90 deg
20
10
0
−10
−20
130
40
150
160
Y coordinate (mm)
- : Surf. opening
○ : Crack tip

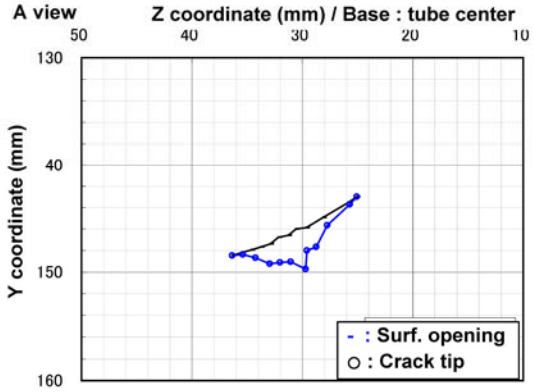
A view
Z coordinate (mm) / Base : tube center
50
40
30
20
10
130
40
150
160
Y coordinate (mm)
- : Surf. opening
○ : Crack tip

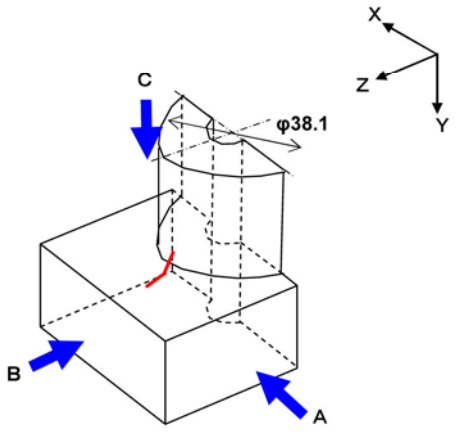
X
Z
Y
C
φ38.1
B
A

Overview

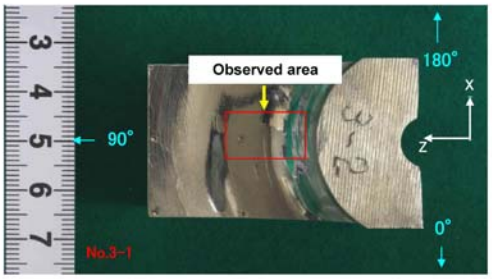

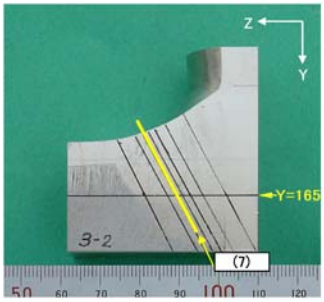

Macro. photo of cross section

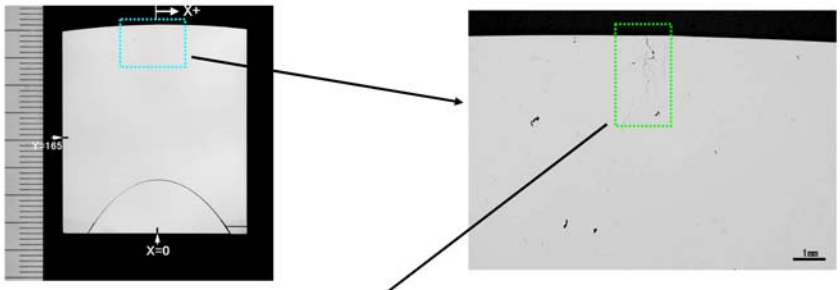

Micro. photo of cross section

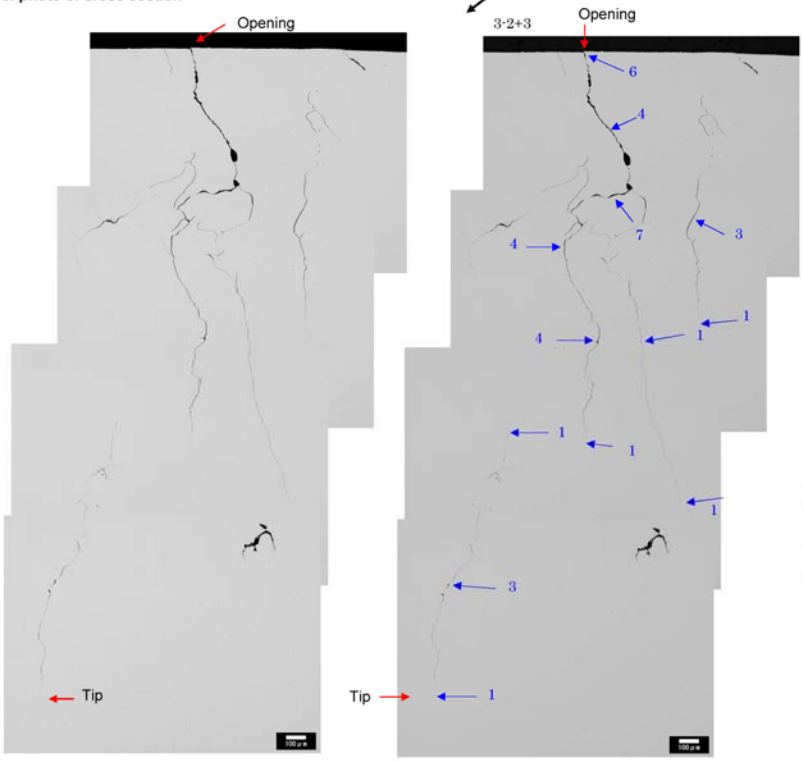

Position		(7)
Depth (mm)	d	3.5
Opening (μm)		6
Tilt (deg) (°)		10
Position of surf. opening (mm)	y	151.6
	X	-0.5
	Y	146.6
	Z	31.3
Position of crack tip (mm)	X	-1.1
	Y	149.7
	Z	29.7

Typical crack opening data of PINC 5.15-1 (perpendicular to weld)
(Position = (7))

Overview

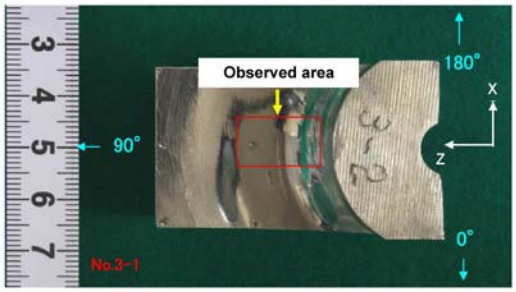

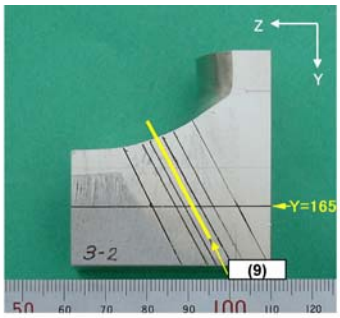

Macro. photo of cross section

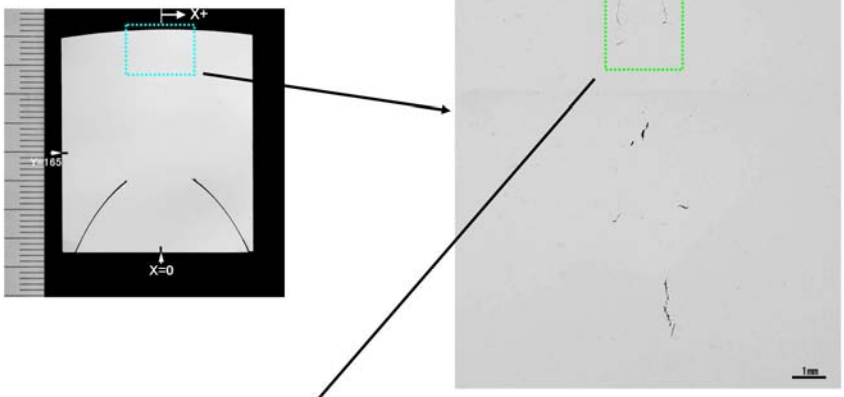

Micro. photo of cross section

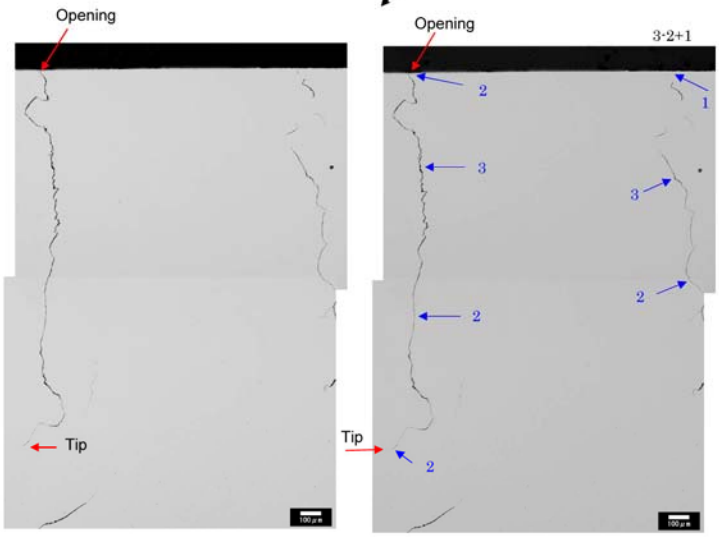

Position		(9)
Depth (mm)	d	2.0
Opening (μm)		2
Tilt (deg) (*)		3
Position of surf. opening (mm)	y	150.3
	X	-0.9
	Y	145.9
	Z	29.6
Position of crack tip (mm)	X	-1.0
	Y	147.6
	Z	28.7

Typical crack opening data of PINC 5.15-1 (perpendicular to weld)
(Position = (9))

(1) Overview

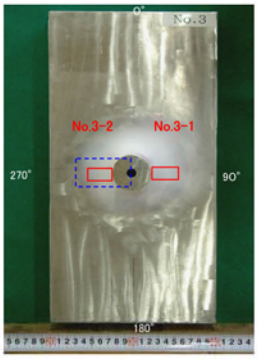

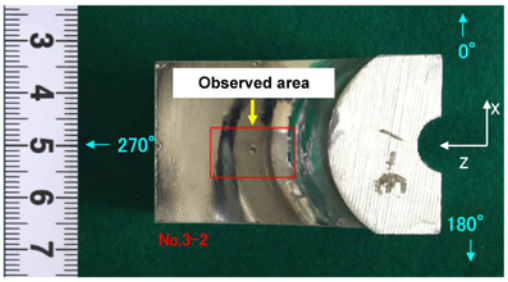

(2) Profile of SCC　　○ : Measured on sliced cross section

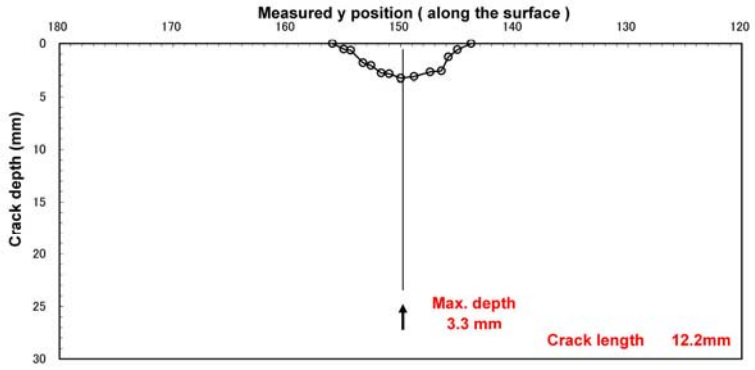

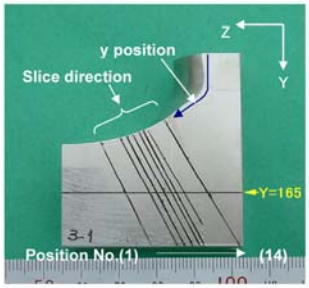

(3) Measured data of SCC

Position		(1)	(2)	(3)	(4)	(5)
Depth (mm)	d	0.0	0.5	0.6	1.8	2.1
Opening (μm)		0	1	1	2	1
Tilt (deg) (*)		—	3	-12	-5	10
Position of surf. opening (mm)	y	156.0	155.0	154.4	153.3	152.6
	X	—	0.4	0.3	-0.2	0.1
	Y	148.7	148.5	148.2	147.7	147.7
	Z	35.2	34.3	33.5	32.7	31.7
Position of crack tip (mm)	X	—	0.3	0.5	-0.1	-0.3
	Y	—	149.0	148.8	149.3	149.6
	Z	—	34.1	33.2	31.9	30.8

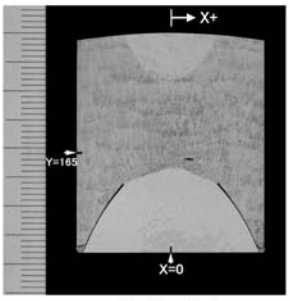

Position (8)

Position		(6)	(7)	(8)	(9)	(10)	(11)	(12)	(13)	(14)
Depth (mm)	d	2.8	2.9	3.3	3.1	2.7	2.6	1.3	0.6	0.0
Opening (μm)		3	131	2	14	3	3	12	1	0
Tilt (deg) (*)		5	18	-7	13	-1	0	22	26	—
Position of surf. opening (mm)	y	151.7	151.0	150.0	148.8	147.4	146.4	145.8	145.0	143.8
	X	-0.1	0.6	-0.4	0.4	-0.8	-0.8	-1.6	-1.7	—
	Y	146.9	146.8	146.1	145.9	145.1	145.1	144.4	143.9	143.3
	Z	31.1	30.2	29.5	28.6	28.0	27.0	26.4	25.6	24.9
Position of crack tip (mm)	X	-0.3	-0.4	0.0	-0.4	-0.8	-0.8	-2.1	-2.0	—
	Y	149.4	149.3	149.1	148.7	147.5	147.4	145.5	144.4	—
	Z	29.9	28.9	28.0	27.2	26.8	25.9	25.8	25.4	—

(*) Measured from radial coordinate of 270 deg. (+ : clockwise)

Results of destructive test on PINC 5.15-2 (perpendicular to weld)

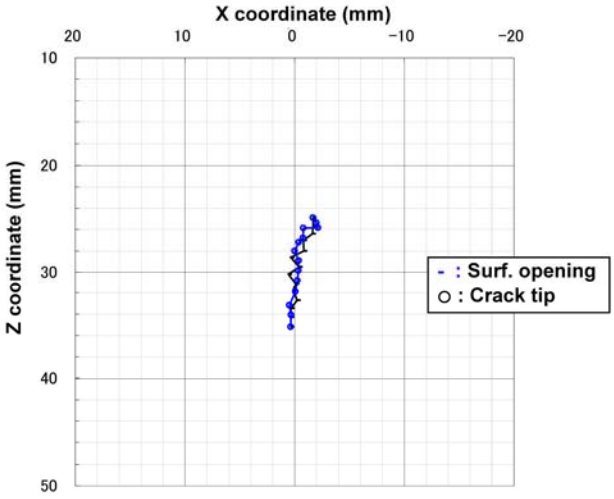
X coordinate (mm)
20
10
0
−10
−20
10
20
30
40
50
Z coordinate (mm)
- : Surf. opening
○ : Crack tip

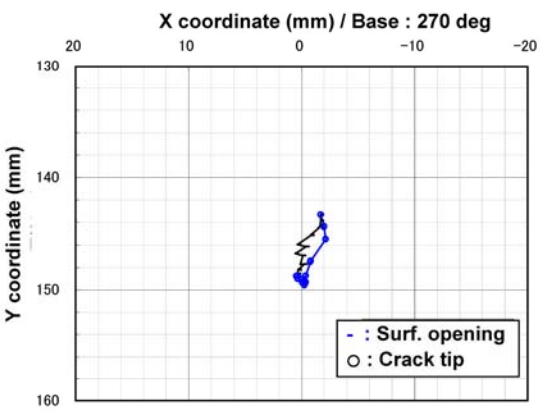
X coordinate (mm) / Base : 270 deg
20
10
0
−10
−20
130
140
150
160
Y coordinate (mm)
- : Surf. opening
○ : Crack tip

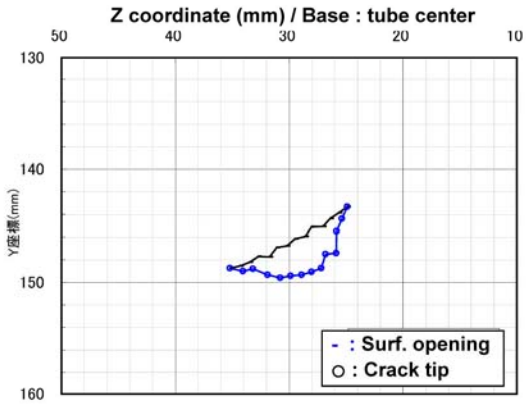
Z coordinate (mm) / Base : tube center
50
40
30
20
10
130
140
150
160
Y座標(mm)
- : Surf. opening
○ : Crack tip

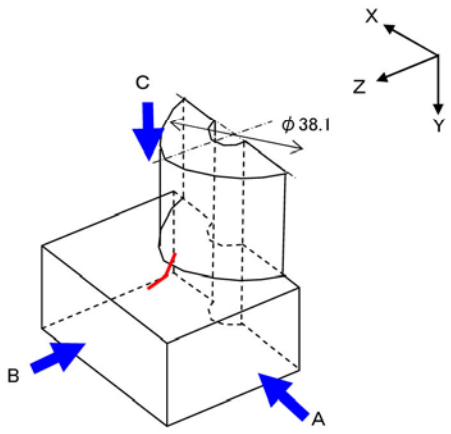
X
Z
Y
C
ϕ38.1
B
A

Overview

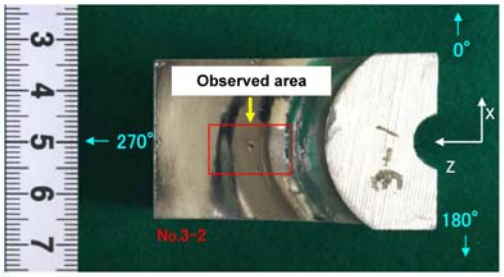

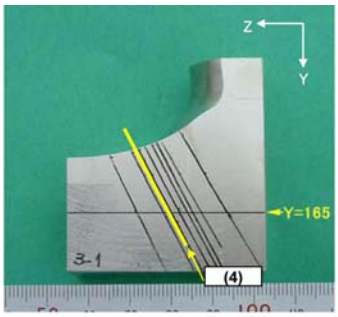

Macro. photo of cross section

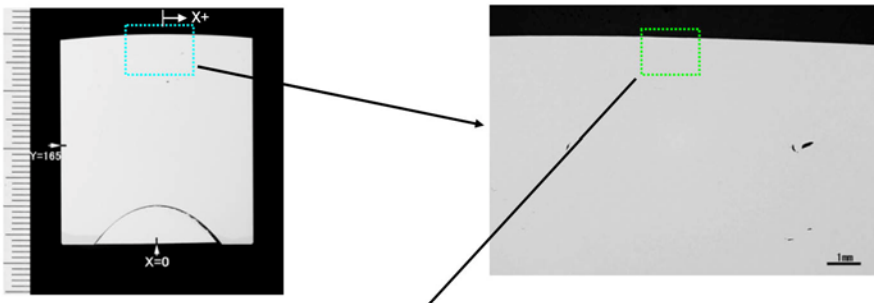

Micro. photo of cross section

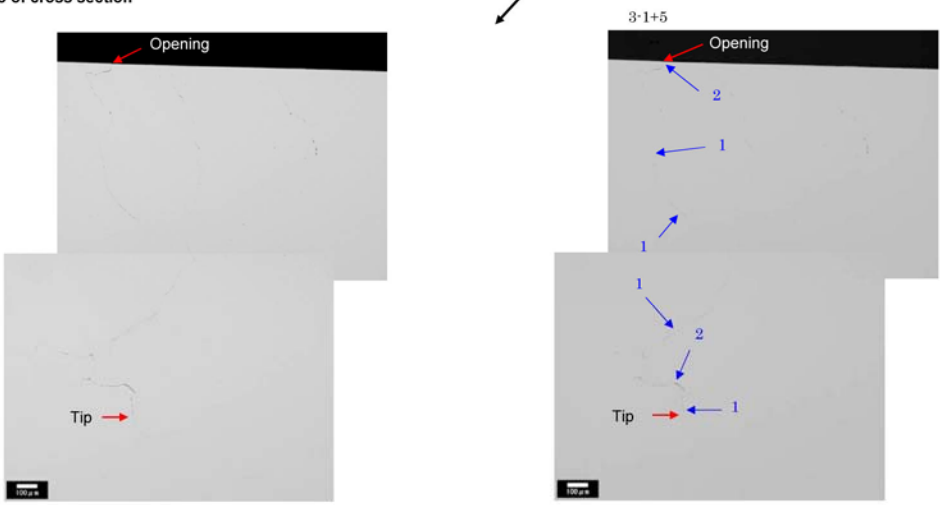

Position		(4)
Depth (mm)	d	1.8
Opening (μm)		2
Tilt (deg) (°)		-5
Position of surf. opening (mm)	y	153.3
	X	-0.2
	Y	147.7
	Z	32.7
Position of crack tip (mm)	X	-0.1
	Y	149.3
	Z	31.9

Typical crack opening data of PINC 5.15-2 (perpendicular to weld)
(Position = (4))

Overview

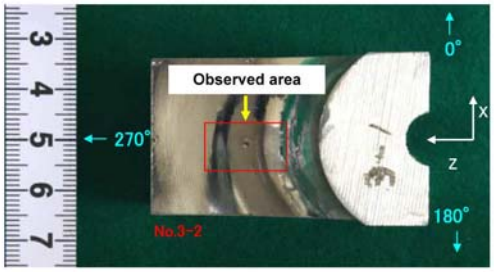

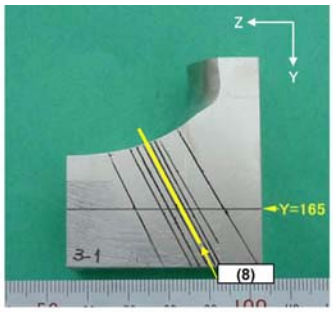

Macro. photo of cross section

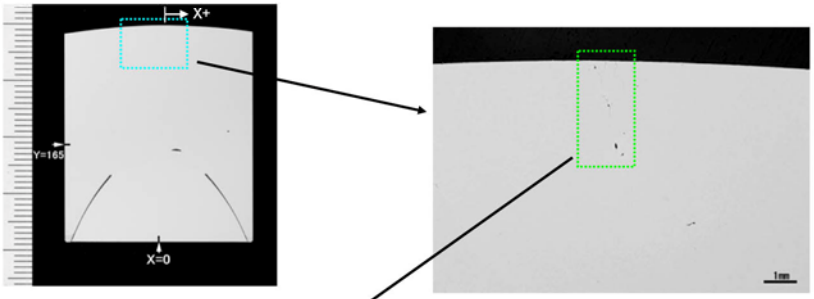

Micro. photo of cross section

3-1+1

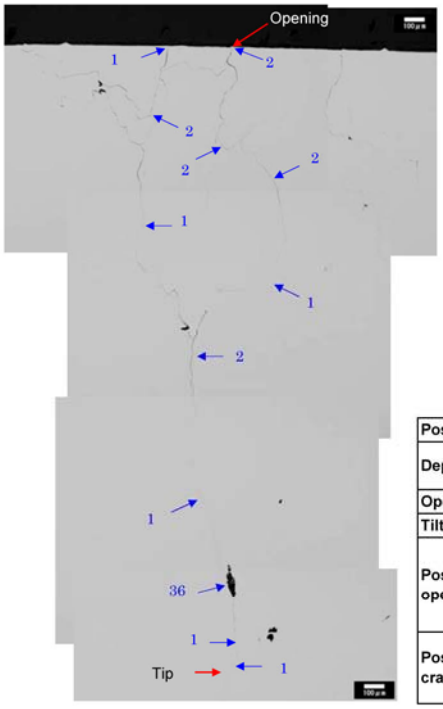

Position		(8)
Depth (mm)	d	3.3
Opening (μm)		2
Tilt (deg) (*)		-7
Position of surf. opening (mm)	y	150.0
	X	-0.4
	Y	146.1
	Z	29.5
Position of crack tip (mm)	X	0.0
	Y	149.1
	Z	28.0

Typical crack opening data of PINC 5.15-2 (perpendicular to weld)
(Position = (8))

(1) Overview

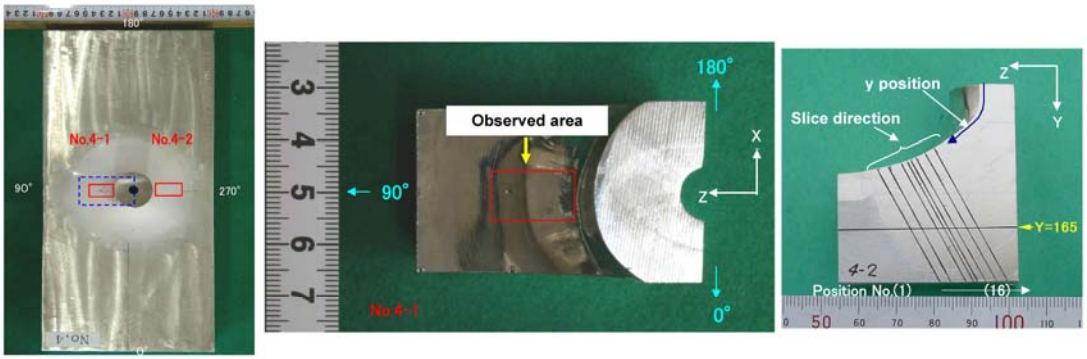

(2) Profile of SCC ○ : Measured on sliced cross section

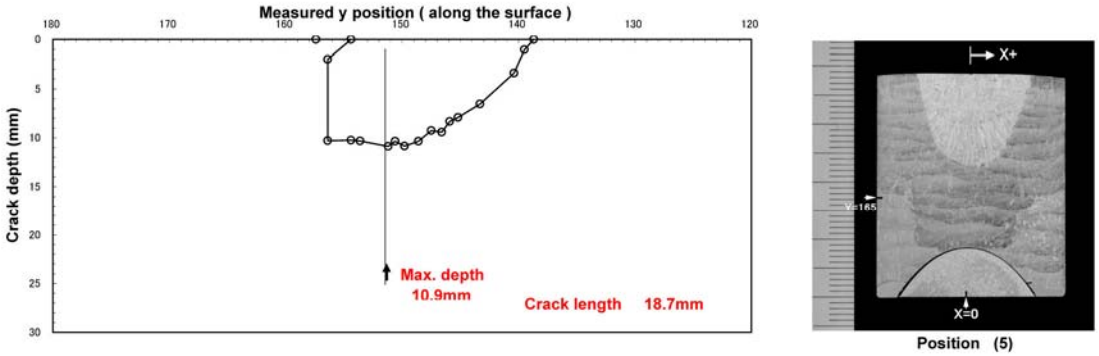

(3) Measured data of SCC

Position		(1)	(2)		(3)	(4)	(5)	(6)	(7)	(8)
Depth (mm)	d	0.0	8.3		10.2	10.3	10.9	10.4	10.8	10.4
Opening (μm)		0	Embeded		2	4	15	5	11	17
Tilt (deg) (*)		—	-		5	3	4	0	2	3
Position of surf. opening (mm)	y	157.4	156.4		154.4	153.6	151.2	150.6	149.8	148.6
	X	—	-1.1	-1.1	1.2	0.8	0.7	0.1	1.2	1.4
	Y	147.5	147.3	149.0	146.8	146.6	145.6	145.4	144.9	144.6
	Z	38.8	37.9	37.0	36.2	35.3	32.8	31.9	31.1	30.3
Position of crack tip (mm)	X	—	1.2		0.3	0.2	0.0	0.1	0.9	0.9
	Y	—	156.5		156.0	155.9	155.3	154.7	154.6	153.9
	Z	—	33.3		31.6	30.6	27.9	27.2	26.3	25.6

Position		(9)	(10)	(11)	(12)	(13)	(14)	(15)	(16)
Depth (mm)	d	9.3	9.4	8.3	7.9	6.6	3.4	1.0	0.0
Opening (μm)		528	5	90	339	5	3	1	0
Tilt (deg) (*)		5	4	17	-1	-3	24	16	—
Position of surf. opening (mm)	y	147.5	146.6	145.9	145.2	143.3	140.4	139.5	138.7
	X	2.0	2.0	2.0	0.0	-0.3	1.3	2.2	—
	Y	144.0	143.7	143.0	142.8	141.3	139.3	138.7	138.1
	Z	29.6	28.7	28.1	27.1	25.9	23.9	23.2	22.5
Position of crack tip (mm)	X	1.3	1.3	-0.5	0.1	0.0	-0.2	1.9	—
	Y	152.3	152.2	150.5	149.9	147.2	142.3	139.6	—
	Z	25.4	24.5	24.3	23.6	23.0	22.4	22.8	—

(*) Measured from radial coordinate of 90 deg. (+ : clockwise)

Results of destructive test on PINC 5.16-1 (perpendicular to weld)

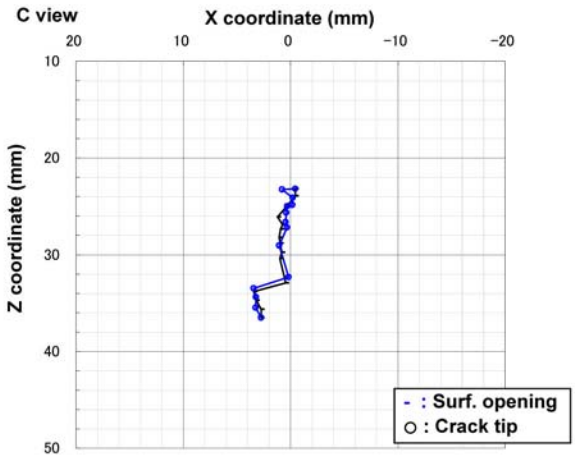
C view
X coordinate (mm)
20
10
0
−10
−20
10
20
30
40
50
Z coordinate (mm)
- : Surf. opening
○ : Crack tip

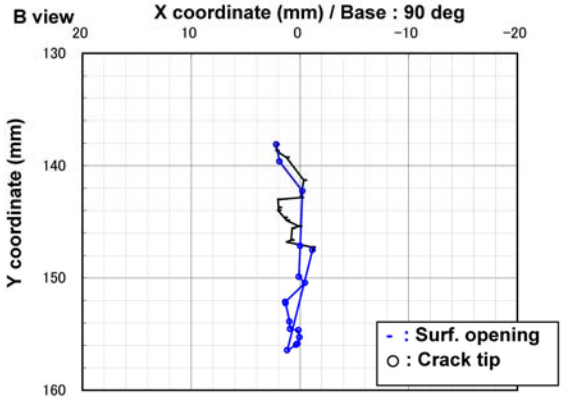
B view
X coordinate (mm) / Base : 90 deg
20
10
0
−10
−20
130
140
150
160
Y coordinate (mm)
- : Surf. opening
○ : Crack tip

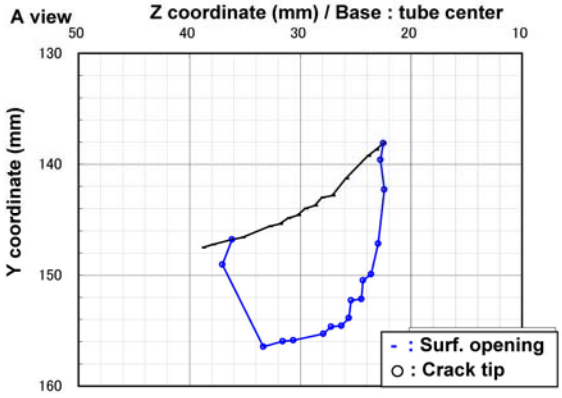
A view
Z coordinate (mm) / Base : tube center
50
40
30
20
10
130
140
150
160
Y coordinate (mm)
- : Surf. opening
○ : Crack tip

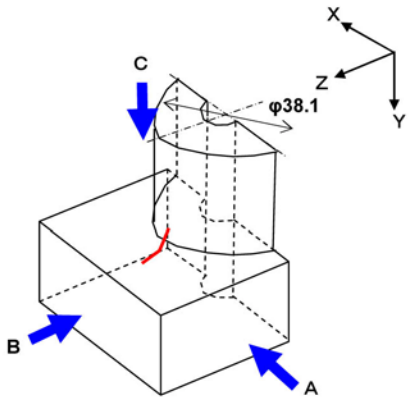
X
Z
Y
C
φ38.1
B
A

Overview

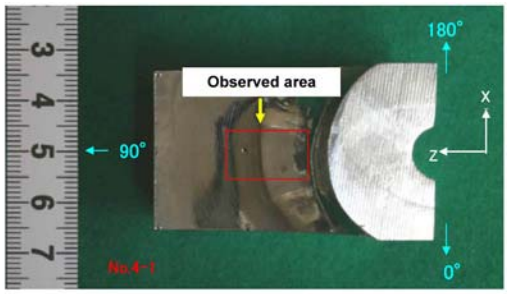

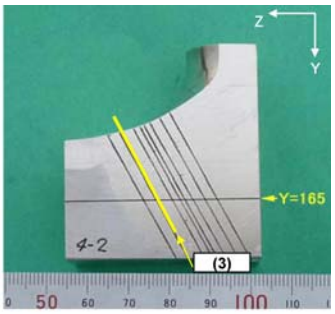

Macro. photo of cross section

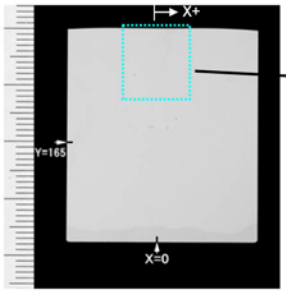

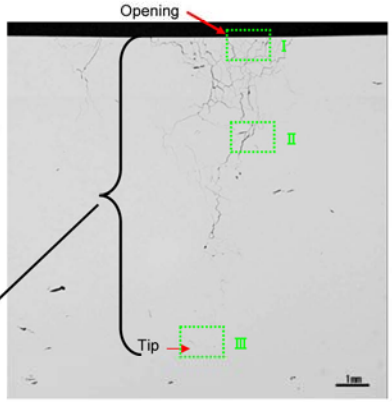

Micro. photo of cross section

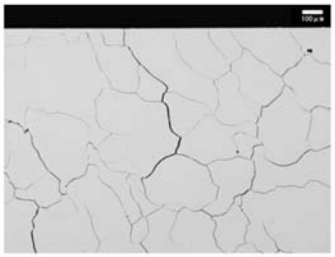

Surface opening

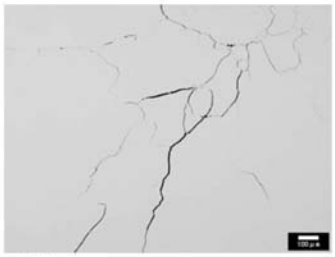

Middle

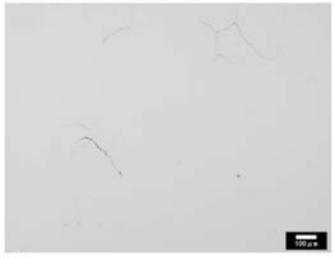

Tip

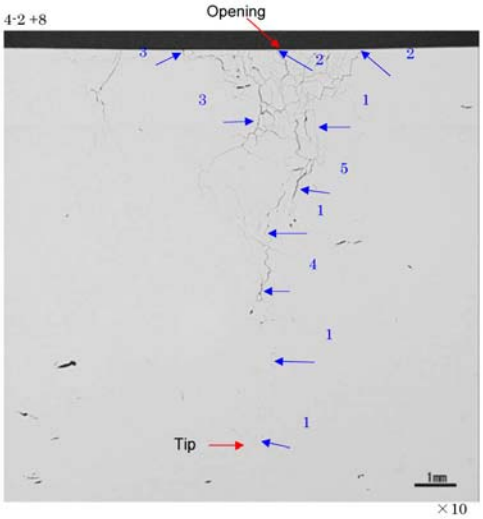

Position		(3)
Depth (mm)	d	10.2
Opening (μm)		2
Tilt (deg) (*)		5
Position of surf. opening (mm)	y	154.4
	X	1.2
	Y	146.8
	Z	36.2
Position of crack tip (mm)	X	0.3
	Y	156.0
	Z	31.6

Typical crack opening data of PINC 5.16-1 (perpendicular to weld)
(Position = (3))

Overview

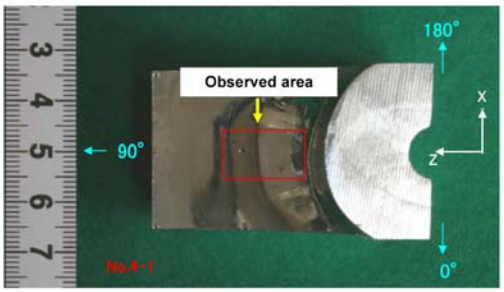

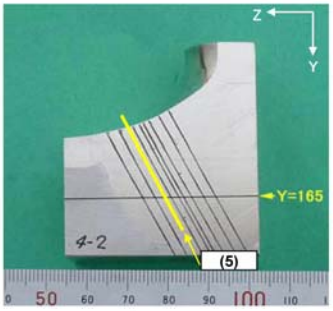

Macro. photo of cross section

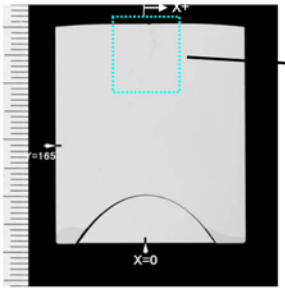

Opening

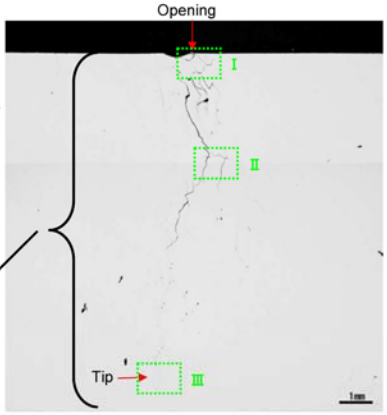

Micro. photo of cross section

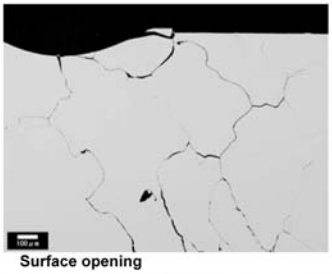

Surface opening

Middle

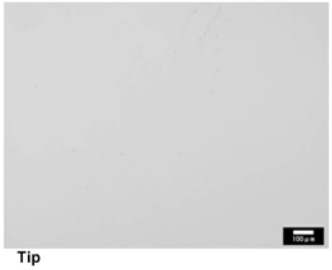

Tip

4-2 +4 Opening

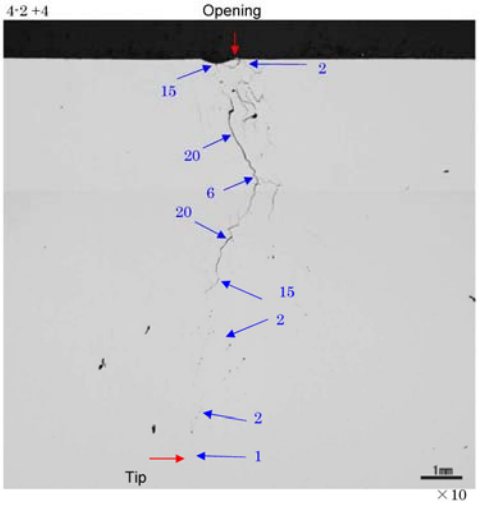

×10

Position		(5)
Depth (mm)	d	10.9
Opening (μm)		15
Tilt (deg) (*)		4
Position of surf. opening (mm)	y	151.2
	X	0.7
	Y	145.6
	Z	32.8
Position of crack tip (mm)	X	0.0
	Y	155.3
	Z	27.9

Typical crack opening data of PINC 5.16-1 (perpendicular to weld)
(Position = (5))

Overview

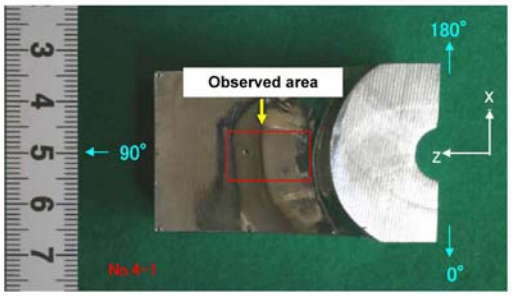

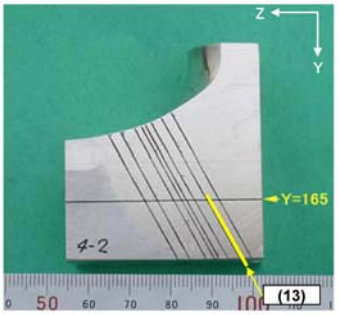

Macro. photo of cross section

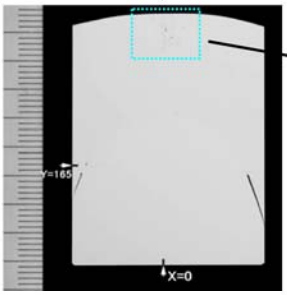

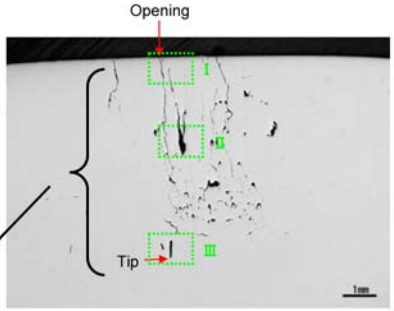

Micro. photo of cross section

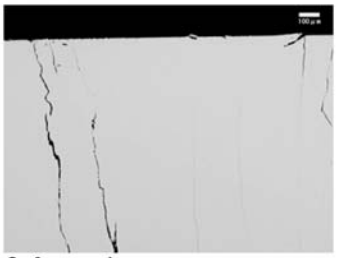

Surface opening

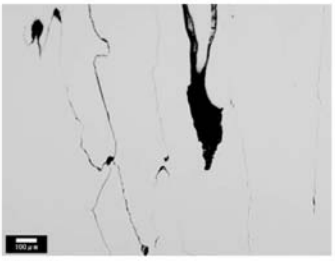

Middle

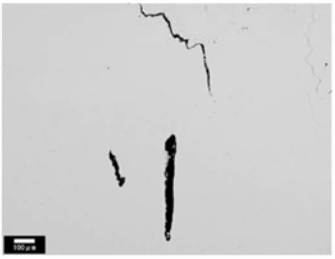

Tip

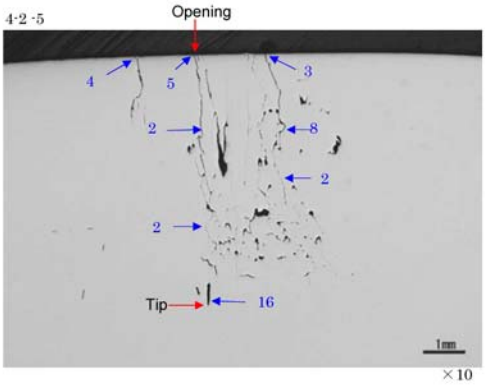

×10

Position		(13)
Depth (mm)	d	6.6
Opening (μm)		5
Tilt (deg) (*)		-3
Position of surf. opening (mm)	y	143.3
	X	-0.3
	Y	141.3
	Z	25.9
Position of crack tip (mm)	X	0.0
	Y	147.2
	Z	23.0

Typical crack opening data of PINC 5.16-1 (perpendicular to weld)
(Position = (13))

(1) Overview

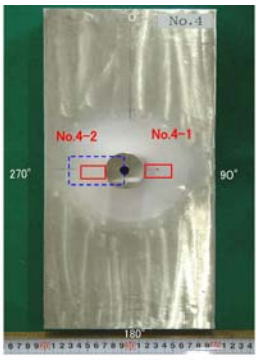

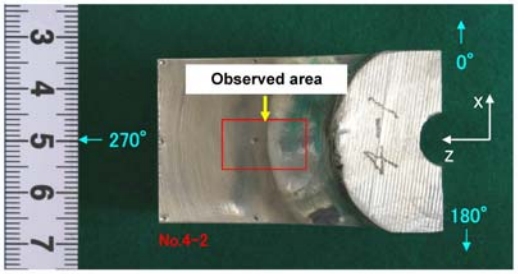

(2) Profile of SCC ○ : Measured on sliced cross section

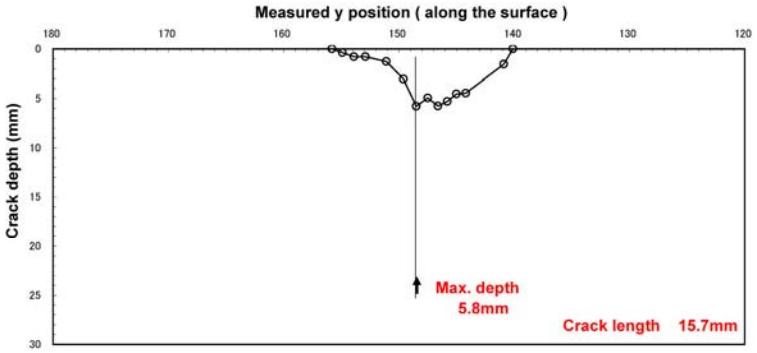

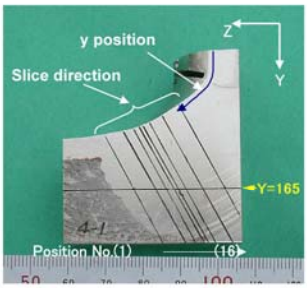

(3) Measured data of SCC

Position		(1)	(2)	(3)	(4)	(5)
Depth (mm)	d	0.0	0.4	0.8	0.8	1.3
Opening (μm)		0	1	1	3	3
Tilt (deg) (*)		—	-55	-1	0	12
Position of surf. opening (mm)	y	155.8	154.9	153.9	152.9	151.1
	X	—	2.7	3.2	3.4	0.4
	Y	148.1	147.8	147.7	147.5	147.3
	Z	36.5	35.6	34.7	33.8	32.9
Position of crack tip (mm)	X	—	3.3	3.2	3.4	0.2
	Y	—	148.2	148.4	148.2	148.5
	Z	—	35.5	34.4	33.5	32.3

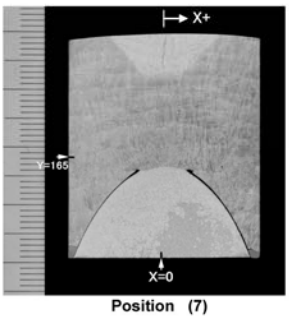

Position (7)

Position		(6)	(7)	(8)	(9)	(10)	(11)	(12)	(13)	(14)
Depth (mm)	d	3.0	5.8	5.0	5.7	5.3	4.5	4.5	1.5	0.0
Opening (μm)		9	8	10	7	4	8	32	13	0
Tilt (deg) (*)		-1	5	6	7	7	12	18	-39	—
Position of surf. opening (mm)	y	149.6	148.5	147.5	146.6	145.8	145.0	144.2	140.9	140.1
	X	1.0	0.8	0.9	1.1	0.9	0.7	1.2	-0.4	—
	Y	146.3	145.6	145.5	144.7	144.4	143.4	142.9	140.3	139.7
	Z	30.4	29.8	28.8	28.2	27.3	26.9	26.1	23.9	23.2
Position of crack tip (mm)	X	1.0	0.3	0.4	0.4	0.3	-0.2	-0.2	0.8	—
	Y	149.0	150.8	149.9	149.8	149.2	147.4	146.9	141.7	—
	Z	29.0	27.2	26.6	25.6	25.0	24.9	24.1	23.2	—

(*) Measured from radial coordinate of 270 deg. (+ : clockwise)

Results of destructive test on PINC 5.16-2 (perpendicular to weld)

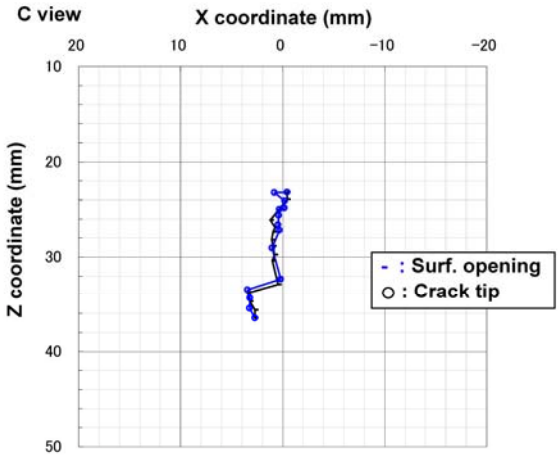
C view
X coordinate (mm)
20
10
0
−10
−20
10
20
30
40
50
Z coordinate (mm)
- : Surf. opening
○ : Crack tip

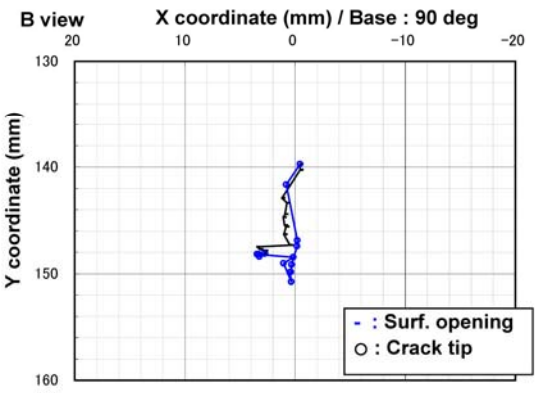
B view
X coordinate (mm) / Base : 90 deg
20
10
0
−10
−20
130
140
150
160
Y coordinate (mm)
- : Surf. opening
○ : Crack tip

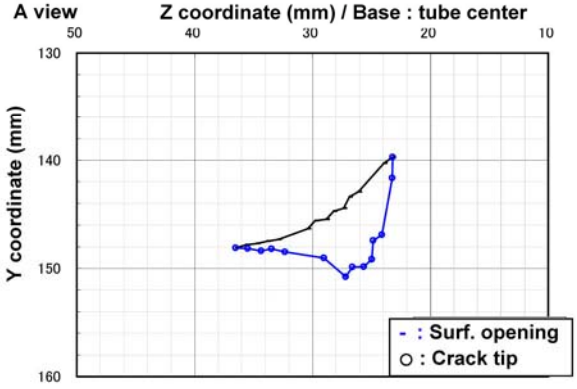
A view
Z coordinate (mm) / Base : tube center
50
40
30
20
10
130
140
150
160
Y coordinate (mm)
- : Surf. opening
○ : Crack tip

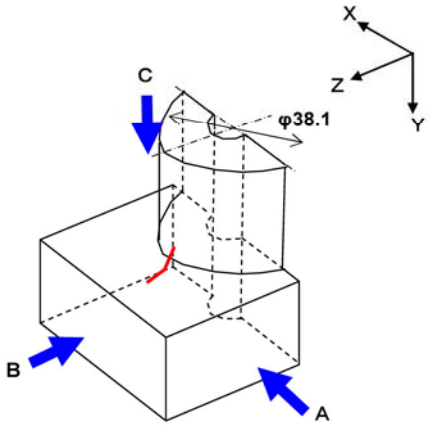
X
Z
Y
C
φ38.1
B
A

Overview

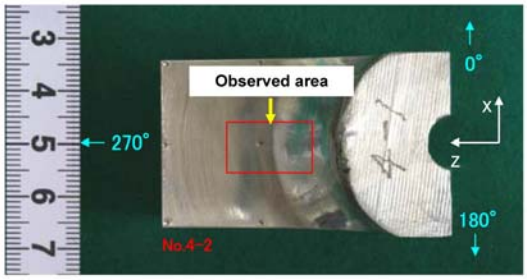

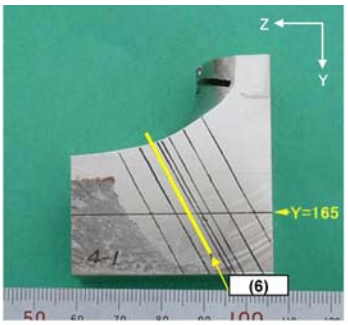

Macro. photo of cross section

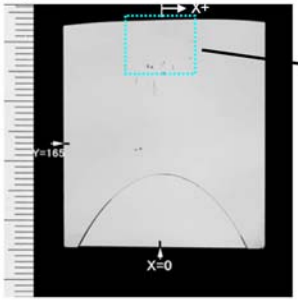

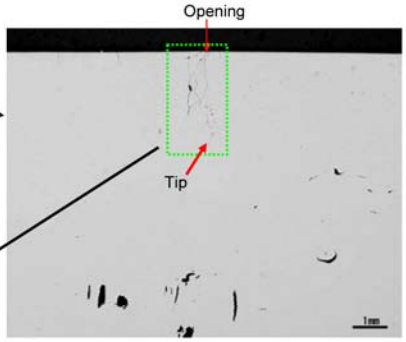

Micro. photo of cross section

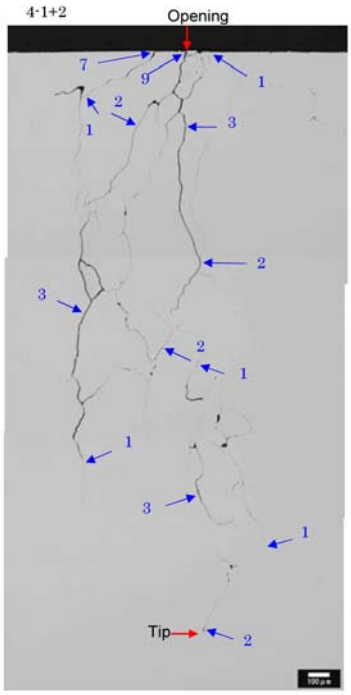

Position		(6)
Depth (mm)	d	3.0
Opening (μm)		9
Tilt (deg) (*)		-1
Position of surf. opening (mm)	y	149.6
	X	1.0
	Y	146.3
	Z	30.4
Position of crack tip (mm)	X	1.0
	Y	149.0
	Z	29.0

Typical crack opening data of PINC 5.16-2 (perpendicular to weld)
(Position = (6))

Overview

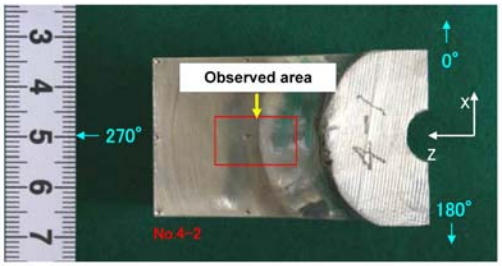

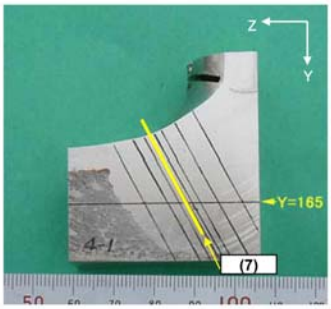

Macro. photo of cross section

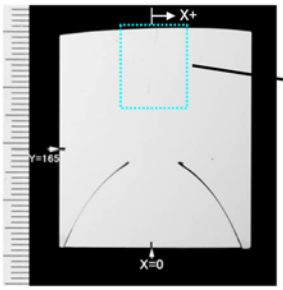

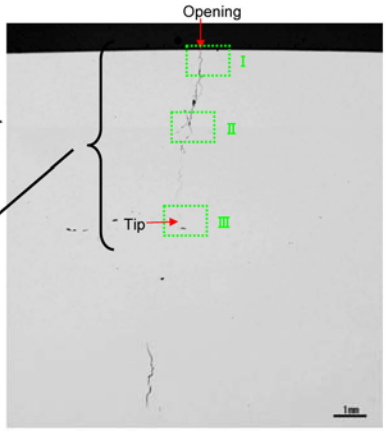

Micro. photo of cross section

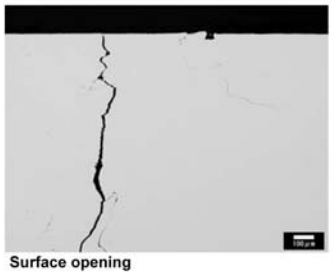

Surface opening

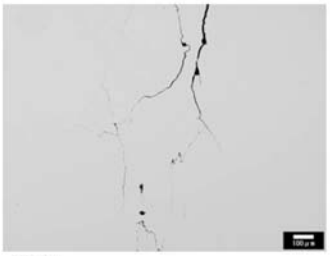

Middle

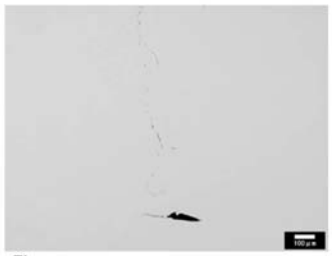

Tip

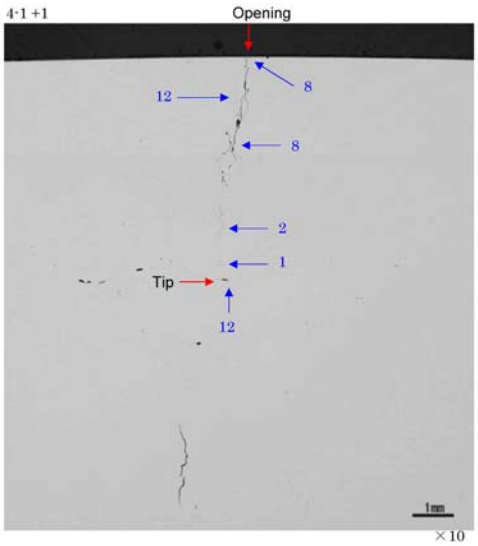

Position		(7)
Depth (mm)	d	5.8
Opening (μm)		8
Tilt (deg) (*)		5
Position of surf. opening (mm)	y	148.5
	X	0.8
	Y	145.6
	Z	29.8
Position of crack tip (mm)	X	0.3
	Y	150.8
	Z	27.2

Typical crack opening data of PINC 5.16-2 (perpendicular to weld)
(Position = (7))

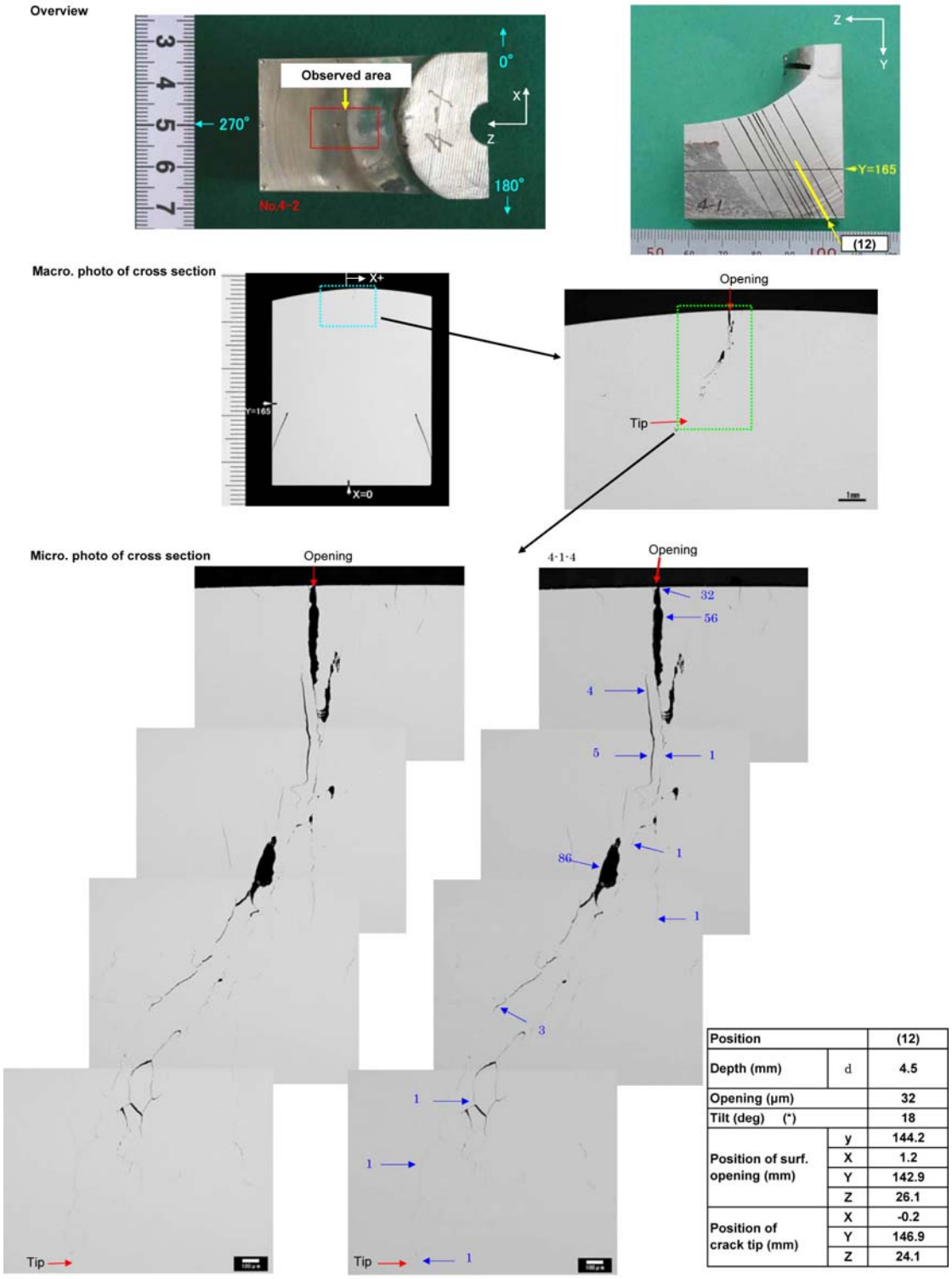

Position		(12)
Depth (mm)	d	4.5
Opening (μm)		32
Tilt (deg) (°)		18
Position of surf. opening (mm)	y	144.2
	X	1.2
	Y	142.9
	Z	26.1
Position of crack tip (mm)	X	-0.2
	Y	146.9
	Z	24.1

Typical crack opening data of PINC 5.16-2 (perpendicular to weld)
(Position = (12))

Appendix C

PINC Data Compilation

Appendix C

PINC BMI Block Data Compilation

AF Pardini
R Mathews

Sample	Flaw	Angle	PNNL ECT Magnitude
5.6	Flaw 1	45	0.72
5.6	Flaw 2	135	1.74
5.6	Flaw 3	180	1.07
5.6	Flaw 4	225	1.25
5.6	Flaw 5	255	NR
5.6	Flaw 6	315	1.44
5.7	Flaw 1	15	2.35
5.7	Flaw 2	165	1.67
5.7	Flaw 3	300	2.32
5.9	Flaw 1	15	0.51
5.9	Flaw 2	75	NR
5.9	Flaw 3	195	NR
5.9	Flaw 4	345	1.33
5.10	Flaw 1	45	2.69
5.10	Flaw 2	75	1.79
5.10	Flaw 3	225	NR
5.10	Flaw 4	255	1.9
5.10	Flaw 5	285	NR
5.10	Flaw 6	315	1.96
5.13	No. 1-1	0	2.45
5.13	No. 1-2	180	1.62
5.14	No. 2-1	0	3.92
5.14	No. 2-2	180	1.39
5.15	No. 3-1	90	2.94
5.15	No. 3-2	270	4.01
5.16	No. 4-1	90	4.42
5.16	No. 4-2	270	7.08
Japan EDM 1	Largest	NA	1.69
Japan EDM 2	Largest	NA	2.43
Japan Ref. 1	Largest	NA	1.76
Japan Ref. 2	Largest	NA	3.52
Cal Std.	5 mm	NA	2.58
Cal Std.	5 mm	NA	2.44
Cal Std.	1 mm	NA	1.96
Cal Std.	1 mm	NA	1.36

Flaw	Observations	POD	ECT
Surf 5.9.2	6	0.167	0
Surf 5.9.3	6	0.167	0
Surf 5.10.3	6	0	0
Surf 5.10.5	6	0.167	0
Surf 5.9.1	6	0.333	0.51
Surf 5.6.1	4	0.75	0.72
Surf 5.6.3	4	0.75	1.07
Surf 5.6.4	4	0.75	1.25
Surf 5.9.4	6	0.167	1.33
Surf 5.14.2	4	0.75	1.39
Surf 5.6.6	4	0.75	1.44
Surf 5.13.2	4	0.5	1.62
Surf 5.7.2	6	0.833	1.67
Surf 5.6.2	4	0.75	1.74
Surf 5.10.2	6	0	1.79
Surf 5.10.4	6	0.5	1.9
Surf 5.10.6	6	0	1.96
Surf 5.7.1	6	0.667	2.35
Surf 5.13.1	4	0.75	2.45
Surf 5.10.1	6	0.167	2.69
Surf 5.15.1	4	0.75	2.94
Surf 5.14.1	4	1	3.92
Surf 5.15.2	4	0.5	4.01
Surf 5.16.1	4	0.75	4.42
Surf 5.16.2	4	0.75	7.08

C.1 Calibration/Verification Standard

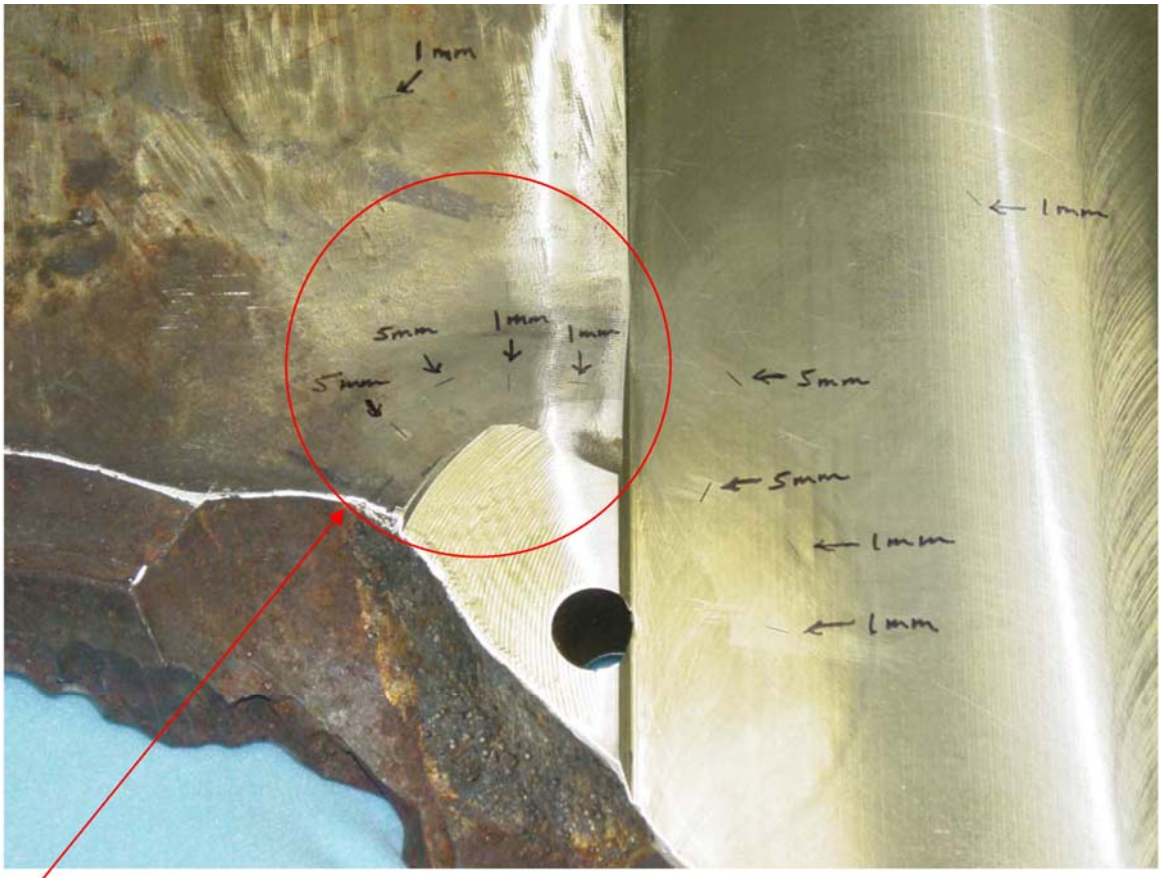

Two Larger Flaws are 4-mm Long × 5-mm Deep × 0.203-mm Wide

Two Smaller Flaws are 4-mm Long × 1-mm Deep × 0.102-mm Wide

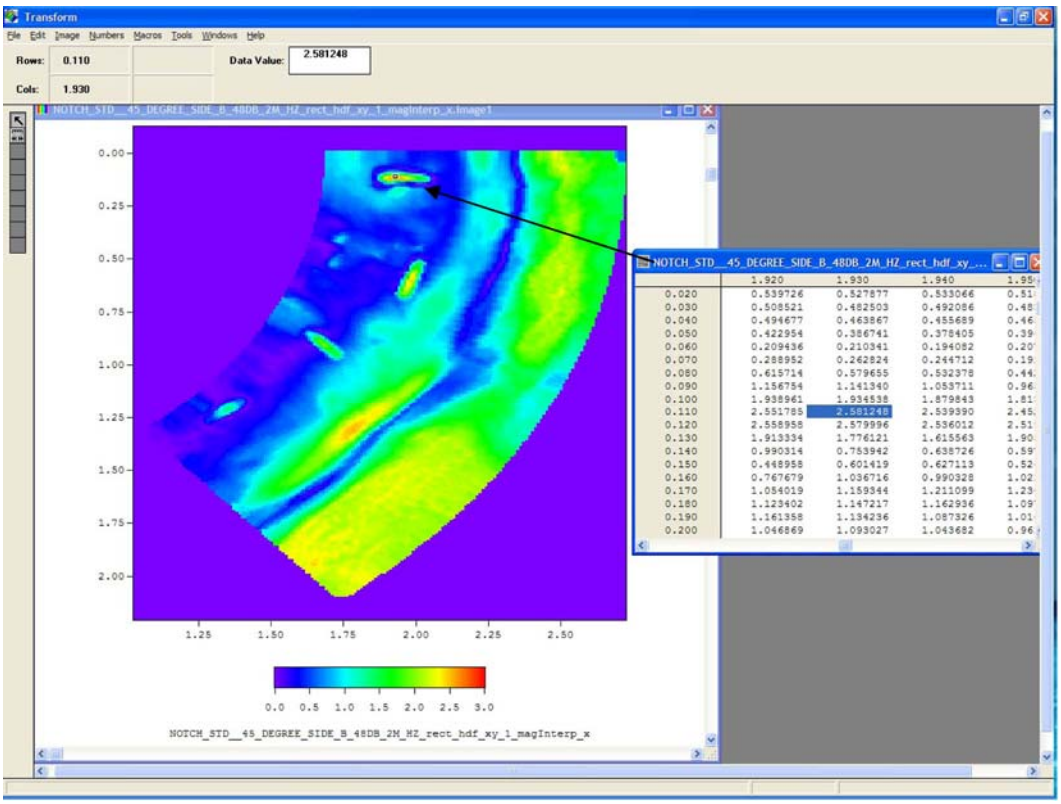
Transform
File Edit Image Numbers Macros Tools Windows Help
Rows: 0.110
Cols: 1.930
Data Value: 2.581248
NOTCH_STD__45_DEGREE_SIDE_B_48DB_2M_HZ_rect_hdf_xy_1_magInterp_x

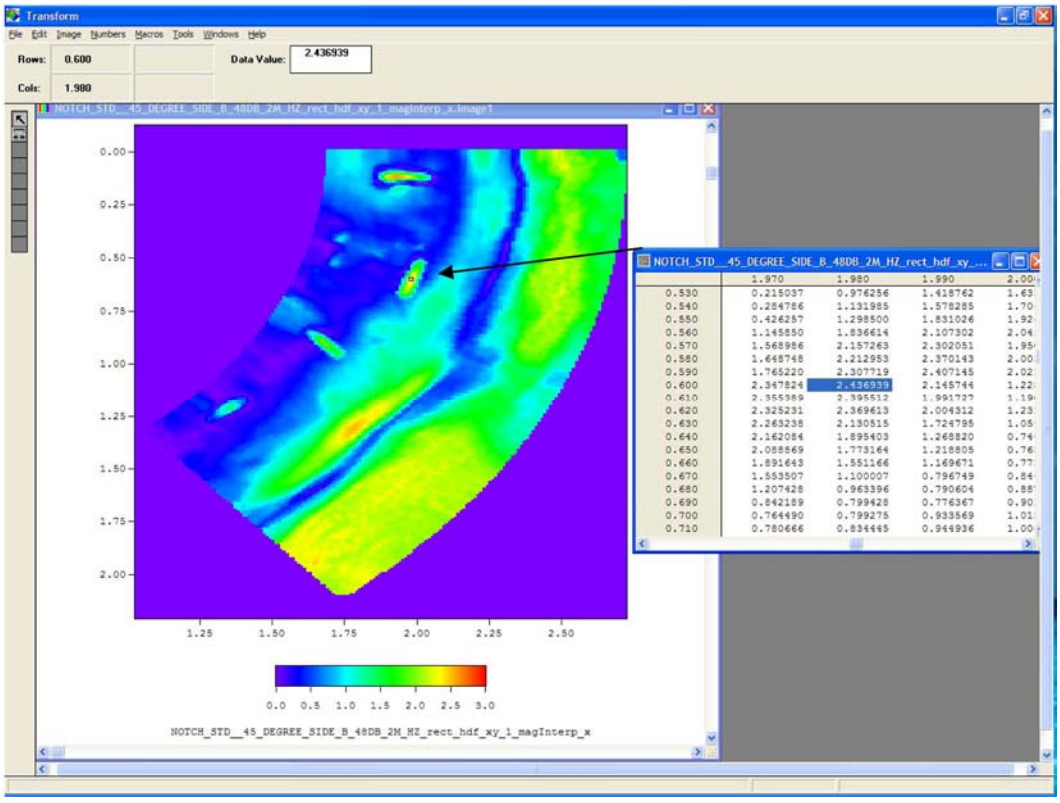
Transform
File Edit Image Numbers Macros Tools Windows Help
Rows: 0.600
Cols: 1.980
Data Value: 2.436939
NOTCH_STD__45_DEGREE_SIDE_B_48DB_2M_HZ_rect_hdf_xy_1_magInterp_x

C.2 PINC 5.7

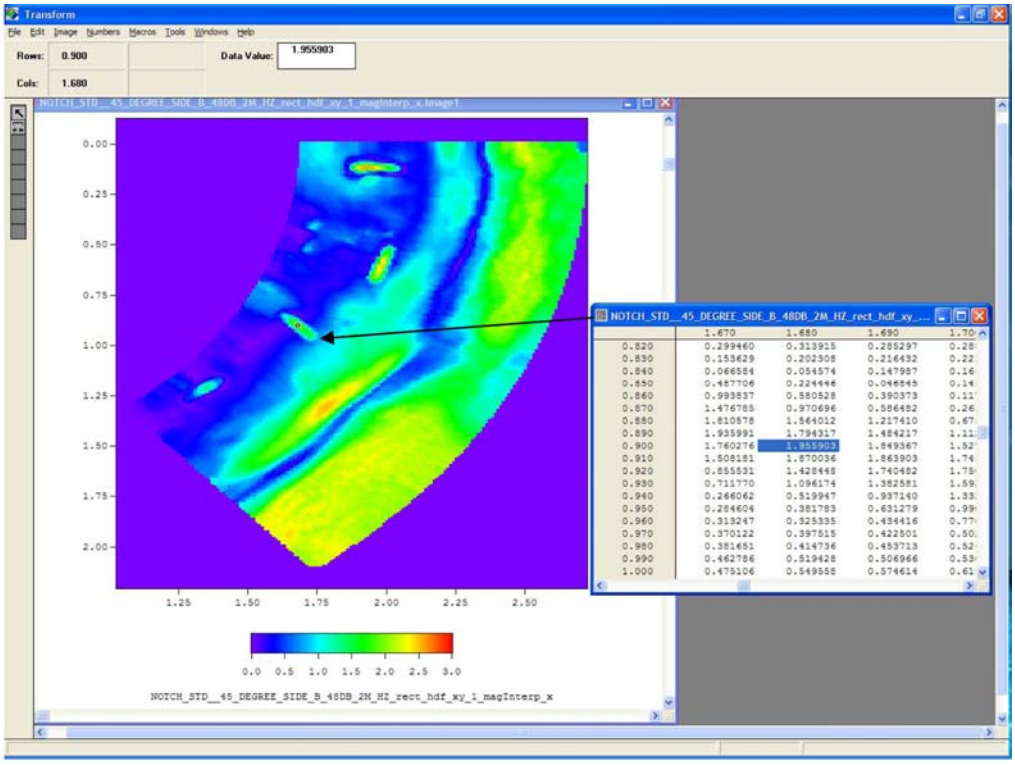
Transform
File Edit Image Numbers Macros Tools Windows Help
Rows: 0.900
Cols: 1.680
Data Value: 1.955903
NOTCH_STD__45_DEGREE_SIDE_B_48DB_2M_HZ_rect_hdf_xy_1_magInterp_x.Image1
NOTCH_STD__45_DEGREE_SIDE_B_48DB_2M_HZ_rect_hdf_xy_....
NOTCH_STD__45_DEGREE_SIDE_B_48DB_2M_HZ_rect_hdf_xy_1_magInterp_x

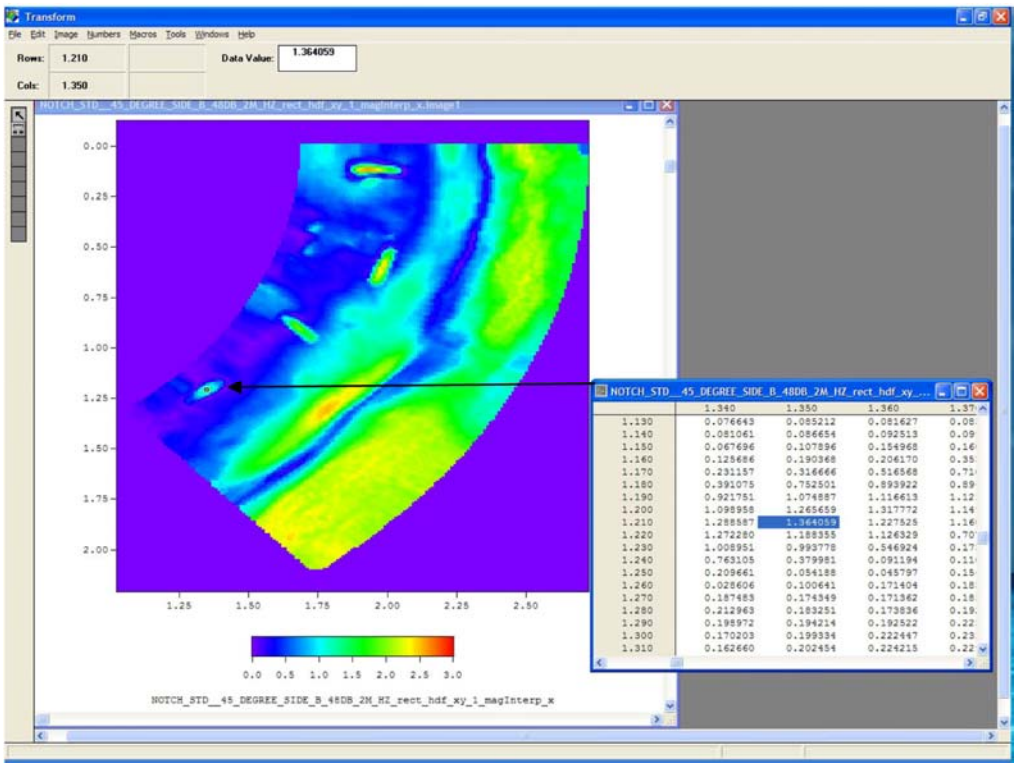
Transform
File Edit Image Numbers Macros Tools Windows Help
Rows: 1.210
Cols: 1.350
Data Value: 1.364059
NOTCH_STD__45_DEGREE_SIDE_B_48DB_2M_HZ_rect_hdf_xy_1_magInterp_x.Image1
NOTCH_STD__45_DEGREE_SIDE_B_48DB_2M_HZ_rect_hdf_xy_....
NOTCH_STD__45_DEGREE_SIDE_B_48DB_2M_HZ_rect_hdf_xy_1_magInterp_x

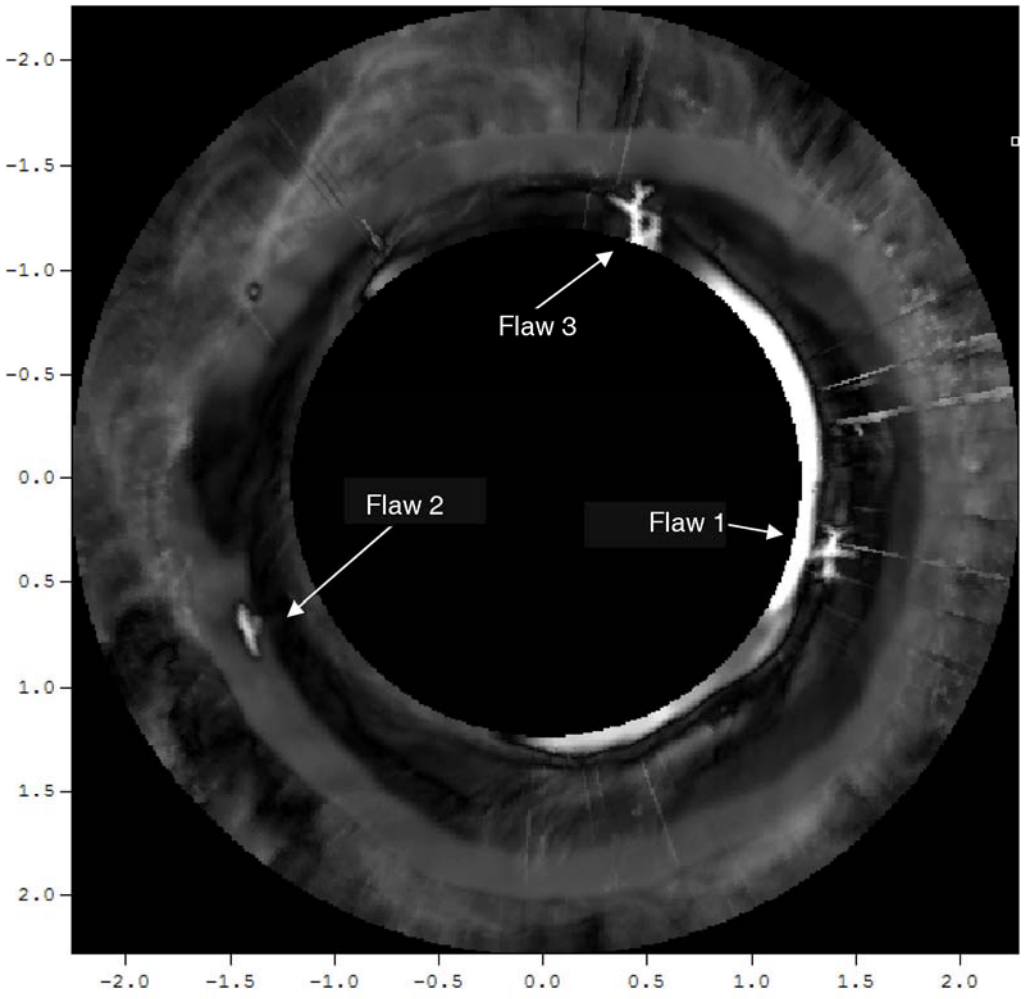

PINC_5_7_RADIAL_360_SCAN_1A_12_19_07_rect_hdf_xy_1_magInterp

C.2.1 Flaw 3

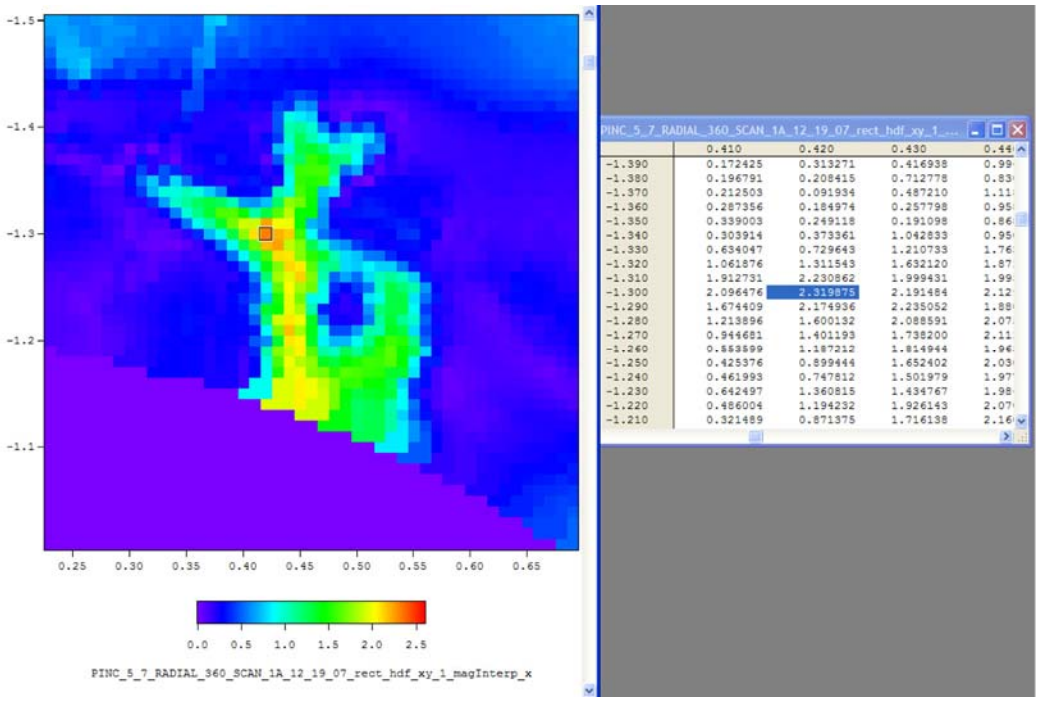

C.2.2 Flaw 1

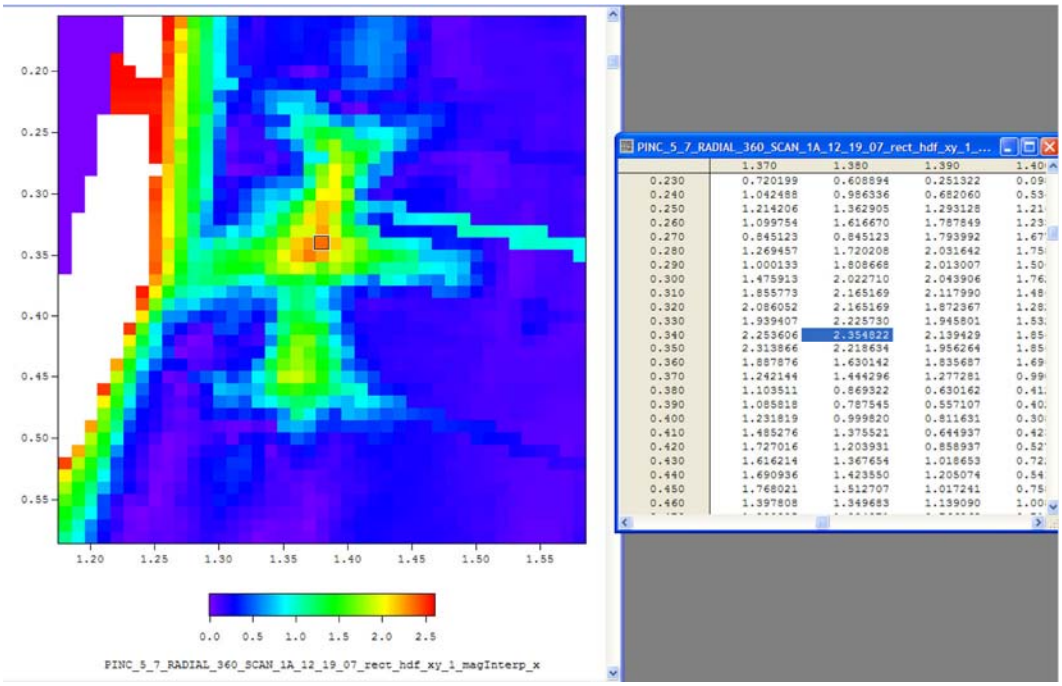

C.2.3 Flaw 2

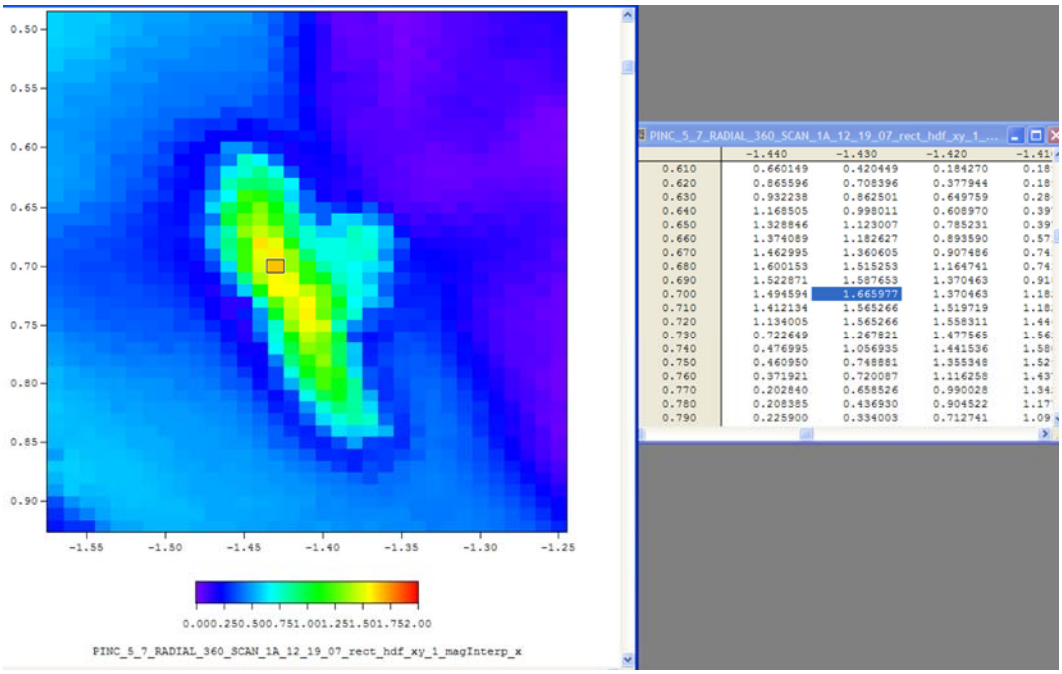
0.50
0.55
0.60
0.65
0.70
0.75
0.80
0.85
0.90
-1.55
-1.50
-1.45
-1.40
-1.35
-1.30
-1.25
0.000.250.500.751.001.251.501.752.00
PINC_5_7_RADIAL_360_SCAN_1A_12_19_07_rect_hdf_xy_1_magInterp_x
PINC_5_7_RADIAL_360_SCAN_1A_12_19_07_rect_hdf_xy_1_...
-1.440 -1.430 -1.420
0.610 0.660149 0.420449 0.184270
0.620 0.865596 0.708396 0.377944
0.630 0.932238 0.862501 0.649759
0.640 1.168505 0.998011 0.608970
0.650 1.328846 1.123007 0.785231
0.660 1.374089 1.182627 0.893590
0.670 1.462995 1.360605 0.907486
0.680 1.600153 1.515253 1.164741
0.690 1.522871 1.587653 1.370463
0.700 1.494594 1.665977 1.370463
0.710 1.412134 1.565266 1.519719
0.720 1.134005 1.565266 1.558311
0.730 0.722649 1.267821 1.477565
0.740 0.476995 1.056935 1.441536
0.750 0.460950 0.748881 1.355348
0.760 0.371921 0.720087 1.116258
0.770 0.202840 0.658526 0.990028
0.780 0.208385 0.436930 0.904522
0.790 0.225900 0.334003 0.712741

C.3 PINC 5.8

No flaws were identified in PINC 5.8. A fabricated area was, however, identified and shown in the following image.

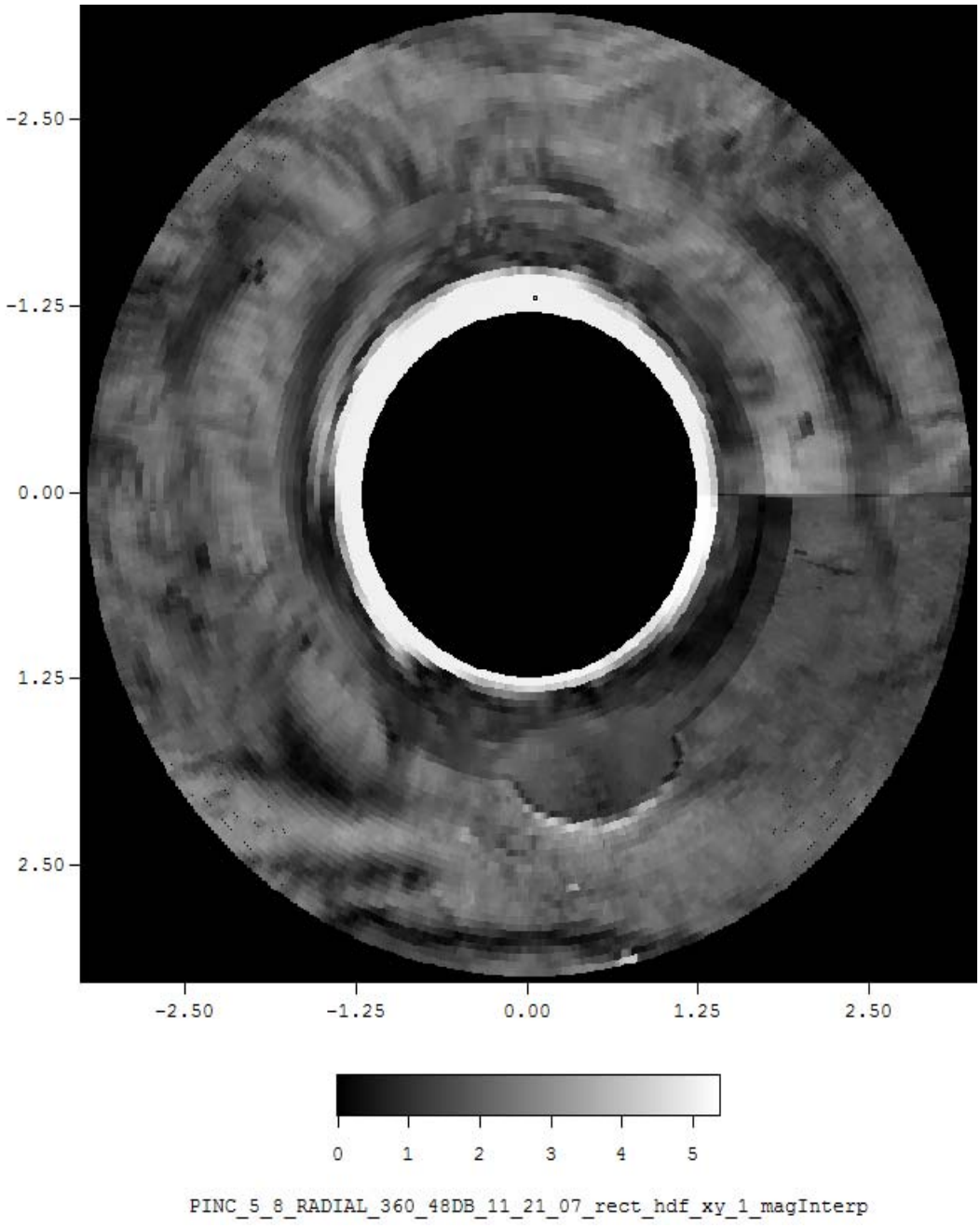

C.4 PINC 5.9

Two flaws were visible on PINC 5.9. The image below shows the magnitude of the edge of the fabrication.

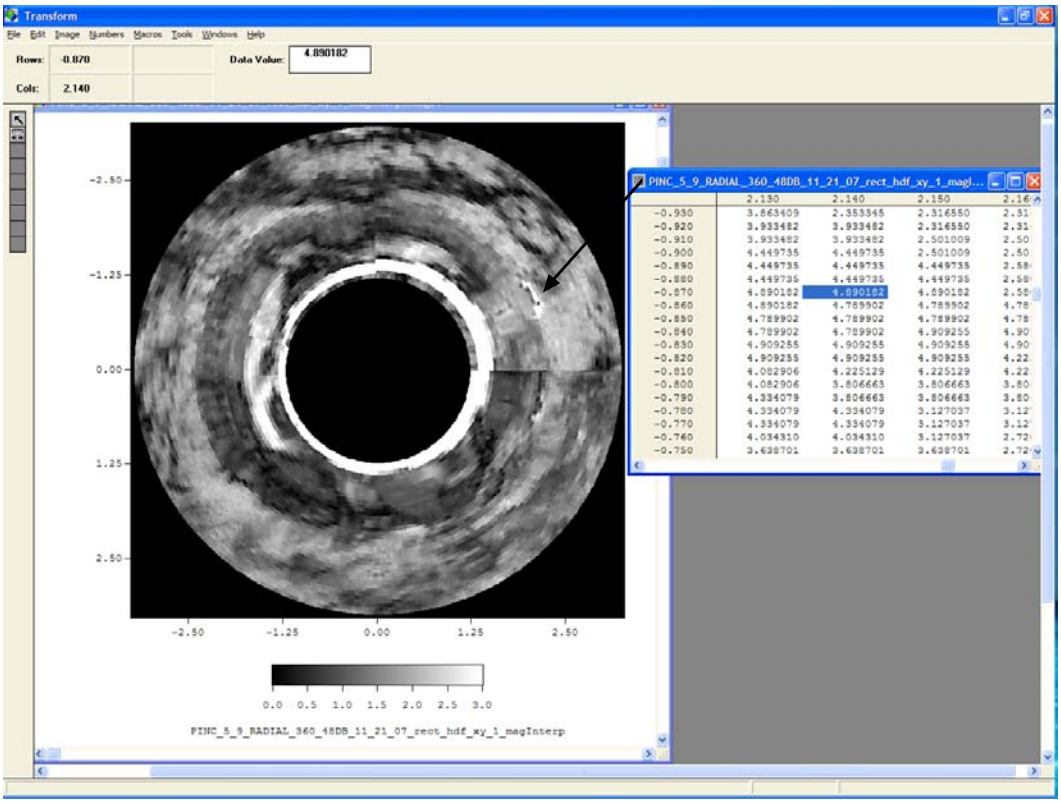

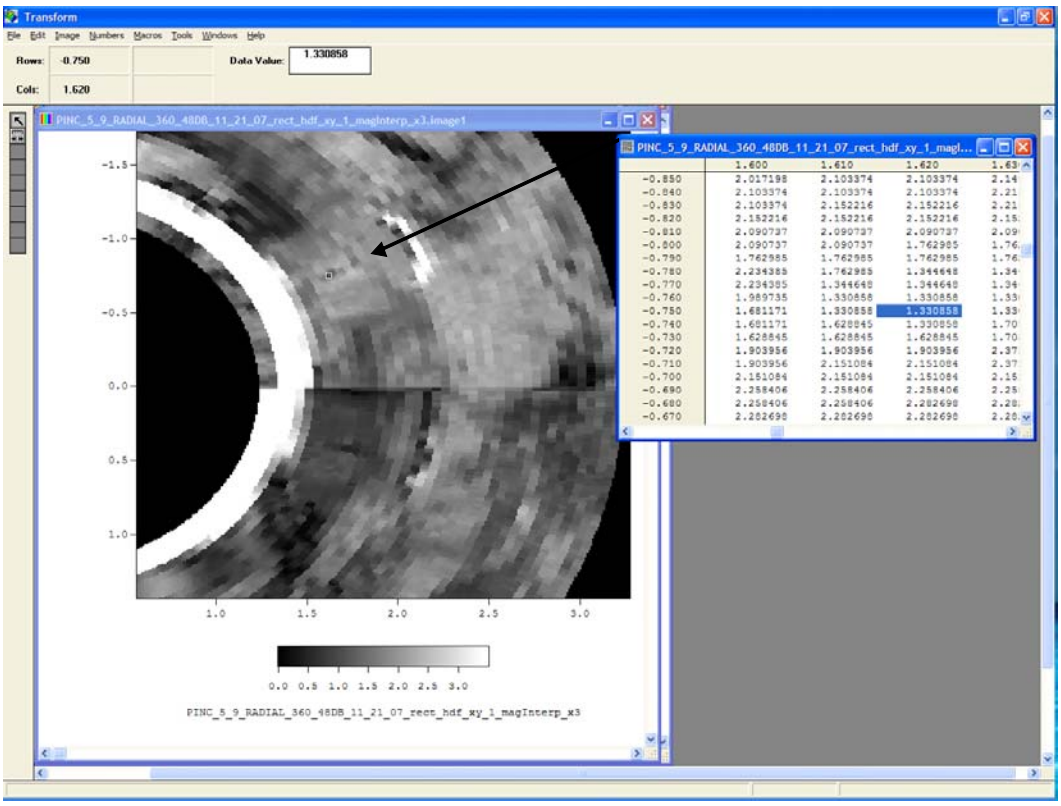
Transform
File Edit Image Numbers Macros Tools Windows Help
Rows: -0.750
Cols: 1.620
Data Value: 1.330858
PINC_5_9_RADIAL_360_48DB_11_21_07_rect_hdf_xy_1_magInterp_x3.image1
PINC_5_9_RADIAL_360_48DB_11_21_07_rect_hdf_xy_1_magI...
PINC_5_9_RADIAL_360_48DB_11_21_07_rect_hdf_xy_1_magInterp_x3

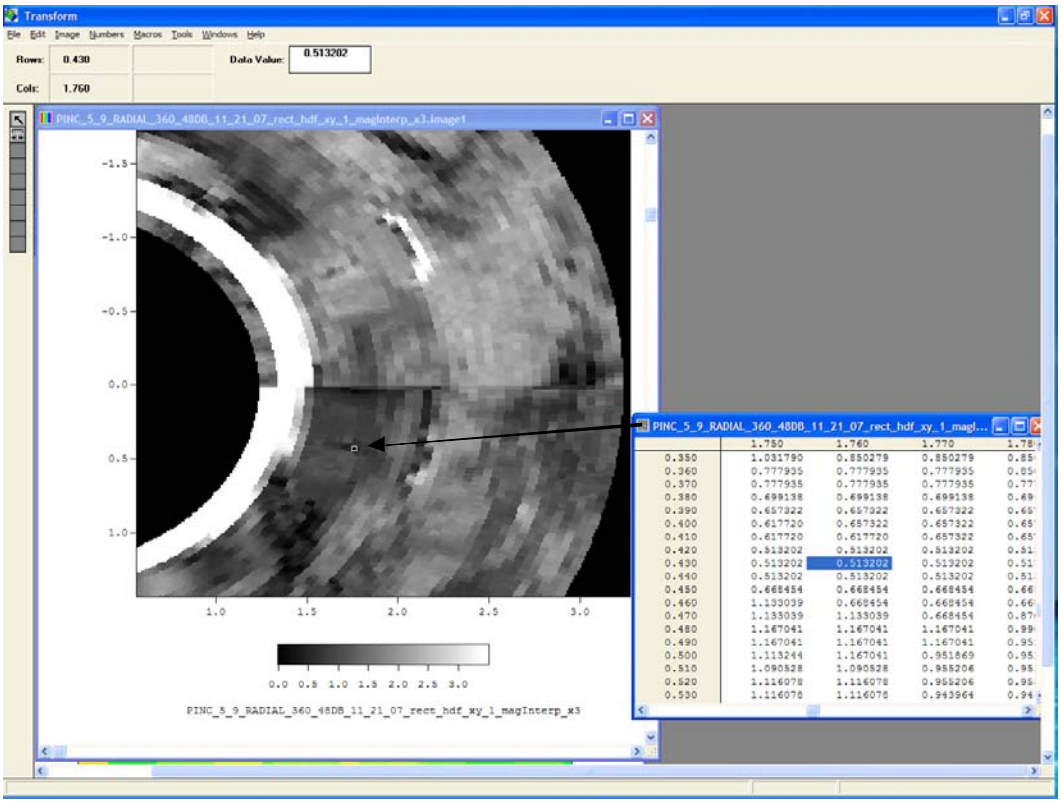
Transform
File Edit Image Numbers Macros Tools Windows Help
Rows: 0.430
Cols: 1.760
Data Value: 0.513202
PINC_5_9_RADIAL_360_48DB_11_21_07_rect_hdf_xy_1_magInterp_x3.image1
PINC_5_9_RADIAL_360_48DB_11_21_07_rect_hdf_xy_1_magI...
PINC_5_9_RADIAL_360_48DB_11_21_07_rect_hdf_xy_1_magInterp_x3

C.5 PINC 5.10

General magnitude of the fabrication area.

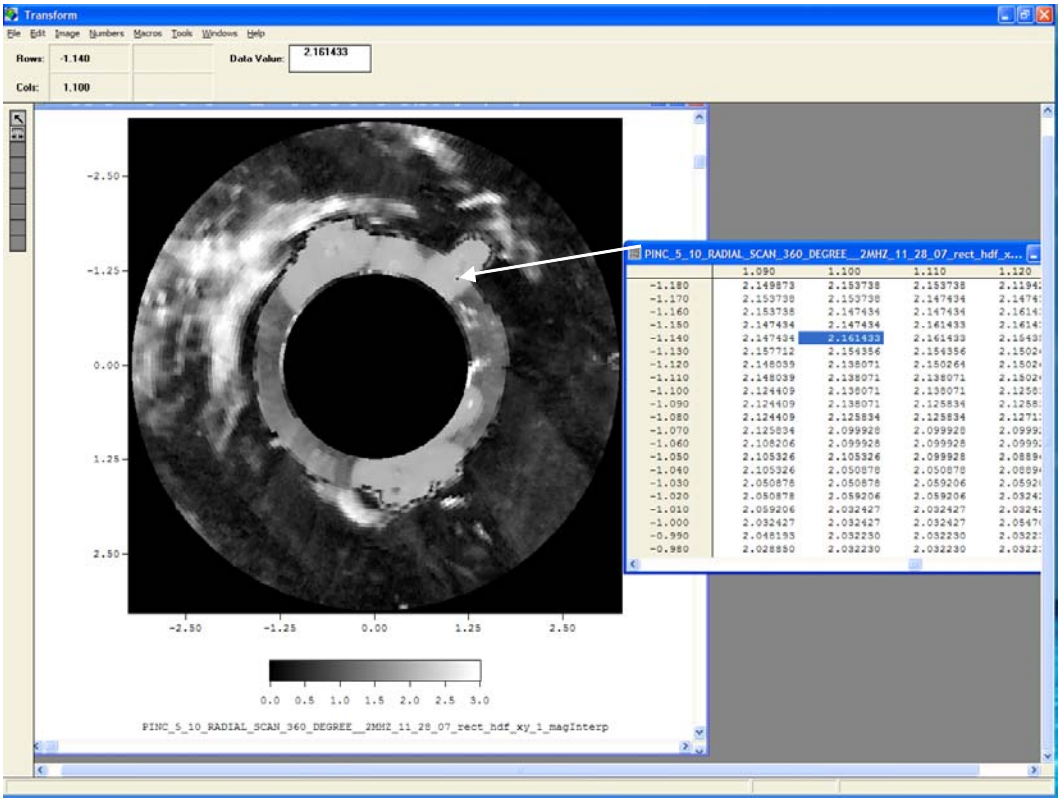

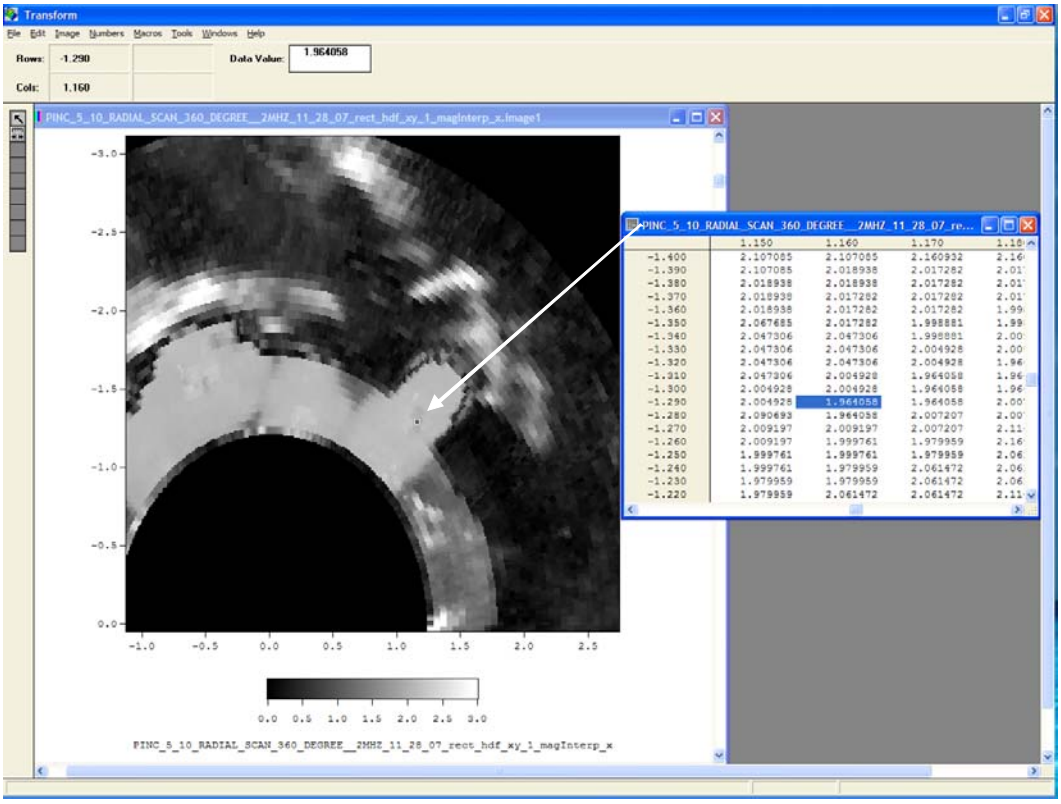
Transform
File Edit Image Numbers Macros Tools Windows Help
Rows: -1.290
Cols: 1.160
Data Value: 1.964058
PINC_5_10_RADIAL_SCAN_360_DEGREE__2MHZ_11_28_07_rect_hdf_xy_1_magInterp_x.Image1
PINC_5_10_RADIAL_SCAN_360_DEGREE__2MHZ_11_28_07_re...
PINC_5_10_RADIAL_SCAN_360_DEGREE__2MHZ_11_28_07_rect_hdf_xy_1_magInterp_x

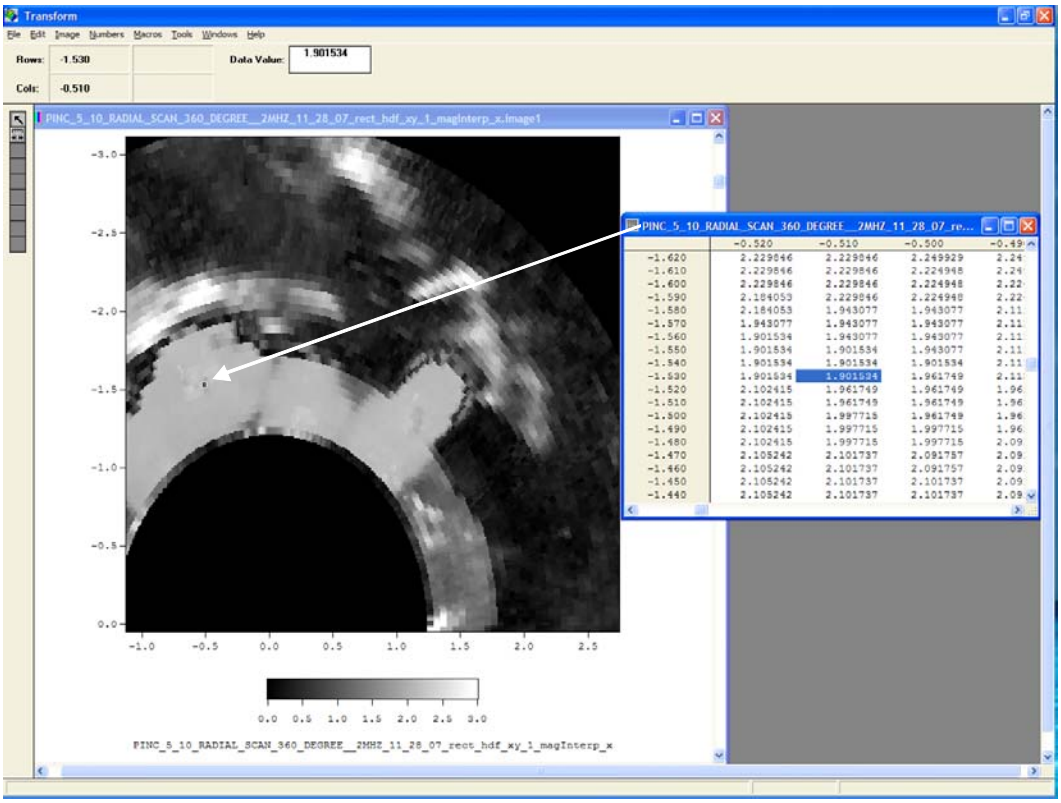
Transform
File Edit Image Numbers Macros Tools Windows Help
Rows: -1.530
Cols: -0.510
Data Value: 1.901534
PINC_5_10_RADIAL_SCAN_360_DEGREE__2MHZ_11_28_07_rect_hdf_xy_1_magInterp_x.Image1
PINC_5_10_RADIAL_SCAN_360_DEGREE__2MHZ_11_28_07_re...
PINC_5_10_RADIAL_SCAN_360_DEGREE__2MHZ_11_28_07_rect_hdf_xy_1_magInterp_x

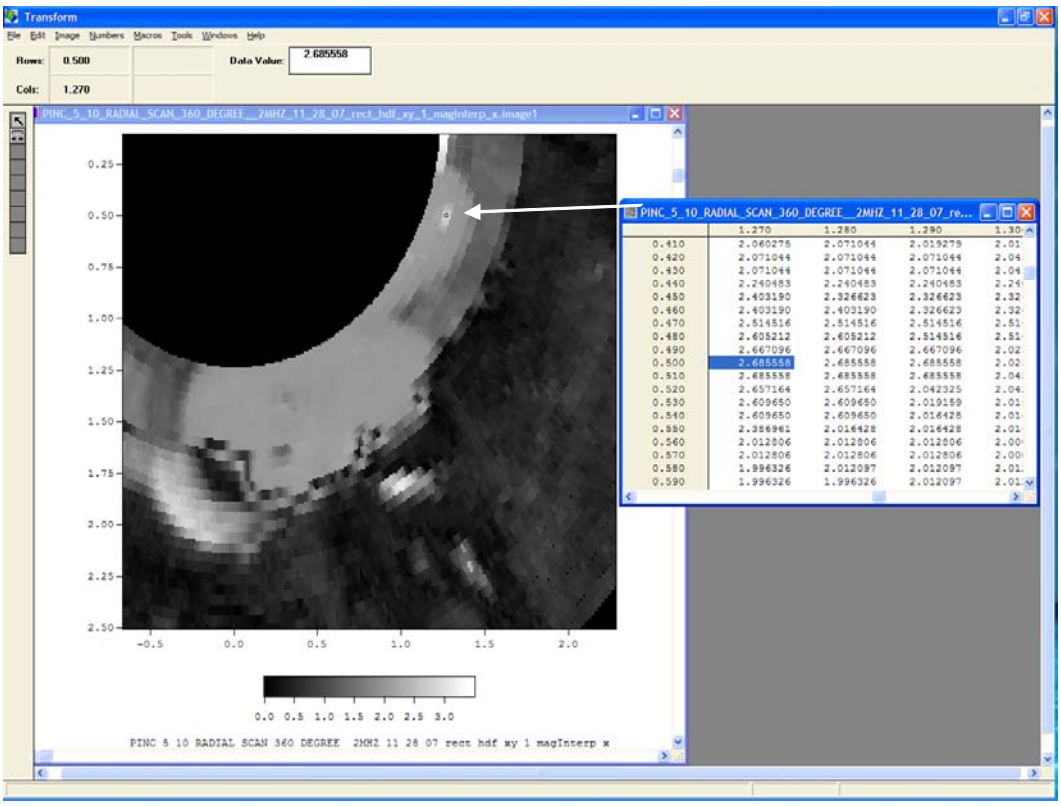
Transform
File Edit Image Numbers Macros Tools Windows Help
Rows: 0.500
Cols: 1.270
Data Value: 2.685558
PINC_5_10_RADIAL_SCAN_360_DEGREE__2MHZ_11_28_07_rect_hdf_xy_1_magInterp_x.image1
PINC_5_10_RADIAL_SCAN_360_DEGREE__2MHZ_11_28_07_re...
PINC 5 10 RADIAL SCAN 360 DEGREE 2MHZ 11 28 07 rect hdf xy 1 magInterp x

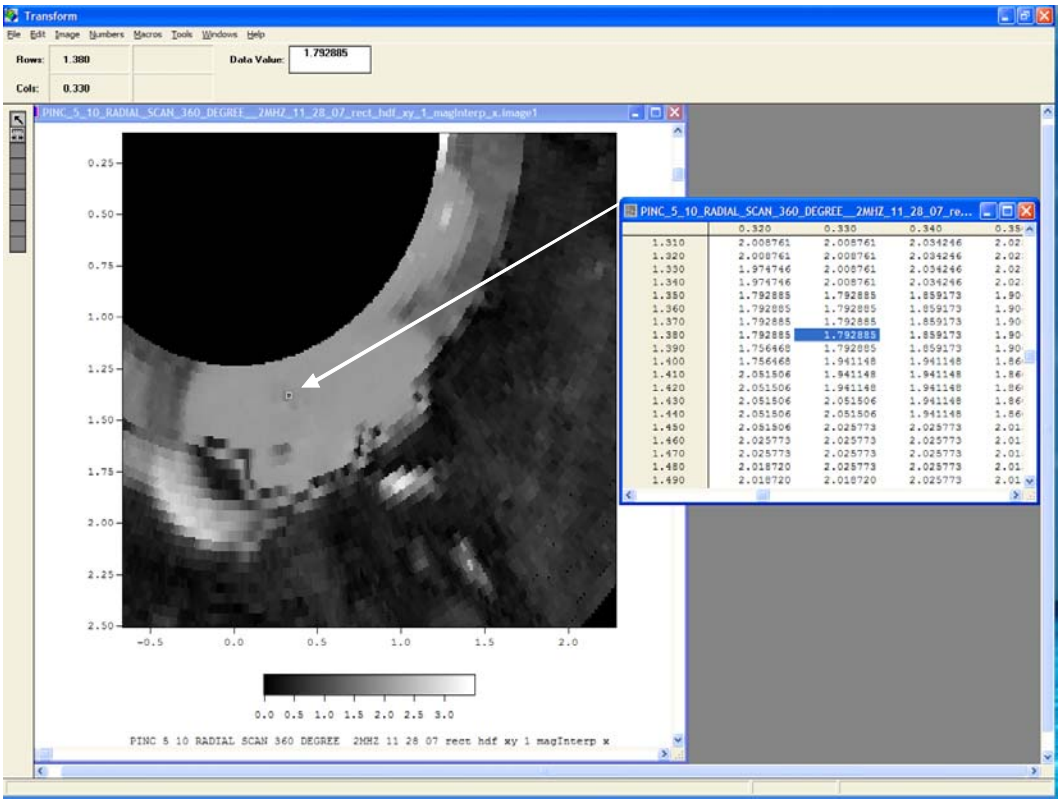
Transform
File Edit Image Numbers Macros Tools Windows Help
Rows: 1.380
Cols: 0.330
Data Value: 1.792885
PINC_5_10_RADIAL_SCAN_360_DEGREE__2MHZ_11_28_07_rect_hdf_xy_1_magInterp_x.image1
PINC_5_10_RADIAL_SCAN_360_DEGREE__2MHZ_11_28_07_re...
PINC 5 10 RADIAL SCAN 360 DEGREE 2MHZ 11 28 07 rect hdf xy 1 magInterp x

Here is another image that we used in a different report which shows six flaws. It is a stretch to say you can see them all unless you know what you are looking for. In the example shown above, we point to a different area for the flaw location. We would need to zero in on the flaw and scan at high resolution to identify.

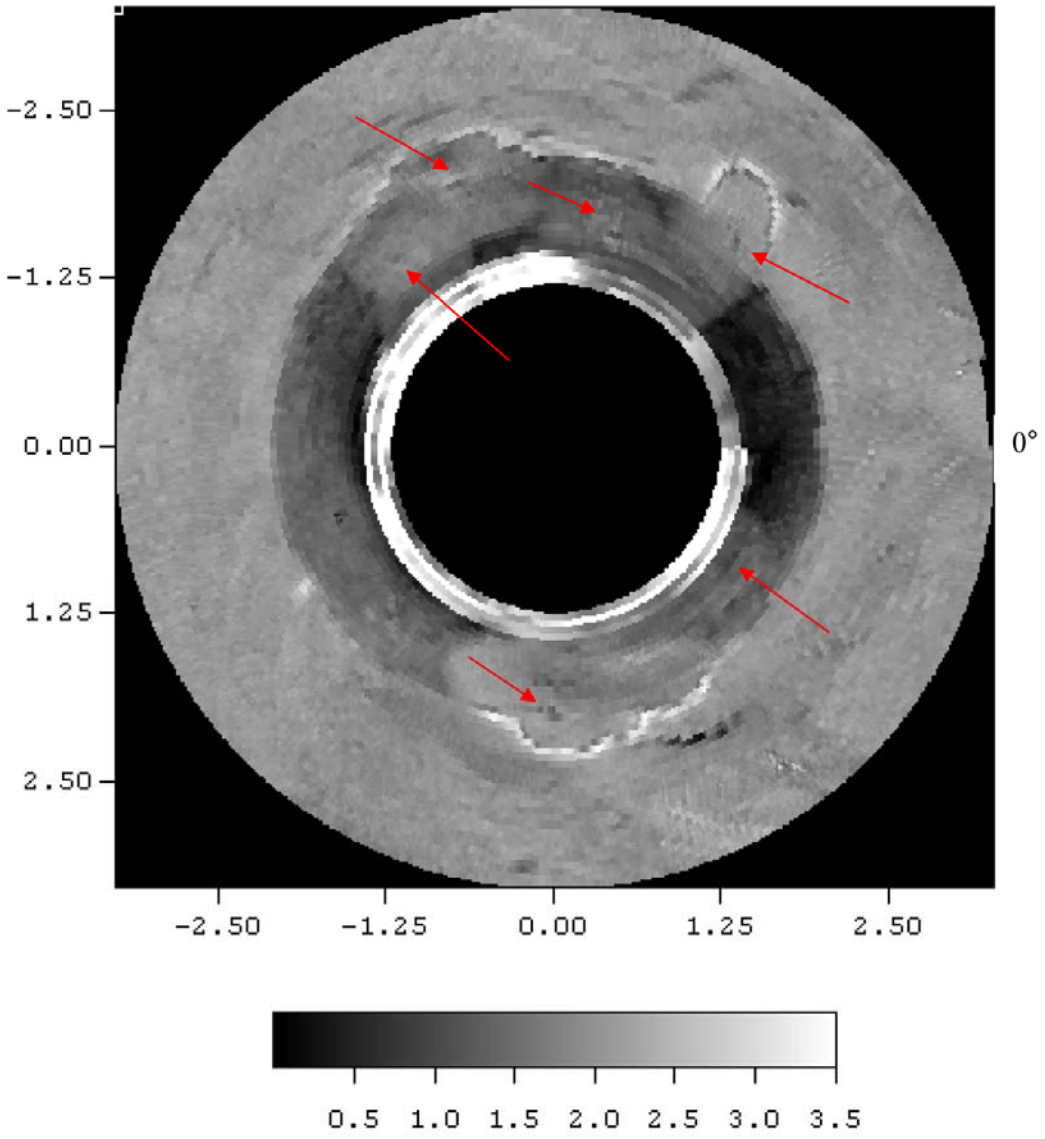

C.6 PINC 5.11

General area magnitude.

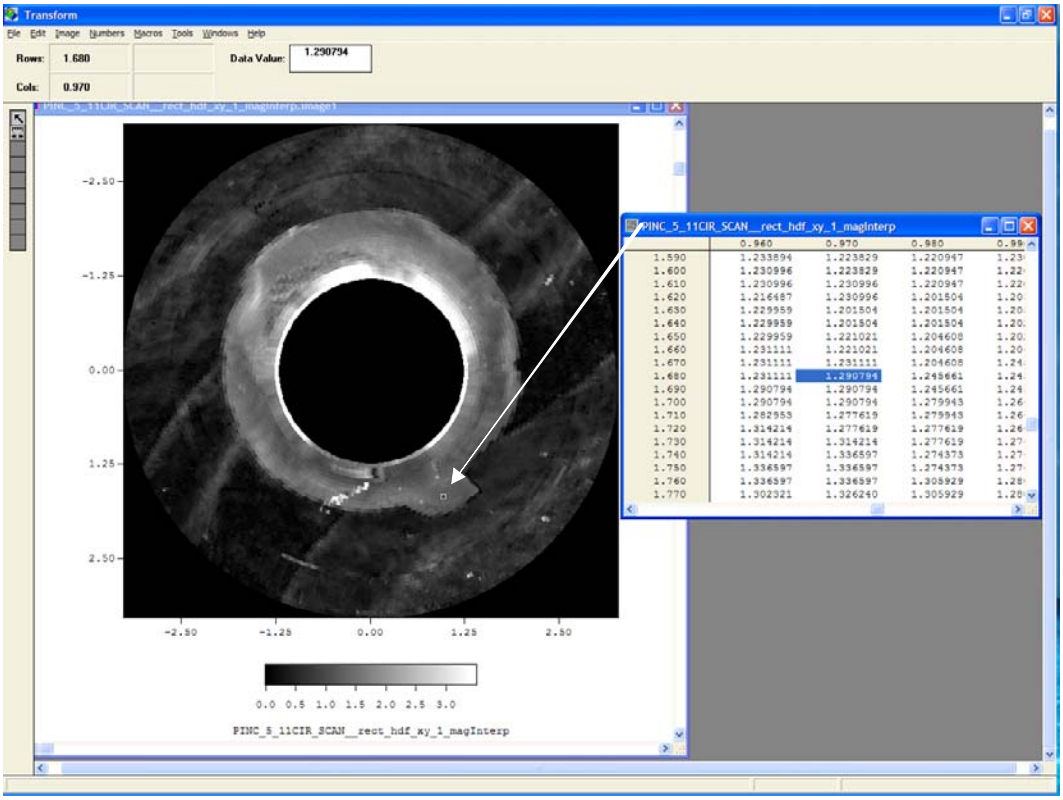

C.7 PINC 5.12

General area magnitude.

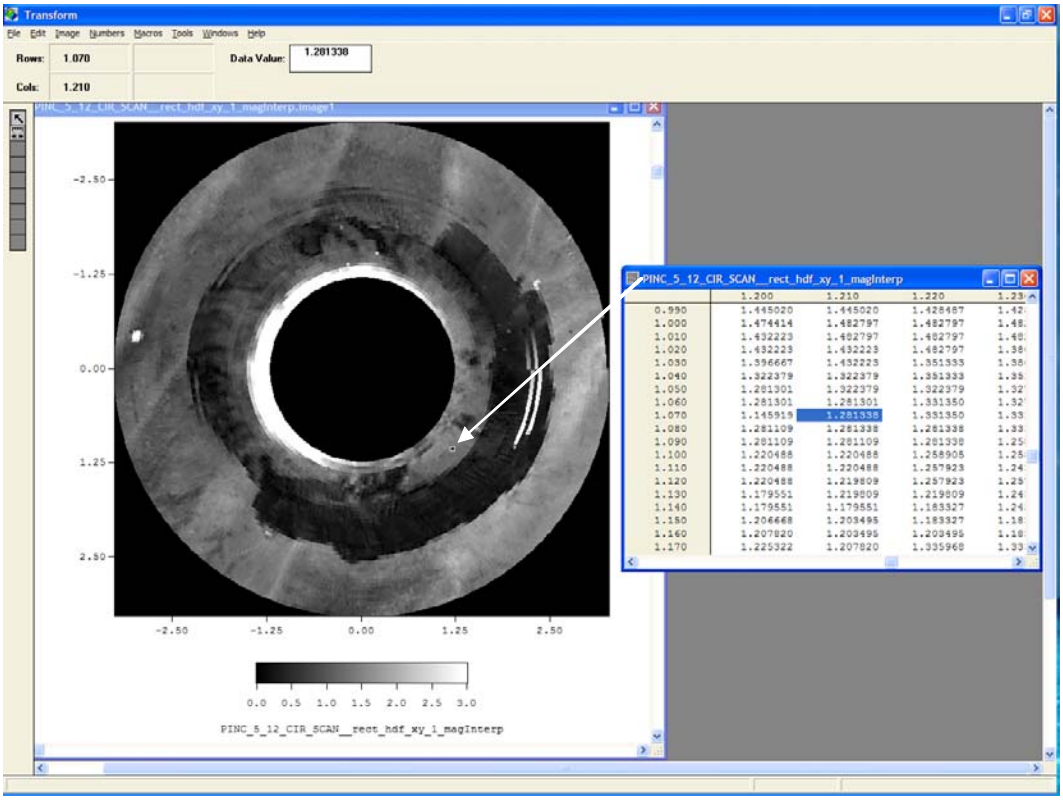

C.8 PINC 5.6

Five indications for sure; the sixth is a guess.

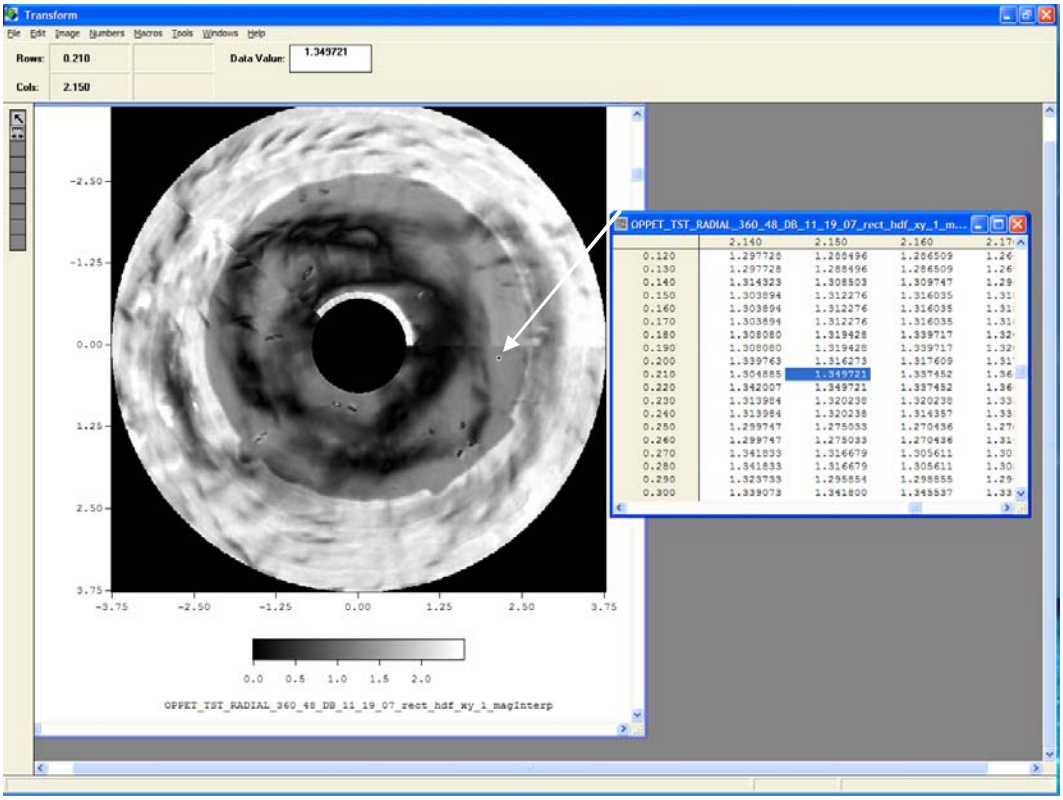

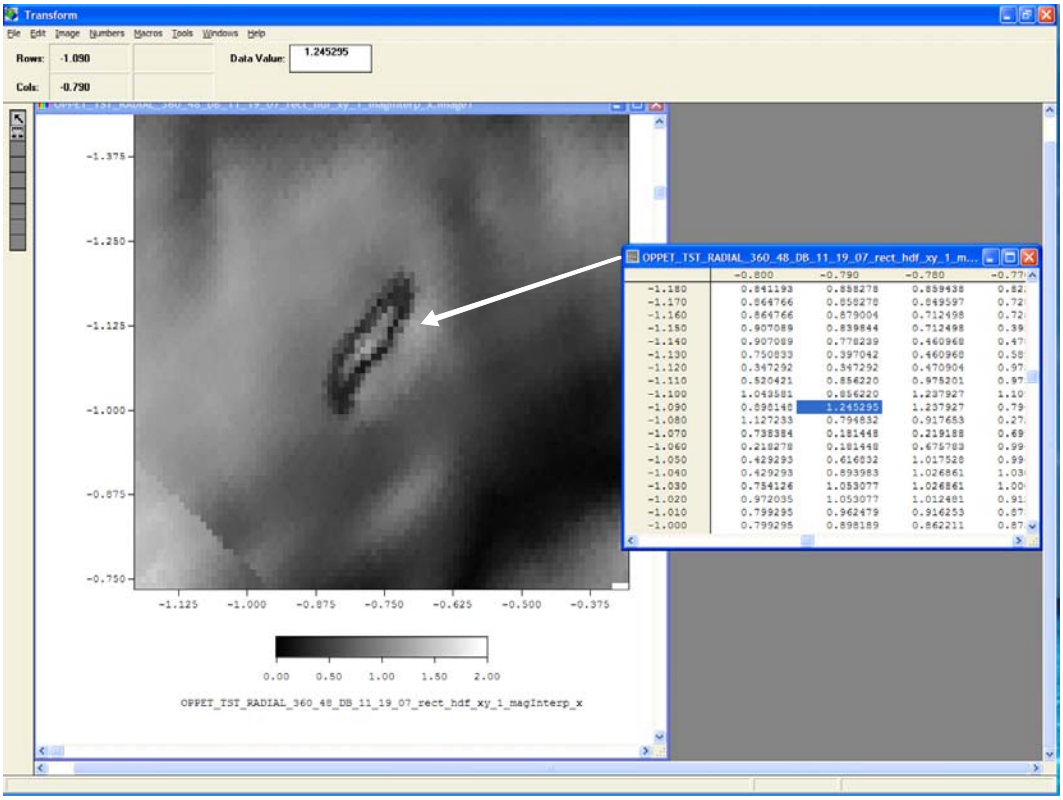
Transform
File Edit Image Numbers Macros Tools Windows Help
Rows: -1.090
Cols: -0.790
Data Value: 1.245295
OPPET_TST_RADIAL_360_48_DB_11_19_07_rect_hdf_xy_1_magInterp_x

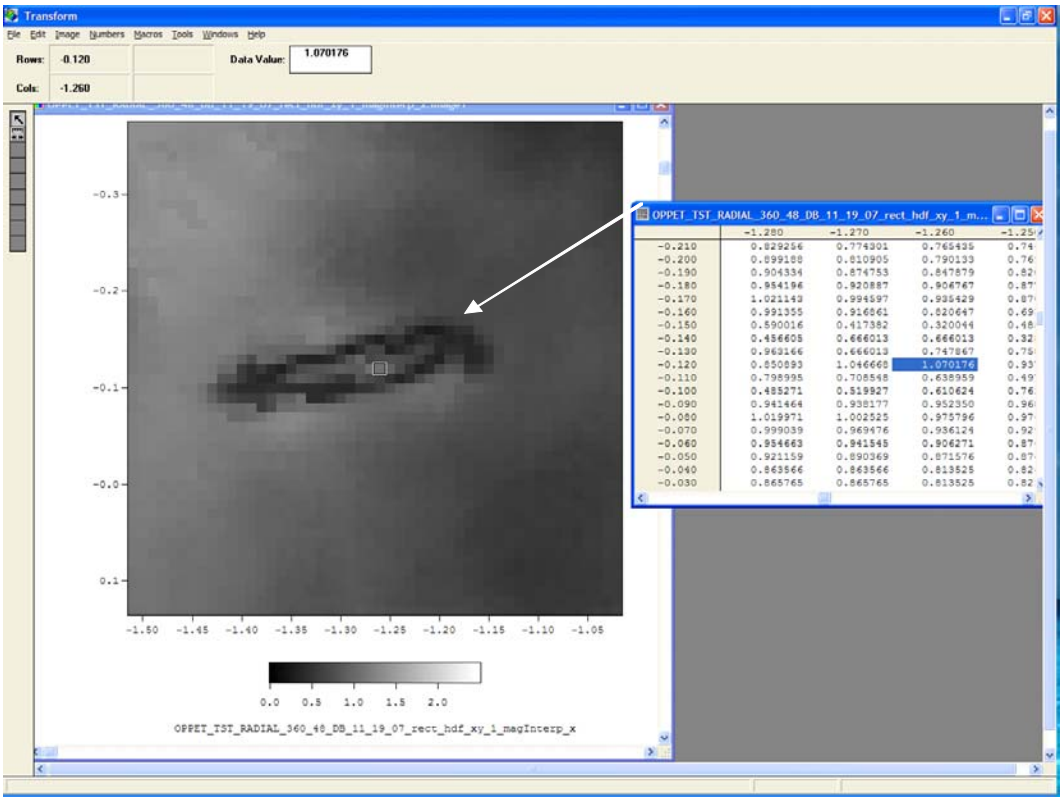
Transform
File Edit Image Numbers Macros Tools Windows Help
Rows: -0.120
Cols: -1.260
Data Value: 1.070176
OPPET_TST_RADIAL_360_48_DB_11_19_07_rect_hdf_xy_1_magInterp_x

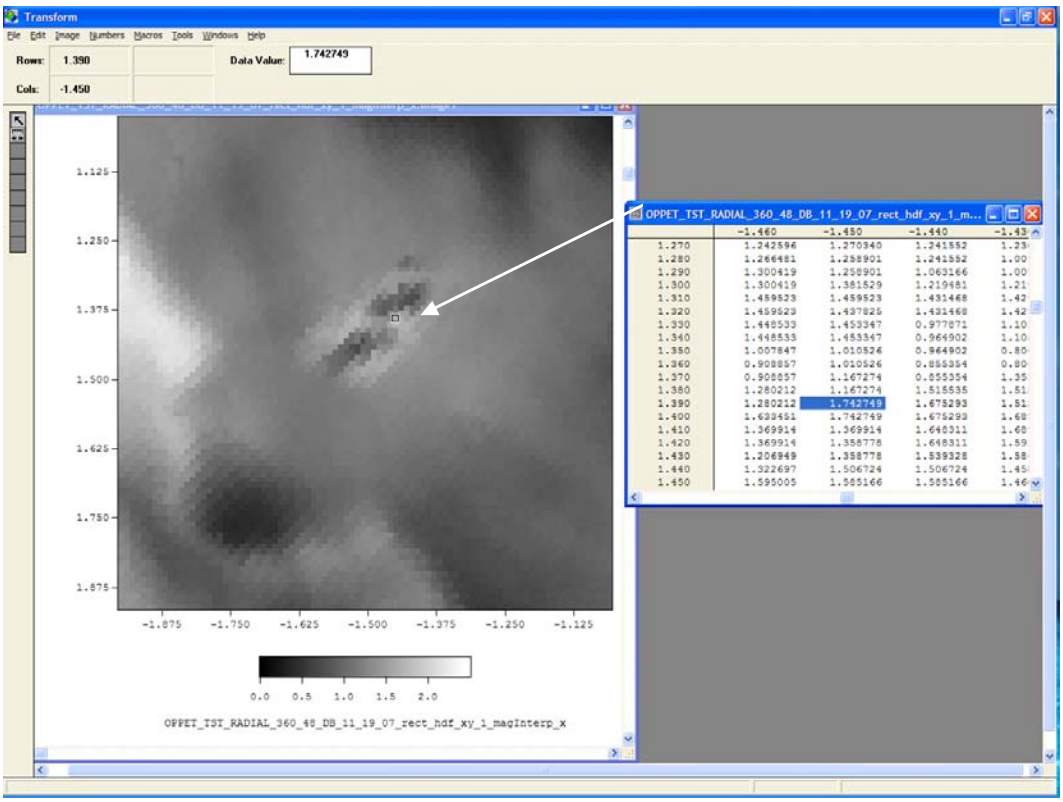
Transform
File Edit Image Numbers Macros Tools Windows Help
Rows: 1.390
Cols: -1.450
Data Value: 1.742749
OPPET_TST_RADIAL_360_48_DB_11_19_07_rect_hdf_xy_1_magInterp_x

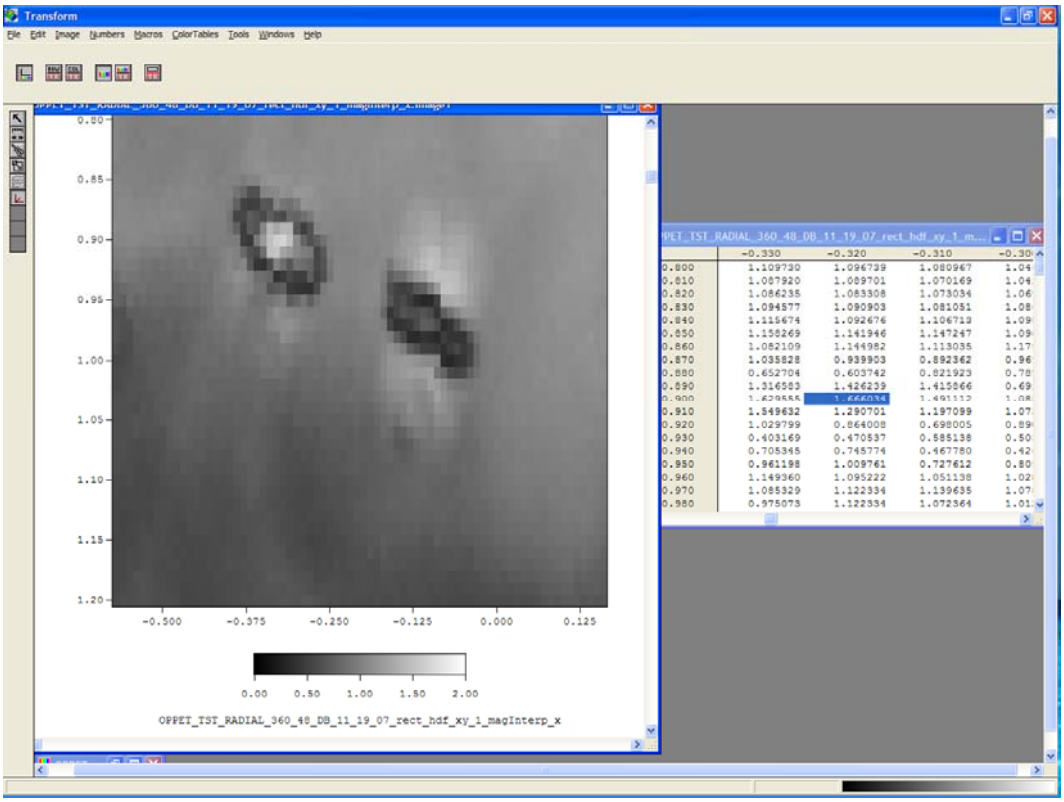
Transform
File Edit Image Numbers Macros ColorTables Tools Windows Help
OPPET_TST_RADIAL_360_48_DB_11_19_07_rect_hdf_xy_1_magInterp_x

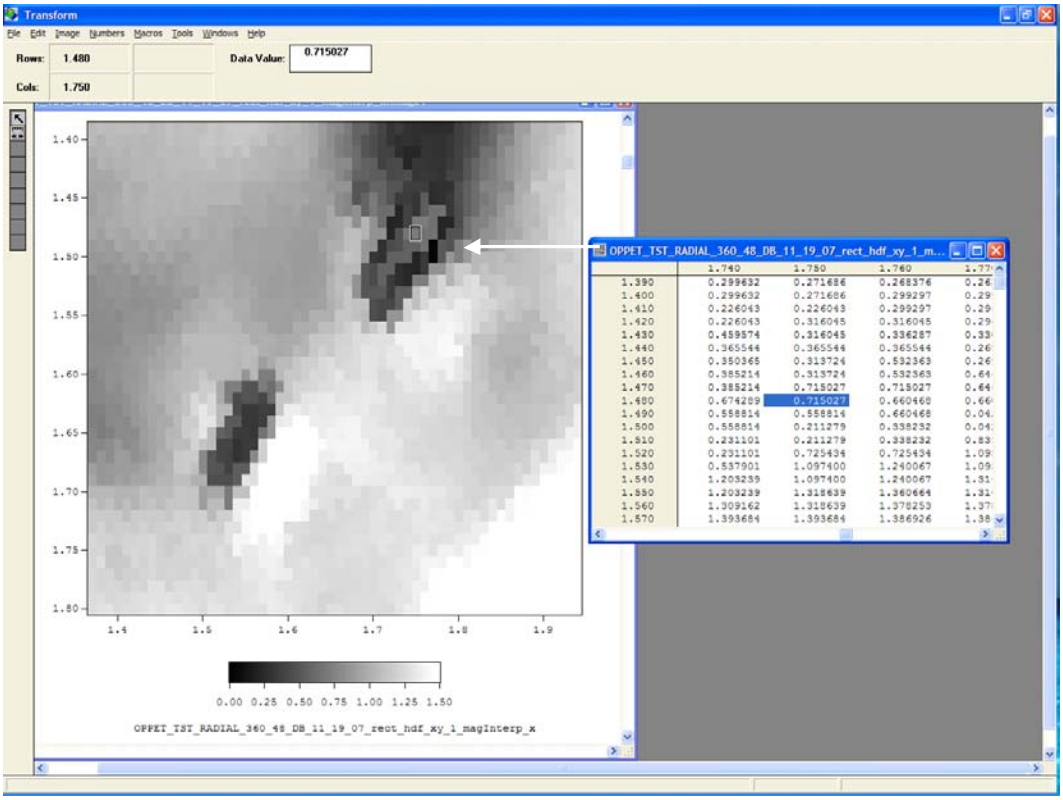
Transform
File Edit Image Numbers Macros Tools Windows Help
Rows: 1.480
Cols: 1.750
Data Value: 0.715027
OPPET_TST_RADIAL_360_48_DB_11_19_07_rect_hdf_xy_1_m...
OPPET_TST_RADIAL_360_48_DB_11_19_07_rect_hdf_xy_1_magInterp_x

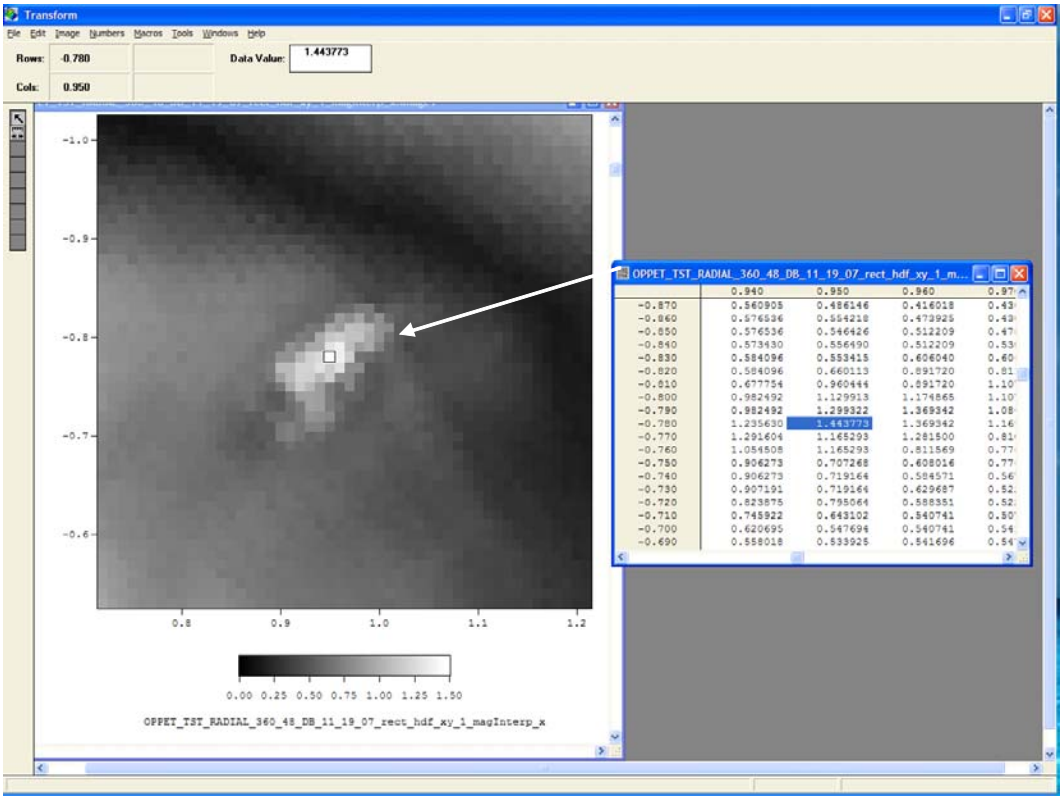
Transform
File Edit Image Numbers Macros Tools Windows Help
Rows: -0.780
Cols: 0.950
Data Value: 1.443773
OPPET_TST_RADIAL_360_48_DB_11_19_07_rect_hdf_xy_1_m...
OPPET_TST_RADIAL_360_48_DB_11_19_07_rect_hdf_xy_1_magInterp_x

C.9 Japanese Samples

C.9.1 EDM Sample Block 1

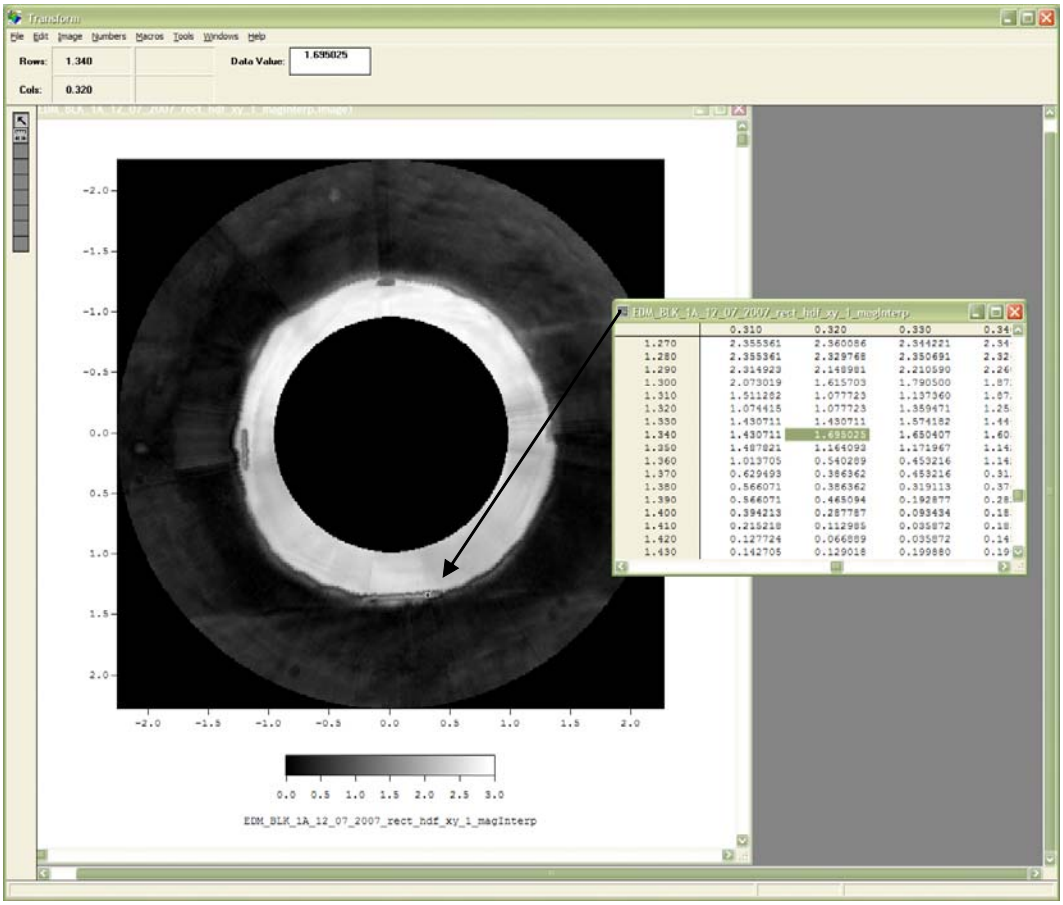

C.9.2 EDM Sample Block 2

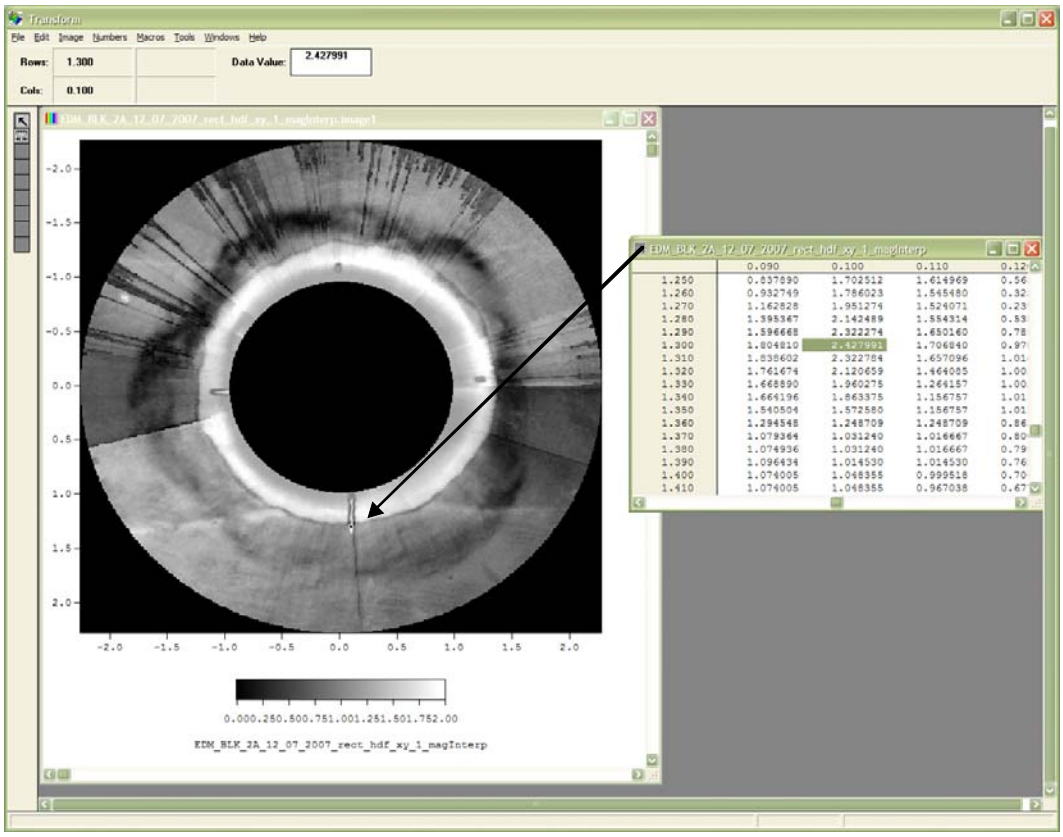

C.9.3 Reference Block 1

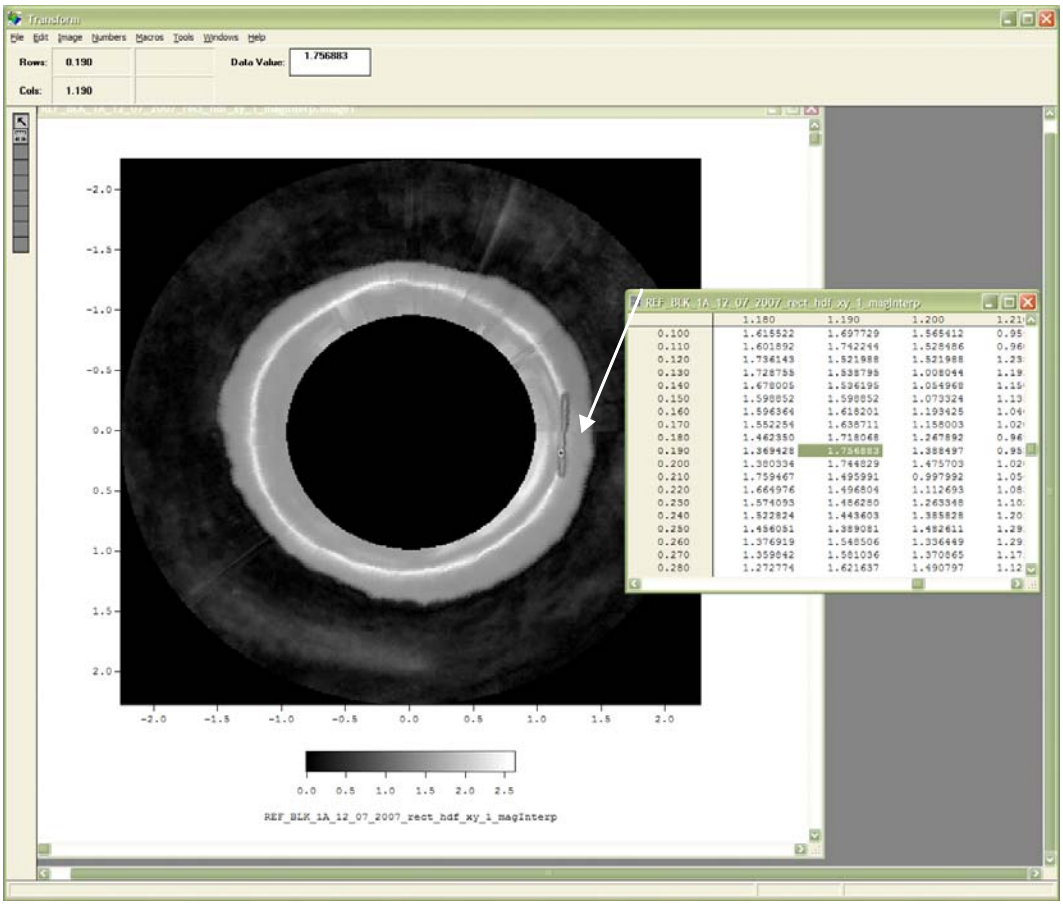

C.9.4 Reference Block 2

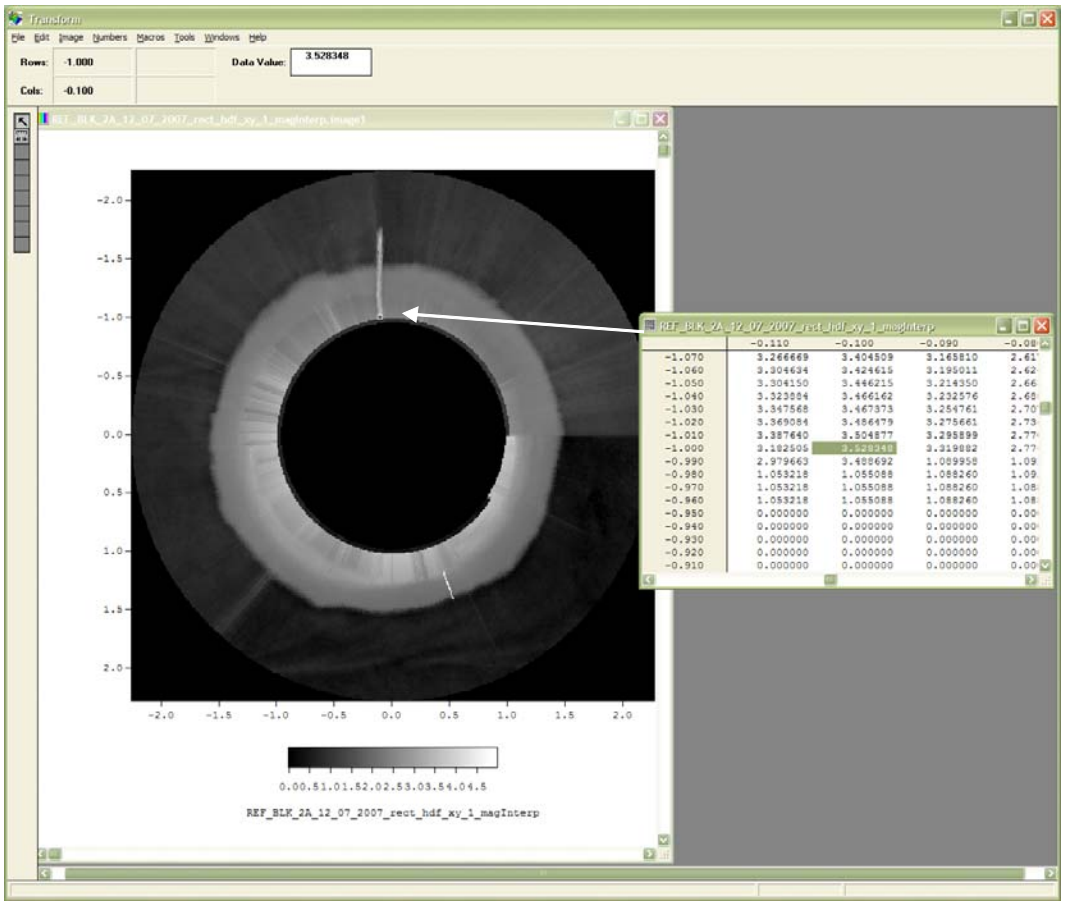

C.10 PINC 5.13

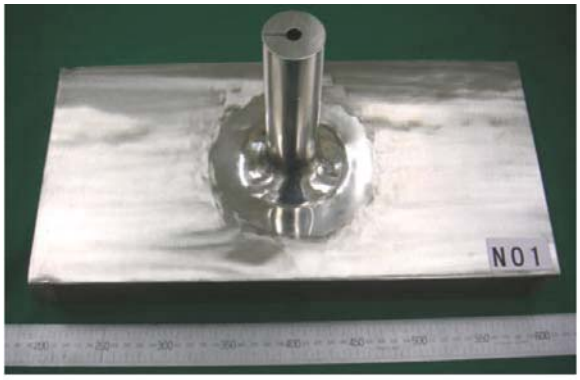
N01

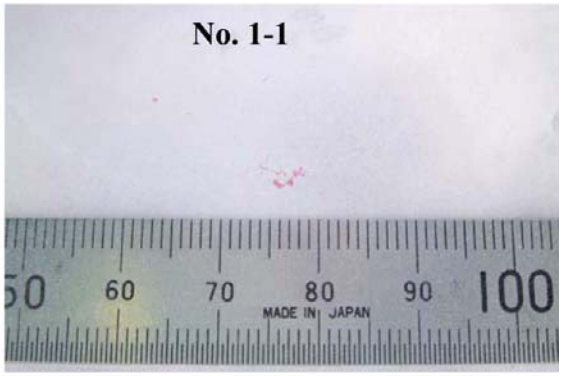
No. 1-1
60
70
80
90
100
MADE IN JAPAN

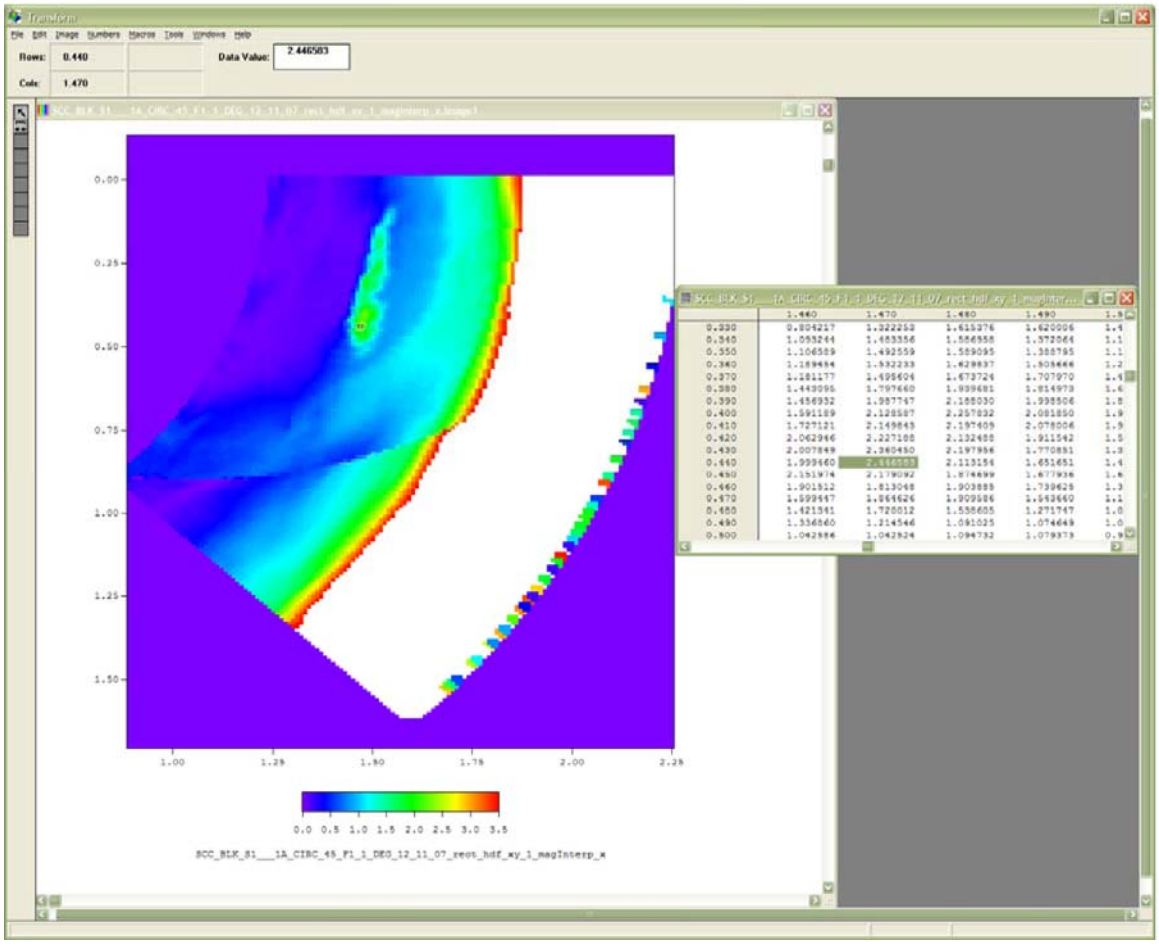
Transform
File Edit Image Numbers Macros Tools Windows Help
Rows: 0.440
Cols: 1.470
Data Value: 2.446503

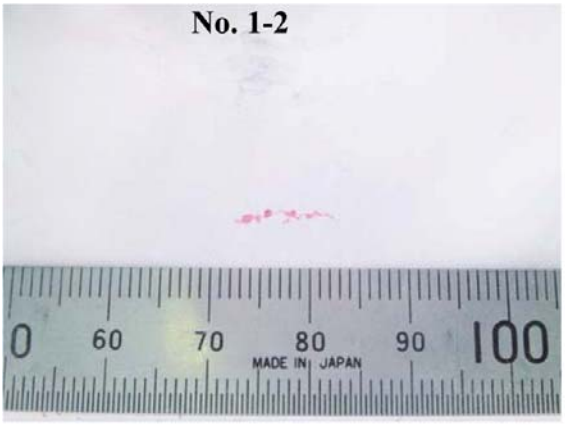
No. 1-2
0
60
70
80
90
100
MADE IN JAPAN

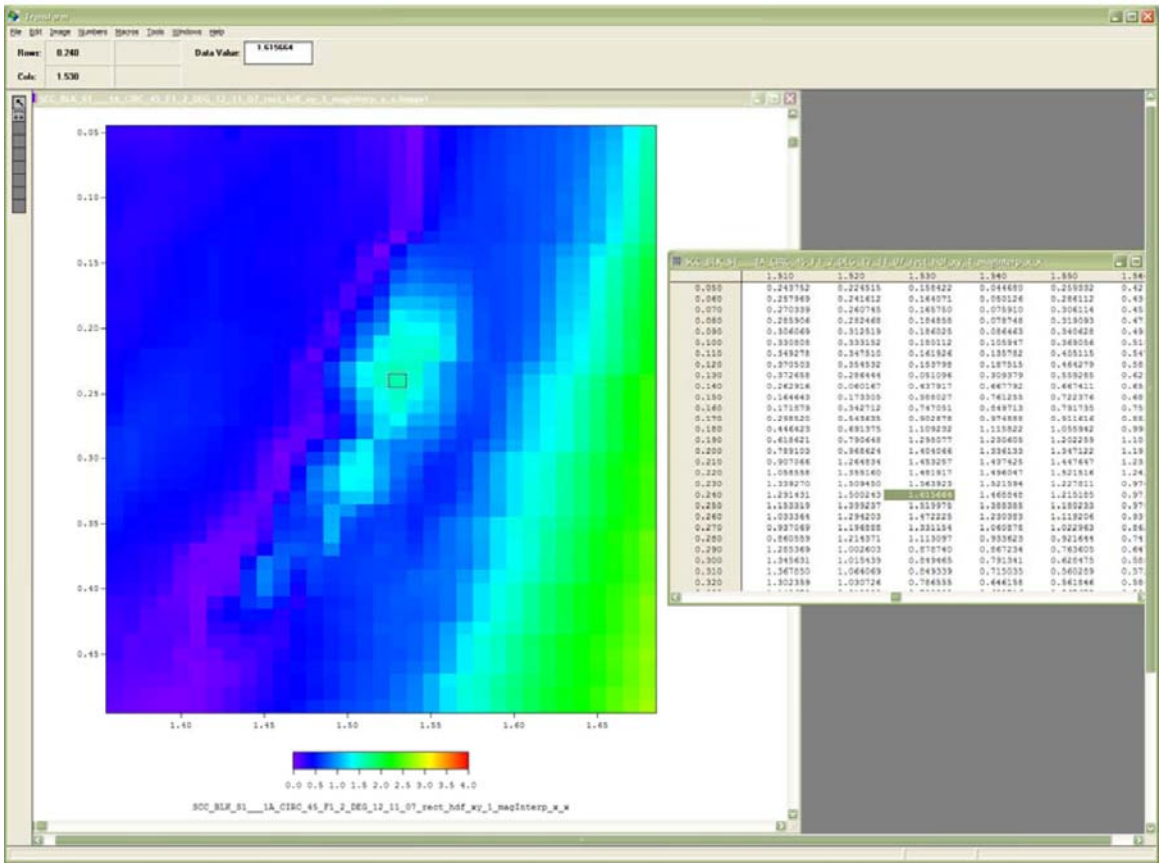

C.11 PINC 5.14

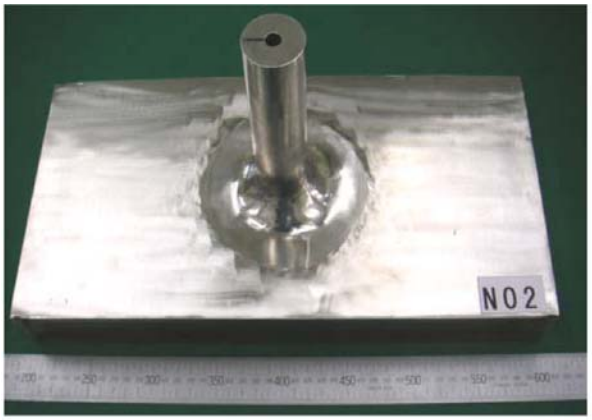

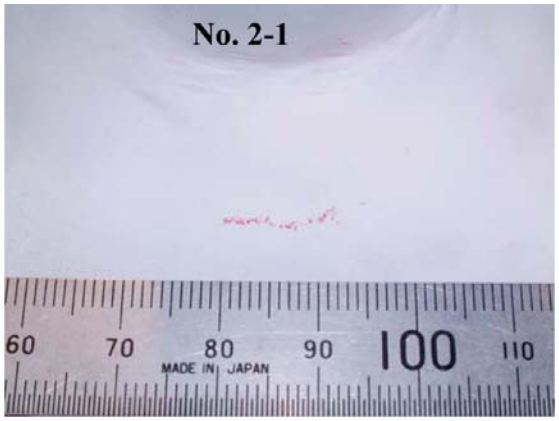

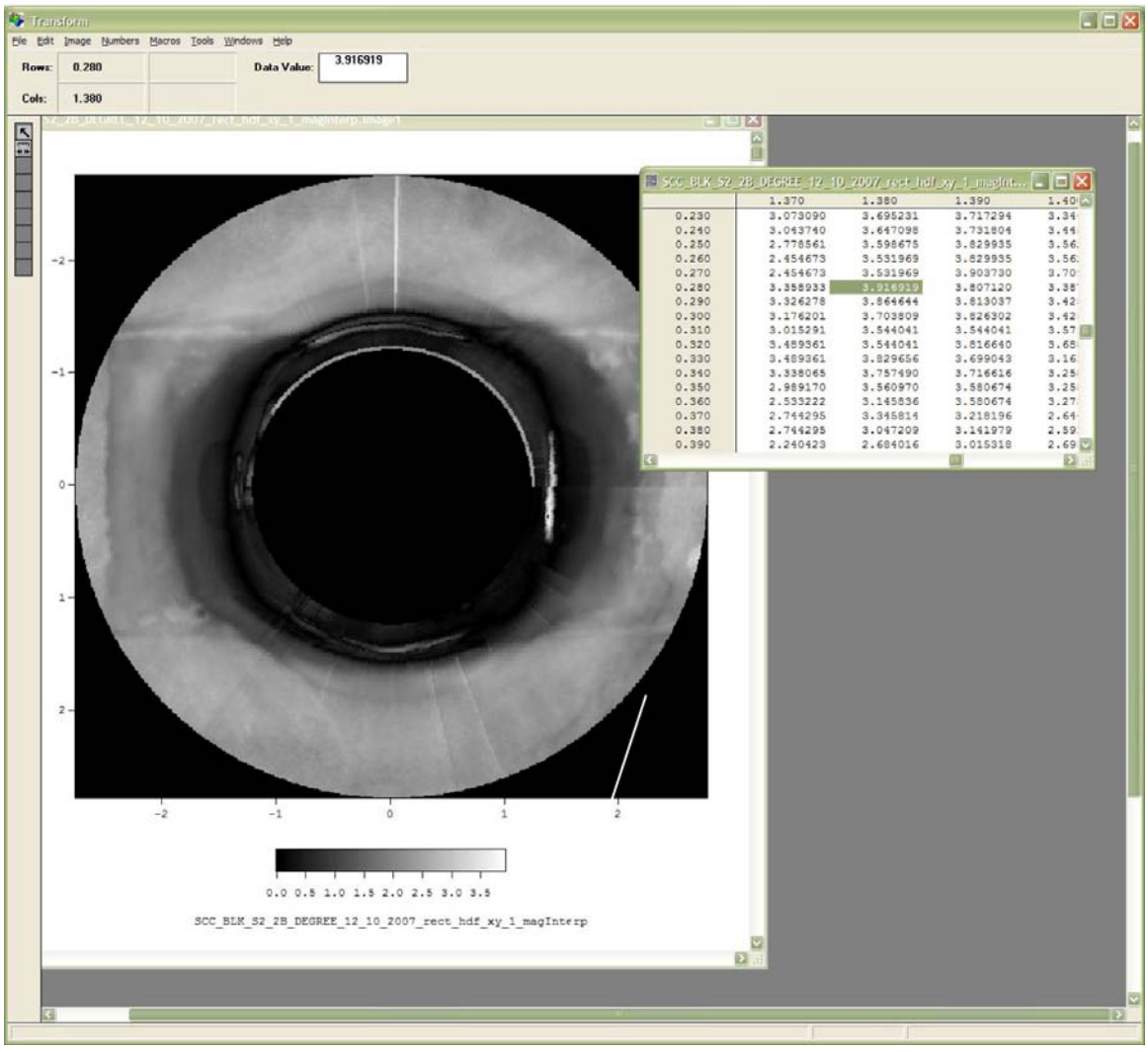

	1.370	1.380	1.390	1.40
0.230	3.073090	3.695231	3.717294	3.34
0.240	3.043740	3.647098	3.731804	3.44
0.250	2.778561	3.598675	3.829935	3.56
0.260	2.454673	3.531969	3.829935	3.56
0.270	2.454673	3.531969	3.903730	3.70
0.280	3.358933	3.916919	3.807120	3.38
0.290	3.326278	3.864644	3.813037	3.42
0.300	3.176201	3.703809	3.826302	3.42
0.310	3.015291	3.544041	3.544041	3.57
0.320	3.489361	3.544041	3.816640	3.68
0.330	3.489361	3.829656	3.699043	3.16
0.340	3.338065	3.757490	3.716616	3.25
0.350	2.989170	3.560970	3.580674	3.25
0.360	2.533222	3.145836	3.580674	3.27
0.370	2.744295	3.345814	3.218196	2.64
0.380	2.744295	3.047209	3.141979	2.59
0.390	2.240423	2.684016	3.015318	2.69

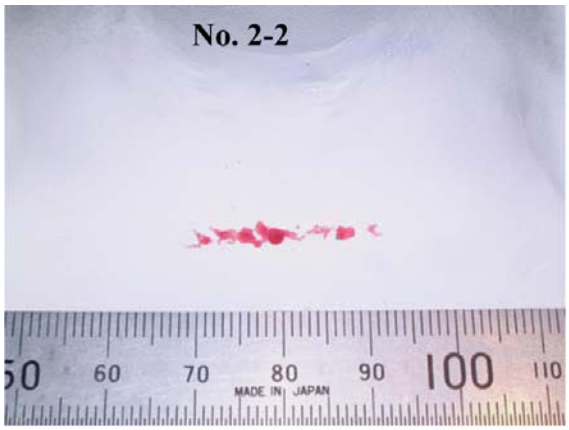
No. 2-2
60
70
80
90
100
110
MADE IN JAPAN

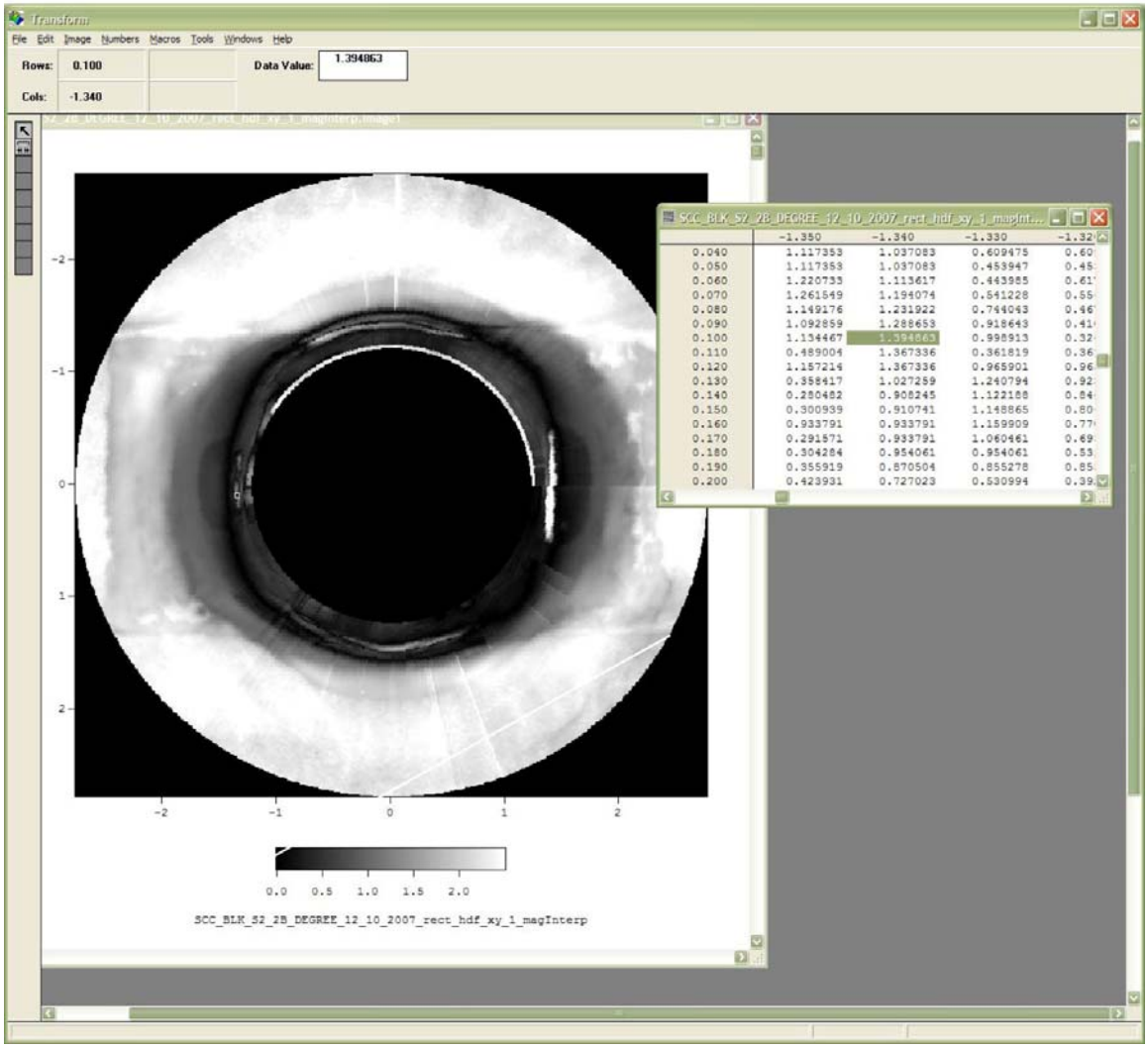
Transform
File Edit Image Numbers Macros Tools Windows Help
Rows: 0.100
Cols: -1.340
Data Value: 1.394863
SCC_BLK_S2_2B_DEGREE_12_10_2007_rect_hdf_xy_1_magInterp
-1.350 -1.340 -1.330
0.040 1.117353 1.037083 0.609475
0.050 1.117353 1.037083 0.453947
0.060 1.220733 1.113617 0.443985
0.070 1.261549 1.194074 0.541228
0.080 1.149176 1.231922 0.744043
0.090 1.092859 1.288653 0.918643
0.100 1.154467 1.394863 0.998913
0.110 0.489004 1.367336 0.361819
0.120 1.157214 1.367336 0.965901
0.130 0.358417 1.027259 1.240794
0.140 0.280482 0.908245 1.122188
0.150 0.300939 0.910741 1.148865
0.160 0.933791 0.933791 1.159909
0.170 0.291571 0.933791 1.060461
0.180 0.304284 0.954061 0.954061
0.190 0.355919 0.870504 0.855278
0.200 0.423931 0.727023 0.530994
0.0 0.5 1.0 1.5 2.0
SCC_BLK_S2_2B_DEGREE_12_10_2007_rect_hdf_xy_1_magInterp

C.12 PINC 5.15

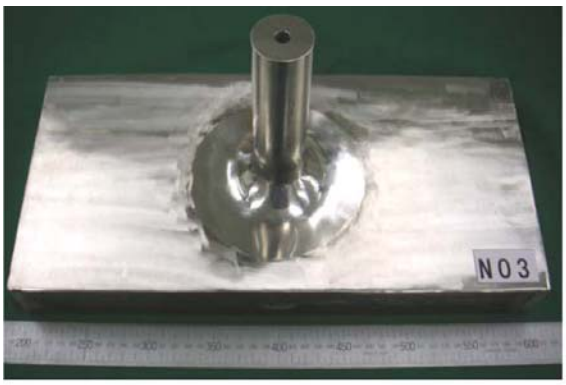
N03

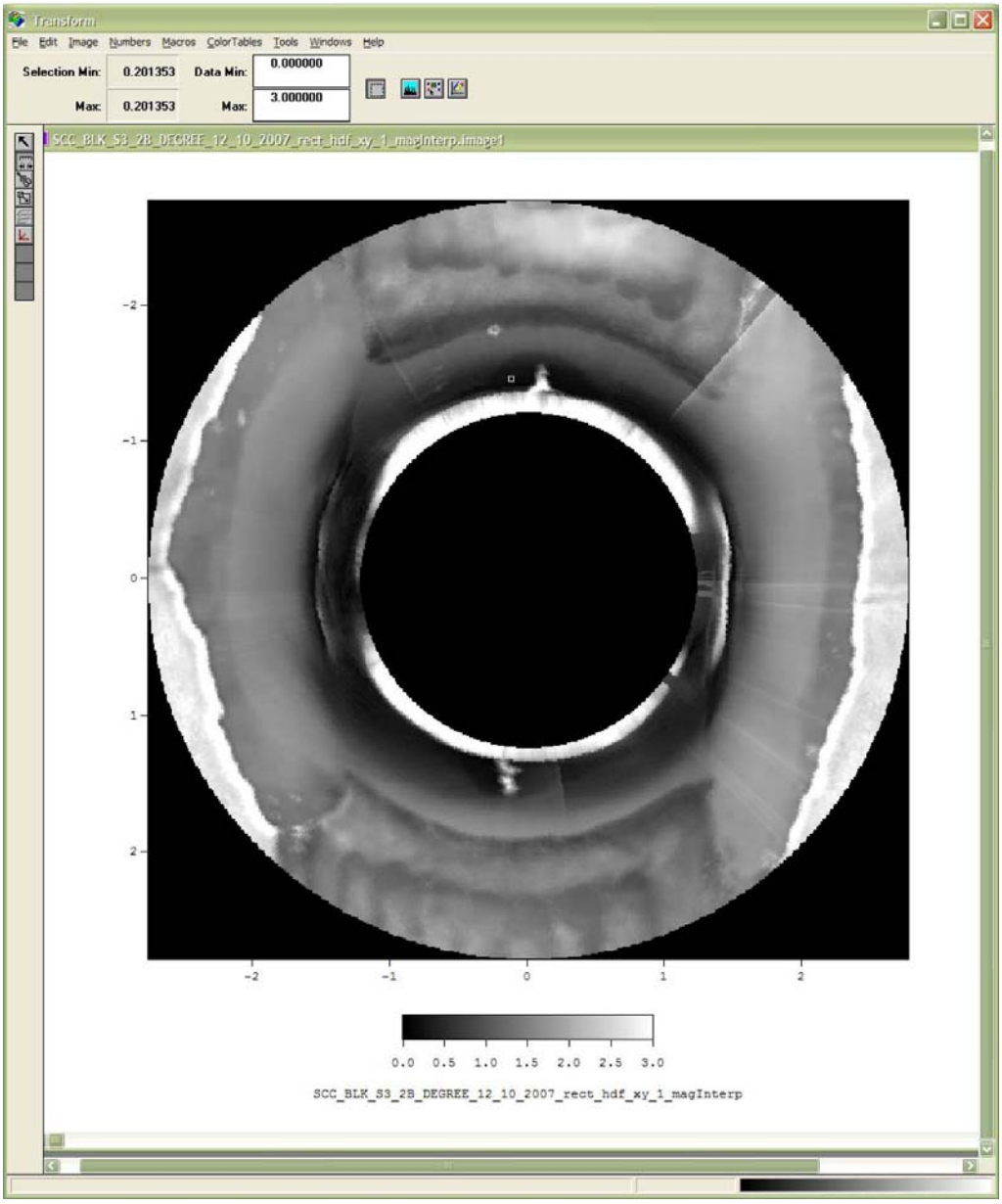
Transform
File Edit Image Numbers Macros ColorTables Tools Windows Help
Selection Min: 0.201353
Max: 0.201353
Data Min: 0.000000
Max: 3.000000
SCC_BLK_S3_2B_DEGREE_12_10_2007_rect_hdf_xy_1_magInterp.image1
-2
-1
0
1
2
0.0 0.5 1.0 1.5 2.0 2.5 3.0
SCC_BLK_S3_2B_DEGREE_12_10_2007_rect_hdf_xy_1_magInterp

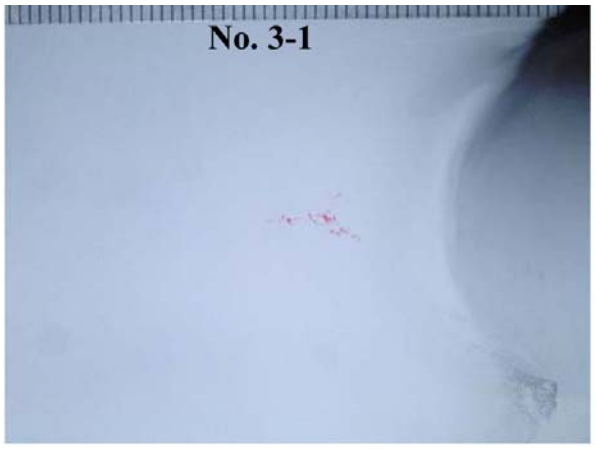
No. 3-1

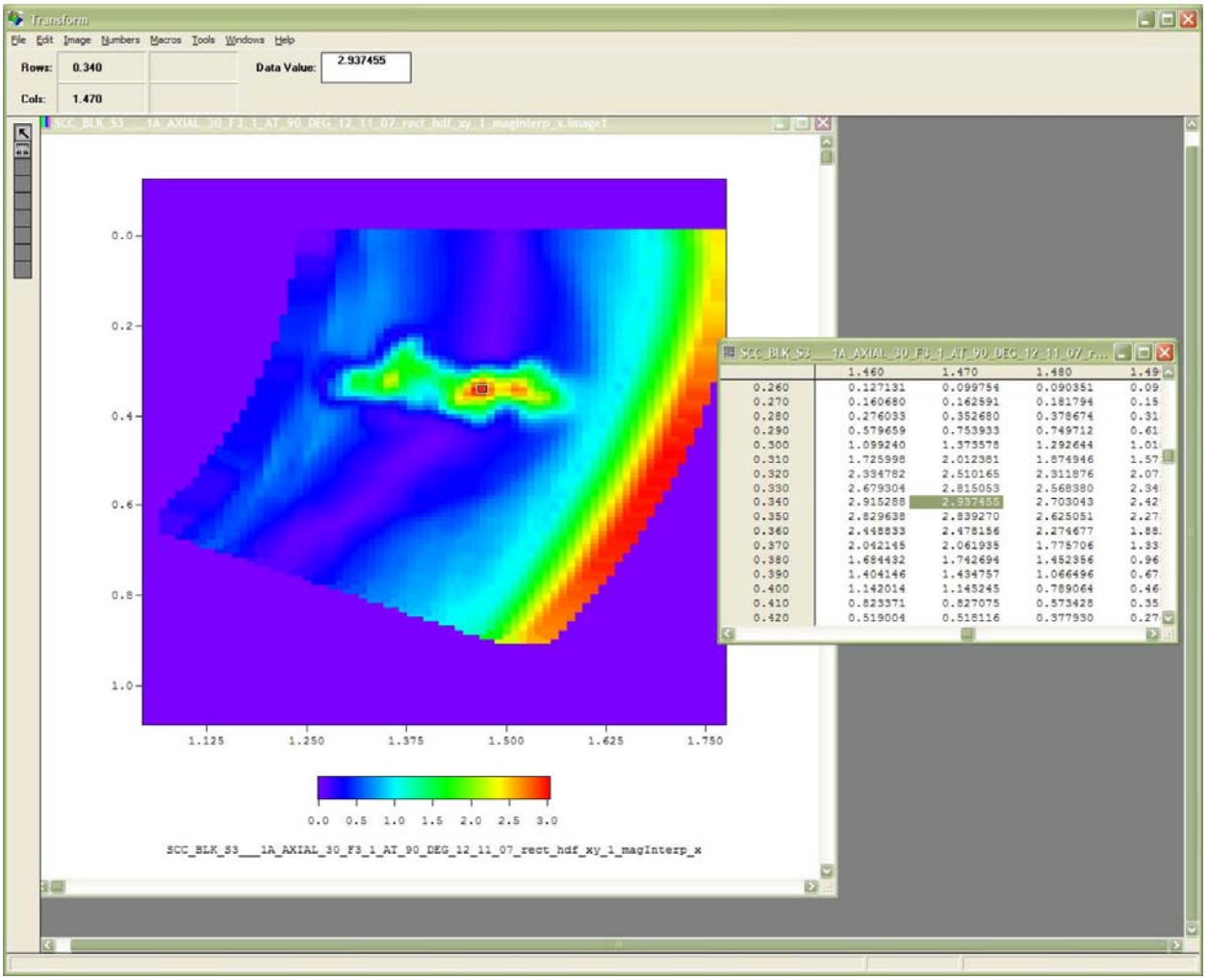
Transform
File Edit Image Numbers Macros Tools Windows Help
Rows: 0.340
Cols: 1.470
Data Value: 2.937455
SCC_BLK_S3___1A_AXIAL_30_F3_1_AT_90_DEG_12_11_07_rect_hdf_xy_1_magInterp_x
1.460 1.470 1.480
0.260 0.127131 0.099754 0.090351
0.270 0.160680 0.162591 0.181794
0.280 0.276033 0.352680 0.378674
0.290 0.579659 0.753933 0.749712
0.300 1.099240 1.373578 1.292644
0.310 1.725998 2.012381 1.874946
0.320 2.334782 2.510165 2.311876
0.330 2.679304 2.815053 2.568380
0.340 2.915288 2.937455 2.703043
0.350 2.829638 2.839270 2.625051
0.360 2.448833 2.478156 2.274677
0.370 2.042145 2.061935 1.775706
0.380 1.684432 1.742694 1.452356
0.390 1.404146 1.434757 1.066496
0.400 1.142014 1.145245 0.789064
0.410 0.823371 0.827075 0.573428
0.420 0.519004 0.518116 0.377930
0.0 0.2 0.4 0.6 0.8 1.0
1.125 1.250 1.375 1.500 1.625 1.750
0.0 0.5 1.0 1.5 2.0 2.5 3.0
SCC_BLK_S3___1A_AXIAL_30_F3_1_AT_90_DEG_12_11_07_rect_hdf_xy_1_magInterp_x

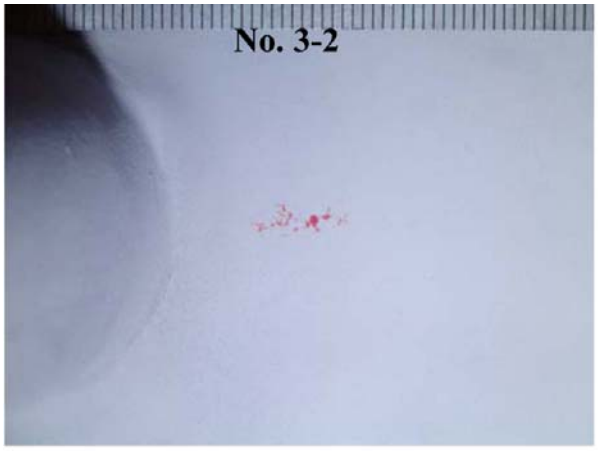
No. 3-2

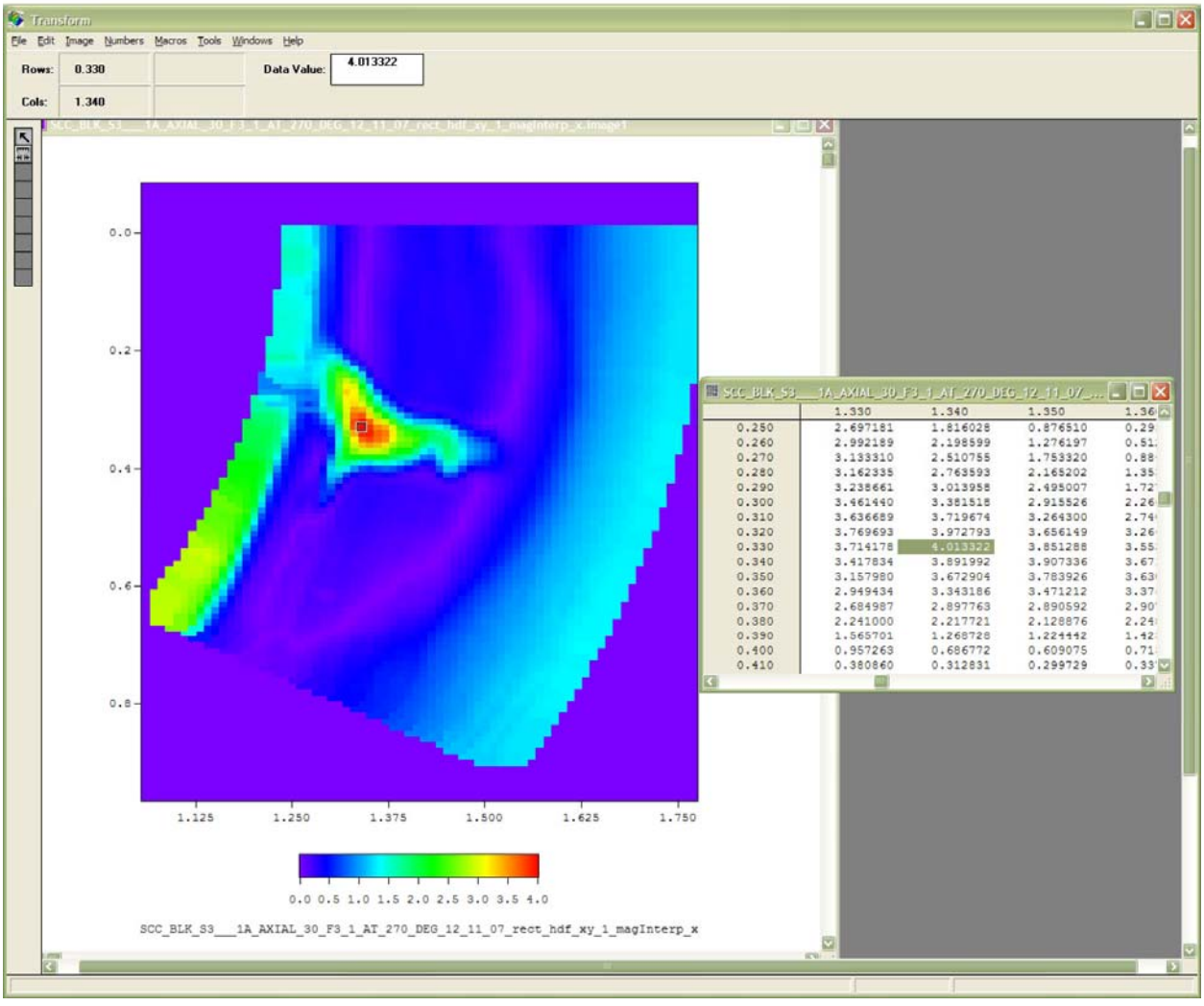
Transform
File Edit Image Numbers Macros Tools Windows Help
Rows: 0.330
Cols: 1.340
Data Value: 4.013322
0.0
0.2
0.4
0.6
0.8
1.125 1.250 1.375 1.500 1.625 1.750
0.0 0.5 1.0 1.5 2.0 2.5 3.0 3.5 4.0
SCC_BLK_S3___1A_AXIAL_30_F3_1_AT_270_DEG_12_11_07_rect_hdf_xy_1_magInterp_x
1.330 1.340 1.350
0.250 2.697181 1.816028 0.876510
0.260 2.992189 2.198599 1.276197
0.270 3.133310 2.510755 1.753320
0.280 3.162335 2.763593 2.165202
0.290 3.238661 3.013958 2.495007
0.300 3.461440 3.381518 2.915526
0.310 3.636689 3.719674 3.264300
0.320 3.769693 3.972793 3.656149
0.330 3.714178 4.013322 3.851288
0.340 3.417834 3.891992 3.907336
0.350 3.157980 3.672904 3.783926
0.360 2.949434 3.343186 3.471212
0.370 2.684987 2.897763 2.890592
0.380 2.241000 2.217721 2.128876
0.390 1.565701 1.268728 1.224442
0.400 0.957263 0.686772 0.609075
0.410 0.380860 0.312831 0.299729

C.13 PINC 5.16

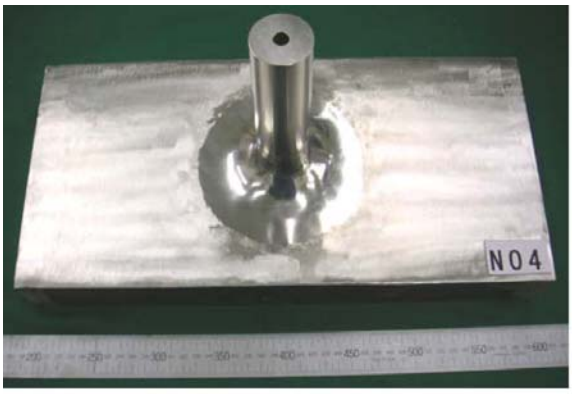

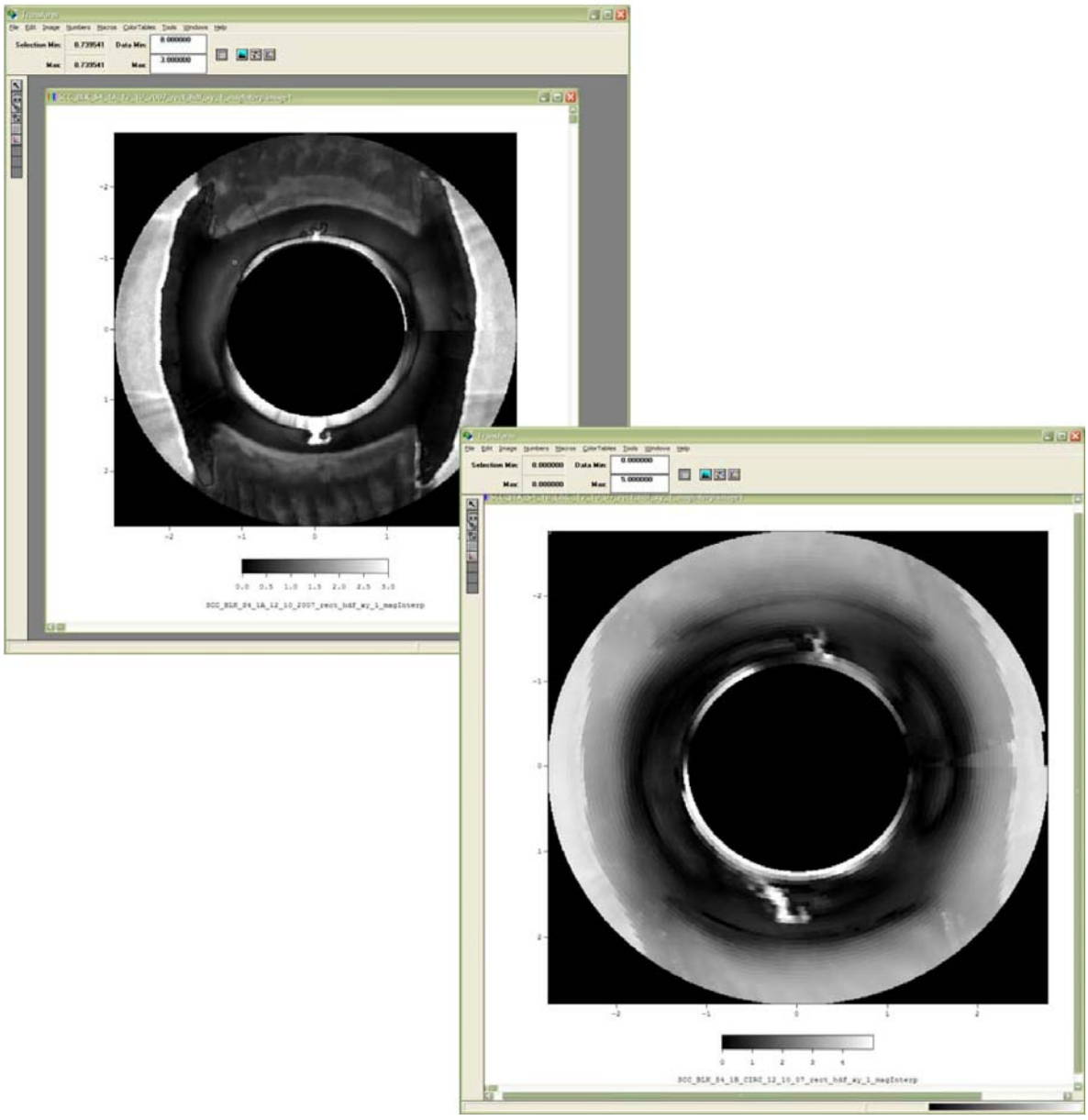

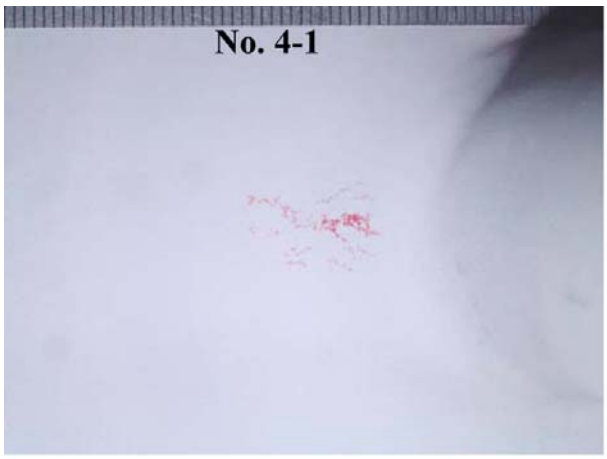
No. 4-1

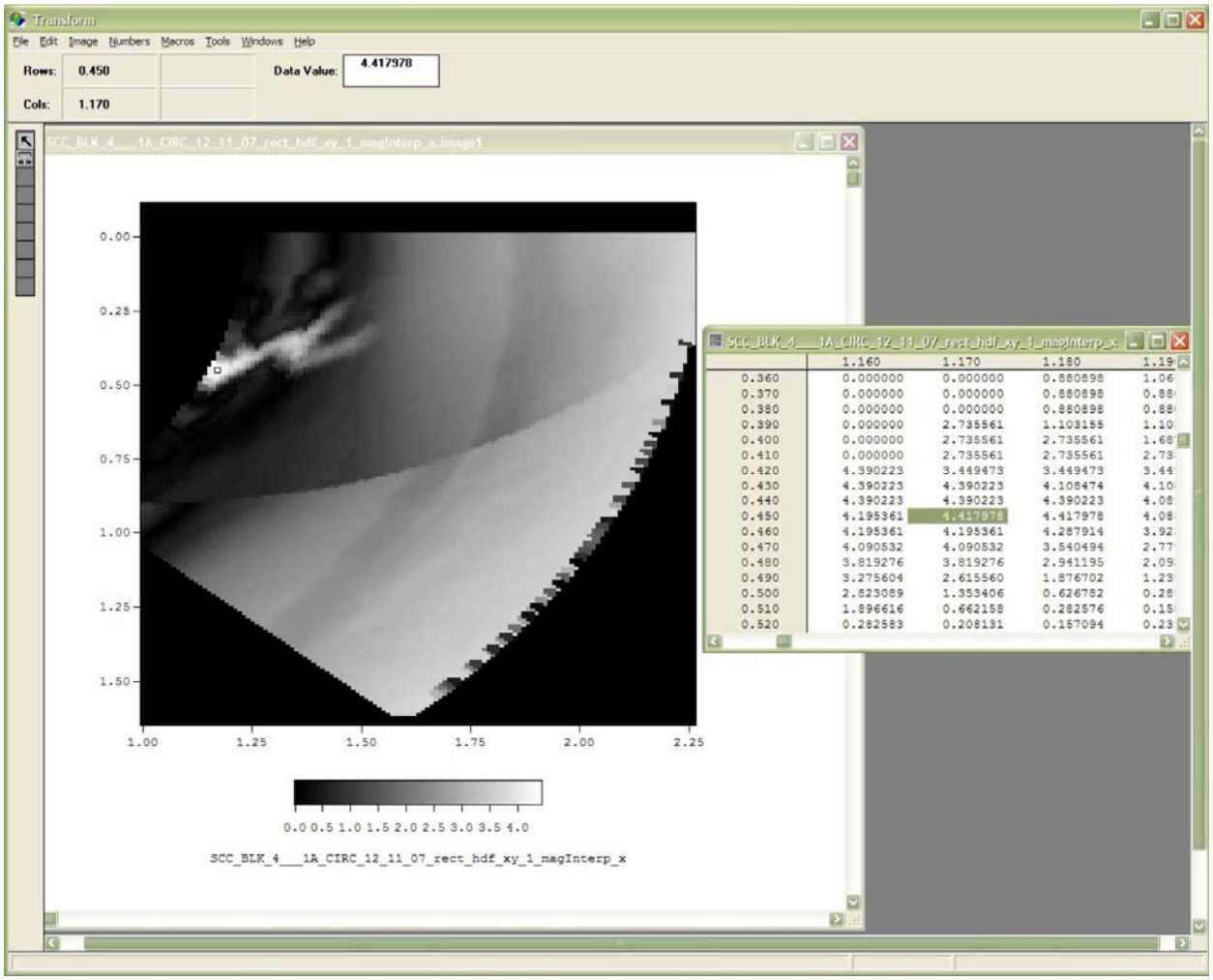
Transform
File Edit Image Numbers Macros Tools Windows Help
Rows: 0.450
Cols: 1.170
Data Value: 4.417978
SCC_BLK_4___1A_CIRC_12_11_07_rect_hdf_xy_1_magInterp_x.image1
0.00
0.25
0.50
0.75
1.00
1.25
1.50
1.00 1.25 1.50 1.75 2.00 2.25
0.0 0.5 1.0 1.5 2.0 2.5 3.0 3.5 4.0
SCC_BLK_4___1A_CIRC_12_11_07_rect_hdf_xy_1_magInterp_x
SCC_BLK_4___1A_CIRC_12_11_07_rect_hdf_xy_1_magInterp_x
1.160 1.170 1.180 1.19
0.360 0.000000 0.000000 0.880898 1.06
0.370 0.000000 0.000000 0.880898 0.88
0.380 0.000000 0.000000 0.880898 0.88
0.390 0.000000 2.735561 1.103155 1.10
0.400 0.000000 2.735561 2.735561 1.68
0.410 0.000000 2.735561 2.735561 2.73
0.420 4.390223 3.449473 3.449473 3.44
0.430 4.390223 4.390223 4.108474 4.10
0.440 4.390223 4.390223 4.390223 4.08
0.450 4.195361 4.417978 4.417978 4.08
0.460 4.195361 4.195361 4.287914 3.92
0.470 4.090532 4.090532 3.540494 2.77
0.480 3.819276 3.819276 2.941195 2.09
0.490 3.275604 2.615560 1.876702 1.29
0.500 2.823089 1.353406 0.626782 0.28
0.510 1.896616 0.662158 0.282576 0.15
0.520 0.282583 0.208131 0.157094 0.23

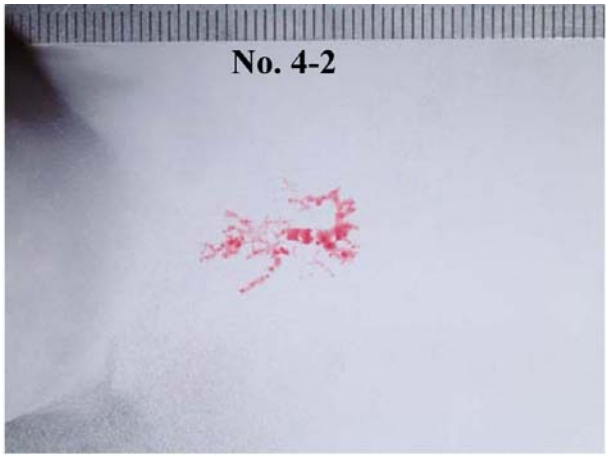
No. 4-2

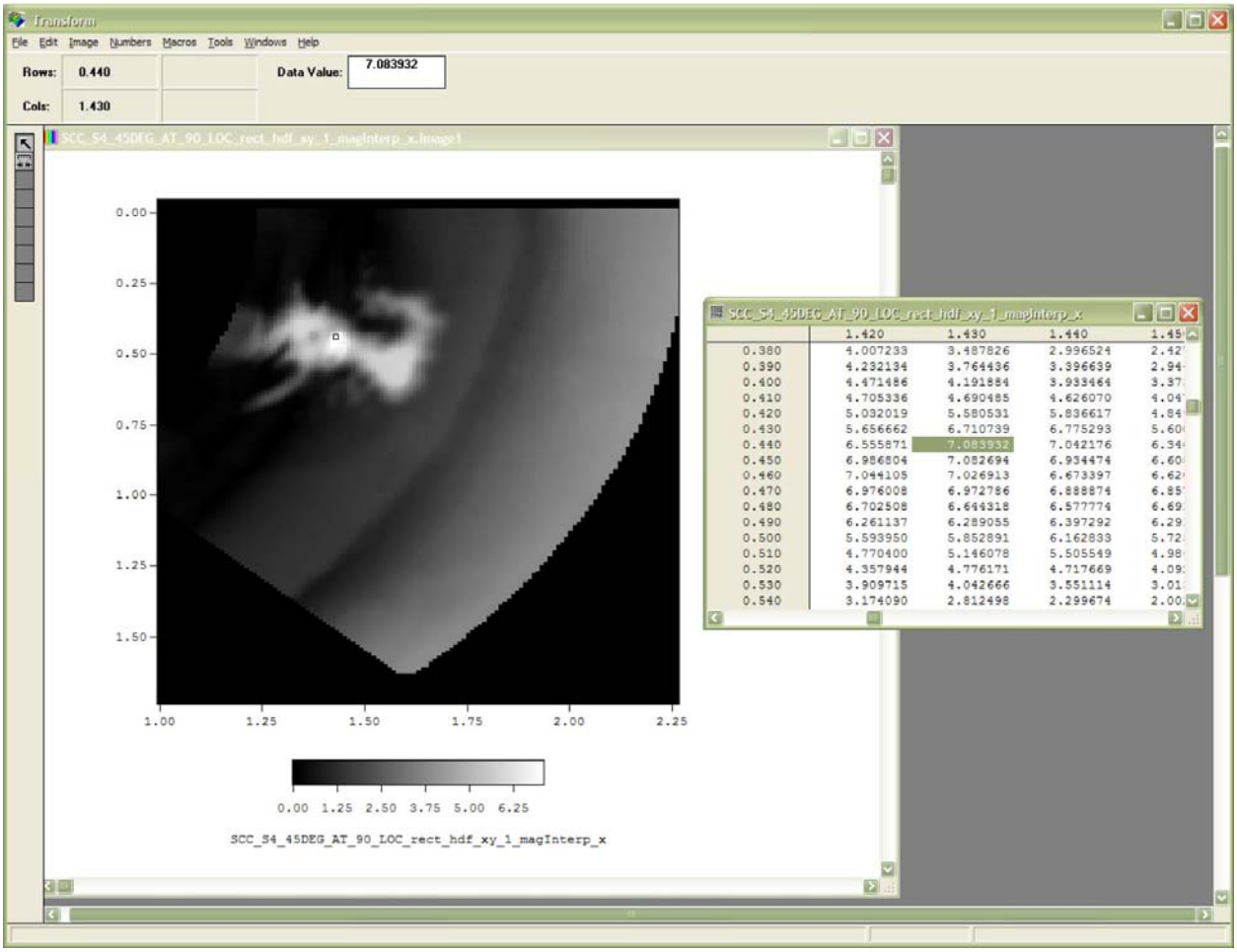
Transform
File Edit Image Numbers Macros Tools Windows Help
Rows: 0.440
Cols: 1.430
Data Value: 7.083932
SCC_S4_45DEG_AT_90_LOC_rect_hdf_xy_1_magInterp_x:Image1
0.00
0.25
0.50
0.75
1.00
1.25
1.50
1.00 1.25 1.50 1.75 2.00 2.25
0.00 1.25 2.50 3.75 5.00 6.25
SCC_S4_45DEG_AT_90_LOC_rect_hdf_xy_1_magInterp_x
SCC_S4_45DEG_AT_90_LOC_rect_hdf_xy_1_magInterp_x
1.420 1.430 1.440 1.45
0.380 4.007233 3.487826 2.996524
0.390 4.232134 3.764436 3.396639
0.400 4.471486 4.191884 3.933464
0.410 4.705336 4.690485 4.626070
0.420 5.032019 5.580531 5.836617
0.430 5.656662 6.710739 6.775293
0.440 6.555871 7.083932 7.042176
0.450 6.986804 7.082694 6.934474
0.460 7.044105 7.026913 6.673397
0.470 6.976008 6.972786 6.888874
0.480 6.702508 6.644318 6.577774
0.490 6.261137 6.289055 6.397292
0.500 5.593950 5.852891 6.162833
0.510 4.770400 5.146078 5.505549
0.520 4.357944 4.776171 4.717669
0.530 3.909715 4.042666 3.551114
0.540 3.174090 2.812498 2.299674

Distribution

No. of
Copies

Name
Organization
Address
City, State and Zip Code

Name
Organization
Address
Address line 2
COUNTRY

Organization
Address
City, State and Zip Code
Name
Name
Name
Name
Name (#)

No. of
Copies

Name
Organization
Address
City, State and Zip Code

Internal Distribution
Pacific Northwest National Laboratory
P.O. Box 999
Richland, WA 99352

Name	Mailstop
Name	Mailstop
Name	Mailstop
Name	Mailstop
Name	(PDF)

Pacific Northwest
NATIONAL LABORATORY

Proudly Operated by **Battelle** *Since 1965*

U.S. DEPARTMENT OF
ENERGY

902 Battelle Boulevard
P.O. Box 999
Richland, WA 99352
1-888-375-PNNL (7665)
www.pnl.gov